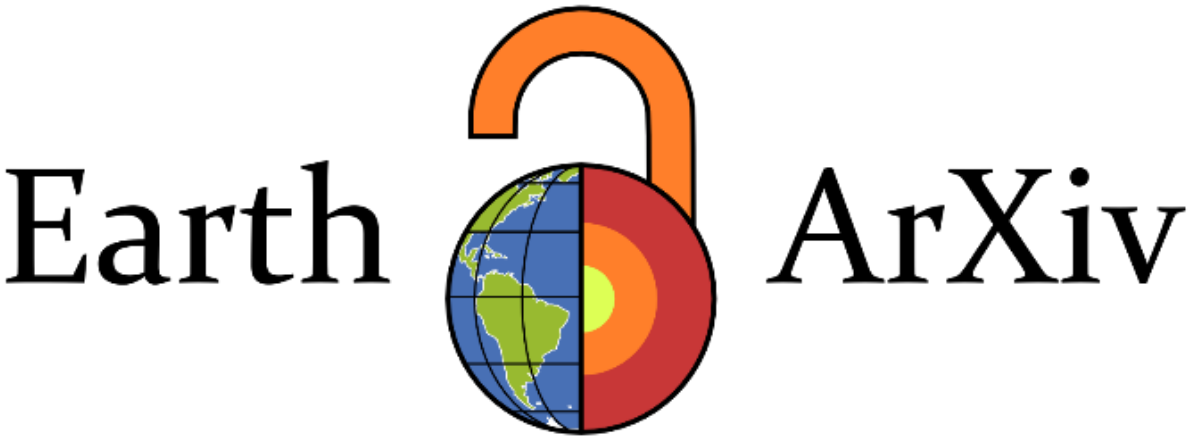

Peer review status:

This is a non-peer-reviewed preprint submitted to EarthArXiv.

Interplay between supercontinents and accretionary orogens recorded in 200 million years of metallogeny

Yanbo Cheng[1] *, Phil Gilmore[1, 2], Michael Doublier[1], Karol Czarnota[1], Chris Lewis[1], Holly Taylor[1], Andrew Clark[1], Liam Pitt[1], David Mole[1], Yue Wang[3], Sebastien Meffre[4], Adrienne Brotodewo[5], Ross Cayley[6], Cameron Cairns[6], Antony Burnham[1, 3], Tom Wise[7]

1 Geoscience Australia, Canberra 2609, Australia

2 Geoscience, Exploration and Mineral Systems, Newcastle 2300, Australia

3 Research School of Earth Sciences, The Australian National University, Canberra 2601, Australia

4 Earth Sciences, University of Tasmania, Hobart 7006, Australia

5 MinEx CRC, Future Industries Institute, Adelaide University, Adelaide 5005, Australia

6 The Geological Survey of Victoria, Melbourne 3002, Australia

7 The Geological Survey of South Australia, Adelaide, 5000, Australia

* Correspondence: yanbo.cheng@ga.gov.au

Abstract

The assembly of supercontinents and the evolution of accretionary orogens are one of the most fundamental drivers of Earth's lithospheric architecture and mineral endowment. Here we reconstruct the 200 million years metallogenic history of the mainland Australian part of the Delamerian convergent margin, a pivotal segment of the East Gondwana paleo-Pacific margin that archives the transition from Rodinian fragmentation to terminal Gondwana assembly. Our analysis reveals that the region's mineral potential is a non-random result of sequential tectonic switching and specific magmatic priming. Magmatic fertility was governed by a narrow window of high hydration, deep-seated fractionation, and elevated oxidation states driven by the recycling of continental and oceanic sediments during multiple tectonic switching events. Integrated geological, geochemical, geochronological, and sulphur isotope evidence identifies four temporally distinct mineralisation events – from Neoproterozoic orthomagmatic Ni-Cu to Siluro-Devonian intrusion-related Au formations. Unlike the specialised "copper factories" of the Andes or the reduced magmatic systems of Japan, the Delamerian convergent margin functions as a diverse "general store" of strategic resources and critical minerals preserved beneath widespread post-mineralisation sedimentary cover. This 200 million years record demonstrates how the interactions between supercontinent and accretionary orogens are translated into four distinctive metallogenic belts within one coherent mineral province.

Introduction

The assembly and dispersal of supercontinents are one of the most fundamental drivers of Earth's lithospheric architecture, regulating geodynamics, and the distribution of global mineral wealth (Cawood et al., 2021). Although the spatial concentration of giant ore deposits is often attributed to localised crustal processes, the first-order control remains the long-term geodynamic evolution of continental margins during major plate reorganisations (e.g., Richards, 2015). The 5,000 km long paleo-Pacific margin of East Gondwana archives a pivotal transition from the fragmentation of Rodinia to the terminal assembly of Gondwana—a tectonic trajectory that provides a favourable laboratory for examining how the interplay of supercontinents and accretionary orogens primes a continental margin to enable a multi-commodity metallogenic province.

A notably well-preserved and accessible portion of the East Gondwana margin is present in eastern Australia. These rocks record the transition from a Neoproterozoic passive margin to a convergent margin that has continued throughout the Phanerozoic and led to the formation of several extensive accretionary orogenic systems, collectively called the Australian Tasmanides. The accretionary orogenic systems young from west to east as: (1) the Cambrian Delamerian Orogen (its eastern half comprising Cambrian deformation superimposed over the Neoproterozoic Rodinian passive margin succession, and its eastern half comprised of a convergent margin complex); (2) the Neoproterozoic to Devonian Mossman Orogen and Thomson Orogen; (3) the Ordovician-Devonian Lachlan Orogen; and (4) the Carboniferous-Triassic New England Orogen. Combined, they constitute the eastern one-third of the continent. Apparently obliquely offset and therefore allochthonous to the mainland geology, but sharing key characteristics (Cayley, 2011; Schofield et al., 2018; Habib et al., 2023), Western Tasmania / King Island together with a portion of central Victoria exhibits Cambrian (Tyennan) orogenesis contemporary with the Delamerian Orogeny, superimposed onto Proterozoic continental crust and including similar Cambrian calc-alkaline igneous successions (Crawford et al., 1996; Cayley et al., 2002; Corbett et al., 2014). The older parts of the Tasmanides geology continues into central Queensland, largely concealed beneath basin successions.

The Delamerian Orogen represents rocks first deformed by the late Cambrian ~500 Ma orogeny and records a change from a passive to convergent margin in the early Cambrian ~530 Ma (Glen 2005). Rocks that record the onset of convergent margin activity are well-preserved and well-exposed along the eastern half of the Delamerian Orogen in NSW and Victoria and encountered in multiple drillholes in northeast South Australia and southwest Queensland and are the focus of this study. Herein, the rocks are referred to as the Delamerian convergent margin. These rocks record not only the onset of paleo-Pacific convergent margin activity in the Cambrian, but also younger distal back-arc tectono-magmatic events driven by stress changes related to the staggered migration of the convergent margin and associated arc system to the east. Multidisciplinary analysis of these rocks and their contained mineralisation reveal four metallogenic regions: the Koonenberry, Lock Lilly-Kars/Wintlow, Nanyah–Glenelg and Stavely. Together, these regions preserve four temporally distinct mineralisation events: (1) Neoproterozoic orthomagmatic Ni–Cu systems developed during continental attenuation; (2) Cambrian volcanic-hosted massive sulfide (VHMS) and porphyry–epithermal systems related to magmatic arc activity (Mortensen et al., 2015; Schofield et al., 2018); (3) Ordovician–Silurian orogenic gold during a discrete crustal thickening event (Willman et al., 2010; Cayley et al., 2011; Bierlein et al., 2024); and (4) Siluro-Devonian porphyry and intrusion-related gold (IRG) systems related to far-field

extension driven by younger, outboard subduction (Bierlein et al., 2002). This diversity in deposit types (with more details in Appendix 1), preserved over a 200-million-year interval from rifting through subduction to post-orogenic overprinting processes, is the subject of this study.

This metallogenic breadth is a direct consequence of tectonic switching and specific magmatic priming. We propose that prospective magmatic fertility in the Delamerian convergent margin was regulated by a narrow window of hydration content and oxidation states, driven by the recycling of continental and oceanic sediments during the transition between different tectonic regimes. Furthermore, while high uplift orogens, such as in the Andes, generally lose their associated deposits due to subsequent erosion, (Sillitoe, 2018; Farrar et al., 2023), mineralisation in the Delamerian convergent margin is often preserved due to moderate shortening and limited erosion, such as in the Stavely region of Victoria. By integrating new geochronological, geochemical, and sulphur isotope datasets related to the transition from passive to convergent margin of Eastern Gondwana in the Australian Tasmanides, we demonstrate how the interplay of supercontinent cycles and accretionary processes create a diverse metallogenic landscape essential for the global supply of strategic resources and critical minerals.

The supercontinents, passive and convergent margins, and accretionary orogens of the Tasmanides

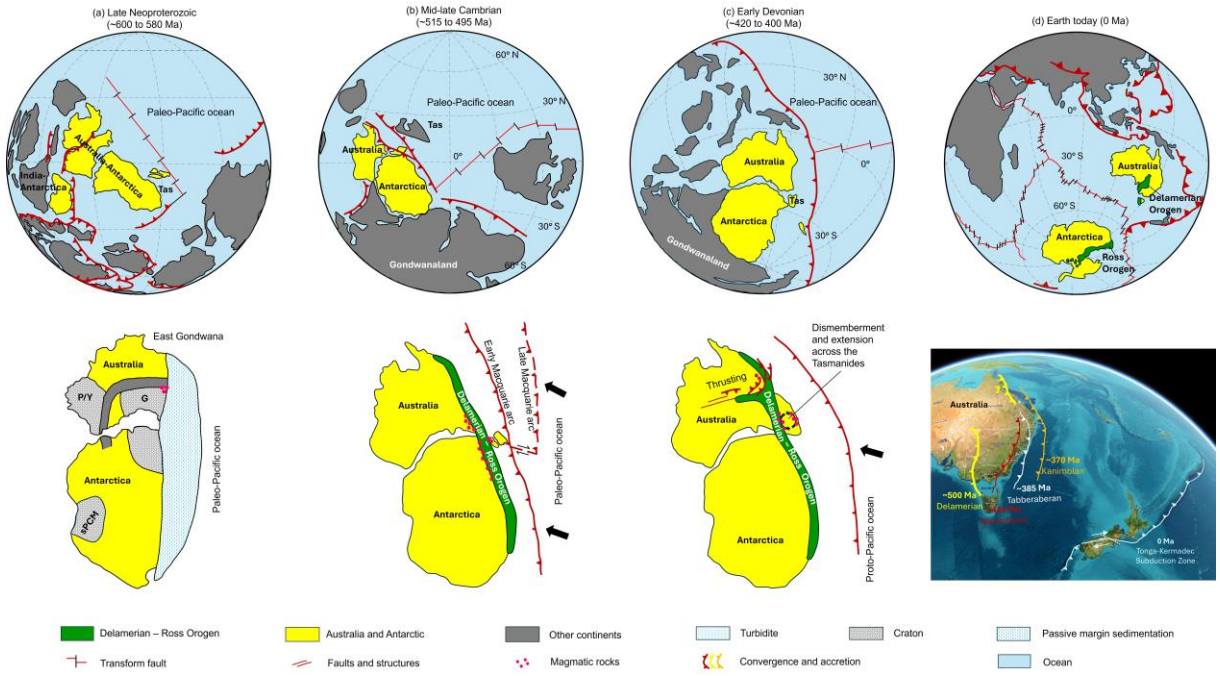

Figure 1 Paleogeographic reconstructions illustrating the tectonic evolution of the Delamerian–Ross Orogen along the eastern Gondwana paleo-Pacific margin from the (a) Late Neoproterozoic (~600-580 Ma), (b) Mid-late Cambrian (~515-495 Ma), (c) Early Devonian (~420-400 Ma) to (d) the present day (0 Ma). Figure modified from Li and Powell (2001), Collins and Pisarevsky (2005), Foster (2013), Champion et al., (2016), Merdith et al., (2017) and Glen and Cooper (2021).

The geodynamic framework of the Delamerian Orogen, as part of the Delamerian convergent margin, is rooted in two successive supercontinent cycles: the fragmentation of Rodinia and the terminal assembly of Gondwana (Cawood, 2005; Li et al., 2008). Episodic lithospheric extension between ca. 830 Ma and 580 Ma established a series of magmatic and non-magmatic passive margins along the Tasman Line (Direen and Crawford, 2003; Merdith et al., 2021). The rifting sequences record the final attenuation of continental lithosphere and the birth of the nascent paleo-Pacific Ocean (Crawford et al., 1997; Lloyd et al., 2022). The lithospheric attenuation between 600 and 580 Ma is preserved in the Glenelg River Complex (South Australia) and Mount Arrowsmith Volcanics (New South Wales) as fragments of a hyper-extended continental margin (Greenfield et al., 2011; Gibson et al., 2015; Schofield et al., 2018; Mulder et al., 2020). During this interval, the VanDieland microcontinent—incorporating parts of the West Tasmania Terrane and the Selwyn Block—has been interpreted to have drifted from the Gondwanan margin, initiating independent drift into a nascent marginal basin (Moore et al., 2015; Glen and Cooper, 2021). Alternative interpretations suggest that only parts of this microcontinent have a rift/drift origin (e.g., Schofield et al., 2018) The geodynamic framework and its relationship to the continental architecture evolution are outlined in Fig. 1.

The long-lived passive margin regime was terminated by a geodynamic reorganisation at ca. 515 ± 5 Ma, triggered by terminal suturing of Gondwana along the internal Mozambique and Kuunga sutures (Boger and Miller, 2004; Foden et al., 2006). The associated continental collision diverted tectonic energy to the supercontinent's periphery, forcing increased convergence rates and the initiation of west-dipping subduction along the previously rifted margins of Australia and Antarctica (Fig. 1b; Rossetti et al., 2011). The event marked the inception of the Delamerian Orogen in southeastern Australia and the structurally active phase of the Ross Orogeny in Antarctica (Glen and Cooper, 2021). In the authochthonous part of the mainland Australian sector, this convergent phase established a series of contemporaneous magmatic arcs including, from south to north, the Stavely Arc in present-day western Victoria, magmatic rocks with arc affinities in the Loch Lilly-Kars and Lake Wintlow belts and the Mount Wright Arc in New South Wales with related magmatism spanning 15-20 Myr (Greenfield et al., 2011; Clark et al., 2024).

The earliest dated stages of subduction along the Gondwana margin are preserved as boninitic juvenile arc rocks (ca. 514 Ma) in the Glenelg Zone, reflecting high-temperature melting of a depleted mantle wedge above a newly foundering slab (Kemp, 2003). Farther east in Victoria, boninitic juvenile arc rocks as old as 520 Ma occur in the Heathcote Volcanic Group but appear to be part of an intra-oceanic arc developed some distance east of Gondwana (Crawford and Keays, 1987; VandenBerg et al., 2000; Squire et al., 2006; Schofield et al., 2018).

The Gondwana margin system displays changes in subduction dynamics along its length. The northern parts of the system in NSW remained semi-stationary with respect to Gondwana, while further south rollback related extension, easterly arc migration and segmentation, and back-arc basin formation became increasingly prevalent, most pronounced in the vicinity of the Stavely Arc. Here, juvenile boninitic to andesitic magmatism in the Stavely Arc is coeval with extension, voluminous sedimentation and back-arc magmatism in the Kanmantoo Trough and Glenelg Zone to its west (Jago et al., 2003; Curtis et al., 2022; Cayley et al., 2011).

Arc magmatism ceased following the main stage of the Delamerian Orogeny at ~500 Ma (e.g., Foden et al., 2002; Schofield et al., 2018). Multiple studies ascribe this phase of orogenesis to the collision of a microcontinent such as VanDieland (e.g., Cayley, 2011; Glen and Cooper, 2021) or Hay-Booligal Zone (Greenfield et al., 2011). This event was followed by locally voluminous A-type magmatism, including the Padthaway Ridge in South Australia (Foden et al., 2002). This magmatism represents a post-orogenic extensional setting and may have been related to slab break-off (Foden et al., 2020).

Following the Delamerian Orogeny, arc magmatism migrated outboard. The geological evidence preserved in western Victoria favours the initiation of a new volcanic arc in a new position farther outboard, rather than rapid slab rollback from the Gondwana margin. This is because intervening intra-oceanic-style crust is older than the Delamerian Orogeny and older even than the onset of Gondwana margin arc magmatism (VandenBerg, 1992; Cayley, 2011). The Ordovician volcanic arc, active between 490 and 460 Ma, is the Macquarie Arc and its formation heralded the onset of the Lachlan Orogen (e.g., Foster and Gray, 2000). A predominantly extensional back arc regime prevailed until the Benambran Orogeny (ca. 445–435 Ma), which recorded the closure of marginal basins and the structural docking of intra-oceanic systems with the continental margin (e.g., Glen and Cooper, 2021). The interval between 430 and 390 Ma was defined by continued tectonic switching that further matured the newly accreted crustal architecture (e.g., Foster and Goscombe, 2013). This interval was also characterised by widespread felsic-dominated magmatism (both peraluminous and metaluminous) that occurred across the Lachlan Orogen and parts of the Delamerian convergent margin, reflecting widespread extension associated with subduction rollback (e.g., Cayley, 2015; Moresi et al., 2014), including advection of mantle heat into the crust during extensional phases (e.g., Chappell et al., 1988; Collins & Richards, 2008). Orogenic pulses, including the Bindian (ca. 420-410 Ma) and Tabberabberan (ca. 390–380 Ma), further amalgamated diverse terranes into the modern stable continental framework of eastern Australia (e.g., Champion et al., 2016).

Tectono-stratigraphic and metallogenic evolution of the Delamerian convergent margin

The Delamerian convergent margin of southeastern Australia preserves sequences of Neoproterozoic–Cambrian continental-margin accretion along the paleo-Pacific margin of Gondwana (Gilmore et al., 2025). Four metallogenic belts—the Koonenberry Belt (KB), Loch Lilly–Kars Belt (LLKB), Anabama–Glenelg Belt (AGB), and Stavely Belt (SB)—can be distinguished based on their metallogenic inventory, magmatic history and position within the Delamerian convergent margin, spanning an inboard-to-outboard transect from the ancient continental margin to the distal arc system. The synthesis presented in Fig. 2 integrates stratigraphic, geochemical, metamorphic, geochronological, and metallogenic data from the Archaean to the Cambrian, with post-accretion intraplate activity continuing into the Devonian, to reconstruct the temporal and spatial architecture of the margin and evaluate its prospectivity for mineral systems.

The stratigraphy associated with the four metallogenic belts records three first-order phases of basin development superimposed on Archaean–Paleoproterozoic basement (Fig. 2). An initial phase of Rodinian rifting (~830–635 Ma) produced mafic-dominated sequences carrying OIB to N-MORB geochemical affinities consistent with incipient continental breakup (Wingate et al., 1998; Morand et al., 2003; Gilmore et al., 2025). Gairdner Large Igneous Province (LIP) magmatism at ca. 827 Ma is recorded as dyke swarms and gabbroic intrusions, including the Little Broken Hill Gabbro in the

Curnamona Province (827 ± 9 Ma; Wingate et al., 1998). A later phase of passive-margin thermal subsidence (~635–530 Ma) accumulated deep-water turbidite sequences, whose metapelitic and metagreywacke assemblages recorded a protracted sedimentation history (Turner et al., 2022). This was followed by the most tectonically dynamic period (~530–360 Ma), which encompasses multiple cycles of subduction initiation, arc construction, orogenesis, and post-orogenic collapse. It is during this interval that the margin's most significant mineral systems operated.

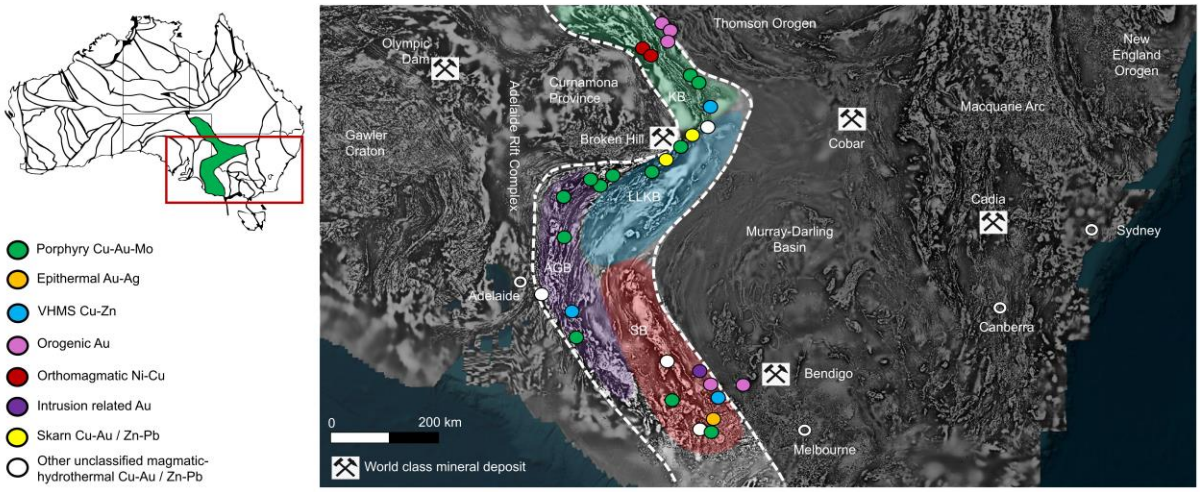

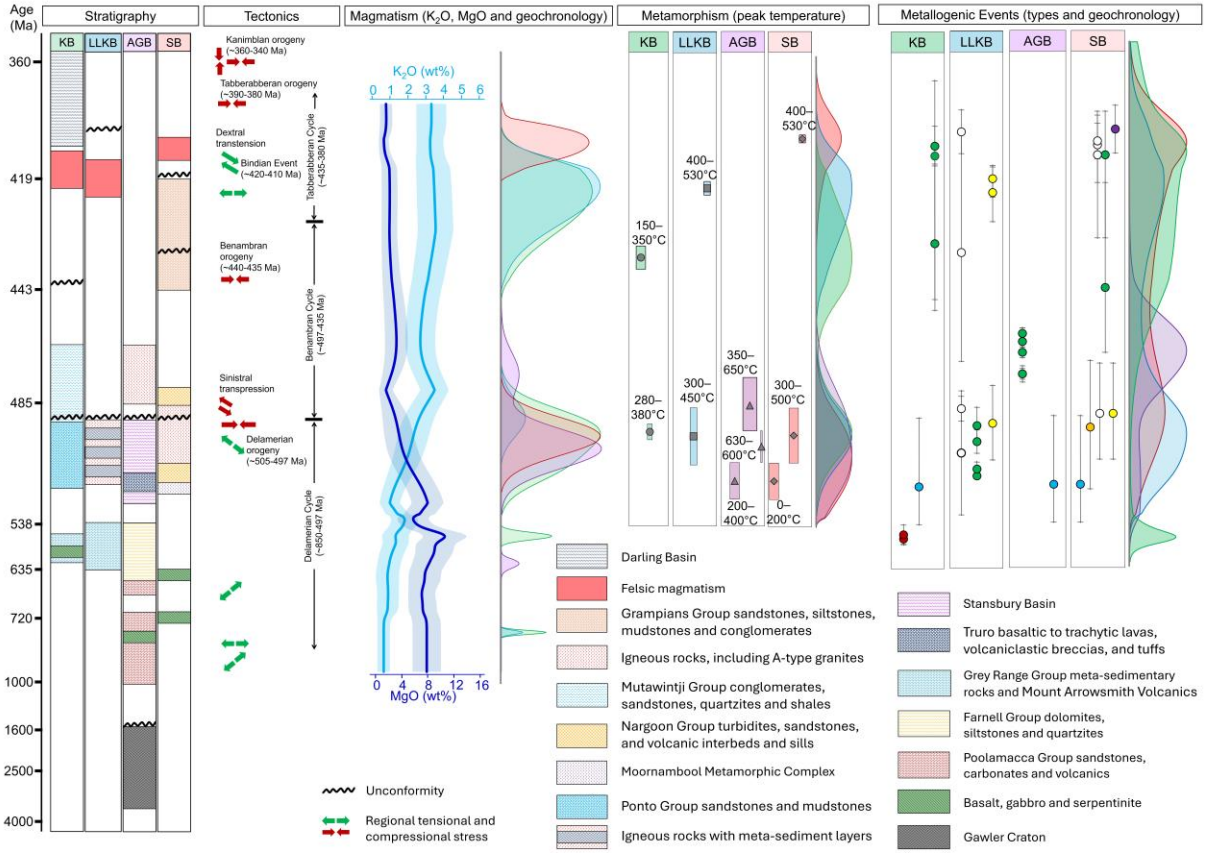

Figure 2 Integrated geological framework for the Delamerian convergent margin showing the interrelationship between stratigraphy, tectonic stress variations, tectonic cycles, geochronology and geochemistry of magmatic history, peak metamorphism temperatures, and ages of mineralisation across the four metallogenic belts, including the Koonenberry Belt (KB), Loch Lilly–Kars Belt (LLKB), Anabama–Glenelg Belt (AGB), and Stavely Belt (SB) of the Delamerian convergent margin. The density curves of (1) magmatism are for the timing of magmatic pulses in KB (green), LLKB (blue), AGB (purple) and SB (red); (2) metamorphism are for the peak temperatures of each regional metamorphic events in KB (green), LLKB (blue), AGB (purple) and SB (red); and (3) ages of metallogenic events in KB (green), LLKB (blue), AGB (purple) and SB (red).

Magmatic evolution across the margin is characterised by systematic compositional shifts that track the transition from rift through arc to post-orogenic settings (Fig. 2). The K_2O and MgO trends of collective magmatic rocks, shown as Gaussian-weighted mean curves with uncertainty envelopes, reveal a margin-wide pattern: mafic, low-K_2O rift basalts dominate the Neoproterozoic record, giving way to medium-K calc-alkaline suites during the Cambrian (~530–495 Ma), before the emergence of high-K post-tectonic magmatism in the Siluro-Devonian (~440–360 Ma). The boninitic-to-calc-alkaline arc sequence of SB—spanning ~525–500 Ma and culminating in the Mount Stavely Volcanic Complex (507.34 ± 0.38 Ma) and Victor Porphyry (503.84 ± 0.30 Ma) (Lewis et al., 2017)—represents the most complete Cambrian arc stratigraphy documented in the Ross–Delamerian Orogen. Magmatic pulse density curves derived from Gaussian kernel density estimation (KDE, bandwidth = 8 Ma) of margin-wide magmatic rocks confirm a dominant Cambrian pulse in all the terranes except the AGB, with secondary Devonian pulses peaking at approximately 415 Ma in LLKB and KB and approximately 405 Ma in SB, consistent with far-field Lachlan Fold Belt reactivation (Foden et al., 2020). Note that the ~490-470 Ma magmatic rocks in the AGB may be underrepresented in this dataset due to poor outcrops.

Metamorphic conditions vary markedly across the margin and provide critical constraints on crustal architecture (Fig. 2). The KB records the peak temperatures ~280–380°C of greenschist facies in most of the region, with lower amphibolite facies are found in the hanging wall of major faults (Greenfield et al., 2011), consistent with an island arc or back-arc environment of subduction-related arc setting. The LLKB attained lower to middle greenschist facies (~300–450°C) during Cambrian regional metamorphism and generated andalusite-stable contact aureoles (~400–530°C) around Devonian monzodioritic intrusions (Gilmore et al., 2025). The AGB records the most extreme metamorphic conditions in the orogen: Buchan-type high-temperature low-pressure (HTLP) metamorphism at ~630–660°C and only 3–4 kbar during ~515–505 Ma (e.g., Morand et al., 2003), possibly driven by lithospheric delamination and asthenospheric upwelling (Turner et al., 2022). This anomalous thermal event produced syn-kinematic migmatites, multiple generations of peraluminous and metaluminous granites (Curtis et al., 2022; Turner et al., 2022). The SB experienced the lowest prograde metamorphic grade among all four belts, with syn-arc burial metamorphism reaching only zeolite to prehnite–pumpellyite facies (<200°C) before rising to mid-greenschist conditions (~300–500°C) during Delamerian contractional burial (Schofield et al., 2018). East of the SB, the accretionary Stawell Zone includes contemporary high-pressure metamorphic rocks (Phillips et al., 2002; Miller et al., 2015) uplifted in the Moyston Fault hanging wall (Cayley & Taylor, 2001; Cayley et al., 2011).

Metallogenic events over time reveal temporal clustering that defines four distinct mineralising episodes (Fig. 2; Appendices 2a and 2b). The earliest episode (~590–580 Ma) is represented by orthomagmatic Ni–Cu mineralisation of Mount Arrowsmith area in the KB, associated with Neoproterozoic rift volcanism. The Cambrian episode (~525–495 Ma) encompasses VHMS Cu–Zn tectonised at mid-crustal levels in accretionary wedge crust (e.g., Mount Ararat; Cayley & Taylor, 2001), high-level porphyry Cu–Au (e.g., Thursday's Gossan) in the SB (Cairns et al., 2018), porphyry Cu–Au and skarn Zn–Pb in LLKB (e.g., Scropes Range), and VHMS Cu-Zn in KB (e.g., Grasmere). The Cambrian metallogenic events preserve the densest clusters of arc-related mineralisation in the margin. A third episode (~480–460 Ma) is recorded exclusively in the AGB as porphyry Cu–Mo mineralisation at Netley Hill and Anabama Hill (Hong et al., 2023), broadly coeval with Ordovician regional extension following Delamerian stabilisation. The fourth episode (~425–399 Ma) featured by Devonian porphyry Cu–Au in the KB and LLKB (424–415 Ma), magmatic-hydrothermal activities including the intrusion-related Au within the SB and the adjacent overthrusted accretionary wedge rocks (412–405 Ma) and Stawell (~399 Ma). Metallogenic kernel density estimation (KDE) analysis (bandwidth = 10 Ma) confirms that the KB, SB and LLKB exhibit a strong pulse of Devonian activity (Fig. 2). The AGB's metallogenic activity peaked in the Ordovician, and the Neoproterozoic events are predominately in the KB.

Crustal evolution and porphyry Cu–Au fertility

The generation of mineral systems along the Delamerian convergent margin represents a cumulative effect of geodynamic, petrological, and geochemical parameters. Analysis of magmatic evolution across KB, LLKB, AGB and SB reveals that mineral fertility is fundamentally regulated by the depth of differentiation, melt hydration state, and the redox evolution of the sub-arc mantle. These factors define a series of narrow prospective windows in which mantle-derived, superhydrous, and highly oxidised magmas were successfully delivered to the upper crust, during distinct cycles of arc development and crustal reactivation. The oxidation state (fO_2) of these magmas, often reaching ΔFMQ +1 to +2 (Fig. 3), acted as the primary influence on metal transport. High fO_2 dictated sulphur speciation, favouring soluble sulphate (SO_4^{2-}) over sulphide (S^{2-}), thereby preventing premature precipitation of magmatic sulphides that would otherwise sequester chalcophile elements such as Cu and Au from the melt (Jugo, 2009; Sun et al., 2013).

During arc development (520–495 Ma), the margin exhibited a bipartite isotopic architecture. The SB was characterised by highly juvenile signatures, with εHf(t) values reaching +10 to +14, whereas magmatic rocks from the remainder of the Delamerian convergent margin show more reworked, older crustal values (Fig. 3a). Consistent with Scheibner and Basden (1998) and Greenfield et al. (2011), this further suggests that the Stavely Arc was located a significant distance offshore by at least ~510 Ma – concordant with evidence of opening of a wide and hot back arc basin in the position of the Glenelg Zone by this time (Kemp, 2009; Cayley et al., 2011; Schofield et al., 2018). Notably, magmatic oxidation and hydration proxies trended upward throughout the evolution of the Stavely Arc: the earliest known arc phases from which data are available (~515 Ma) were largely reduced and dry but evolved into a Cu-Au fertile state (oxidised and hydrous) by approximately 500 Ma (Fig. 3c). It is proposed that this transient fertility peak in the Stavely Arc was driven either by a slab-tear event that exposed high-temperature hydrothermal source material from the subducting oceanic crust to the mantle wedge (e.g., Mole et al., 2025), or the arc initiated oblique to the continental margin thus created different margin

setting from north to south with more continental flavour in north (e.g., KB and LLKB) and more oceanic in south (e.g., SB) (Greenfield et al., 2011).

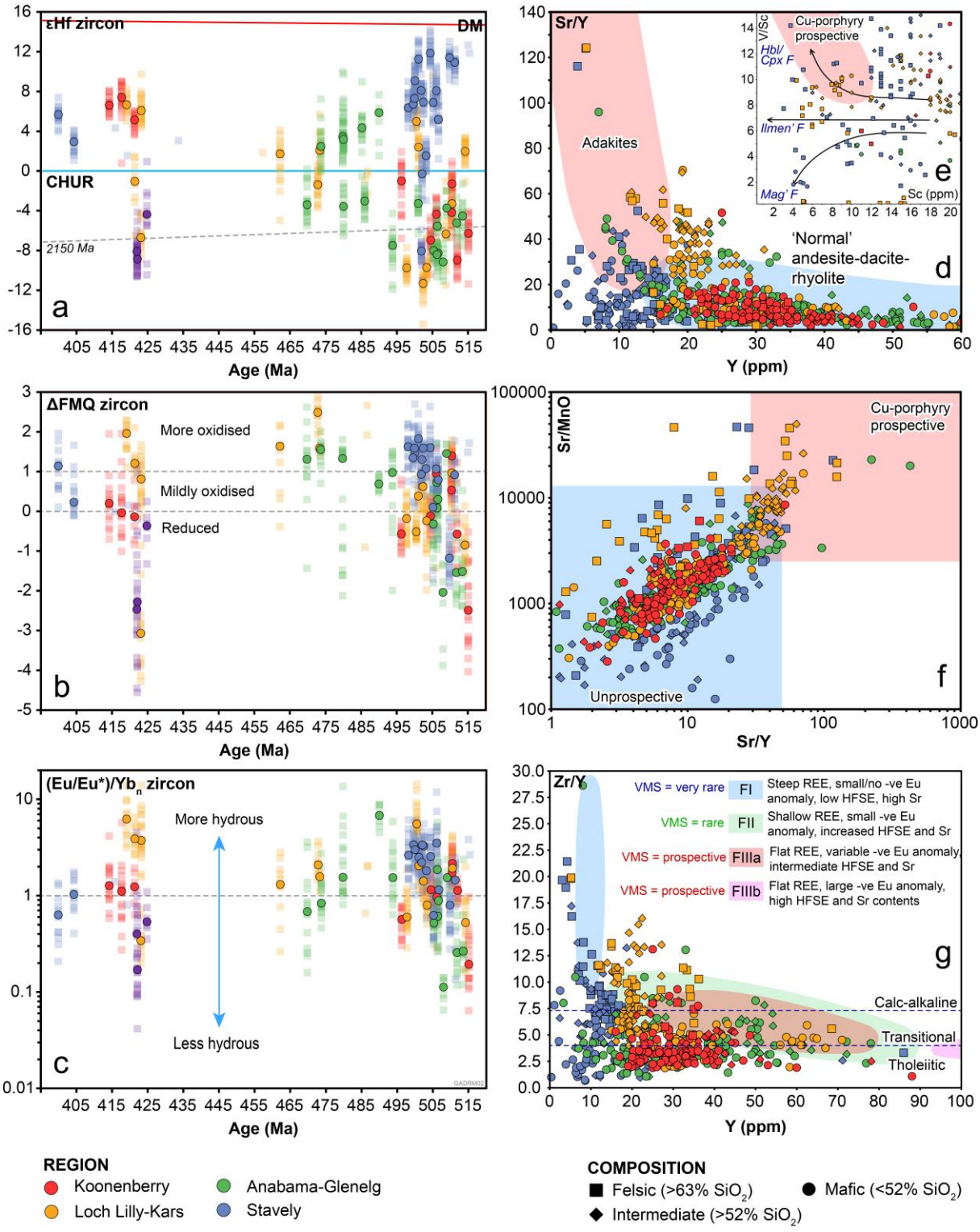

Figure 3 Igneous rocks prospective fertility indicators to demonstrate the variation of magma sources, crustal maturity, evolution history, oxidation and water content of igneous rocks from Cambrian and Devonian along the Delamerian convergent margin. (a) zircon εHf (t) versus Age (Ma); (b) zircon ΔFMQ versus Age (Ma) (Loucks et al., 2020); (c) zircon $(Eu/Eu^*)/Yb_n$ versus Age (Ma) (Lu et al., 2019); (d) whole rock Sr/Y ratio versus Y concentrations (inset (e) whole rock V/Sc ratio versus Sc concentrations) (Lee et al., 2005; Loucks et al., 2014); (f) whole rock Sr/MnO versus Sr/Y ratios (Loucks et al., 2014); and (g) whole rock Zr/Y ratios versus Y concentrations (Pearce and Norry, 1979).

Following the cessation of arc magmatism and the terminal phase of the Delamerian Orogeny that deformed the arc and closed and imbricated the back-arc basin at ~500 Ma, post-orogenic A-type magmatism (~490–460 Ma) persisted for approximately 30 Myr in a post-orogenic extensional setting, interpreted to reflect either a slab break off event after the Delamerian Orogeny (Foden et al., 2020), or interactions between Cambrian and early Ordovician volcanic arc (e.g., the Macquarie Arc) events (Hong et al., 2023). During this interval, εHf(t) values remained predominantly juvenile, often exceeding the radiogenic signatures of the preceding arc phase (Fig. 3a), while magmatic water contents steadily decreased towards 460 Ma (Fig. 3c). Geochemically, part of this cluster within the 'prospective' field of the Sr/MnO versus Sr/Y diagram, characterised by Sr/Y ratios >40 and Sr/MnO ratios >2,500 (Fig. 3f). These ratios serve as diagnostic proxies for high-pressure differentiation in a thickened crustal root (>40 km), where early precipitation of amphibole and garnet sequestered Y and MnO, while suppression of plagioclase prevented early depletion of Sr (Loucks, 2014: Chiaradia, 2015).

After a magmatic hiatus of approximately 30 Myr, additional magmatism overprinted parts of the Delamerian convergent margin between 430 and 390 Ma. Magmatism occurred in the central-north segments (the LLKB and KB) from approximately 425 Ma, followed by subaerial volcanism and (in parts) shallow granite emplacement in the Stavely and Stawell Zones from approximately 415 Ma. This magmatic cycle, a distal expression of ongoing Lachlan orogeneis father east, produced highly productive igneous rocks: both the LLKB and KB exhibit juvenile, oxidised, and hydrous magmatism. In the LLKB, Devonian monzonitic porphyries carry strong fertility signals, including high Sr/Y and V/Sc (>10) ratios, aligning with amphibole fractionation with some plotting within the porphyry Cu field (Taylor et al., 2026; Fig. 3d, e).

Magmatic fertility in a global context

Four independent geochemical proxies collectively demonstrate that magmatic fertility across Delamerian convergent margin was neither uniform nor proportional to tectonic activity, but instead defined by a narrow interval of crustal maturity, water content and oxidation state (Fig. 4, Appendix 3).

The SB records the clearest fertile signature for porphyry Cu mineralisation. Late-stage porphyry phases such as the Victor quartz monzodiorite yield Sr/Y of 31–58 and La/Yb of 44–53—The Sr/Y ratio exceeds the Cu-fertility threshold of 35 (Loucks, 2014), and the La/Yb ratio suggests magma equilibration with a garnet-bearing residue at crustal depths exceeding approximately 40 km (Chiaradia, 2015). V/Sc ratios of 13.8–16.3 plot well above the Loucks (2014) threshold at equivalent SiO_2 concentrations of 61–64 wt.%, confirming magnetite-series, oxidised crystallisation conditions. This interpretation is independently corroborated by ΔFMQ values of +1.5 to +2.5, which lie within the Cu-

fertile field defined by Richards (2015), and by zircon (Eu/Eu*)/Yb of 1.1–1.35 paired with (Ce/Nd)/Y of 0.118–0.14 – both exceeding the fertile thresholds of 0.7 and 0.09, respectively (Lu et al., 2016; Loucks et al., 2024). Crucially, the SB occupies a geochemical field overlapping directly with Oyu Tolgoi and Erdenet in all four discrimination spaces, reinforcing the analogy with the Central Asian Orogenic Belt (CAOB). Relative to the Andean giants—El Teniente, Los Pelambres, and Quellaveco—the SB achieves comparable ΔFMQ and zircon oxidation parameters but falls short of the adakitic Sr/Y values (75–157) diagnostic of the thickest Andean crust (>50 km), consistent with a hyperextended margin and possibly less evolved crustal column during the Cambrian arc stage (Schofield et al., 2018).

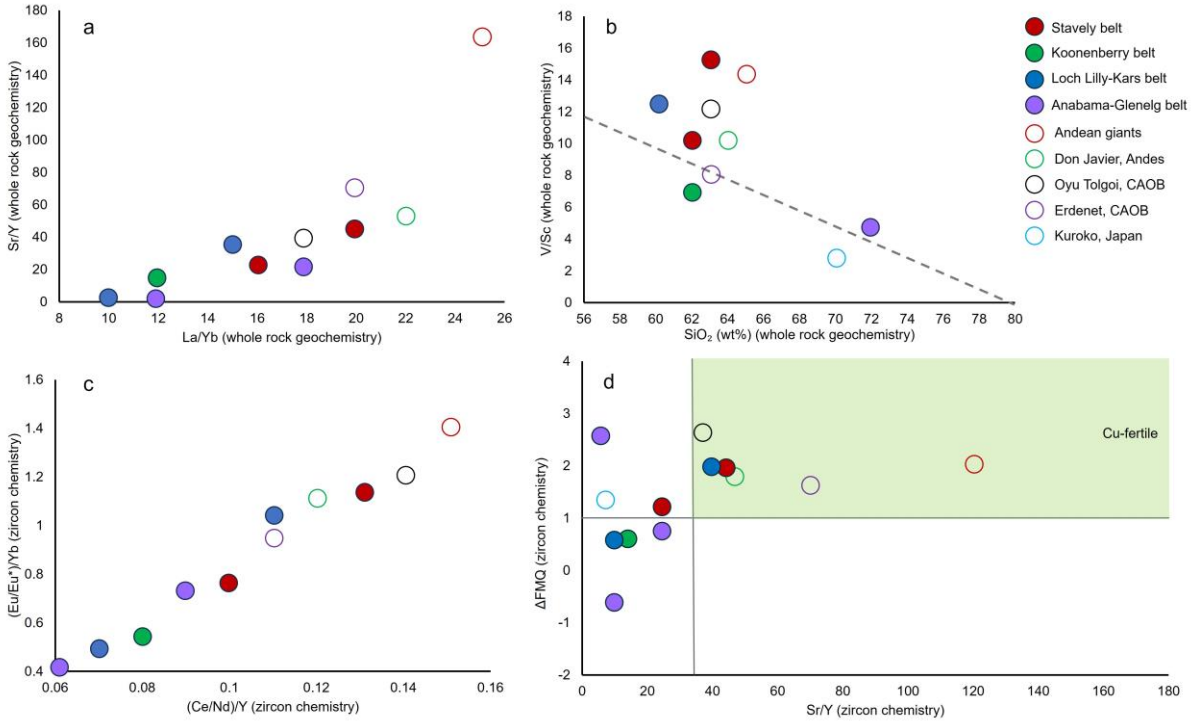

Figure 4 Comparison on whole rock geochemical magma fertility indicators between the four metallogenic belts of the Delamerian convergent margin (Koonenberry Belt (KB), Loch Lilly–Kars Belt (LLKB), Anabama–Glenelg Belt (AGB), and Stavely Belt (SB)) and their global analogues (including the supergiant deposits in Andes, Don Javier area of the Andes, Oyu Tolgoi area of the Central Asian Orogenic Belt (CAOB), Erdenet area of the CAOB and the Kuroko area of Japan). (a) La/Yb versus Sr/Y (whole rock geochemistry); (b) SiO_2 (wt%) versus V/Sc (whole rock geochemistry); (c) (Ce/Nd)/Y versus (Eu/Eu*)/Yb (zircon chemistry); and (d) Sr/Y versus ΔFMQ (zircon chemistry). To reveal their differences and similarities, this figure only displays the average values of datasets from each region. Details including data sources and further interpretations can be found in Appendices 3 and 4.

The LLKB reveals a temporally bifurcated fertility record. Its Devonian monzodiorite suite (Sr/Y 47–48, ΔFMQ +1.8 to +2.0, V/Sc 12.8) satisfies all Cu fertility thresholds and clusters with the SB in the fertile quadrant of the ΔFMQ–Sr/Y diagram. By contrast, Cambrian arc equivalents from the same belt (Sr/Y 14.4, V/Sc 4.3, ΔFMQ +0.5) fall entirely below critical thresholds, suggesting that fertile

magmatic conditions were not inherent to the local arc development but were acquired through post-collisional crustal thickening and dehydration during the Benambran orogenic cycle (Baatar et al., 2020).

The contrasting response of the Cambrian magmatic rocks (>495 Ma) in AGB is equally diagnostic. Its peraluminous granites—with ΔFMQ of –0.7, Sr/Y of 6.8, V/Sc of 3.8, and zircon (Eu/Eu*)/Yb of 0.42—plot alongside the Kuroko back-arc felsic volcanics across all fertility proxies, occupying the most reduced, garnet-poor, and oxidation-deficient corner of each diagram. The elevated $\delta^{18}O$ values (7.5–8.1‰) (Mole et al., 2025) and strongly negative εHf(t) of –6 to –10 (Fig. 3a) recorded by these granites confirm that extensive recycling of supracrustal sediment buffered the magmatic fO_2 downward, precluding sulphur speciation conditions necessary for Cu–Au endowment. This suite represents a fundamentally distinct metallogeny driven by crustal assimilation rather than mantle-flux oxidation.

The 480–460 Ma porphyry Cu-Mo prospects of the AGB show compelling fertility indicators. Zircon chemistry yields high Eu/Eu* (>0.3), elevated 1000×(Eu/Eu*)/Y (>1), and low Dy/Yb (<0.3), with over 90% of analyses falling within global fertile porphyry fields. Rayleigh fractionation modelling confirms prevalent garnet-amphibole crystallization under hydrous conditions, suppressing plagioclase and driving progressive magmatic evolution favorable for metal enrichment. Zircon oxybarometry records moderately high oxidation states (ΔFMQ +0.7 to +3.1), broadly consistent with the Cu-fertile field defined by Richards (2015), promoting sulfur transport into exsolving ore fluids. Apatite volatile systematics reveal magmatic S (37–909 ppm) and Cl (0.30–3.01 wt%) enrichment concentrated in the most porphyritic intrusive phases. Notably, however, these oxidation and hydration signatures fall short of those recorded in the giant Andean porphyry systems and remain comparable to CAOB-style deposits, reflecting the post-subduction rather than mature arc character of the causative magmas, collectively confirming the region's potential for porphyry Cu-Mo mineralization (Hong et al., 2023, 2024).

The KB is definitively barren across all four proxies—ilmenite-series arc tholeiites (ΔFMQ <+1, V/Sc <5, Sr/Y <15) consistent only with a VHMS-prospective submarine volcanic setting (Figs. 3 and 4), as evidenced by the Grasmere and Cymbric Vale deposits.

The four metallogenic belts developed in and around the Delamerian convergent margin each represents a distinct ore-forming archetype, illuminated by belt-by-belt comparison with globally documented analogues across multiple dimensions: geological setting and crustal architecture, geochemical fertility thresholds, and resource endowment benchmarks (Appendix 4). Analogues across three global convergent margin accretionary systems (CAOB, Central Andes, Japanese archipelago) corroborate the relative strength of each pairing and identify the SB as the priority Cu–Au porphyry exploration target, with a high level of confidence when compared with the giant mineralised porphyries of the CAOB (e.g., Oyu Tolgoi).

Sulphur isotope signatures as a sequential tectonic archive across orogenic cycles

The sulphur isotope record of the Delamerian convergent margin metallogenic system spans four isotopically distinct regimes, each governed by a specific tectonic environment and a characteristic dominant sulphur reservoir (Fig. 5; Appendix 5). Across approximately 200 million years, these regimes constitute a geochemical narrative of the convergent margin evolution, in which $\delta^{34}S$ functions not merely as a fluid tracer but as a sequential tectonic archive, recording the successive opening,

maturation, onset of convergence, possible micro-continent collision, and roll-back of the proto-Pacific arc system.

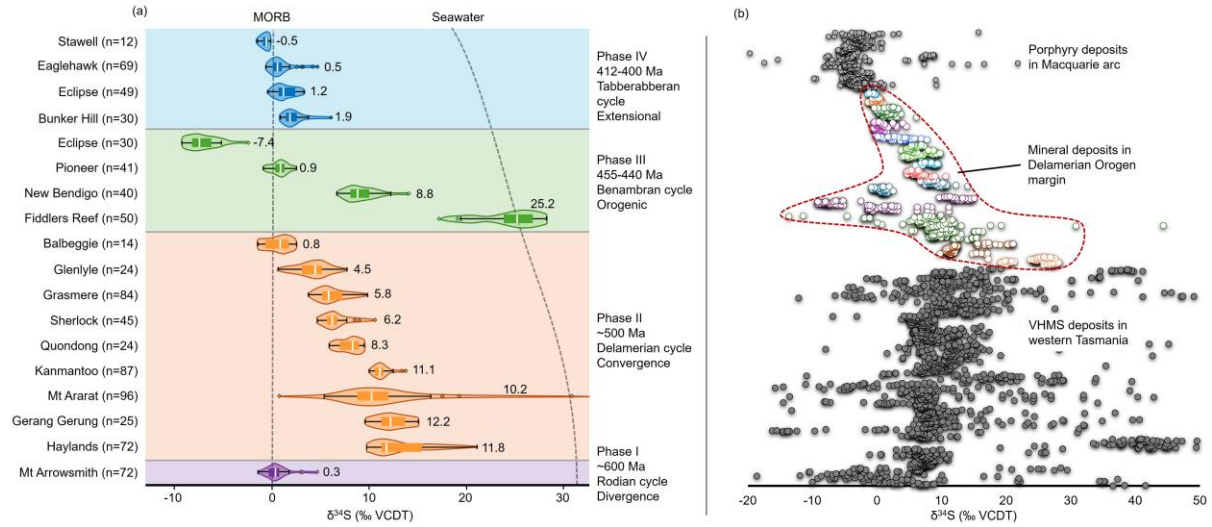

Figure 5 $\delta^{34}S$ isotope distributions of sulphide minerals from mineral deposits in the Delamerian convergent margin compared with adjacent regional deposit populations. Data of the mineral deposits in the Delamerian convergent margin has been collected in this study. S isotope compositions of the VHMS mineral deposits associated with Mt Read Volcanics in western Tasmania are from ISOTAS (2002), and the S isotope data of the porphyry deposits in Macquarie Arc (New South Wales) are from Heithersay and Walshe (1995), Radclyffe (1995), Howland-Rose (1996), Harris (1997), Bastrakov (2001), Lickfold (2002), Wilson et al., (2007) and Zukowski et al., (2014).

(a) Violin plots showing the distribution of $\delta^{34}S$ values (‰ VCDT) for individual mineral deposits, grouped and colour-coded by tectonic phase and orogenic cycle. Dashed lines denote end-member sulphur reservoirs: mid-ocean ridge basalt (MORB) at $\delta^{34}S \approx 0$‰, reflecting the depleted mantle sulphur reservoir, and Cambrian–Ordovician seawater sulphate at $\delta^{34}S \approx +30$‰ (Hough et al., 2012), consistent with coeval marine evaporite records. Median values are annotated to the right of each violin. Four tectonic phases are distinguished.

(b) Bivariate density plot comparing $\delta^{34}S$ values (‰ VCDT) of Delamerian convergent margin mineral deposits (coloured open circles, outlined by red dashed field) against two regional reference populations: (1) porphyry Au–Cu deposits of the intra-oceanic Macquarie Arc (light grey circles, upper population); and (2) Cambrian volcanic-hosted massive sulphide (VHMS) deposits of the Mount Read Volcanics, western Tasmania (dark grey circles, lower dense cluster). The Delamerian convergent margin deposits (red-outlined field) occupy an intermediate isotopic space straddling the MORB and seawater endmembers, lying between the porphyry population and the Tasmanian VHMS field, and record the integrated sulphur isotope signature of a long-lived accretionary orogen cycling through successive convergent, collisional, and extensional tectonic regimes from ~600 to ~400 Ma.

Regime I 600-580 Ma: Rodinian rifting and the mantle baseline

A rifting episode at 600–580 Ma was developed in eastern Australia, characterised by rift-related igneous activities (Glen, 2005). The Mount Arrowsmith mafic–ultramafic magmatism of northwestern New South Wales (~585 Ma; Gilmore et al., 2025) represents the oldest evidence of a metallogenic event in the Delamerian convergent margin and the most primitive in isotopic terms: $\delta^{34}S$ values of −1.39 to +4.6‰ (mean +0.4‰, n = 72) across both pyrite and chalcopyrite, recording sulphur exsolved directly from an asthenospheric melt during passive-margin rifting along the Rodinian supercontinent margin. Other Neoproterozoic to Cambrian basalts in southeastern Australia, which are interpreted to be remnants of the Rodinian margin, reflect mantle decompression during extension and rifting of the Australian–East Antarctic craton (Glen and Cooper, 2021). The MORB-like $\delta^{34}S$ signature of Mount Arrowsmith attest to an asthenospheric mantle source, delivering primitive sulphur to a juvenile passive margin rift basin. This primordial sulphur-isotope baseline is not observed until the final post-orogenic granite suite restores near-zero $\delta^{34}S$ signature approximately 200 million years later (Fig. 5), through an entirely different geological mechanism.

Regime II 515-495 Ma: Cambrian convergence – a multi-process sulphur system

The establishment of convergent margin activity and subsequent orogenesis along the eastern Gondwana margin led to arc magmatism and seafloor hydrothermal activity and culminated in formation of a west-verging fold-thrust belt in the inboard Adelaide Fold Belt (Glen, 2005; Foden et al., 2006). The ~500 Ma metallogenic event displays by far the most isotopically diverse dataset, spanning a 22‰ range within a ~20 Myr window, as five different sulphur reservoirs operated simultaneously at different positions across the arc–back-arc–continental margin system associated with the evolution of the Delamerian convergent margin.

At the SB, oxidised, calc-alkaline metaluminous magmas exsolved sulphur-bearing fluids injected into juvenile Cambrian volcanic basement without sulphur crustal contamination (e.g., Balbeggie, Victoria; mean +0.6‰). At shallow volcanic levels in the Stavely Arc, the epithermal mineralisation at Glenlyle, Victoria (+4.1‰) records a moderate Cambrian seawater sulphate (~+30‰; Hough et al., 2012) contribution from open-system thermochemical sulphate reduction (TSR), intermediate between the pure magmatic endmember and seawater-reduced VHMS systems. The Grasmere (+6.3‰) and Sherlock (+6.4‰) VHMS deposits of the KB and AGB record steady-state open-system TSR of Cambrian seawater sulphate at approximately 19–20% mixing fraction. These values are consistent with the global VHMS TSR model and comparable to the Miocene Kuroko back-arc vent systems of the Hokuroku Basin, Japan (Sato, 1977; Yamada and Yoshida, 2011). Accretionary wedge-hosted VHMS mineralisation at Mount Ararat, Victoria (mean +11.2‰, outliers to +44.4‰) departs from this stable open-vent regime: its extreme pyrite outliers require closed-system Rayleigh bacterial sulphate reduction (BSR) in isolated sub-seafloor pore-water cells. Given its accretionary wedge context east of the SB, Mount Ararat VHMS can be considered exotic. Meanwhile, Kanmantoo, South Australia (mean +11.1‰), records a fifth simultaneous process: a metamorphosed syn-sedimentary seafloor exhalative deposit whose sulphur signature was thoroughly homogenised by amphibolite-facies metamorphism during the ca. 500 Ma Delamerian Orogeny. Therefore, the exceptional isotopic tightness of the Kanmantoo distribution is an indication of tectonic and metamorphic overprinting during the Delamerian Orogeny, rather than the isotope fractionation processes during mineralisation.

Regime III 445–435 Ma: The Benambran Orogeny – metamorphic devolatilisation and marine sulphur inheritance

The 445–435 Ma Benambran Orogeny was the major mineralising event in the Stawell and Bendigo structural zones of Victoria, related to accretion of the Vandieland microcontinent to the Gondwana plate, and to the development of crustal-scale fault systems that acted as fluid pathways and structural traps for metamorphic hydrothermal fluids (Willman et al., 2010; Cayley et al., 2011; Phillips et al., 2012). This event records the most elevated $\delta^{34}S$ in the entire dataset and simultaneously produced the largest spread of values, with the diagnostic signature of metamorphic devolatilisation acting on compositionally heterogeneous basement. Orogenic gold deposits formed at approximately 440 Ma in the western Lachlan Orogen involved circulation of metamorphic fluids through greenschist- to amphibolite-facies Cambrian to Ordovician metasedimentary sequences, with fluid chemistry impacted by devolatilisation reactions in the turbidite (Bierlein et al., 2004).

Fiddlers Reef, Victoria (mean +24.5‰, range +17.25 to +28.3‰), marks the isotopic maximum associated with this event. Its mean $\delta^{34}S$ value represents approximately 98% of coeval Silurian seawater sulphate (+25‰; Hough et al., 2012), potentially related to large-scale prograde metamorphic devolatilisation of Cambrian sediments and marine interflow units of the Stawell Zone. In-situ pyrite zoning records the structural dynamics of this devolatilisation in crystallographic detail: cores at +26.7‰ capture the earliest, deepest metamorphic fluid carrying the maximum marine sulphur load from Cambrian basement; rims at +22.4‰ record the progressive dilution of this fluid by contributions from shallower crustal sources as Benambran fold-thrust propagation widened the fluid catchment.

The contrast between Fiddlers Reef and two coeval deposits in the same Benambran event encapsulates the foundational principle of this study. New Bendigo (mean +9.1‰), hosted in Ordovician Warratta Group turbidites, records approximately 34% coeval seawater sulphate fraction in its metamorphic fluid—a predictable consequence of Ordovician turbidite devolatilisation greenschist-facies conditions during the Benambran Orogeny. Pioneer (mean +1.1‰), despite its similar host rocks and structural position within the same orogenic event, yields $\delta^{34}S$ values (+0.6 to +1.7‰) irreconcilable with any metamorphic fluid leaching a marine sedimentary source. Its near-zero isotopic signature instead falls within the range of magmatic-hydrothermal systems associated with reduced granites, pointing to an intrusion-related gold (IRG) style sulphur source from a subsurface reduced granitic intrusion, making Pioneer a candidate for the intrusion-related gold–orogenic gold continuum (Bierlein and McKnight, 2005). Therefore, the $\delta^{34}S$ values provide the chemical fingerprint that distinguishes these endmembers: where the source is metamorphic marine sediment, $\delta^{34}S$ inherits the marine sulphate budget; where the source is magmatic sulphur, $\delta^{34}S$ approaches zero regardless of the host environment.

Regime IV 420–400 Ma: Far-field extension and the reduced granite sulphur buffer

Following the Benambran Orogeny, the middle Silurian saw widespread extension as the Pacific plate boundary migrated eastward before a new westward-dipping subduction zone persisting into the late Devonian (Cayley, 2015; Moresi et al., 2014). At this time, the Delamerian convergent margin became a far-field region subject to extension, rifting, felsic intrusion and volcanism associated with the Tabberabberan tectonic cycle (Collins, 2002; Glen, 2005). Early Devonian granitic plutons of predominantly metaluminous and peraluminous composition were emplaced at approximately 420–400 Ma.

The $\delta^{34}S$ consequences of this transition in the Delamerian convergent margin are explicit. The Eaglehawk skarn, New South Wales (+0.7‰), Bunker Hill porphyry, New South Wales (+2.1‰), Eclipse porphyry, New South Wales (+1.4‰), and IRG mineralisation at Stawell, Victoria (−0.6‰) collectively define a near-zero $\delta^{34}S$ cluster across three different styles of mineralisation. The approximately 25‰ drop from the Benambran metamorphic peak (~440 Ma, ~+24.5‰) at Fiddlers Reef to Stawell's post-orogenic IRG deposit (~400 Ma, ~–0.5‰) in 40 million years is a significant geochemical signature of tectonic regime change. This change in $\delta^{34}S$ is a quantitative marker of the shift from compressional crustal thickening and metamorphic marine-sulphur leaching to extensional decompression and magmatic sulphur buffering. The tightness of the Stawell IRG cluster is itself diagnostic: at no other point in the 200 million years record does a mineral system produce such isotopic uniformity, reflecting the chemical dominance of an isotopically homogeneous magmatic sulphur source—the Stawell Granite (~400 Ma, Arne et al., 1998)—operating as a closed-system sulphur buffer that overrode the ambient marine sulphur budget of the surrounding Cambrian turbidite host rocks, despite similar rocks having yielded $\delta^{34}S$ up to +28‰ at Fiddlers Reef ~40 million years earlier.

Overall, a discrete phase of Au-Cu mineralisation associated with late Silurian to early Devonian (~420–400 Ma) magmatism is widely distributed along the Delamerian convergent margin reflects a mineralogically and isotopically distinct process operated synchronously with the emplacement of Devonian plutons, overprinting earlier metamorphism-dominated orogenic Au.

Heterogeneous geological processes and metallogenic diversity

The spatial and temporal distribution of mineral deposits is a non-random consequence of the convergence between lithospheric architecture, geodynamic regimes, and magmatic evolution (Sillitoe and Perelló, 2005; Huston et al., 2023). The four metallogenic belts identified here occupy a versatile middle ground between two metallogenic endmembers of accretionary orogenic systems—the Central Andes and the Japanese archipelago—hosting a broad spectrum of mineral deposits including orthomagmatic Cu-Ni, VHMS, porphyry, epithermal, orogenic Au, and IRG. This diversity contrasts sharply with the Central Andes, where a long history of terrane accretion against a rigid cratonic basement has developed long-lived, trans-lithospheric structural corridors and a constrained volcanic regime whereby fertile magmas and fluids are focused into preeminent Cu–Mo–Au belts (Farrar et al., 2023). In contrast, the Japanese archipelago is dominated by weak inter-plate coupling and trench retreat, a configuration that produces widespread ash-flow caldera flare-ups that explosively discharge potential ore-forming fluids into the atmosphere (Sillitoe, 2018). The Japanese system is further constrained by interactions with carbon-rich lithologies in its underlying accretionary complexes, resulting in reduced, ilmenite-series magmas that lock up chalcophile elements at depth and produce mineralisation dominated by Sn and W rather than Cu (Sillitoe, 2018). These architectural differences influence magma fertility: the Andean margin produces oxidised, hydrous, high-Sr/Y magmas in thickened crustal MASH (Melting, Assimilation, Storage, and Homogenisation) zones during contractional pulses, optimising the accumulation of fluid-rich magma in large, shallow-level chambers and facilitating the formation of deposits such as Chuquicamata (Sillitoe and Perelló, 2005). In contrast, the retreating convergent margin regime in the Japanese archipelago has produced significant VHMS mineralisation.

The Delamerian convergent margin avoids these extremes, exhibiting widespread plutonic and volcanic calc-alkaline magmatism with mixed fertility characteristics that account for its noted metallogenic breadth. The prospectivity of Delamerian convergent margin is further modulated by significant post-mineralisation preservation. The Andes suffer from high surface uplift and rapid exhumation, which expose deep porphyry cores but often destroy shallow epithermal lithocaps (Sillitoe and Perelló, 2005). Potential porphyry environments in Japan remain largely concealed by young, shallowly eroded volcanoes and highlighted by the presence of epithermal mineralisation. In contrast, a wide variety of mineral deposits are present in the four metallogenic belts identified in the Delamerian convergent margin of southeast Australia. This is likely due to the limited amount of uplift and erosion experienced following the Delamerian Orogeny and subsequent orogenic cycles, which helped locally to preserve prospective rocks of the Cambrian arc and back-arc systems. Therefore, while the Andes function as a specialised "copper factory" and Japan as a volatile, reduced laboratory, the Delamerian convergent margin serves as a diverse "general store", preserving a wide array of mineral products beneath locally variable thickness sedimentary cover.

Supercontinent cyclicity as a first-order control on metallogenic architecture

The Delamerian convergent margin metallogenic record, spanning approximately 200 Myr from Rodinian rifting to post-orogenic far field overprinting, provides a definitive empirical framework for understanding how supercontinent cyclicity generates a multi-commodity mineral province.

Temporal clustering reflects geodynamic punctuation. The four metallogenic events are not randomly distributed through time but correspond to discrete geodynamic transitions: (i) the approximately 585 Ma rifting pulse records mantle-sourced sulphur during Rodinian fragmentation; (ii) the approximately 520 Ma Cambrian event coincides with a change from passive margin to active subduction, generating the greatest isotopic and deposit-type diversity; (iii) the approximately 440 Ma Benambran pulse records metamorphic devolatilisation of a marine sedimentary pile undergoing crustal thickening; and (iv) the approximately 430 to 410 Ma magmatic pulse in the Delamerian convergent margin documents localised magmatism probably driven by far-field events in the Lachlan Orogen to the east. Each pulse represents a discrete geodynamic event in the supercontinent evolutionary cycle, confirming that metallogenetic events are fundamentally encoded by secular changes in tectonic processes (Huston et al., 2023).

The sulphur isotope system is a quantitative tectonic barometer. The approximately 25‰ excursion in $\delta^{34}S$ values from Fiddlers Reef (+24.5‰, ~440 Ma) to IRG mineralisation at Stawell (−0.6‰, ~400 Ma) over just 40 Myr constitutes a dramatic geochemical signature of a change in stress regime. This shift records the transition from compressional crustal thickening—in which prograde metamorphism devolatilises a marine sedimentary sulphur reservoir—to extension and decompression melting controlled by a reduced magmatic sulphur buffer. The exceptional internal consistency of the Stawell IRG cluster demonstrates that the ore-fluid sulphur budget was entirely dominated by a single closed-system magmatic source. This $\delta^{34}S$ stratigraphy constitutes a quantitative tectonic barometer with resolution sufficient to discriminate individual orogenic phases within a broader accretionary cycle.

A metallogenic archetype distinct from the Andean and Japanese endmembers. Unlike the Andean system, in which rigid cratonic backstops and long-lived translithospheric fault corridors focus Cu–Mo–Au endowment into a narrow belt, the Delamerian convergent margin's heterogeneous crustal

563 architecture—alternating between juvenile arc segments (SB, εHf = +8 to +14) and reworked crustal
564 domains (AGB, εHf = −6 to −10)—generates a laterally diverse array of deposit types across a broad
565 tectono-stratigraphic transect. Unlike the Japanese system, in which ilmenite-series magmatism and
566 interaction with carbon-rich accretionary complexes suppress porphyry Cu potential, the Delamerian
567 convergent margin repeatedly achieved magnetite-series oxidation states (ΔFMQ = +1 to +3) during
568 Gondwana suturing. The result is a "general store" of metallogeny rather than a specialised commodity
569 factory.

570 **Preservation: a legacy of regional extension and tectonic quiescence.** Unlike in the Andes, the
571 extensional tectonics that prevailed during most of the Cambrian in the Delamerian Orogen, combined
572 with moderate compression and crustal thickening during the Delamerian Orogeny, and episodes of
573 cover sedimentation (e.g., Grampians Group upon the SB) and transtension thereafter have resulted in
574 the preservation of a wide variety of types of mineral deposits. Even, locally, Cambrian epithermal
575 deposits (e.g., Glenyle) have been discovered in the SB. Limited subsequent tectonic activity also
576 contributed to the preservation of these deposits under relatively thin post-mineral cover (<200 m) across
577 large parts of the Delamerian convergent margin.

578 **Implications for mineral prospectivity.** The 200 Myr record of tectonic activity in the Delamerian
579 convergent margin discussed here demonstrates that the most productive windows for magmatic-
580 hydrothermal mineralisation occur at specific inflection points in the supercontinent cycle: at the
581 lithospheric extension and rifting associated with passive margin and supercontinent fragmentation;
582 transition from active subduction to subsequential orogenesis initiation; during metamorphic
583 devolatilisation after peak orogenesis; and during post-orogenic extensional collapse. These inflection
584 points can be identified in ancient and modern orogens worldwide using the combined geochemical
585 fingerprints developed here: the geological and temporospatial framework, zircon εHf and trace element
586 systematics, prospective magma fertility proxies, and $\delta^{34}S$ reservoir discrimination. The tectono-
587 metallogenic framework established for the Delamerian convergent margin thus provides a transferable
588 analytical template for evaluating mineral prospectivity in convergent margins as part of supercontinent
589 evolution cyclicity (Huston et al., 2023), with direct relevance to the global supply of strategic resources
590 and critical minerals.

Acknowledgements

Geoscience Australia acknowledges the Traditional Custodians of the lands on which the samples used in this study were collected. I. Williams is thanked for measuring and processing SHRIMP U–Pb isotopes for titanite samples, which greatly enhanced the accuracy of the geochronological framework for metallogenic events along the Delamerian convergent margin. R. Stern assisted in the design and implementation of in-situ sulphur isotope measurements on sulphide minerals, and J. Wu prepared samples to facilitate the analytical procedures; their contributions are greatly appreciated. We thank S. Gilbert at the University of Adelaide for assistance with LA-ICP-MS in-situ mica Rb–Sr and siderite Lu–Hf geochronological analyses at Adelaide Microscopy, and R. Maas at the University of Melbourne for assistance with fluorite Sm–Nd geochronological data collection. We are grateful to B. Reid (Stawell Gold Mines), S. Cochrane (Navarre Minerals Limited), and S. Robson (Battery Minerals) for discussions during fieldwork in western Victoria. The authors thank colleagues from the Geological Survey of New South Wales, Geological Survey of South Australia, and Geological Survey of Victoria for assistance with drill core sampling and for sharing their expertise on the rocks and geology of the Delamerian convergent margin. A. Budd, J. Cloutier and I. Schroder provided constructive comments on an earlier version of this manuscript.

Appendix Captions

Appendix 1 Locations, genetic types and characteristics of key mineral deposits in the Delamerian convergent margin, Australia, including the detailed information on examined drill holes and analysed samples in this study.

Appendix 2A Detailed new geochronological dataset of key mineral deposits in the Delamerian convergent margin, Australia. The datasets include titanite and apatite U-Pb ages by LA-ICP-MS, mica ^{40}Ar-^{39}Ar ages by MC-MS, mica Rb-Sr and siderite Lu-Hf ages by LA-ICP-MS, and fluorite Sm-Nd by ID-TIMS.

Appendix 2B Isochron plots of geochronology of samples from mineral deposits in the Delamerian Convergent margin, southeast Australia.

Appendix 3 Geochemical fertility data compilation on key mineral deposits in Delamerian convergent margin and global tectono-metallogenic analogues.

Appendix 4 Global tectono-metallogenic analogues with the 4 metallogenic belts of the Delamerian Orogen margin, southeast Australia.

Appendix 5 Sulphur isotopes of the key sulphide minerals (pyrite, chalcopyrite, sphalerite, pyrrhotite and galena) from mineral deposits in the Delamerian Convergent margin, southeast Australia.

Appendix 6 Analytical methods.

References

Arne, D. C., Bierlein, F. P., McNaughton, N., Wilson, C. J. L. & Morand, V. J. Timing of gold mineralisation in western and central Victoria, Australia: new constraints from SHRIMP II analysis of zircon grains from felsic intrusive rocks. *Ore Geol. Rev.* **13**, 251–273 (1998).

Baatar, B., Parra-Avila, L. A., Fiorentini, M. L., Plitt, P. & Crawford, A. J. Porphyry Cu fertility of the Loch Lilly–Kars Belt, Western New South Wales, Australia. *Aust. J. Earth Sci.* **67**, 75–87 (2020).

Bierlein, F. P., Arne, D. C. & Cartwright, I. Stable isotope (C, O, S) systematics in alteration haloes associated with orogenic gold mineralisation in the Victorian gold province, SE Australia. *Geochem. Explor. Environ. Anal.* **4**, 191–211 (2004a).

Bierlein, F. P., Arne, D. C., Foster, D. A. & Reynolds, P. A geochronological framework for orogenic gold mineralisation in central Victoria, Australia. *Miner. Deposita* **36**, 741–767 (2001).

Bierlein, F. P., Christie, A. B. & Smith, P. K. A comparison of orogenic gold mineralisation in central Victoria (AUS), western South Island (NZ) and Nova Scotia (CAN): implications for variations in the endowment of Palaeozoic metamorphic terrains. *Ore Geol. Rev.* **25**, 125–168 (2004b).

Bierlein, F. P., Gray, D. R. & Foster, D. A. Metallogenic relationships to tectonic evolution — the Lachlan Orogen, Australia. *Earth Planet. Sci. Lett.* **202**, 1–13 (2002).

Bierlein, F. P. & McKnight, S. Possible intrusion-related gold systems in the western Lachlan Orogen, southeast Australia. *Econ. Geol.* **100**, 385–398 (2005).

Boger, S. D. & Miller, J. M. Terminal suturing of Gondwana and the onset of the Ross–Delamerian Orogeny: the cause and effect of an Early Cambrian reconfiguration of plate motions. *Earth Planet. Sci. Lett.* **219**, 35–48 (2004).

Cairns, C. P. et al. Stavely Project – Historical Mineral Exploration Data Compilation. Stavely Project Report 2, Geological Survey of Victoria, Department of Economic Development, Jobs, Transport and Resources (2018).

Cawood, P. A. Terrane assembly and the Tasmanides: a Gondwana odyssey. in *Terrane Processes at the Margins of Gondwana* Geol. Soc. Lond. Spec. Publ. 246 (2005).

Cawood, P. A., Martin, E. L., Murphy, J. B. & Pisarevsky, S. A. Gondwana's interlinked peripheral orogens. *Earth Planet. Sci. Lett.* **568**, 117057 (2021).

Cayley, R. A. The giant Lachlan Orocline — a powerful new predictive tool for mineral exploration under cover across eastern Australia. *Aust. Inst. Geosci. Bull.* **62**, 29–38 (2015).

Cayley, R. A. Exotic crustal block accretion to the eastern Gondwanaland margin in the Late Cambrian — Tasmania, the Selwyn Block, and implications for the Cambrian–Silurian evolution of the Ross, Delamerian, and Lachlan orogens. *Gondwana Res.* **19**, 628–649 (2011).

Cayley, R. A. et al. Crustal architecture of central Victoria: results from the 2006 deep crustal reflection seismic survey. *Aust. J. Earth Sci.* **58**, 113–156 (2011).

Cayley, R. A. et al. Results of Deep Seismic Reflection Imaging of the Eastern Delamerian Orogen, South Australia and Western Victoria, Australia. GeoScience Victoria, Department of Primary Industries, Victoria (2011).

Cayley, R. A. & Taylor, D. H. Ararat 1:100 000 Map Area Geological Report. Geological Survey of Victoria Report 115 (2001).

Cayley, R. A. & Taylor, D. H. Grampians Special Map Area Geological Report. Geological Survey of Victoria Report 107 (1997).

667 Cayley, R. A., Taylor, D. H., VandenBerg, A. H. M. & Moore, D. H. Proterozoic–Early Palaeozoic rocks and
668 the Tyennan Orogeny in central Victoria: the Selwyn Block and its tectonic implications. *Aust. J. Earth*
669 *Sci.* **49**, 225–254 (2002).
670 Cherry, D. P. Gold-copper mineralisation at Hill 800, Jamieson Volcanics, eastern Victoria. in *VICMIN98 – The*
671 *Second GPIC Conference on Recent Developments in Victorian Geology and Mineralisation* (eds
672 Hughes, M. J. & Ho, S. E.) Aust. Inst. Geosci. Bull. **24**, 21–28 (1998).
673 Chiaradia, M. Crustal thickness control on Sr/Y signatures of recent arc magmas: an Earth-scale perspective.
674 *Sci. Rep.* **5**, 8115 (2015).
675 Collins, W. J. Hot orogens, tectonic switching, and creation of continental crust. *Geology* **30**, 535–538 (2002).
676 Collins, W. J. & Richards, S. W. Geodynamic significance of S-type granites in circum-Pacific orogens. *Geology*
677 **36**, 559–562 (2008).
678 Corbett, K. D. et al. Cambrian Tasmania. in *Geological Evolution of Tasmania* (eds Corbett, K. D., Quilty, P. G.
679 & Calver, C. R.) Geol. Soc. Aust. Spec. Publ. **24**, 95–240 (2014).
680 Crawford, A. J., Donaghy, A. G., Black, L. P. & Stuart-Smith, P. G. Mt Read Volcanics correlates in western
681 Victoria: a new exploration opportunity. *Aust. Inst. Geosci. Bull.* **20**, 97–102 (1996).
682 Curtis, S. et al. Back-arc extension and inversion during the Delamerian Orogeny. Geological Survey of New
683 South Wales Report GS2021/1733 (2022).
684 Direen, N. G. & Crawford, A. J. The Tasman Line: where is it, what is it, and is it Australia's Rodinian breakup
685 boundary? *Aust. J. Earth Sci.* **50**, 491–502 (2003).
686 Dolgopolova, A. et al. Sr–Nd–Pb–Hf isotope systematics of the Hugo Dummett Cu–Au porphyry deposit (Oyu
687 Tolgoi, Mongolia). *Lithos* **164–167**, 47–64 (2013).
688 Farrar, A. D., Cooke, D. R., Hronsky, J. M. A., Wood, D. G. & Benavides, S. B. A model for the lithospheric
689 architecture of the Central Andes and the localisation of giant porphyry copper deposit clusters. *Econ.*
690 *Geol.* **118**, 1561–1589 (2023).
691 Fergusson, C. L. & Coney, P. J. Implications of a Bengal Fan-type deposit in the Paleozoic Lachlan fold belt of
692 southeastern Australia. *Geology* **20**, 1047–1049 (1992).
693 Foden, J., Elburg, M. A., Dougherty-Page, J. & Burtt, A. The timing and duration of the Delamerian Orogeny:
694 correlation with the Ross Orogen and implications for Gondwana assembly. *J. Geol.* **114**, 189–210
695 (2006).
696 Foden, J., Elburg, M. A., Turner, S., Sandiford, M., O'Callaghan, J. & Mitchell, S. Granite production in the
697 Delamerian Orogen, South Australia. *J. Geol. Soc. Lond.* **159**, 557–575 (2002).
698 Foden, J. et al. Cambro-Ordovician magmatism in the Delamerian Orogeny: implications for tectonic
699 development of the southern Gondwanan margin. *Gondwana Res.* **81**, 490–521 (2020).
700 Franklin, J. M., Gibson, H. L., Jonasson, I. R. & Galley, A. G. Volcanogenic massive sulfide deposits. in
701 *Economic Geology One Hundredth Anniversary Volume* (eds Hedenquist, J. W. et al.) 523–560 (Society
702 of Economic Geologists, 2005).
703 Gardiner, N. J. et al. Contrasting granite metallogeny through the zircon record: a case study from Myanmar.
704 *Sci. Rep.* **7**, 46250 (2017).
705 Gilmore, P. J. et al. The Delamerian Orogen on mainland Australia plotted in time and space. Geoscience
706 Australia Record 2025/03 (2025).
707 Glen, R. A. The Tasmanides of eastern Australia. *Geol. Soc. Lond. Spec. Publ.* **246**, 23–96 (2005).
708 Glen, R. A. & Cooper, R. A. The onset of latest Ediacaran to Cambrian subduction along the East Gondwana
709 margin: a review. *Earth-Sci. Rev.* **220**, 103687 (2021).

710 Glen, R. A., Crawford, A. J., Percival, I. G. & Barron, L. M. Early Ordovician development of the Macquarie
711 Arc, Lachlan Orogen, New South Wales. *Aust. J. Earth Sci.* **54**, 167–179 (2007).
712 Greenfield, J. E., Gilmore, P. J. & Mills, K. J. (compilers). Explanatory Notes for the Koonenberry Belt
713 Geological Maps. Geological Survey of New South Wales Bulletin 35 (2010).
714 Greenfield, J. E., Musgrave, R. J., Bruce, M. C., Gilmore, P. J. & Mills, K. J. The Mount Wright Arc: a Cambrian
715 subduction system developed on the continental margin of East Gondwana, Koonenberry Belt, eastern
716 Australia. *Gondwana Res.* **19**, 650–669 (2011).
717 Habib, U., Meffre, S., Berry, R. & Belousova, E. A. Provenance of lower Paleozoic sedimentary rocks in
718 Tasmania and Waratah Bay, southern Victoria: constraints from detrital zircon hafnium isotopes and
719 trace-element geochemistry. *Aust. J. Earth Sci.* **70**, 175–188 (2023).
720 Haines, P. W. et al. Isotopic and geochemical characterisation of the Cambrian Kanmantoo Group, South
721 Australia. *Aust. J. Earth Sci.* **56**, 1095–1110 (2009).
722 Herrington, R. J., Zaykov, V. V., Maslennikov, V. V., Brown, D. & Puchkov, V. N. Mineral deposits of the
723 Urals and links to geodynamic evolution. in *Economic Geology One Hundredth Anniversary Volume* (eds
724 Hedenquist, J. W. et al.) 1069–1095 (Society of Economic Geologists, 2005).
725 Hong, W. et al. Using zircon and apatite chemistry to fingerprint porphyry Cu–Mo±Au mineralisation in the
726 Delamerian Orogen, South Australia. *Miner. Deposita* **59**, 1–19 (2024).
727 Ishihara, S. The magnetite-series and ilmenite-series granitic rocks. *Mining Geol.* **27**, 293–305 (1977).
728 Kemp, A. I. S. et al. Isotopic evidence for rapid continental growth in an extensional accretionary orogen: the
729 Tasmanides, eastern Australia. *Earth Planet. Sci. Lett.* **284**, 455–466 (2009).
730 Khashgerel, B.-E., Rye, R. O., Hedenquist, J. W. & Kavalieris, I. Geology and reconnaissance stable isotope
731 study of the Oyu Tolgoi porphyry Cu–Au system, South Gobi, Mongolia. *Econ. Geol.* **101**, 503–522
732 (2006).
733 Khashgerel, B.-E., Rye, R. O., Kavalieris, I. & Hayashi, K. Overview of the Oyu Tolgoi porphyry Cu–Au system,
734 Mongolia: geology, geochronology, fluid inclusion, and stable isotope study. *Miner. Deposita* **43**, 493–
735 515 (2008).
736 Kita, N. T. et al. Internal ^{26}Al–^{26}Mg isotope systematics of a Type B CAI: remelting of refractory precursor
737 solids. *Geochim. Cosmochim. Acta* **86**, 37–51 (2012).
738 Lehmann, B. et al. The Bolivian tin province and regional tin distribution in the Central Andes: a reassessment.
739 *Econ. Geol.* **85**, 1044–1058 (1990).
740 Lewis, C. J. et al. New SHRIMP U–Pb zircon ages from the Stavely region, western Victoria: July 2015 – June
741 2017. Geoscience Australia Record 2017/15 (2017).
742 Li, Z. X. et al. Assembly, configuration, and break-up history of Rodinia: a synthesis. *Precambrian Res.* **160**,
743 179–210 (2008).
744 Li, Z. X. & Powell, C. M. An outline of the palaeogeographic evolution of the Australasian region since the
745 beginning of the Neoproterozoic. *Earth-Sci. Rev.* **53**, 237–277 (2001).
746 Lloyd, J. C., Collins, A. S., Blades, M. L., Gilbert, S. E. & Amos, K. J. Early evolution of the Adelaide
747 Superbasin. *Geosciences* **12**, 154 (2022).
748 Loucks, R. R. Distinctive composition of copper-ore-forming arc magmas. *Aust. J. Earth Sci.* **61**, 5–16 (2014).
749 Lu, Y. J., Loucks, R. R., Fiorentini, M. L., Yang, Z. M. & Hou, Z. Q. Fluid flux melting generated postcollisional
750 high Sr/Y copper ore-forming water-rich magmas in Tibet. *Geology* **43**, 583–586 (2015).
751 Lu, Y.-J. et al. Zircon compositions as a pathfinder for porphyry Cu ± Mo ± Au deposits. in *Tectonics and*
752 *Metallogeny of the Tethyan Orogenic Belt* (ed. Richards, J. P.) SEG Spec. Publ. **19**, 329–347 (2016).

Merdith, A. S. et al. Extending full-plate tectonic models into deep time: linking the Neoproterozoic and the Phanerozoic. *Earth-Sci. Rev.* **214**, 103477 (2021).

Miller, J., Phillips, D., Wilson, C. & Dugdale, L. Evolution of a reworked orogenic zone: the boundary between the Delamerian and Lachlan fold belts, southeastern Australia. *Aust. J. Earth Sci.* **52**, 921–940 (2005).

Mole, D., Clark, A., Bodorkos, S. & Lewis, C. New U–Pb SHRIMP zircon geochronology from NDI drilling of the Delamerian Orogen: Loch Lilly–Kars and Lake Wintlow Belts, southwest NSW. Geoscience Australia Record 2024/21 (2024).

Mole, D. et al. Architecture, evolution and fertility of the Delamerian Orogen: insights from zircon. in *Exploring for the Future: Extended Abstracts*. Geoscience Australia, Canberra (2023).

Moore, D. H., Betts, P. G. & Hall, M. Fragmented Tasmania: the transition from Rodinia to Gondwana. *Aust. J. Earth Sci.* **62**, 1–35 (2015).

Morand, V. J. et al. Glenelg Special Map Area Geological Report. Geological Survey of Victoria Report 123 (2003).

Moresi, L., Betts, P., Miller, M. & Cayley, R. Dynamics of continental accretion. *Nature* **508**, 245–248 (2014).

Mortensen, J. K., Gemmell, J. B., McNeill, A. W. & Friedman, R. M. High-precision U–Pb zircon chronostratigraphy of the Mount Read Volcanic Belt in western Tasmania, Australia: implications for VHMS deposit formation. *Econ. Geol.* **110**, 445–468 (2015).

Mulder, J. A. et al. Neoproterozoic opening of the Pacific Ocean recorded by multi-stage rifting in Tasmania, Australia. *Earth-Sci. Rev.* **201**, 102941 (2020).

Perry, V. Geochemistry of the Loch Lilly–Kars volcanics and correlation along the Tasman Line, Eastern Australia. BSc (Hons) thesis, Univ. of Newcastle (2021).

Phillips, G. N. et al. Gold: historical wealth, future potential. in *Geology of Victoria* 3rd edn (ed. Birch, W. D.) 377–433 (Geological Society of Australia, 2012).

Porter, T. M. The geology, structure and mineralisation of the Oyu Tolgoi porphyry copper–gold–molybdenum deposits, Mongolia: a review. *Geosci. Front.* **7**, 375–407 (2016).

Purdom, S. R. Genesis of a possible IRGS deposit near Stawell, Victoria. BSc (Hons) thesis, Univ. of Tasmania (2024).

Reed, A. R. Pre-Tabberabberan deformation in eastern Tasmania: a southern extension of the Benambran orogeny. *Aust. J. Earth Sci.* **48**, 785–796 (2001).

Richards, J. P. High Sr/Y arc magmas and porphyry Cu ± Mo ± Au deposits: just add water. *Econ. Geol.* **106**, 1075–1081 (2011).

Richards, J. P. The oxidation state, and sulfur and Cu contents of arc magmas: implications for metallogeny. *Lithos* **233**, 27–45 (2015).

Sato, T. Kuroko deposits: their geology, geochemistry and origin. in *Volcanic Processes in Ore Genesis*. Geol. Soc. Lond. Spec. Publ. **7**, 153–161 (1977).

Schofield, A. et al. Regional Geology and Mineral Systems of the Stavely Arc, Western Victoria. Geoscience Australia Record 2018/02 (2018).

Shen, P., Pan, H., Hattori, K., Cooke, D. R. & Seitmuratova, E. Large Paleozoic and Mesozoic porphyry deposits in the Central Asian Orogenic Belt: geodynamic settings, magmatic sources, and genetic models. *Gondwana Res.* **58**, 161–194 (2018).

Sillitoe, R. H. Porphyry copper systems. *Econ. Geol.* **105**, 3–41 (2010).

Sillitoe, R. H. & Perelló, J. Andean copper province: tectonomagmatic settings, deposit types, metallogeny, exploration, and discovery. in *Economic Geology One Hundredth Anniversary Volume* (eds Hedenquist, J. W. et al.) 845–890 (Society of Economic Geologists, 2005).

797 Sillitoe, R. H. Why no porphyry copper deposits in Japan and South Korea? *Resour. Geol.* **68**, 107–125 (2018).
798 Soejono, I. et al. Buchan-type metamorphism in the Mongolian Altai: lithogeochemistry, P–T conditions and
799 comparison with the Delamerian analogue. *Geol. Mag.* **158**, 2059–2080 (2021).
800 Squire, R. J. et al. Cambrian backarc-basin basalt in western Victoria related to evolution of a continent-dipping
801 subduction zone. *Aust. J. Earth Sci.* **53**, 707–719 (2006).
802 Turner, S. et al. A comparison of granite genesis in the Adelaide Fold Belt and Glenelg River Complex using
803 U–Pb, Hf and O isotopes in zircon. *J. Petrol.* **63**, egac102 (2022).
804 Turner, S. P. et al. Source of the Lachlan fold belt flysch linked to convective removal of the lithospheric mantle
805 and rapid exhumation of the Delamerian–Ross fold belt. *Geology* **24**, 941–944 (1996).
806 VandenBerg, A. H. M. Kilmore 1:50 000 Map Geological Report. Geological Survey of Victoria Report 91
807 (1991).
808 VandenBerg, A. H. M. et al. The Tasman Fold Belt System in Victoria. Geological Survey of Victoria Special
809 Publication (2000).
810 Wainwright, A. J. et al. Devonian and Carboniferous arcs of the Oyu Tolgoi porphyry Cu–Au district, South
811 Gobi region, Mongolia. *GSA Bull.* **123**, 306–328 (2011).
812 White, A. J. R. & Chappell, B. W. Granitoid types and their distribution in the Lachlan Fold Belt, SE Australia.
813 *Geol. Soc. Am. Mem.* **159**, 21–34 (1983).
814 Willman, C. E. et al. Crustal-scale fluid pathways and source rocks in the Victorian gold province, Australia:
815 insights from deep seismic reflection profiles. *Econ. Geol.* **105**, 895–915 (2010).
816 Wingate, M. T. D., Campbell, I. H., Compston, W. & Gibson, G. M. Ion microprobe U–Pb ages for
817 Neoproterozoic basaltic magmatism in south-central Australia and implications for the breakup of
818 Rodinia. *Precambrian Res.* **87**, 135–159 (1998).
819 Yamada, R. & Yoshida, T. Relationships between Kuroko volcanogenic massive sulfide (VMS) deposits, felsic
820 volcanism, and island arc development in the northeast Honshu arc, Japan. *Miner. Deposita* **46**, 431–448
821 (2011).
822 Ye, Z. et al. Geology and geochronology of the Don Javier Cu–Mo porphyry deposit, southern Peru. *Ore Geol.*
823 *Rev.* **143**, 104777 (2022).

Interplay between supercontinents and accretionary orogens recorded in 200 million years of metallogeny

Appendix 1 Characteristics of Mineral Deposits in the Delamerian Convergent Margin, Australia

Yanbo Cheng[1] *, Phil Gilmore[1, 2], Michael Doublier[1], Karol Czarnota[1], Chris Lewis[1], Holly Taylor[1], Andrew Clark[1], Liam Pitt[1], David Mole[1], Yue Wang[3], Sebastien Meffre[4], Adrienne Brotodewo[5], Ross Cayley[6], Cameron Cairns[6], Antony Burhnam[1, 3], Tom Wise[7], Adrian Fabris[7]

1 Geoscience Australia, Canberra 2609, Australia
2 Geoscience, Exploration and Mineral Systems, Newcastle 2300, Australia
3 Research School of Earth Sciences, The Australian National University, Canberra 2601, Australia
4 Earth Sciences, University of Tasmania, Hobart 7006, Australia
5 MinEx CRC, Future Industries Institute, Adelaide University, Adelaide 5005, Australia
6 The Geological Survey of Victoria, Melbourne 3002, Australia
7 The Geological Survey of South Australia, Adelaide, 5000, Australia

* Correspondence: yanbo.cheng@ga.gov.au

Introduction

This Supplementary Appendix presents the complete mineralogical characterisation dataset for 21 mineral prospects examined as part of the Delamerian Characterisation and Discovery framework of Geoscience Australia. Data include: (i) downhole HyLogger hyperspectral signatures (SWIR, TIR and VNIR); (ii) drill core specimen petrography; (iii) thin-section reflected-light photomicrographs; and (iv) Automated Mineralogy maps produced by the Advanced Mineral Identification and Characterisation System (AMICS) or Mineral Liberation Analysis (MLA).

Prospects are grouped by tectonic belt and geographic region, following the Delamerian Orogen framework from north to south: (1) New South Wales — Loch Lilly–Kars Belt; (2) New South Wales — Koonenberry Belt; (3) New South Wales — Warratta Inlier; (4) South Australia — Kanmantoo–Glenelg River Zone; and (5) Victoria — Grampians–Stavely Belt. Within each Part, prospects are presented in the sequence of their original Appendix numbering.

Each prospect entry comprises three standardised tables: (A) Sample List — borehole collar and sample interval data; (B) Mineralisation Characteristics — mineral assemblages resolved by analytical method; and (C) Mineralogical Textures and Paragenesis — interpretive synthesis of mineral paragenesis. Figure references at the end of each entry direct the reader to the associated image atlas (embedded in the detailed Appendix files identified by number).

For prospects without detailed individual appendix files, all data are compiled here from the consolidated Delamerian Mineral Prospect Summary report. Abbreviations used throughout are listed in the consolidated Mineral Abbreviation Legend at the end of this document.

Table 1 Summary of the studied key mineral deposits and prospects in Delamerian convergent margin

Deposit types	Mineral deposits	States	Borehole Names	Latitude	Longitude	Datum
Epithermal	Glenyle	Victoria	GDD003	-37.4135	142.7339	GDA94
Epithermal	Glenyle	Victoria	GDD006	-37.4089	142.7343	GDA94
Epithermal	Glenyle	Victoria	GDD008	-37.4105	142.7339	GDA94
IRG	Stawell	Victoria	SSDD0001	-37.0599	142.8005	GDA94
Mafic-ultramafic magmatic	Mount Arrowsmith	New South Wales	DH 119113	-30.164	141.668	GDA94
Mafic-ultramafic magmatic	Mount Arrowsmith	New South Wales	DH 119114	-30.164	141.668	GDA94
Mafic-ultramafic magmatic	Mount Arrowsmith	New South Wales	DMDD2	-30.2347	141.8687	GDA94
Orogenic Au	Fiddlers Reef	Victoria	YEHRIP01	-37.056	143.379	GDA94
Orogenic gold	Good Friday	New South Wales	AWGF02	-29.5985	141.8078	GDA94
Orogenic gold	New Bendigo	New South Wales	AWNB05	-29.6527	141.9043	GDA94
Orogenic gold	Pioneer	New South Wales	AWPN01A	-29.5436	141.8414	GDA94
Orogenic gold	Pioneer	New South Wales	AWPN02A	-29.5436	141.8414	GDA94
Porphyry	Bunker Hill	New South Wales	DDH3	-30.9312	142.6185	GDA94
Porphyry	Eclipse	New South Wales	DDH2	-30.9447	142.6228	GDA94
Porphyry	Follies Tank	New South Wales	DD90DL19	-31.883	142.6406	GDA94
Porphyry	Follies Tank	New South Wales	DD90DL20	-31.8828	142.6428	GDA94
Porphyry	Quondong	New South Wales	NBH011	-32.7314	141.4544	GDA94
Porphyry	Wahratta	New South Wales	CP2	-31.9705	141.9506	GDA94
Porphyry	Wahratta	New South Wales	DD96WA3	-31.9642	142.0011	GDA94
Porphyry	Eclipse	Victoria	ED003	-37.1811	142.1274	GDA94
Porphyry	Resolution (Irvine)	Victoria	RD002	-37.191	142.863	GDA94
Porphyry	Balbeggie	Victoria	SB1DH1	-37.6519	142.6114	GDA94
Skarn	Eaglehawk	New South Wales	DD95EHK3	-32.3588	141.6937	GDA94
Skarn	Eaglehawk	New South Wales	NBH004	-32.3514	141.688	GDA94
Skarn	Scropes Range	New South Wales	DD92DL23	-31.894	142.3793	GDA94
Skarn	Scropes Range	New South Wales	DD92DL22	-31.894	142.3793	GDA94
Skarn	Gerang Gerung	Victoria	GG-01	-36.3572	141.8669	GDA94
VHMS	Mt Ararat	Victoria	Mt Ararat 10	-37.309	142.865	GDA94
VHMS	Mt Ararat	Victoria	Mt Ararat 1	-37.309	142.867	GDA94
VHMS	Grasmere	New South Wales	DD88GR01	-31.3015	142.7147	GDA94
VHMS	Grasmere	New South Wales	DD89GR05	-31.3008	142.7155	GDA94

Deposit types	Mineral deposits	States	Borehole Names	Latitude	Longitude	Datum
VHMS	Grasmere	New South Wales	DD90GR07	-31.3025	142.7144	GDA94
VHMS	Grasmere	New South Wales	ADD-1	-31.287	142.6961	GDA94
VHMS	Grasmere	New South Wales	ADD-2	-31.2872	142.6922	GDA94
VHMS	Sherlock	South Australia	SHR034	-35.3271	139.7717	GDA2020
VHMS	Sherlock	South Australia	SHR026	-35.3457	139.7629	GDA2020
VHMS	Sherlock	South Australia	SHR008	-35.3464	139.7608	GDA2020
VHMS	Haylands	South Australia	DEL10ACD001	-34.1154	139.6212	GDA2020

Note there are identical and similar names of key prospects throughout the project area:

- There is an Eclipse prospect in the Stavely region of Victoria and in the Wertago area of the Koonenberry Belt in NSW.
- The Wahratta prospect is east of Broken Hill, NSW, whilst the Warratta Inlier near Tibooburra (NSW) hosts orogenic gold prospects (e.g., Pioneer, Good Friday, New Bendigo).

S1.1 Eaglehawk prospect

Loch Lilly–Kars Belt, New South Wales

(A) Sample List

Sample No.	Sample ID	Borehole	From (m)	To (m)	Notes
8012591	2022440177	DD95EHK3	167.00	167.10	Sulfides and hydrothermal alteration
9651901	202256532620008	NBH004	165.10	165.50	Sulfides and hydrothermal alteration
9651902	202256532620009	NBH004	171.10	171.50	Sulfides and hydrothermal alteration
9651903	202256532620010	NBH004	185.50	185.70	Sulfides and hydrothermal alteration
8012635	2022440221	NBH004	190.30	190.40	Sulfides and hydrothermal alteration
9651904	202256532620011	NBH004	195.40	195.60	Sulfides and hydrothermal alteration

(B) Mineralisation Characteristics

Data Type	Mineral Assemblage
Hyperspectral SWIR	*Ms, Bt, Sme, Chl, Amp, Car, Kln*
Hyperspectral TIR	*Qtz, Kfsp, Pl, Ms, Bt, Sme, Chl, Amp, Grt, Ol, Px, Car, Kln*
Hyperspectral VNIR	*Gth, Hem*
Drill core specimen	*Py, Grt, Px*
Thin section	*Py, Po, Grt, Px, Ttn, Fsp*
AMICS mineral map	*Ab, An, Ap, Cal, Di, Py, Ttn, Ep*

(C) Mineralogical Textures and Paragenesis

Category	Description
Texture	Skarn minerals including garnet, pyroxene and epidote are found at Eaglehawk. Sulfides in the two examined drill holes are interpreted to be related to retrograde skarn hydrothermal alteration.
Paragenesis	Garnet and pyroxene formed earlier than sulfides. Pyrite formed earlier than pyrrhotite.

(D) Supplementary Figure Reference

Supplementary Figures *include (1) Downhole HyLogger hyperspectral images and summaries of drill holes DD95EHK3 and NBH004, Eaglehawk prospect, Loch Lilly–Kars Belt, NSW; (2) Drill core photographs and reflected-light photomicrographs of representative ore samples (skarn sulfides and hydrothermal alteration assemblages); (3) BSE images and AMICS mineral maps showing Ab–An–Di–Py–Ttn–Ep mineral assemblages.*

S1.1 The Eaglehawk prospect, Loch Lilly-Kars Belt, New South Wales

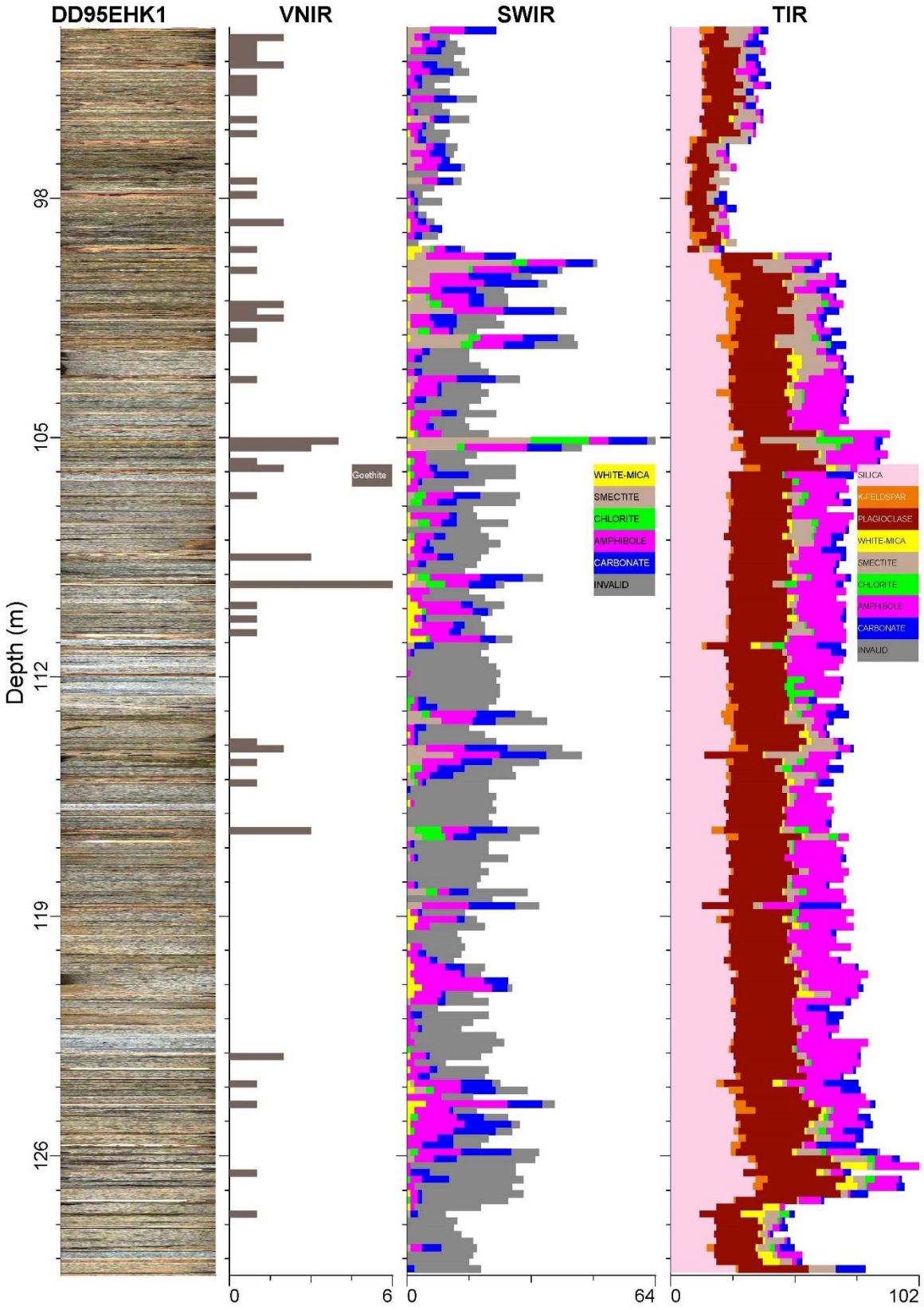

Figure 1 Downhole HyLogger hyperspectral image of the hole DD95EHK1, Eaglehawk prospect, Loch Lilly-Kars Belt, New South Wales, Australia.

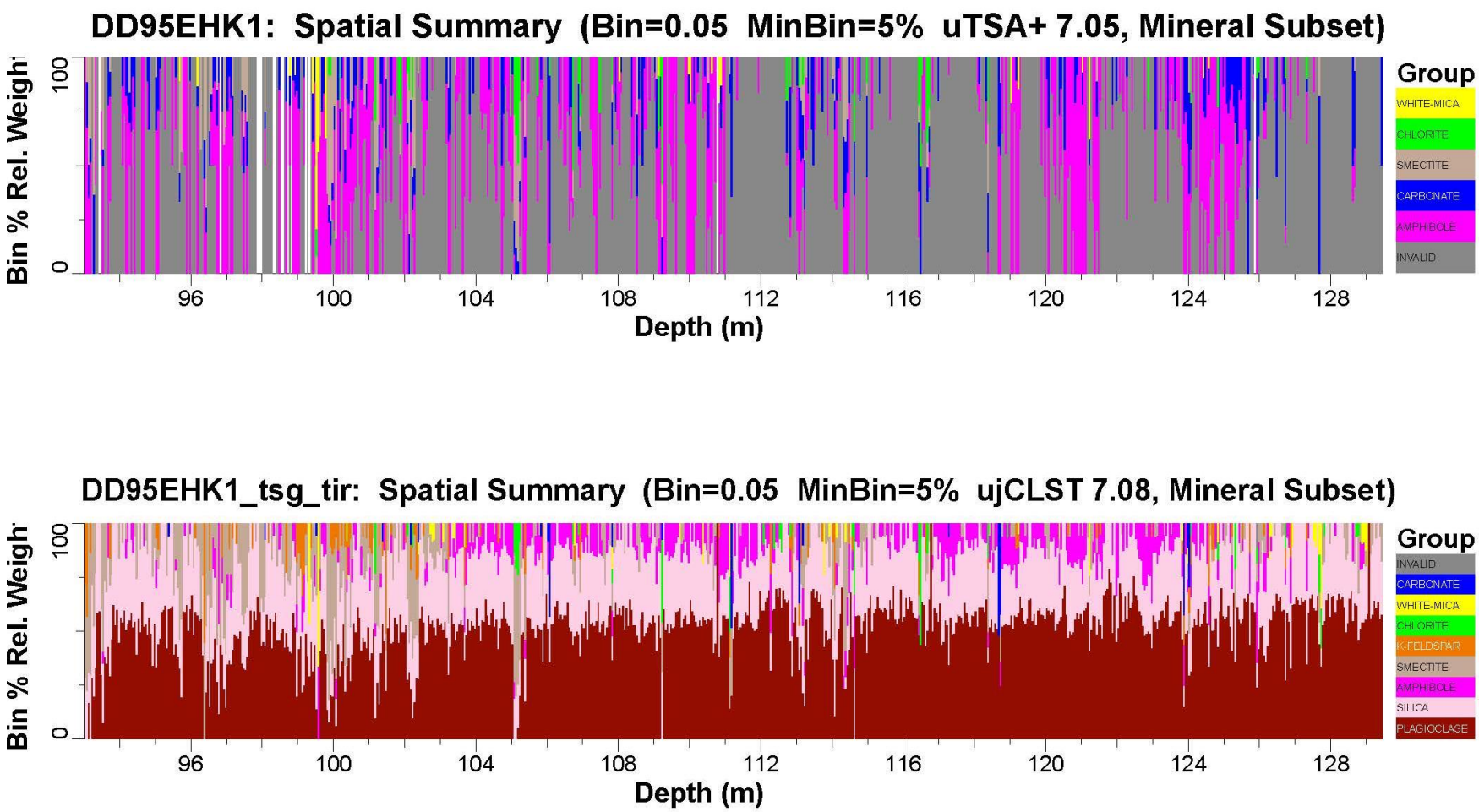

Figure 2 Summary of the HyLogger hyperspectral image of the hole DD95EHK1, Eaglehawk prospect, Loch Lilly-Kars Belt, New South Wales, Australia.

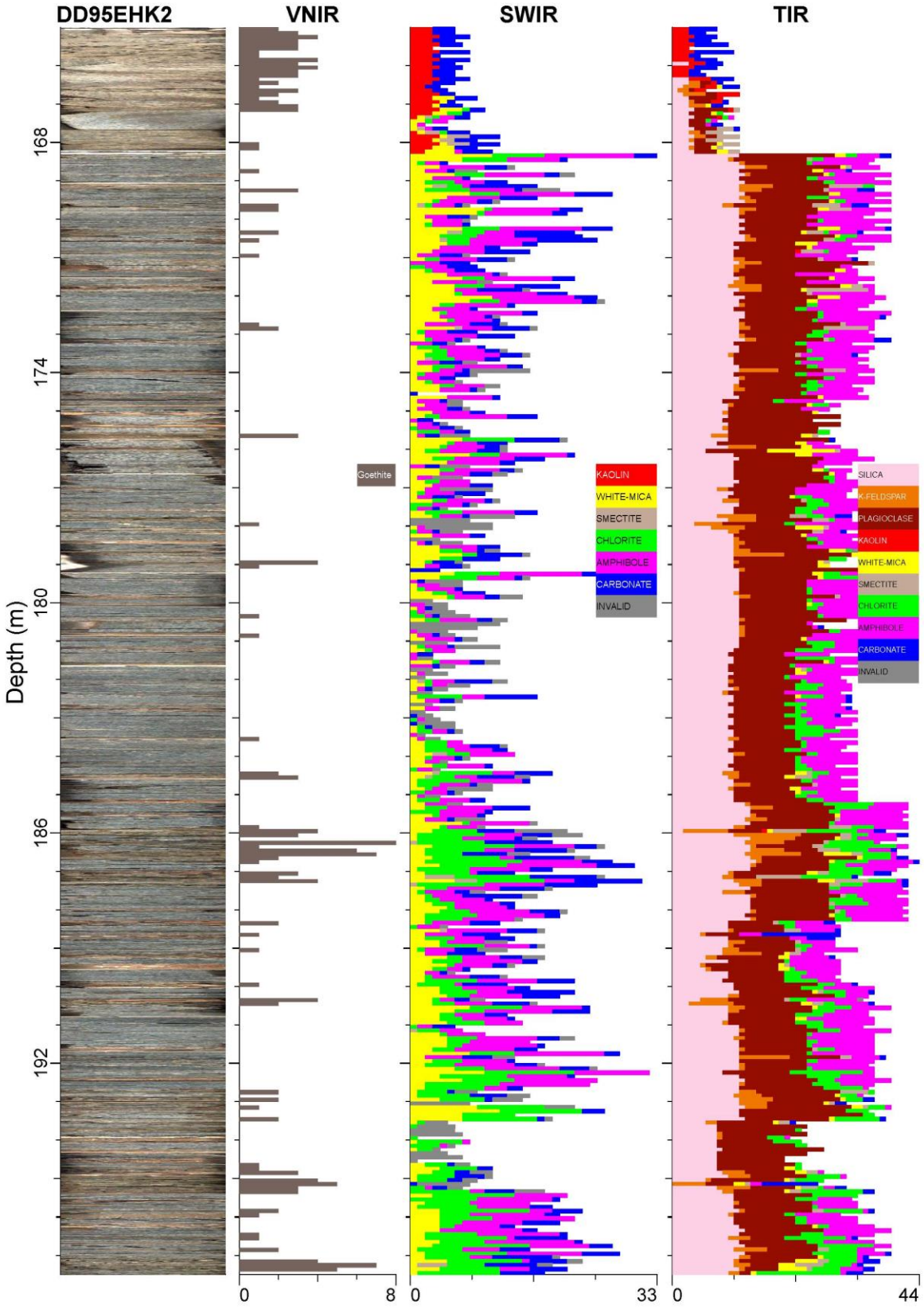

Figure 3 Downhole HyLogger hyperspectral image of the hole DD95EHK2, Eaglehawk prospect, Loch Lilly Kars region, New South Wales, Australia.

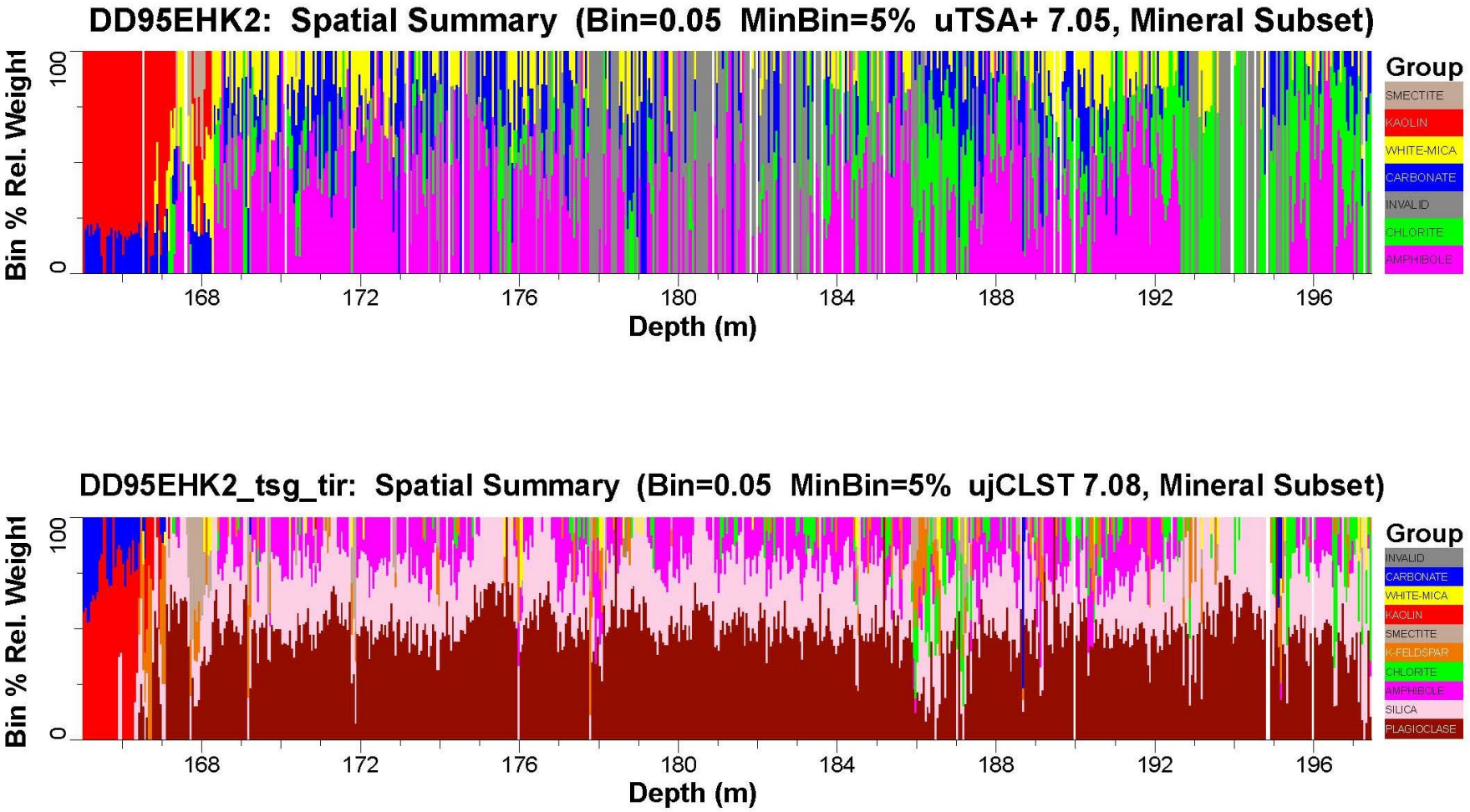

Figure 4 Summary of the HyLogger hyperspectral image of the hole DD95EHK2, Eaglehawk prospect, Loch Lilly-Kars Belt, New South Wales, Australia.

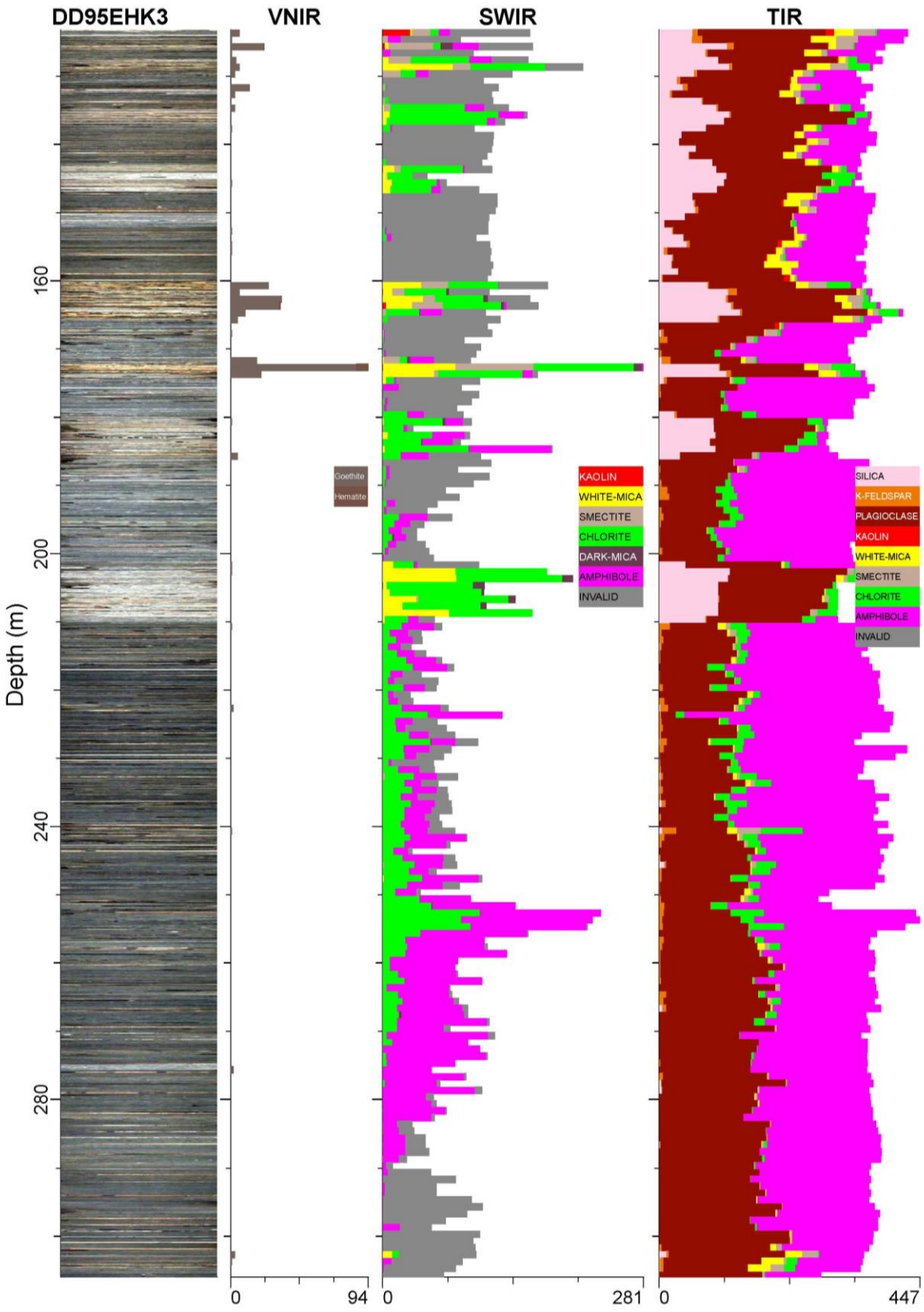

Figure 5 Downhole HyLogger hyperspectral image of the hole DD95EHK3, Eaglehawk prospect, Loch Lilly-Kars Belt, New South Wales, Australia.

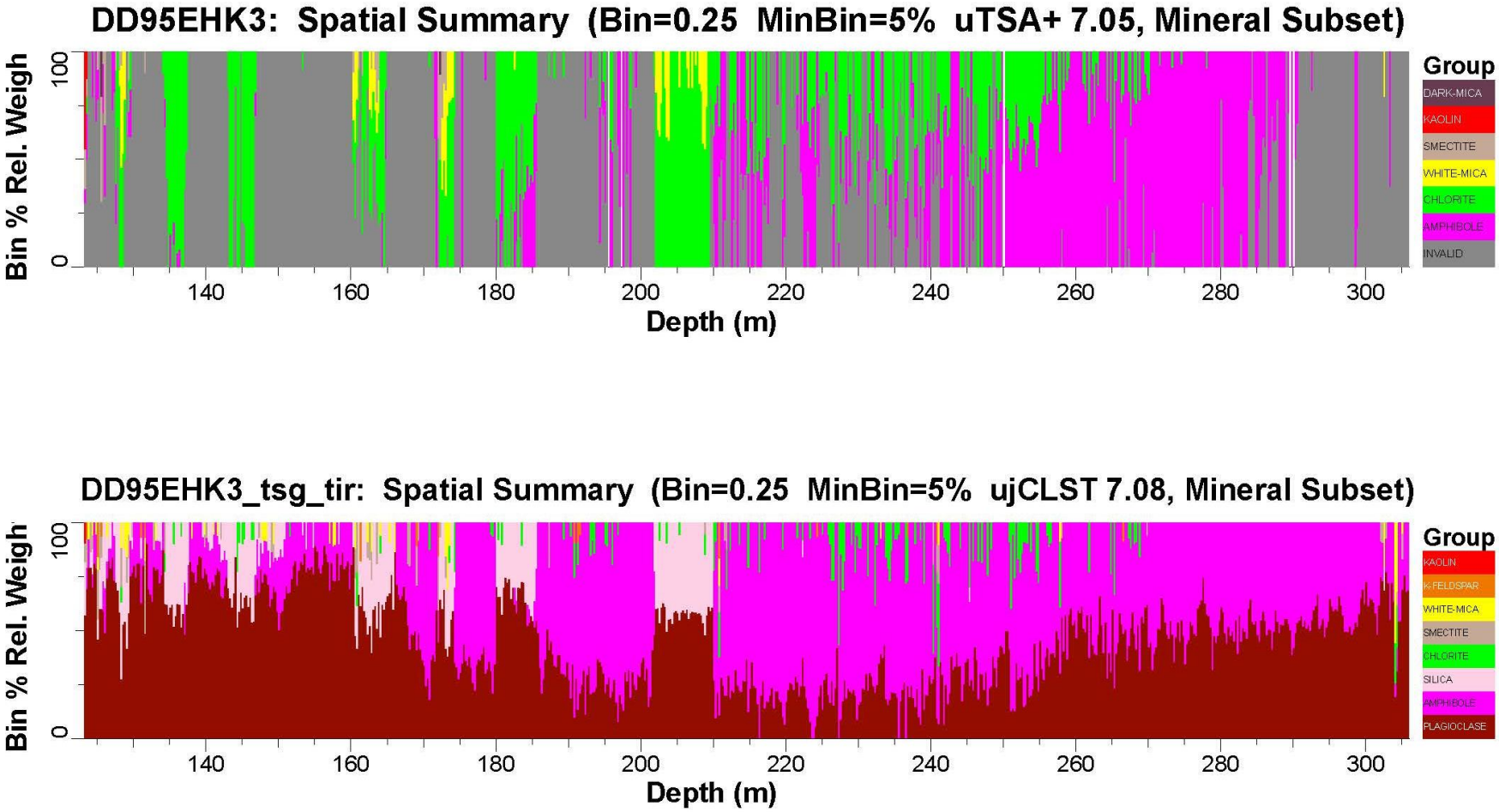

Figure 6 Summary of the HyLogger hyperspectral image of the hole DD95EHK3, Eaglehawk prospect, Loch Lilly-Kars Belt, New South Wales, Australia.

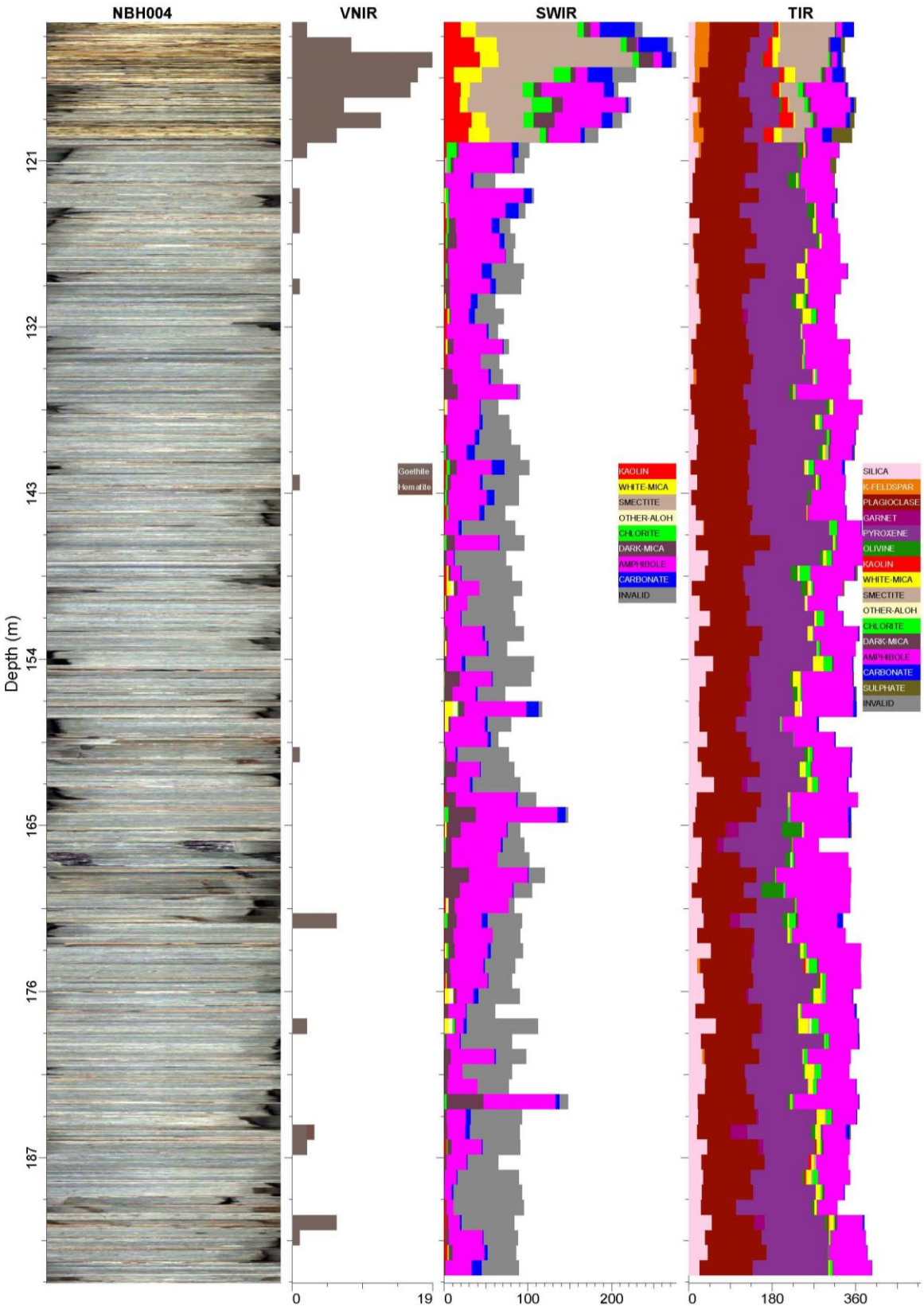

Figure 7 Downhole HyLogger hyperspectral image of the hole NBH004, Eaglehawk prospect, Loch Lilly-Kars Belt, New South Wales, Australia.

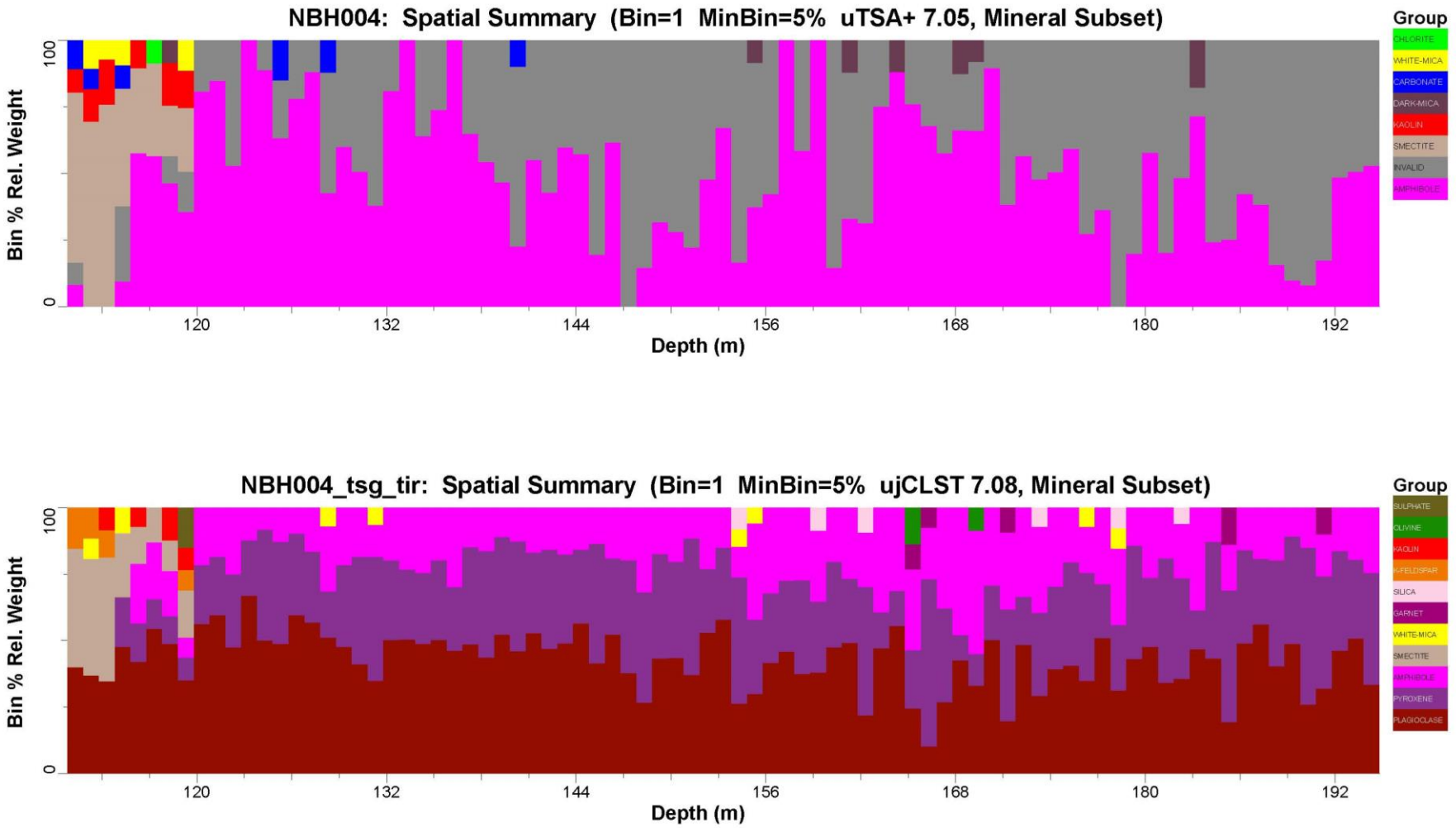

Figure 8 Summary of the HyLogger hyperspectral image of the hole NBH004, Eaglehawk prospect, Loch Lilly-Kars Belt, New South Wales, Australia.

Sample ID	Prospect	Borehole Name	From (m)	To (m)	Note
2022330048	Eaglehawk	NBH004	195.4	195.6	Sulfide ore and hydrothermal alteration

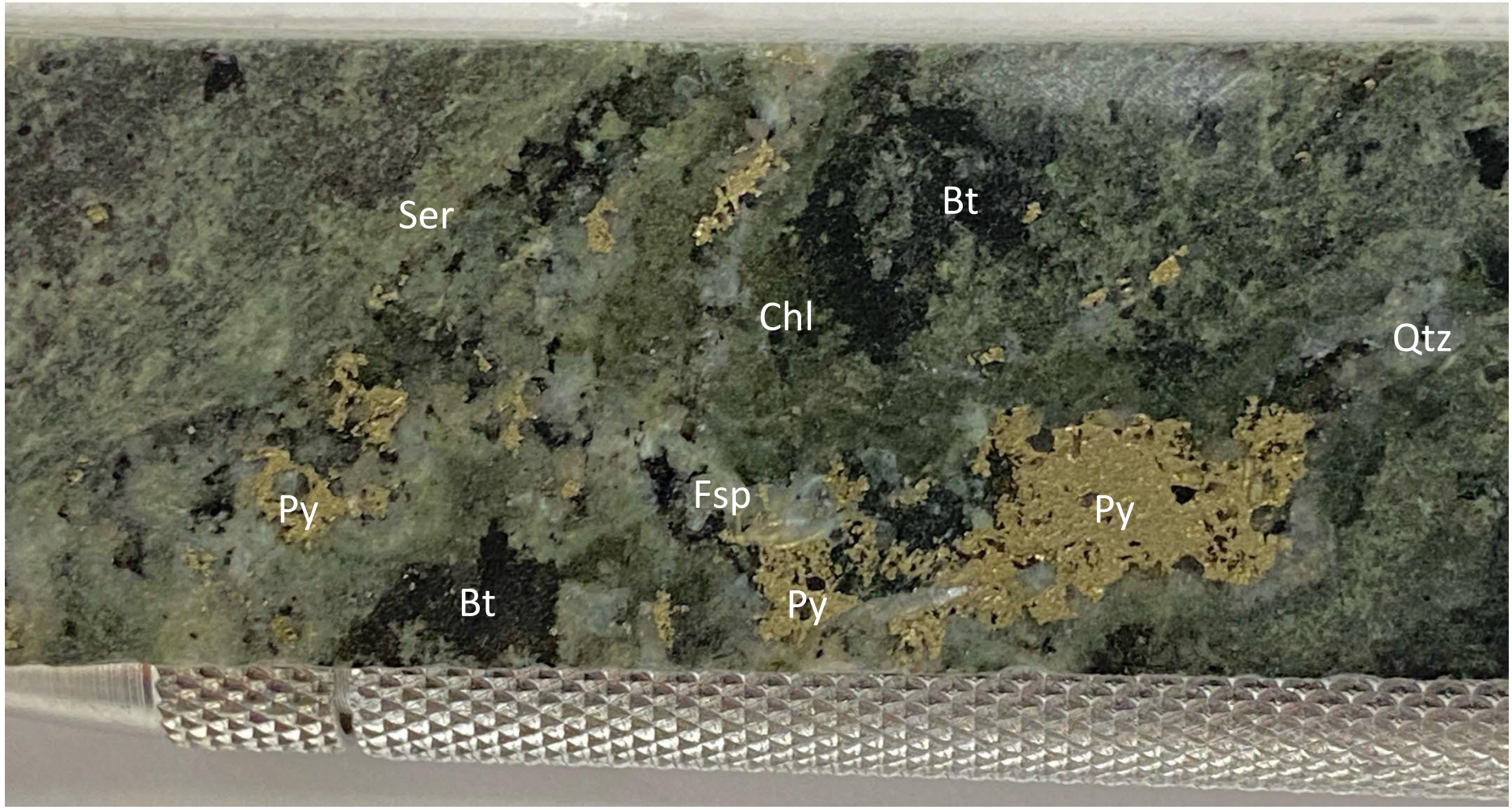

Figure 9 Photos of the drill core sample 2022330048 from drill hole NBH004 of the Eaglehawk prospect, Loch Lilly-Kars Belt, New South Wales, Australia. Py-pyrite; Qtz-quartz; Chl-chlorite; Bt-biotite; Ser-sericite; Fsp-feldspar.

Sample ID	Prospect	Borehole Name	From (m)	To (m)	Note
2022330048	Eaglehawk	NBH004	195.4	195.6	Sulfide and hydrothermal alteration

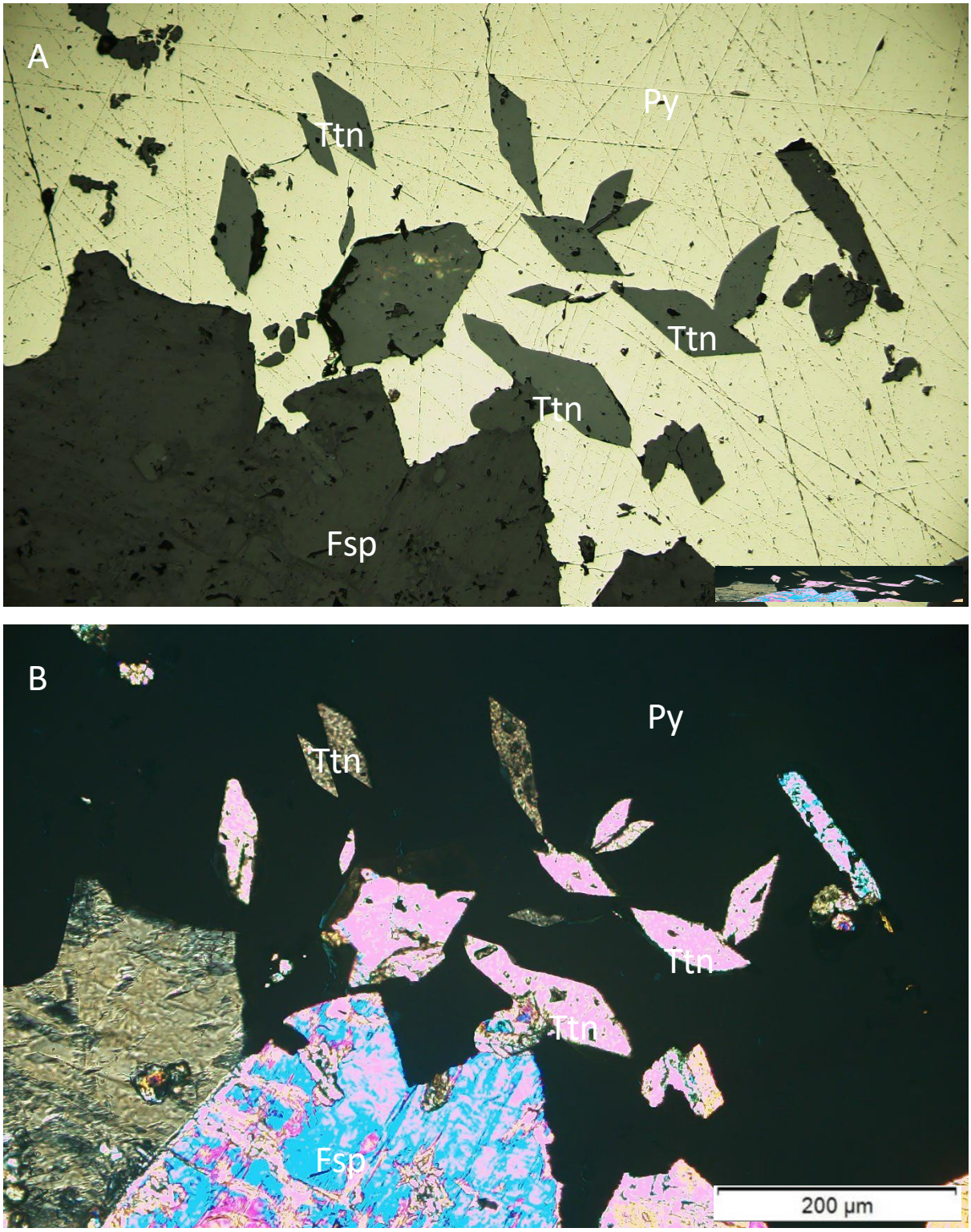

Figure 10 A: Reflective light photomicrograph of skarn alteration and associated sulfide of the sample 2022330047 from drill hole NBH004 of the Eaglehawk prospect, Loch Lilly-Kars Belt, New South Wales, Australia. B: Cross polarized light photomicrograph of A. Ttn-titanite; Fsp-feldspar; Py-pyrite.

Sample ID	Prospect	Borehole Name	From (m)	To (m)	Note
2022330048	Eaglehawk	NBH004	195.4	195.6	Sulfide and hydrothermal alteration

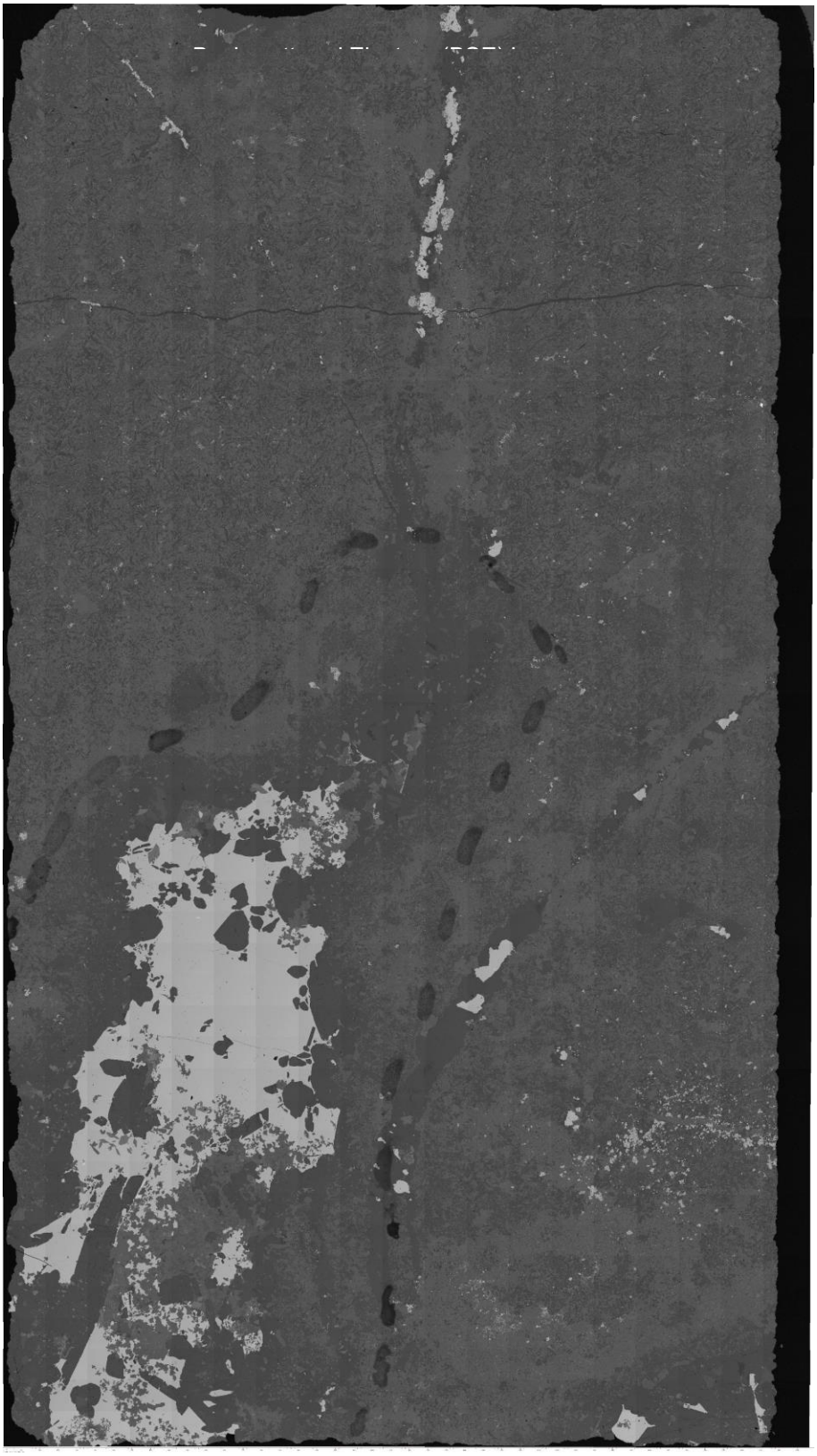

Figure 11 Backscattered electron (BSE) image of the sample 2022330048 from drill hole NBH004 of the Eaglehawk prospect, Loch Lilly-Kars Belt, New South Wales, Australia.

Sample ID	Prospect	Borehole Name	From (m)	To (m)	Note
2022330048	Eaglehawk	NBH004	195.4	195.6	Sulfide and hydrothermal alteration

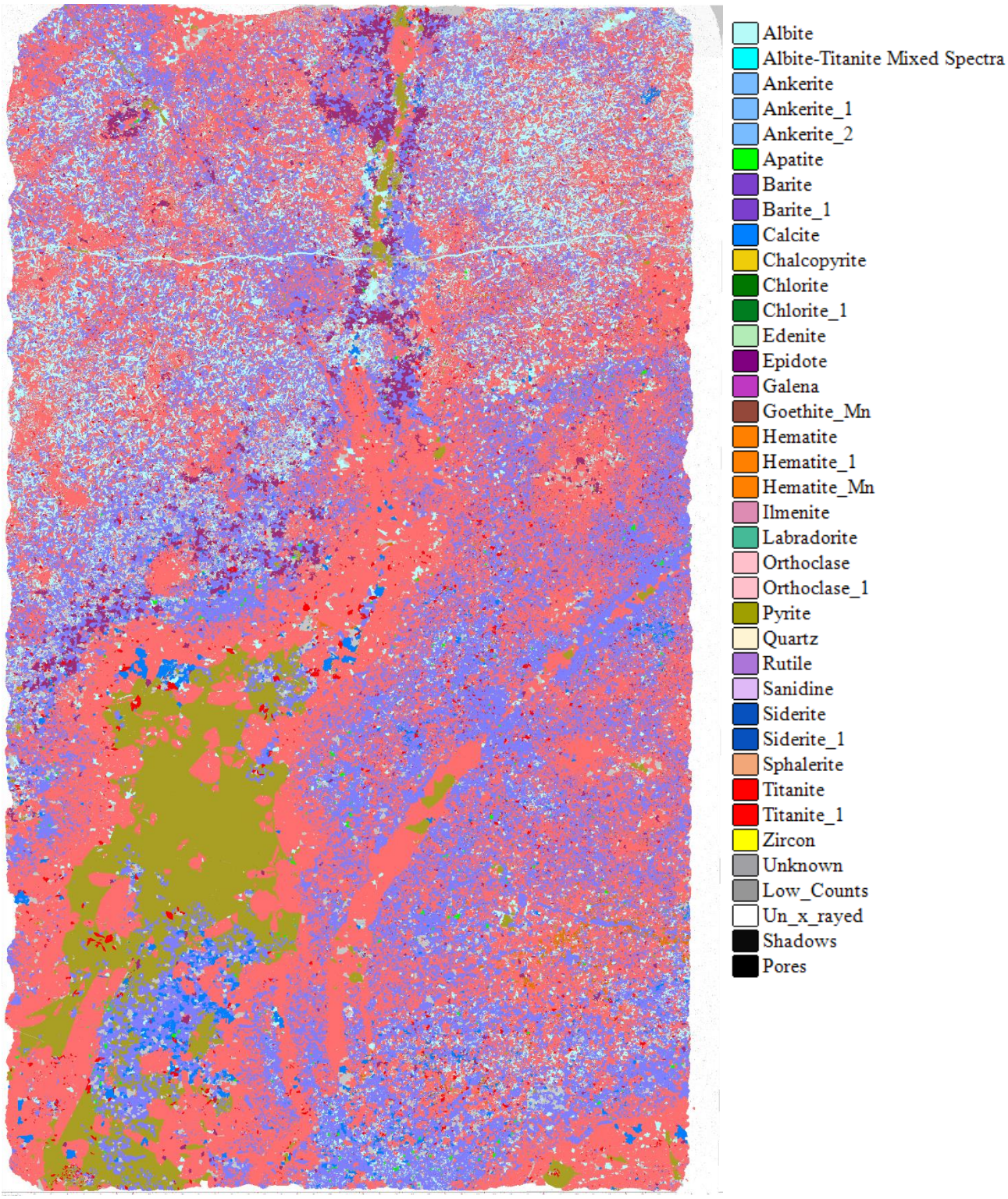

Figure 12 Mineral Liberation Analysis (MLA) mineral map of the sample 2022330048 from drill hole NBH004 of the Eaglehawk prospect, Loch Lilly-Kars Belt, New South Wales, Australia.

Sample ID	Prospect	Borehole Name	From (m)	To (m)	Note
2022330047	Eaglehawk	NBH004	185.5	185.7	Sulfide ore and hydrothermal alteration

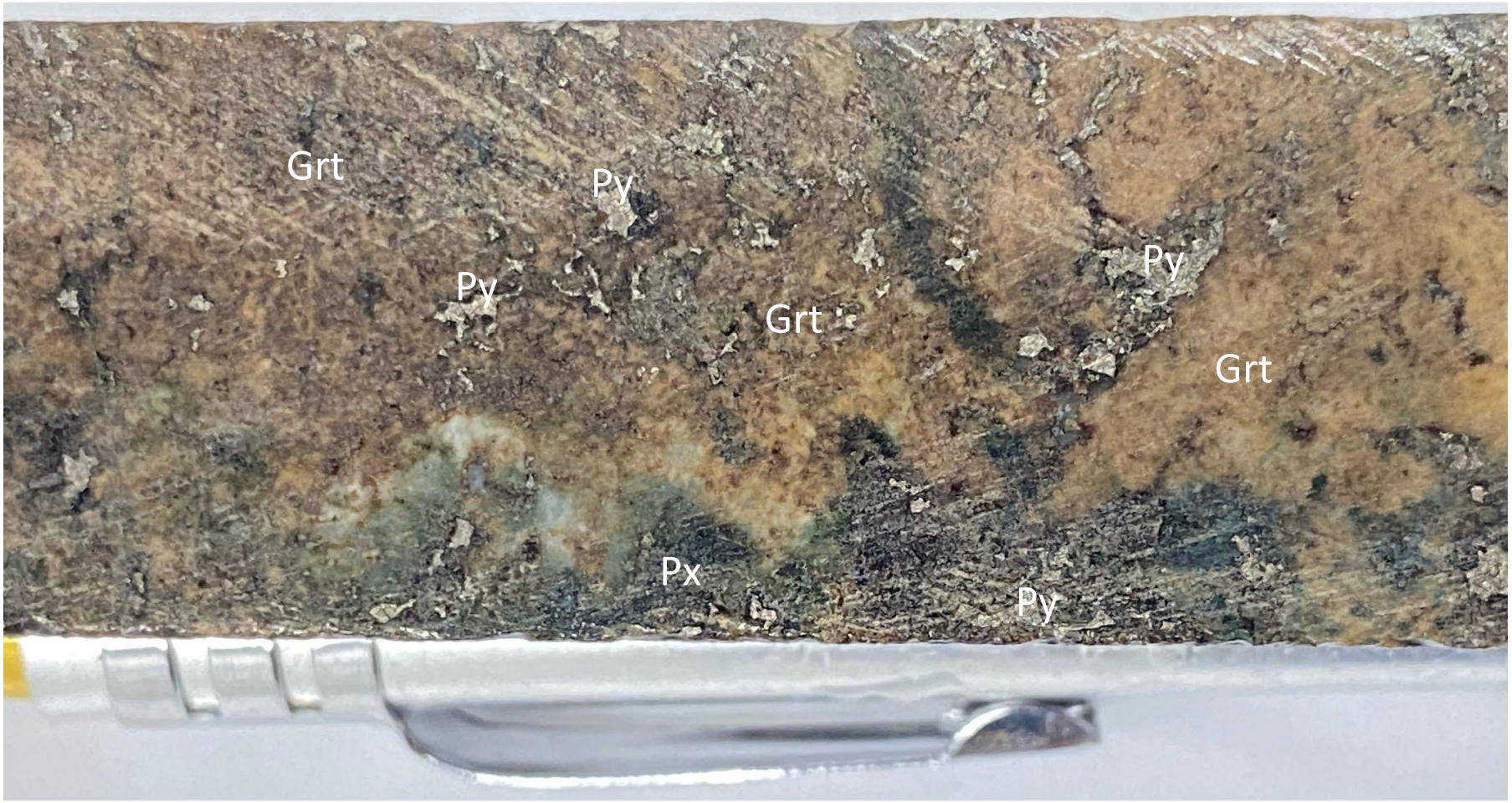

Figure 13 Photos of the drill core sample 2022330047 from drill hole NBH004 of the Eaglehawk prospect, Loch Lilly-Kars Belt, New South Wales, Australia. Grt-garnet; Px-pyroxene; Py-pyrite.

Sample ID	Prospect	Borehole Name	From (m)	To (m)	Note
2022330047	Eaglehawk	NBH004	185.5	185.7	Sulfide and hydrothermal alteration

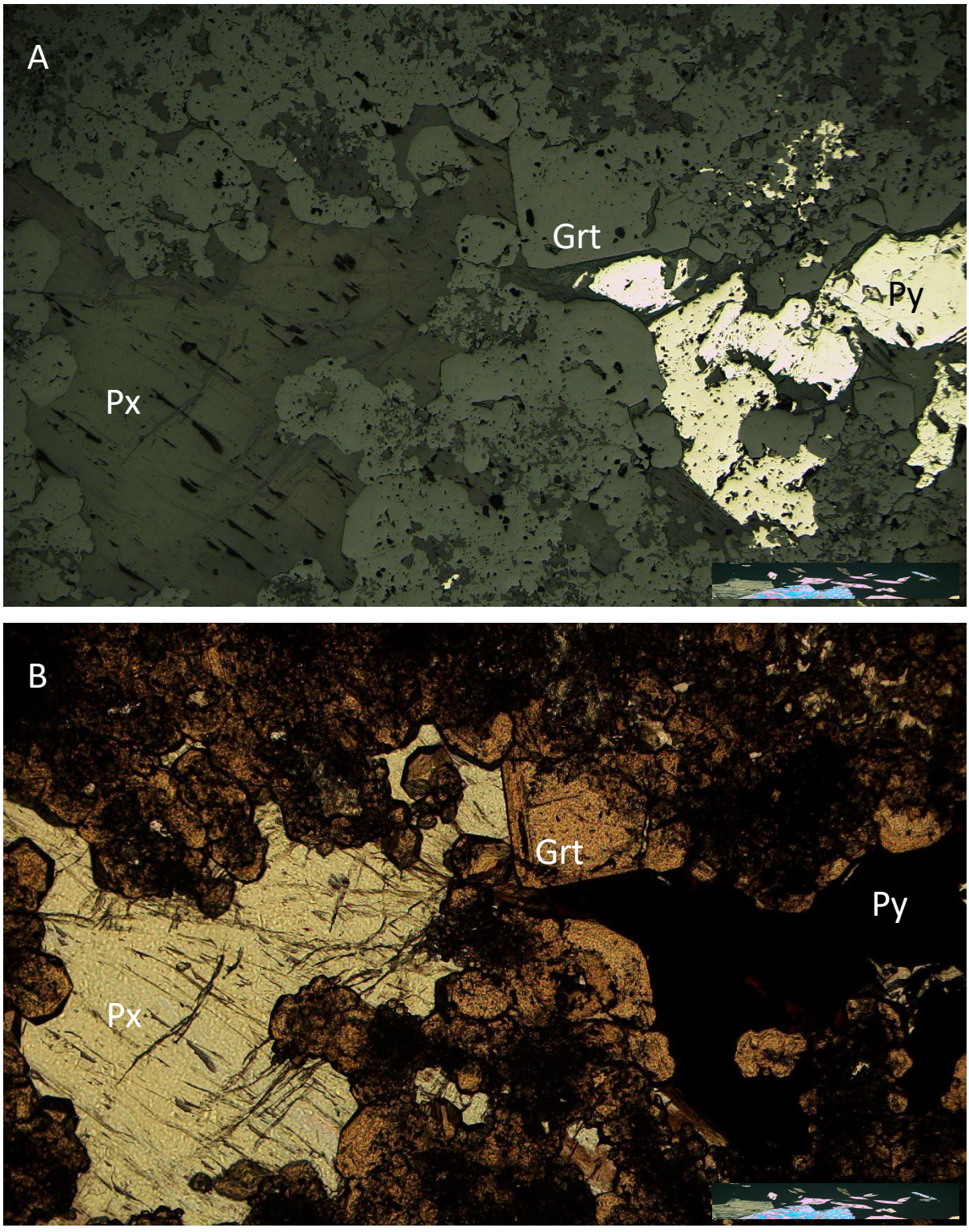

Figure 14 A: Reflective light photomicrograph of skarn alteration and associated sulfide of the sample 2022330047 from drill hole NBH004 of the Eaglehawk prospect, Loch Lilly-Kars Belt, New South Wales, Australia. B: Plain light photomicrograph of A. Grt-garnet; Px-pyroxene; Py-pyrite.

Sample ID	Prospect	Borehole Name	From (m)	To (m)	Note
2022330047	Eaglehawk	NBH004	185.5	185.7	Sulfide and hydrothermal alteration

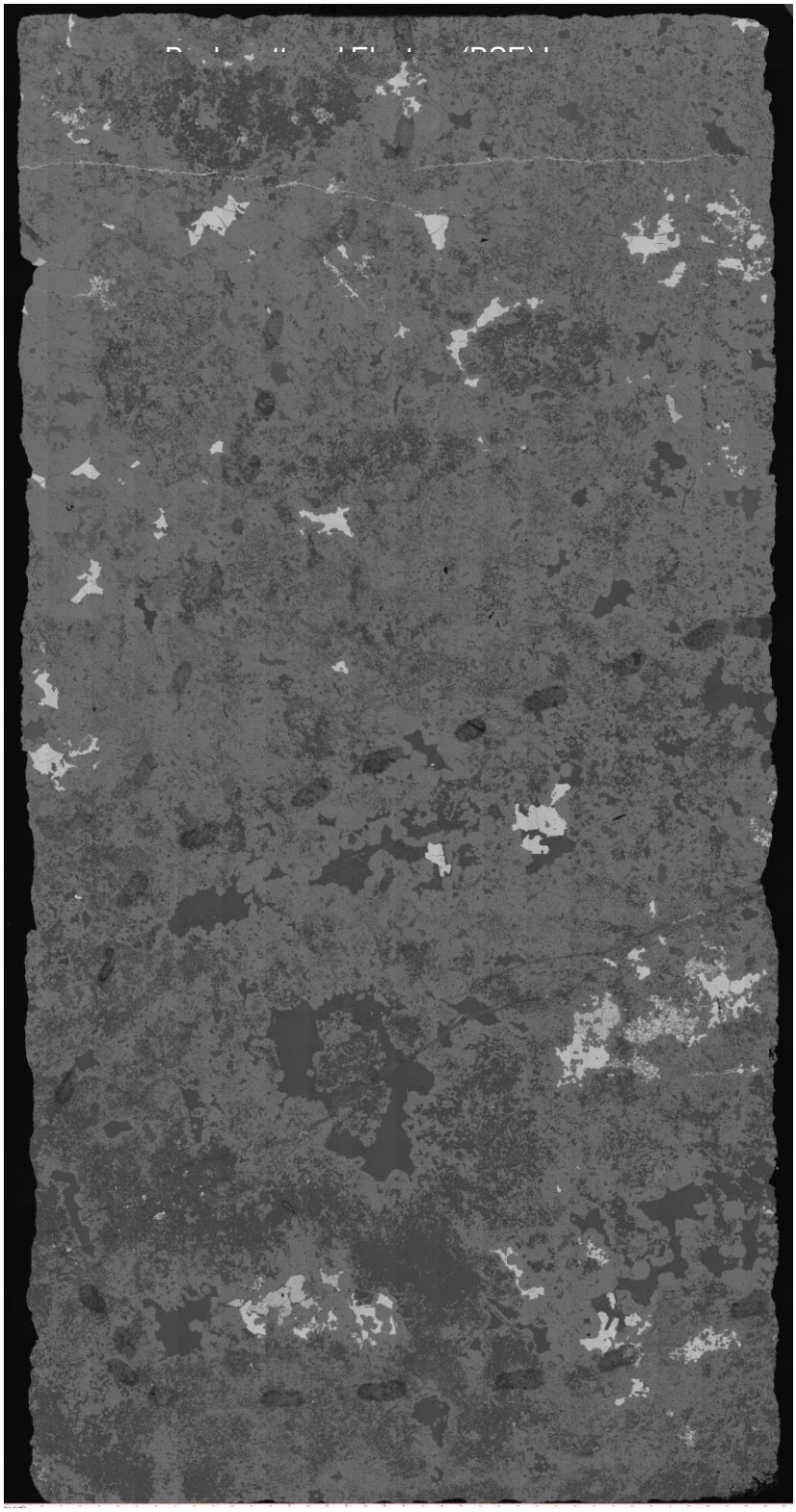

Figure 15 Backscattered electron (BSE) image of the sample 2022330047 from drill hole NBH004 of the Eaglehawk prospect, Loch Lilly-Kars Belt, New South Wales, Australia.

Sample ID	Prospect	Borehole Name	From (m)	To (m)	Note
2022330047	Eaglehawk	NBH004	185.5	185.7	Sulfide and hydrothermal alteration

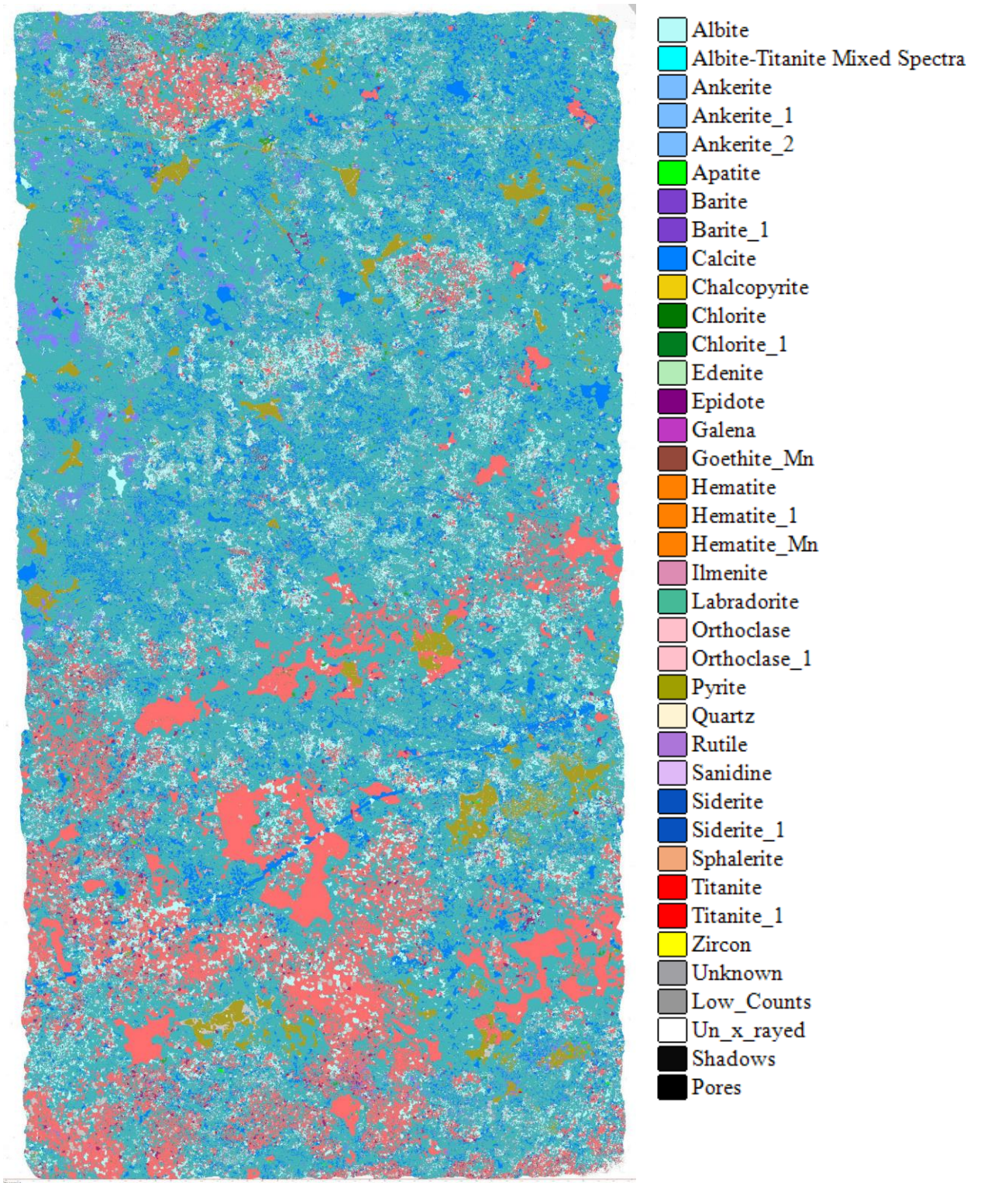

Figure 16 Mineral Liberation Analysis (MLA) mineral map of the sample 2022330047 from drill hole NBH004 of the Eaglehawk prospect, Loch Lilly-Kars Belt, New South Wales, Australia.

Sample ID	Prospect	Borehole Name	From (m)	To (m)	Note
2022330045	Eaglehawk	NBH004	165.1	165.5	Sulfide ore and hydrothermal alteration

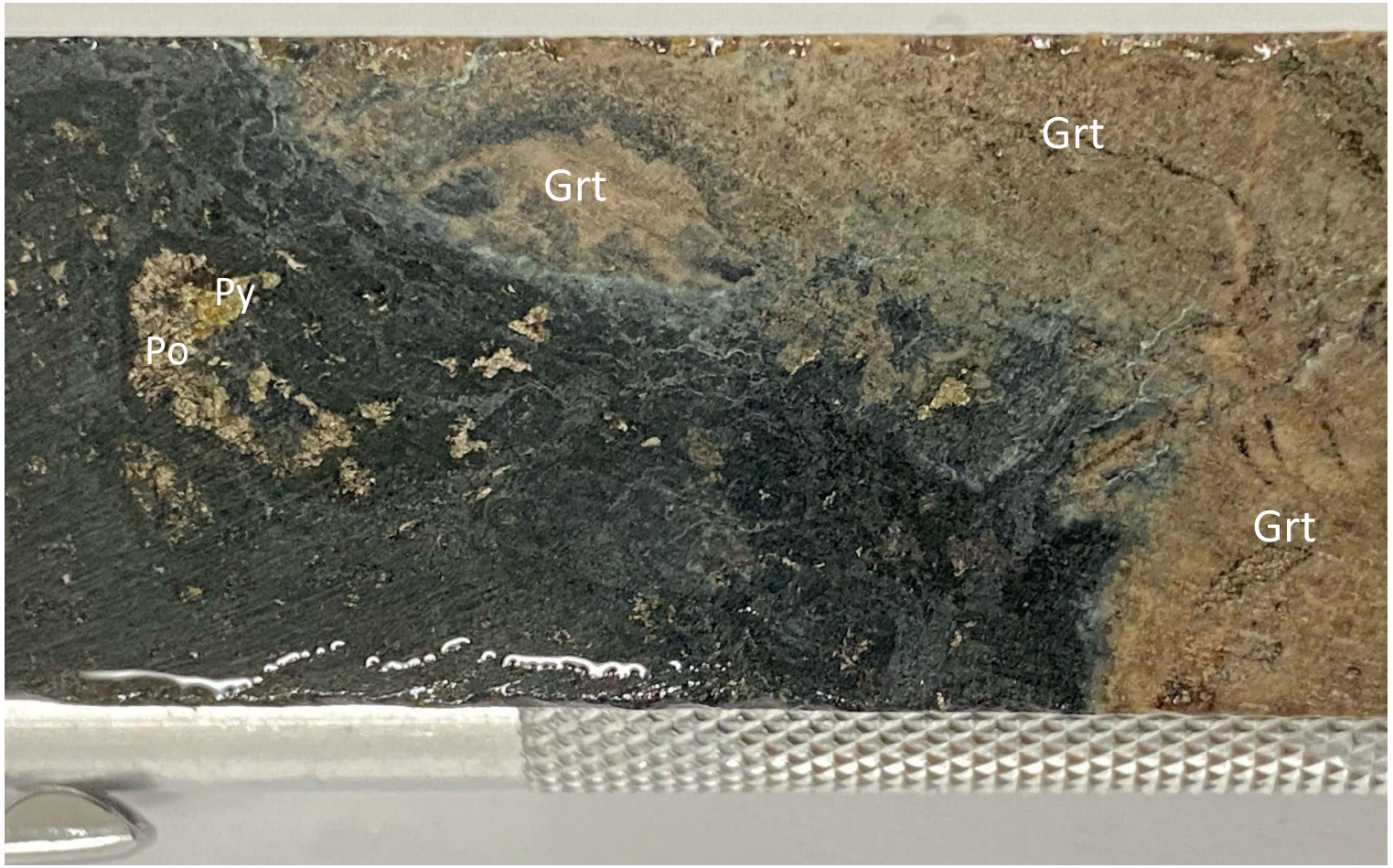

Figure 17 Photos of the drill core sample 2022330045 from drill hole NBH004 of the Eaglehawk prospect, Loch Lilly-Kars Belt, New South Wales, Australia. Grt-garnet; Px-pyroxene; Py-pyrite; Po-pyrrhotite.

Sample ID	Prospect	Borehole Name	From (m)	To (m)	Note
2022330045	Eaglehawk	NBH004	165.1	165.5	Sulfide and hydrothermal alteration

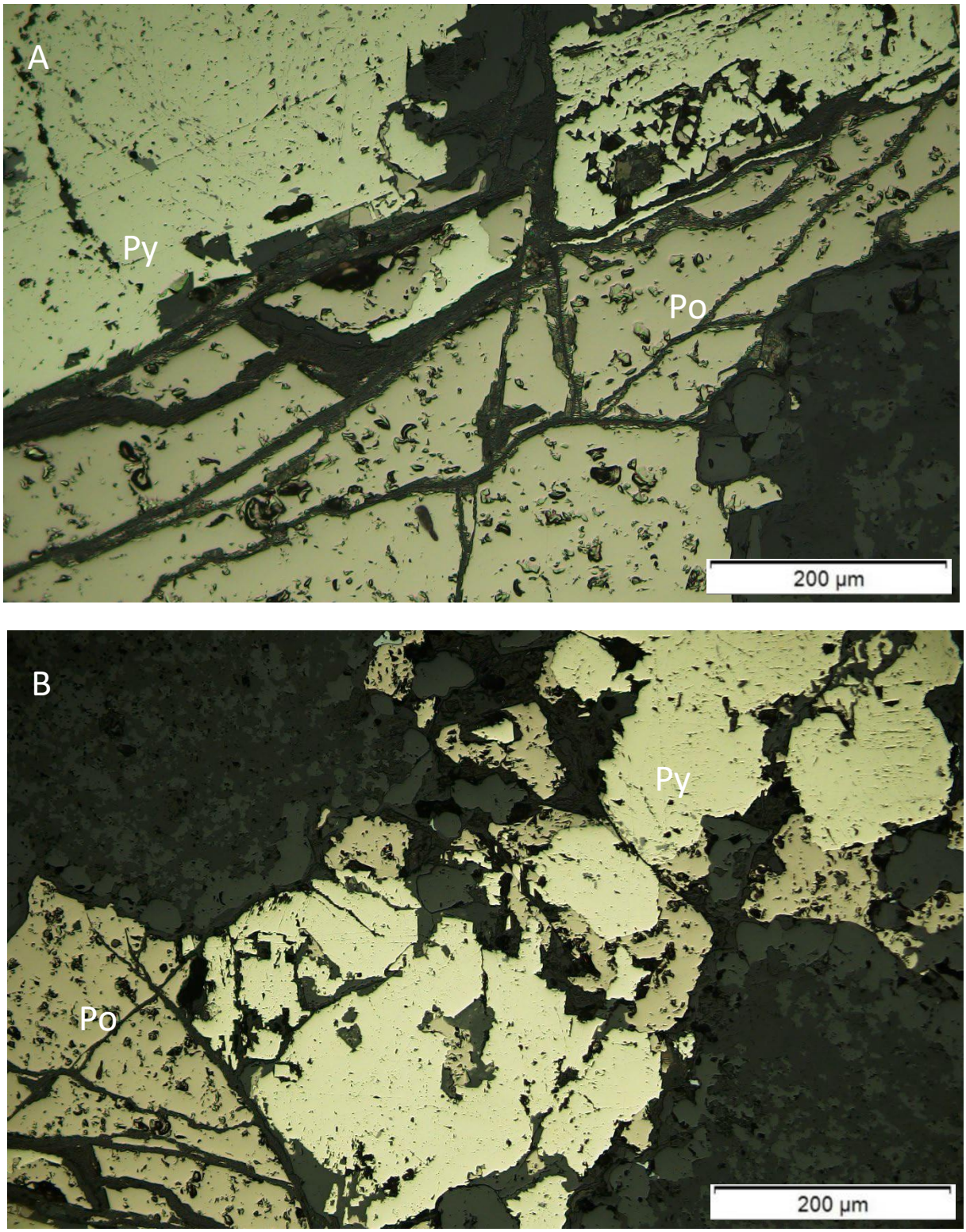

Figure 18 A and B: Reflective light photomicrograph of Py and Po of the sample 2022330045 from drill hole NBH004 of the Eaglehawk prospect, Loch Lilly-Kars Belt, New South Wales, Australia. Grt-garnet; Px-pyroxene; Py-pyrite; Po-pyrrhotite.

Sample ID	Prospect	Borehole Name	From (m)	To (m)	Note
2022440177	Eaglehawk	DD95EHK3	167	167.1	Sulfide ore and hydrothermal alteration

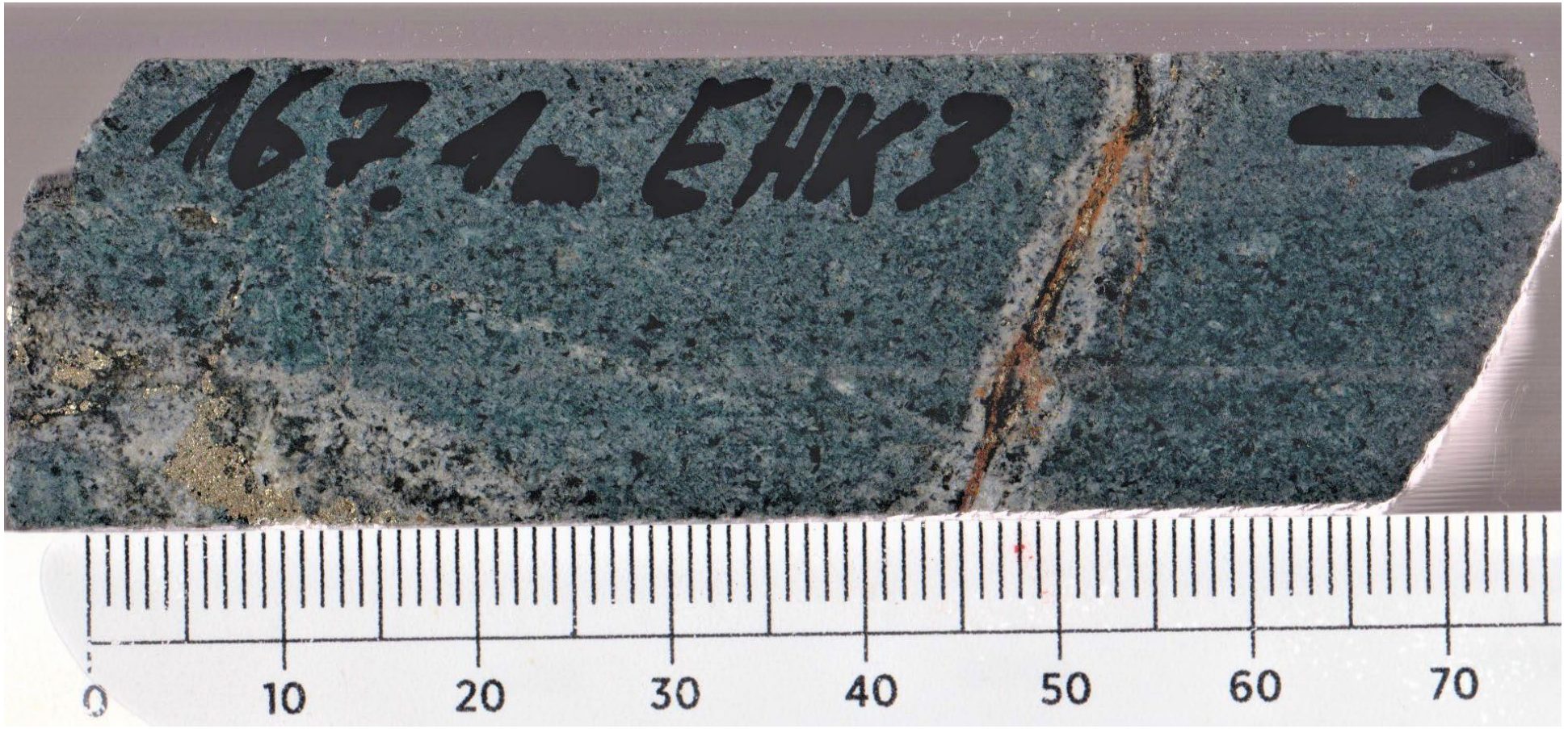

Figure 19 Photos of the drill core sample 2022440177 from drill hole DD95EHK3 of the Eaglehawk prospect, Loch Lilly-Kars Belt, New South Wales, Australia.

Sample ID	Prospect	Borehole Name	From (m)	To (m)	Note
2022440221	Eaglehawk	NBH004	190.3	190.4	Sulfide ore and hydrothermal alteration

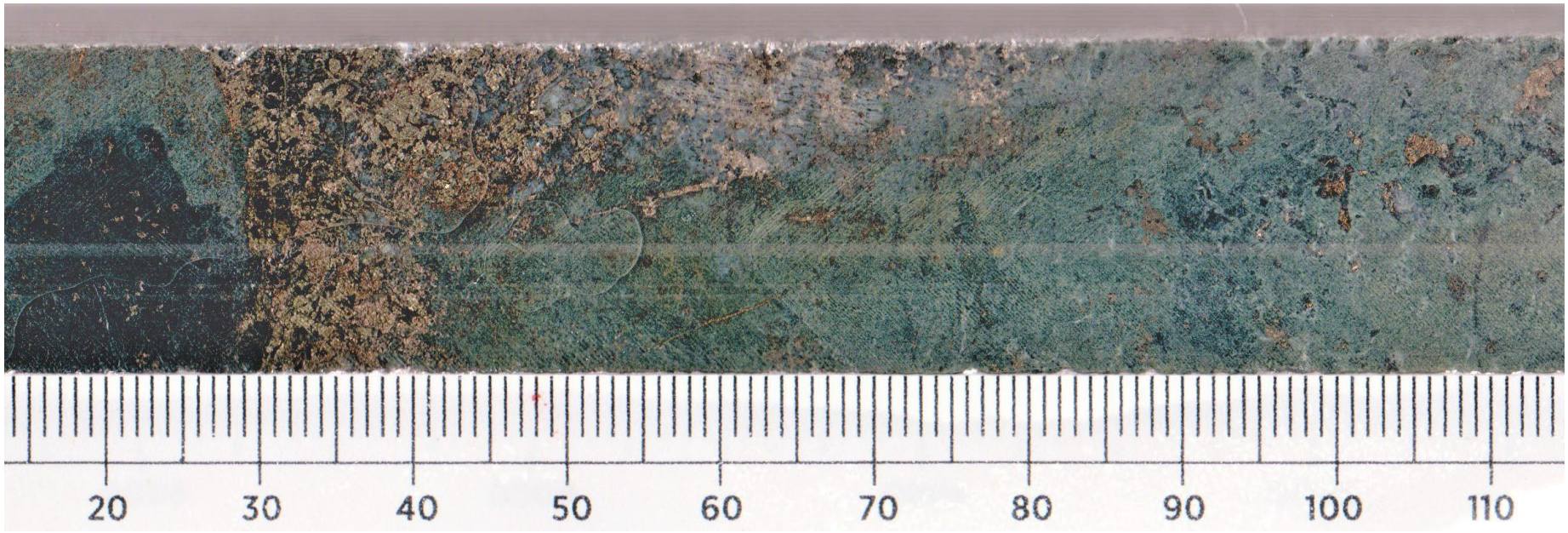

Figure 20 Photos of the drill core sample 2022440221 from drill hole NBH004 of the Eaglehawk prospect, Loch Lilly-Kars Belt, New South Wales, Australia.

Sample ID	Prospect	Borehole Name	From (m)	To (m)	Note
2022330043	Eaglehawk	NBH004	171.1	171.5	Sulfide ore and hydrothermal alteration

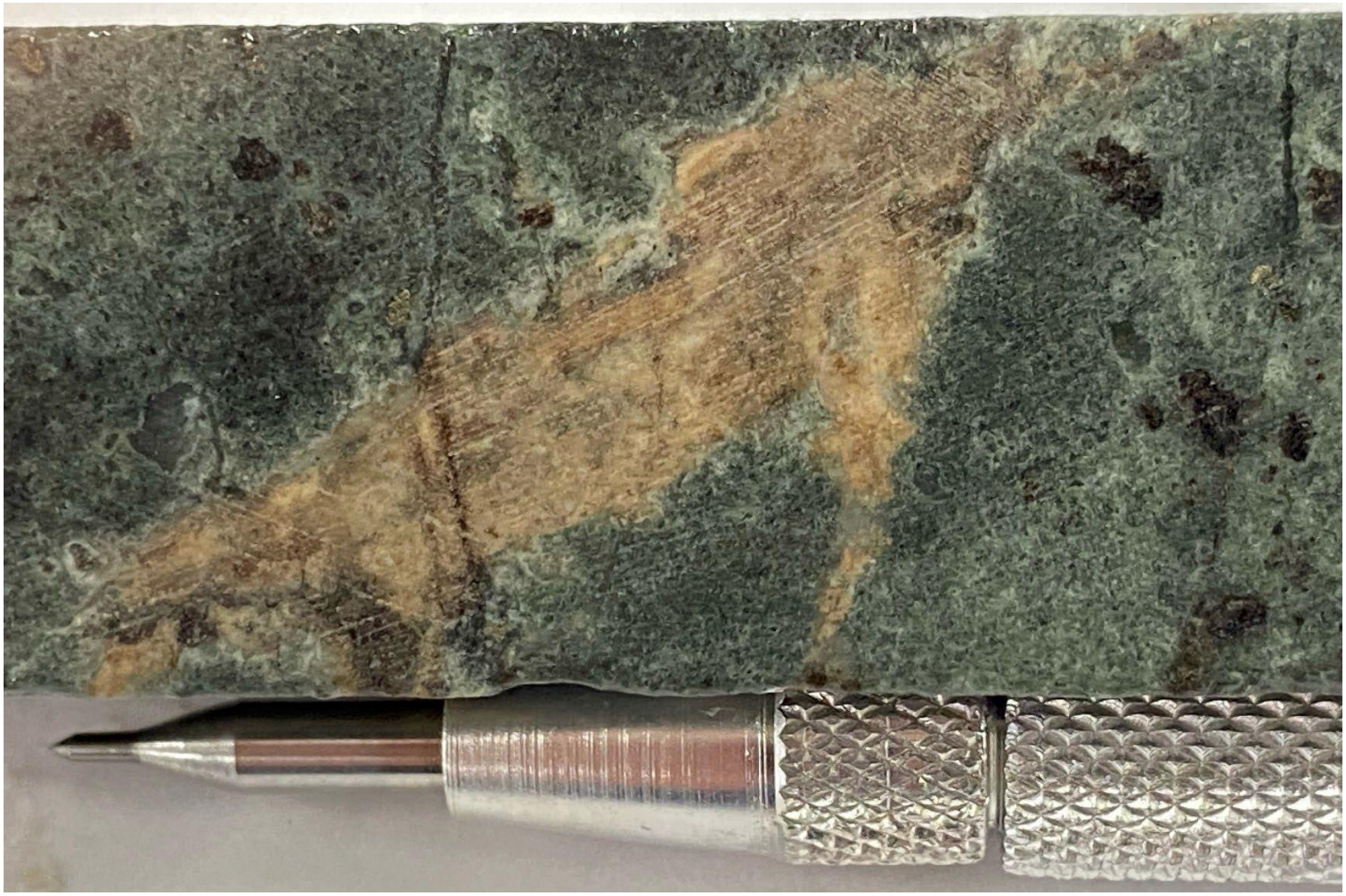

Figure 21 Photos of the drill core sample 2022330043 from drill hole NBH004 of the Eaglehawk prospect, Loch Lilly-Kars Belt, New South Wales, Australia.

S1.2 Scropes Range prospect

Loch Lilly–Kars Belt, New South Wales

Detailed image data: Appendix 2 (individual data file)

(A) Sample List

Sample No.	Sample ID	Borehole	From (m)	To (m)	Notes
9651897	202256532620004	DD92DL23	52.20	52.30	Sulfide ore and hydrothermal alteration
9651896	202256532620003	DD92DL22	82.70	82.90	Sulfide ore and hydrothermal alteration

(B) Mineralisation Characteristics

Data Type	Mineral Assemblage
Hyperspectral SWIR	*Ms, Chl, Car, sulfate*
Hyperspectral TIR	*Qtz, Kfsp, Pl, Ms, Chl, Amp, Car, Kln, sulfate*
Hyperspectral VNIR	*Gth, Hem*
Drill core specimen	*Qtz, Gn*
Thin section	*Gn, Py*
AMICS mineral map	*Or, Qtz, Gn, Py, Cpy, Brt, Ap, Ttn*

(C) Mineralogical Textures and Paragenesis

Category	Description
Texture	Scropes Range is a Zn-rich prospect. Mineralisation is associated with brecciation; sphalerite occurs within a quartz–fluorite–calcite matrix.
Paragenesis	Galena formed later than pyrite, precipitated by a lower-temperature hydrothermal fluid. Fine calcite veins represent the latest hydrothermal activity.

(D) Supplementary Figure Reference

Supplementary Figures *include (1) Downhole HyLogger hyperspectral images and summaries of drill holes DD92DL22 and DD92DL23; and (2) Drill core photographs, reflected-light photomicrographs, and BSE/MLA mineral maps of sulfide ore (Gn–Py–Cpy–Brt assemblage), samples 2022330033 and 2022330030.*

S1.2 The Scropes Range prospect, Loch Lilly-Kars Belt, New South Wales

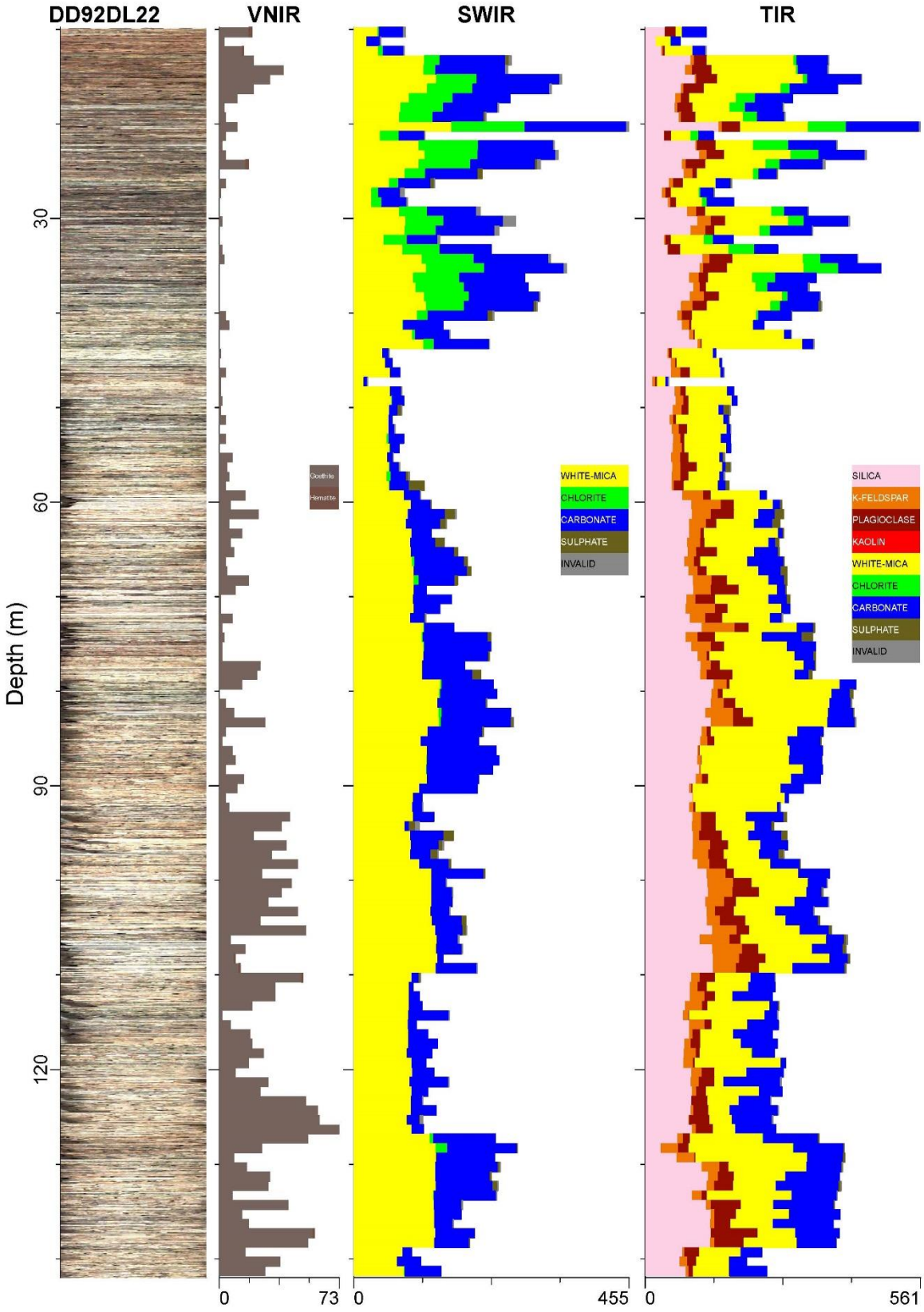

Figure 1 Downhole hylogger hyperspectral image of the hole DD92DL22 of the Scropes Range prospect, Loch Lilly-Kars Belt, New South Wales, Australia.

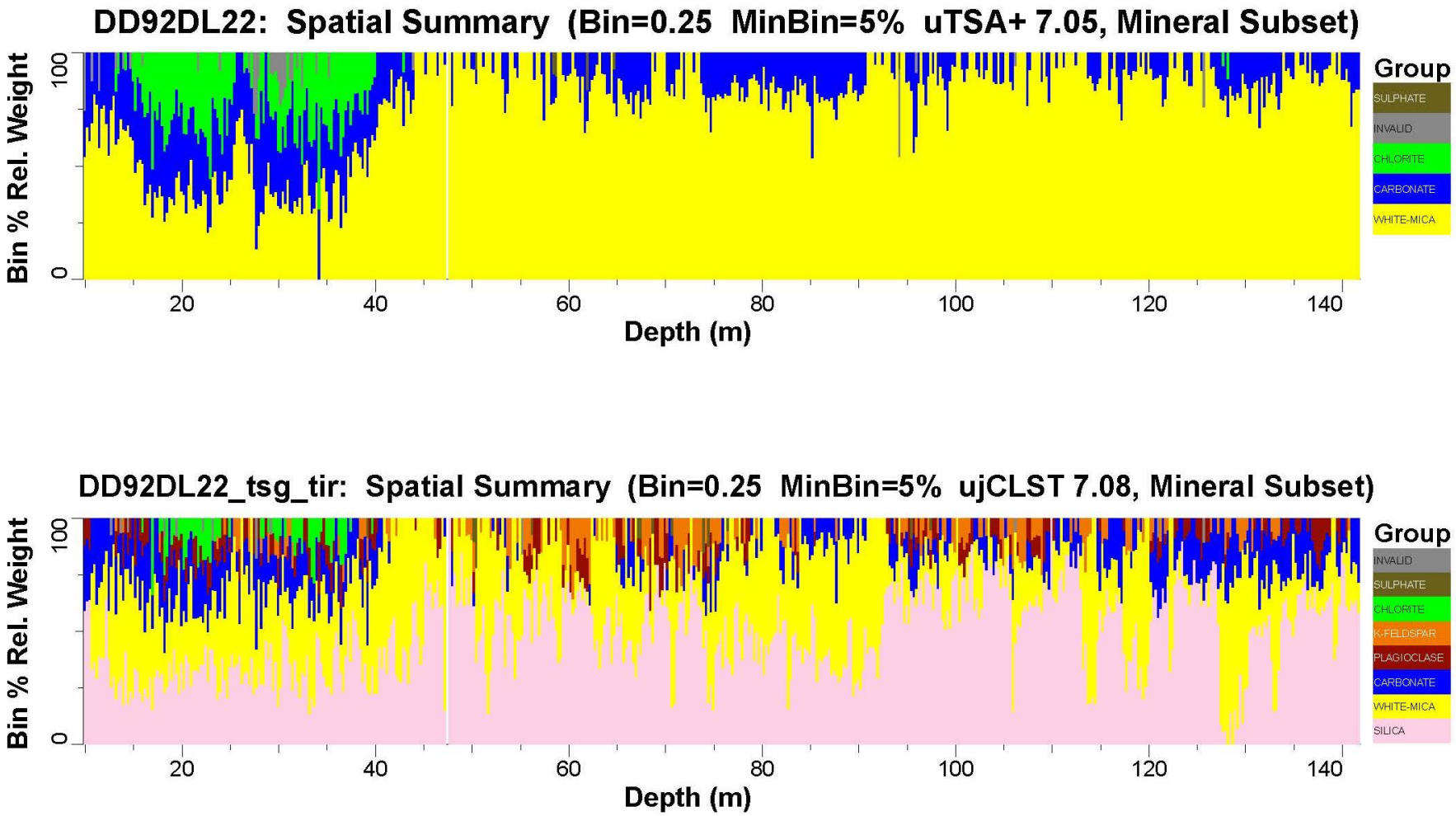

Figure 2 Summary of the hylogger hyperspectral image of the hole DD92DL22 of the Scropes Range prospect, Loch Lilly-Kars Belt, New South Wales, Australia.

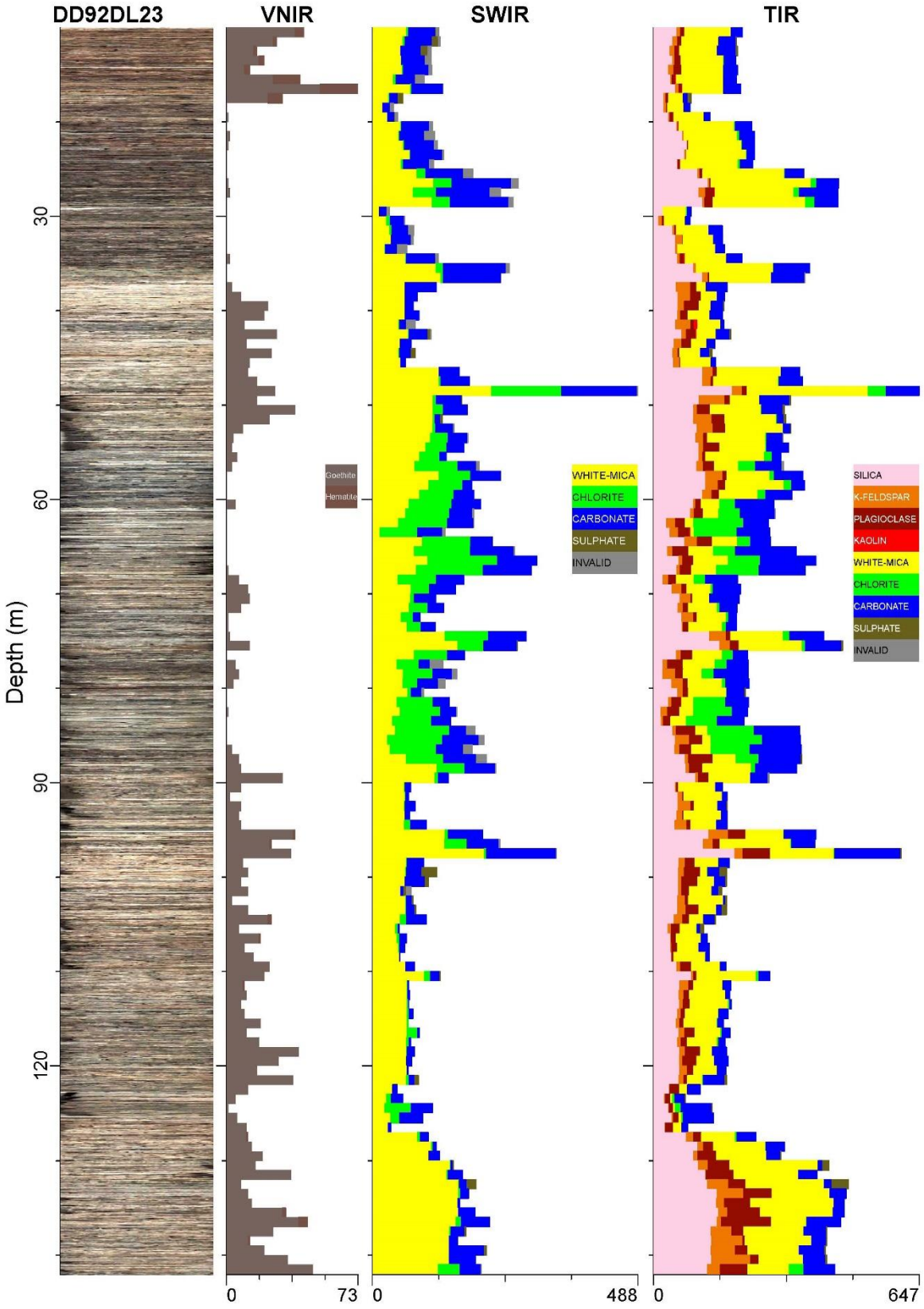

Figure 3 Downhole hylogger hyperspectral image the hole DD92DL23 of the Scropes Range prospect, Loch Lilly-Kars Belt, New South Wales, Australia.

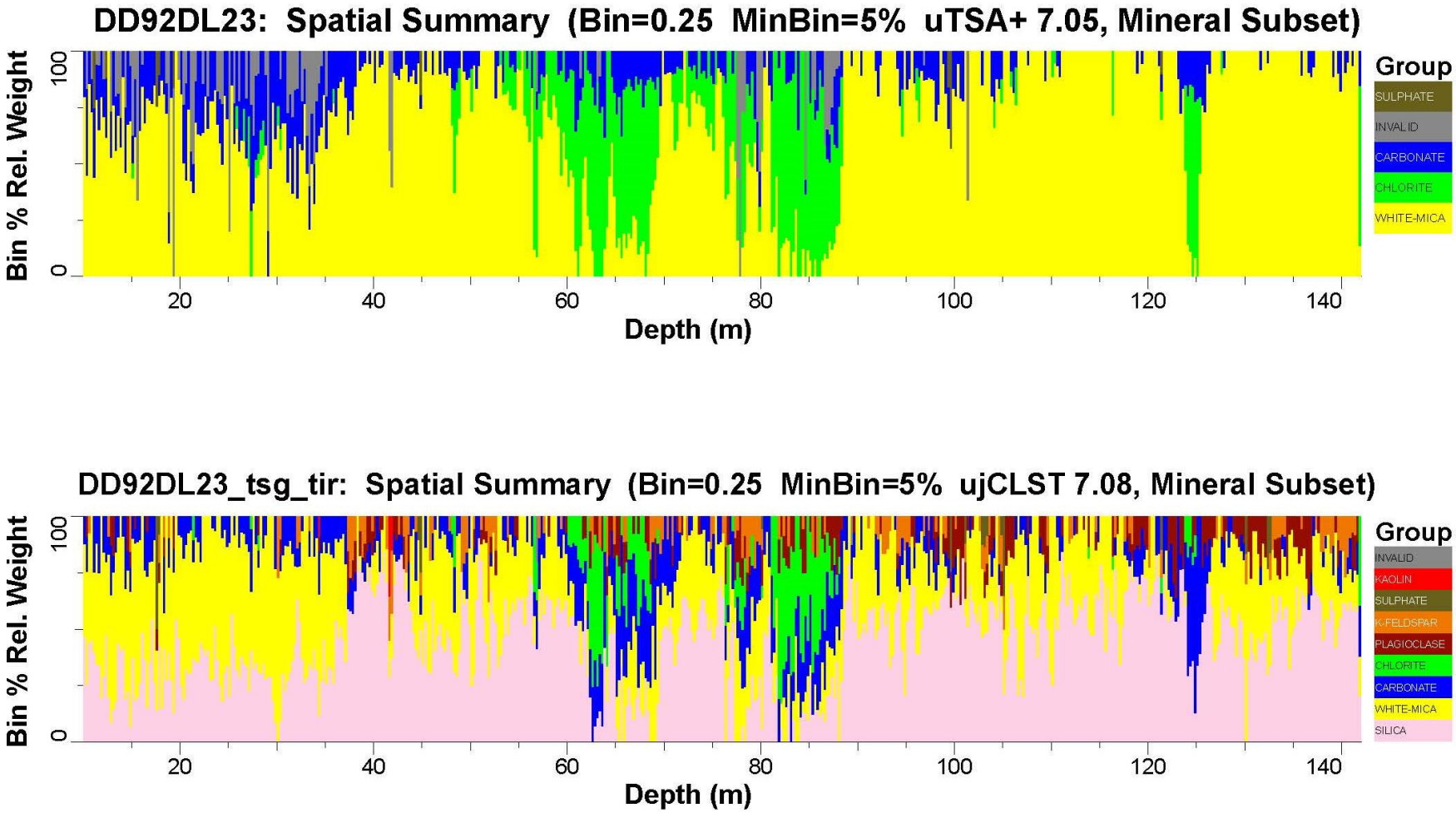

Figure 4 Summary of the hylogger hyperspectral image of the hole DD92DL23 of the Scropes Range prospect, Loch Lilly-Kars Belt, New South Wales, Australia.

Sample ID	Prospect	Borehole Name	From (m)	To (m)	Note
2022330033	Scropes Range	DD92DL22	82.7	82.9	Sulfide ore and hydrothermal alteration

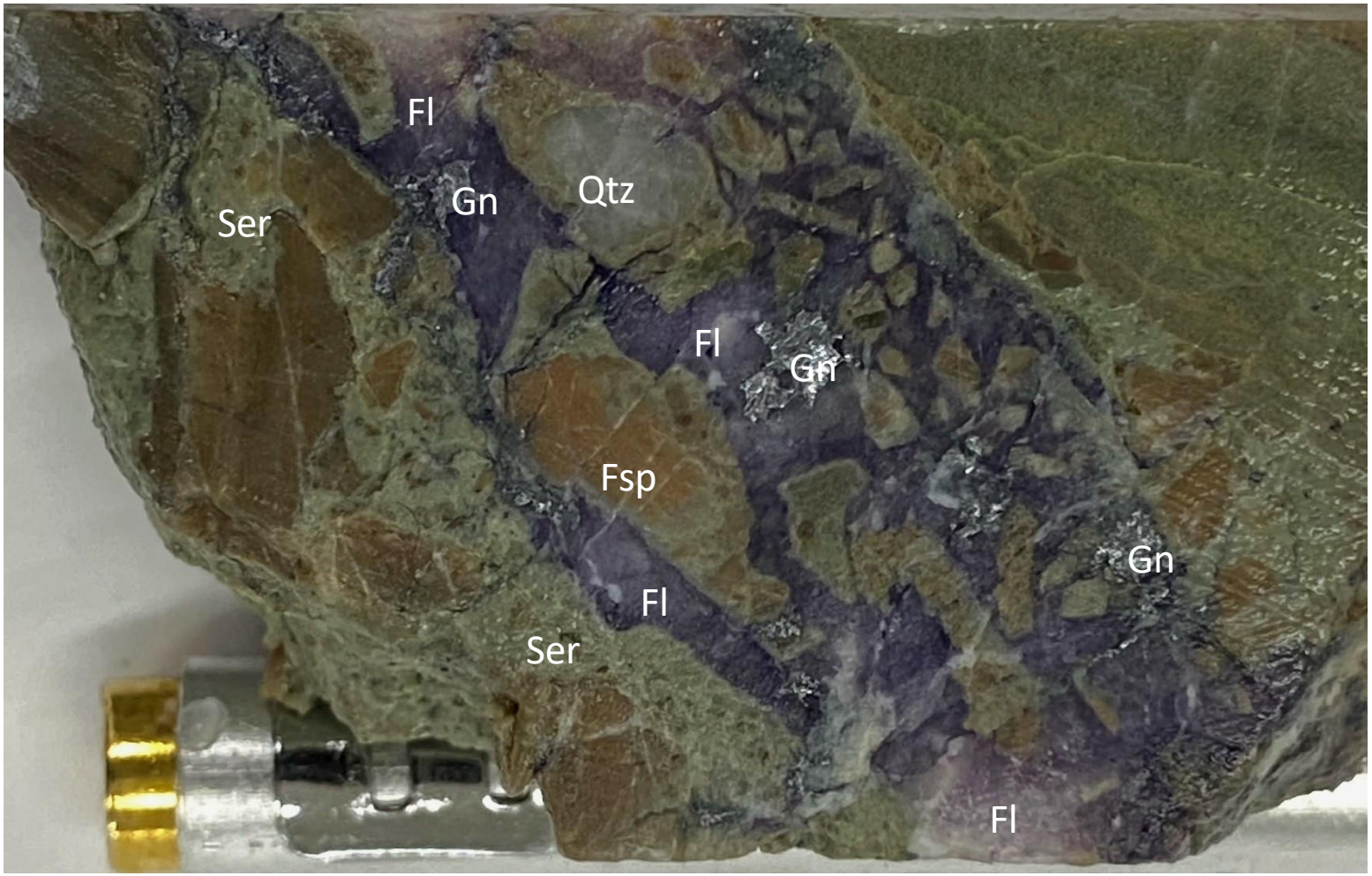

Figure 5 Photos of the drill core sample 2022330033 from drill hole DD92DL23 of the Scropes Range prospect, Loch Lilly-Kars Belt, New South Wales, Australia. Fl-fluorite; Gn-galena; Ser-sericite; Qtz-quartz; Fsp-feldspar.

Sample ID	Prospect	Borehole Name	From (m)	To (m)	Note
2022330033	Scropes Range	DD92DL22	82.7	82.9	Sulfide ore and hydrothermal alteration

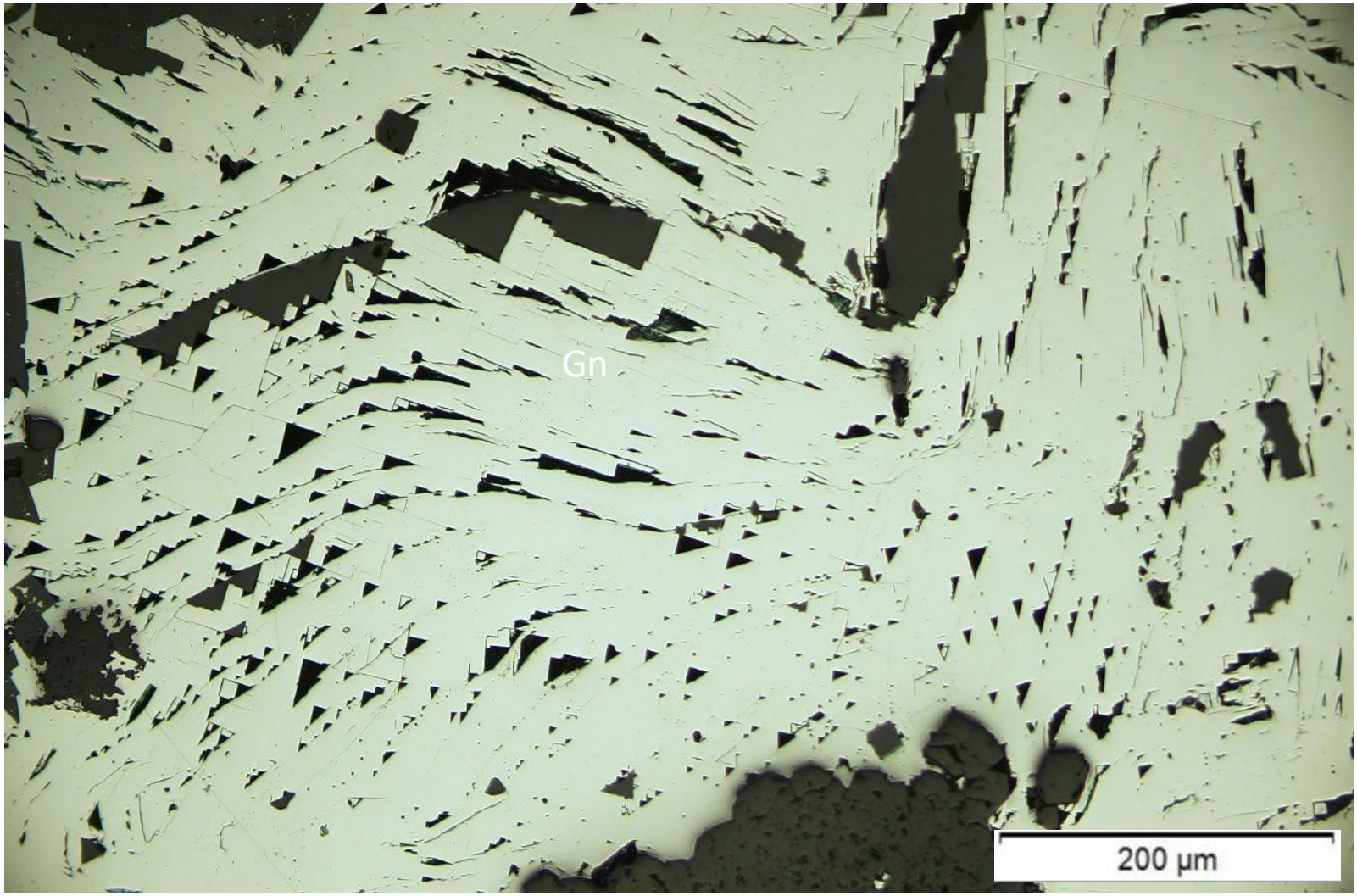

Figure 6 Reflective light photomicrograph of the sample 2022330033 from drill hole DD92DL23 of the Scropes Range prospect, Loch Lilly-Kars Belt, New South Wales, Australia. Gn-galena.

Sample ID	Prospect	Borehole Name	From (m)	To (m)	Note
2022330033	Scropes Range	DD92DL22	82.7	82.9	Sulfide and hydrothermal alteration

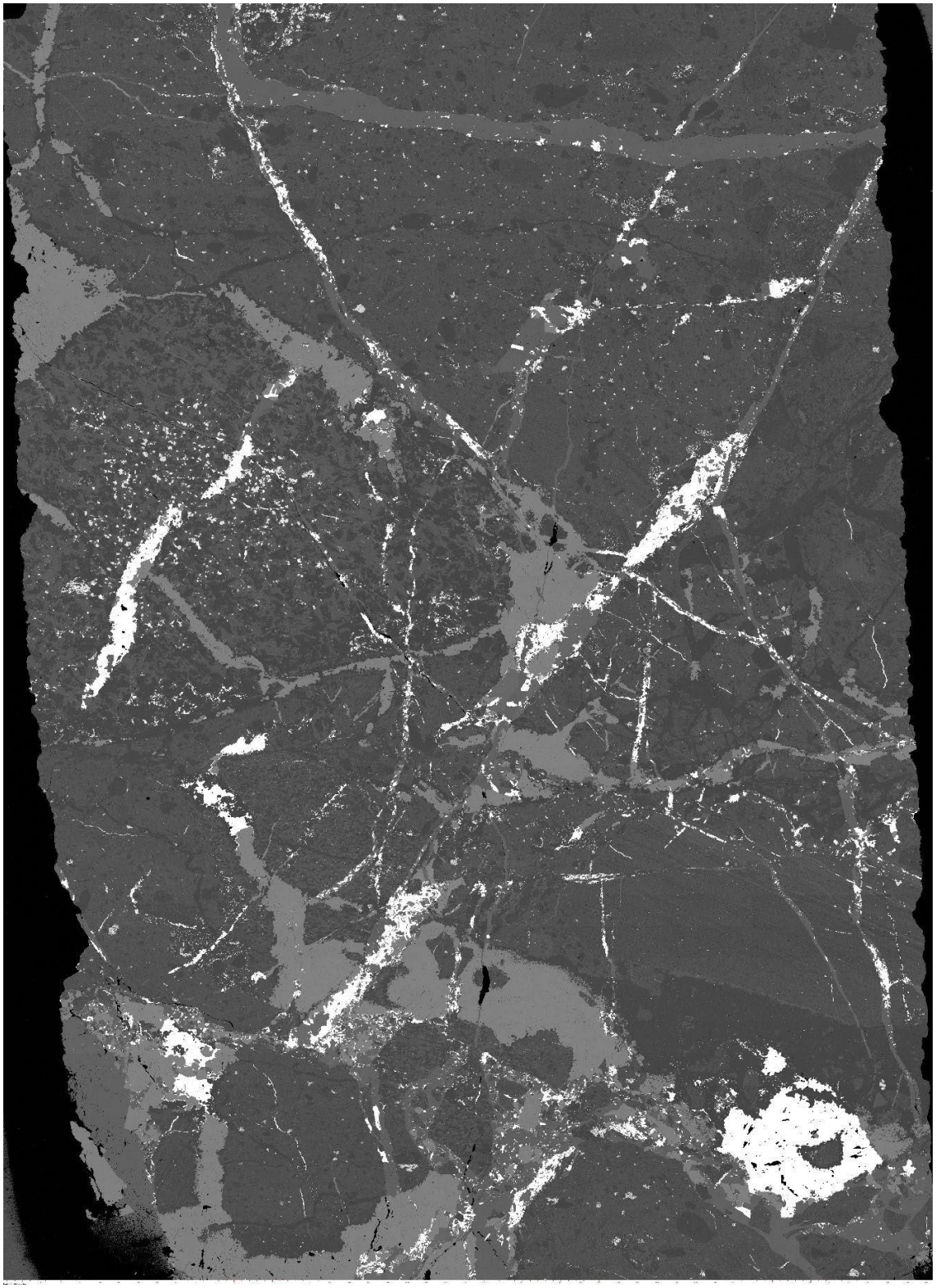

Figure 7 Backscattered electron (BSE) image of the sample 2022330033 from drill hole DD92DL23 of the Scropes Range prospect, Loch Lilly-Kars Belt, New South Wales, Australia.

Sample ID	Prospect	Borehole Name	From (m)	To (m)	Note
2022330033	Scropes Range	DD92DL22	82.7	82.9	Sulfide and hydrothermal alteration

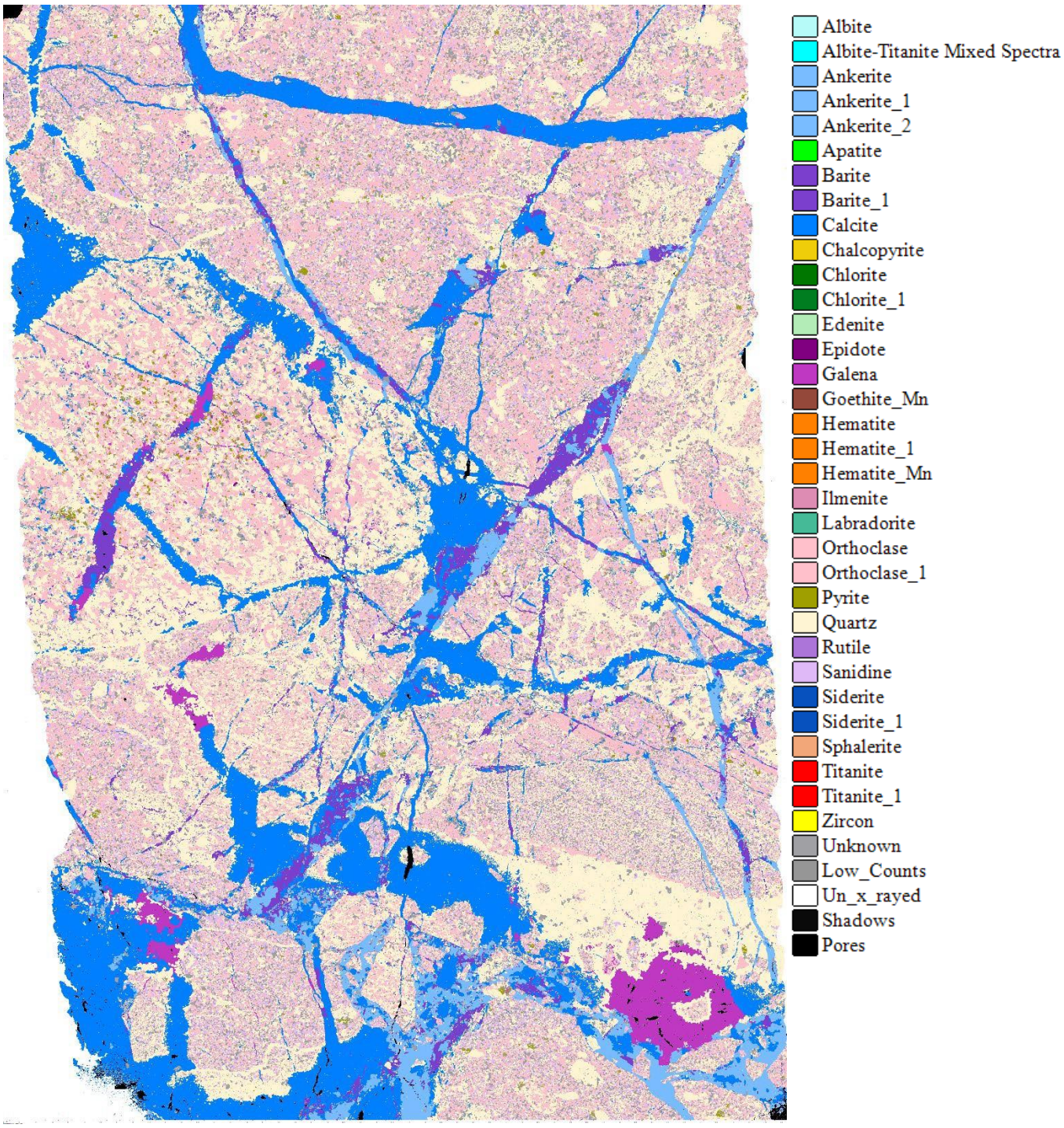

Figure 8 Mineral Liberation Analysis (MLA) mineral map of the sample 2022330033 from drill hole DD92DL23 of the Scropes Range prospect, Loch Lilly-Kars Belt, New South Wales, Australia.

Sample ID	Prospect	Borehole Name	From (m)	To (m)	Note
2022330030	Scropes Range	DD92DL23	52.2	52.3	Sulfide ore and hydrothermal alteration

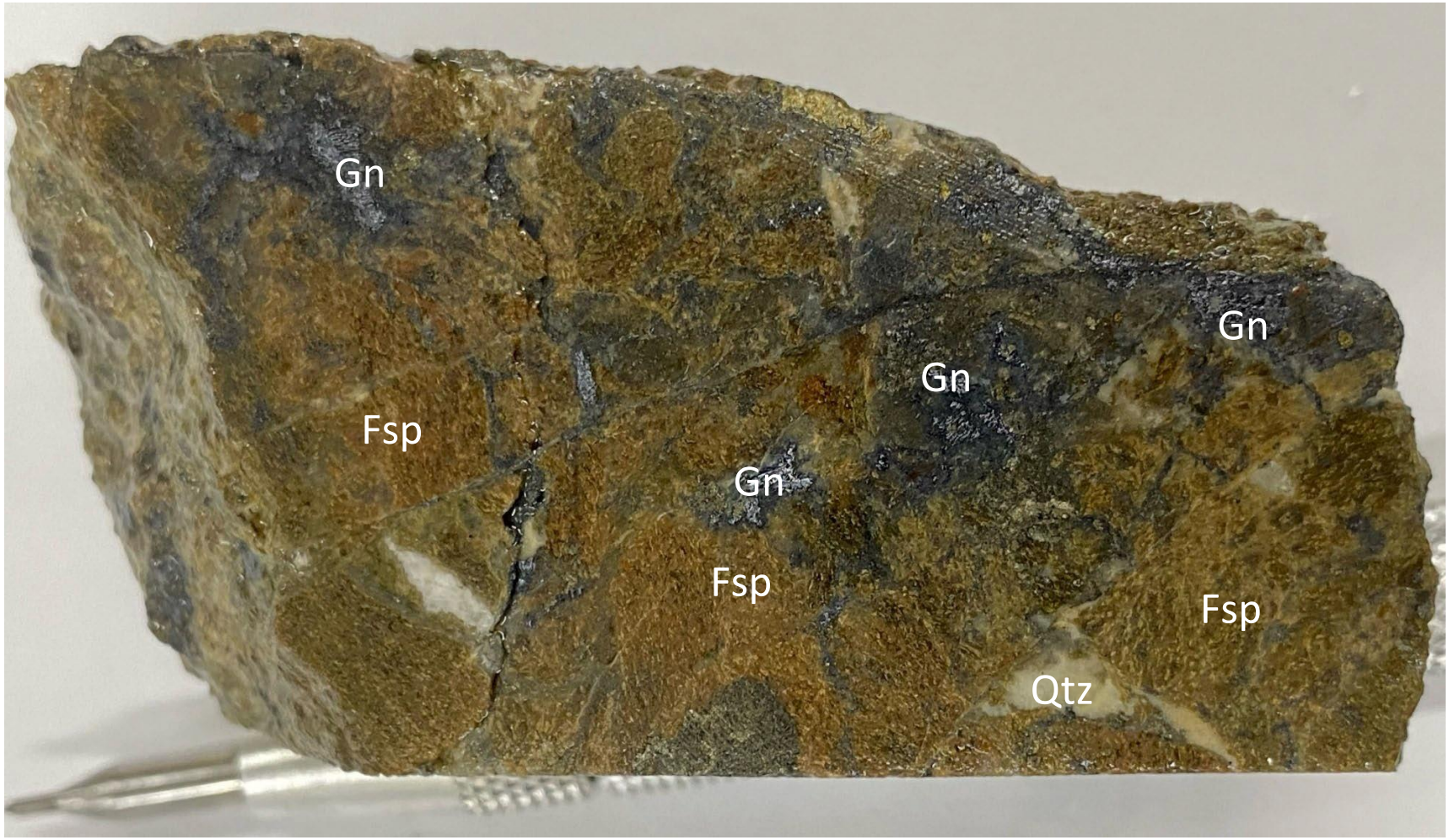

Figure 9 Photos of the drill core sample 2022330030 from drill hole DD92DL23 of the Scropes Range prospect, Loch Lilly-Kars Belt, New South Wales, Australia. Gn-galena; Fsp-feldspar; Qtz-quartz.

Sample ID	Prospect	Borehole Name	From (m)	To (m)	Note
2022330030	Scropes Range	DD92DL23	52.2	52.3	Sulfide ore and hydrothermal alteration

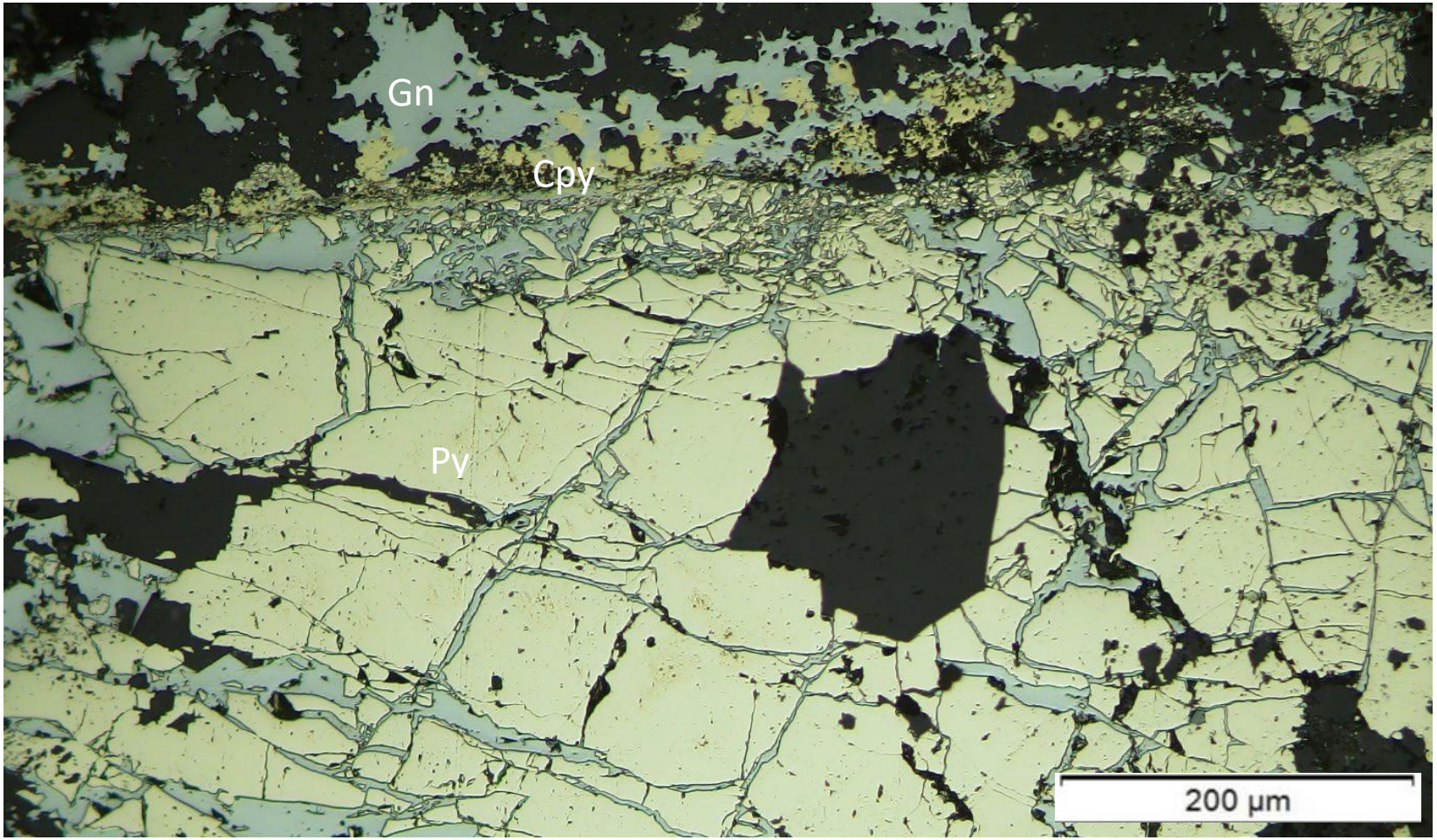

Figure 10 Reflective light photomicrograph of the sample 2022330030 from drill hole DD92DL23 of the Scropes Range prospect, Loch Lilly-Kars Belt, New South Wales, Australia. Gn-galena; Py-pyrite; Cpy-chalcopyrite.

Sample ID	Prospect	Borehole Name	From (m)	To (m)	Note
2022330030	Scropes Range	DD92DL23	52.2	52.3	Sulfides and hydrothermal alteration

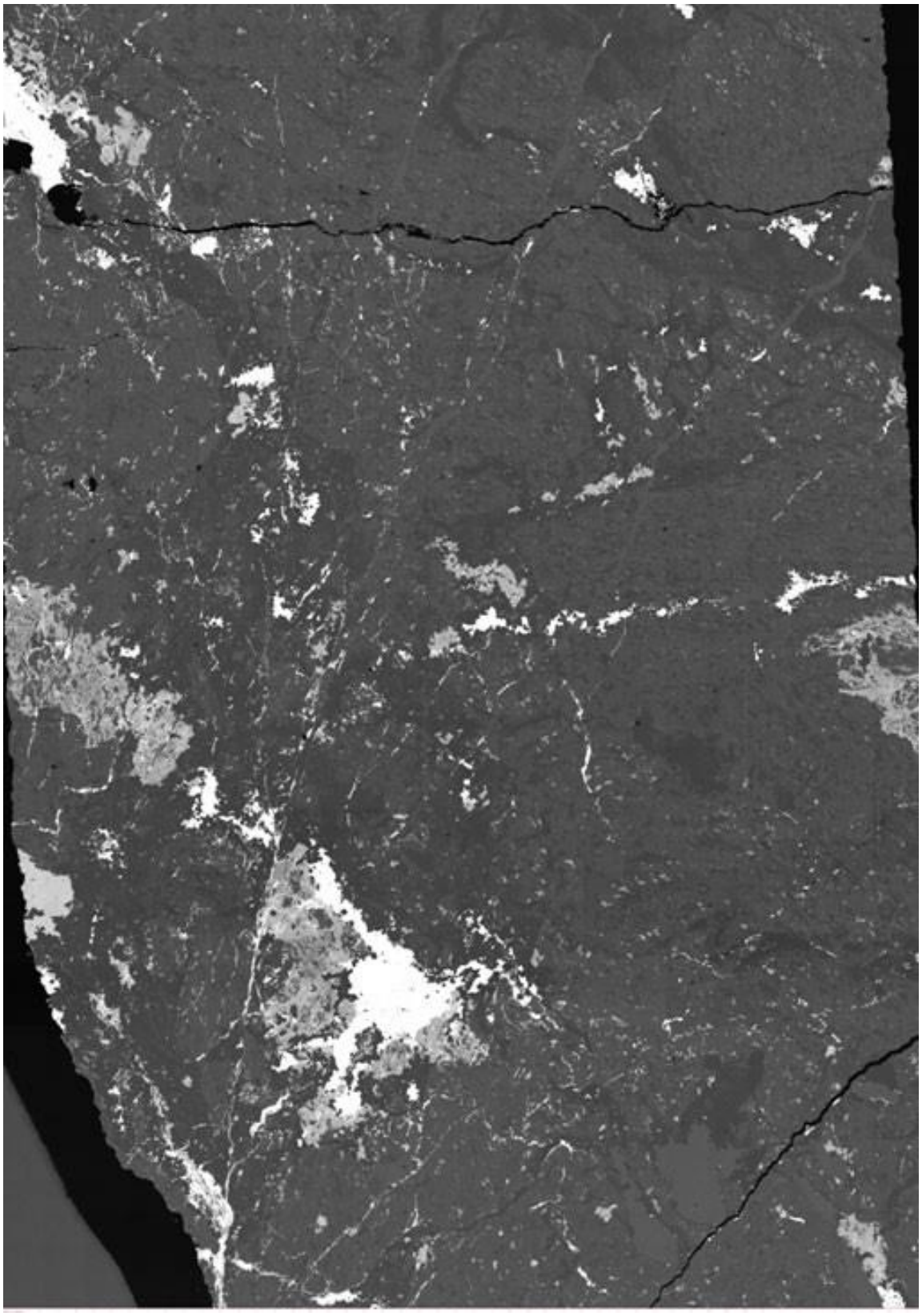

Figure 11 Backscattered electron (BSE) image of the sample 2022330030 from drill hole DD92DL23 of the Scropes Range prospect, Loch Lilly-Kars Belt, New South Wales, Australia.

Sample ID	Prospect	Borehole Name	From (m)	To (m)	Note
2022330030	Scropes Range	DD92DL23	52.2	52.3	Sulfides and hydrothermal alteration

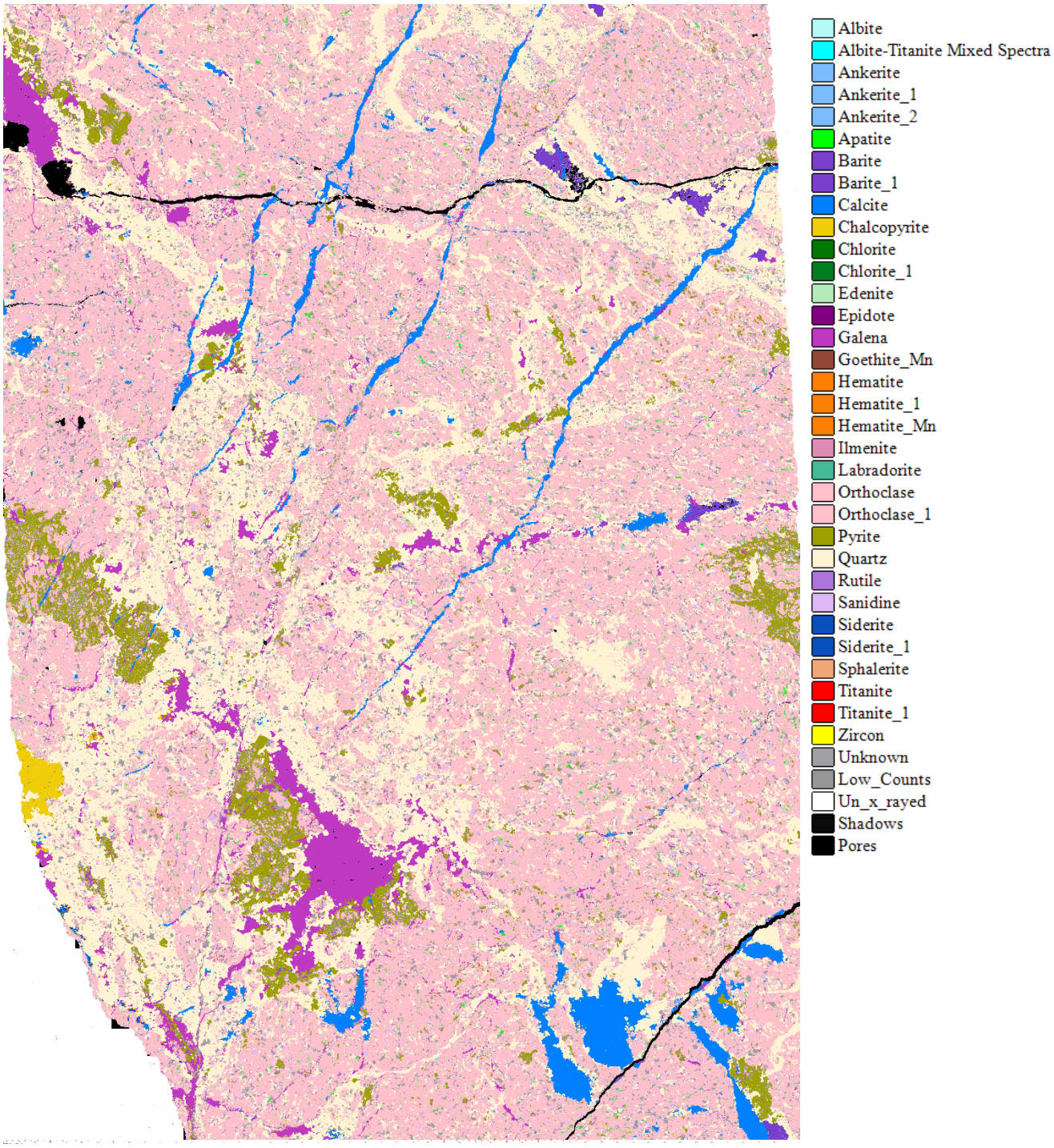

Figure 12 Mineral Liberation Analysis (MLA) mineral map of the sample 2022330030 from drill hole DD92DL23 of the Scropes Range prospect, Loch Lilly-Kars Belt, New South Wales, Australia.

S1.3 Wahratta prospect

Loch Lilly–Kars Belt, New South Wales

Detailed image data: Appendix 3 (individual data file)

(A) Sample List

Sample No.	Sample ID	Borehole	From (m)	To (m)	Notes
9651894	202256532620001	CP2	389.80	390.00	Sulfide ore and hydrothermal alteration
9651895	202256532620002	CP2	427.10	427.20	Sulfide ore and hydrothermal alteration
9651898	202256532620005	DD96WA3	842.30	842.40	Sulfide ore and hydrothermal alteration
9651899	202256532620006	DD96WA3	947.80	948.00	Sulfide ore and hydrothermal alteration
9651900	202256532620007	DD96WA3	1052.80	1053.20	Sulfide ore and hydrothermal alteration

(B) Mineralisation Characteristics

Data Type	Mineral Assemblage
Hyperspectral SWIR	*Ms, Sme, Chl, Ep, Amp, Car, Kln, sulfate*
Hyperspectral TIR	*Qtz, Kfsp, Pl, Px, Ms, Sme, Chl, Car, Amp, Ep, sulfate, phosphate*
Hyperspectral VNIR	*Gth, Hem*
Drill core specimen	*Qtz, Kfsp, Bt, Ser, Pl, Py, Cal*
Thin section	*Qtz, Py, Fsp, Ap, Ab*
AMICS mineral map	*Or, Qtz, Hem, Py, Ep, Chl, Cal, Ank, Ed, Ap, Ttn*

(C) Mineralogical Textures and Paragenesis

Category	Description
Texture	Features of porphyry-type mineralisation are present, including a suite of magmatic-hydrothermal alteration mineral assemblages. Note: cover sequence extends to ~820 m in this area.
Paragenesis	Sulfides occur as veins together with biotite, albite and K-feldspar hosted in porphyritic intrusive rocks. Quartz–feldspar–pyrite veins crosscut organic-rich shale.

(D) Supplementary Figure Reference

Supplementary Figures *include (1) Downhole HyLogger hyperspectral images and summaries of drill holes CP2, CP3 and DD96WA3; and (2) Drill core photographs, reflected-light photomicrographs, BSE images and MLA mineral maps of sulfide veins and hydrothermal alteration assemblages, samples 2022330070, 2022330063, 2022330068, 2022330036 and 2022330037.*

S1.3 The Wahratta prospect, Loch Lilly-Kars Belt, New South Wales

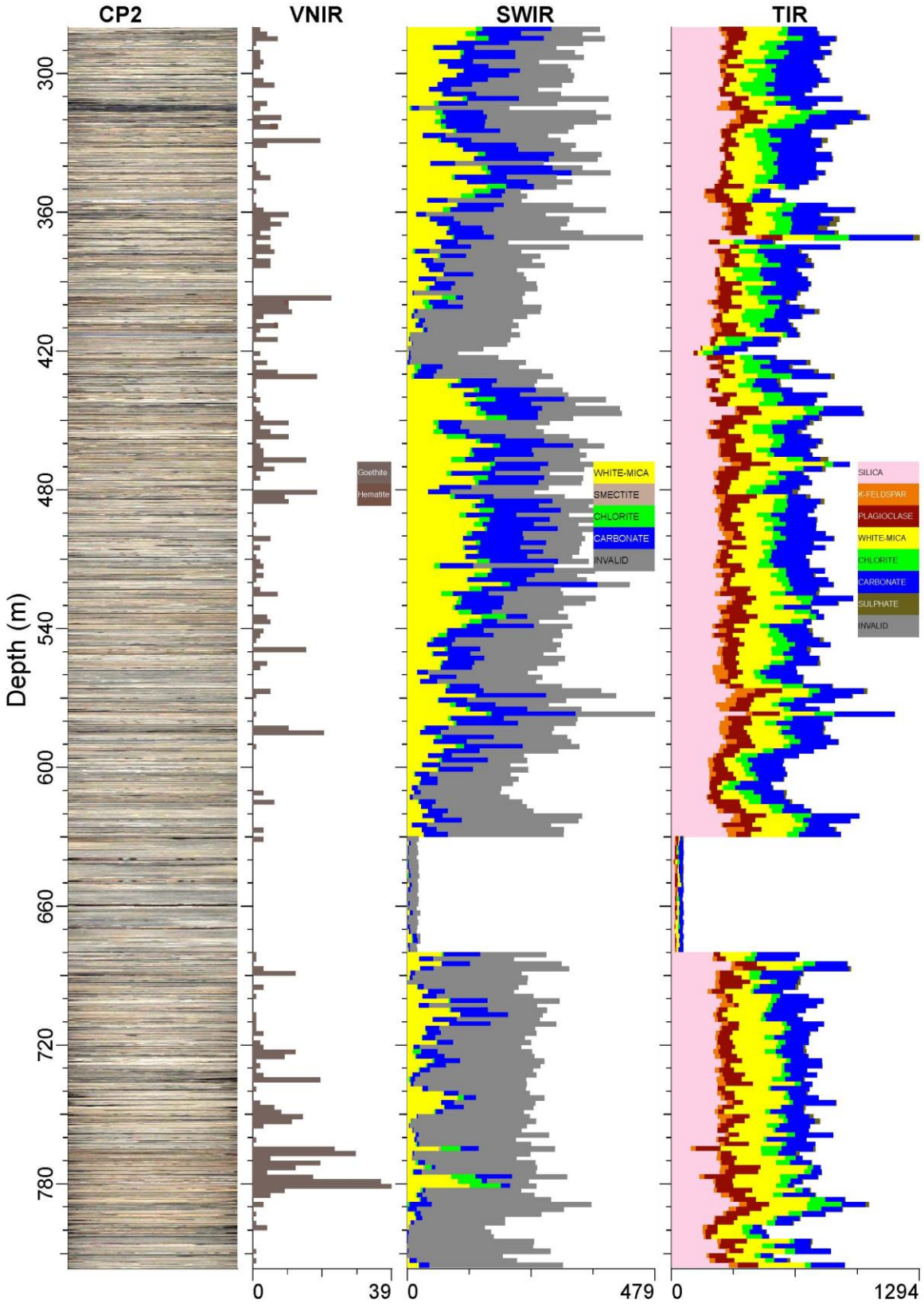

Figure 1 Downhole hylogger hyperspectral image of the hole CP2, Wahratta prospect, Loch Lilly-Kars Belt, New South Wales, Australia. Note the cover is to ~820m in this area.

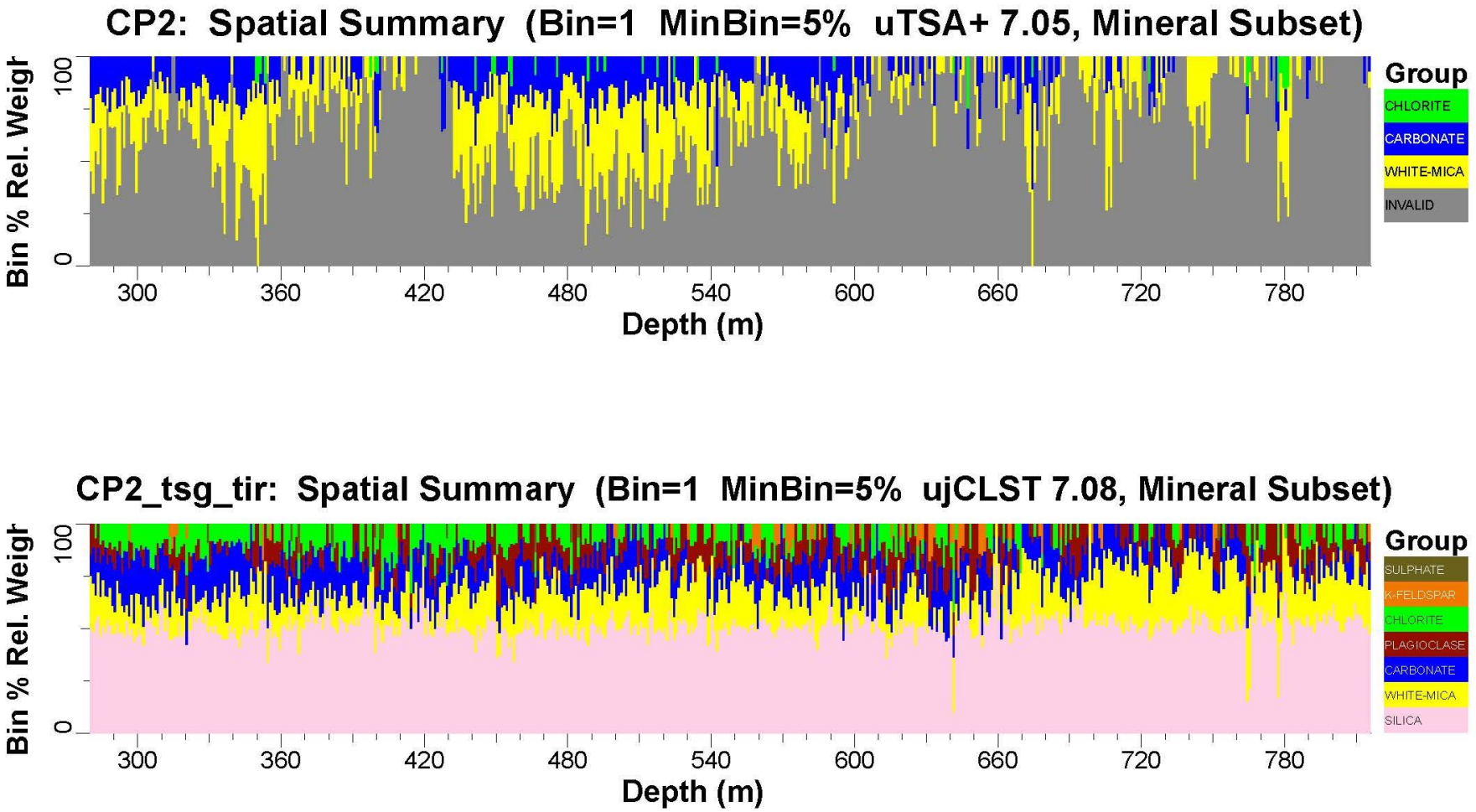

Figure 2 Summary of the hylogger hyperspectral image of the hole CP2, Wahratta prospect, Loch Lilly-Kars Belt, New South Wales, Australia. Note the cover is to ~820m in this area.

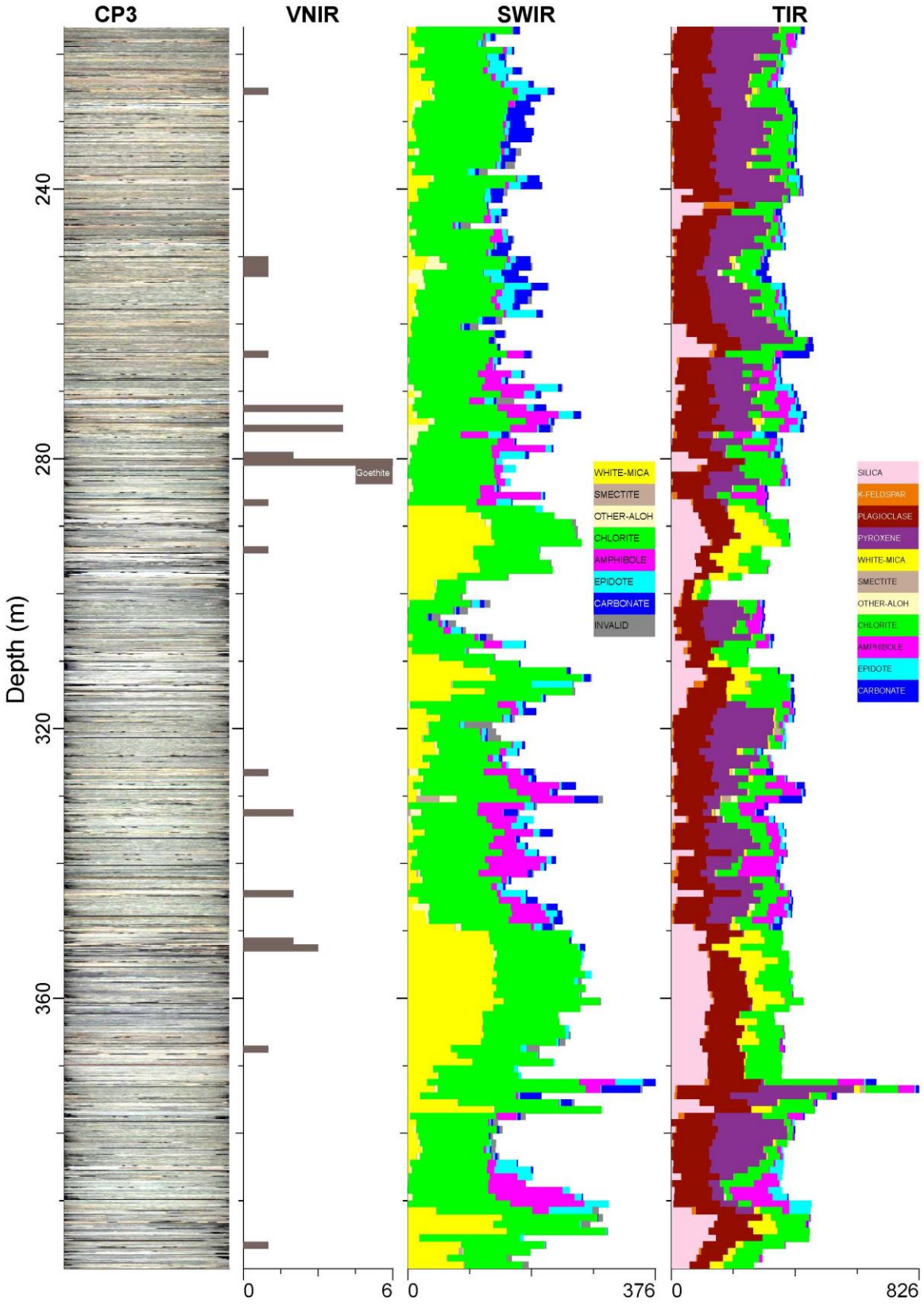

Figure 3 Downhole hylogger hyperspectral image of the hole CP3, Wahratta prospect, Loch Lilly-Kars Belt, New South Wales, Australia. Note the cover is to ~820m in this area.

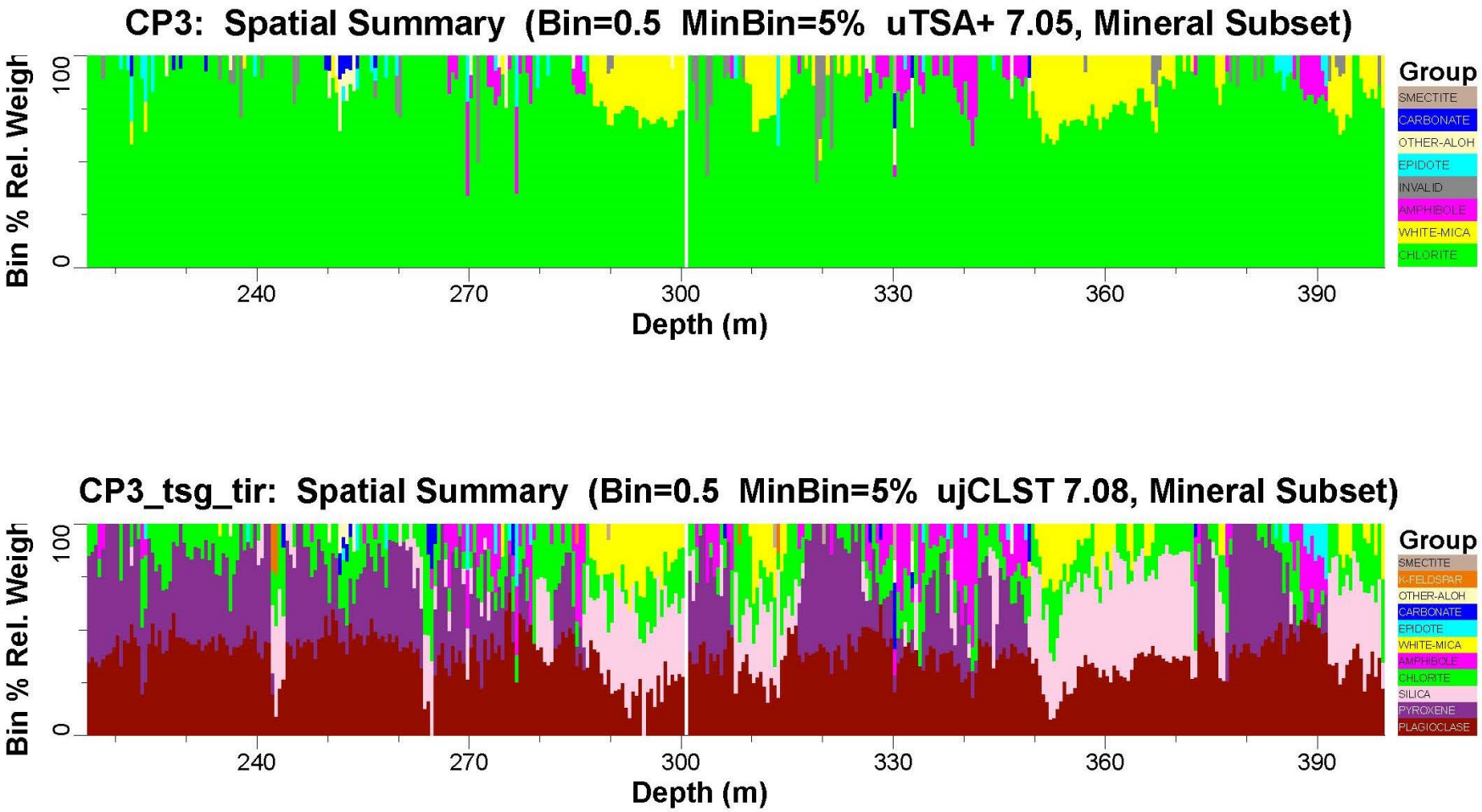

Figure 4 Summary of the hylogger hyperspectral image of the hole CP3, Wahratta prospect, Loch Lilly-Kars Belt, New South Wales, Australia. Note the cover is to ~820m in this area.

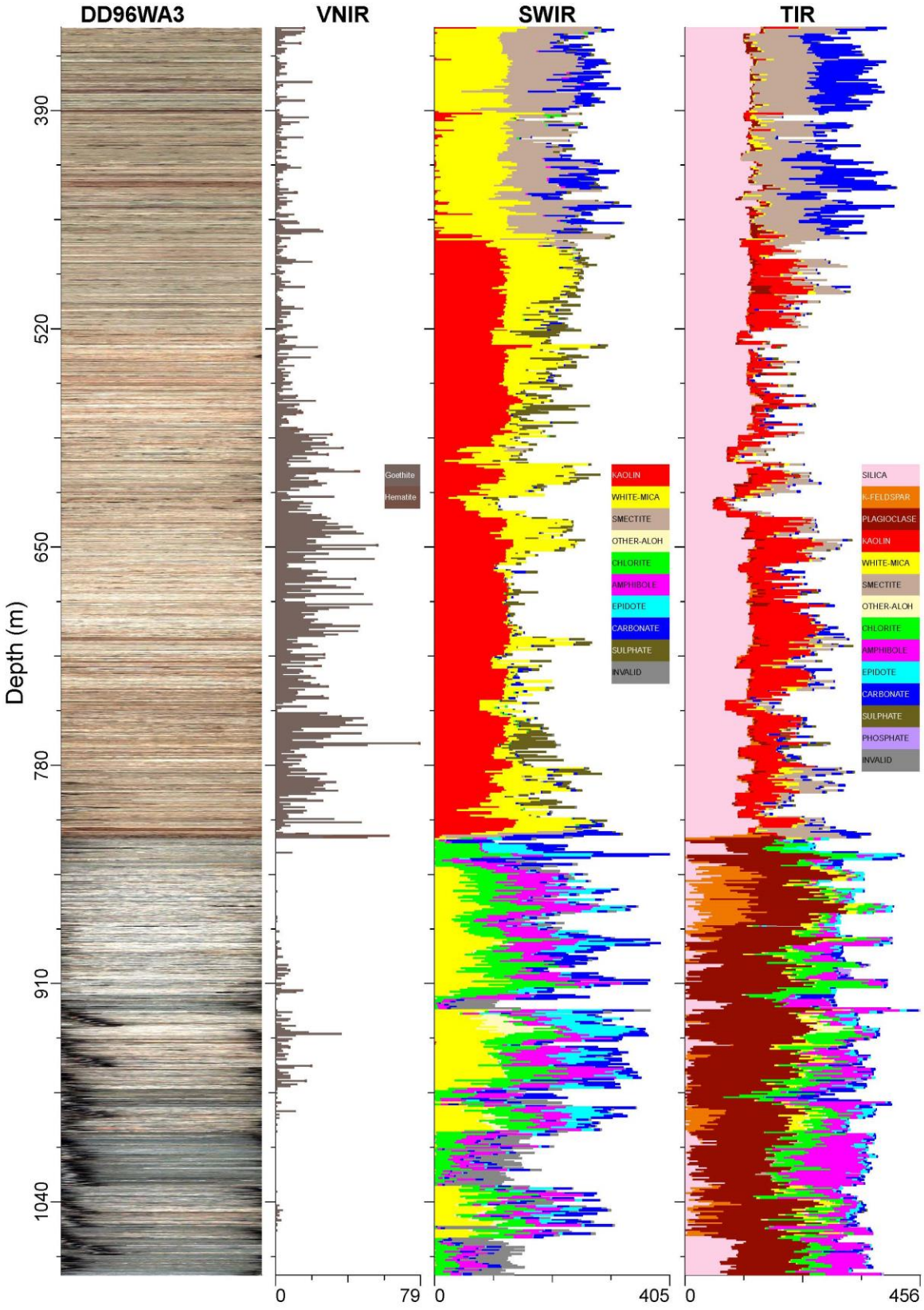

Figure 5 Downhole hylogger hyperspectral image of the hole DD96WA3, Wahratta prospect, Loch Lilly-Kars Belt, New South Wales, Australia. Note the cover is to ~820m in this area.

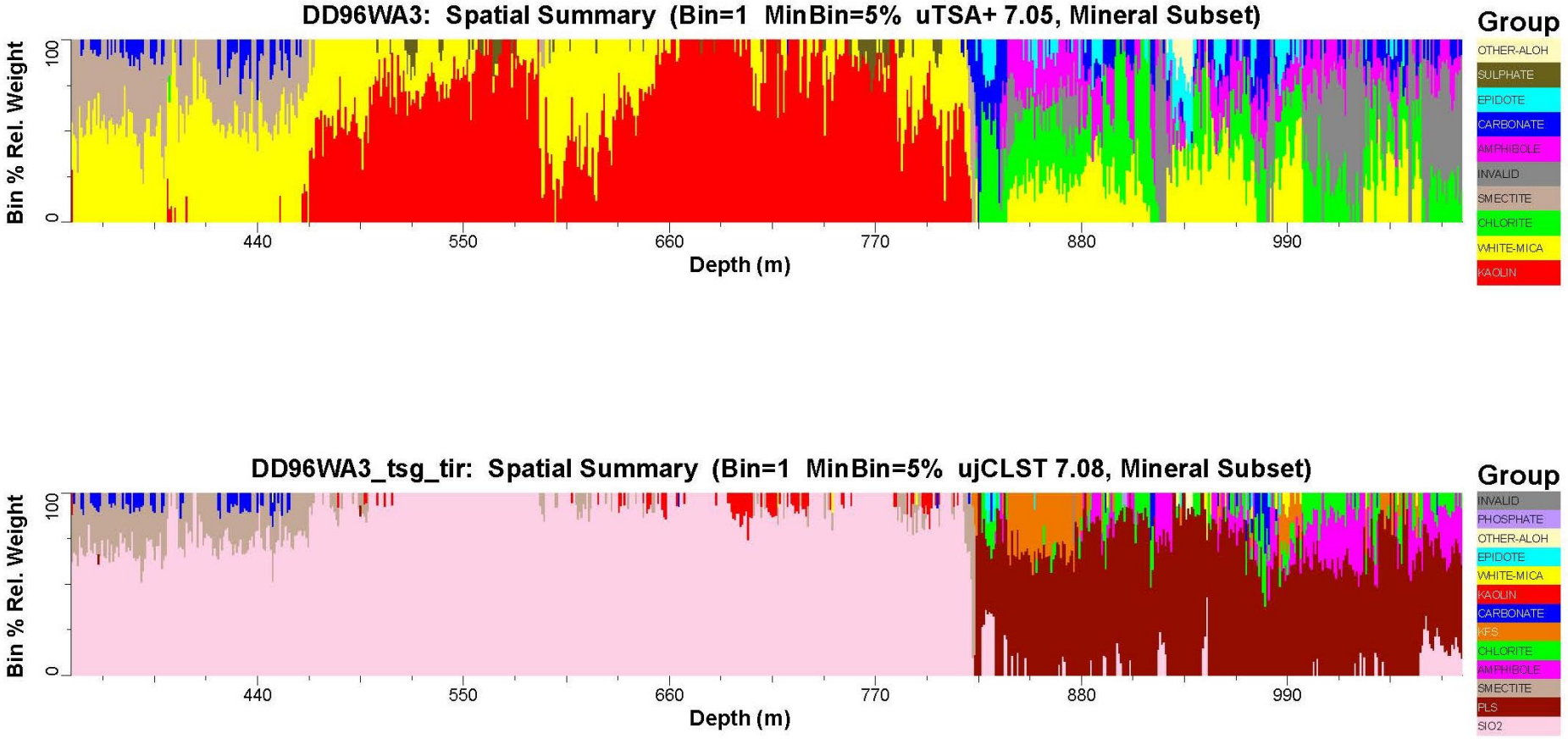

Figure 6 Summary of the hylogger hyperspectral image of the hole DD96WA3, Wahratta prospect, Loch Lilly-Kars Belt, New South Wales, Australia. Note the cover is to ~820m in this area.

Sample ID	Prospect	Borehole Name	From (m)	To (m)	Note
2022330070	Wahratta	DD96WA3	1052.75	1053.2	Sulfide ore and hydrothermal alteration

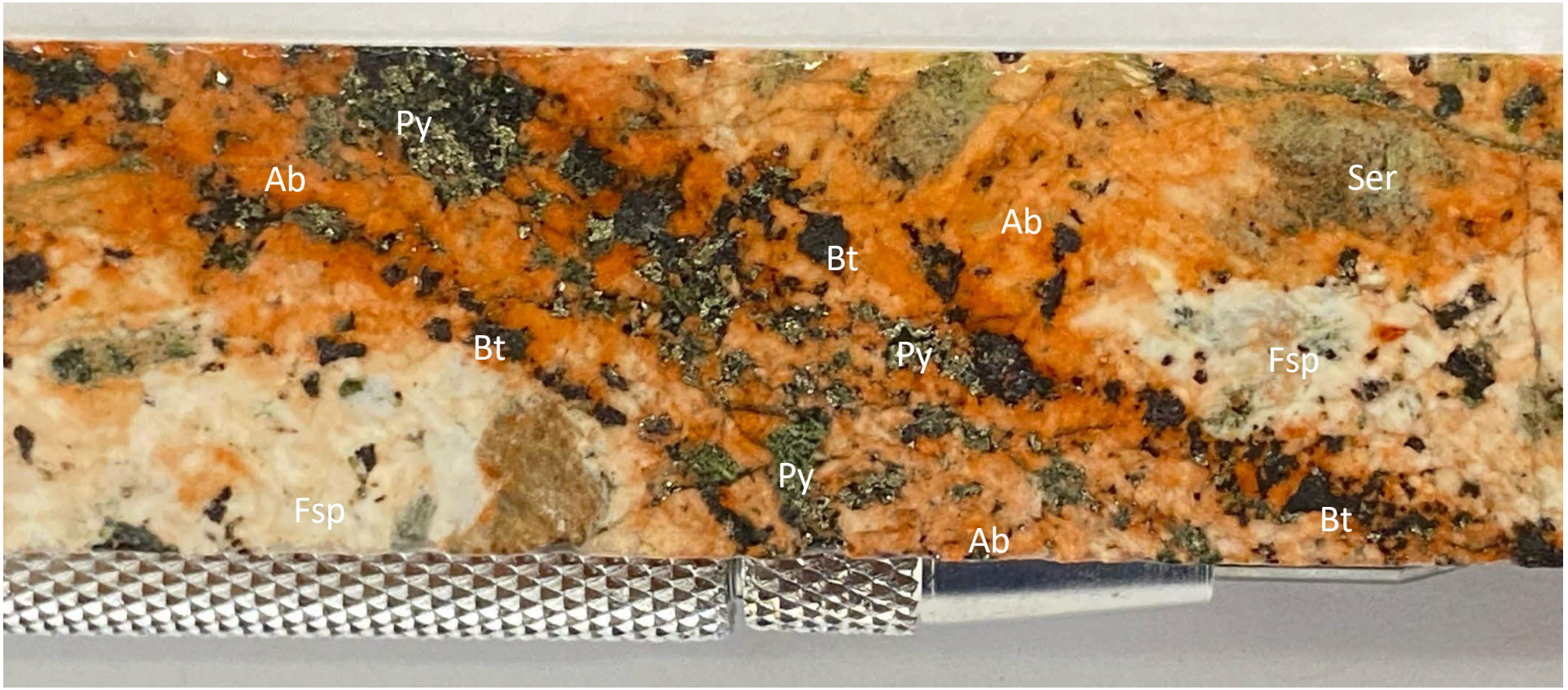

Figure 7 Photos of the drill core sample 2022330070 from drill hole DD96WA3 of the Wahratta prospect, Loch Lilly-Kars Belt, New South Wales, Australia. Py-pyrite; Bt-biotite; Fsp-feldspar; Ab-albite; Ser-sericite.

Sample ID	Prospect	Borehole Name	From (m)	To (m)	Note
2022330070	Wahratta	DD96WA3	1052.75	1053.2	Sulfide ore and hydrothermal alteration

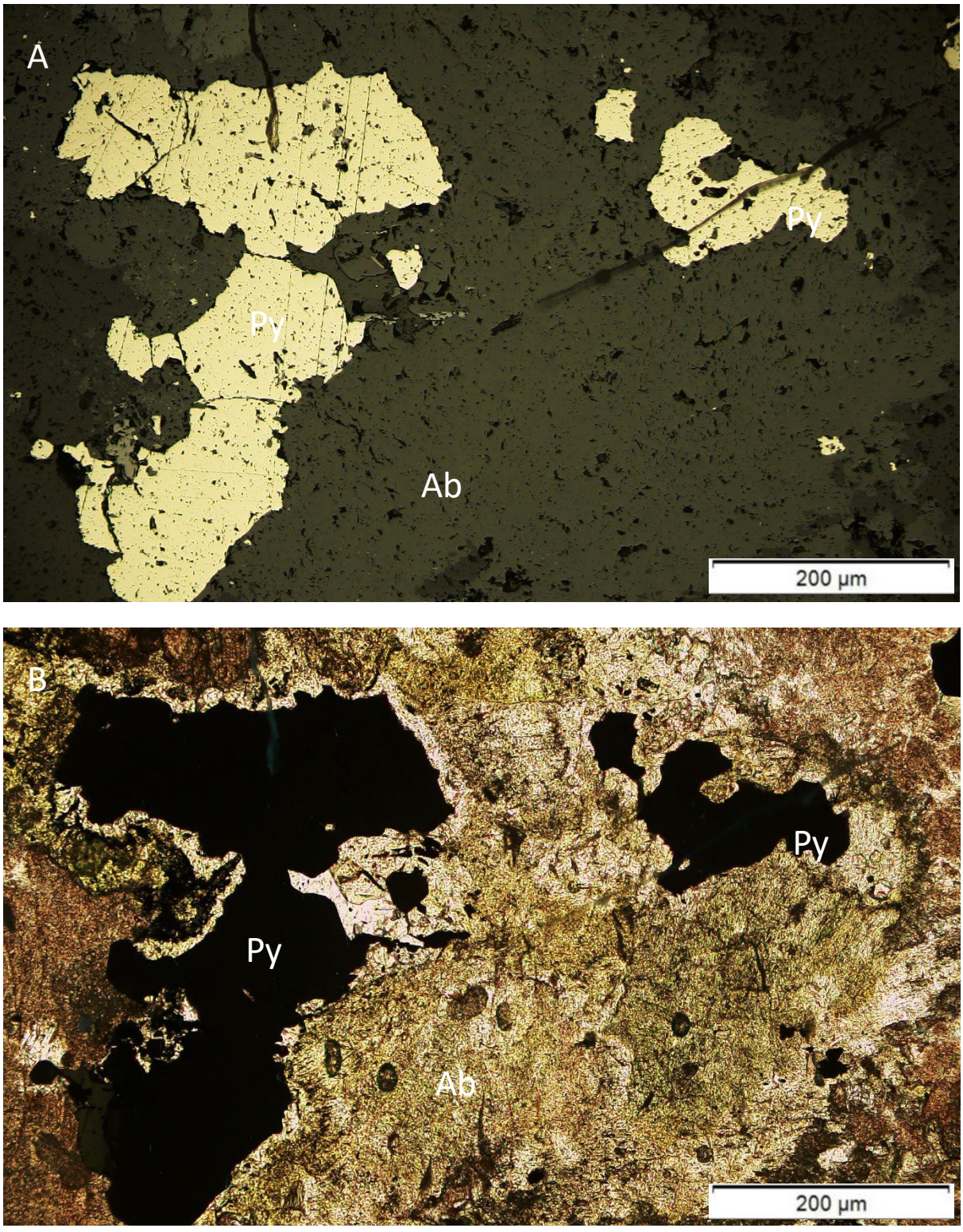

Figure 8 A: Reflective light photomicrograph of the sample 2022330070 from drill hole DD96WA3 of the Wahratta prospect, Loch Lilly-Kars Belt, New South Wales, Australia. B: Cross polarized light photomicrograph of A. Ab-albite; Py-pyrite.

Sample ID	Prospect	Borehole Name	From (m)	To (m)	Note
2022330070	Wahratta	DD96WA3	1052.75	1053.2	Sulfide ore and hydrothermal alteration

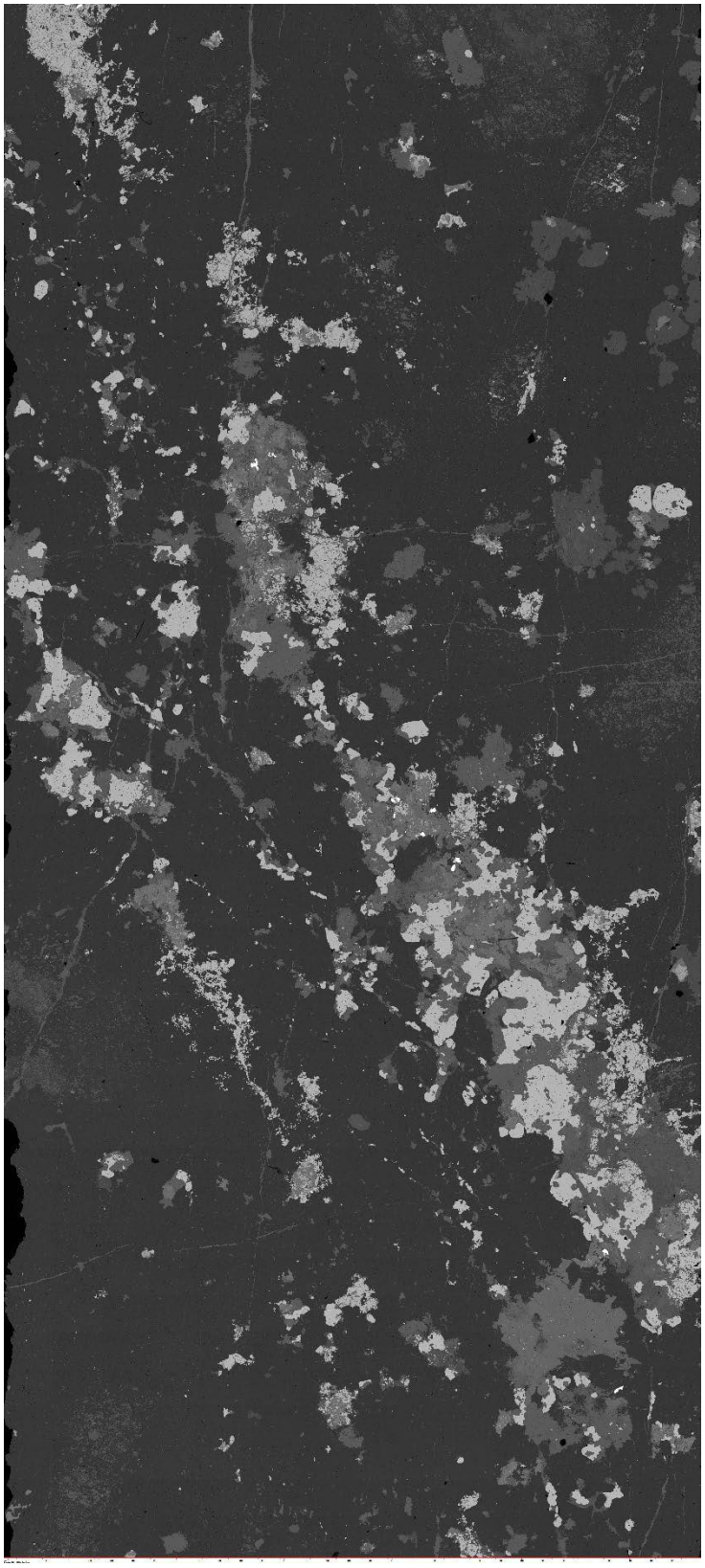

Figure 9 Backscattered electron (BSE) image of the sample 2022330070 from drill hole DD96WA3 of the Wahratta prospect, Loch Lilly-Kars Belt, New South Wales, Australia.

Sample ID	Prospect	Borehole Name	From (m)	To (m)	Note
2022330070	Wahratta	DD96WA3	1052.75	1053.2	Sulfide ore and hydrothermal alteration

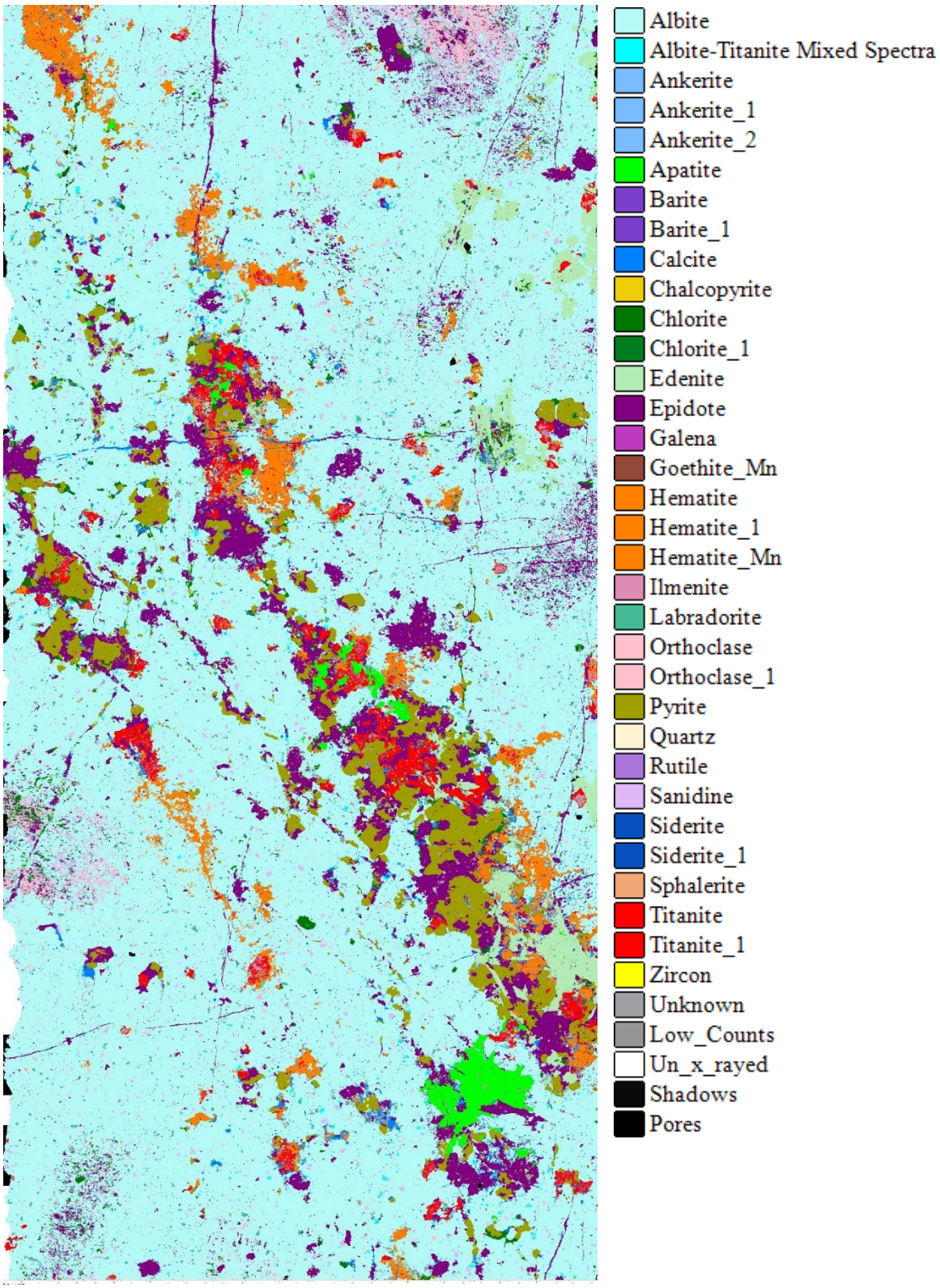

Figure 10 Mineral Liberation Analysis (MLA) mineral map of the sample 2022330070 from drill hole DD96WA3 of the Wahratta prospect, Loch Lilly-Kars Belt, New South Wales, Australia.

Sample ID	Prospect	Borehole Name	From (m)	To (m)	Note
2022330063	Wahratta	DD96WA3	842.25	842.35	Sulfide ore and hydrothermal alteration

Figure 11 Photos of the drill core sample 2022330063 from drill hole DD96WA3 of the Wahratta prospect, Loch Lilly-Kars Belt, New South Wales, Australia.

Sample ID	Prospect	Borehole Name	From (m)	To (m)	Note
2022330063	Wahratta	DD96WA3	842.25	842.35	Sulfide and hydrothermal alteration

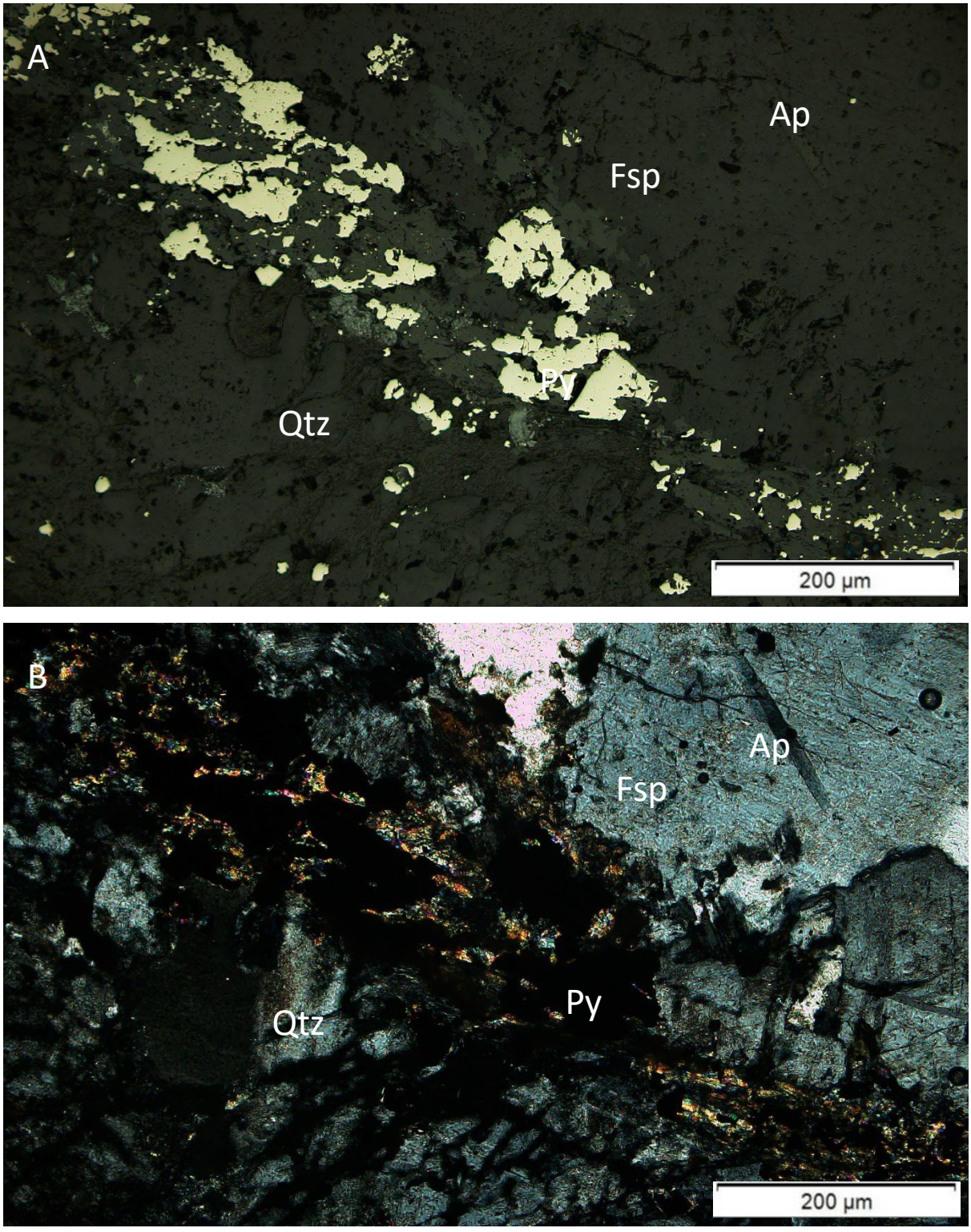

Figure 12 A: Reflective light photomicrograph of the sample 2022330063 from drill hole DD96WA3 of the Wahratta prospect, Loch Lilly-Kars Belt, New South Wales, Australia. B: Cross polarized light photomicrograph of A. Qtz-quartz; Py-pyrite; Fes-feldspar; Ap-apatite.

Sample ID	Prospect	Borehole Name	From (m)	To (m)	Note
2022330063	Wahratta	DD96WA3	842.25	842.35	Sulfide and hydrothermal alteration

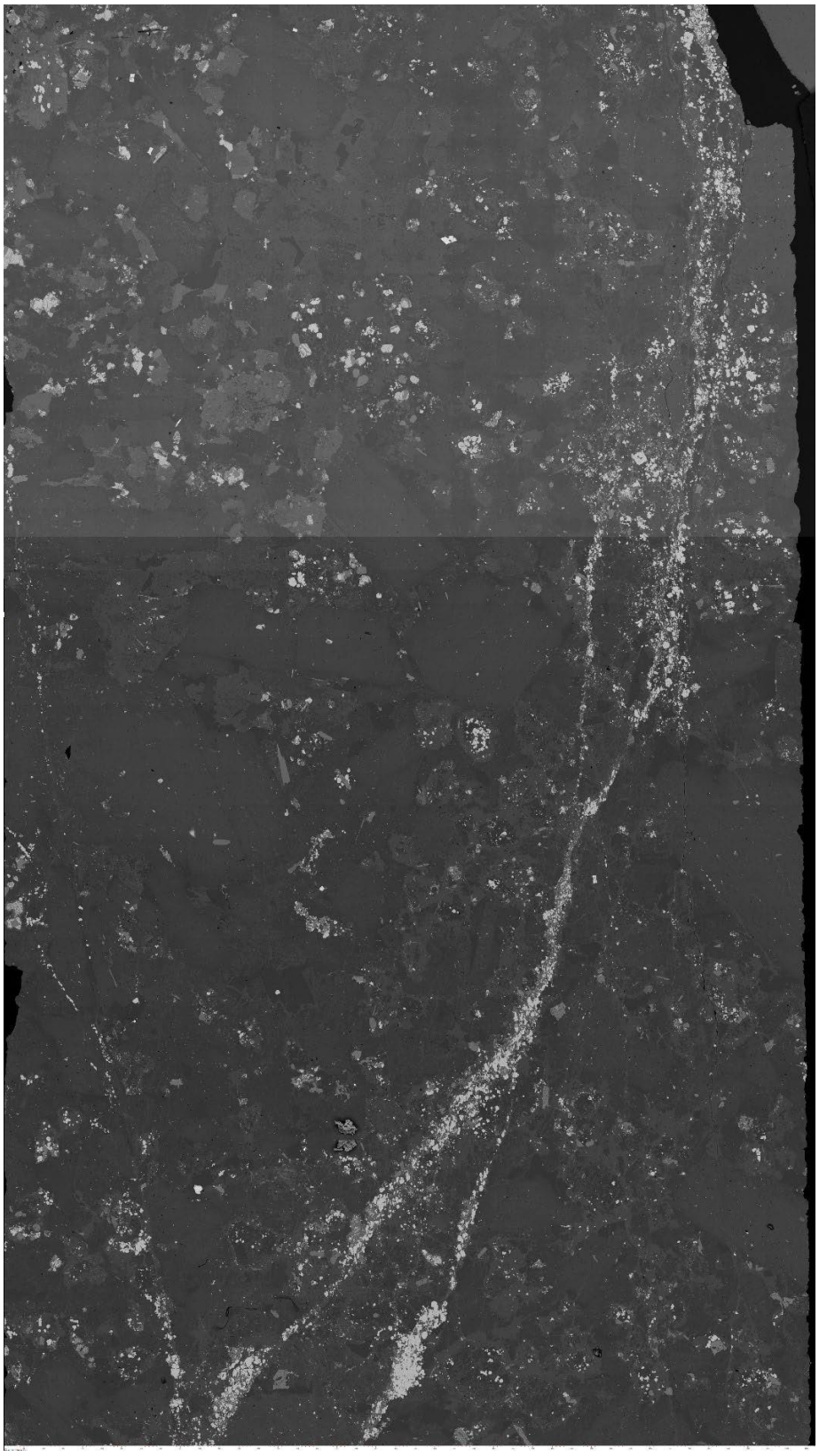

Figure 13 Backscattered electron (BSE) image of the sample 2022330063 from drill hole DD96WA3 of the Wahratta prospect, Loch Lilly-Kars Belt, New South Wales, Australia.

Sample ID	Prospect	Borehole Name	From (m)	To (m)	Note
2022330063	Wahratta	DD96WA3	842.25	842.35	Sulfide and hydrothermal alteration

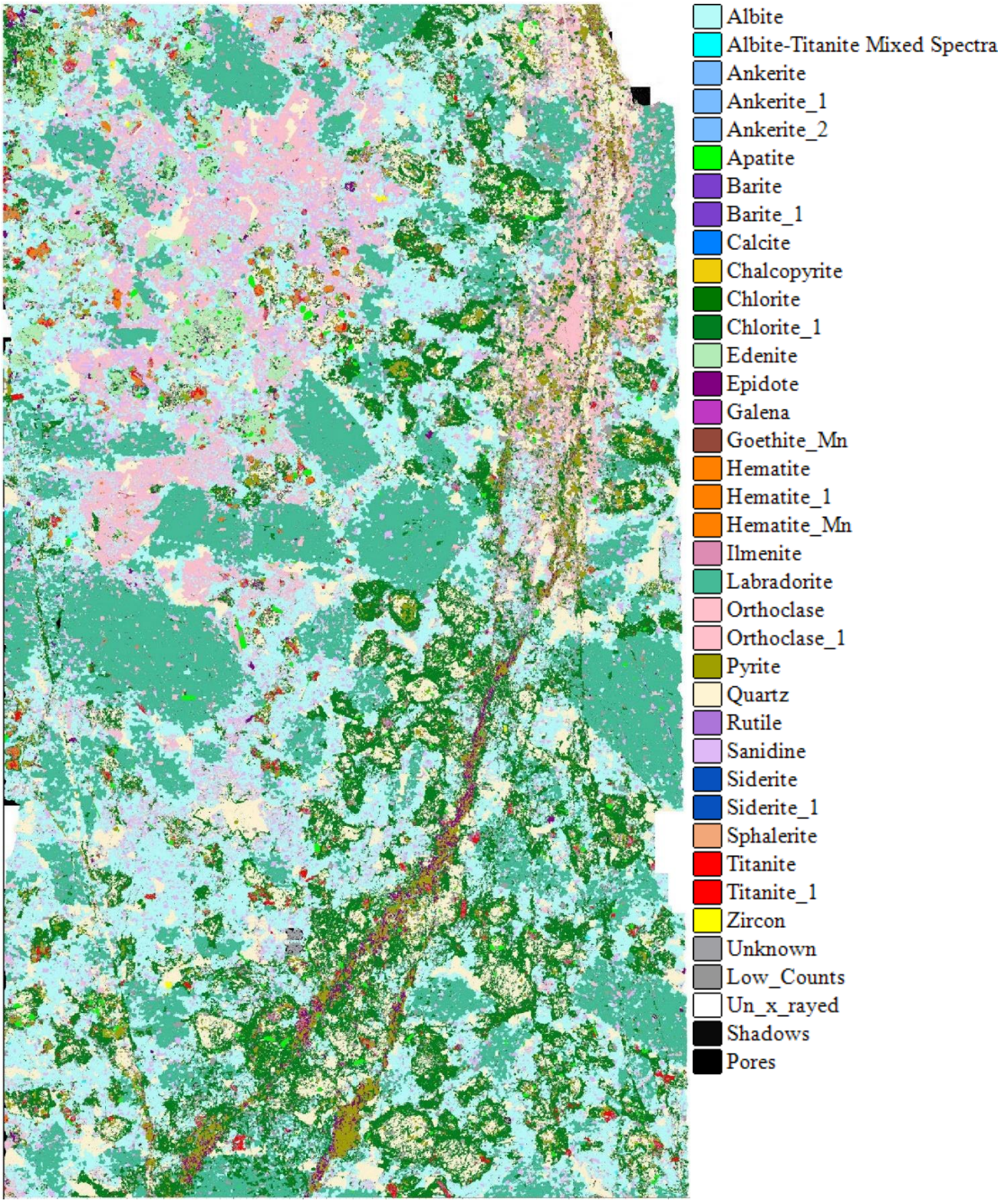

Figure 14 Mineral Liberation Analysis (MLA) mineral map of the sample 2022330063 from drill hole DD96WA3 of the Wahratta prospect, Loch Lilly-Kars Belt, New South Wales, Australia.

Sample ID	Prospect	Borehole Name	From (m)	To (m)	Note
2022330068	Wahratta	DD96WA3	947.8	948	Sulfide ore and hydrothermal alteration

Figure 15 Photos of the drill core sample 2022330068 from drill hole DD96WA3 of the Wahratta prospect, Loch Lilly-Kars Belt, New South Wales, Australia.

Sample ID	Prospect	Borehole Name	From (m)	To (m)	Note
2022330036	Wahratta	CP2	389.8	390	Sulfide ore and hydrothermal alteration

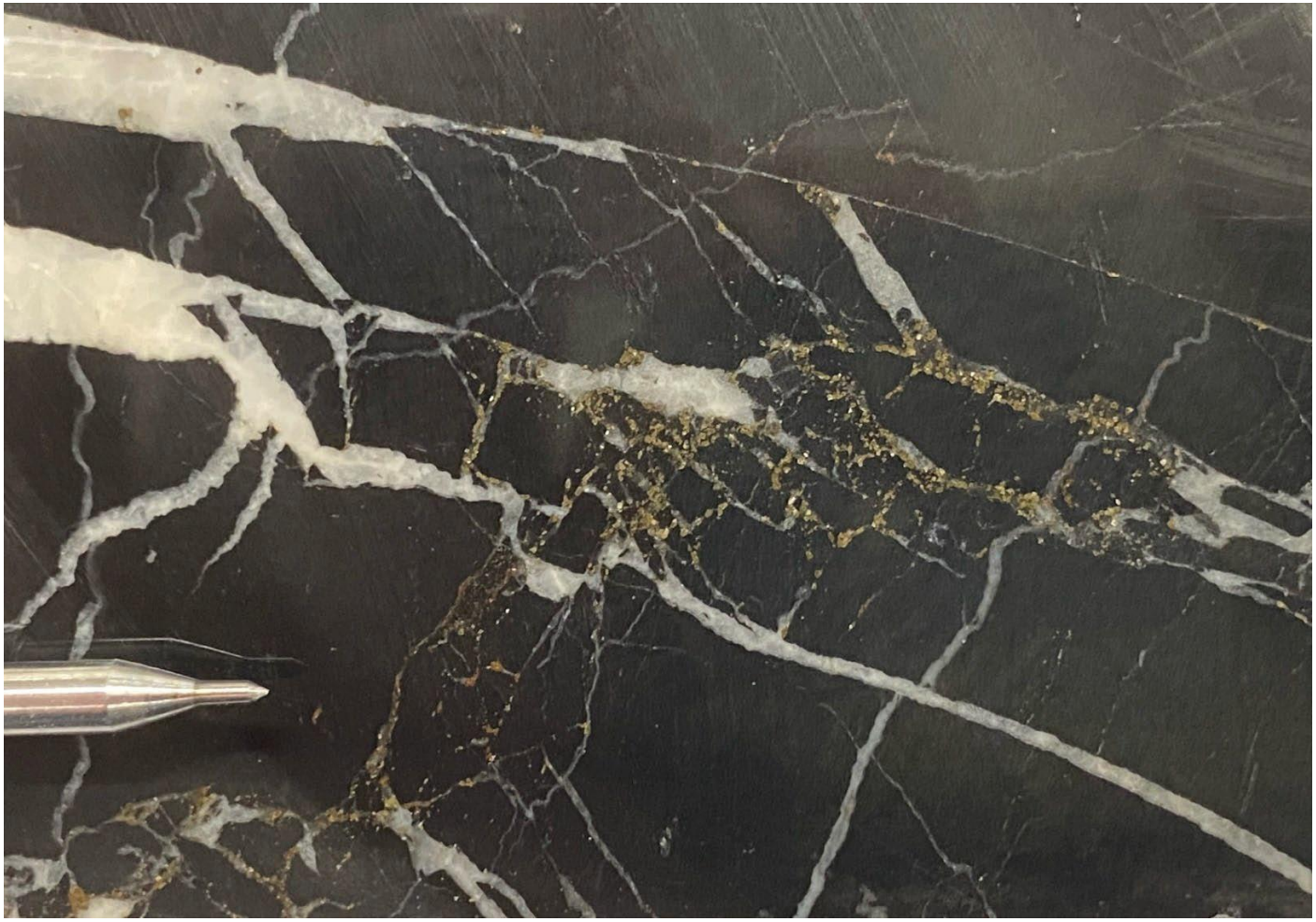

Figure 16 Photos of the drill core sample 2022330036 from drill hole CP2 of the Wahratta prospect, Loch Lilly-Kars Belt, New South Wales, Australia.

Sample ID	Prospect	Borehole Name	From (m)	To (m)	Note
2022330037	Wahratta	CP2	427.1	427.2	Sulfide ore and hydrothermal alteration

Figure 17 Photos of the drill core sample 2022330037 from drill hole CP2 of the Wahratta prospect, Loch Lilly-Kars Belt, New South Wales, Australia.

S1.4 Quondong prospect

Loch Lilly–Kars Belt, New South Wales

Detailed image data: Appendix 4 (individual data file)

(A) Sample List

Sample No.	Sample ID	Borehole	From (m)	To (m)	Notes
9651905	2022330093	NBH011	244.30	244.40	Sulfide ore and hydrothermal alteration
9651906	2022330094	NBH011	271.20	271.60	Sulfide ore and hydrothermal alteration

(B) Mineralisation Characteristics

Data Type	Mineral Assemblage
Hyperspectral SWIR	*Ms, Chl, Ep, Amp, Car*
Hyperspectral TIR	*Qtz, Kfsp, Pl, Px, Ms, Chl, Car, Amp, Ep*
Hyperspectral VNIR	*Gth*
Drill core specimen	*Kfsp, Ep, Py*
Thin section	*Mgt, Py, Ep*
AMICS mineral map	*Ab, Or, Py, Cpy, Chl, Cal, Ap, Ttn, Zrn*

(C) Mineralogical Textures and Paragenesis

Category	Description
Texture	The protolith of the wall rocks at Quondong is intermediate-to-mafic in composition.
Paragenesis	Three alteration generations are identified: (1) early K-feldspar–albite alteration; (2) albite-dominant vein emplacement; (3) late epidote veins. Pyrite is associated with the early K-feldspar–albite stage; chalcopyrite is confined to the latest epidote veins.

(D) Supplementary Figure Reference

Supplementary Figures *include (1) Downhole HyLogger hyperspectral image and summary of drill hole NBH011; and (2) Drill core photographs, reflected-light photomicrographs, BSE images and MLA mineral maps showing Kfsp–Ep–Py–Cpy alteration zoning, samples 2022330094 and 2022330093.*

S1.4 The Quondong prospect, Loch Lilly-Kars Belt, New South Wales

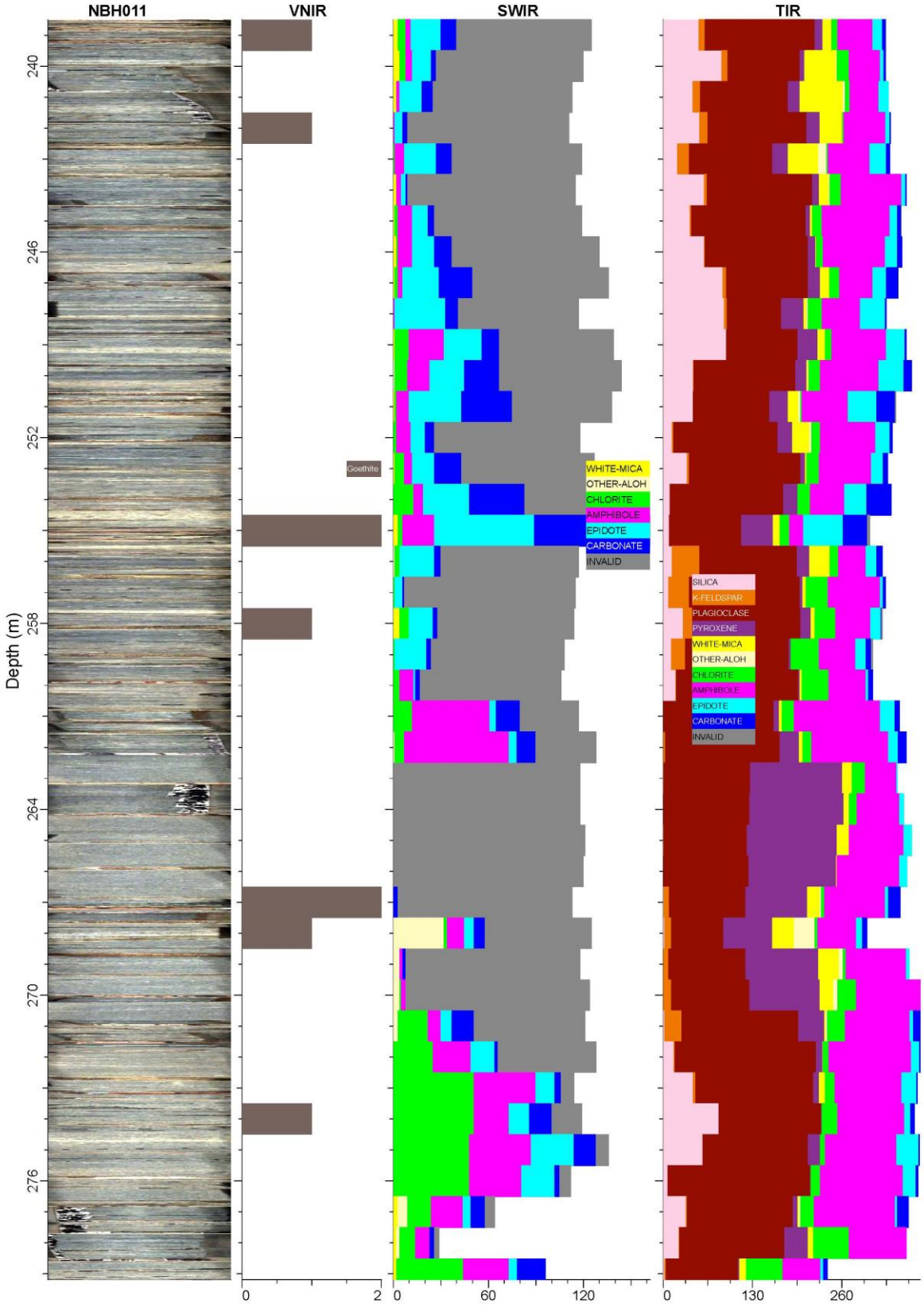

Figure 1 Downhole hylogger hyperspectral image of the hole NBH011 of the Quondong prospect, Loch Lilly-Kars Belt, New South Wales, Australia.

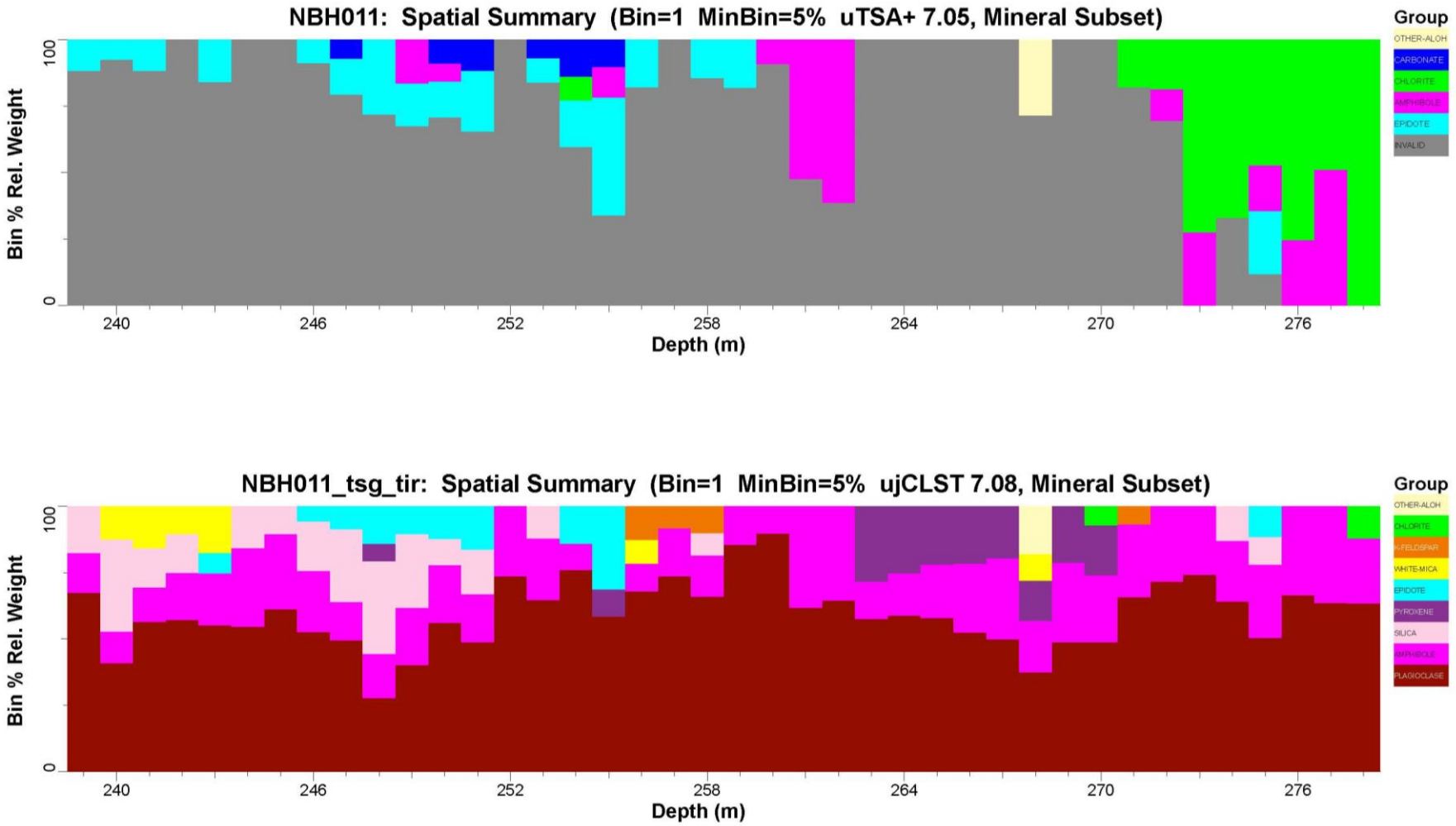

Figure 2 Summary of the hylogger hyperspectral image of the hole NBH011 of the Quondong prospect, Loch Lilly-Kars Belt, New South Wales, Australia.

Sample ID	Prospect	Borehole Name	From (m)	To (m)	Note
2022330094	Quondong	NBH011	271.2	271.6	Sulfide ore and hydrothermal alteration

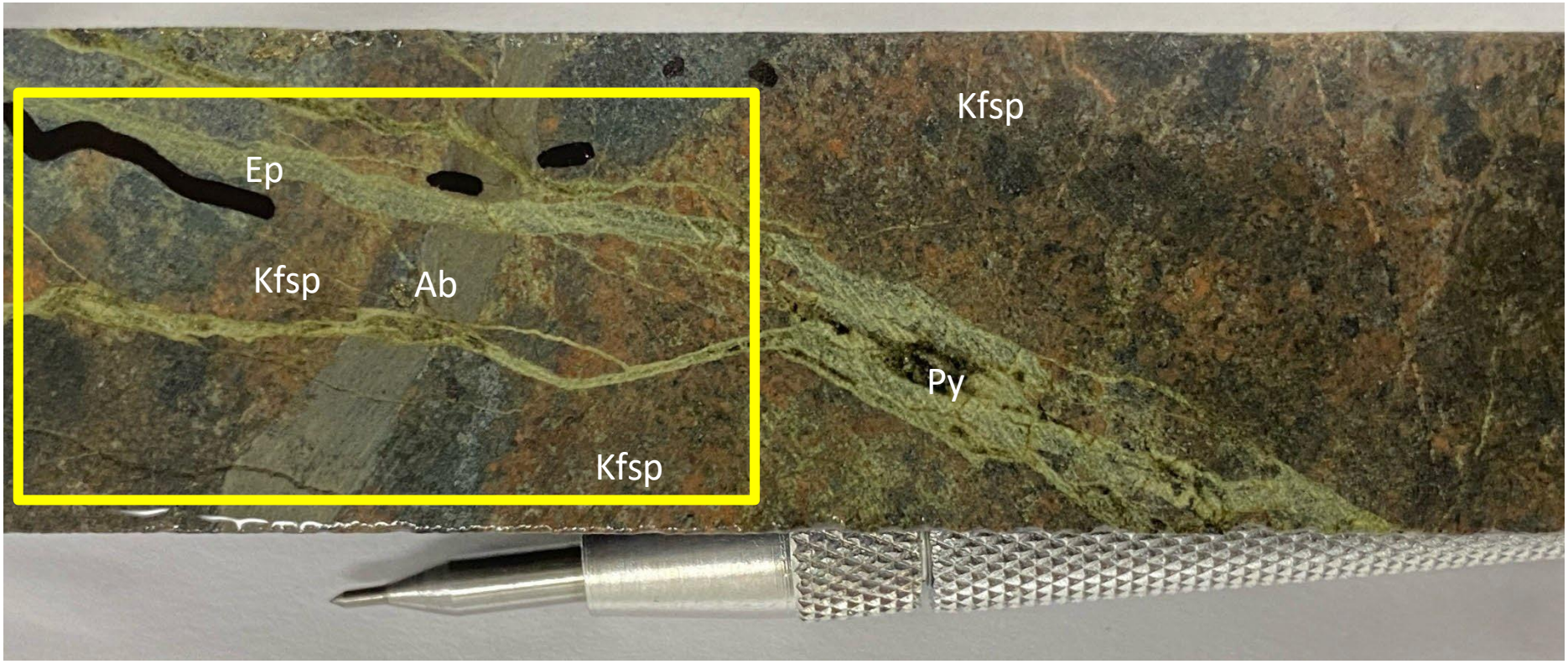

Figure 3 Photos of the drill core sample 2022330094 from drill hole NBH011 of the Quondong prospect, Loch Lilly-Kars Belt, New South Wales, Australia. Ep-epidote; Kfsp-K-felsdspar; Ab-albite; Py-pyrite.

Sample ID	Prospect	Borehole Name	From (m)	To (m)	Note
2022330094	Quondong	NBH011	271.2	271.6	2022330094

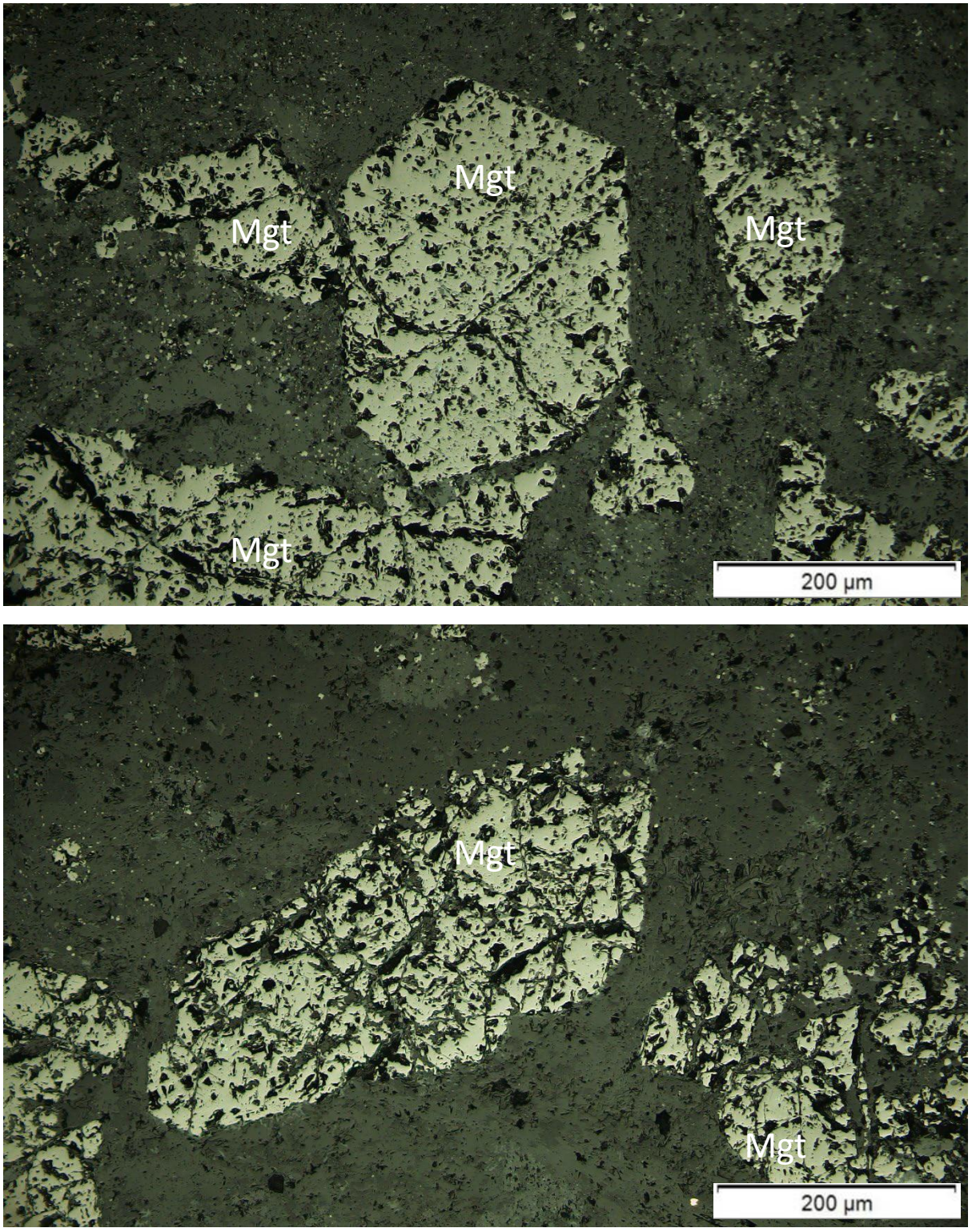

Figure 4 Reflective light photomicrograph of the sample 2022330094 from drill hole NBH011 of the Quondong prospect, Loch Lilly-Kars Belt, New South Wales, Australia. Mgt-magnetite.

Sample ID	Prospect	Borehole Name	From (m)	To (m)	Note
2022330094	Quondong	NBH011	271.2	271.6	2022330094

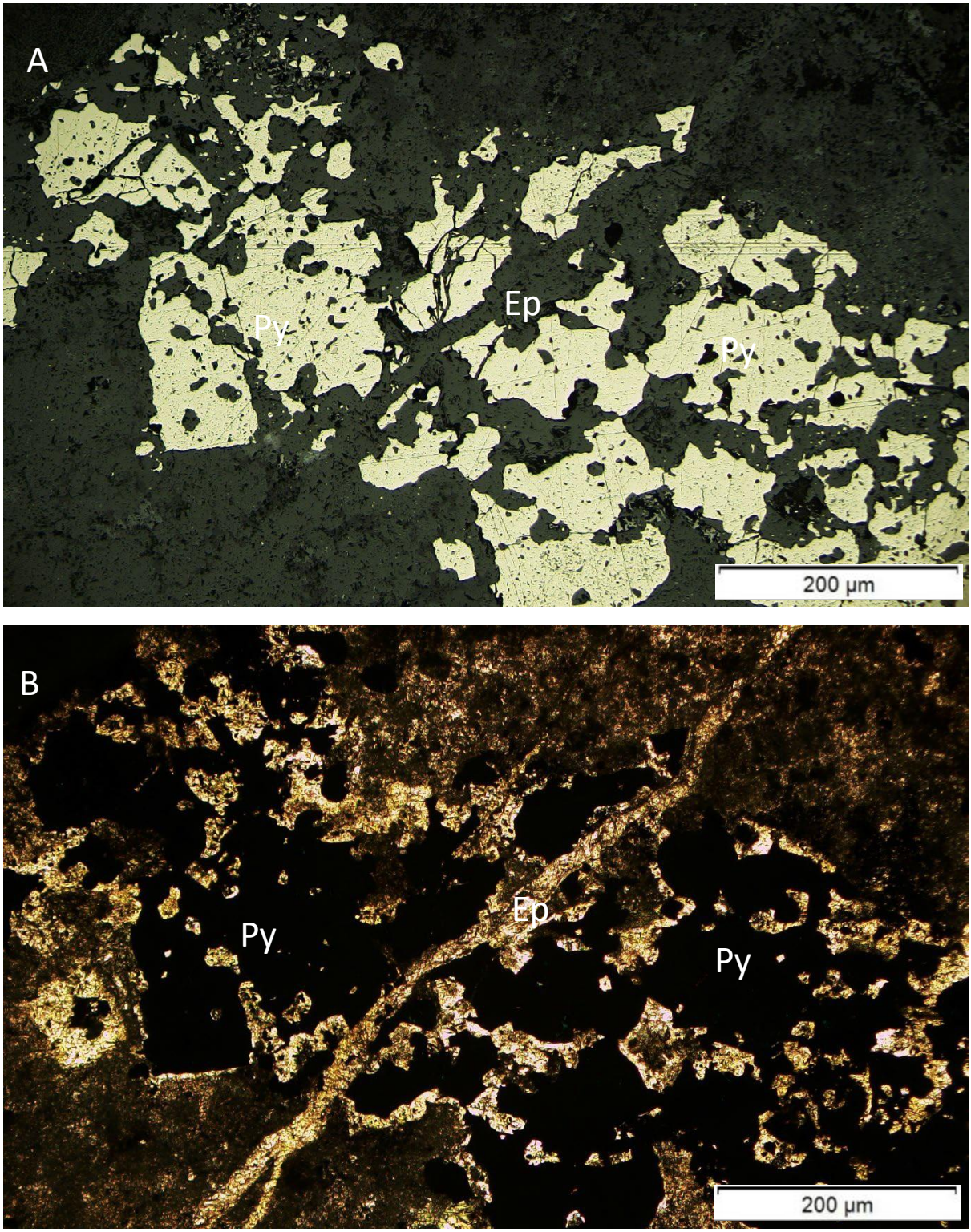

Figure 5 A: Reflective light photomicrograph of the sample 2022330094 from drill hole NBH011 of the Quondong prospect, Loch Lilly-Kars Belt, New South Wales, Australia. B: Plain light photomicrograph of A. Py-pyrite; Ep-epidote.

Sample ID	Prospect	Borehole Name	From (m)	To (m)	Note
2022330094	Quondong	NBH011	271.2	271.6	2022330094

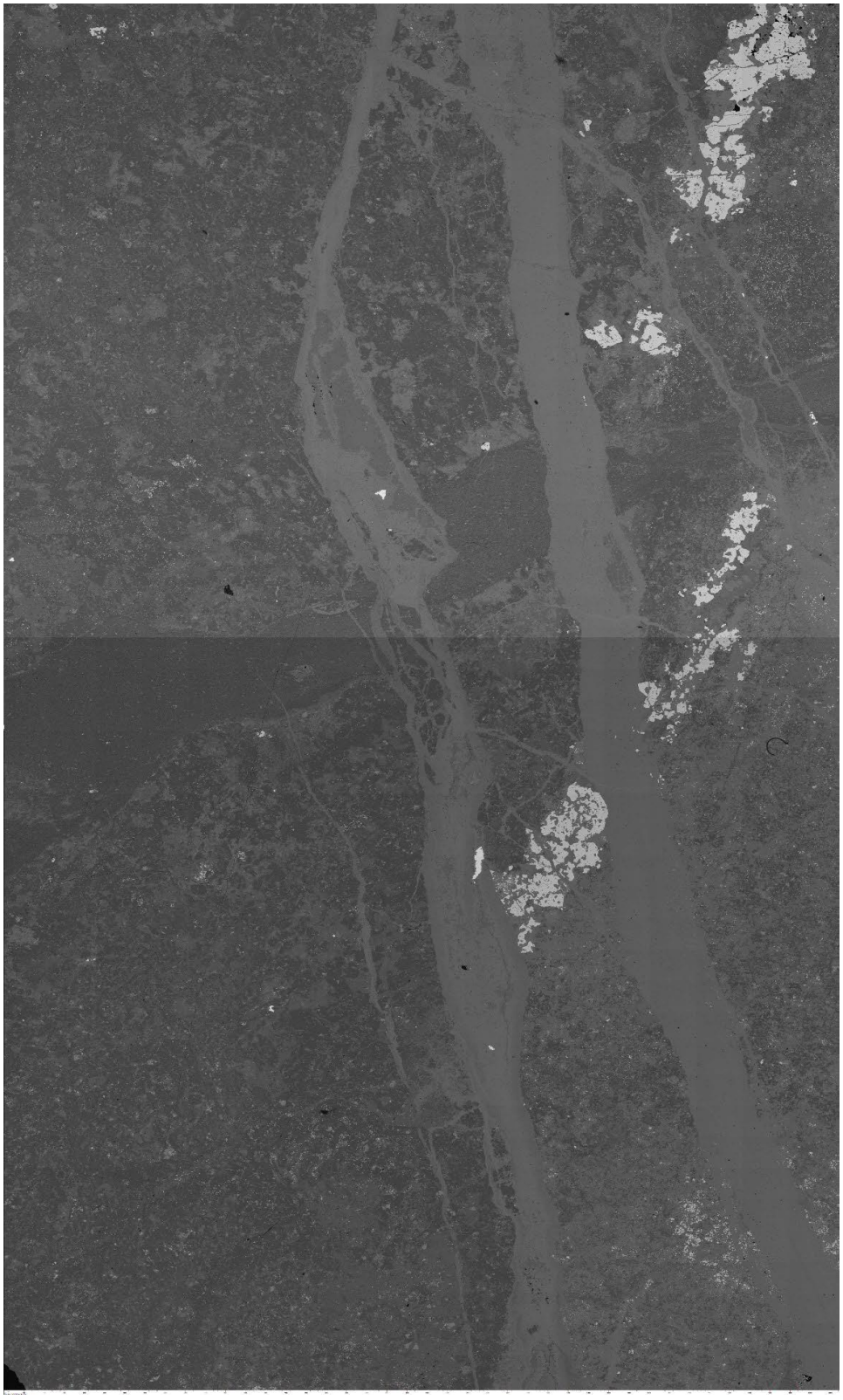

Figure 6 Backscattered electron (BSE) image of the sample 2022330094 from drill hole NBH011 of the Quondong prospect, Loch Lilly-Kars Belt, New South Wales, Australia.

Sample ID	Prospect	Borehole Name	From (m)	To (m)	Note
2022330094	Quondong	NBH011	271.2	271.6	2022330094

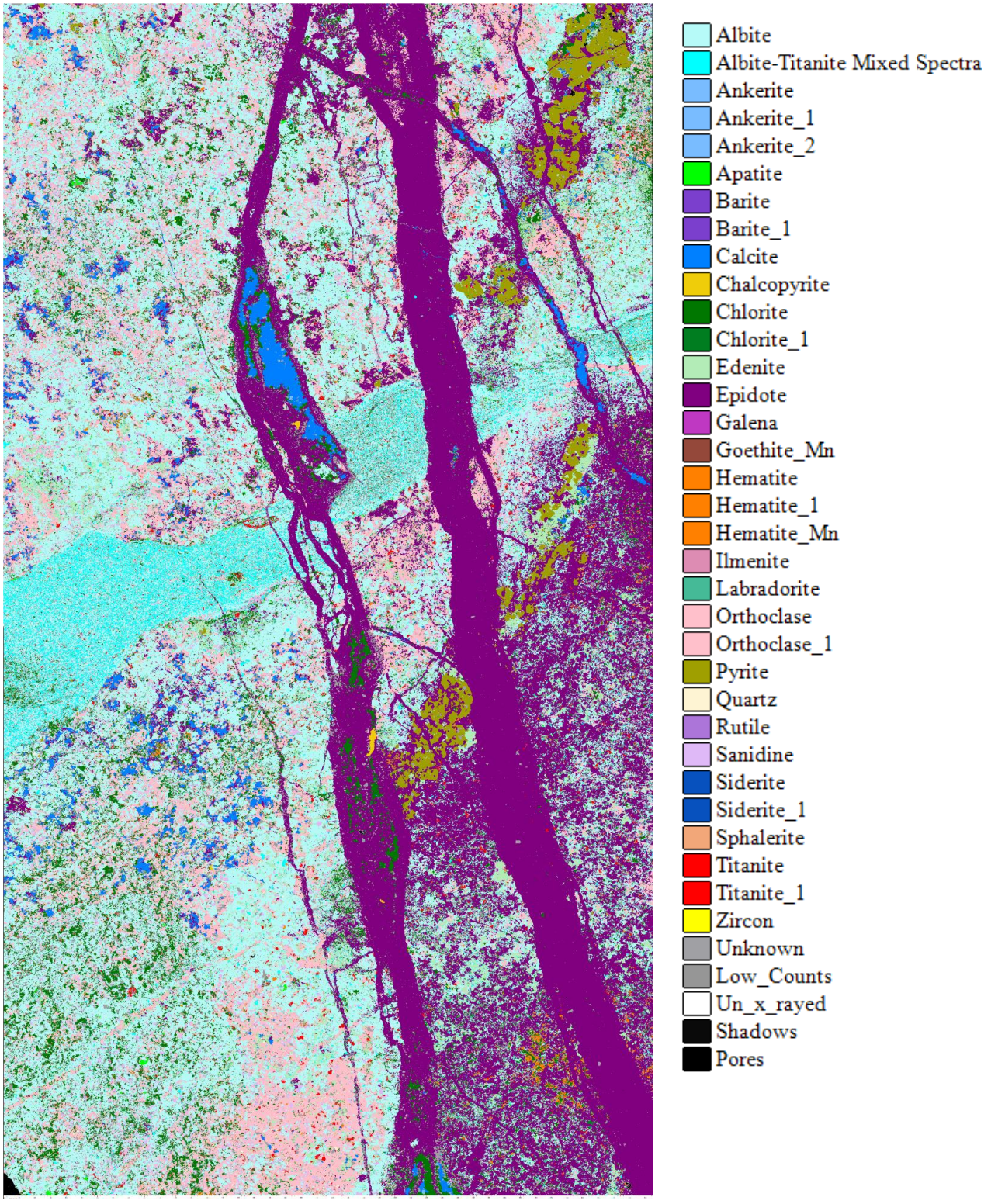

Figure 7 Mineral Liberation Analysis (MLA) mineral map of the sample 2022330094 from drill hole NBH011 of the Quondong prospect, Loch Lilly-Kars Belt, New South Wales, Australia.

Sample ID	Prospect	Borehole Name	From (m)	To (m)	Note
2022330093	Quondong	NBH011	244.3	244.4	Sulfide ore and hydrothermal alteration

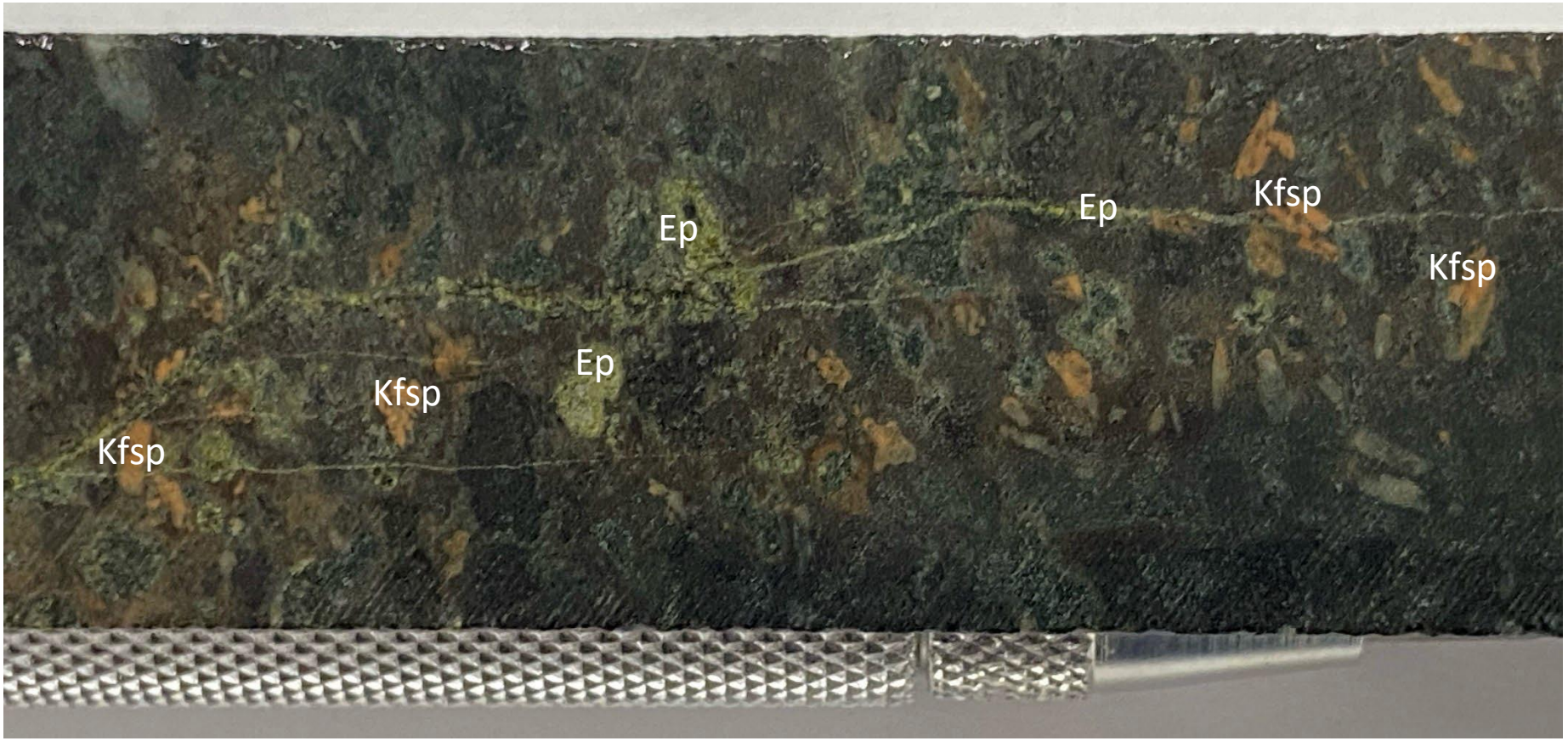

Figure 8 Photos of the drill core sample 2022330093 from drill hole NBH011 of the Quondong prospect, Loch Lilly-Kars Belt, New South Wales, Australia. Kfsp-K-feldspar; Ep-epidote.

S1.5 Follies Tank prospect

Loch Lilly–Kars Belt, New South Wales

Detailed image data: Appendix 5 (individual data file)

(A) Sample List

Sample No.	Sample ID	Borehole	From (m)	To (m)	Notes
8012540	2022440056	DD90DL20	109.60	109.70	Igneous rocks and hydrothermal alteration
8012535	2022440051	DD90DL19	137.20	137.40	Igneous rocks and hydrothermal alteration

(B) Mineralisation Characteristics

Data Type	Mineral Assemblage
Hyperspectral SWIR	—
Hyperspectral TIR	—
Hyperspectral VNIR	—
Drill core specimen	*Kfsp, Pl, Bt, Qtz, Chl, Py*
Thin section	—
AMICS mineral map	—

(C) Mineralogical Textures and Paragenesis

Category	Description
Texture	Data limited to drill core observation. No HyLogger hyperspectral data or thin section petrography available.
Paragenesis	Pyrite is associated with biotite–chlorite–sericite veins within igneous host rocks.

(D) Supplementary Figure Reference

Supplementary Figures *include Drill core photographs of igneous host rocks with Kfsp–Bt–Qtz–Chl–Py assemblages, samples 2022440051 (DD90DL19) and 2022440056 (DD90DL20).*

S1.5 The Follies Tank prospect, Loch Lilly-Kars Belt, New South Wales

Sample ID	Prospect	Borehole Name	From (m)	To (m)	Note
2022440051	Follies Tank	DD90DL19	137.2	137.4	Igneous rocks and hydrothermal alteration

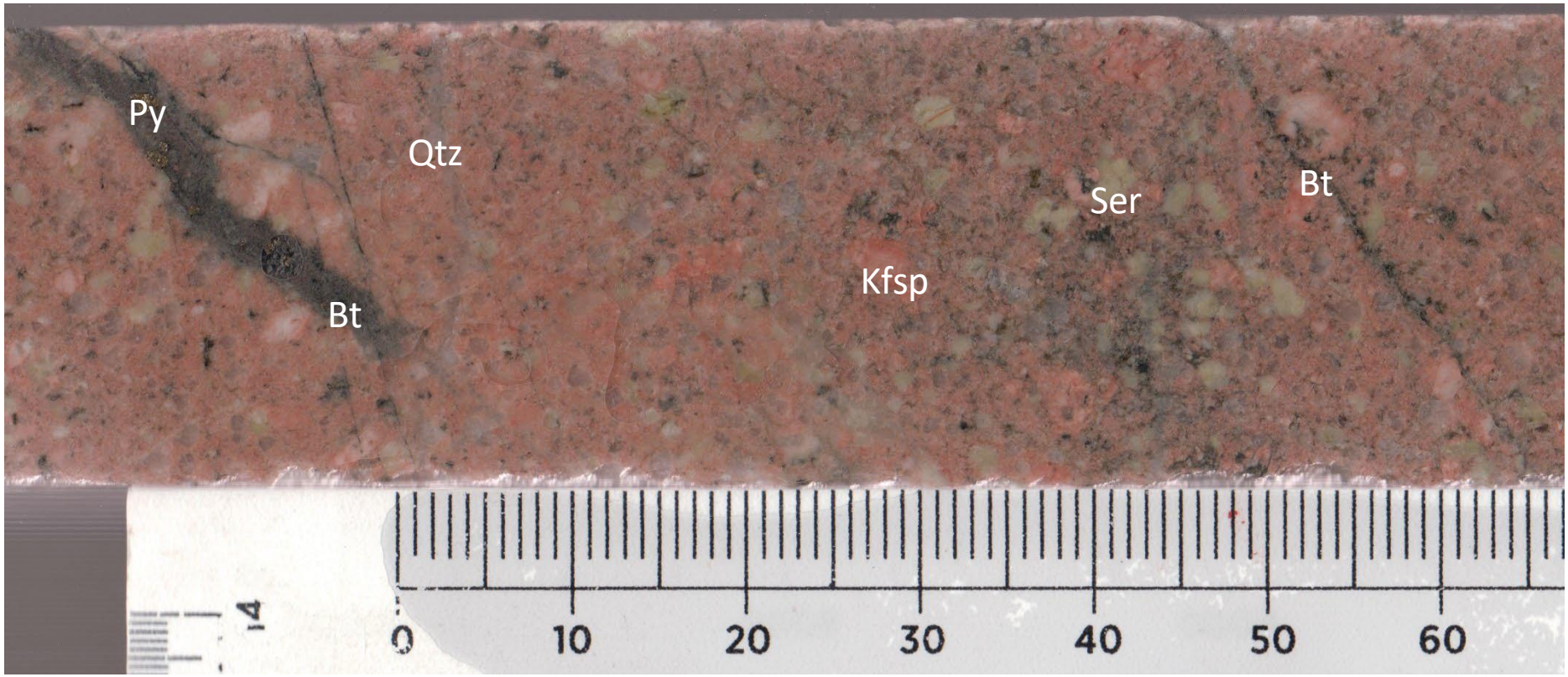

Figure 1 Photos of the drill core sample 2022440051 from drill hole DD90DL19 of the Follies Tank prospect, Loch Lilly-Kars Belt, New South Wales, Australia. Py-pyrite; Bt-biotite; Qtz-quartz; Ser-sericite; Kfsp-K-feldspar.

Sample ID	Prospect	Borehole Name	From (m)	To (m)	Note
2022440056	Follies Tank	DD90DL20	109.6	109.7	Igneous rocks and hydrothermal alteration

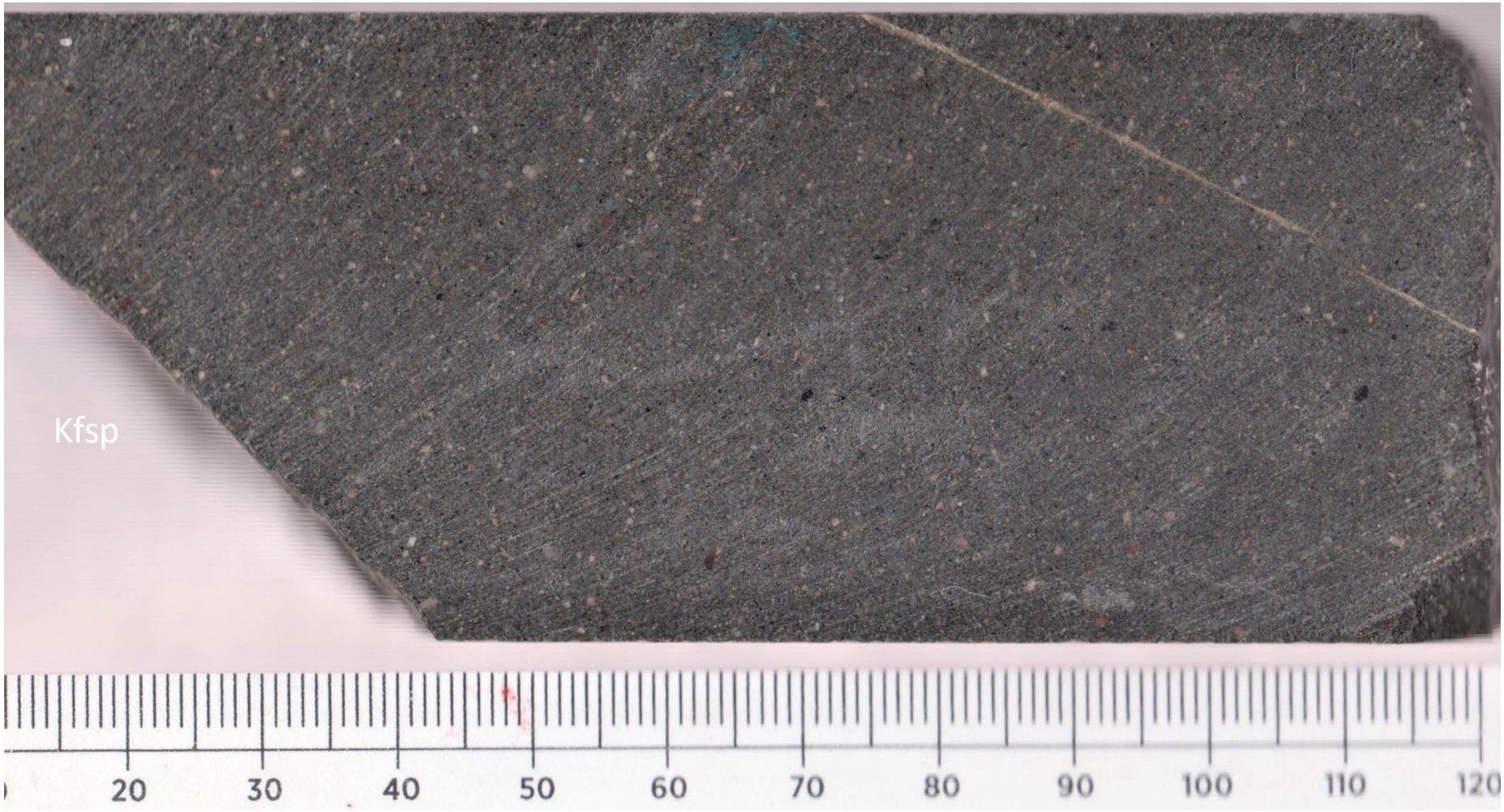

Figure 2 Photos of the drill core sample 2022440056 from drill hole DD90DL20 of the Follies Tank prospect, Loch Lilly-Kars Belt, New South Wales, Australia.

S2.1 Grasmere prospect

Koonenberry Belt, New South Wales

(A) Sample List

Sample No.	Sample ID	Borehole	From (m)	To (m)	Notes
8012463	2022440108	ADD-1	71.50	71.65	Massive sulfide ore
8012466	2022440111	ADD-1	82.90	83.05	Massive sulfide ore
8012469	2022440114	ADD-1	236.60	236.80	Massive sulfide ore
8012470	2022440115	ADD-1	252.77	253.00	Massive sulfide ore
8012471	2022440116	ADD-1	254.09	254.26	Massive sulfide ore
8012472	2022440117	ADD-1	254.76	254.86	Massive sulfide ore
8012473	2022440118	ADD-1	254.86	255.00	Massive sulfide ore
8012474	2022440119	ADD-1	257.11	257.30	Massive sulfide ore
8012476	2022440121	ADD-2	158.20	158.32	Massive sulfide ore
8012477	2022440122	ADD-2	159.15	159.35	Massive sulfide ore
8012514	2022440066	DD88GR01	68.98	69.15	Massive sulfide ore
8012515	2022440067	DD88GR01	70.09	70.29	Massive sulfide ore
8012516	2022440068	DD88GR01	70.96	71.15	Massive sulfide ore
8012517	2022440069	DD88GR01	71.90	72.00	Massive sulfide ore
8012518	2022440070	DD88GR01	91.25	91.31	Massive sulfide ore
8012519	2022440071	DD88GR01	101.51	101.67	Massive sulfide ore
8012522	2022440074	DD88GR01	128.09	128.26	Massive sulfide ore
8012523	2022440075	DD89GR05	121.00	121.10	Massive sulfide ore
8012524	2022440076	DD89GR05	122.60	122.75	Massive sulfide ore
8012525	2022440077	DD89GR05	125.05	125.17	Massive sulfide ore
8012526	2022440078	DD89GR05	125.45	125.50	Massive sulfide ore
8012527	2022440079	DD89GR05	127.30	127.45	Massive sulfide ore
8012528	2022440080	DD89GR05	128.20	128.30	Massive sulfide ore
8012529	2022440081	DD89GR05	129.40	129.45	Massive sulfide ore
8012541	2022440082	DD90GR07	211.80	211.90	Massive sulfide ore

Sample No.	Sample ID	Borehole	From (m)	To (m)	Notes
8012543	2022440084	DD90GR07	219.35	219.45	Massive sulfide ore
8012545	2022440086	DD90GR07	228.90	229.00	Massive sulfide ore

(B) Mineralisation Characteristics

Data Type	Mineral Assemblage
Hyperspectral SWIR	*Ms, Sme, Chl, Amp, Ep, Car, Tur, sulfate*
Hyperspectral TIR	*Qtz, Kfsp, Pl, Kln, Ms, Sme, Chl, Amp, Ep, Car, sulfate*
Hyperspectral VNIR	*Gth, Hem*
Drill core specimen	*Chl, Py, Cpy, Qtz, Cal, Ep*
Thin section	*N/A*
AMICS mineral map	*Qtz, Py, Chl, Ap, Cpy, Sph, Ank, Cal, Hem, Bt, Sid*

(C) Mineralogical Textures and Paragenesis

Category	Description
Texture	Massive sulfide ore with chlorite–epidote–quartz gangue. Tourmaline is present in the SWIR hyperspectral data.
Paragenesis	Chlorite–epidote–quartz–calcite forms the alteration assemblage. Pyrite predates chalcopyrite. Sphalerite and ankerite represent a late-stage hydrothermal overprint.

(D) Supplementary Figure Reference

Supplementary Figures *include HyLogger hyperspectral images of drill holes ADD-1, ADD-2, DD88GR01, DD89GR05 and DD90GR07; drill core photographs and AMICS mineral maps of massive sulfide ore (Py–Cpy–Sph assemblage).*

S2.1 The Grasmere prospect, Koonenberry Belt, New South Wales

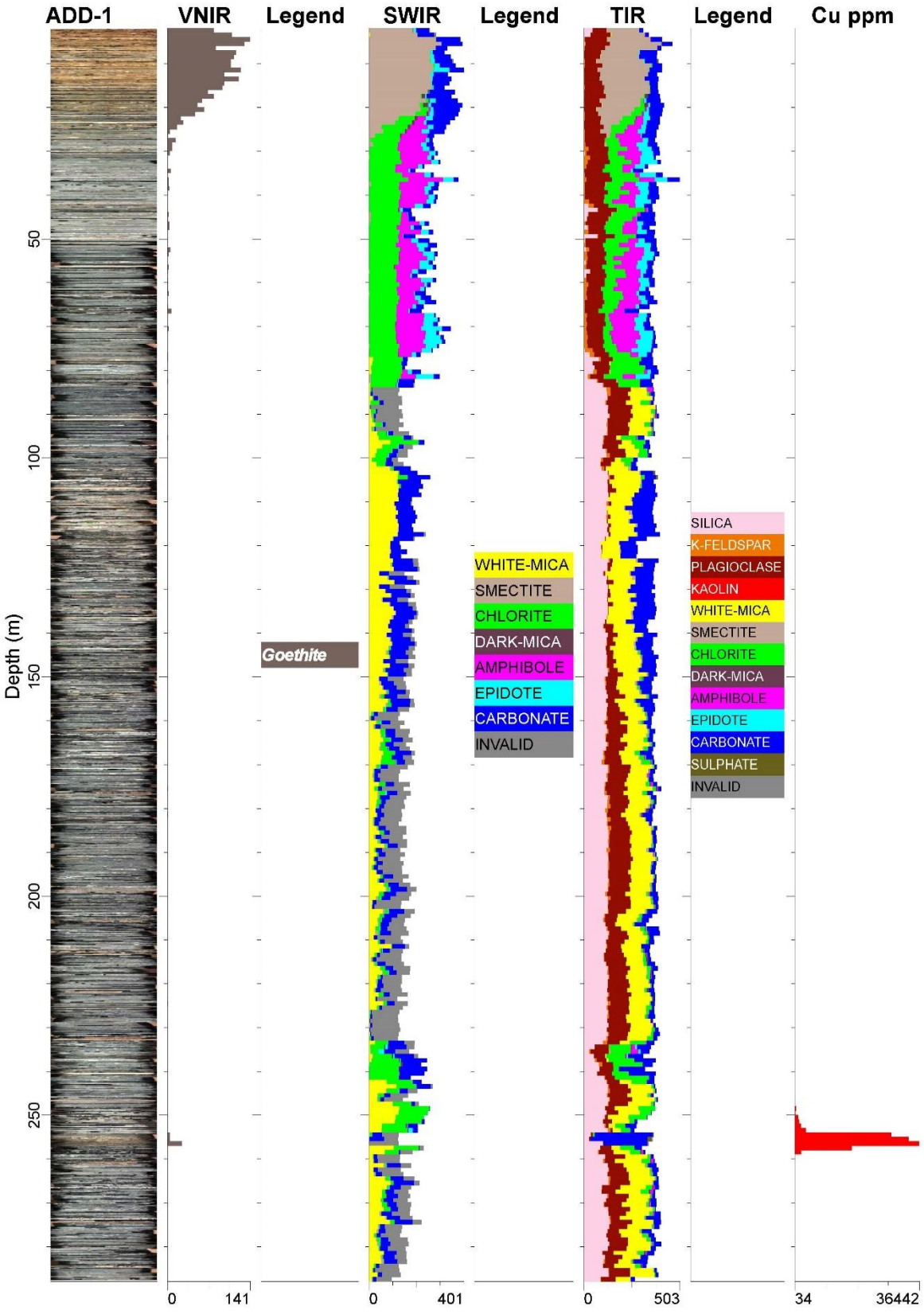

Figure 1 Downhole hylogger hyperspectral image of the hole ADD-1, Grasmere prospect, Koonenberry Belt, New South Wales, Australia. Cu content is up to ~3.6 wt. % at 250-260m depth.

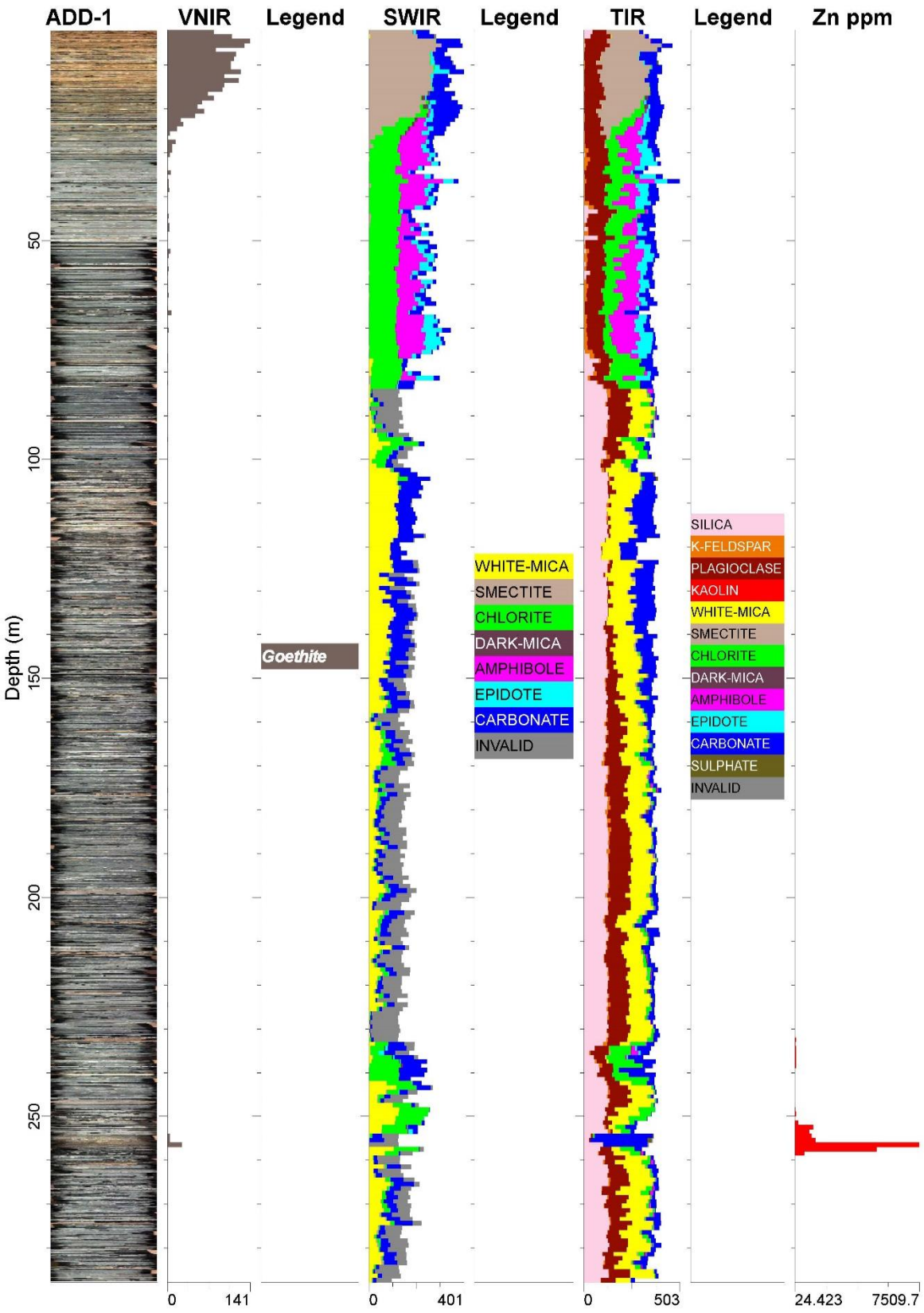

Figure 2 Downhole hylogger hyperspectral image of the hole ADD-1, Grasmere prospect, Koonenberry Belt, New South Wales, Australia. Zn content is up to ~0.75 wt. % at 250-260m depth.

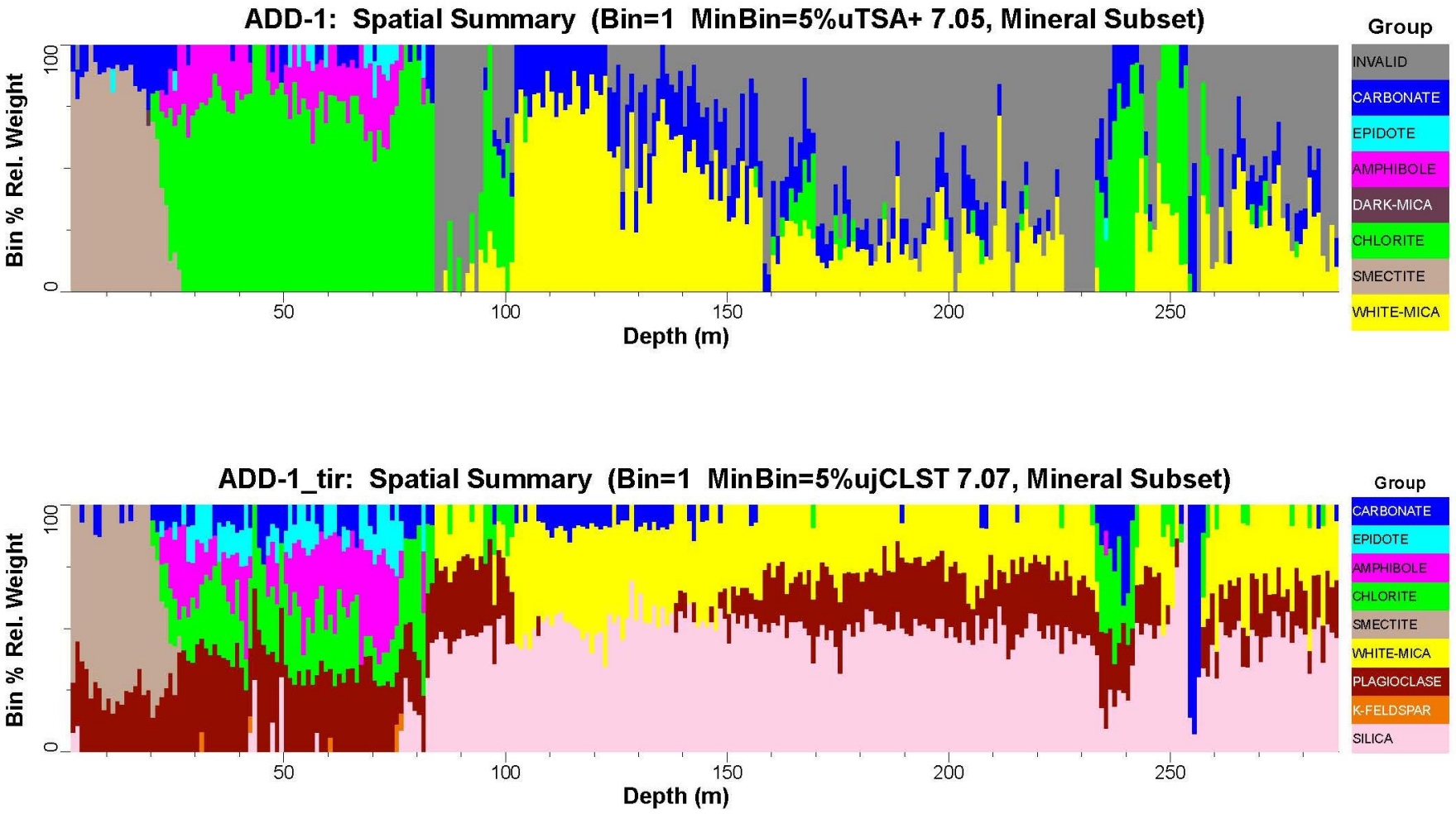

Figure 3 Summary of the hylogger hyperspectral image of the hole ADD-1, Grasmere prospect, Koonenberry Belt, New South Wales, Australia.

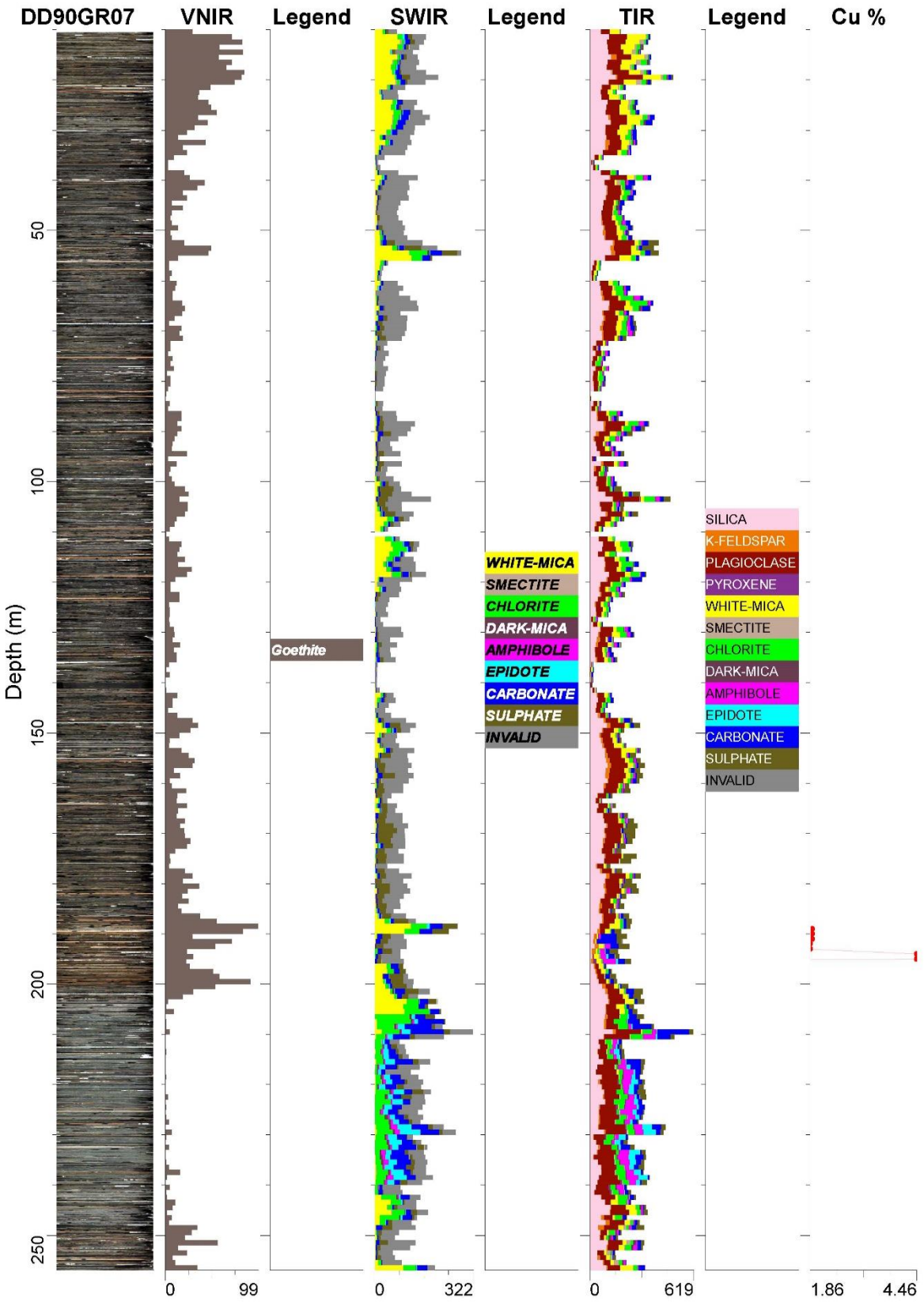

Figure 4 Downhole hylogger hyperspectral image of the hole DD90GR07, Grasmere prospect, Koonenberry Belt, New South Wales, Australia. Cu content is up to ~4.46 wt. % at 190-200m depth.

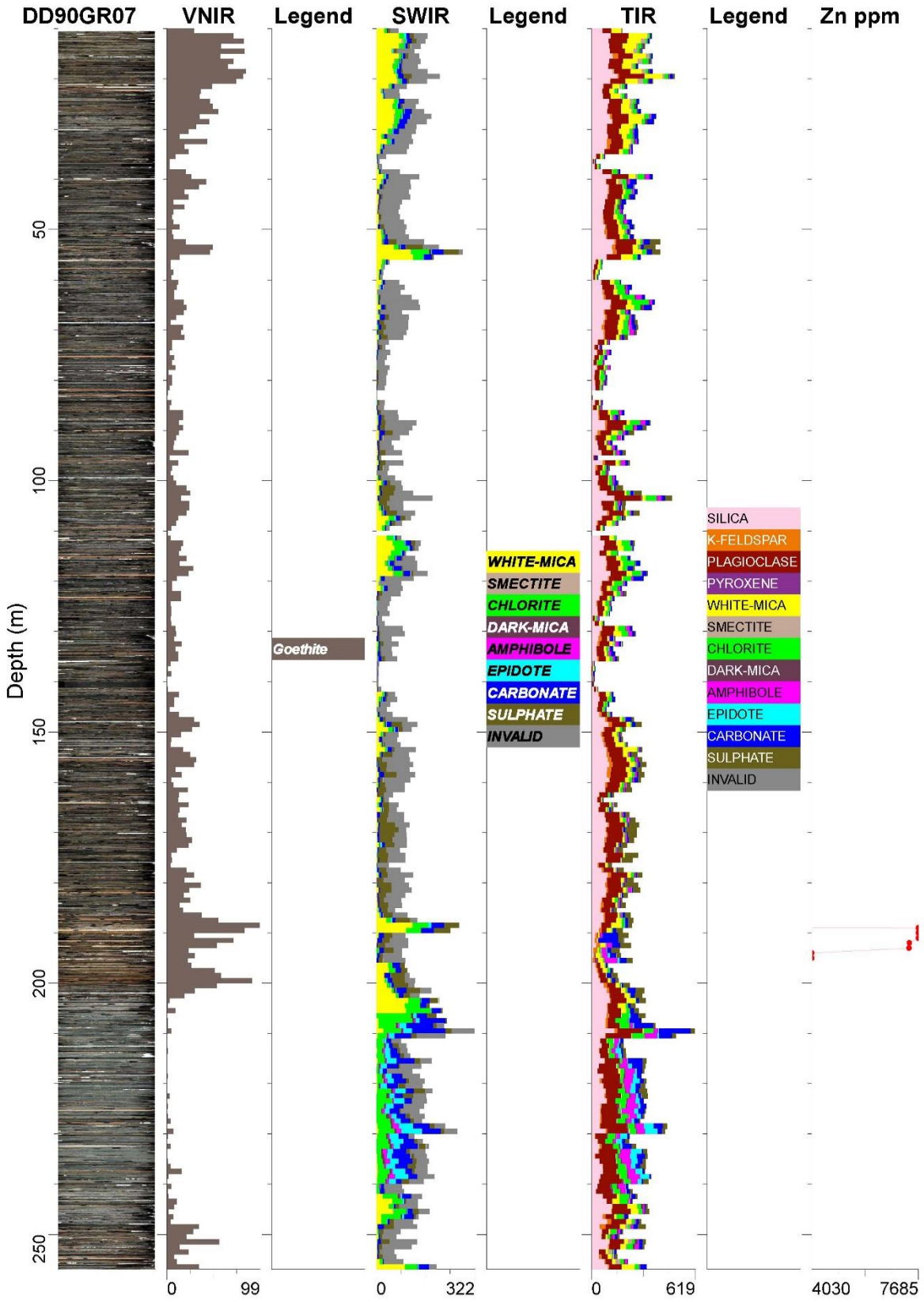

Figure 5 Downhole hylogger hyperspectral image of the hole DD90GR07, Grasmere prospect, Koonenberry Belt, New South Wales, Australia. Zn content is up to ~0.77 wt. % at 190-200m depth.

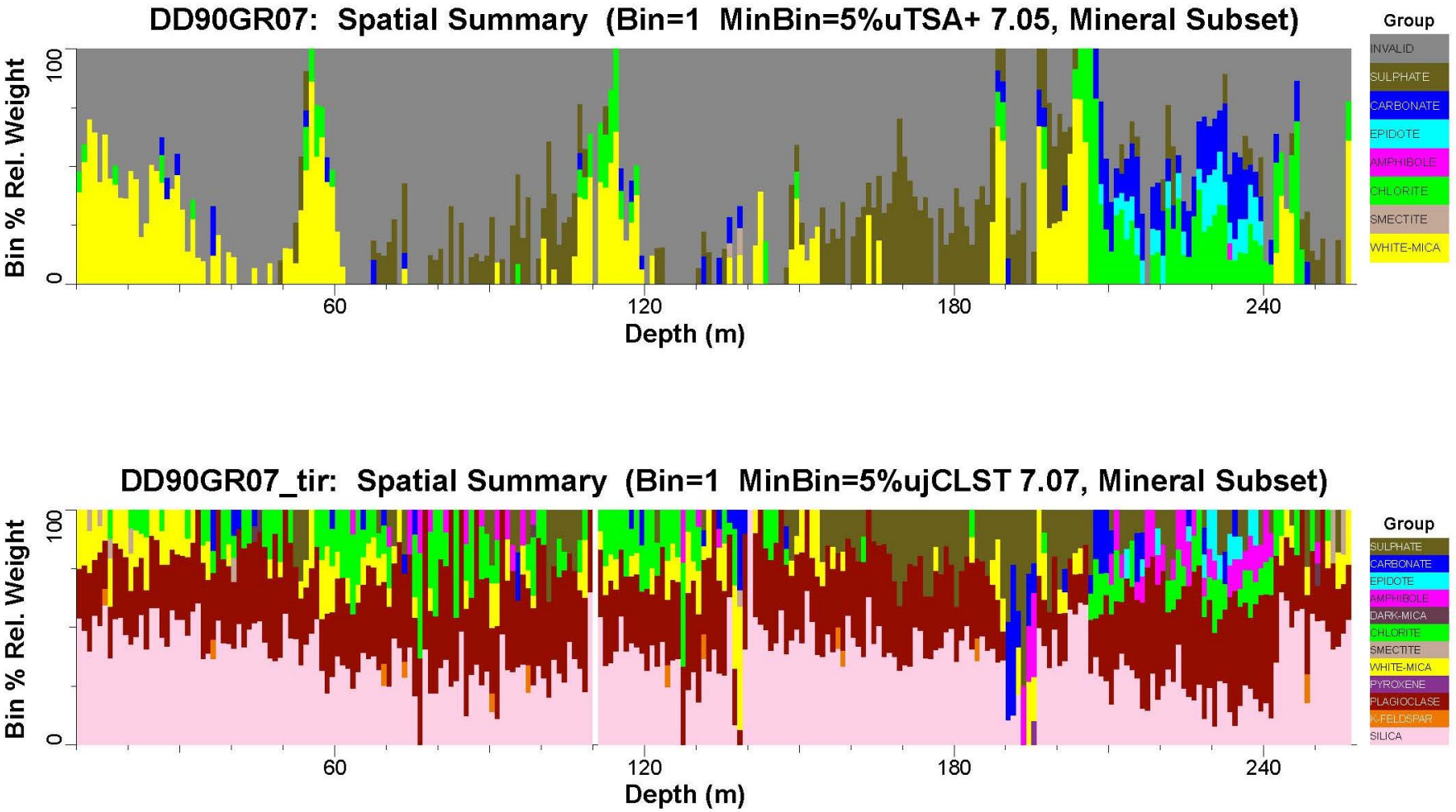

Figure 6 Summary of the hylogger hyperspectral image of the hole DD90GR07, Grasmere prospect, Koonenberry Belt, New South Wales, Australia.

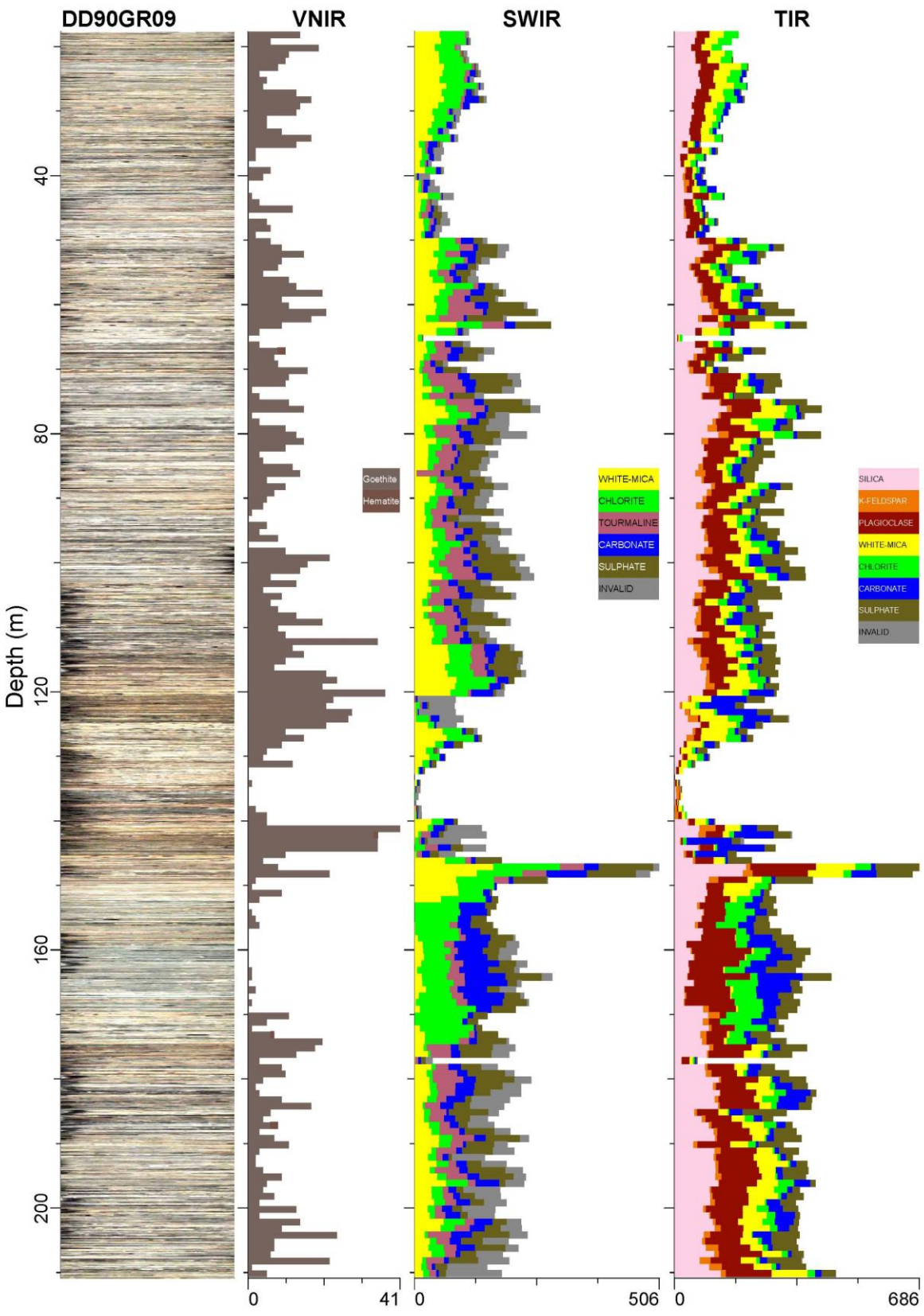

Figure 7 Downhole hylogger hyperspectral image of the hole DD90GR09, Grasmere prospect, Koonenberry Belt, New South Wales, Australia.

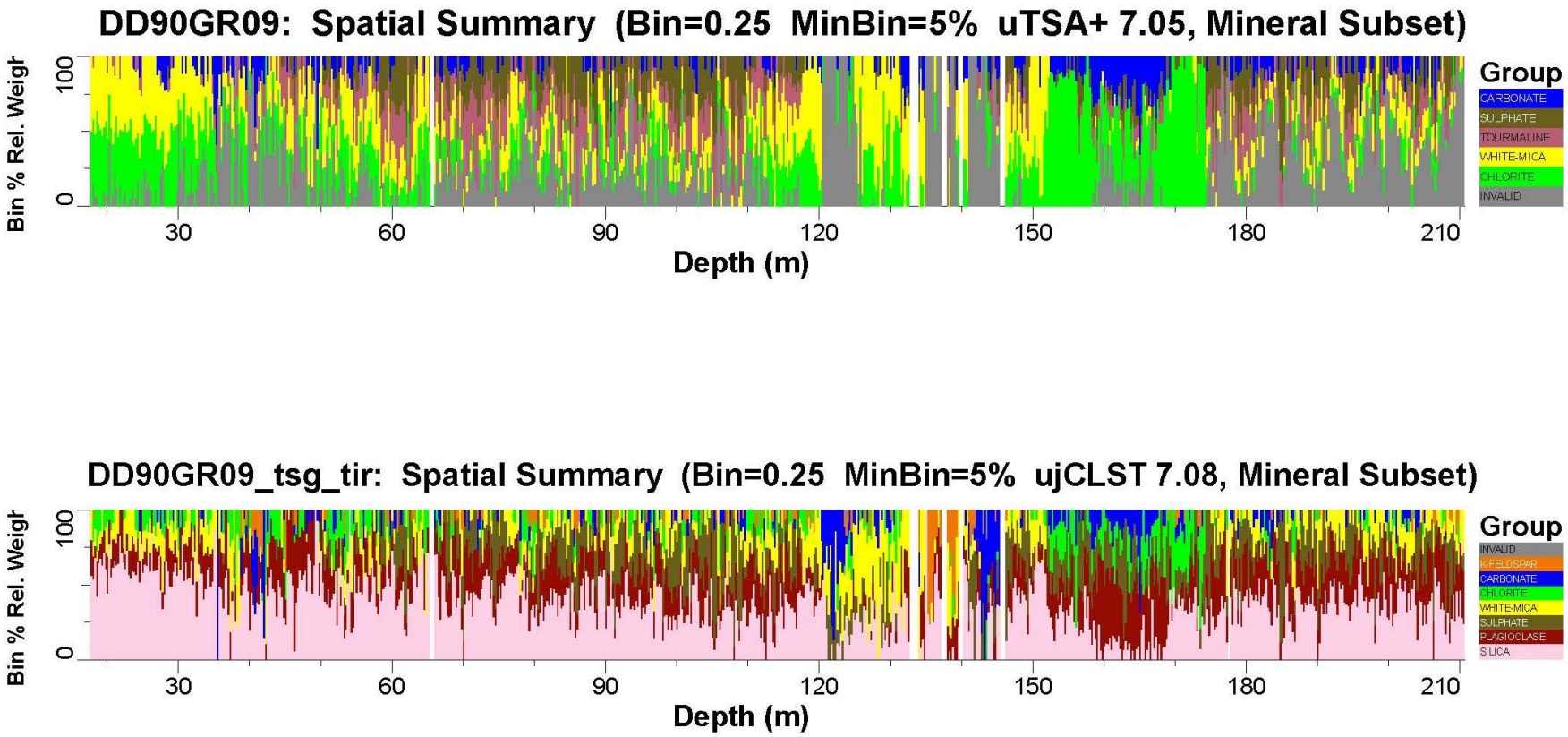

Figure 8 Summary of the hylogger hyperspectral image of the hole DD90GR09, Grasmere prospect, Koonenberry Belt, New South Wales, Australia.

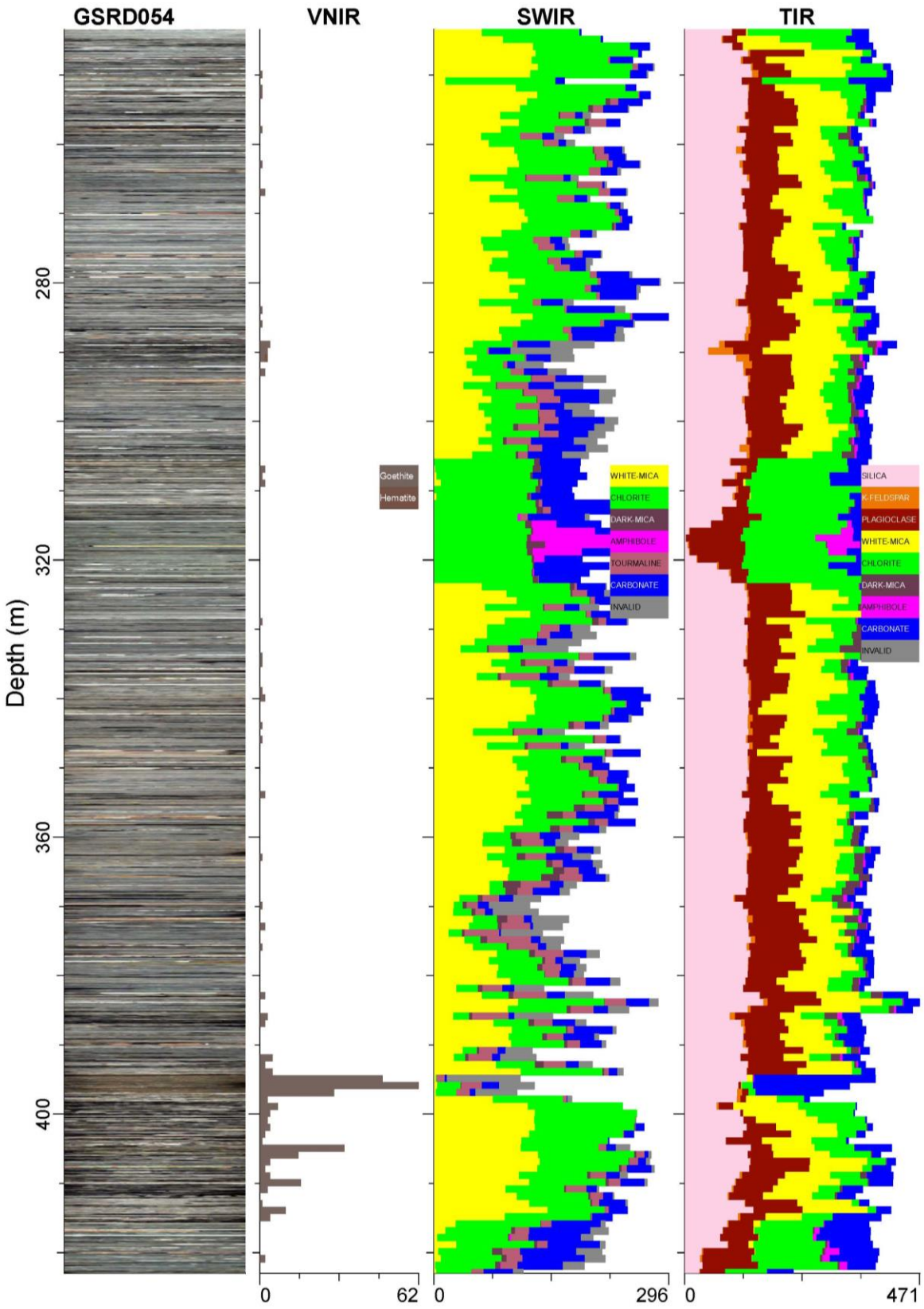

Figure 9 Downhole hylogger hyperspectral image of the hole GSRD054, Grasmere prospect, Koonenberry Belt, New South Wales, Australia.

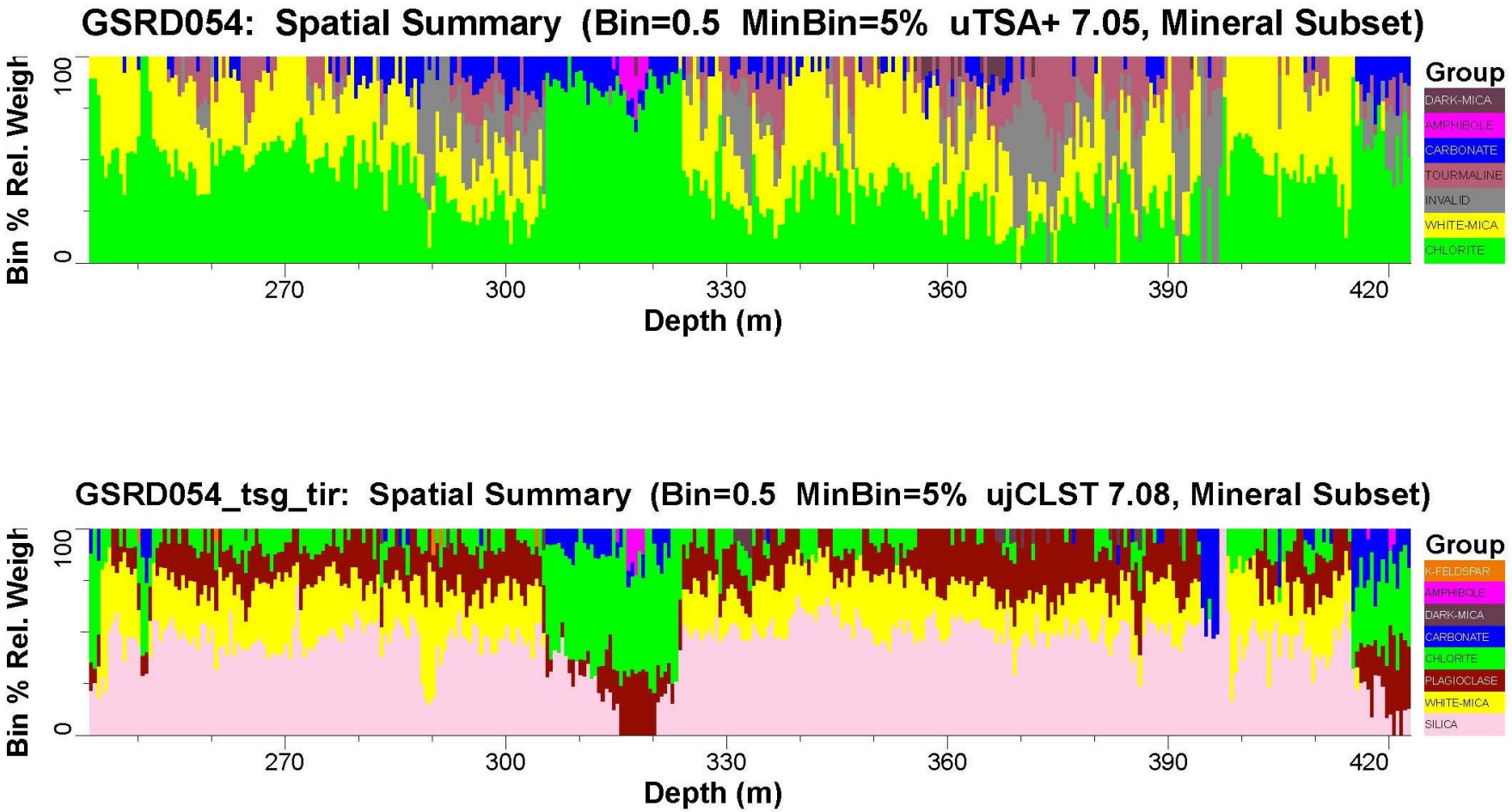

Figure 10 Summary of the hylogger hyperspectral image of the hole GSRD054, Grasmere prospect, Koonenberry Belt, New South Wales, Australia.

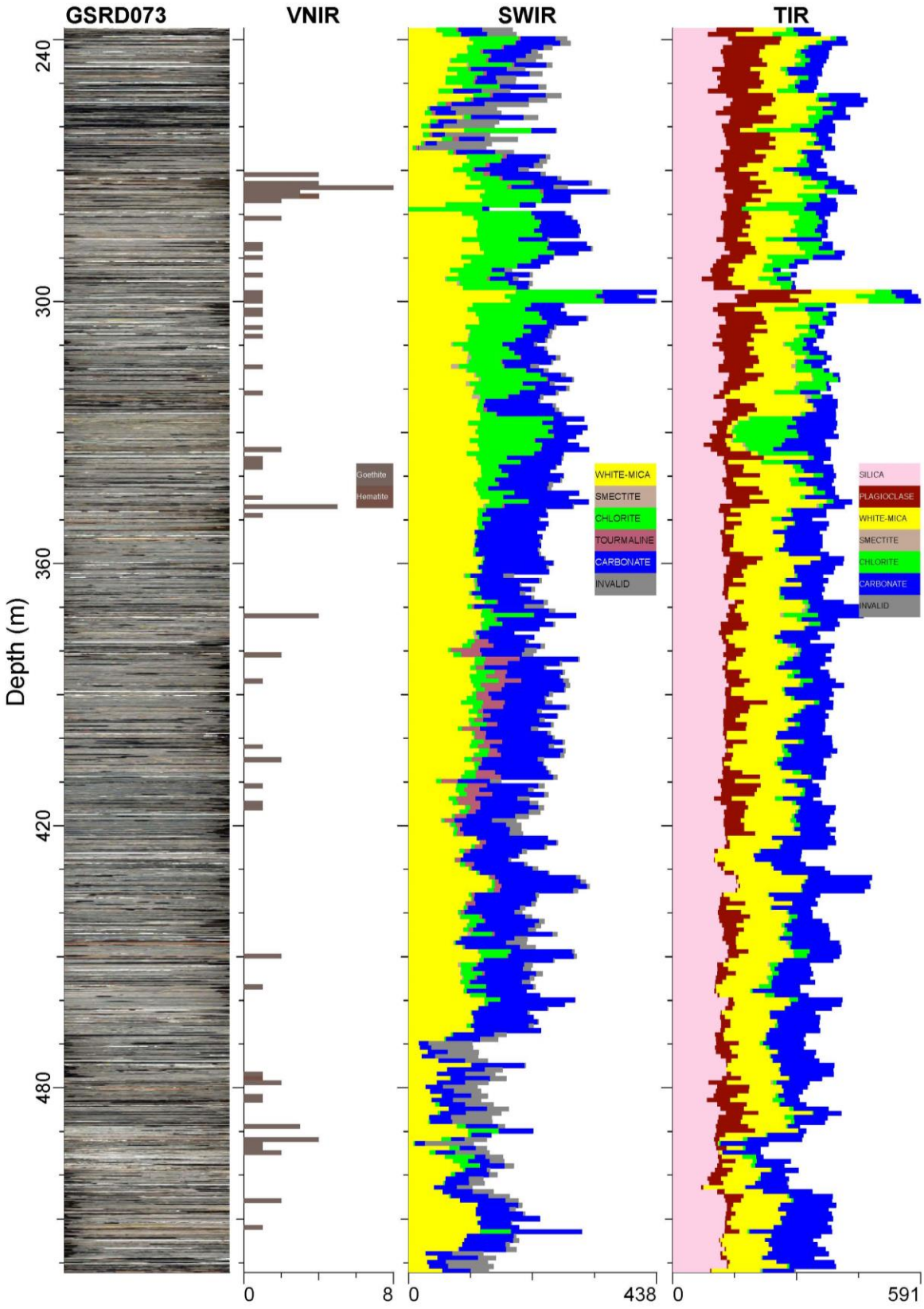

Figure 11 Downhole hylogger hyperspectral image of the hole GSRD073, Grasmere prospect, Koonenberry Belt, New South Wales, Australia.

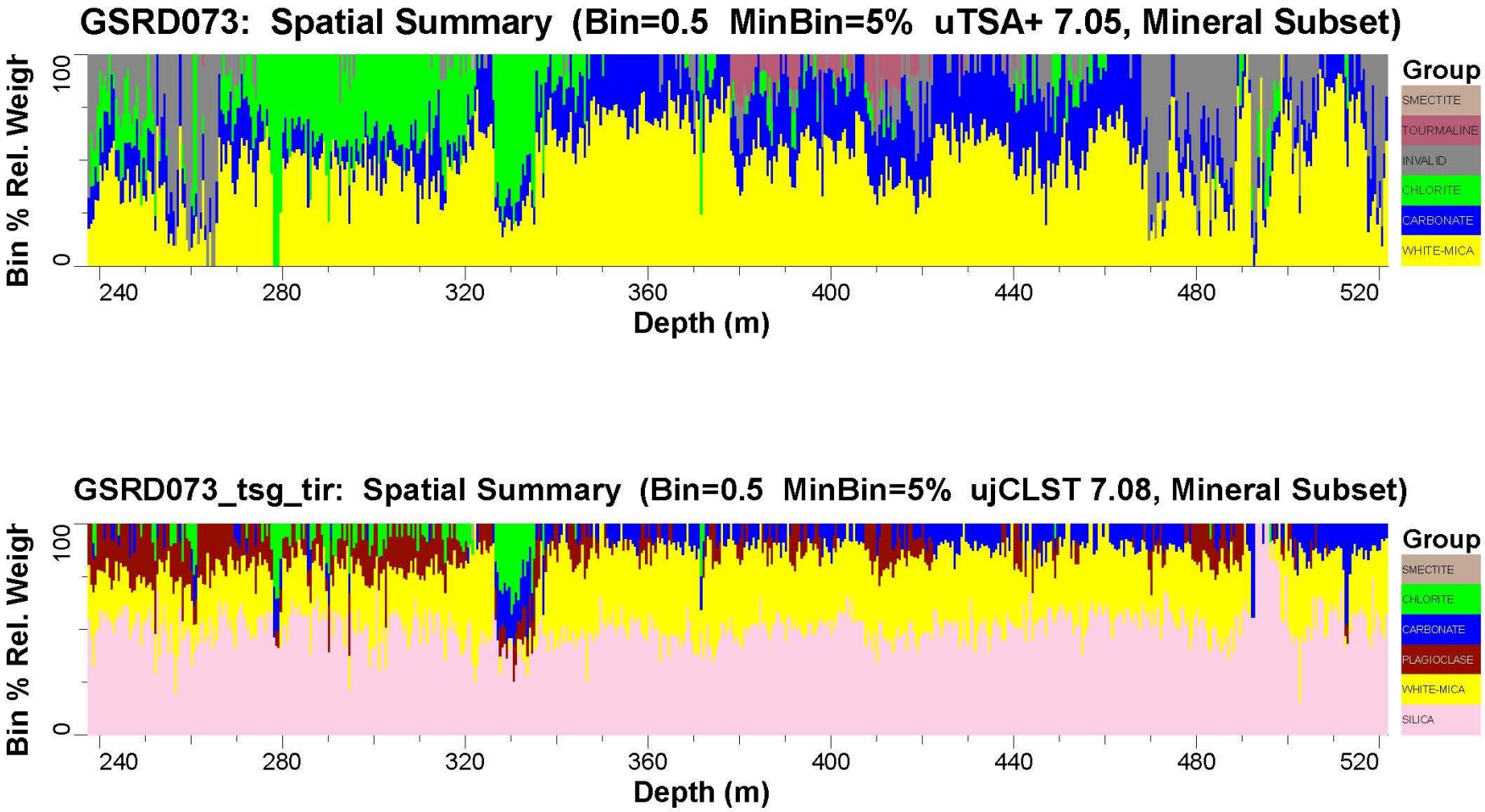

Figure 12 Summary of the hylogger hyperspectral image of the hole GSRD073, Grasmere prospect, Koonenberry Belt, New South Wales, Australia.

Sample ID	Prospect	Borehole Name	From (m)	To (m)	Note
2022440119	Grasmere	ADD-1	257.11	257.3	Massive sulfide ore

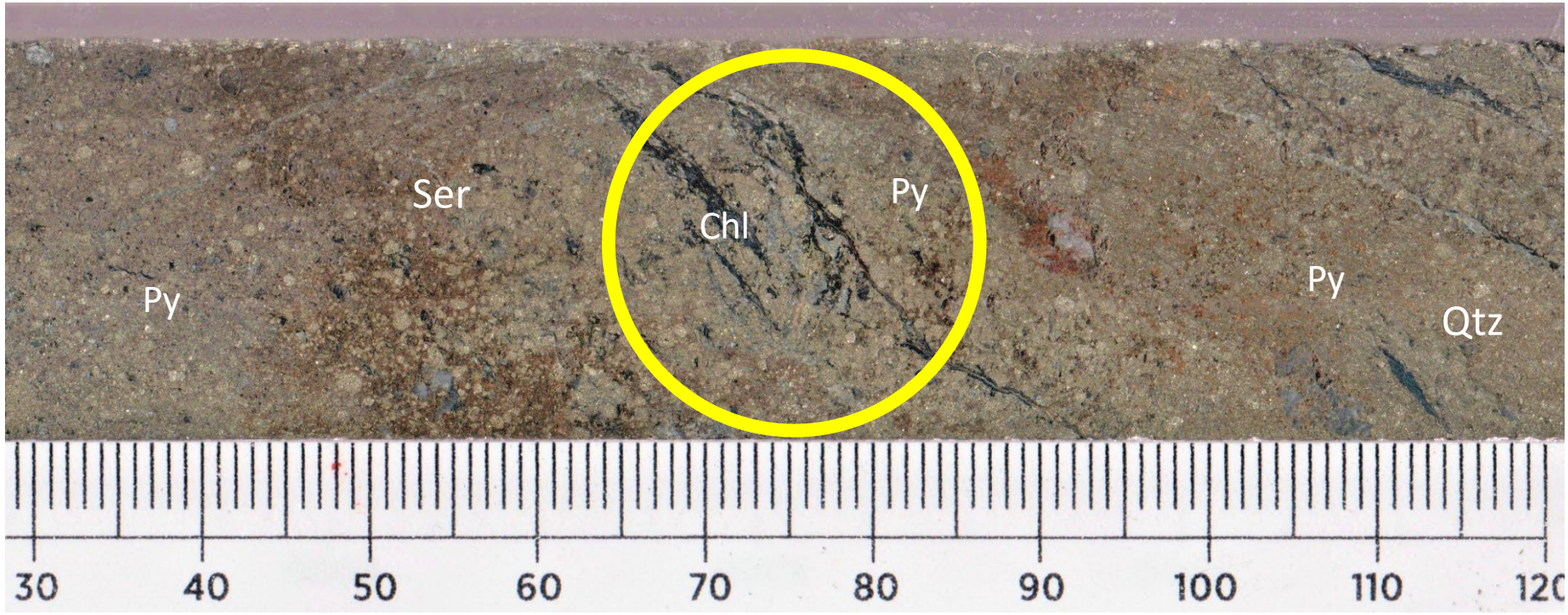

Figure 13 Photos of the drill core sample 2022440119 from drill hole ADD-1 of the Grasmere prospect, Koonenberry Belt, New South Wales, Australia. Py-pyrite; Chl-chlorite.

Sample ID	Prospect	Borehole Name	From (m)	To (m)	Note
2022440119	Grasmere	ADD-1	257.11	257.3	Massive sulfide ore

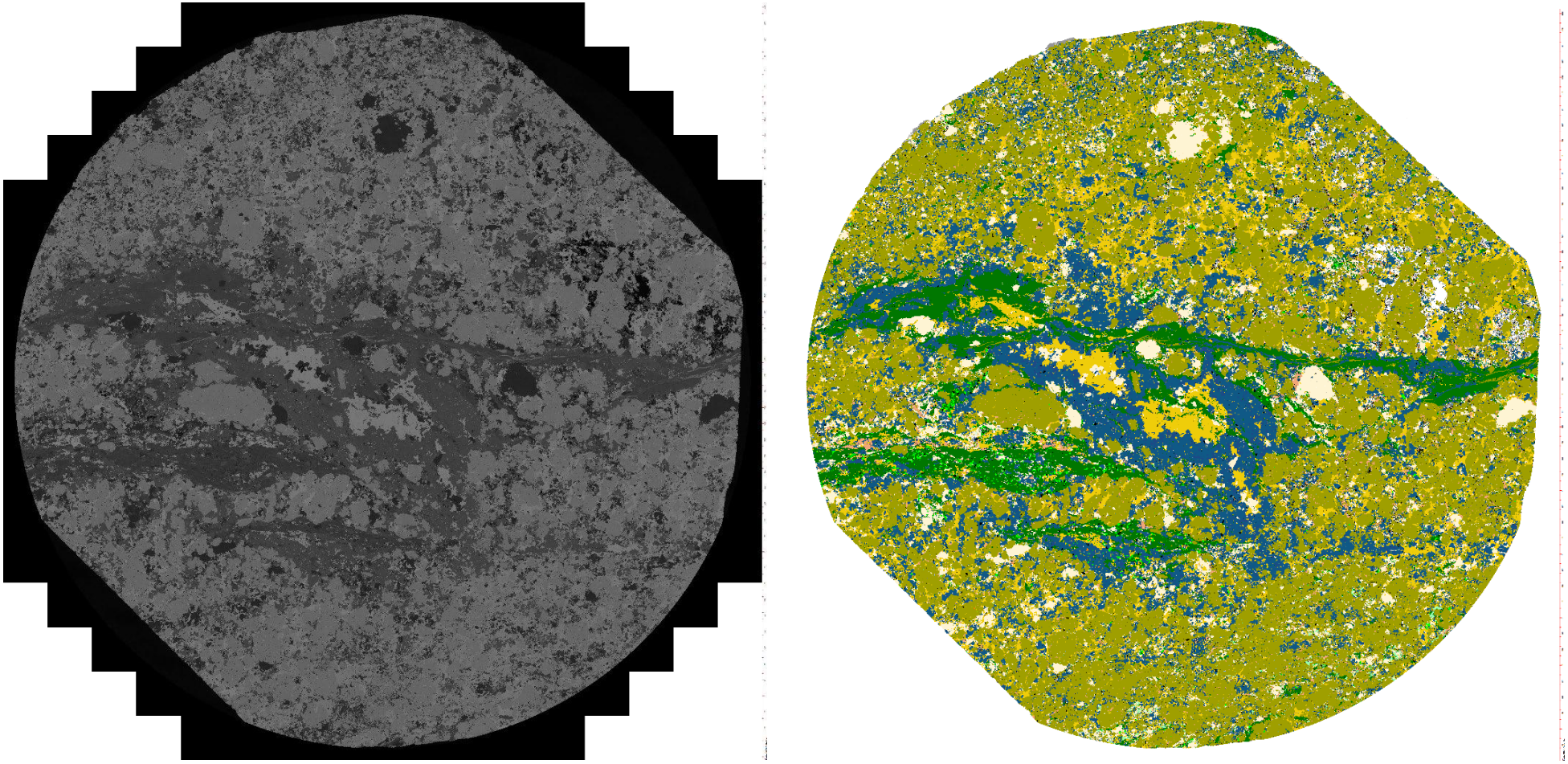

Figure 14 Backscattered electron (BSE) image (left) and Mineral Liberation Analysis (MLA) mineral map (right) of the sample 2022440119 from drill hole ADD-1 of the Grasmere prospect, Koonenberry Belt, New South Wales, Australia. See Figure 47 at the end of this document for the legend of minerals identified using Mineral Liberation Analysis (MLA) mapping.

Sample ID	Prospect	Borehole Name	From (m)	To (m)	Note
2022440066	Grasmere	DD88GR01	68.98	69.15	Massive sulfide ore

Figure 15 Photos of the drill core sample 2022440066 from drill hole DD88GR01 of the Grasmere prospect, Koonenberry Belt, New South Wales, Australia.

Sample ID	Prospect	Borehole Name	From (m)	To (m)	Note
2022440066	Grasmere	DD88GR01	68.98	69.15	Massive sulfide ore

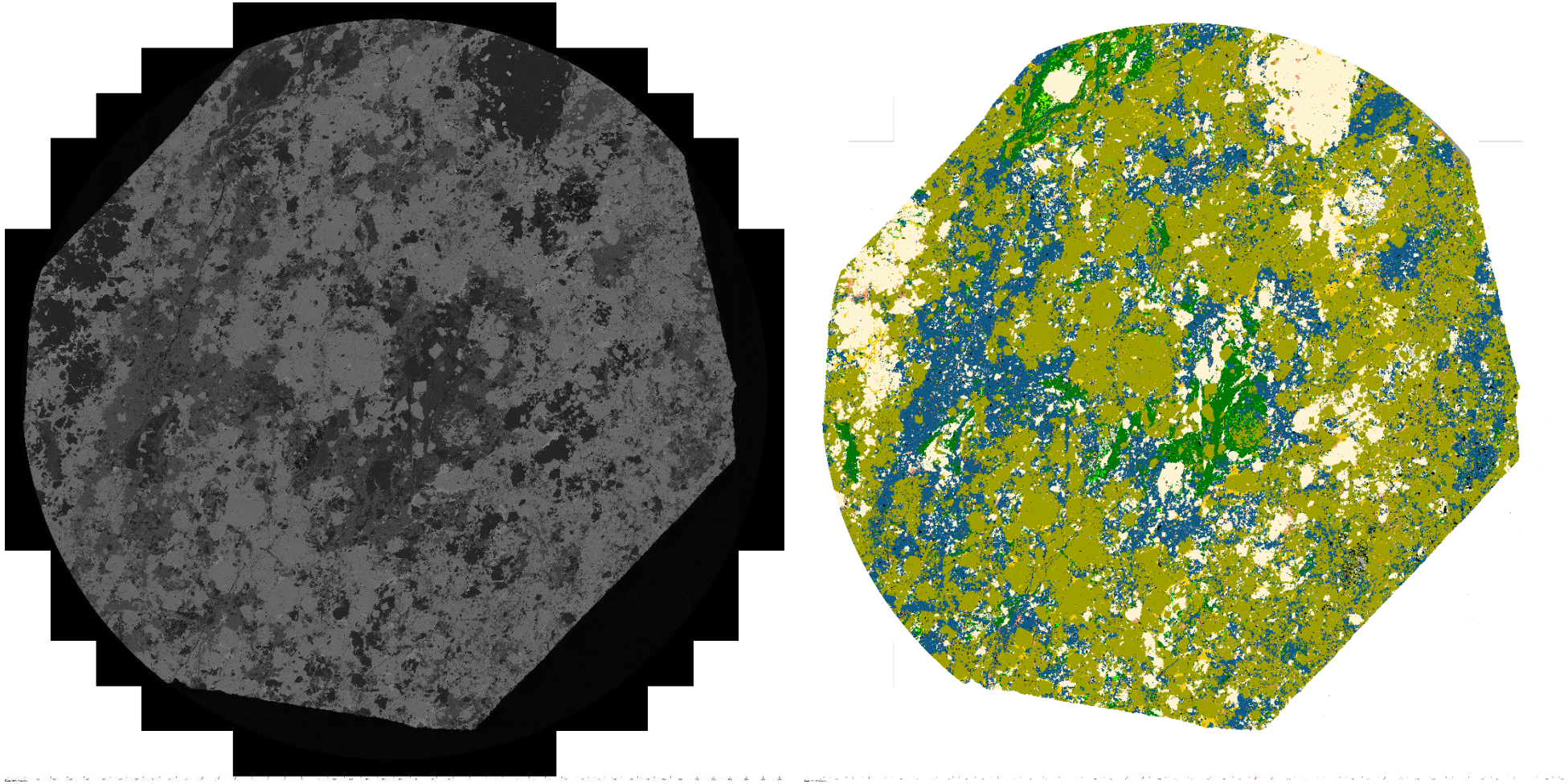

Figure 16 Backscattered electron (BSE) image (left) and Mineral Liberation Analysis (MLA) mineral map (right) of the sample 2022440066 from drill hole DD88GR01 of the Grasmere prospect, Koonenberry Belt, New South Wales, Australia. See Figure 47 at the end of this document for the legend of minerals identified using Mineral Liberation Analysis (MLA) mapping.

Sample ID	Prospect	Borehole Name	From (m)	To (m)	Note
2022440067	Grasmere	DD88GR01	70.09	70.29	Massive sulfide ore

Figure 17 Photos of the drill core sample 2022440067 from drill hole DD88GR01 of the Grasmere prospect, Koonenberry Belt, New South Wales, Australia.

Sample ID	Prospect	Borehole Name	From (m)	To (m)	Note
2022440067	Grasmere	DD88GR01	70.09	70.29	Massive sulfide ore

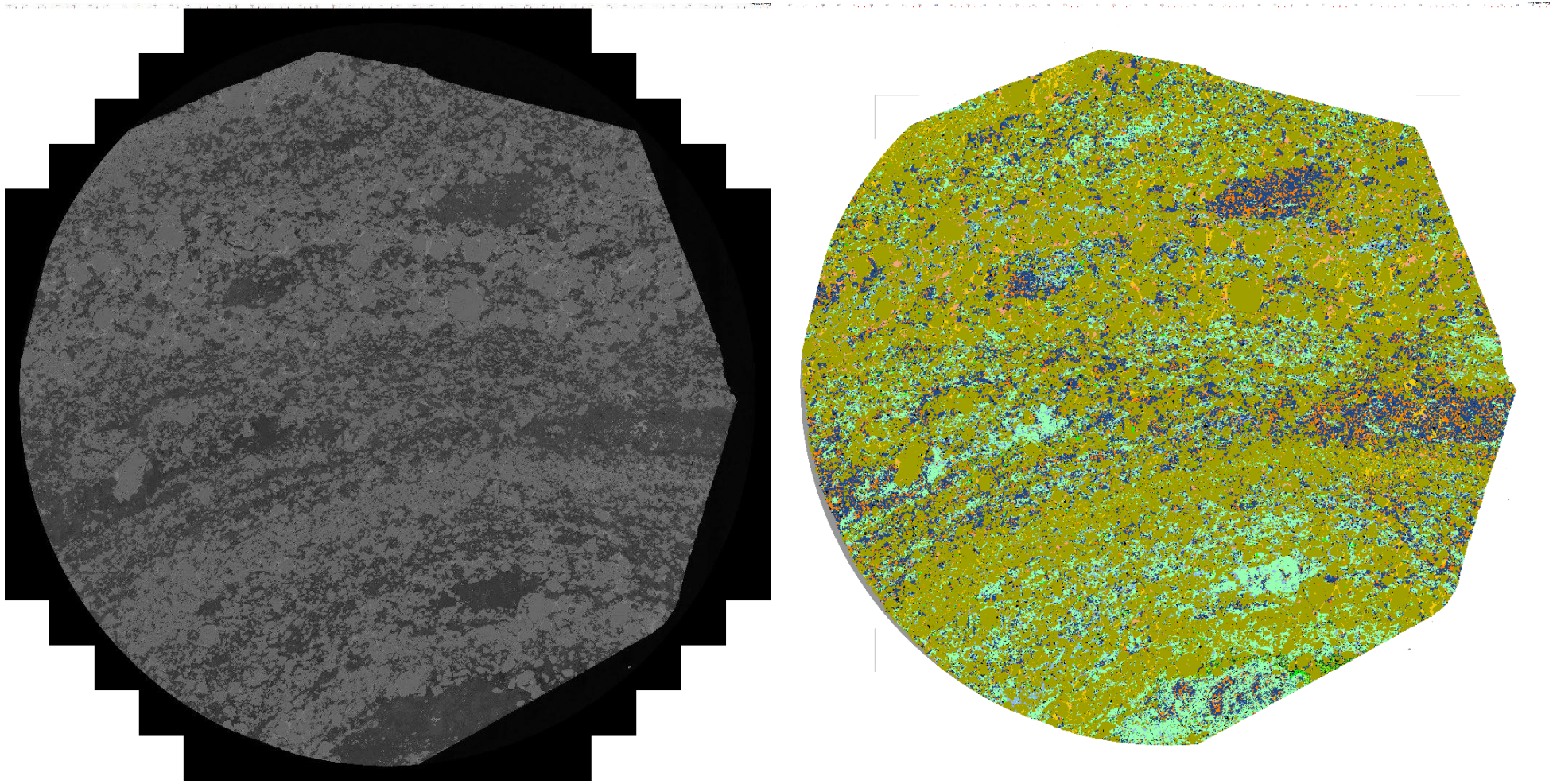

Figure 18 Backscattered electron (BSE) image (left) and Mineral Liberation Analysis (MLA) mineral map (right) of the sample 2022440067 from drill hole DD88GR01 of the Grasmere prospect, Koonenberry Belt, New South Wales, Australia. See Figure 47 at the end of this document for the legend of minerals identified using Mineral Liberation Analysis (MLA) mapping.

Sample ID	Prospect	Borehole Name	From (m)	To (m)	Note
2022440075	Grasmere	DD89GR05	121	121.1	Massive sulfide ore

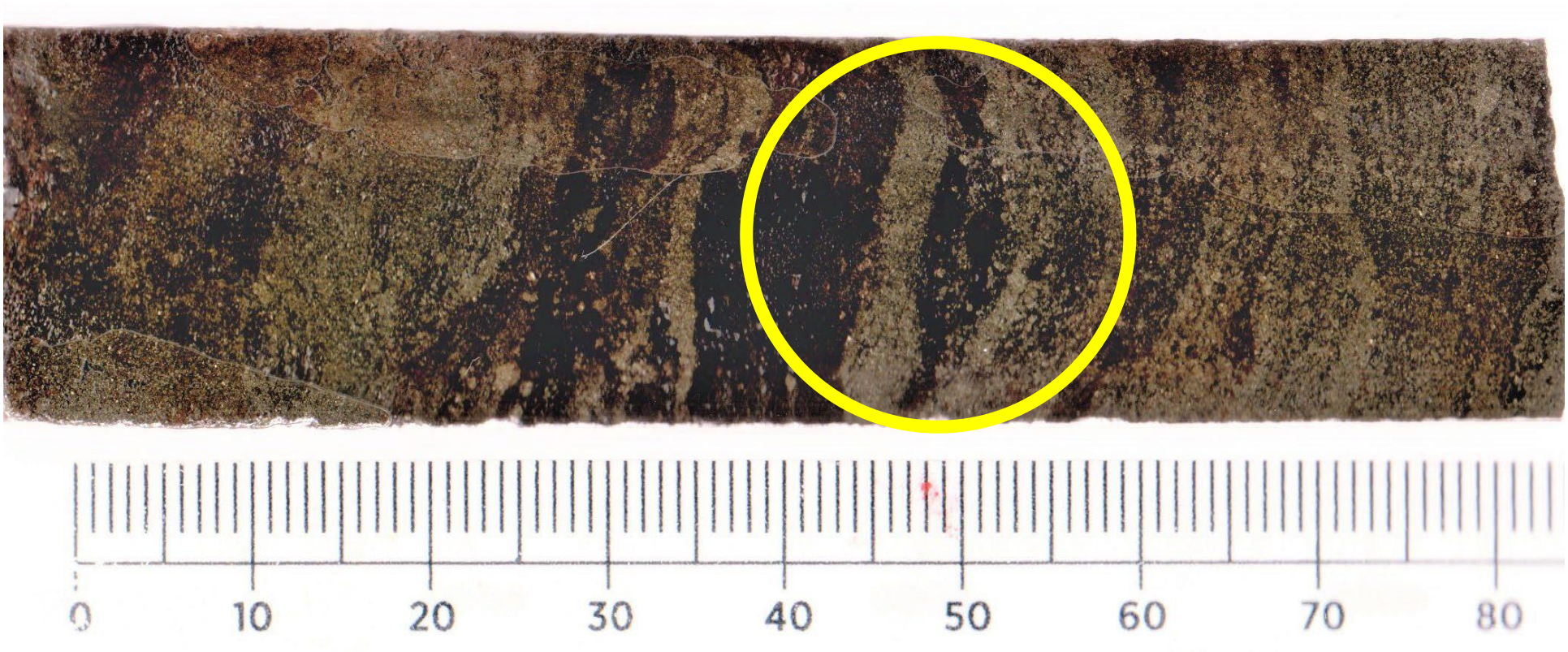

Figure 19 Photos of the drill core sample 2022440075 from drill hole DD88GR05 of the Grasmere prospect, Koonenberry Belt, New South Wales, Australia.

Sample ID	Prospect	Borehole Name	From (m)	To (m)	Note
2022440075	Grasmere	DD89GR05	121	121.1	Massive sulfide ore

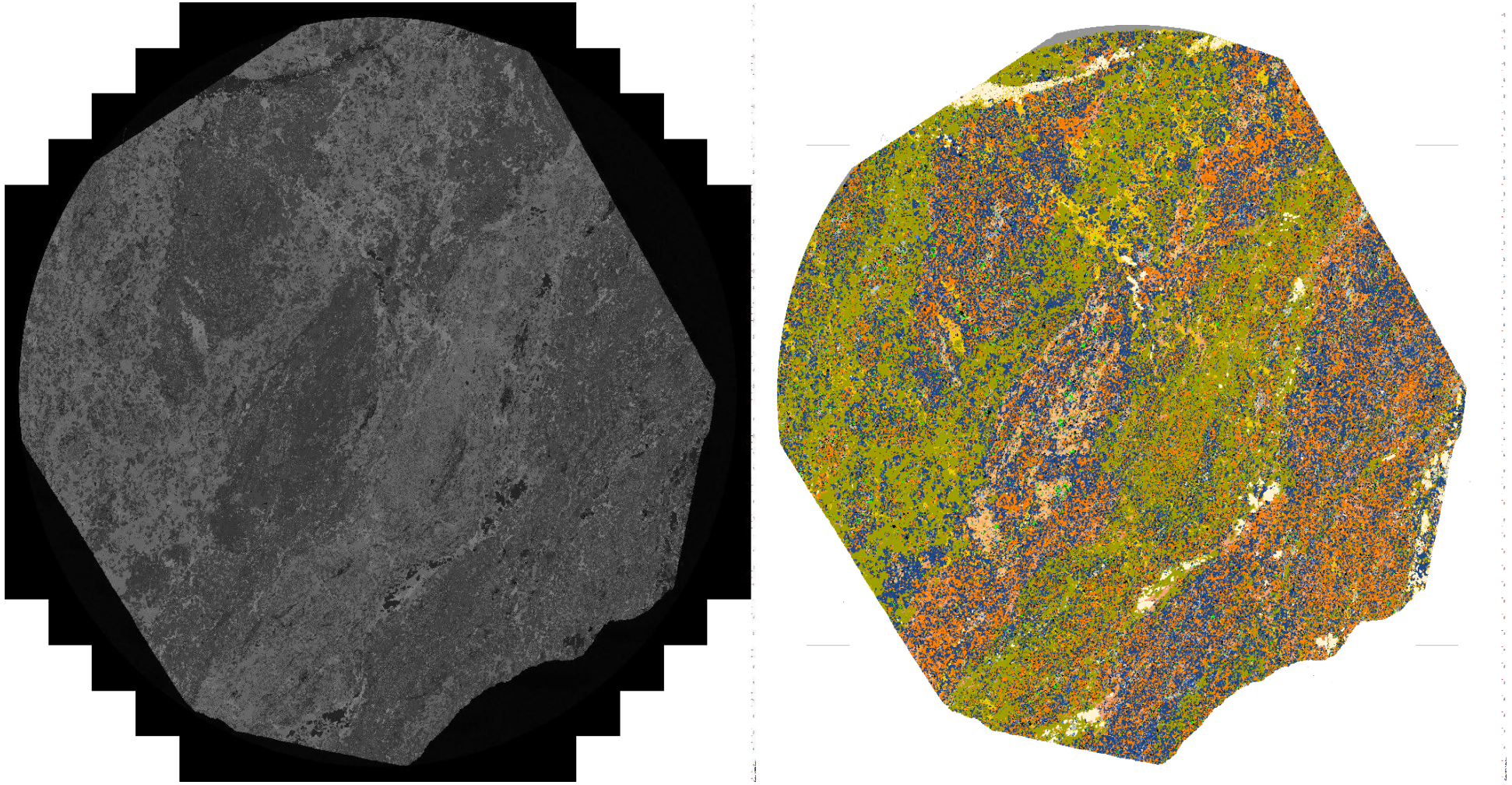

Figure 20 Backscattered electron (BSE) image (left) and Mineral Liberation Analysis (MLA) mineral map (right) of the sample 2022440075 from drill hole DD88GR05 of the Grasmere prospect, Koonenberry Belt, New South Wales, Australia. See Figure 47 at the end of this document for the legend of minerals identified using Mineral Liberation Analysis (MLA) mapping.

Sample ID	Prospect	Borehole Name	From (m)	To (m)	Note
2022440080	Grasmere	DD89GR05	128.2	128.3	Massive sulfide ore

Figure 21 Photos of the drill core sample 2022440080 from drill hole DD88GR05 of the Grasmere prospect, Koonenberry Belt, New South Wales, Australia.

Sample ID	Prospect	Borehole Name	From (m)	To (m)	Note
2022440080	Grasmere	DD89GR05	128.2	128.3	Massive sulfide ore

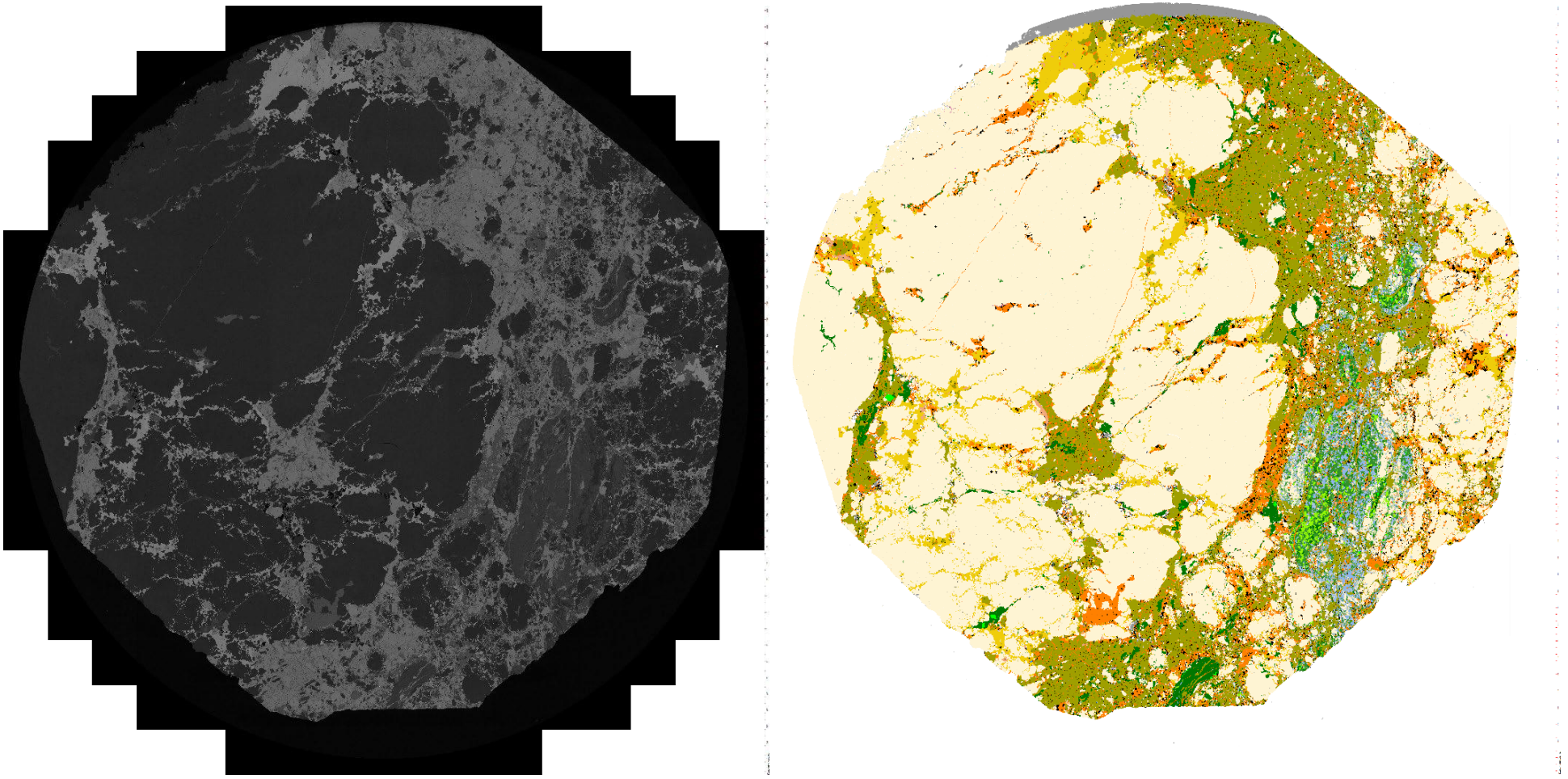

Figure 22 Backscattered electron (BSE) image (left) and Mineral Liberation Analysis (MLA) mineral map (right) of the sample 2022440080 from drill hole DD88GR05 of the Grasmere prospect, Koonenberry Belt, New South Wales, Australia. See Figure 47 at the end of this document for the legend of minerals identified using Mineral Liberation Analysis (MLA) mapping.

Sample ID	Prospect	Borehole Name	From (m)	To (m)	Note
2022440115	Grasmere	ADD-1	252.77	253	Massive sulfide ore

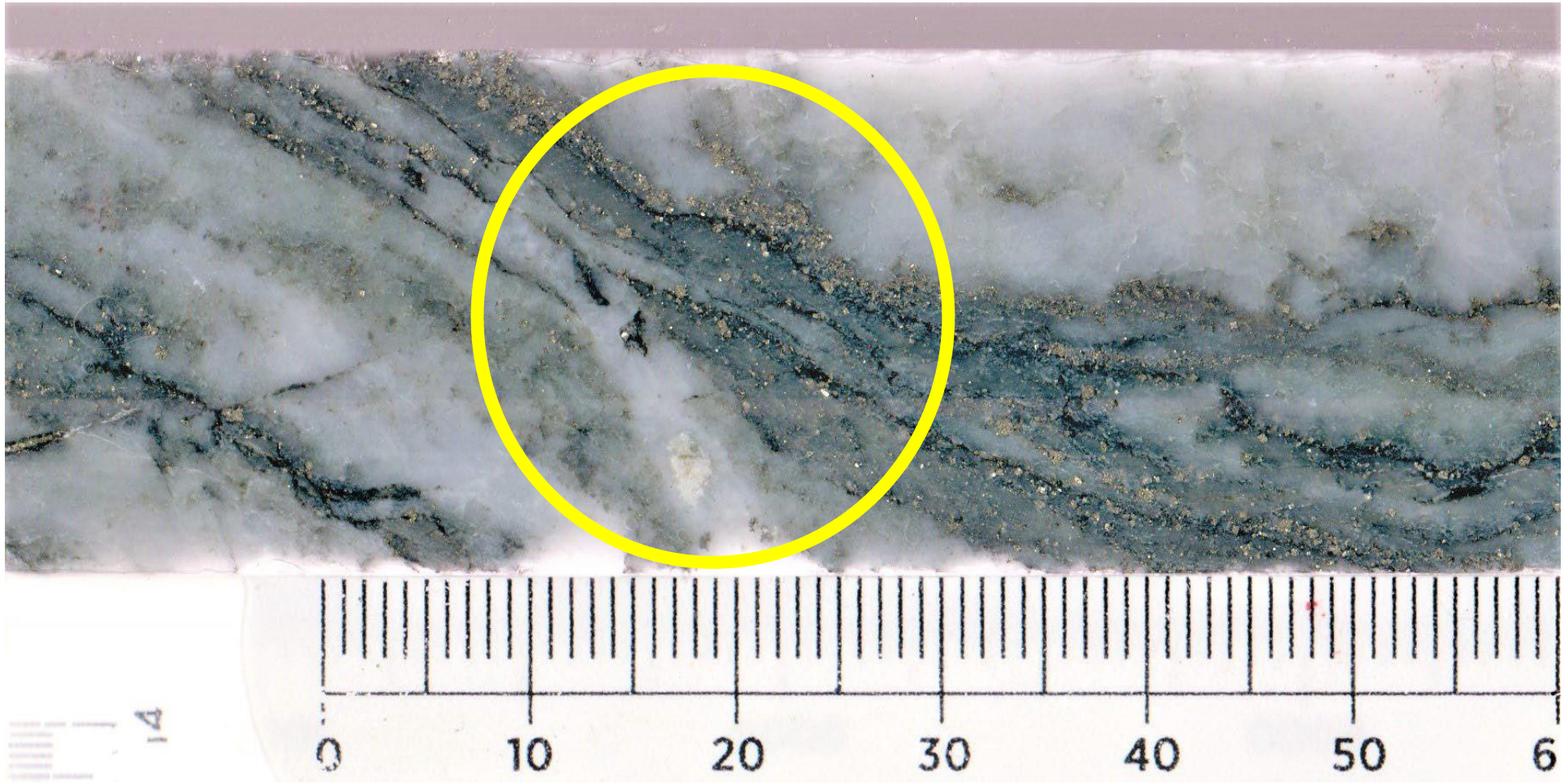

Figure 23 Photos of the drill core sample 2022440115 from drill hole ADD-1 of the Grasmere prospect, Koonenberry Belt, New South Wales, Australia.

Sample ID	Prospect	Borehole Name	From (m)	To (m)	Note
2022440115	Grasmere	ADD-1	252.77	253	Massive sulfide ore

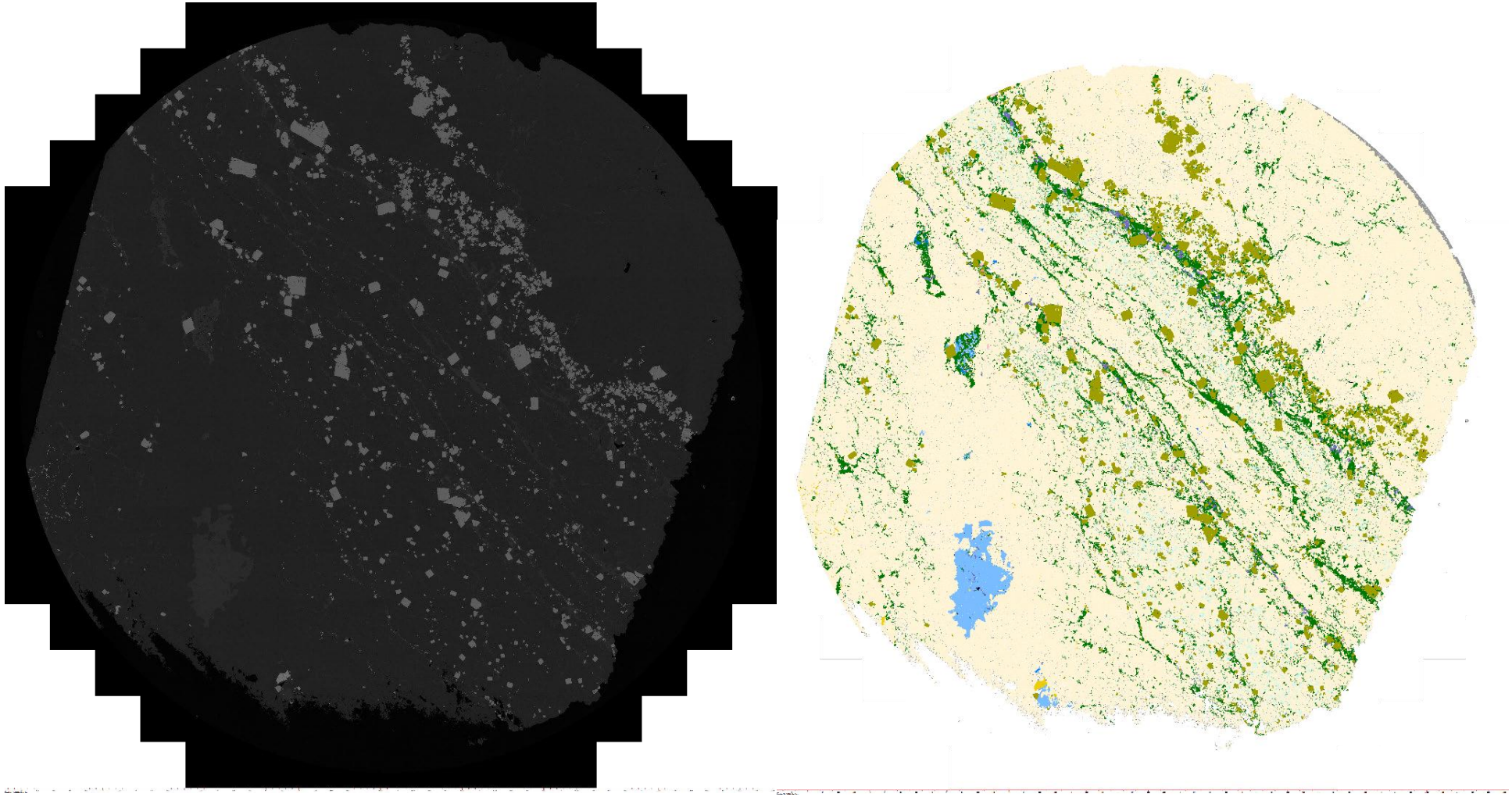

Figure 24 Backscattered electron (BSE) image (left) and Mineral Liberation Analysis (MLA) mineral map (right) of the sample 2022440115 from drill hole ADD-1 of the Grasmere prospect, Koonenberry Belt, New South Wales, Australia. See Figure 47 at the end of this document for the legend of minerals identified using Mineral Liberation Analysis (MLA) mapping.

Sample ID	Prospect	Borehole Name	From (m)	To (m)	Note
2022440117	Grasmere	ADD-1	254.76	254.86	Massive sulfide ore

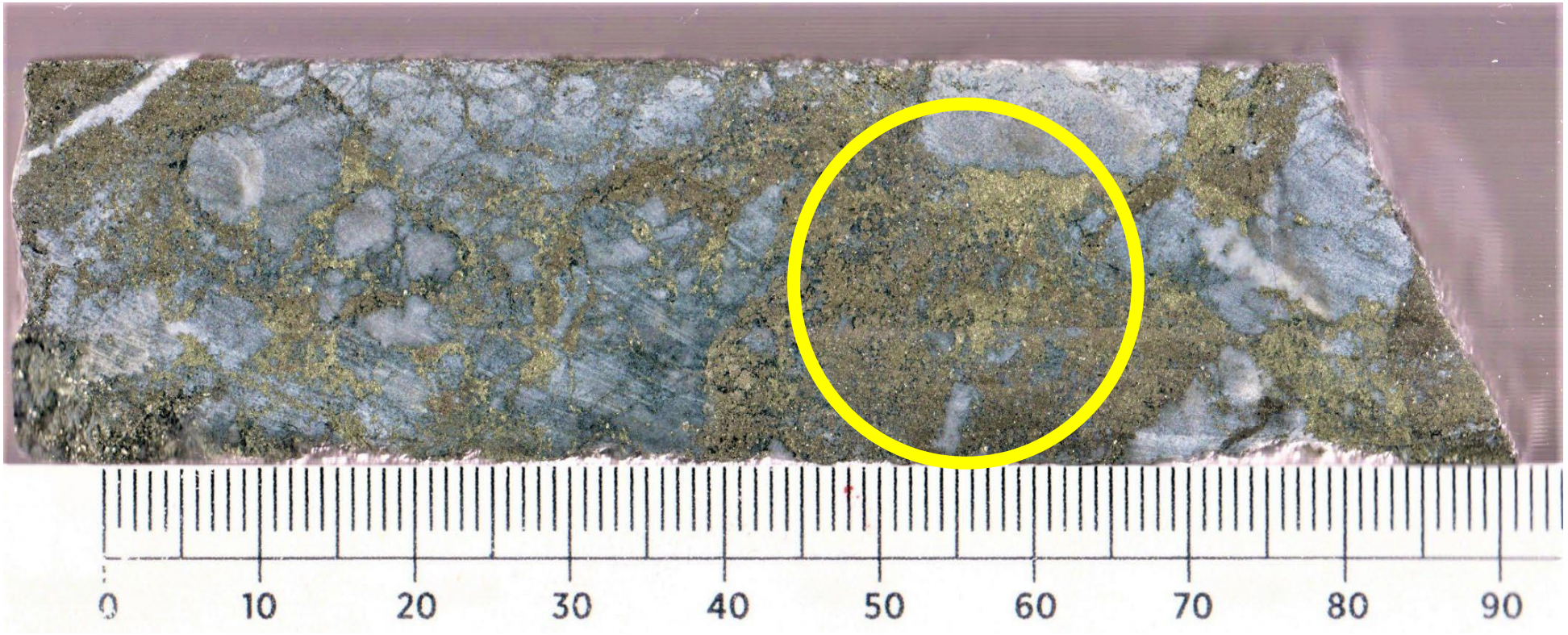

Figure 25 Photos of the drill core sample 2022440117 from drill hole ADD-1 of the Grasmere prospect, Koonenberry Belt, New South Wales, Australia.

Sample ID	Prospect	Borehole Name	From (m)	To (m)	Note
2022440117	Grasmere	ADD-1	254.76	254.86	Massive sulfide ore

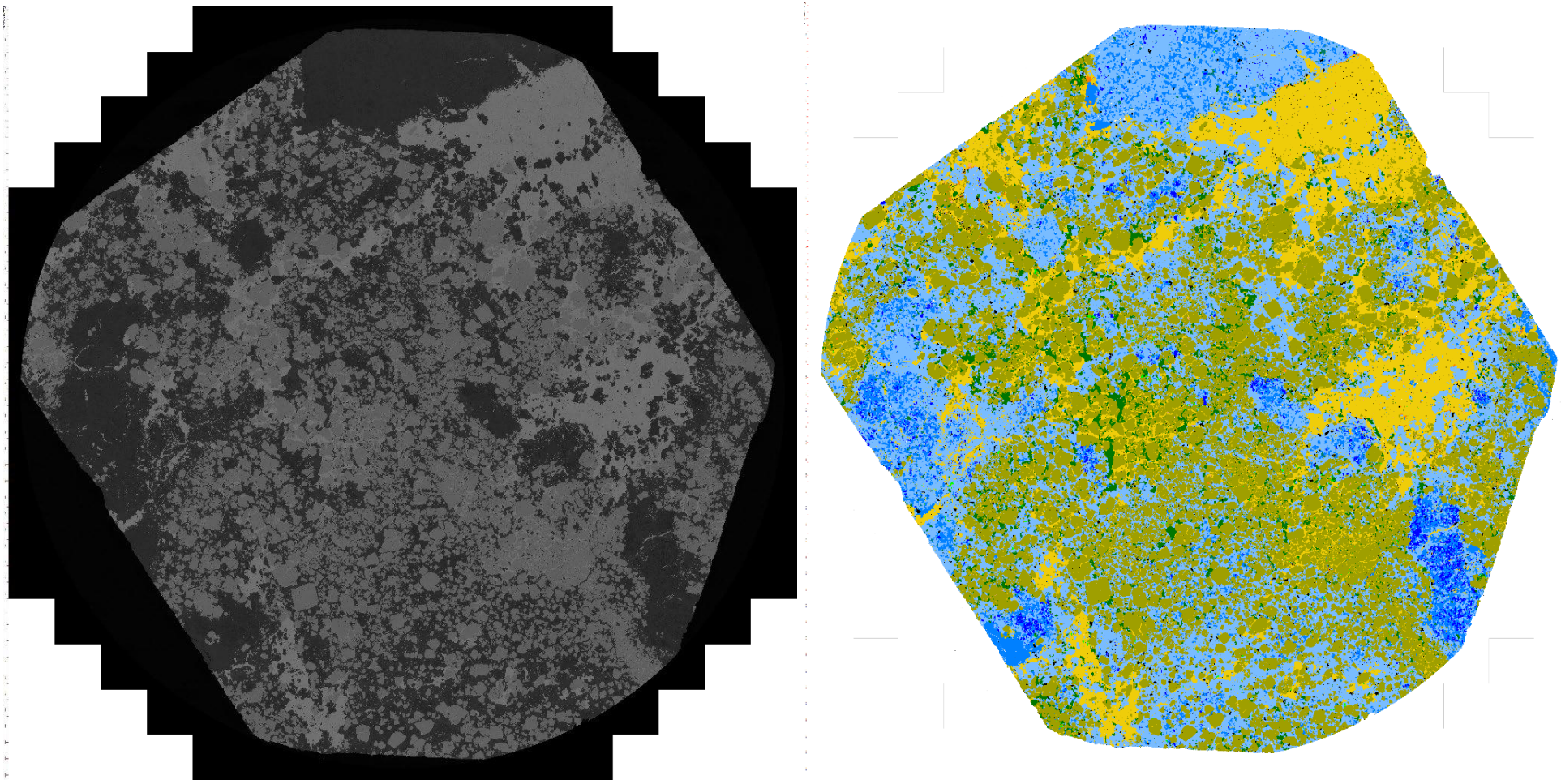

Figure 26 Backscattered electron (BSE) image (left) and Mineral Liberation Analysis (MLA) mineral map (right) of the sample 2022440117 from drill hole ADD-1 of the Grasmere prospect, Koonenberry Belt, New South Wales, Australia. See Figure 47 at the end of this document for the legend of minerals identified using Mineral Liberation Analysis (MLA) mapping.

Sample ID	Prospect	Borehole Name	From (m)	To (m)	Note
2022440121	Grasmere	ADD-2	158.2	158.32	Massive sulfide ore

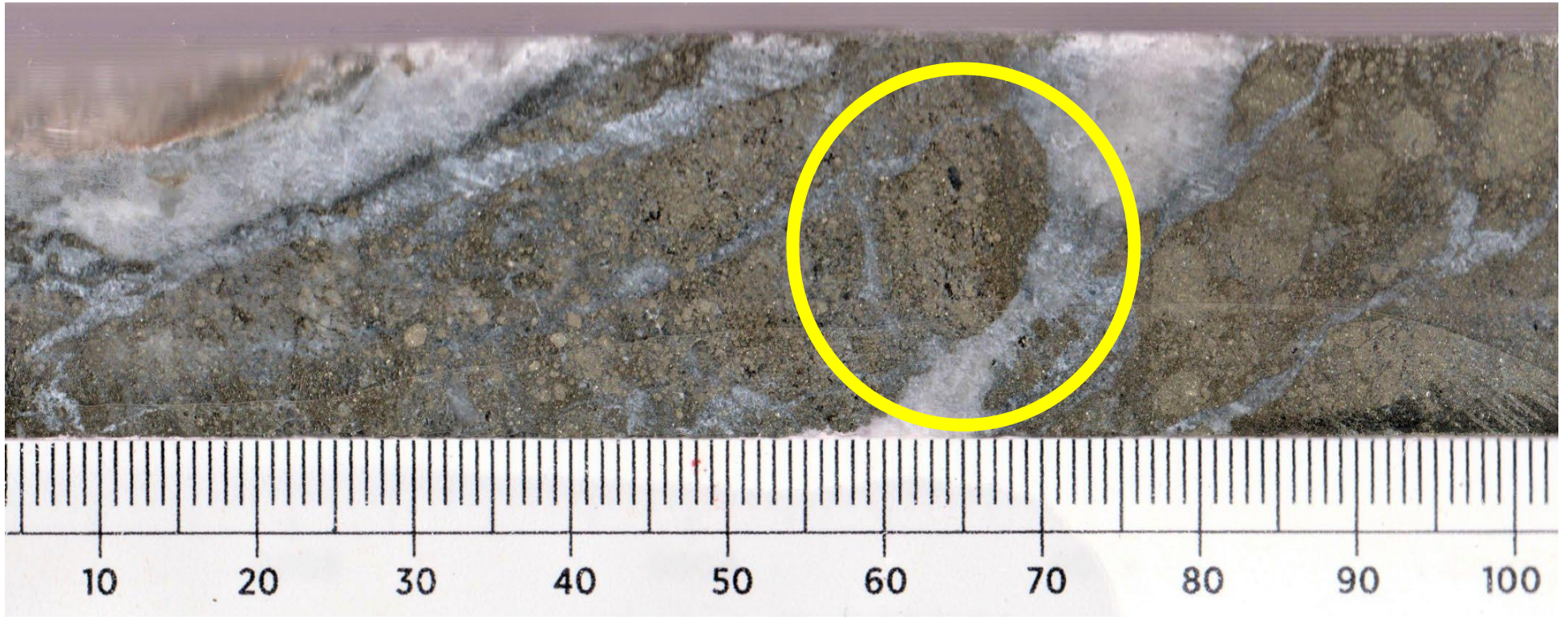

Figure 27 Photos of the drill core sample 2022440121 from drill hole ADD-2 of the Grasmere prospect, Koonenberry Belt, New South Wales, Australia.

Sample ID	Prospect	Borehole Name	From (m)	To (m)	Note
2022440121	Grasmere	ADD-2	158.2	158.32	Massive sulfide ore

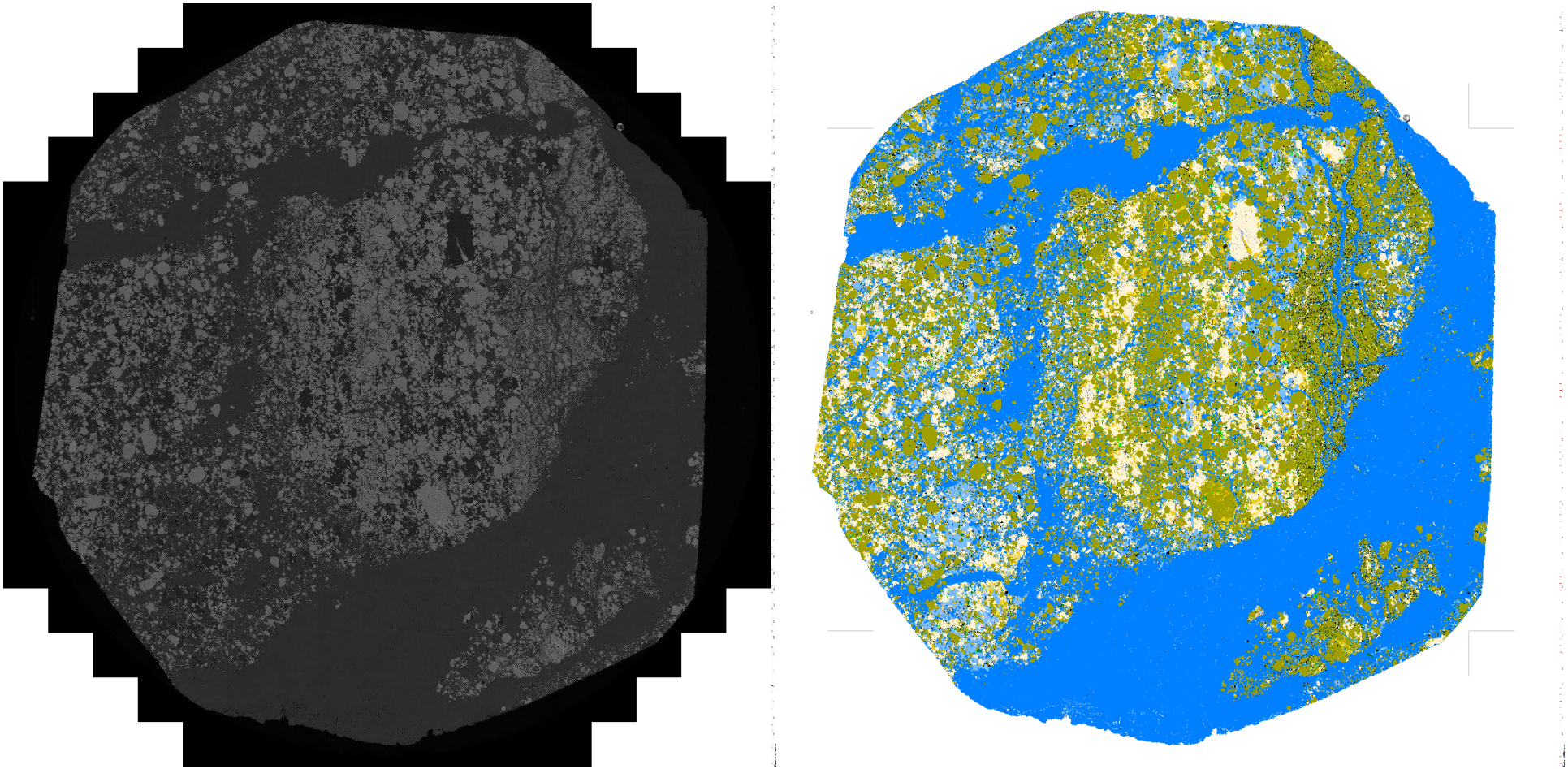

Figure 28 Backscattered electron (BSE) image (left) and Mineral Liberation Analysis (MLA) mineral map (right) of the sample 2022440121 from drill hole ADD-2 of the Grasmere prospect, Koonenberry Belt, New South Wales, Australia. See Figure 47 at the end of this document for the legend of minerals identified using Mineral Liberation Analysis (MLA) mapping.

Sample ID	Prospect	Borehole Name	From (m)	To (m)	Note
2022440122	Grasmere	ADD-2	159.15	159.35	Massive sulfide ore

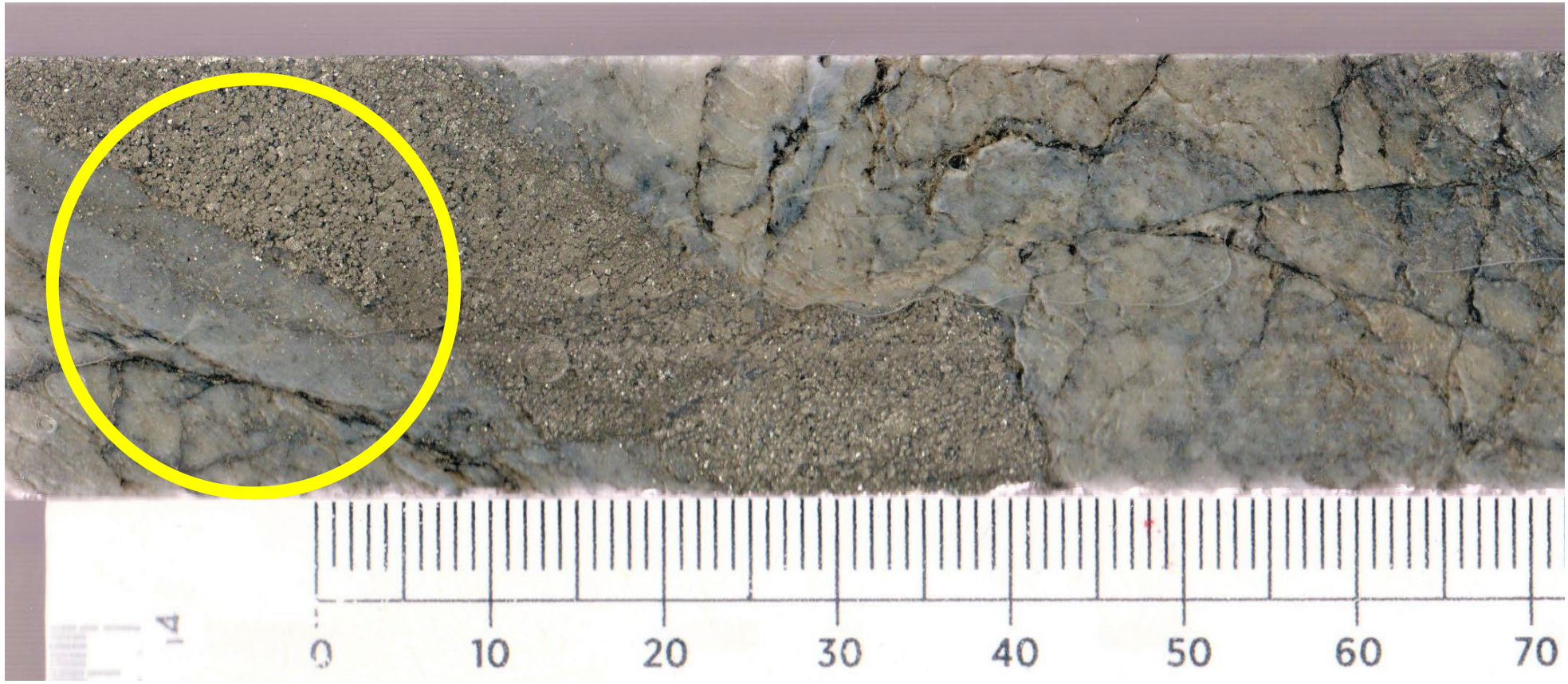

Figure 29 Photos of the drill core sample 2022440122 from drill hole ADD-2 of the Grasmere prospect, Koonenberry Belt, New South Wales, Australia.

Sample ID	Prospect	Borehole Name	From (m)	To (m)	Note
2022440122	Grasmere	ADD-2	159.15	159.35	Massive sulfide ore

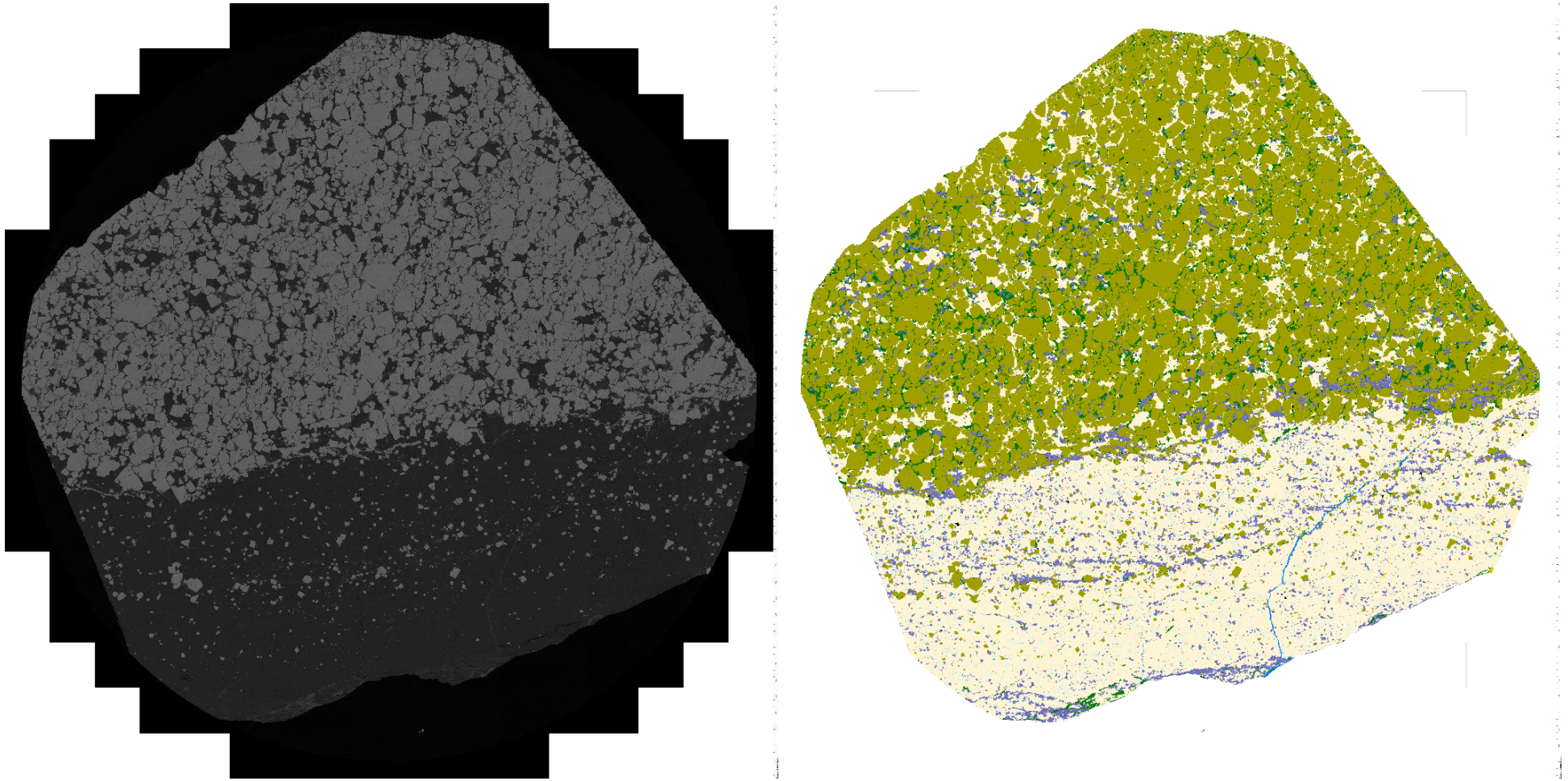

Figure 30 Backscattered electron (BSE) image (left) and Mineral Liberation Analysis (MLA) mineral map (right) of the sample 2022440122 from drill hole ADD-2 of the Grasmere prospect, Koonenberry Belt, New South Wales, Australia. See Figure 47 at the end of this document for the legend of minerals identified using Mineral Liberation Analysis (MLA) mapping.

Sample ID	Prospect	Borehole Name	From (m)	To (m)	Note
2022440068	Grasmere	DD88GR01	70.96	71.15	Massive sulfide ore

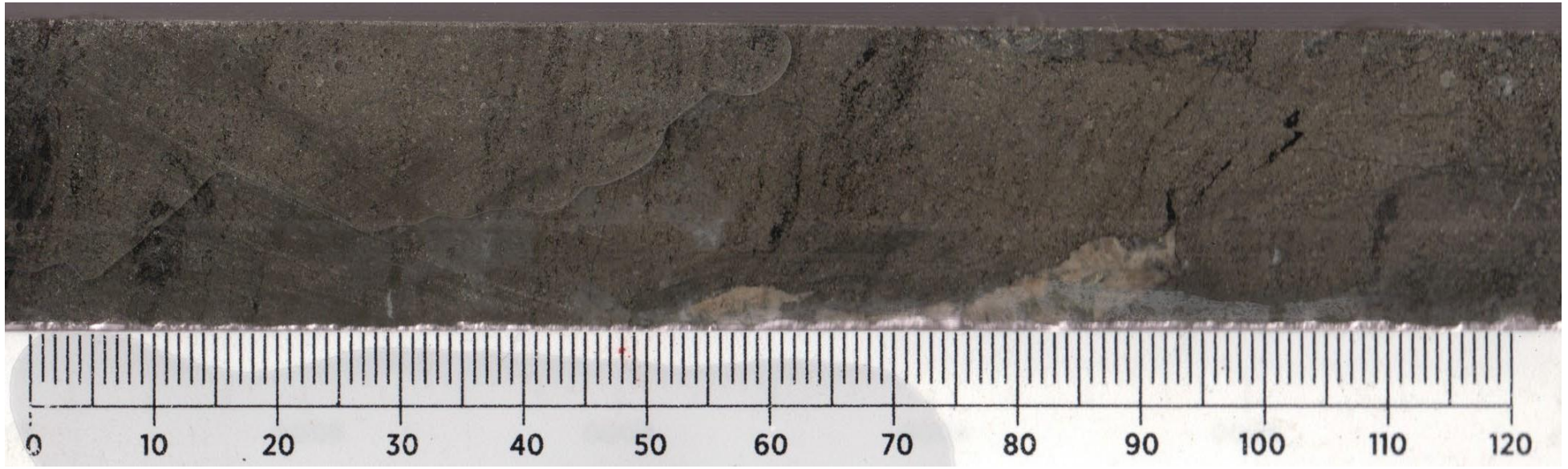

Figure 31 Photos of the drill core sample 2022440068 from drill hole DD88GR01 of the Grasmere prospect, Koonenberry Belt, New South Wales, Australia.

Sample ID	Prospect	Borehole Name	From (m)	To (m)	Note
2022440069	Grasmere	DD88GR01	71.9	72	Massive sulfide ore

Figure 32 Photos of the drill core sample 2022440069 from drill hole DD88GR01 of the Grasmere prospect, Koonenberry Belt, New South Wales, Australia.

Sample ID	Prospect	Borehole Name	From (m)	To (m)	Note
2022440070	Grasmere	DD88GR01	91.25	91.31	Massive sulfide ore

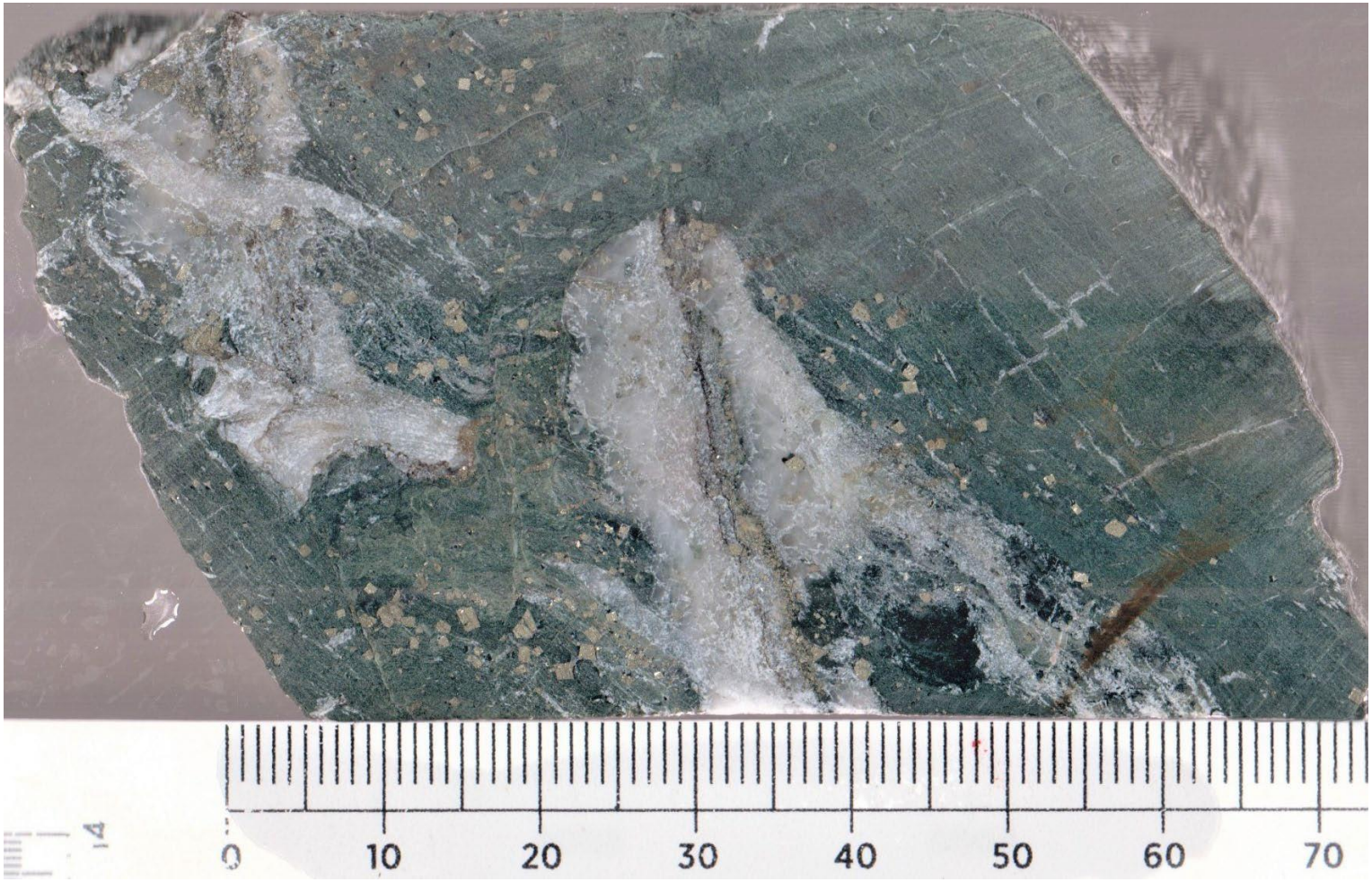

Figure 33 Photos of the drill core sample 2022440070 from drill hole DD88GR01 of the Grasmere prospect, Koonenberry Belt, New South Wales, Australia.

Sample ID	Prospect	Borehole Name	From (m)	To (m)	Note
2022440071	Grasmere	DD88GR01	101.51	101.67	Massive sulfide ore

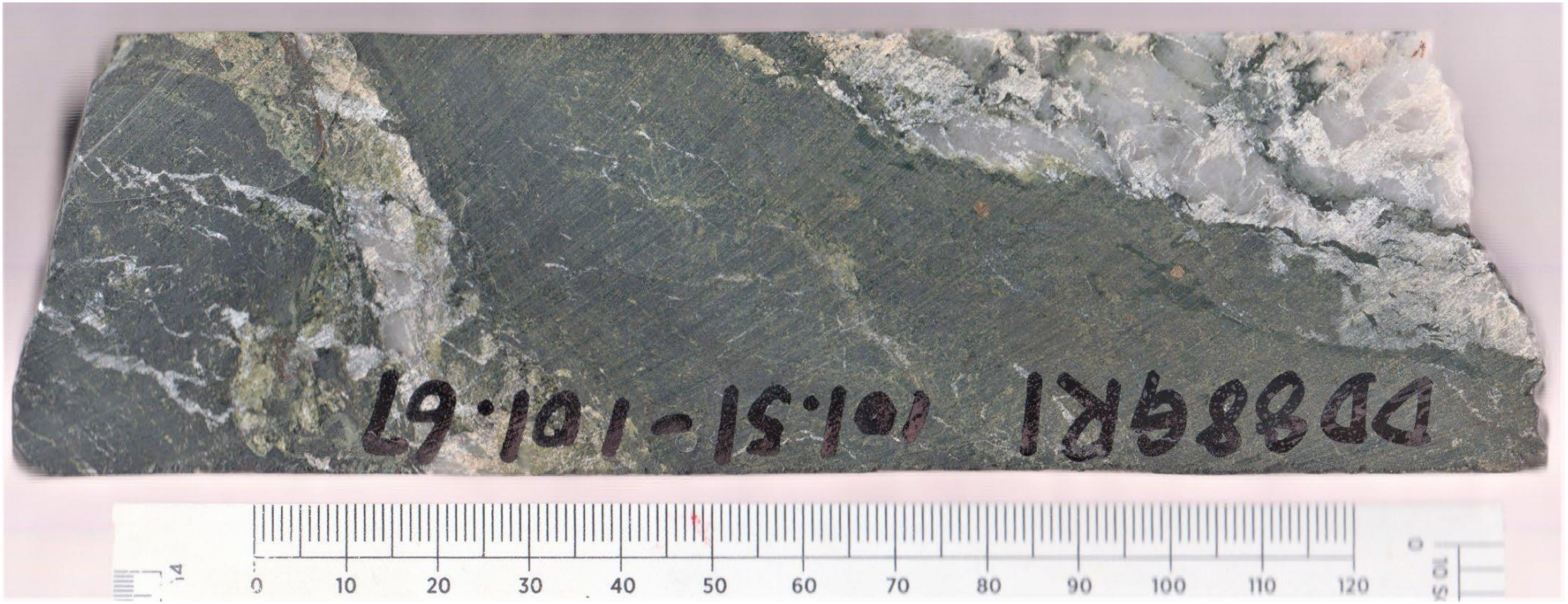

Figure 34 Photos of the drill core sample 2022440071 from drill hole DD88GR01 of the Grasmere prospect, Koonenberry Belt, New South Wales, Australia.

Sample ID	Prospect	Borehole Name	From (m)	To (m)	Note
2022440074	Grasmere	DD88GR01	128.09	128.26	Massive sulfide ore

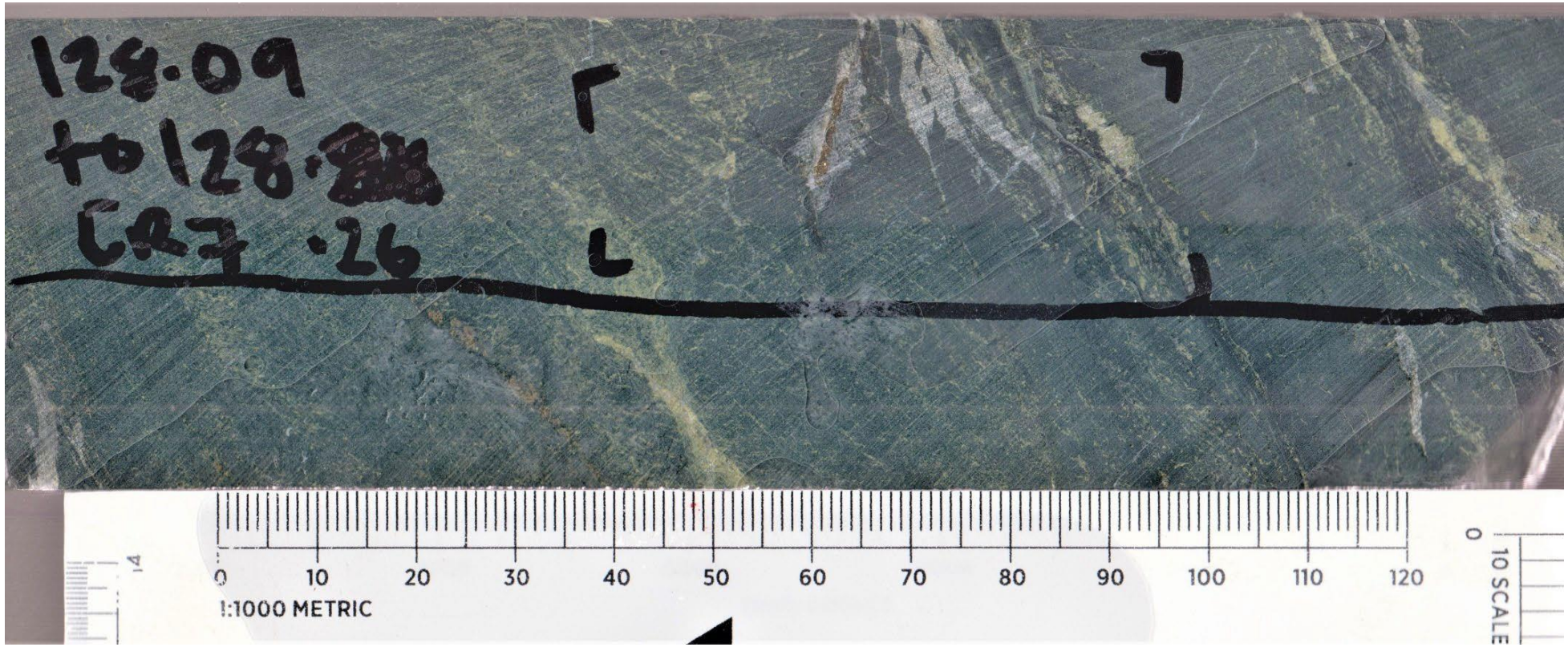

Figure 35 Photos of the drill core sample 2022440074 from drill hole DD88GR01 of the Grasmere prospect, Koonenberry Belt, New South Wales, Australia.

Sample ID	Prospect	Borehole Name	From (m)	To (m)	Note
2022440077	Grasmere	DD89GR05	125.05	125.17	Massive sulfide ore

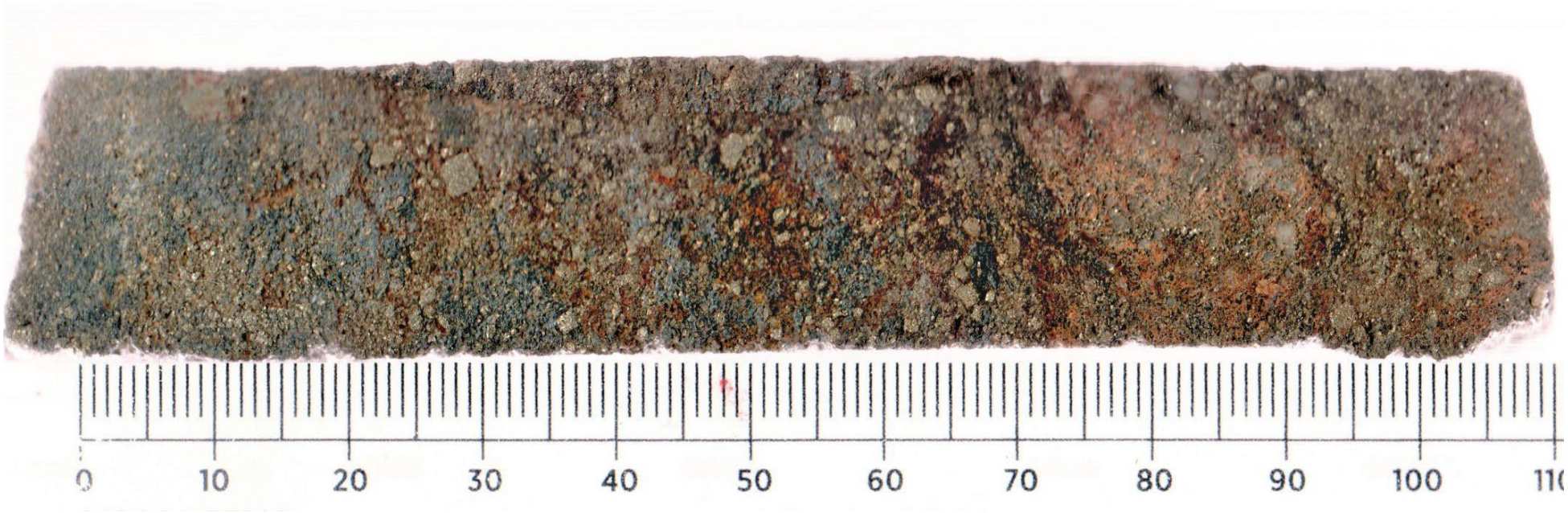

Figure 36 Photos of the drill core sample 2022440077 from drill hole DD88GR05 of the Grasmere prospect, Koonenberry Belt, New South Wales, Australia.

Sample ID	Prospect	Borehole Name	From (m)	To (m)	Note
2022440078	Grasmere	DD89GR05	125.45	125.5	Massive sulfide ore

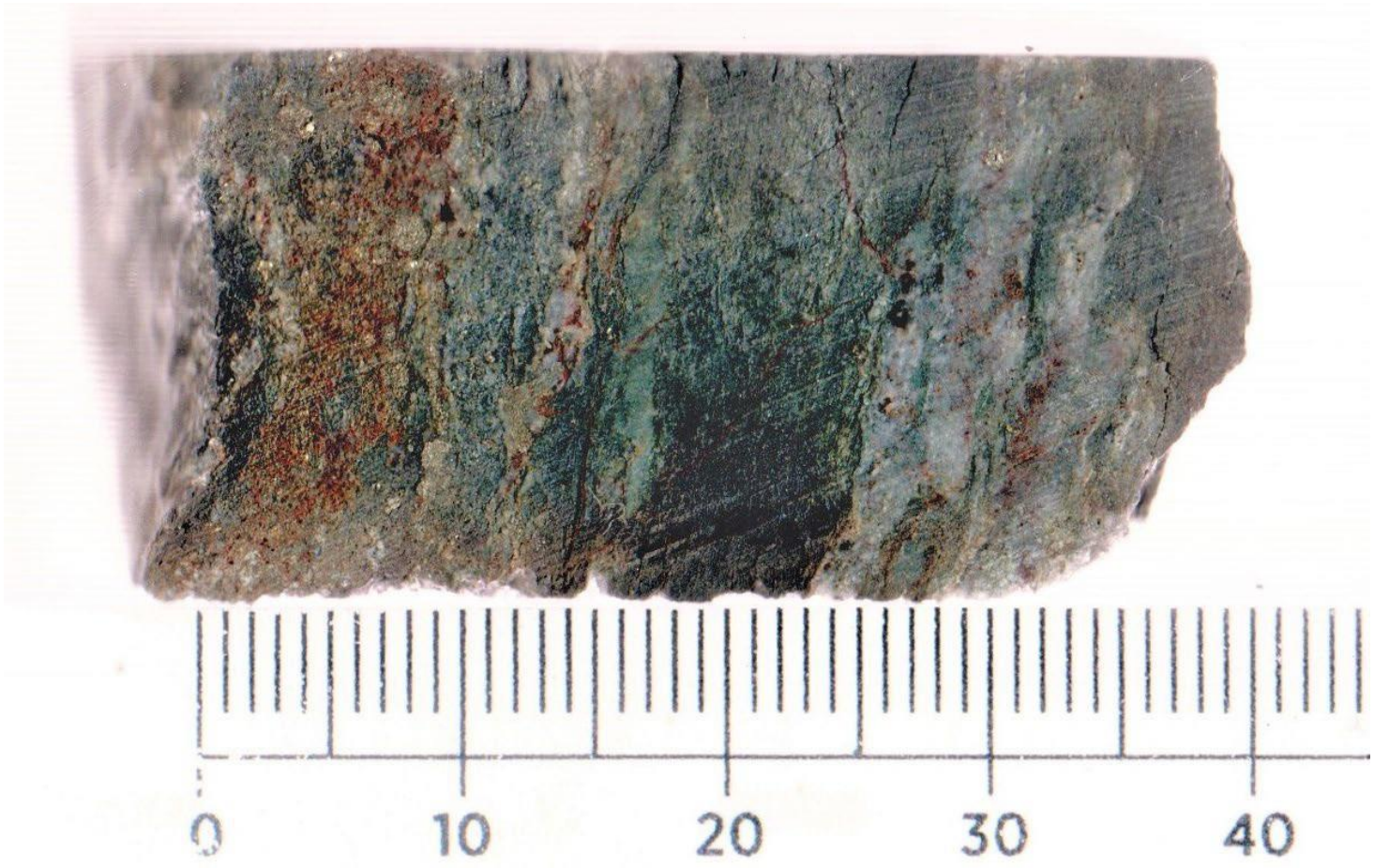

Figure 37 Photos of the drill core sample 2022440078 from drill hole DD88GR05 of the Grasmere prospect, Koonenberry Belt, New South Wales, Australia.

Sample ID	Prospect	Borehole Name	From (m)	To (m)	Note
2022440079	Grasmere	DD89GR05	127.3	127.45	Massive sulfide ore

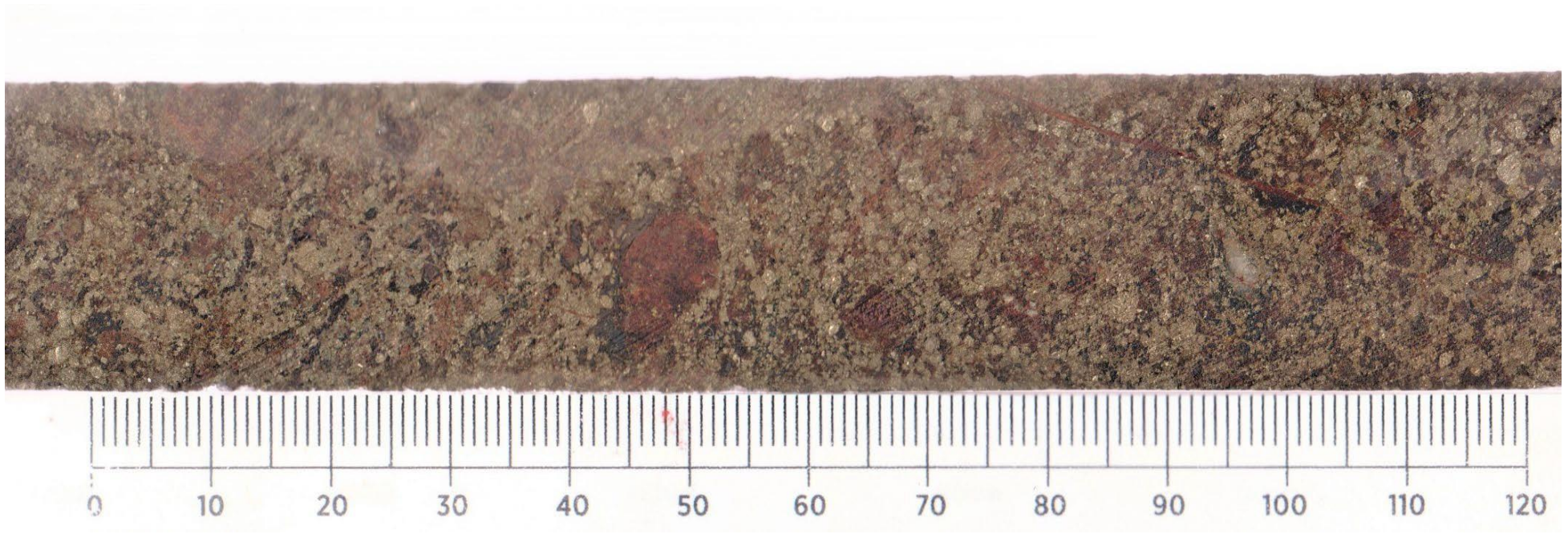

Figure 38 Photos of the drill core sample 2022440079 from drill hole DD88GR05 of the Grasmere prospect, Koonenberry Belt, New South Wales, Australia.

Sample ID	Prospect	Borehole Name	From (m)	To (m)	Note
2022440081	Grasmere	DD89GR05	129.4	129.45	Massive sulfide ore

Figure 39 Photos of the drill core sample 2022440081 from drill hole DD88GR05 of the Grasmere prospect, Koonenberry Belt, New South Wales, Australia.

Sample ID	Prospect	Borehole Name	From (m)	To (m)	Note
2022440082	Grasmere	DD90GR07	211.8	211.9	Massive sulfide ore

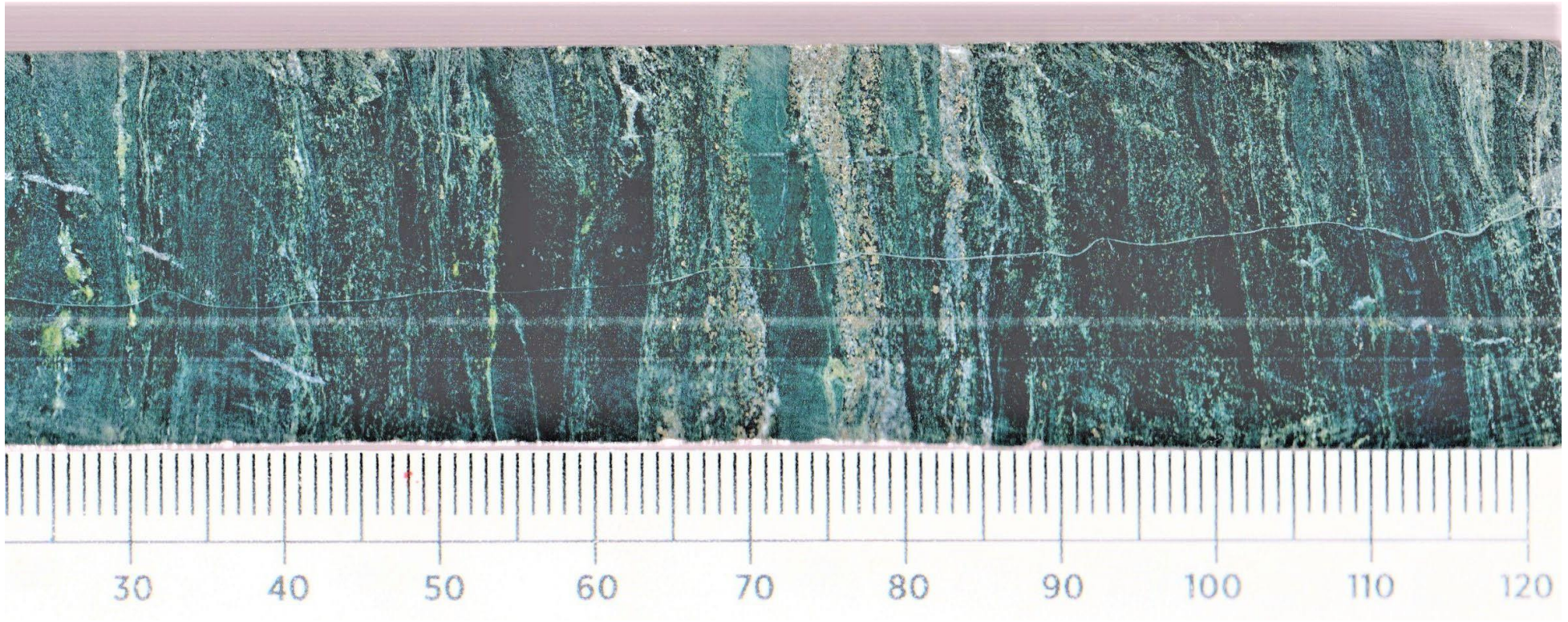

Figure 40 Photos of the drill core sample 2022440082 from drill hole DD88GR07 of the Grasmere prospect, Koonenberry Belt, New South Wales, Australia.

Sample ID	Prospect	Borehole Name	From (m)	To (m)	Note
2022440084	Grasmere	DD90GR07	219.35	219.45	Massive sulfide ore

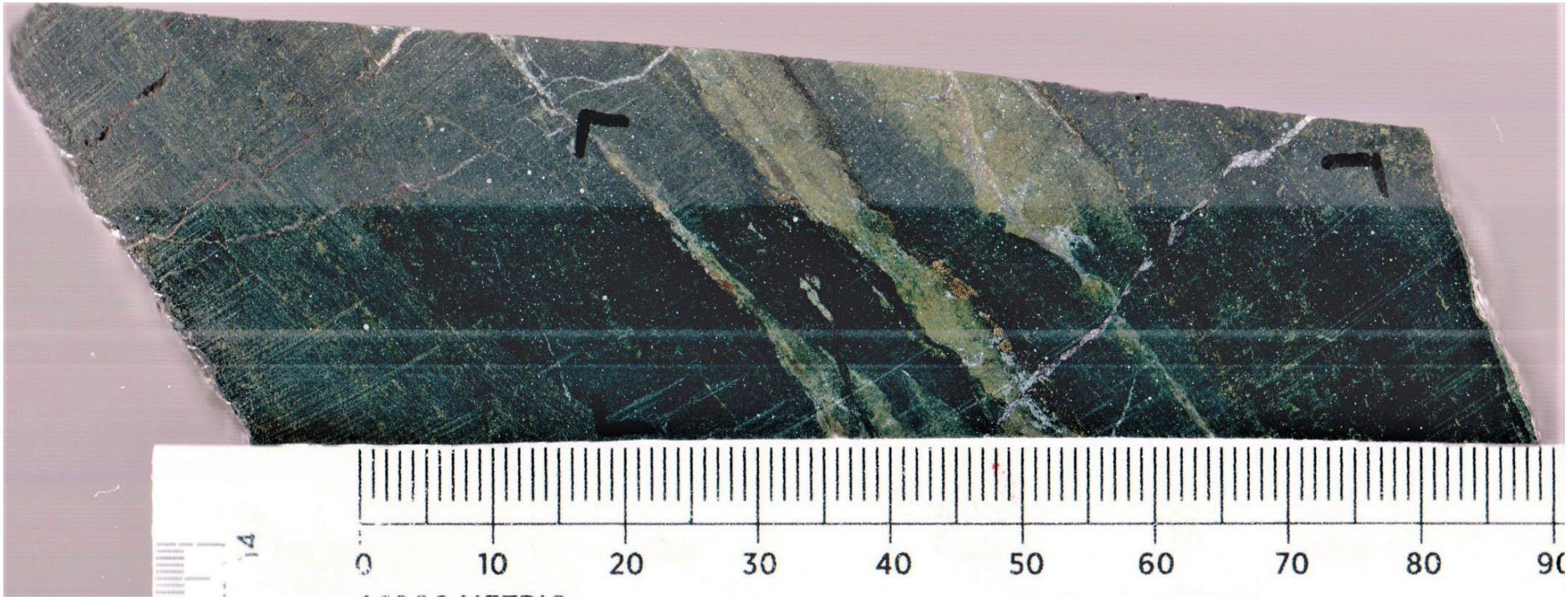

Figure 41 Photos of the drill core sample 2022440084 from drill hole DD88GR07 of the Grasmere prospect, Koonenberry Belt, New South Wales, Australia.

Sample ID	Prospect	Borehole Name	From (m)	To (m)	Note
2022440086	Grasmere	DD90GR07	228.9	229	Massive sulfide ore

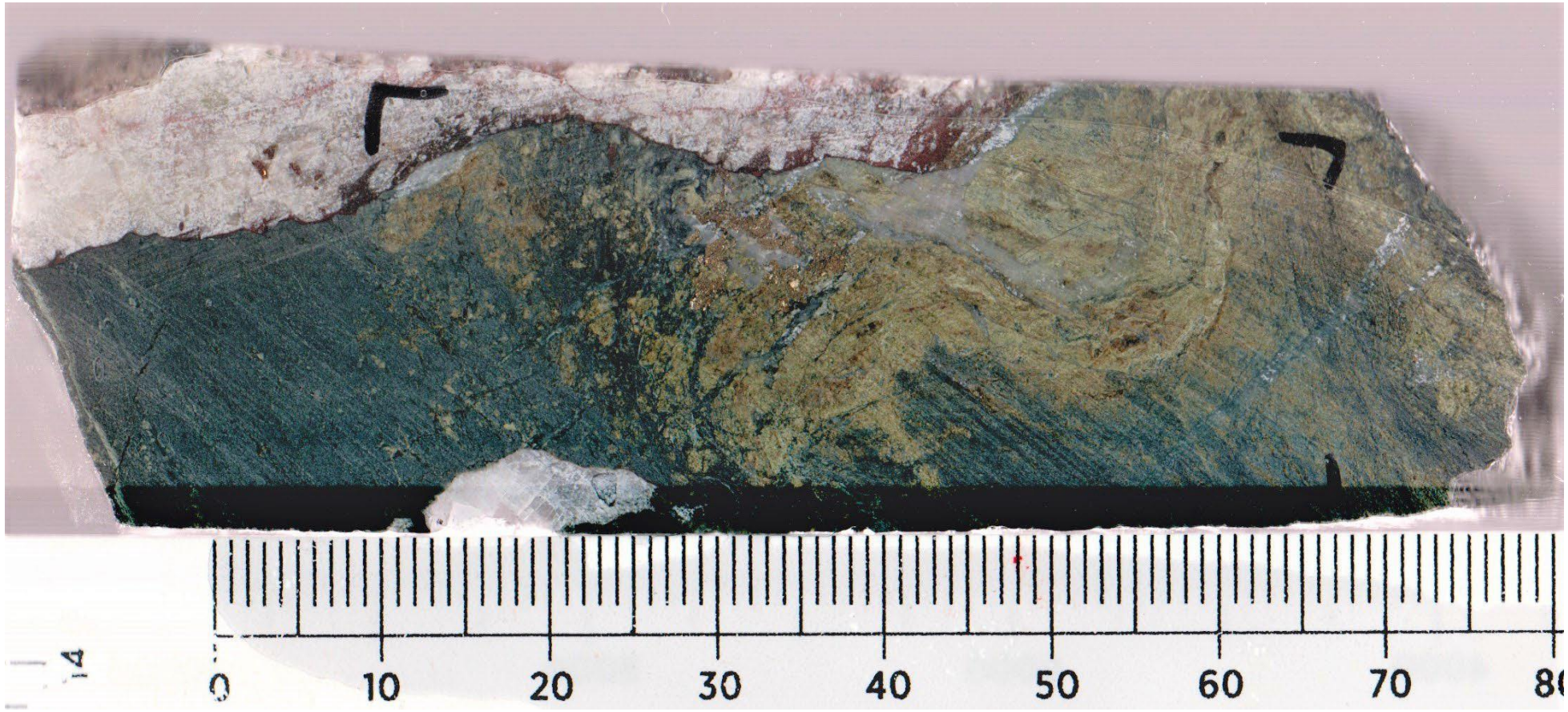

Figure 42 Photos of the drill core sample 2022440086 from drill hole DD88GR07 of the Grasmere prospect, Koonenberry Belt, New South Wales, Australia.

Sample ID	Prospect	Borehole Name	From (m)	To (m)	Note
2022440108	Grasmere	ADD-1	71.5	71.65	Massive sulfide ore

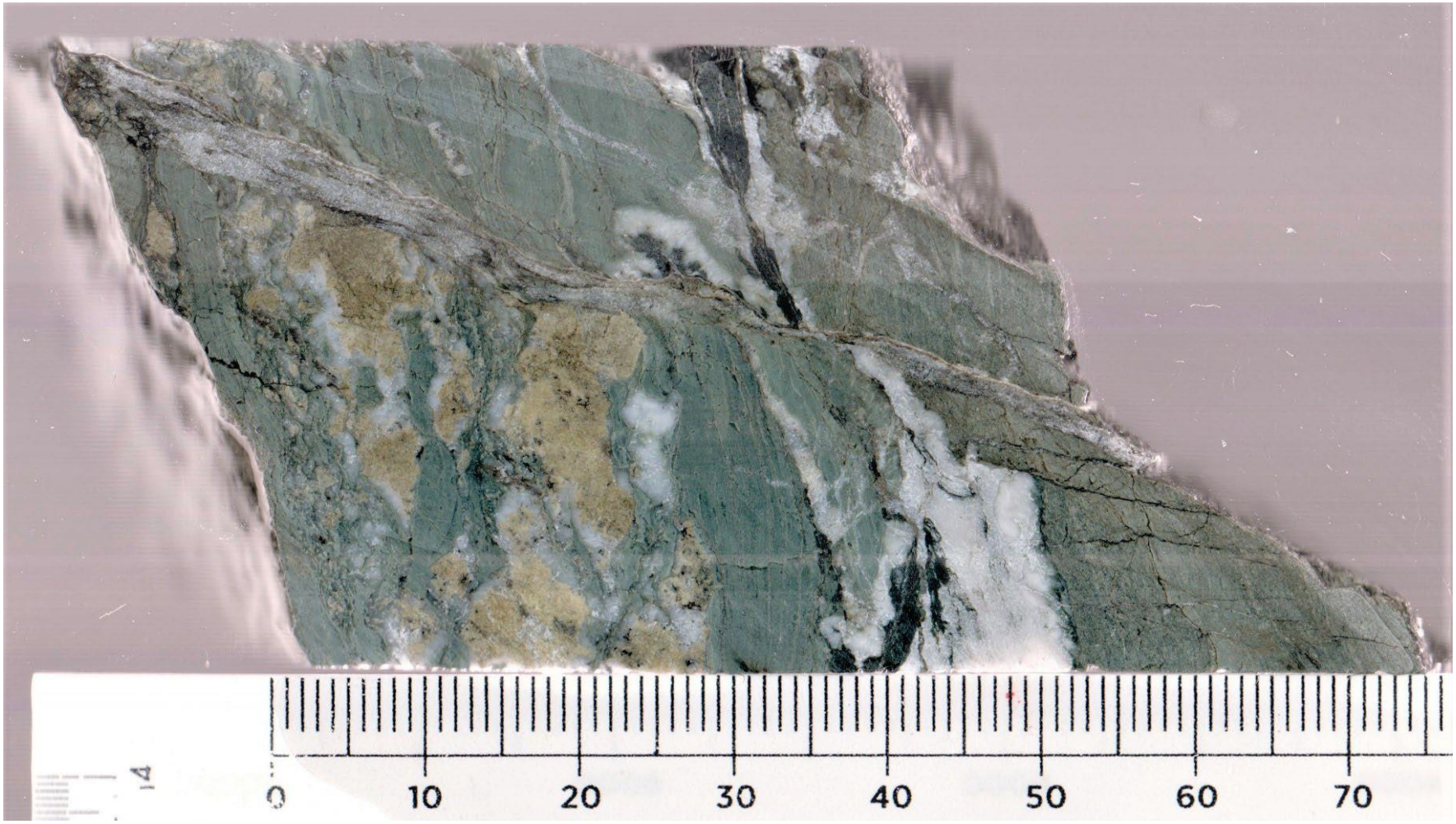

Figure 43 Photos of the drill core sample 2022440108 from drill hole ADD-1 of the Grasmere prospect, Koonenberry Belt, New South Wales, Australia.

Sample ID	Prospect	Borehole Name	From (m)	To (m)	Note
2022440111	Grasmere	ADD-1	82.9	83.05	Massive sulfide ore

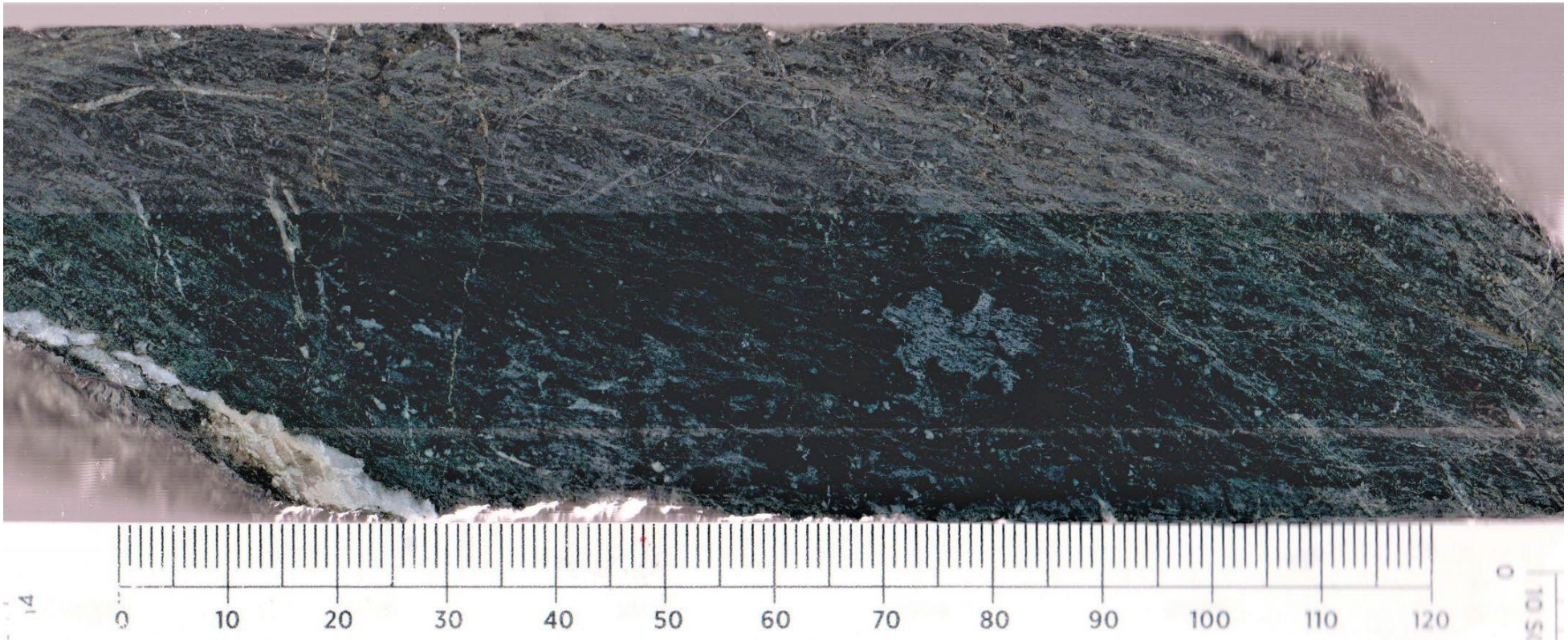

Figure 44 Photos of the drill core sample 2022440111 from drill hole ADD-1 of the Grasmere prospect, Koonenberry Belt, New South Wales, Australia.

Sample ID	Prospect	Borehole Name	From (m)	To (m)	Note
2022440114	Grasmere	ADD-1	236.6	236.8	Massive sulfide ore

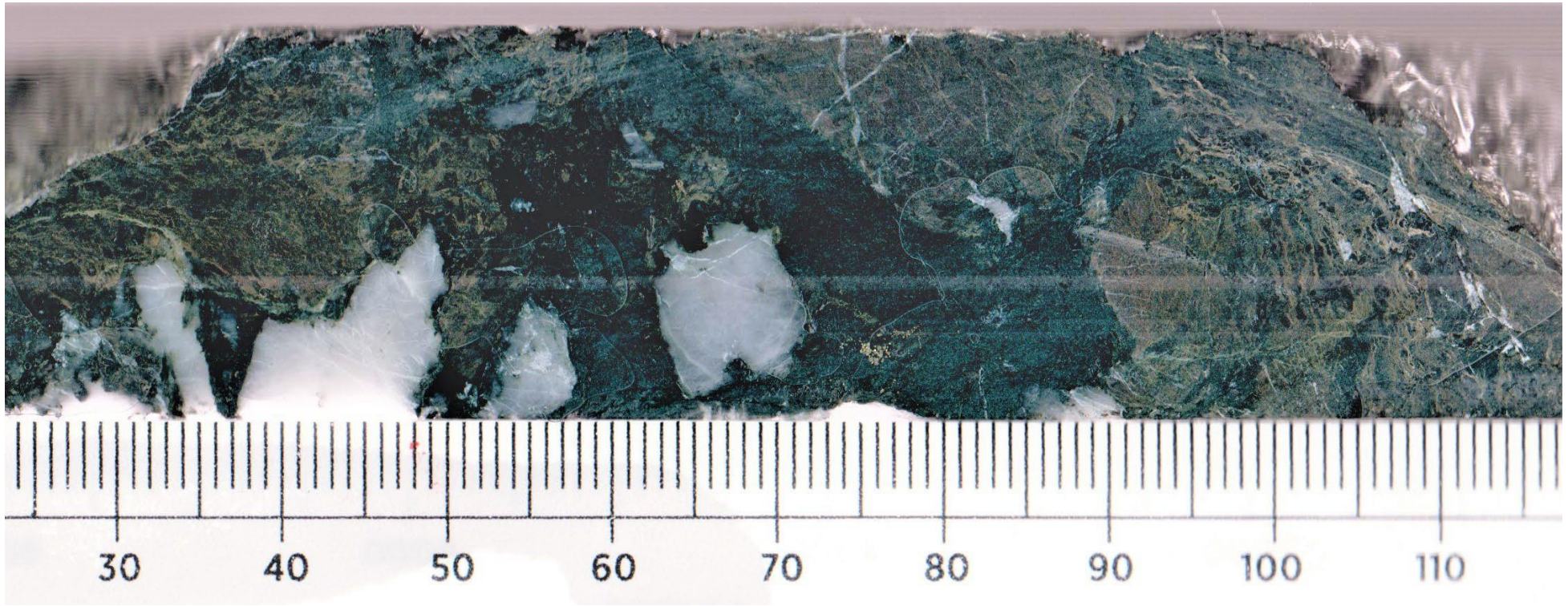

Figure 45 Photos of the drill core sample 2022440114 from drill hole ADD-1 of the Grasmere prospect, Koonenberry Belt, New South Wales, Australia.

Sample ID	Prospect	Borehole Name	From (m)	To (m)	Note
2022440118	Grasmere	ADD-1	254.86	255	Massive sulfide ore

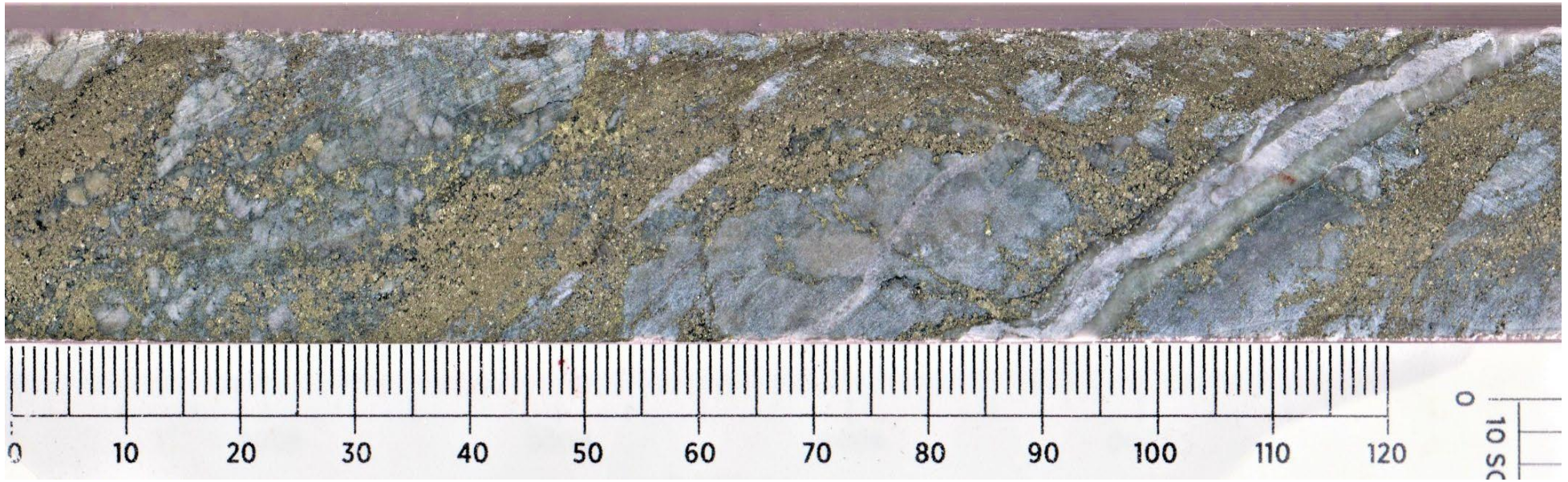

Figure 46 Photos of the drill core sample 2022440118 from drill hole ADD-1 of the Grasmere prospect, Koonenberry Belt, New South Wales, Australia.

S2.2 Eclipse prospect

Wertago Region, New South Wales

Detailed image data: Appendix 7 (individual data file)

(A) Sample List

Sample No.	Sample ID	Borehole	From (m)	To (m)	Notes
8012591b	2022440190	DDH2	414 ft	415 ft	Sulfide ore and hydrothermal alteration
—	2022440189	DDH2	224 ft	225 ft	Sulfide ore and hydrothermal alteration
—	2022440191	DDH2	—	—	Sulfide ore and hydrothermal alteration
—	2022440192	DDH2	—	—	Sulfide ore and hydrothermal alteration
—	2022440187	DDH2	—	—	Sulfide ore and hydrothermal alteration
—	2022440188	DDH2	—	—	Sulfide ore and hydrothermal alteration

(B) Mineralisation Characteristics

Data Type	Mineral Assemblage
Hyperspectral SWIR	—
Hyperspectral TIR	—
Hyperspectral VNIR	—
Drill core specimen	*Py, Qtz, Chl*
Thin section	—
AMICS mineral map	*Py, Qtz, Chl (MLA)*

(C) Mineralogical Textures and Paragenesis

Category	Description
Texture	Sulfide ore consists predominantly of pyrite with quartz and chlorite in legacy drill core intervals (depths recorded in feet, original DDH2 drilled pre-metric).
Paragenesis	Pyrite occurs as disseminated and vein-hosted grains within chlorite-altered host rocks. Quartz veining postdates main pyrite formation.

(D) Supplementary Figure Reference

Supplementary Figures *include drill core photographs of samples 2022440190, 2022440189, 2022440191, 2022440192, 2022440187 and 2022440188 from DDH2; BSE images and MLA mineral maps of Py–Qtz–Chl assemblage. MLA mineral standard legend included.*

S2.2 The Eclipse prospect, Wertago region, New South Wales

Sample ID	Prospect	Borehole Name	From (ft)	To (ft)	Note
2022440190	Eclipse	DDH2	414	415	Sulfide ore and hydrothermal alteration

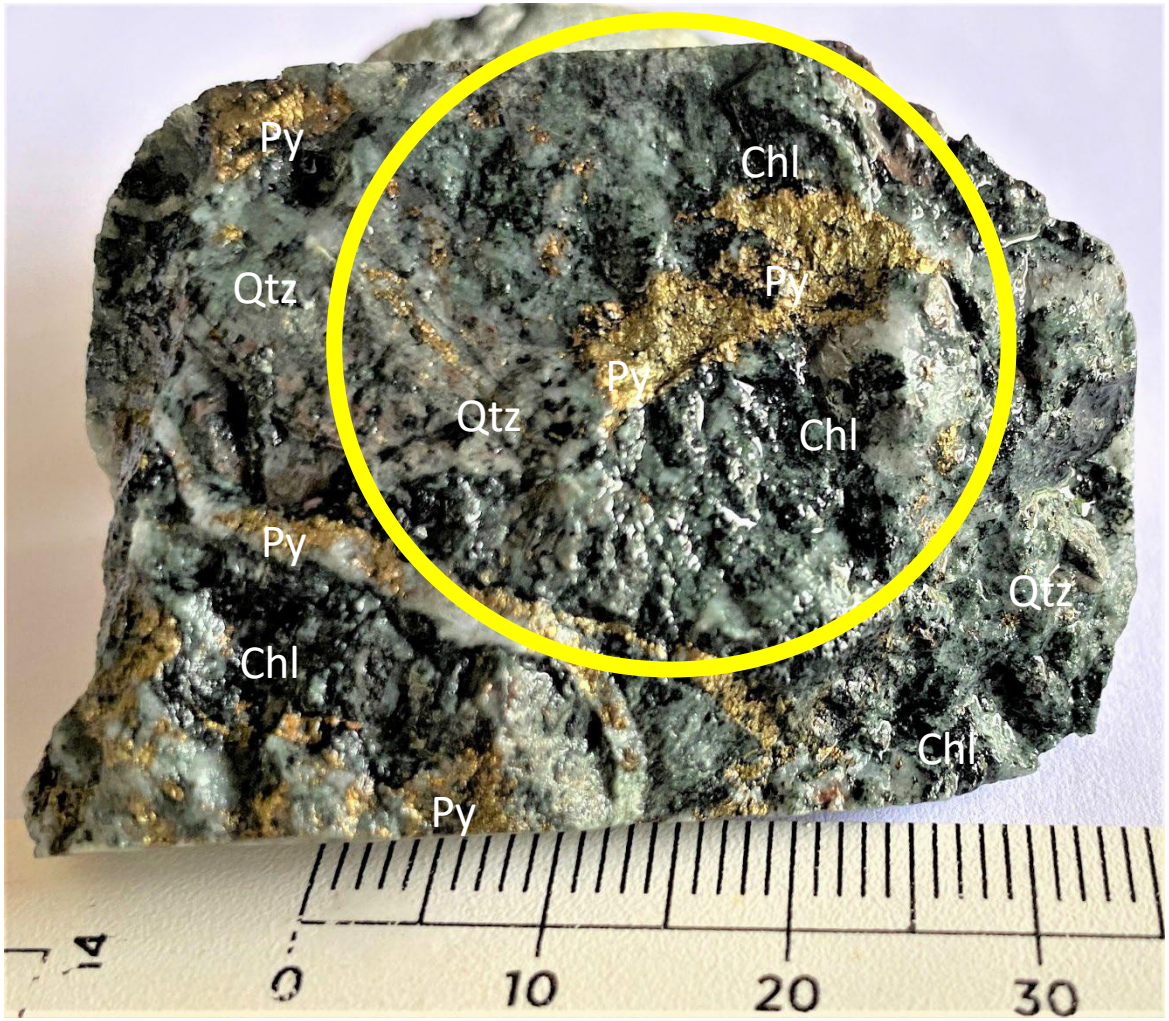

Figure 1 Photos of the drill core sample 2022440190 from drill hole DDH2 of the Eclipse prospect, Wertago region, New South Wales, Australia. Py-pyrite; Qtz-quartz; Chl-chlorite.

Sample ID	Prospect	Borehole Name	From (ft)	To (ft)	Note
2022440190	Eclipse	DDH2	414	415	Sulfide ore and hydrothermal alteration

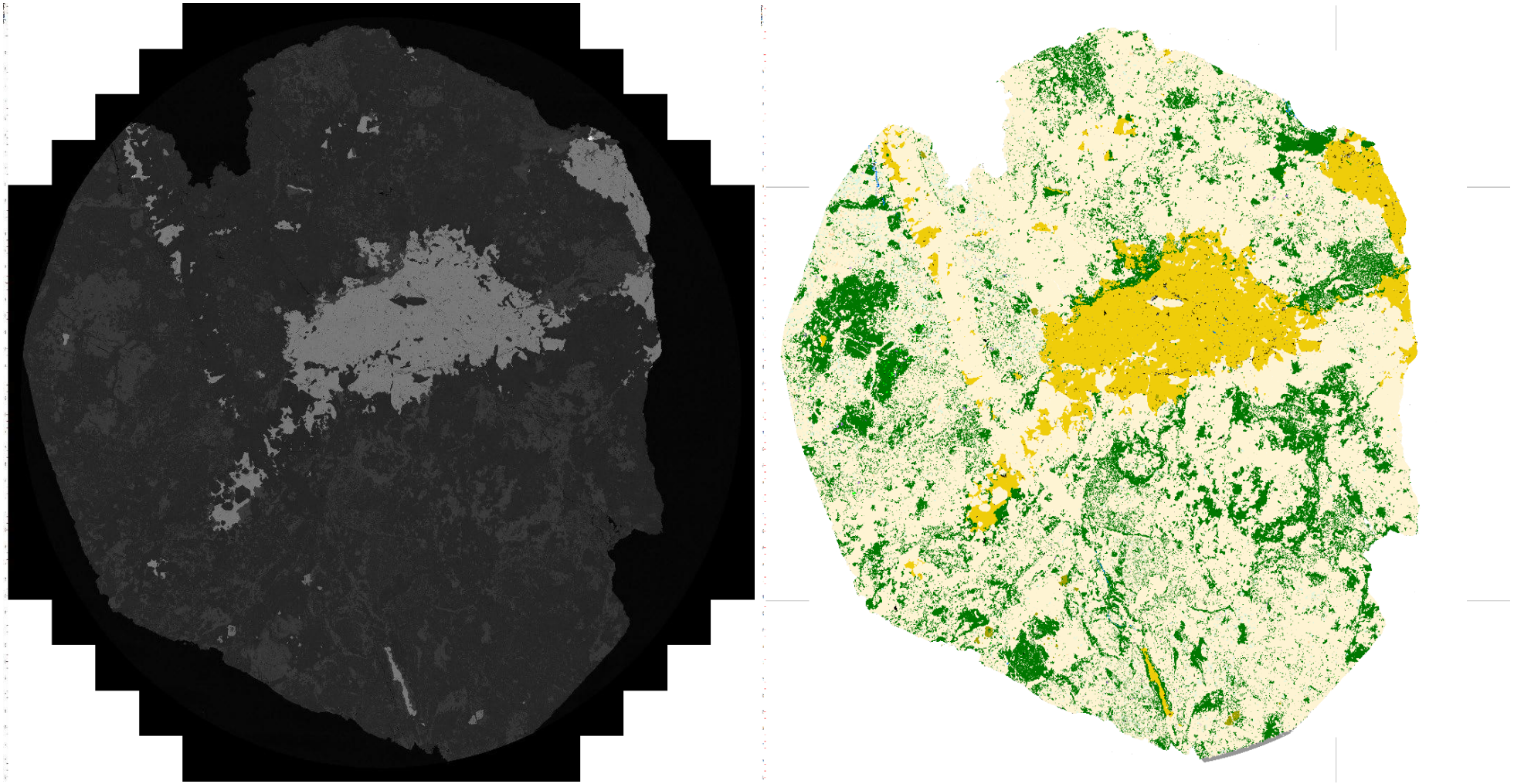

Figure 2 Backscattered electron (BSE) image (left) and Mineral Liberation Analysis (MLA) mineral map (right) of the sample 2022440190 from drill hole DDH2 of the Eclipse prospect, Wertago region, New South Wales, Australia. See Figure 10 at the end of this document for the legend of minerals identified using Mineral Liberation Analysis (MLA) mapping.

Sample ID	Prospect	Borehole Name	From (ft)	To (ft)	Note
2022440189	Eclipse	DDH2	224	225	Sulfide ore and hydrothermal alteration

Figure 3 Photos of the drill core sample 2022440189 from drill hole DDH2 of the Eclipse prospect, Wertago region, New South Wales, Australia.

Sample ID	Prospect	Borehole Name	From (ft)	To (ft)	Note
2022440189	Eclipse	DDH2	224	225	Sulfide ore and hydrothermal alteration

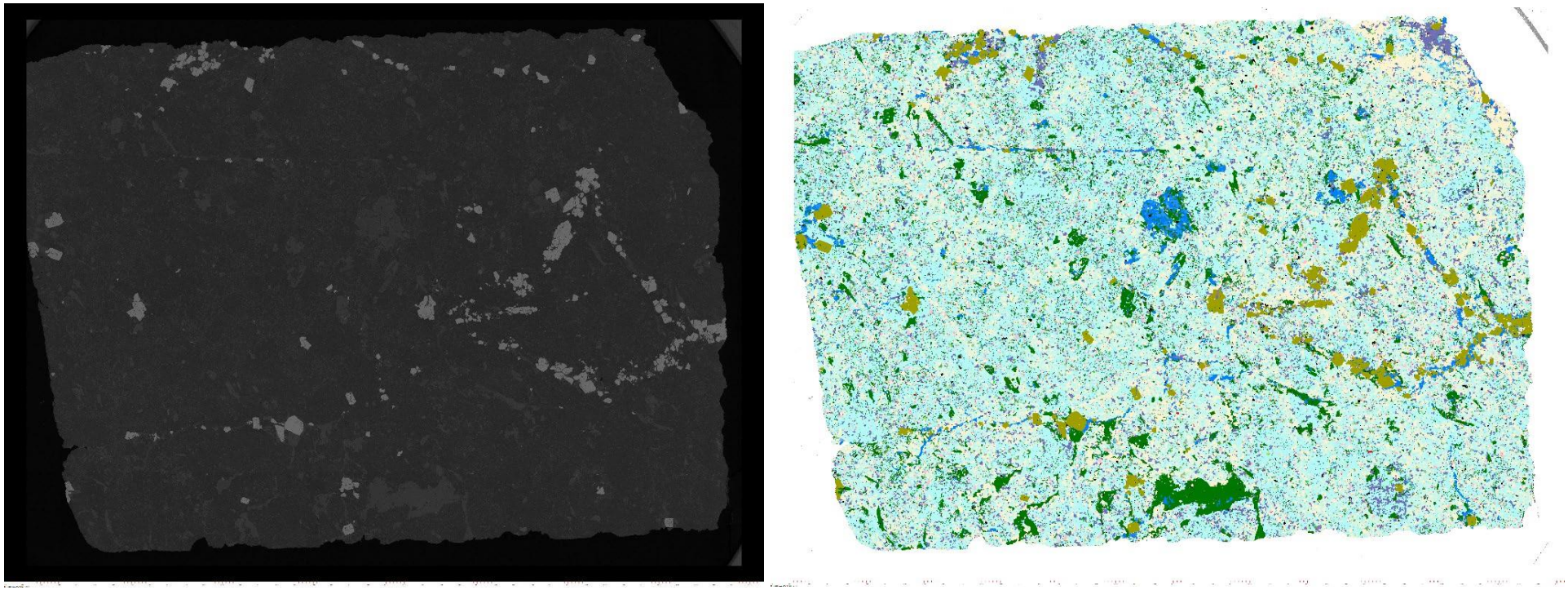

Figure 4 Backscattered electron (BSE) image (left) and Mineral Liberation Analysis (MLA) mineral map (right) of the sample 2022440189 from drill hole DDH2 of the Eclipse prospect, Wertago region, New South Wales, Australia. See Figure 10 at the end of this document for the legend of minerals identified using Mineral Liberation Analysis (MLA) mapping.

Sample ID	Prospect	Borehole Name	From (ft)	To (ft)	Note
2022440191	Eclipse	DDH2	429	430	Sulfide ore and hydrothermal alteration

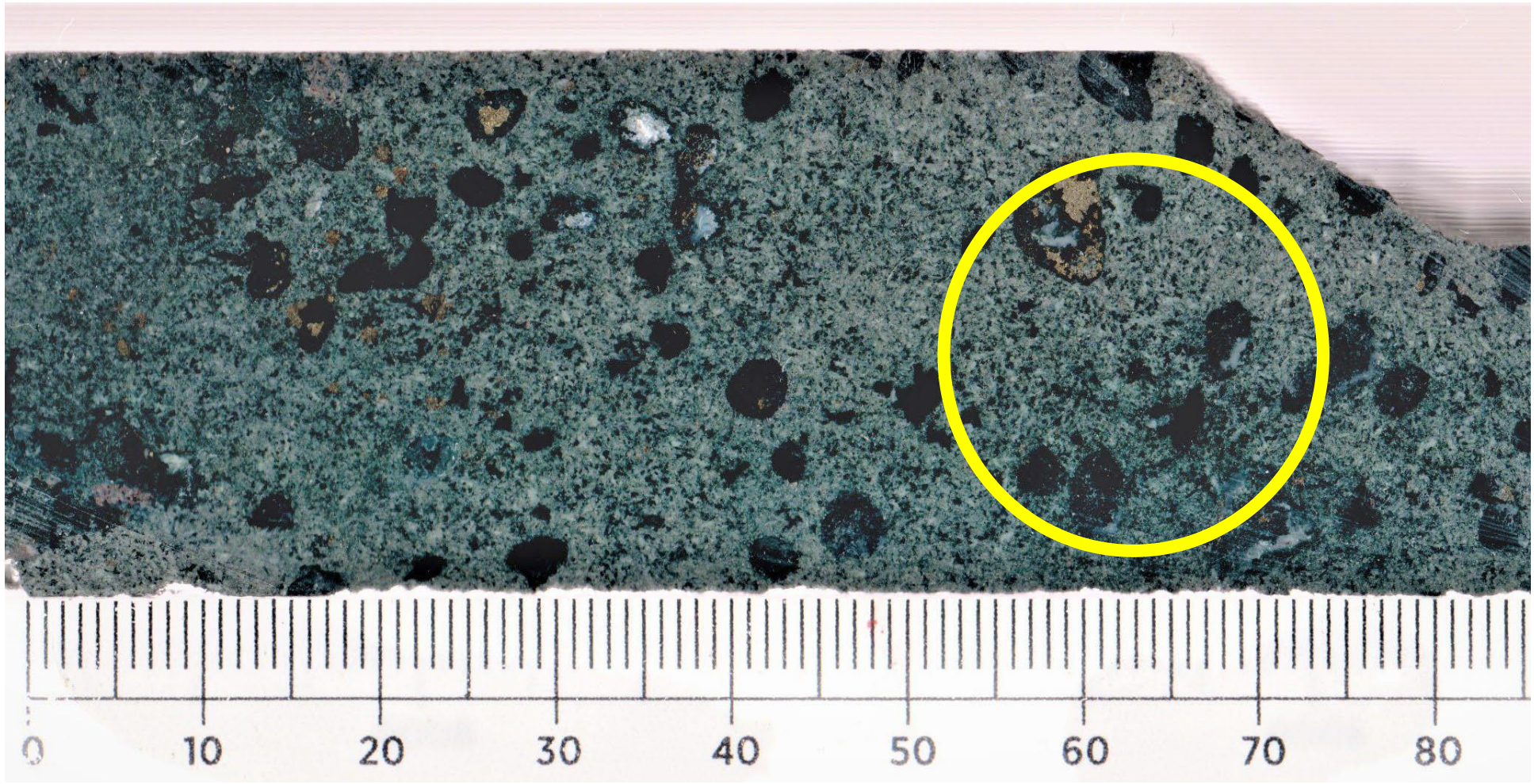

Figure 5 Photos of the drill core sample 2022440191 from drill hole DDH2 of the Eclipse prospect, Wertago region, New South Wales, Australia.

Sample ID	Prospect	Borehole Name	From (ft)	To (ft)	Note
2022440191	Eclipse	DDH2	429	430	Sulfide ore and hydrothermal alteration

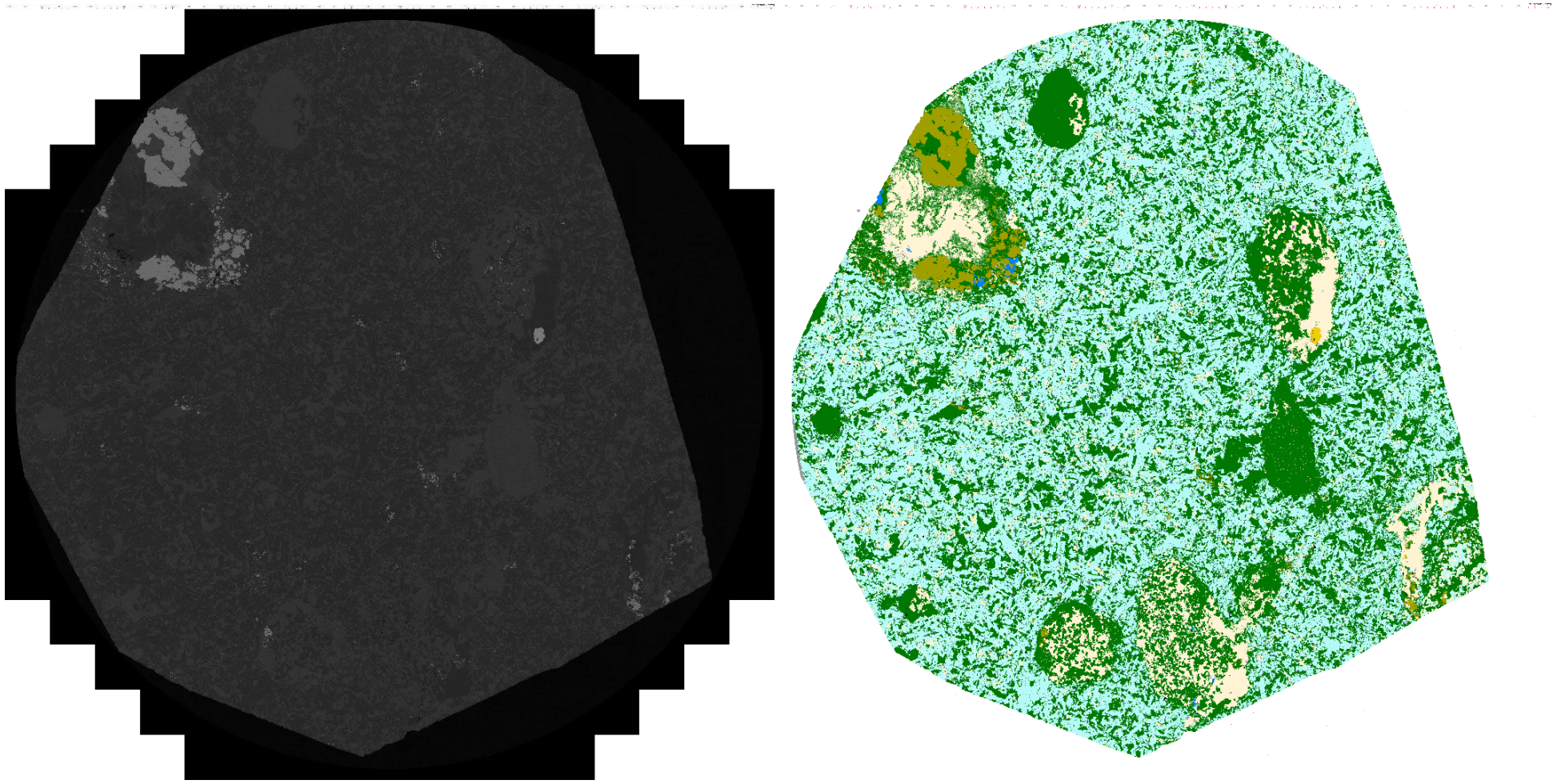

Figure 6 Backscattered electron (BSE) image (left) and Mineral Liberation Analysis (MLA) mineral map (right) of the sample 2022440191 from drill hole DDH2 of the Eclipse prospect, Wertago region, New South Wales, Australia. See Figure 10 at the end of this document for the legend of minerals identified using Mineral Liberation Analysis (MLA) mapping.

Sample ID	Prospect	Borehole Name	From (ft)	To (ft)	Note
2022440192	Eclipse	DDH2	443	444	Sulfide ore and hydrothermal alteration

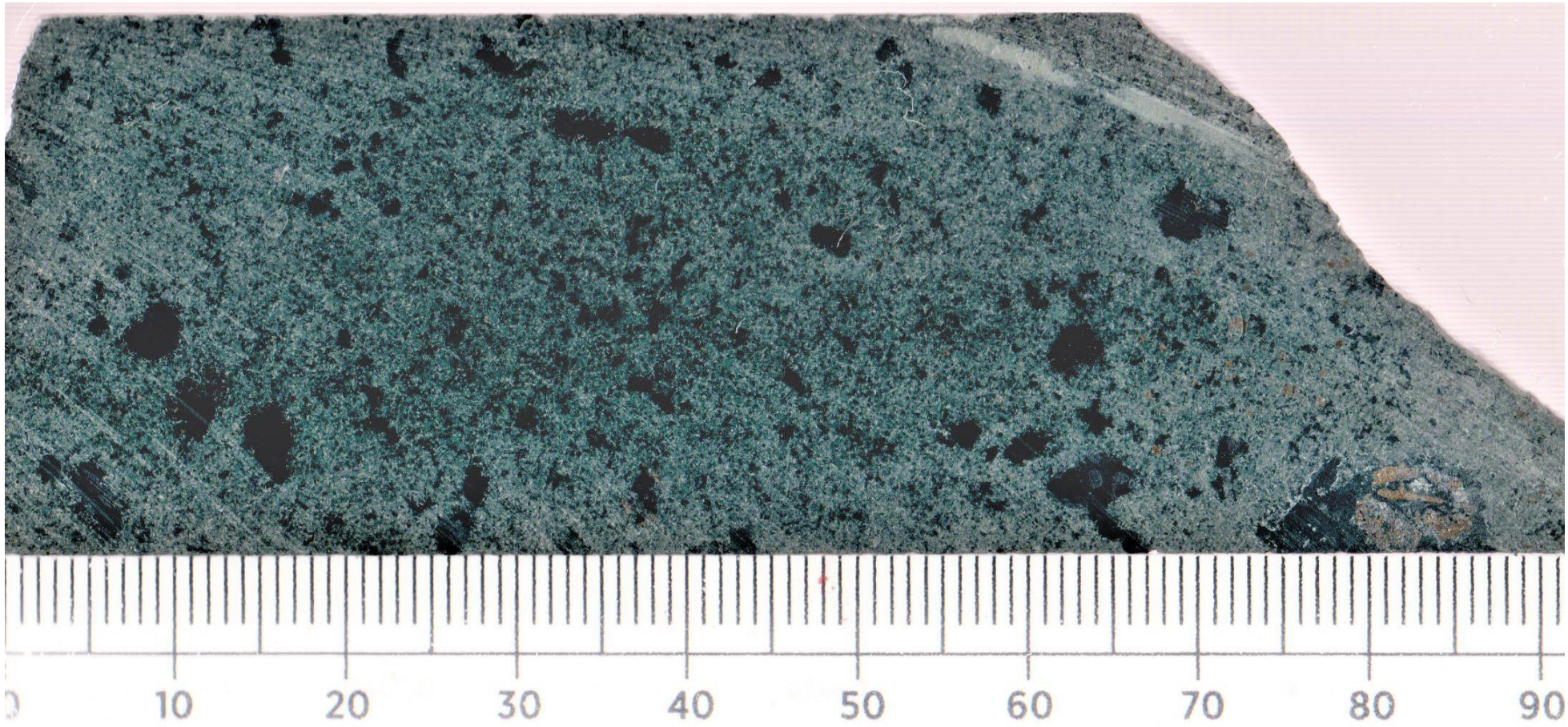

Figure 7 Photos of the drill core sample 2022440192 from drill hole DDH2 of the Eclipse prospect, Wertago region, New South Wales, Australia.

Sample ID	Prospect	Borehole Name	From (ft)	To (ft)	Note
2022440187	Eclipse	DDH2	129	130	Sulfide ore and hydrothermal alteration

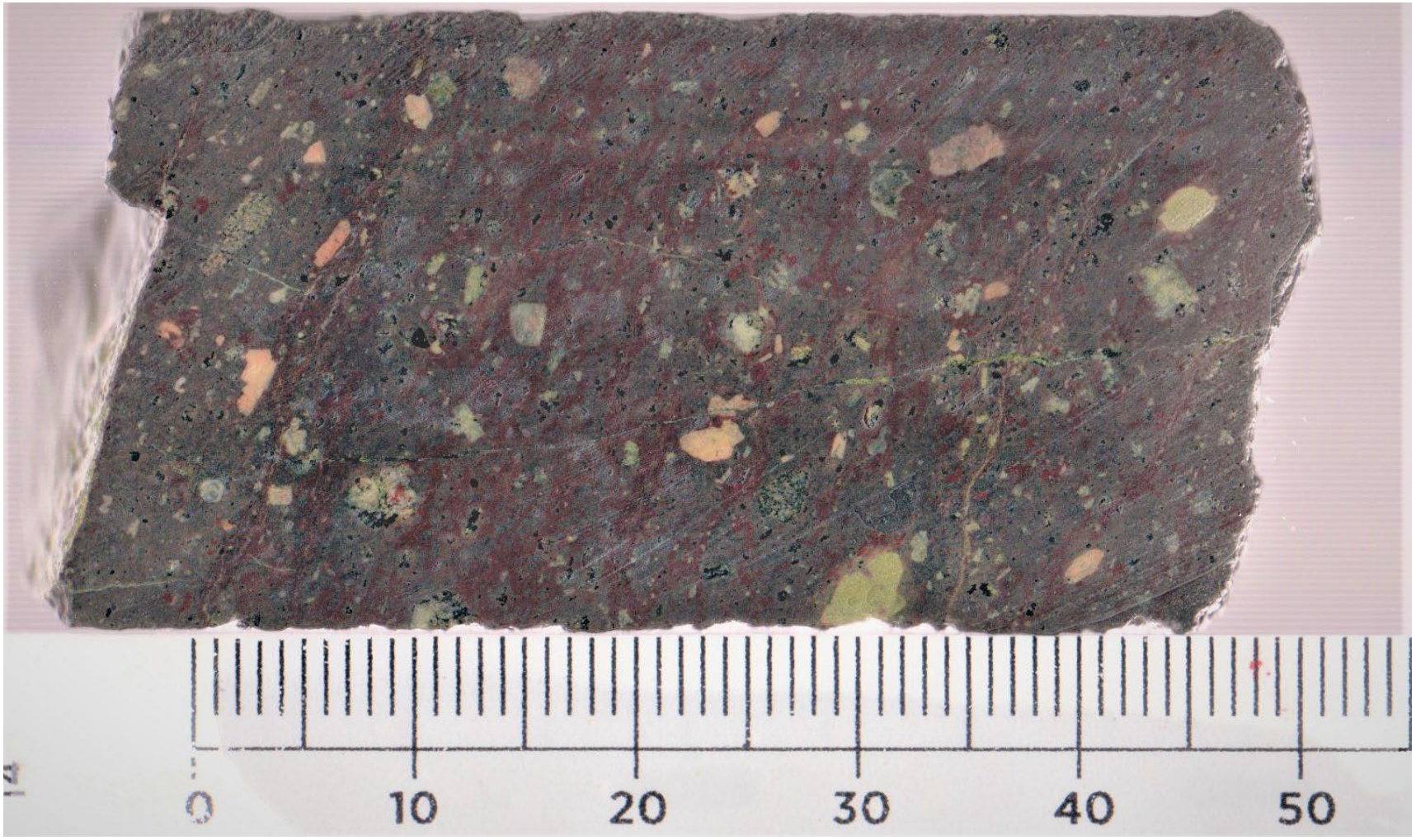

Figure 8 Photos of the drill core sample 2022440187 from drill hole DDH2 of the Eclipse prospect, Wertago region, New South Wales, Australia.

Sample ID	Prospect	Borehole Name	From (ft)	To (ft)	Note
2022440188	Eclipse	DDH2	215	216	Sulfide ore and hydrothermal alteration

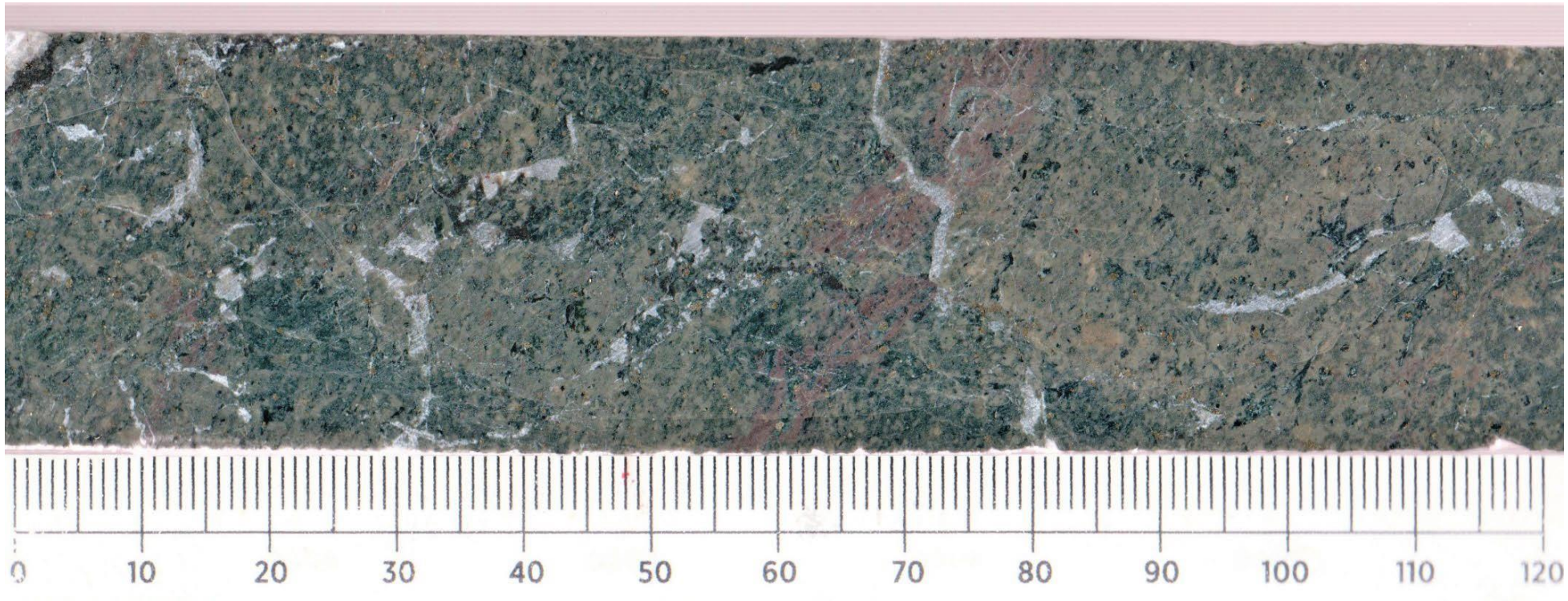

Figure 9 Photos of the drill core sample 2022440188 from drill hole DDH2 of the Eclipse prospect, Wertago region, New South Wales, Australia.

S2.3 Bunker Hill prospect

Wertago Region, New South Wales

Detailed image data: Appendix 8 (individual data file)

(A) Sample List

Sample No.	Sample ID	Borehole	From (m)	To (m)	Notes
8012540b	2022440196	DDH2	355 ft	355.5 ft	Sulfide ore and hydrothermal alteration
—	2022330193	DDH2	—	—	Sulfide ore and hydrothermal alteration
—	2022330194	DDH2	—	—	Sulfide ore and hydrothermal alteration
—	2022330195	DDH2	—	—	Sulfide ore and hydrothermal alteration
—	2022330197	DDH3	—	—	Sulfide ore and hydrothermal alteration

(B) Mineralisation Characteristics

Data Type	Mineral Assemblage
Hyperspectral SWIR	—
Hyperspectral TIR	—
Hyperspectral VNIR	—
Drill core specimen	*Py, Ab, Cal, Kfsp, Qtz, Chl*
Thin section	—
AMICS mineral map	*Py, Ab, Cal, Kfsp, Qtz, Chl (AMICS)*

(C) Mineralogical Textures and Paragenesis

Category	Description
Texture	Pyrite-dominated sulfide mineralisation hosted in albite–K-feldspar–quartz–calcite–chlorite alteration assemblage. Legacy drill core (depths in feet).
Paragenesis	Albite and K-feldspar represent early potassic alteration. Chlorite–calcite overprints the earlier feldspar alteration. Pyrite is associated with both alteration stages.

(D) Supplementary Figure Reference

Supplementary Figures *include (1) Downhole HyLogger hyperspectral image and summary of drill hole DD3; (2) Drill core photographs of samples 2022330196, 2022330193–2022330195 and 2022330197; BSE and AMICS mineral maps. AMICS mineral standard legend included.*

S2.3 The Bunker Hill prospect, Wertago region, New South Wales

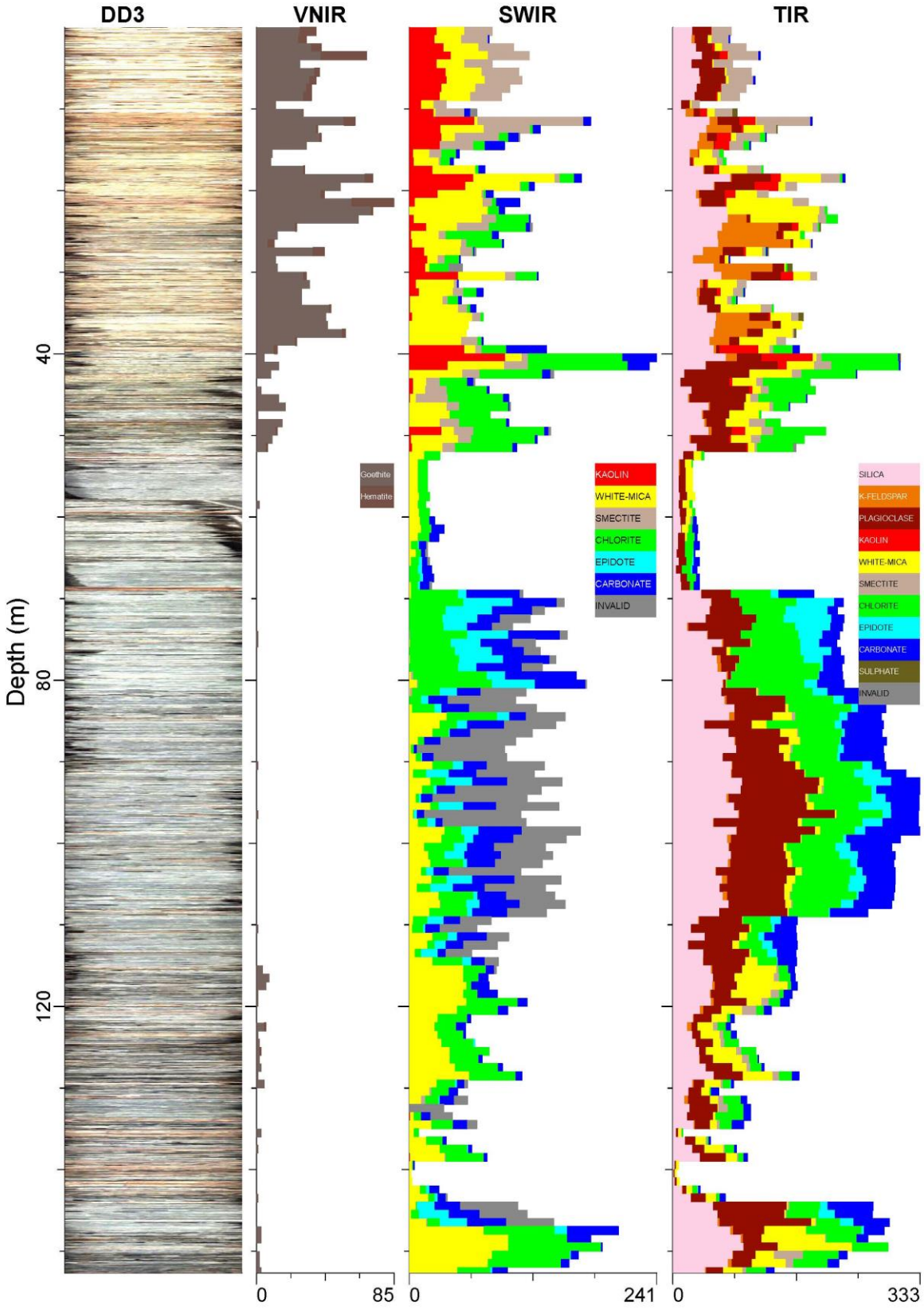

Figure 1 Downhole hylogger hyperspectral image of the hole DD3 of the Bunker Hill prospect, Wertago region, New South Wales, Australia.

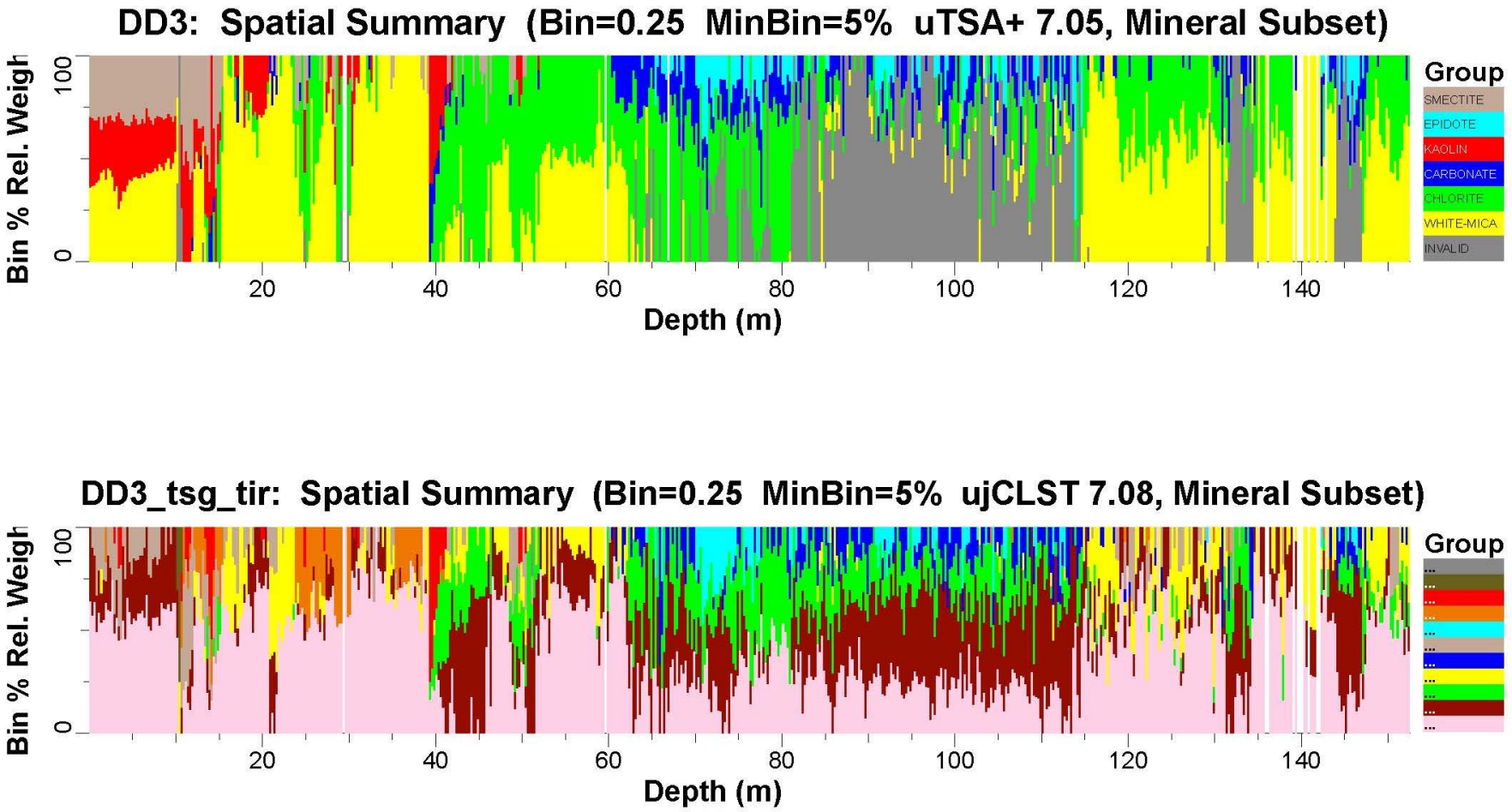

Figure 2 Summary of the hylogger hyperspectral image of the hole DD3 of the Bunker Hill prospect, Wertago region, New South Wales, Australia.

Sample ID	Prospect	Borehole Name	From (ft)	To (ft)	Note
2022440196	Bunker Hill	DDH2	355	355.5	Sulfide ore and hydrothermal alteration

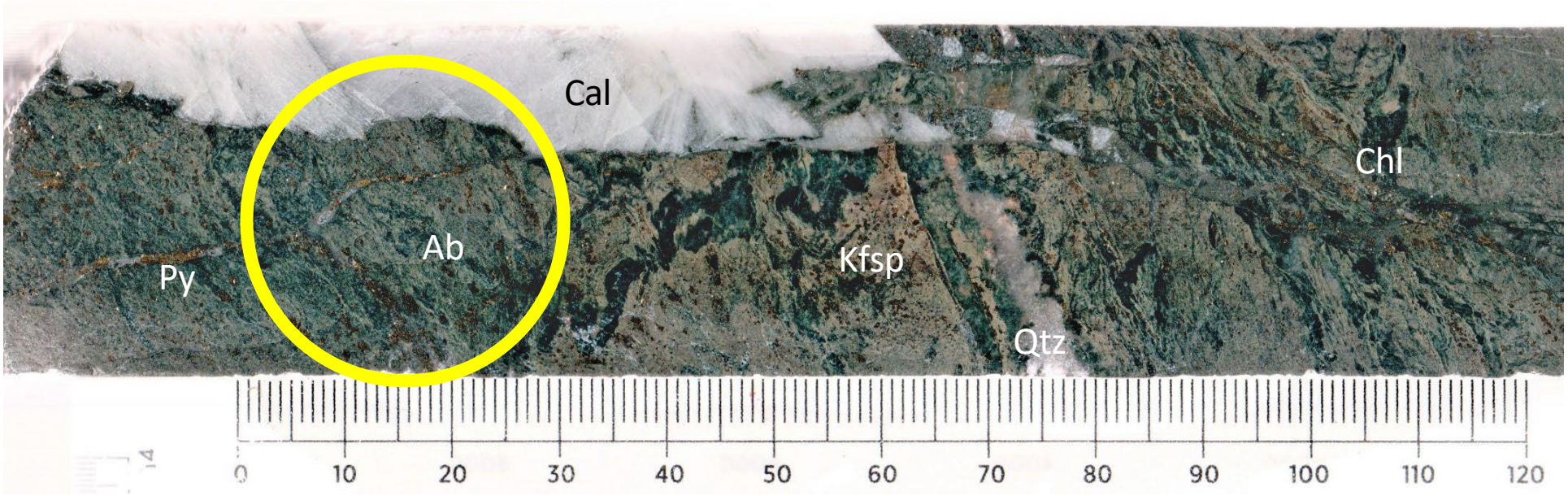

Figure 3 Photos of the drill core sample 2022330196 from drill hole DDH2 of the Bunker Hill prospect, Wertago region, New South Wales, Australia. Py-pyrite; Ab-albite; Cal-calcite; Kfsp-K-feldspar; Qtz-quartz; Chl-chlorite.

Sample ID	Prospect	Borehole Name	From (ft)	To (ft)	Note
2022440196	Bunker Hill	DDH2	355	355.5	Sulfide ore and hydrothermal alteration

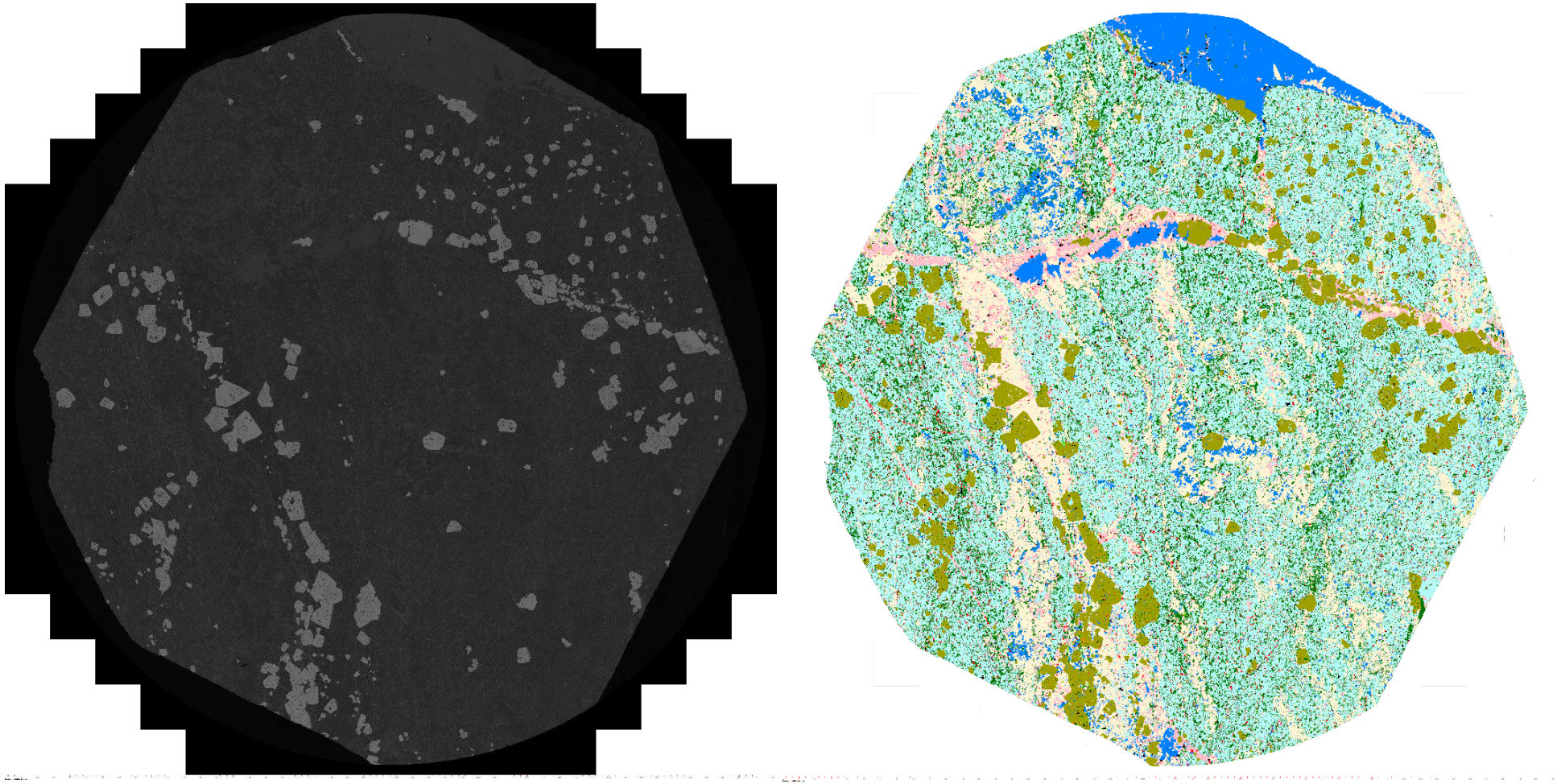

Figure 4 Backscattered electron (BSE) image (left) and Advanced Mineral Identification and Characterization System (AMICS) mineral map (right) of the sample 2022330196 from drill hole DDH2 of the Bunker Hill prospect, Wertago region, New South Wales, Australia. See Figure 9 at the end of this document for the legend of minerals identified using Mineral Liberation Analysis (MLA) mapping.

Sample ID	Prospect	Borehole Name	From (ft)	To (ft)	Note
2022440193	Bunker Hill	DDH2	116	117	Sulfide ore and hydrothermal alteration

Figure 5 Photos of the drill core sample 2022330193 from drill hole DDH2 of the Bunker Hill prospect, Wertago region, New South Wales, Australia.

Sample ID	Prospect	Borehole Name	From (ft)	To (ft)	Note
2022440194	Bunker Hill	DDH2	139	140	Sulfide ore and hydrothermal alteration

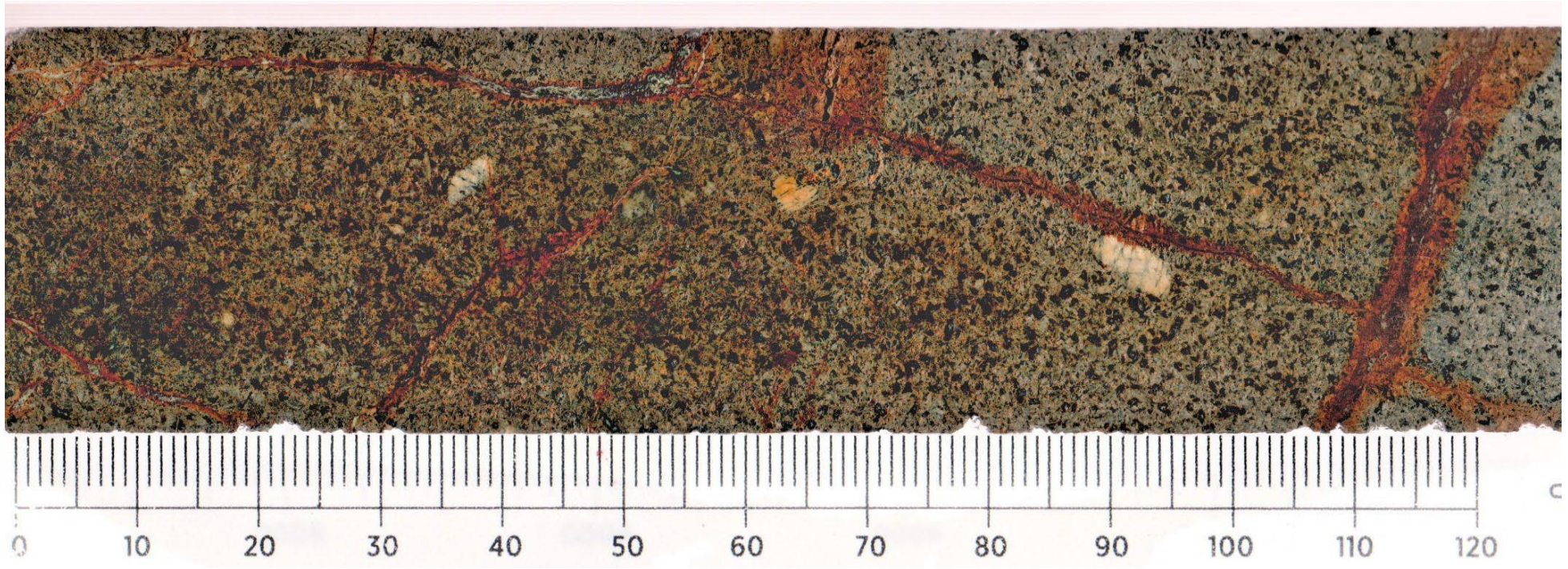

Figure 6 Photos of the drill core sample 2022330194 from drill hole DDH2 of the Bunker Hill prospect, Wertago region, New South Wales, Australia.

Sample ID	Prospect	Borehole Name	From (ft)	To (ft)	Note
2022440195	Bunker Hill	DDH2	354.5	355	Sulfide ore and hydrothermal alteration

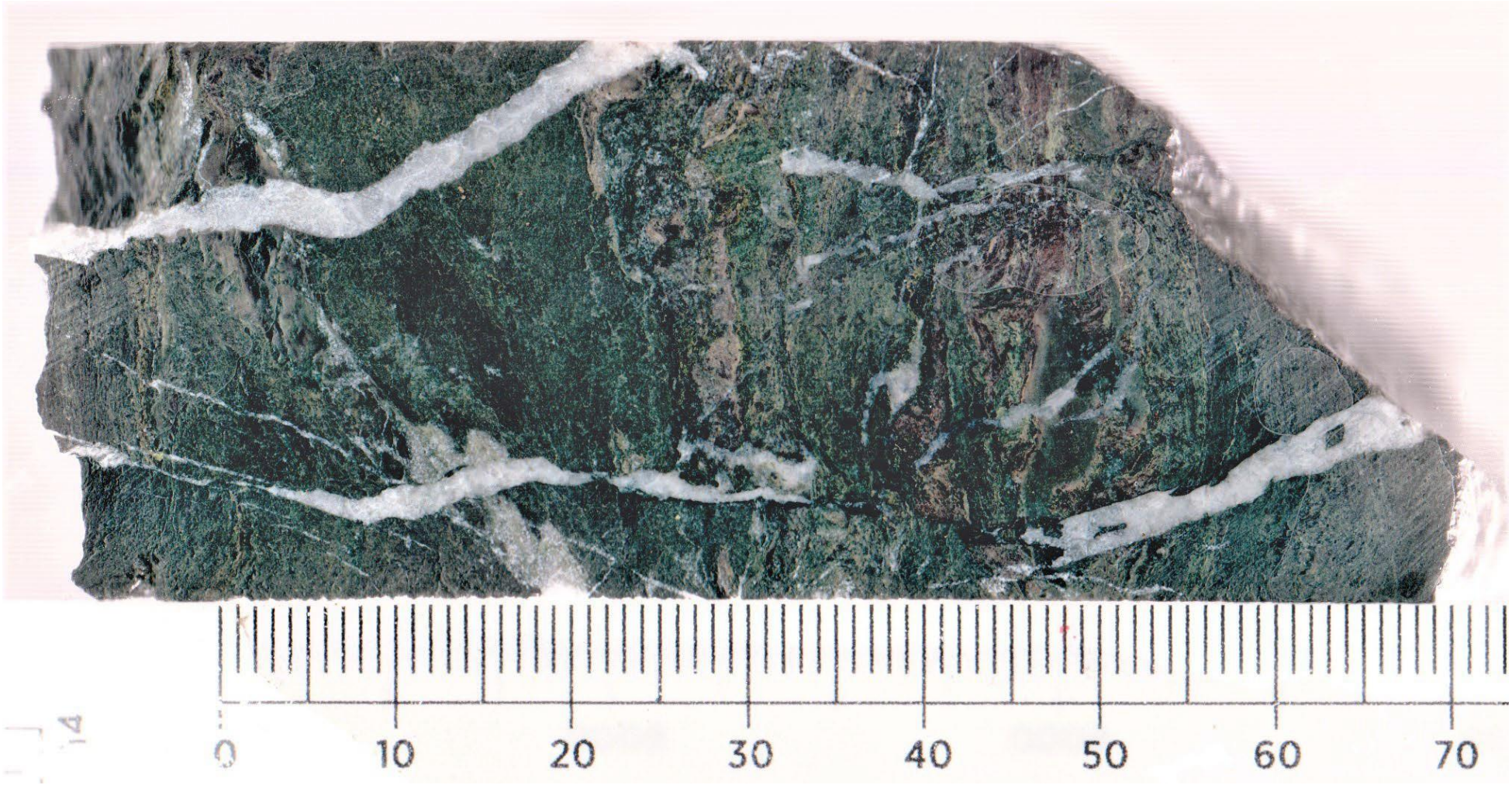

Figure 7 Photos of the drill core sample 2022330195 from drill hole DDH2 of the Bunker Hill prospect, Wertago region, New South Wales, Australia.

Sample ID	Prospect	Borehole Name	From (ft)	To (ft)	Note
2022440197	Bunker Hill	DDH3	355.5	356	Sulfide ore and hydrothermal alteration

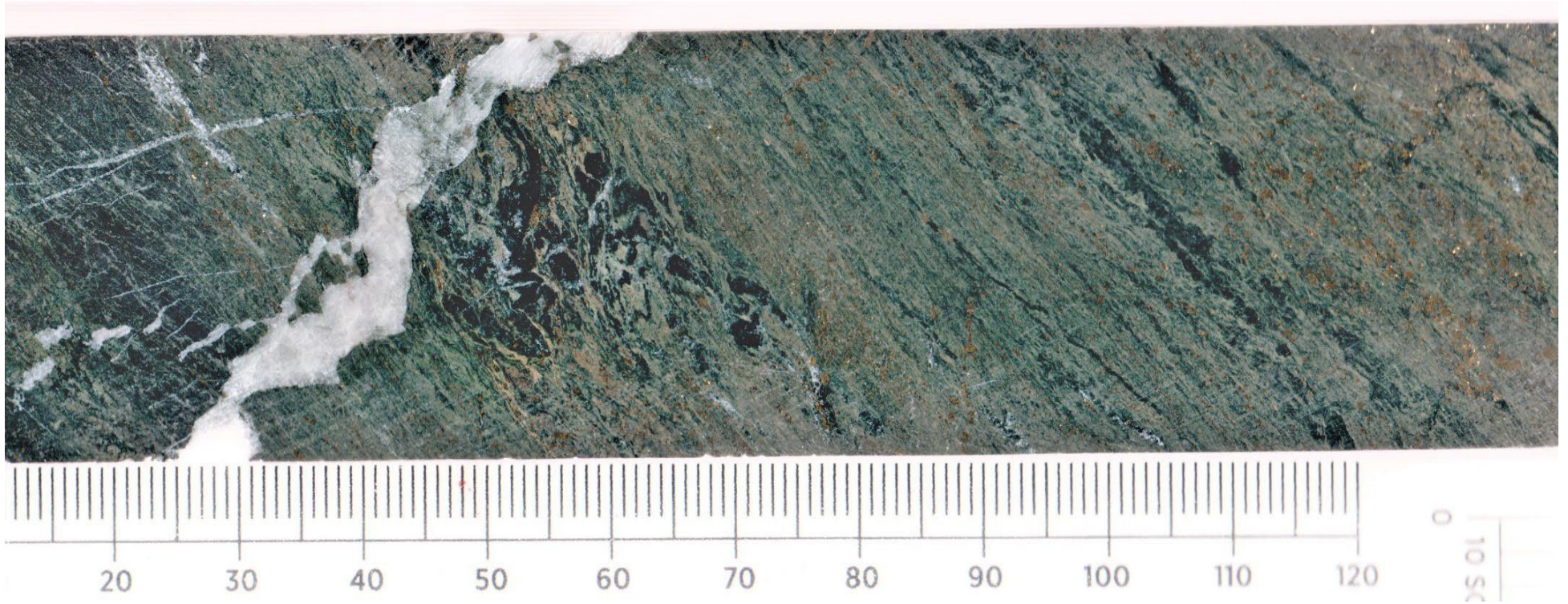

Figure 8 Photos of the drill core sample 2022330197 from drill hole DDH3 of the Bunker Hill prospect, Wertago region, New South Wales, Australia.

S2.4 Mount Arrowsmith prospect

Wertago Region, New South Wales

(A) Sample List

Sample No.	Sample ID	Borehole	From (m)	To (m)	Notes
8012585	2022440183	AWMA01	89.84	90.00	Sulfide ore and hydrothermal alteration
8012586	2022440184	AWMA01	116.40	116.65	Sulfide ore and hydrothermal alteration
8012587	2022440185	AWMA01	118.11	118.25	Sulfide ore and hydrothermal alteration

(B) Mineralisation Characteristics

Data Type	Mineral Assemblage
Hyperspectral SWIR	*Kln, Ms, Sme, Chl, Car*
Hyperspectral TIR	*Qtz, Kfsp, Gth, Hem*
Hyperspectral VNIR	*Gth, Hem*
Drill core specimen	*Py, Fsp, Apy, Cpy, Sph*
Thin section	—
AMICS mineral map	*Qtz, Py, Car, Hem, Fsp, Apy, Cpy, Sph, Ab, Ap, Mnz, Kfsp, Chl, Bt*

(C) Mineralogical Textures and Paragenesis

Category	Description
Texture	Polymetallic sulfide (Py–Apy–Cpy–Sph) hosted in feldspar-bearing igneous rocks with kaolinite–chlorite hydrothermal overprint.
Paragenesis	Arsenopyrite and pyrite predate chalcopyrite and sphalerite. Monazite is present as an accessory phase. Late carbonate veins cut all sulfide generations.

(D) Supplementary Figure Reference

Supplementary Figures *include HyLogger hyperspectral images of drill hole AWMA01 and AMICS mineral maps of polymetallic sulfide assemblage (Py–Apy–Cpy–Sph), samples 2022440183–2022440185.*

S2.4 The Mount Arrowsmith region, New South Wales

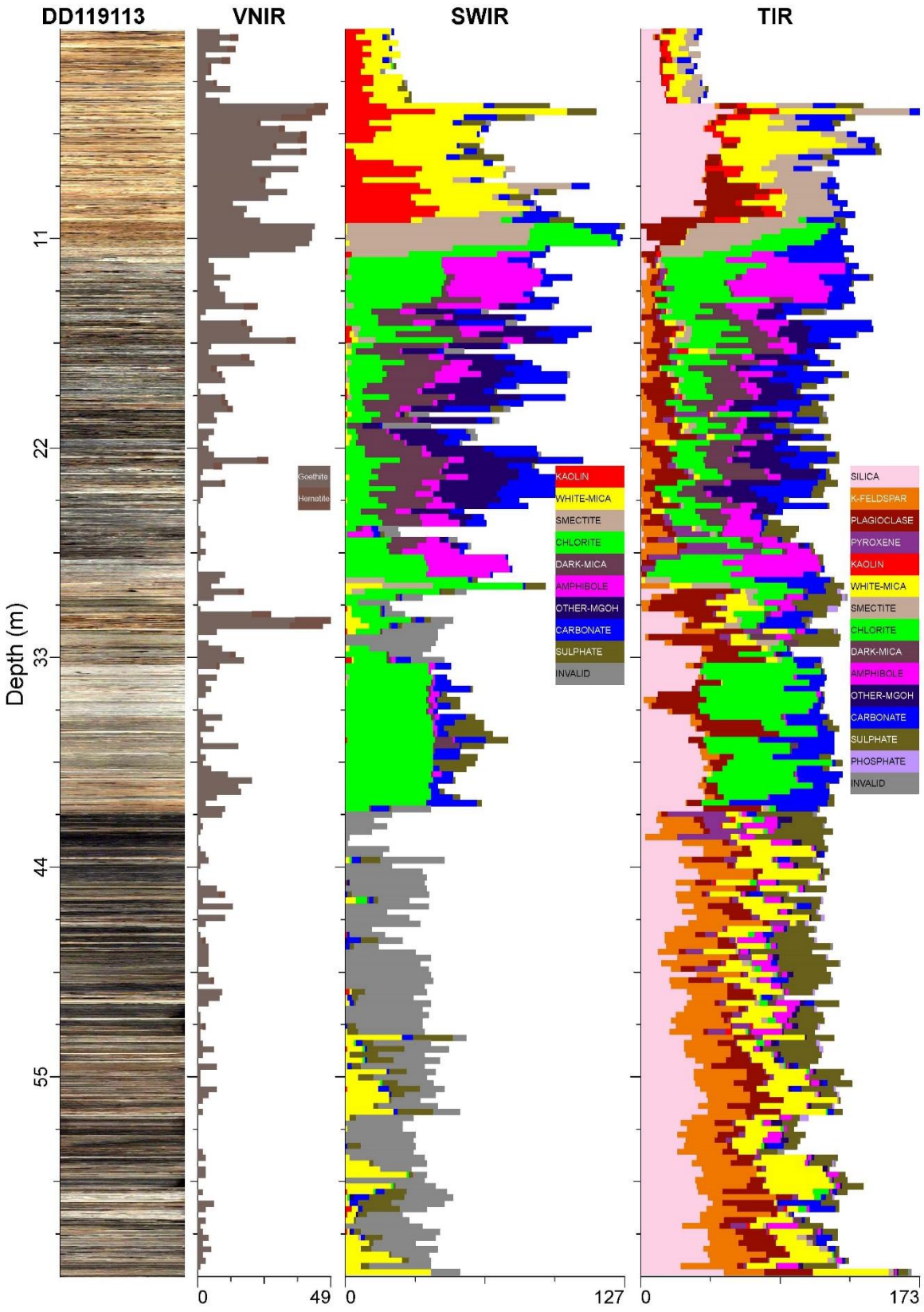

Figure 1 Downhole hylogger hyperspectral image of the hole DD119113, Mount Arrowsmith region, New South Wales, Australia.

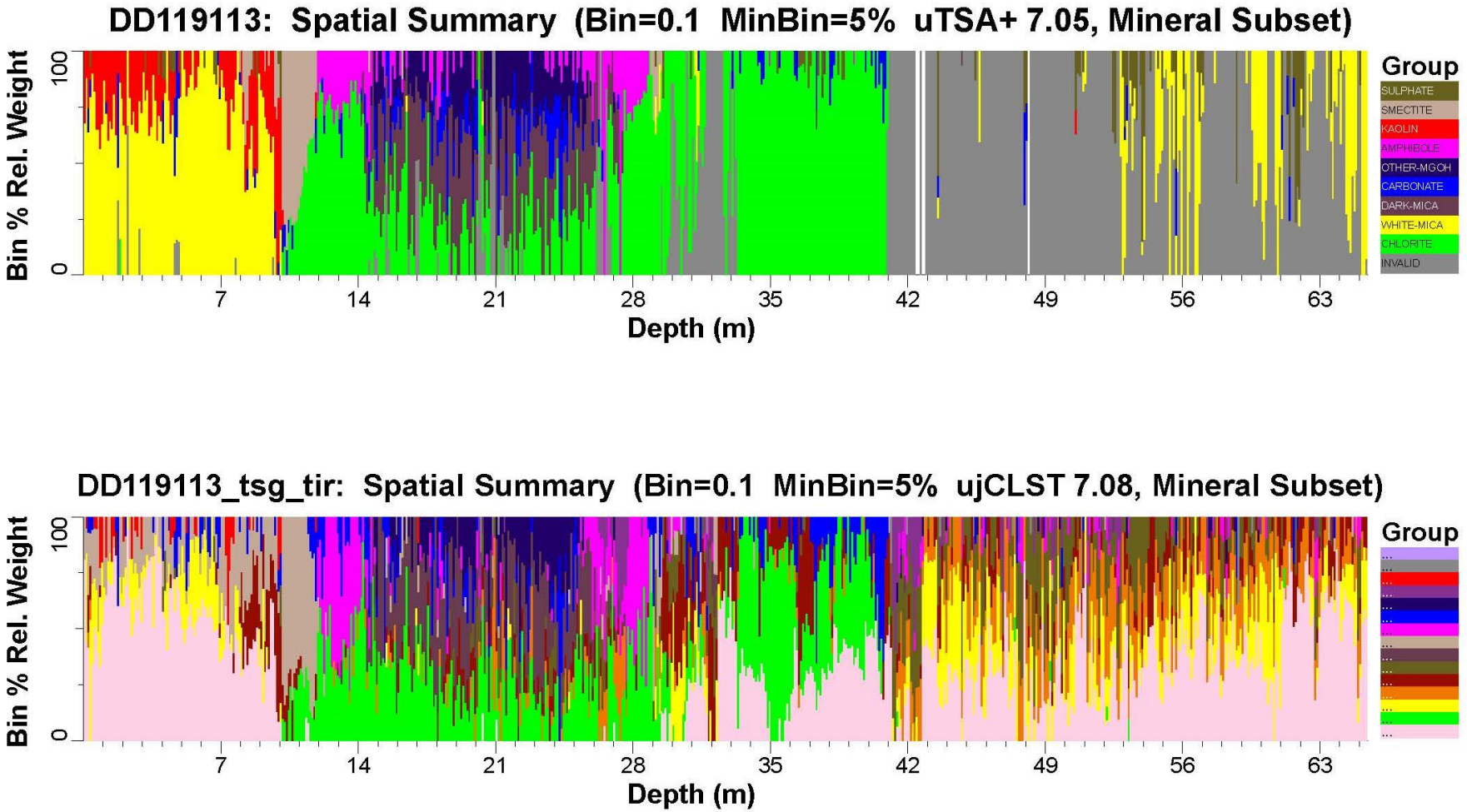

Figure 2 Summary of the hylogger hyperspectral image of the hole DD119113, Mount Arrowsmith region, New South Wales, Australia.

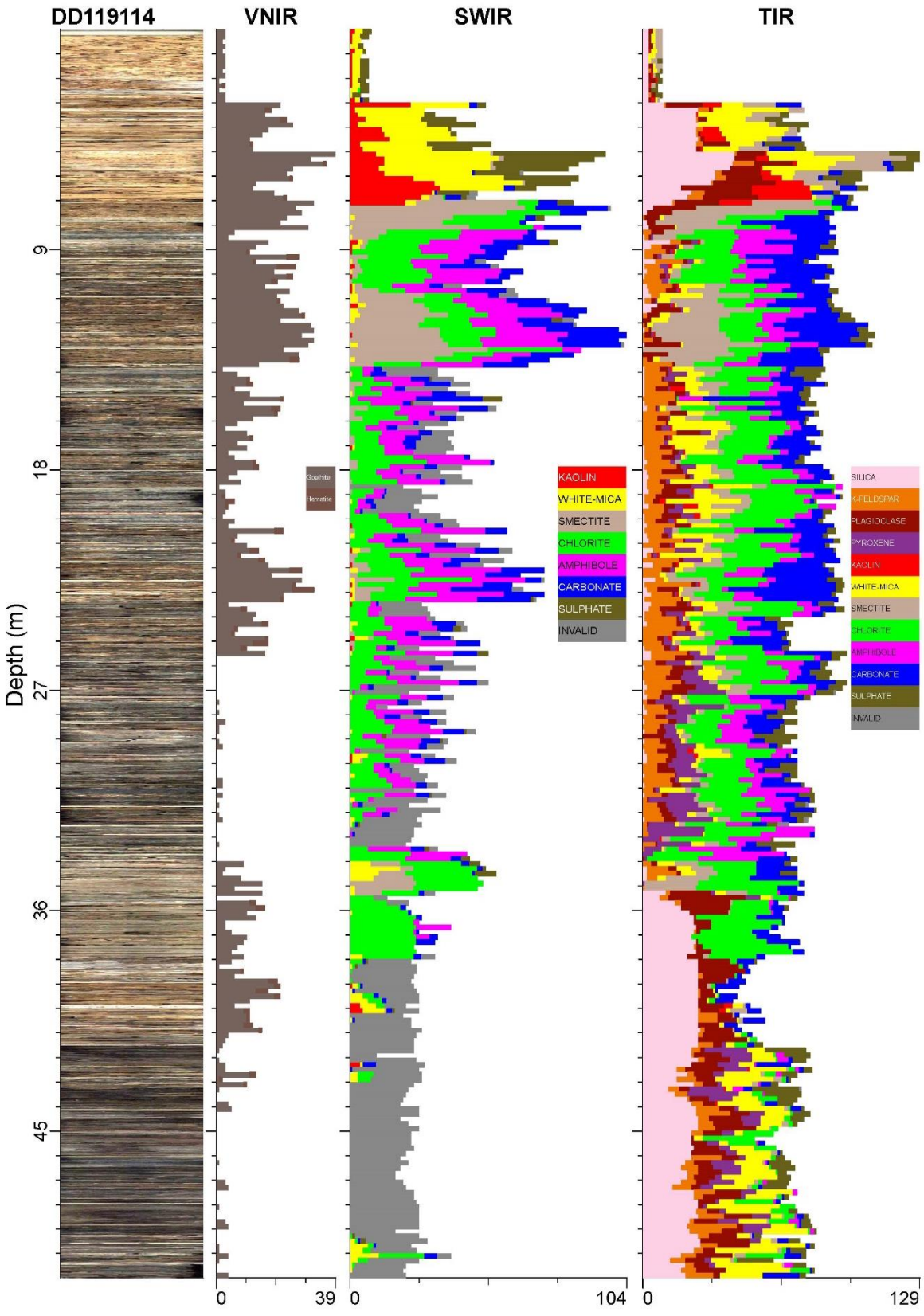

Figure 3 Downhole hylogger hyperspectral image of the hole DD119114, Mount Arrowsmith region, New South Wales, Australia.

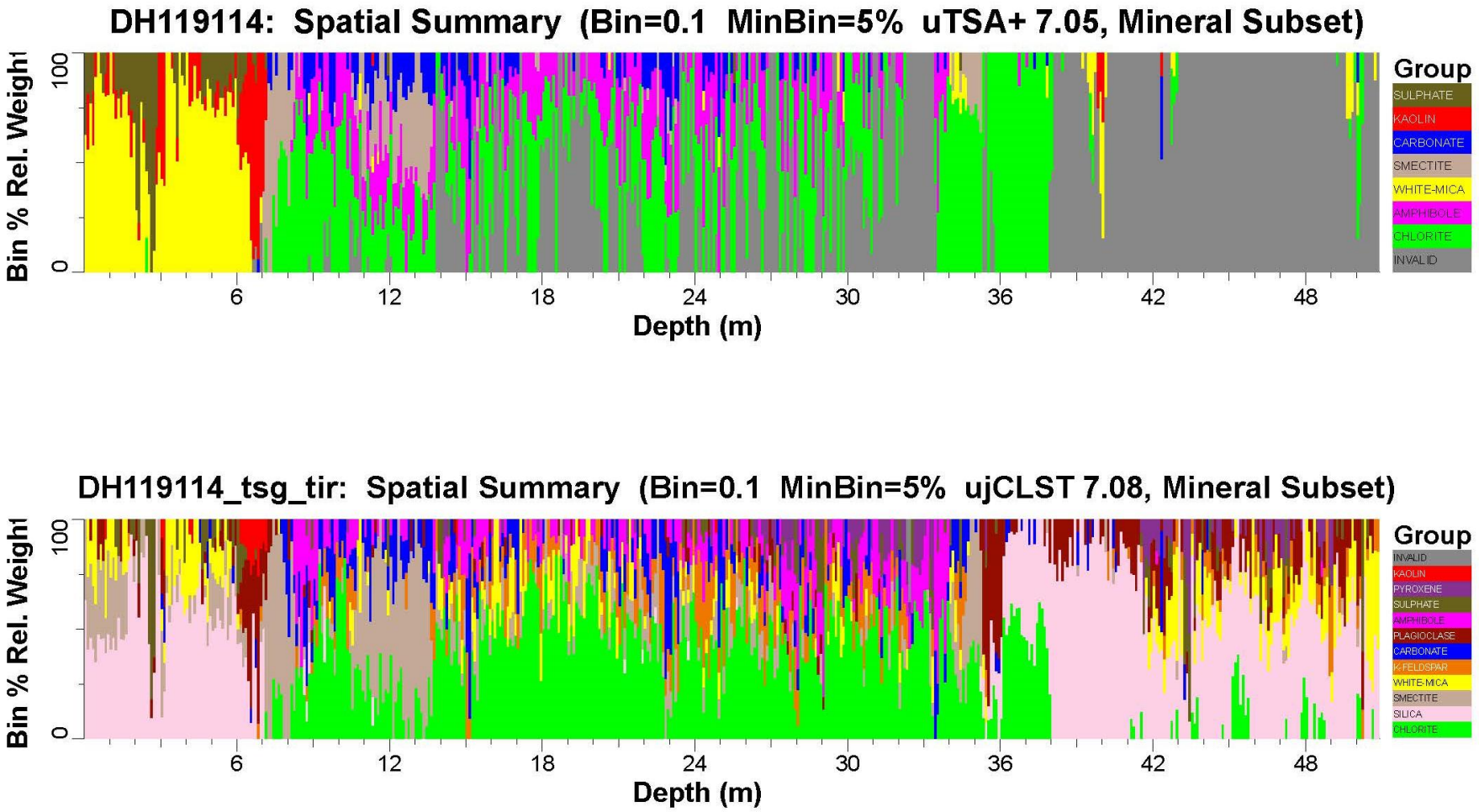

Figure 4 Summary of the hylogger hyperspectral image of the hole DD119114, Mount Arrowsmith region, New South Wales, Australia.

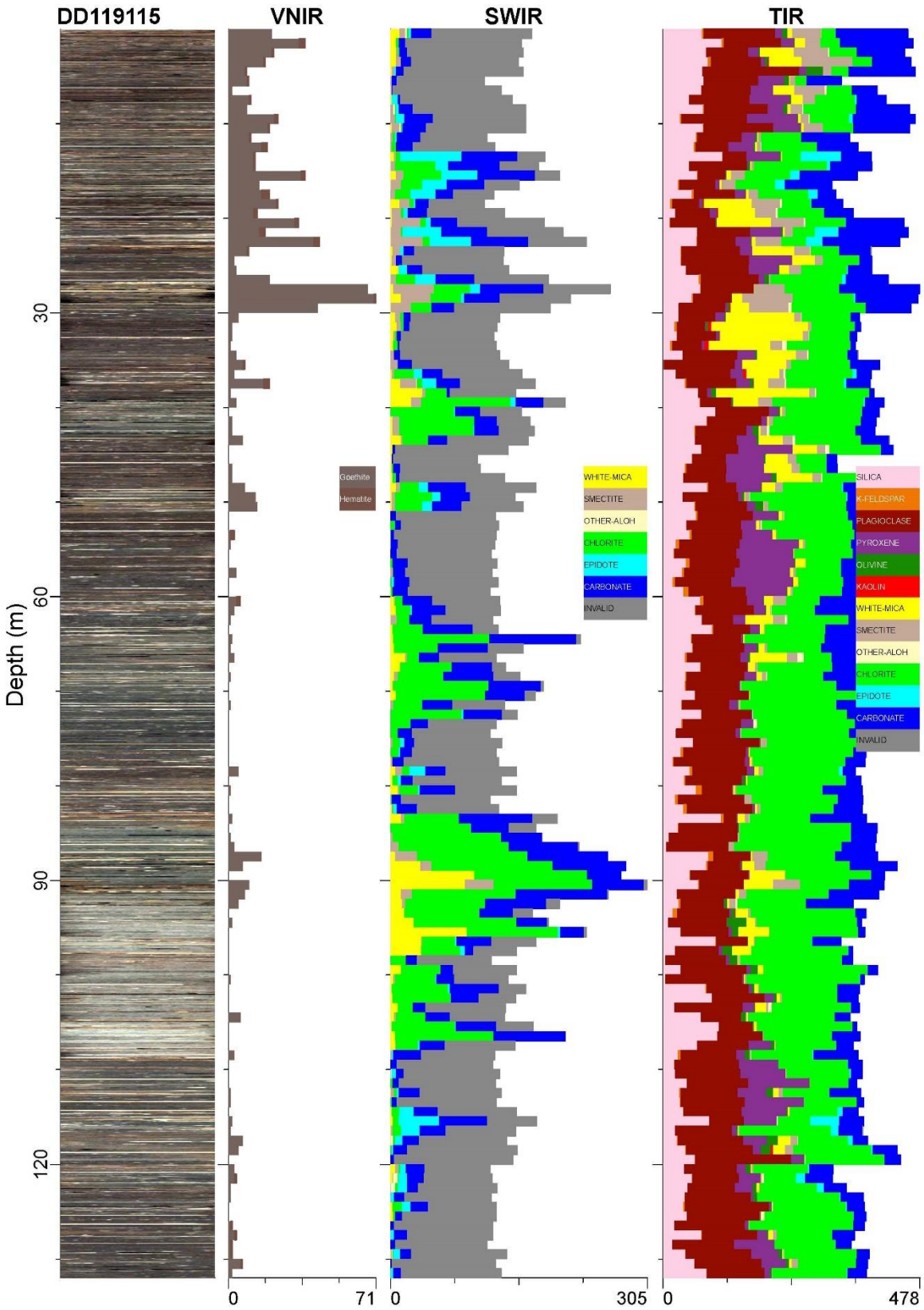

Figure 5 Downhole hylogger hyperspectral image of the hole DD119115, Mount Arrowsmith region, New South Wales, Australia.

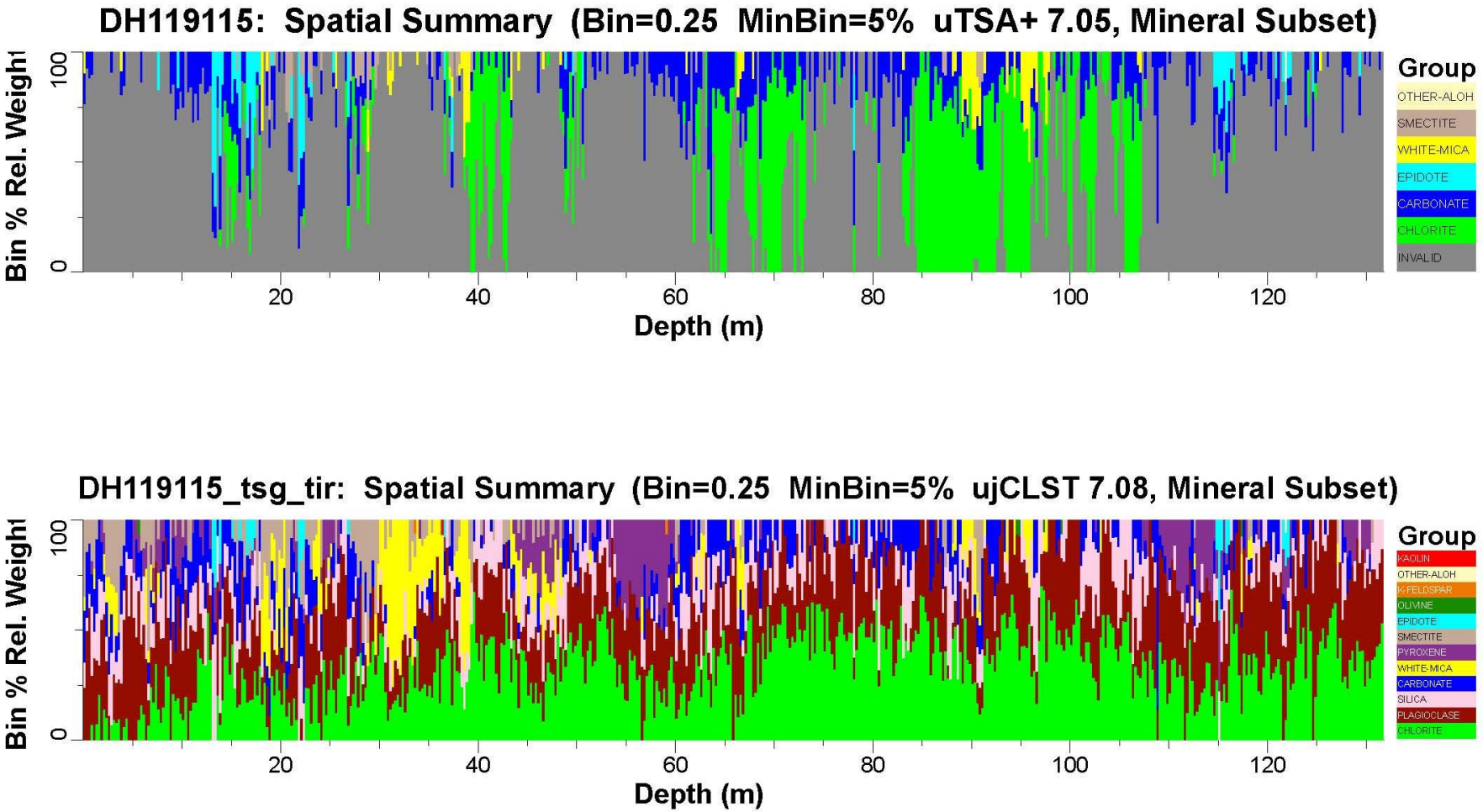

Figure 6 Summary of the hylogger hyperspectral image of the hole DD119115, Mount Arrowsmith region, New South Wales, Australia.

Sample ID	Prospect	Borehole Name	From (m)	To (m)	Note
2022440202	Mount Arrowsmith East	DH 119113	21.3	21.4	Mafic rocks and sulfides

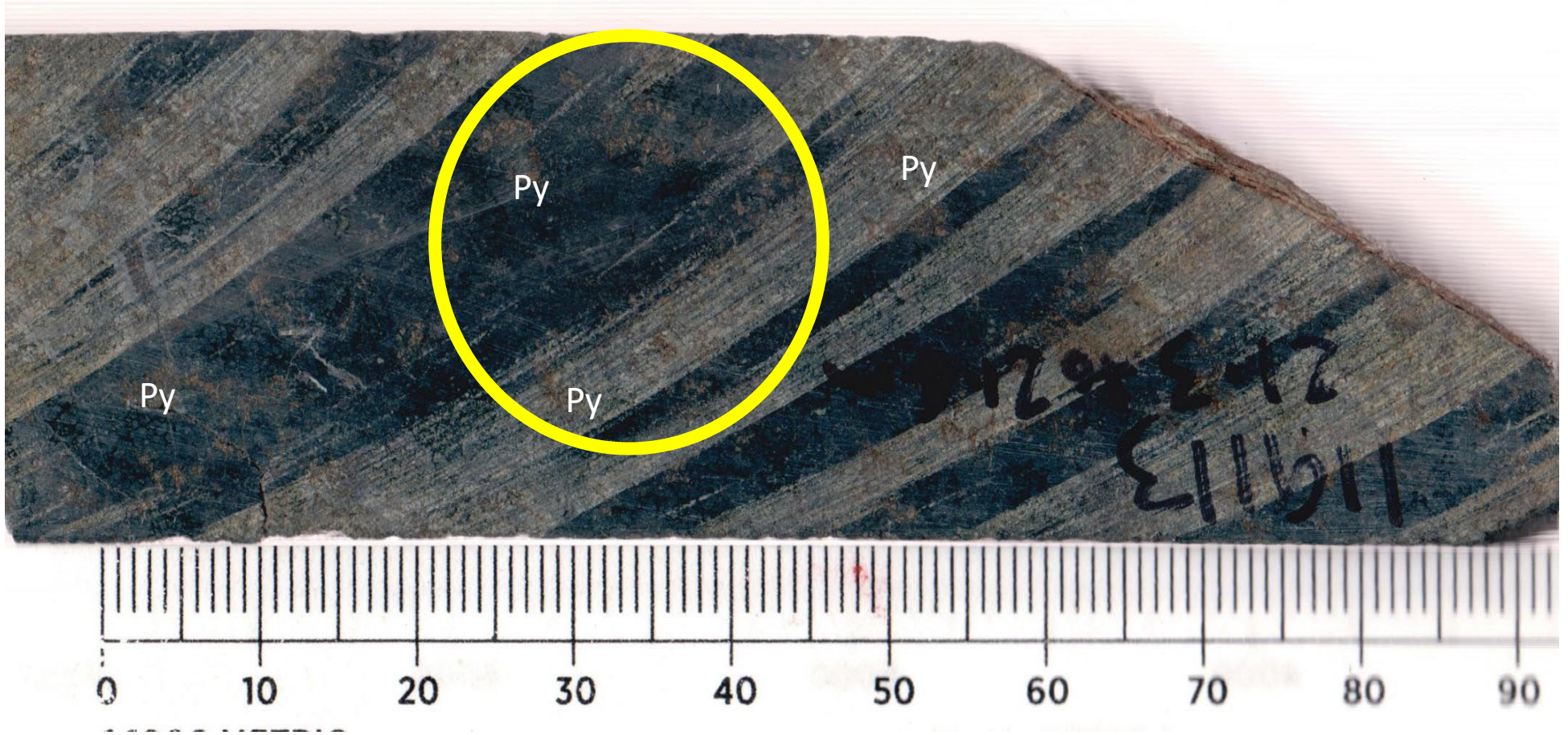

Figure 7 Photos of the drill core sample 2022440202 from drill hole DH 119113 of the Mount Arrowsmith region, New South Wales, Australia. Py-pyrite.

Sample ID	Prospect	Borehole Name	From (m)	To (m)	Note
2022440202	Mount Arrowsmith East	DH 119113	21.3	21.4	Mafic rocks and sulfides

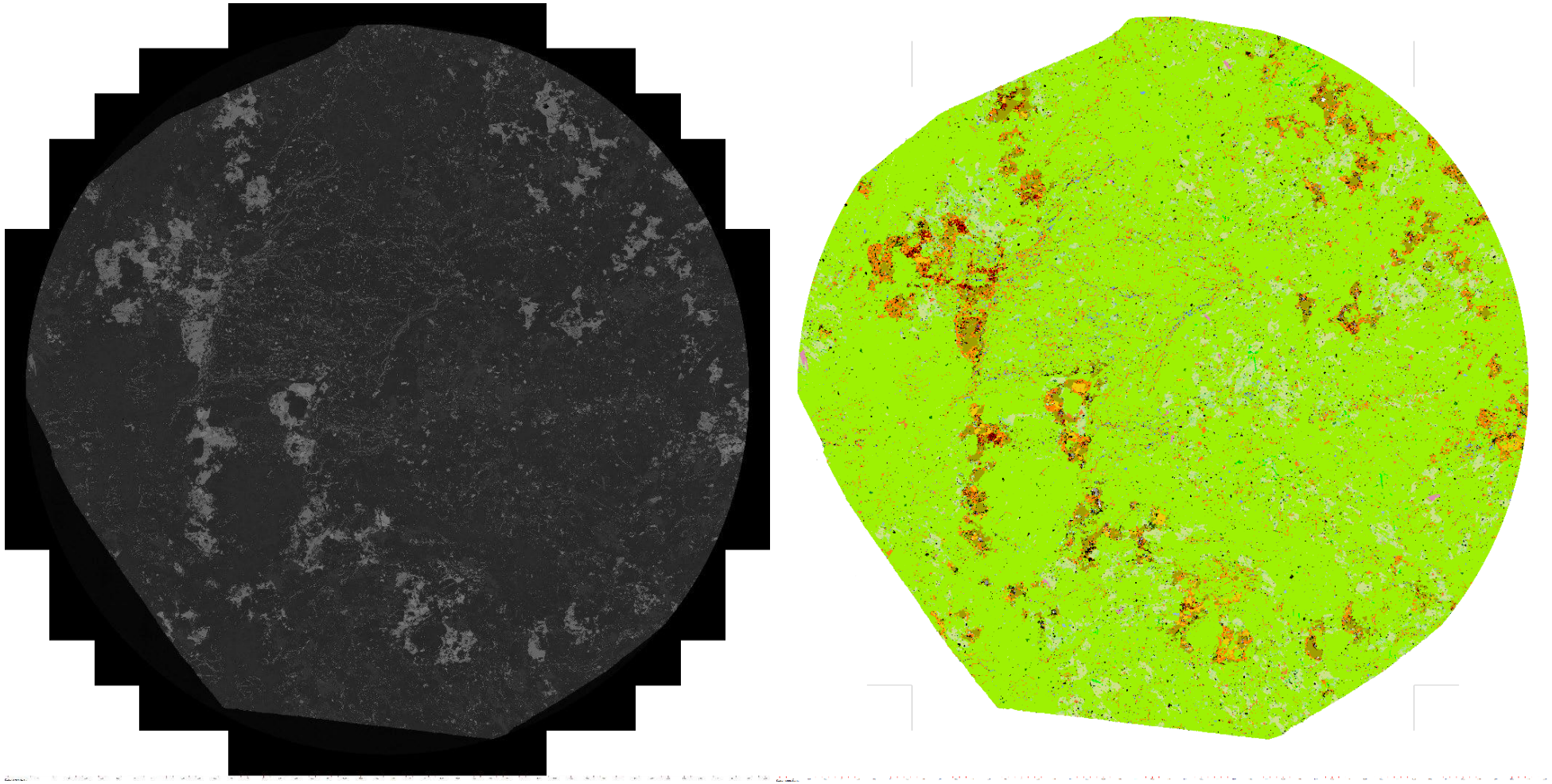

Figure 8 Backscattered electron (BSE) image (left) and Advanced Mineral Identification and Characterization System (AMICS) mineral map (right) of the sample 2022440202 from drill hole DH 119113 of the Mount Arrowsmith region, New South Wales, Australia.

Sample ID	Prospect	Borehole Name	From (m)	To (m)	Note
2022440201	Mount Arrowsmith East	DH 119113	20.4	20.5	Mafic rocks and sulfides

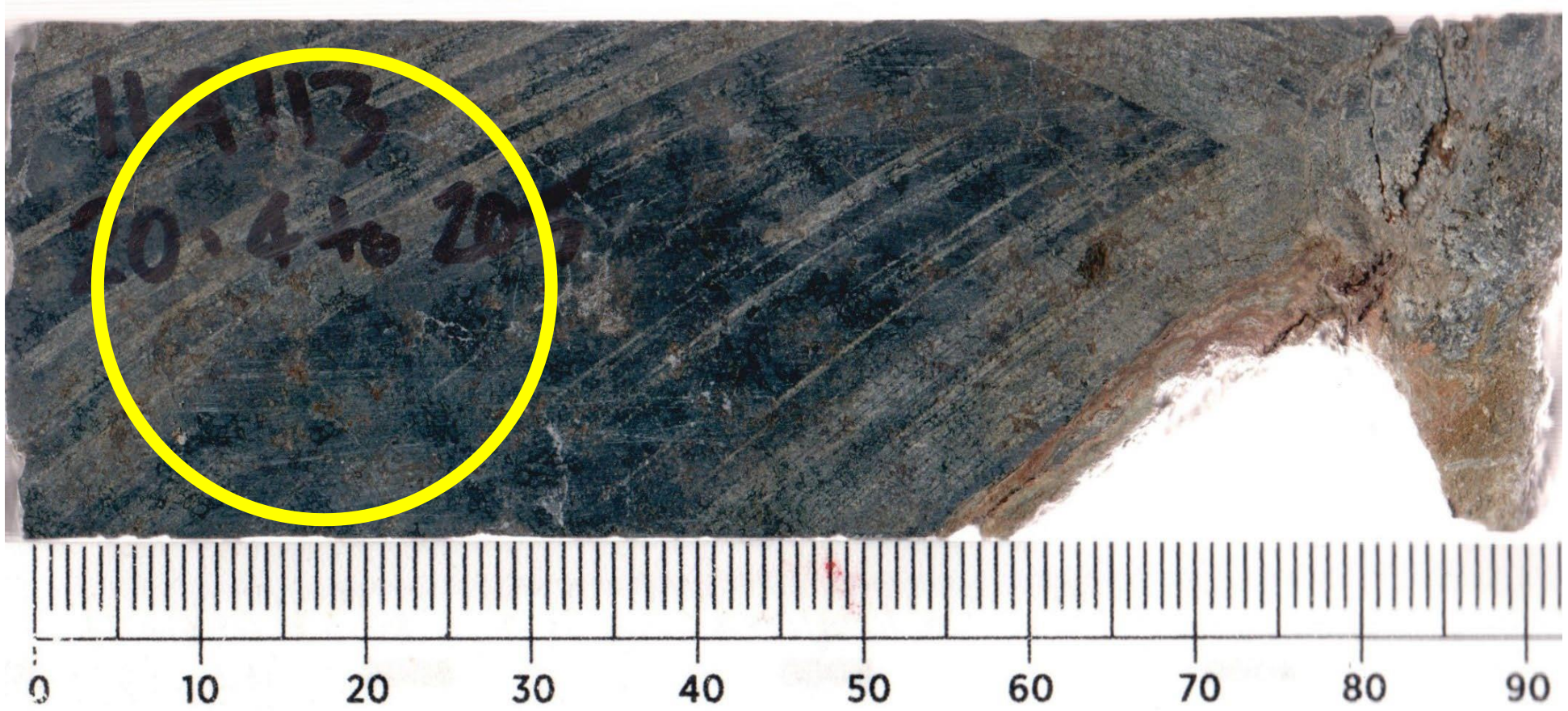

Figure 9 Photos of the drill core sample 2022440201 from drill hole DH 119113 of the Mount Arrowsmith region, New South Wales, Australia. See Figure 25 at the end of this document for the legend of minerals identified using Mineral Liberation Analysis (MLA) mapping.

Sample ID	Prospect	Borehole Name	From (m)	To (m)	Note
2022440201	Mount Arrowsmith East	DH 119113	20.4	20.5	Mafic rocks and sulfides

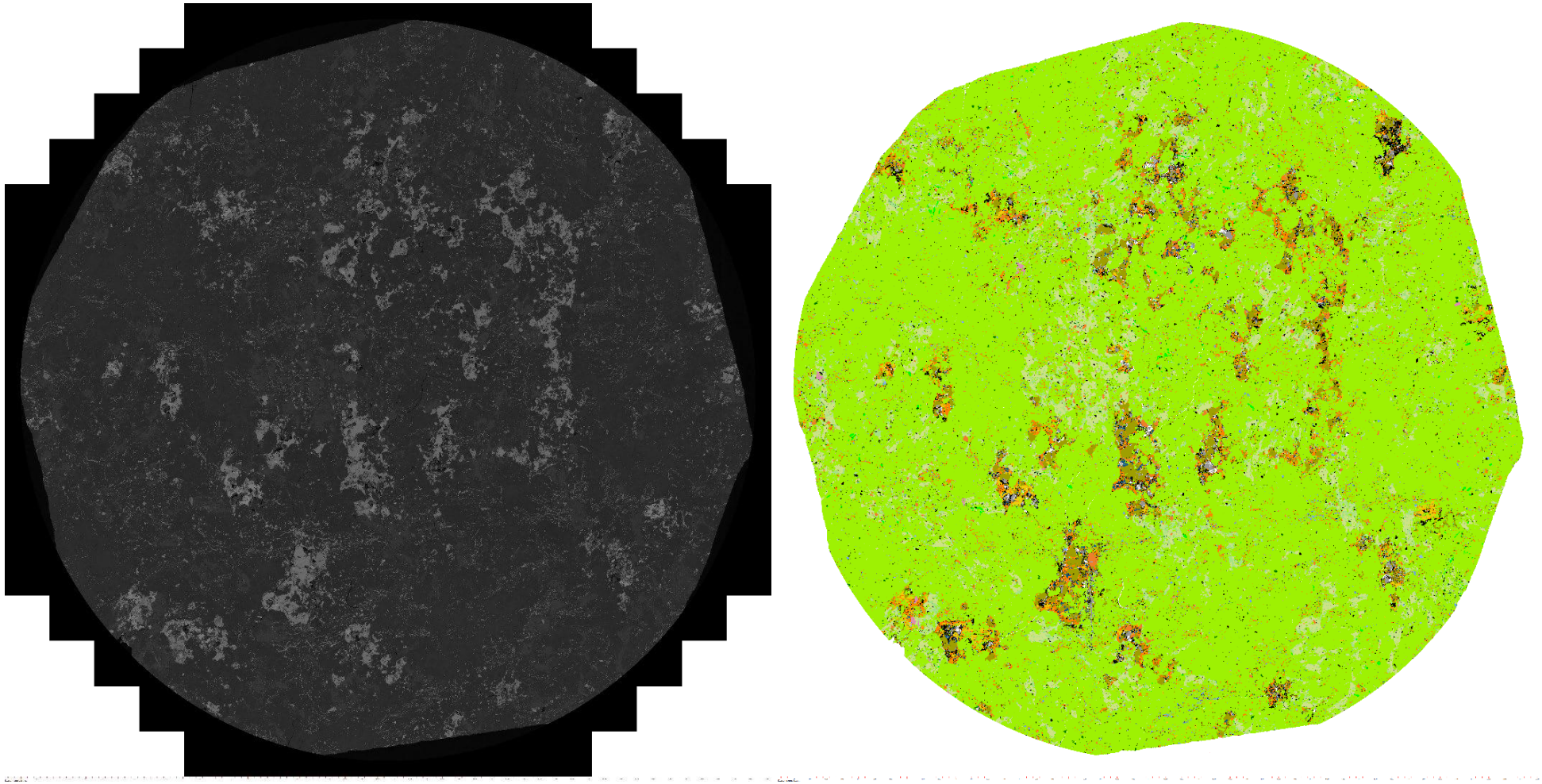

Figure 10 Backscattered electron (BSE) image (left) and Advanced Mineral Identification and Characterization System (AMICS) mineral map (right) of the sample 2022440201 from drill hole DH 119113 of the Mount Arrowsmith region, New South Wales, Australia. See Figure 25 at the end of this document for the legend of minerals identified using Mineral Liberation Analysis (MLA) mapping.

Sample ID	Prospect	Borehole Name	From (m)	To (m)	Note
2022440207	Mount Arrowsmith East	DH 119114	19.32	19.38	Mafic rocks and sulfides

Figure 11 Photos of the drill core sample 2022440207 from drill hole DH 119114 of the Mount Arrowsmith region, New South Wales, Australia.

Sample ID	Prospect	Borehole Name	From (m)	To (m)	Note
2022440207	Mount Arrowsmith East	DH 119114	19.32	19.38	Mafic rocks and sulfides

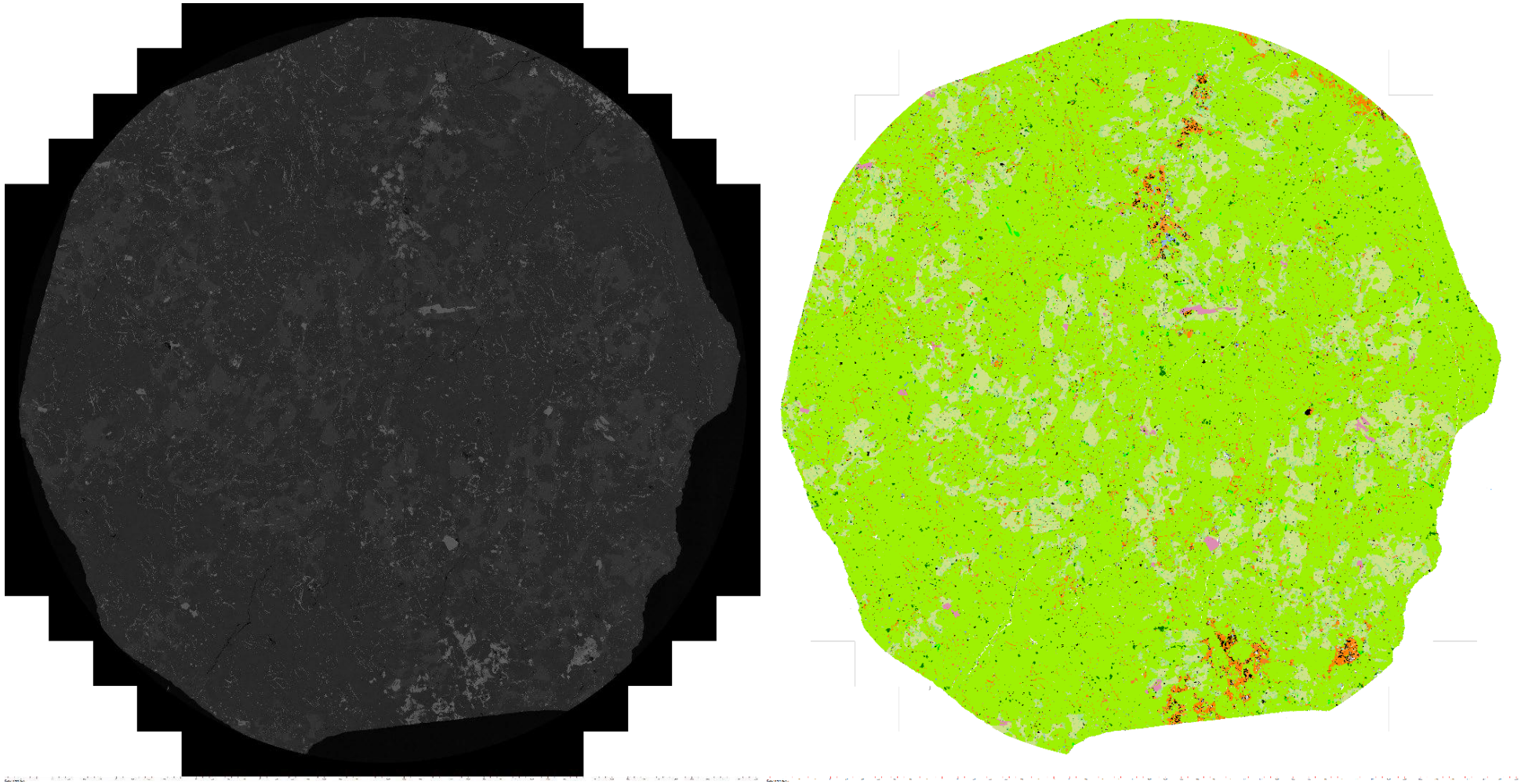

Figure 12 Backscattered electron (BSE) image (left) and Advanced Mineral Identification and Characterization System (AMICS) mineral map (right) of the sample 2022440207 from drill hole DH 119114 of the Mount Arrowsmith region, New South Wales, Australia. See Figure 25 at the end of this document for the legend of minerals identified using Mineral Liberation Analysis (MLA) mapping.

Sample ID	Prospect	Borehole Name	From (m)	To (m)	Note
2022440211	Mount Arrowsmith East	DH 119114	31.8	31.9	Mafic rocks and sulfides

Figure 13 Photos of the drill core sample 2022440211 from drill hole DH 119114 of the Mount Arrowsmith region, New South Wales, Australia.

Sample ID	Prospect	Borehole Name	From (m)	To (m)	Note
2022440211	Mount Arrowsmith East	DH 119114	31.8	31.9	Mafic rocks and sulfides

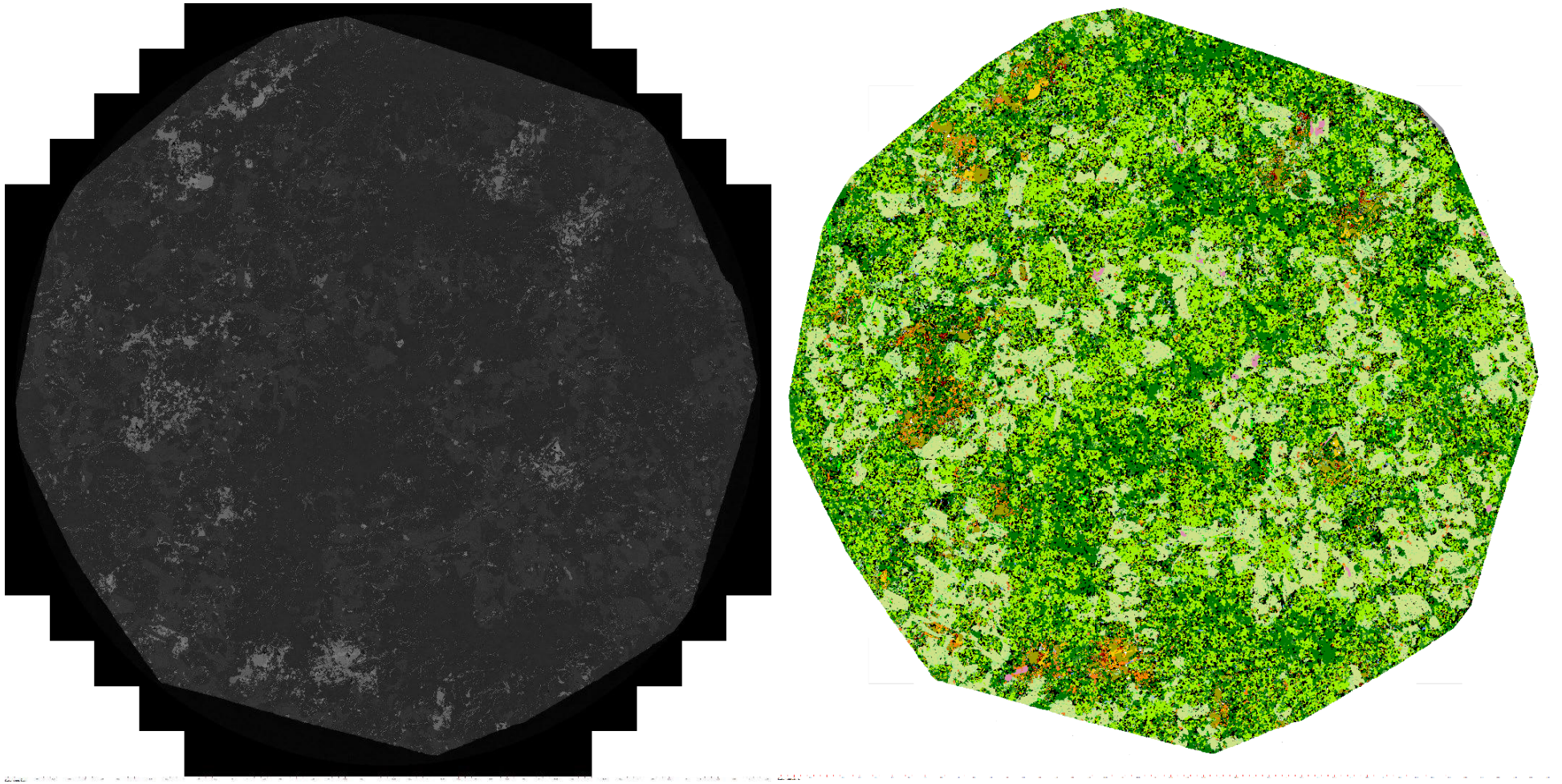

Figure 14 Backscattered electron (BSE) image (left) and Advanced Mineral Identification and Characterization System (AMICS) mineral map (right) of the sample 2022440211 from drill hole DH 119114 of the Mount Arrowsmith region, New South Wales, Australia. See Figure 25 at the end of this document for the legend of minerals identified using Mineral Liberation Analysis (MLA) mapping.

Sample ID	Prospect	Borehole Name	From (m)	To (m)	Note
2022440213	Mount Arrowsmith East	DH 119114	32.8	32.9	Mafic rocks and sulfides

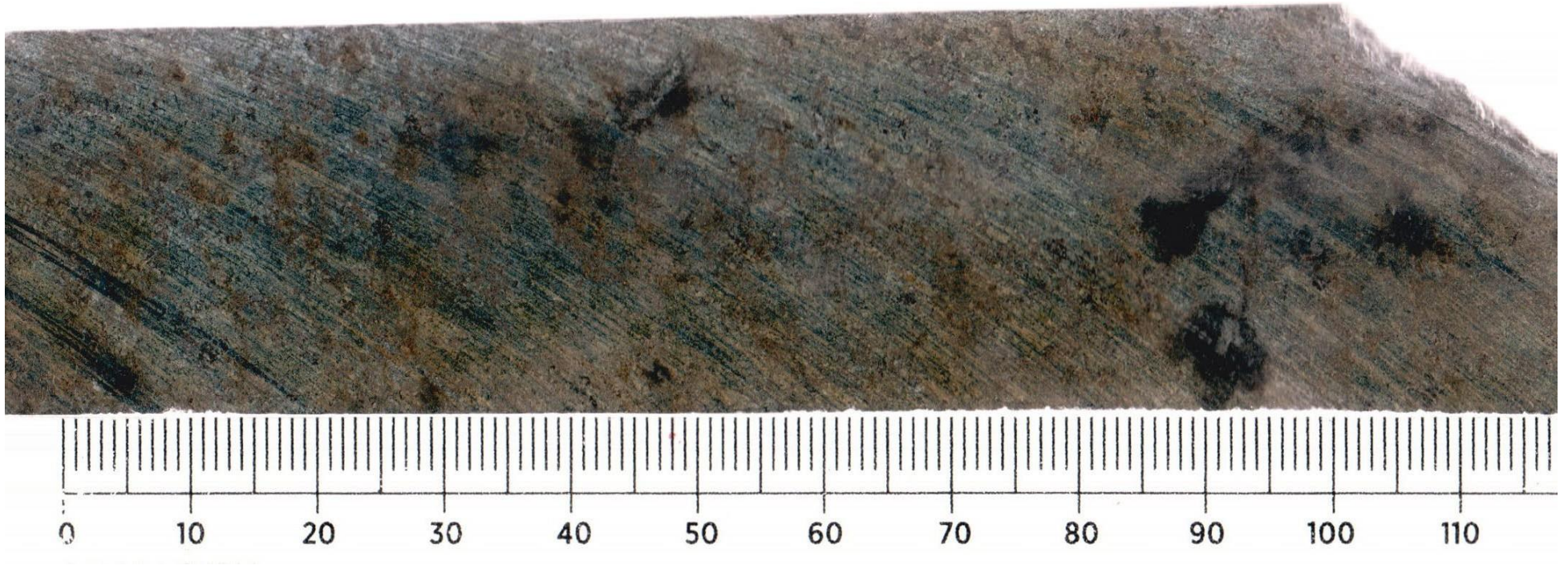

Figure 15 Photos of the drill core sample 2022440213 from drill hole DH 119114 of the Mount Arrowsmith region, New South Wales, Australia.

Sample ID	Prospect	Borehole Name	From (m)	To (m)	Note
2022440213	Mount Arrowsmith East	DH 119114	32.8	32.9	Mafic rocks and sulfides

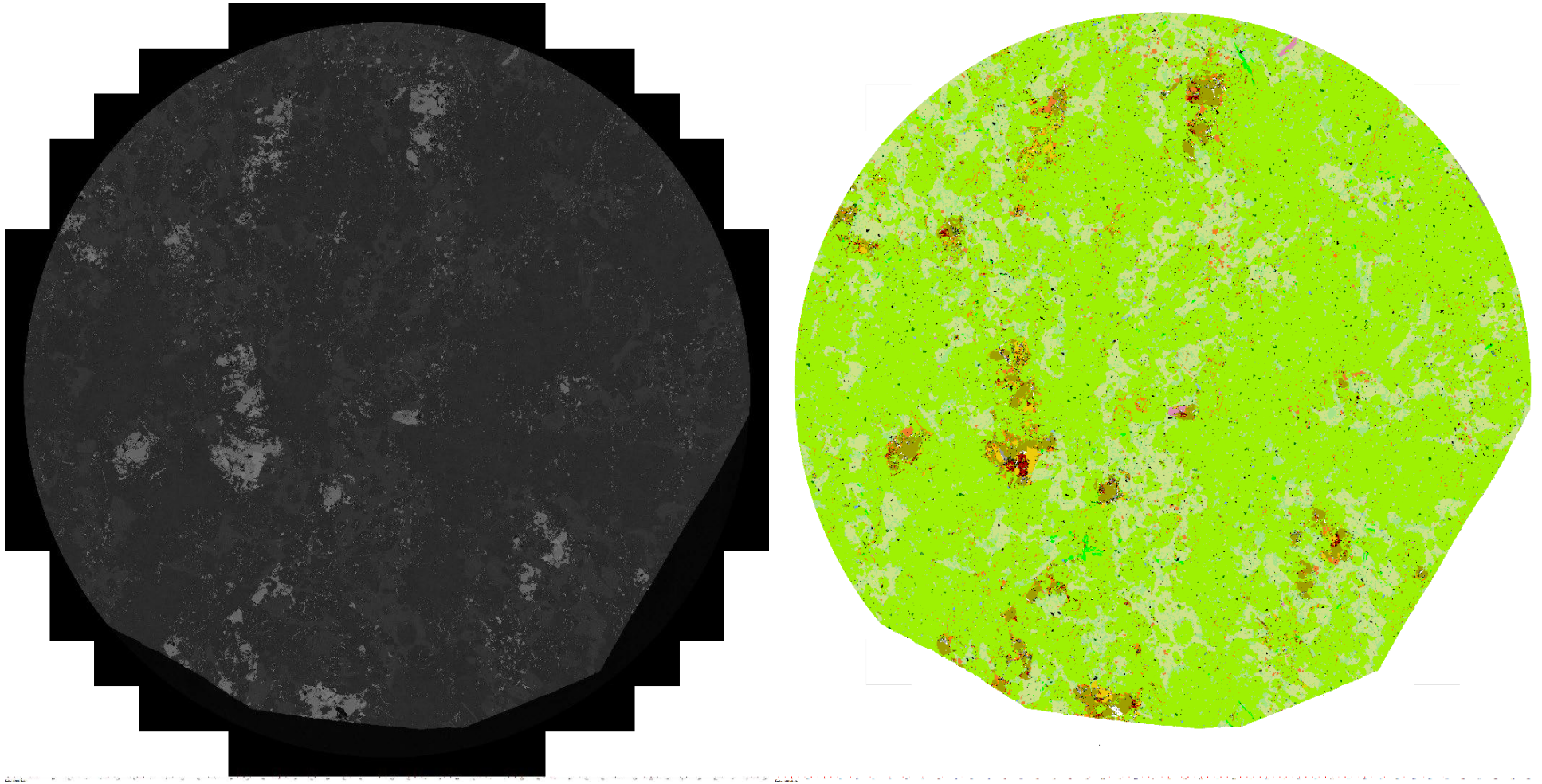

Figure 16 Backscattered electron (BSE) image (left) and Advanced Mineral Identification and Characterization System (AMICS) mineral map (right) of the sample 2022440213 from drill hole DH 119114 of the Mount Arrowsmith region, New South Wales, Australia. See Figure 25 at the end of this document for the legend of minerals identified using Mineral Liberation Analysis (MLA) mapping.

Sample ID	Prospect	Borehole Name	From (m)	To (m)	Note
2022440204	Mount Arrowsmith East	DH 119113	23.25	23.35	Mafic rocks and sulfides

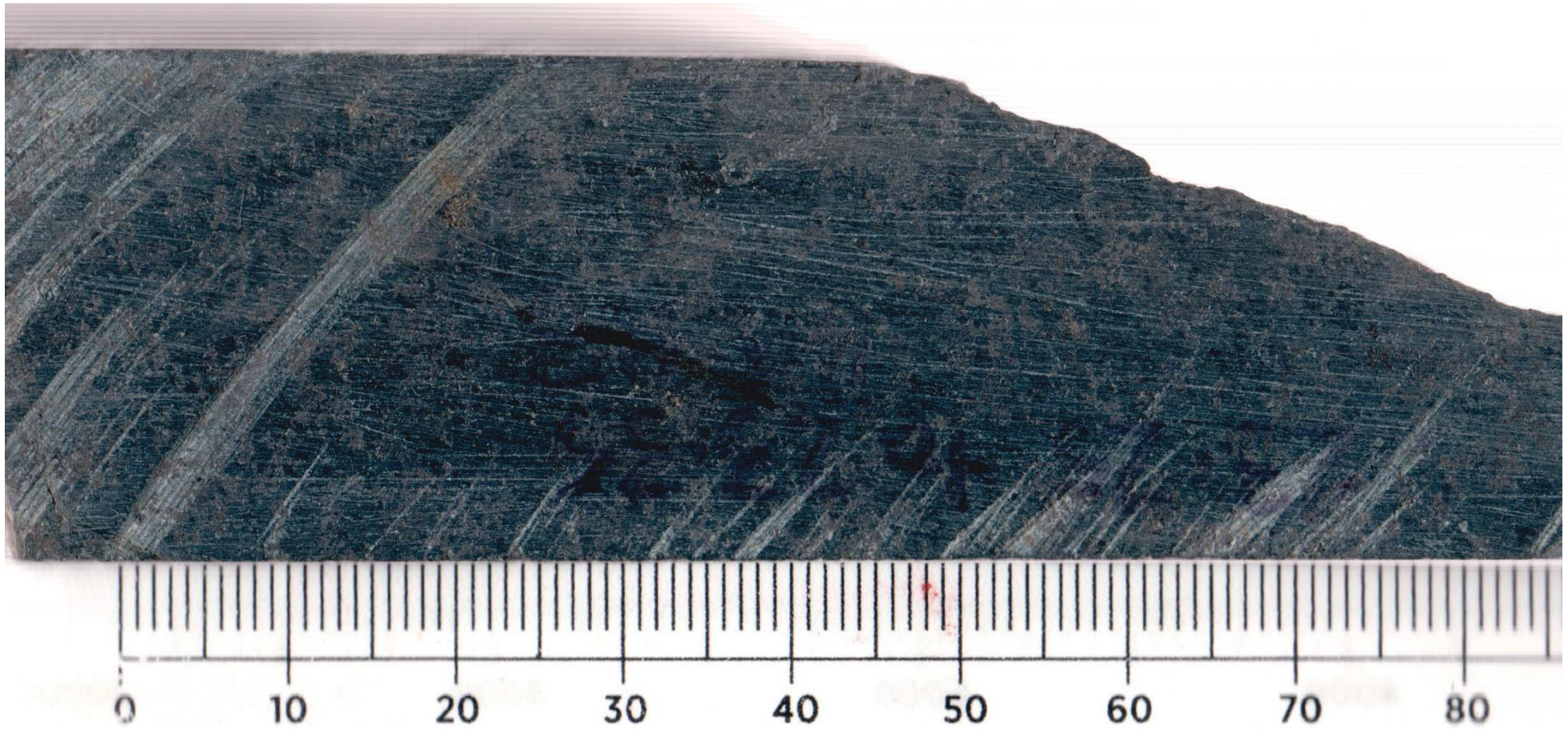

Figure 17 Photos of the drill core sample 2022440204 from drill hole DH 119113 of the Mount Arrowsmith region, New South Wales, Australia.

Sample ID	Prospect	Borehole Name	From (m)	To (m)	Note
2022440199	Mount Arrowsmith East	DH 119113	14.35	14.45	Mafic rocks and sulfides

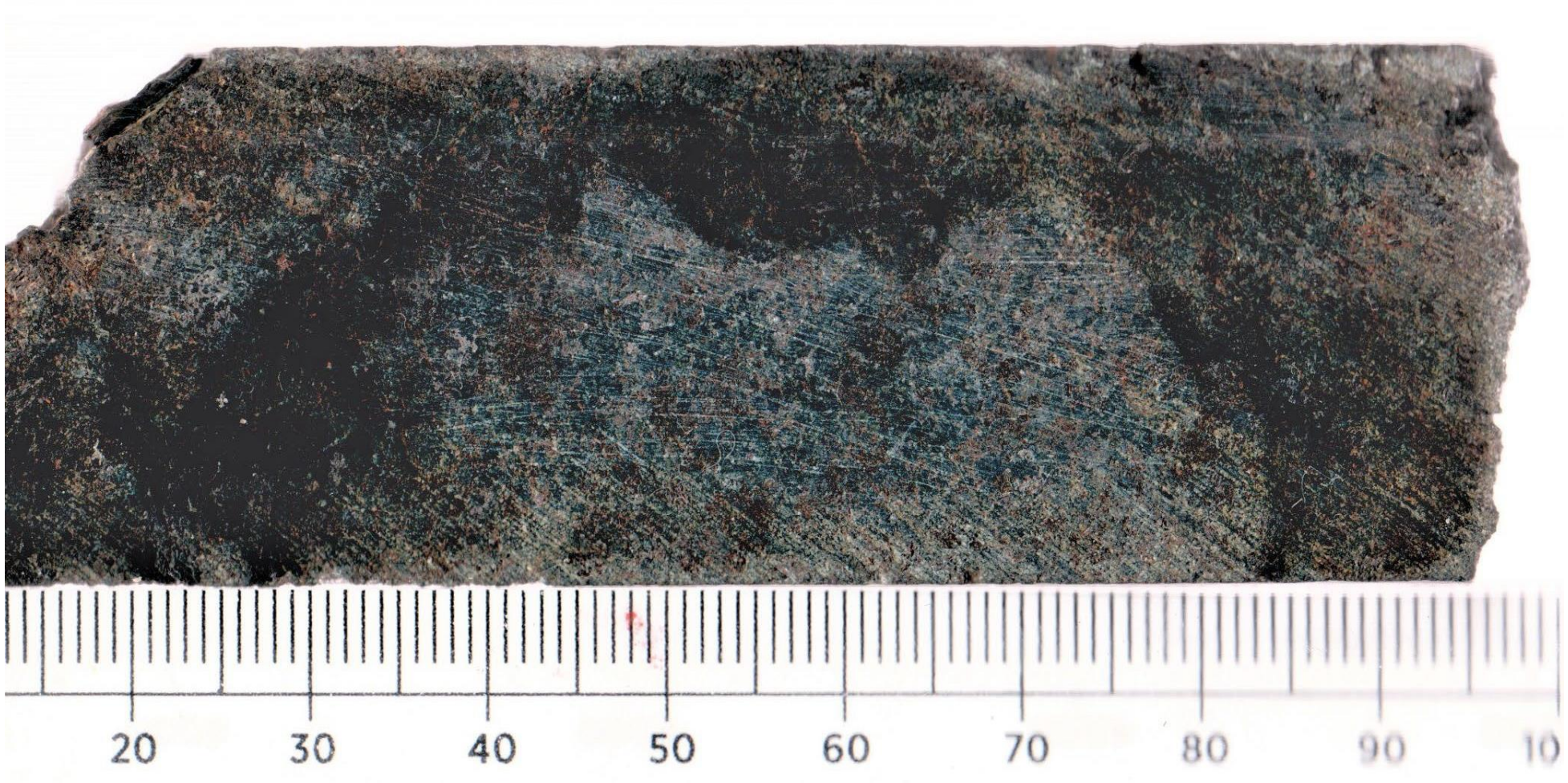

Figure 18 Photos of the drill core sample 2022440199 from drill hole DH 119113 of the Mount Arrowsmith region, New South Wales, Australia.

Sample ID	Prospect	Borehole Name	From (m)	To (m)	Note
2022440208	Mount Arrowsmith East	DH 119114	26.1	26.2	Mafic rocks and sulfides

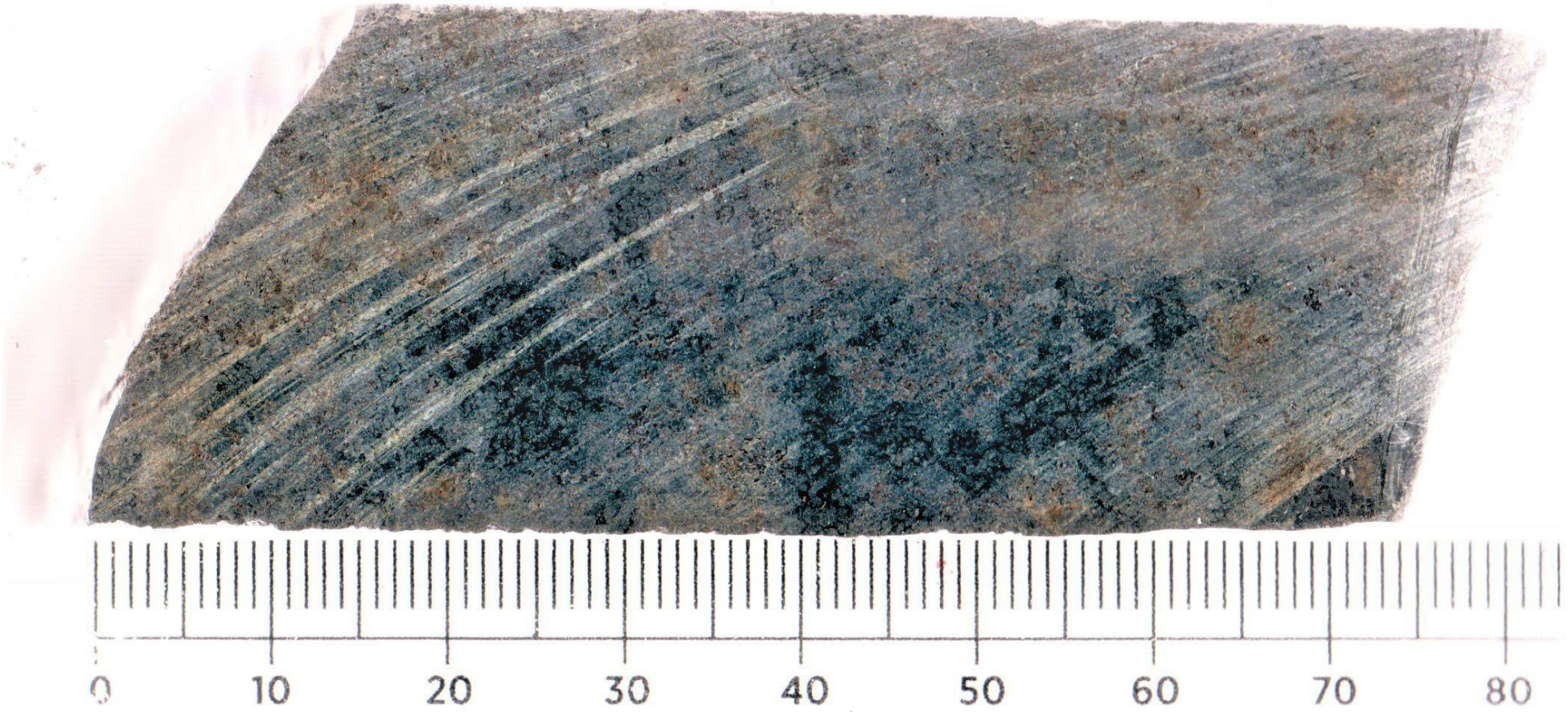

Figure 19 Photos of the drill core sample 2022440208 from drill hole DH 119114 of the Mount Arrowsmith region, New South Wales, Australia.

Sample ID	Prospect	Borehole Name	From (m)	To (m)	Note
2022440211	Mount Arrowsmith East	DH 119114	31.8	31.9	Mafic rocks and sulfides

Figure 20 Photos of the drill core sample 2022440211 from drill hole DH 119114 of the Mount Arrowsmith region, New South Wales, Australia.

Sample ID	Prospect	Borehole Name	From (m)	To (m)	Note
2022440214	Mount Arrowsmith East	DH 119114	33.45	33.65	Mafic rocks and sulfides

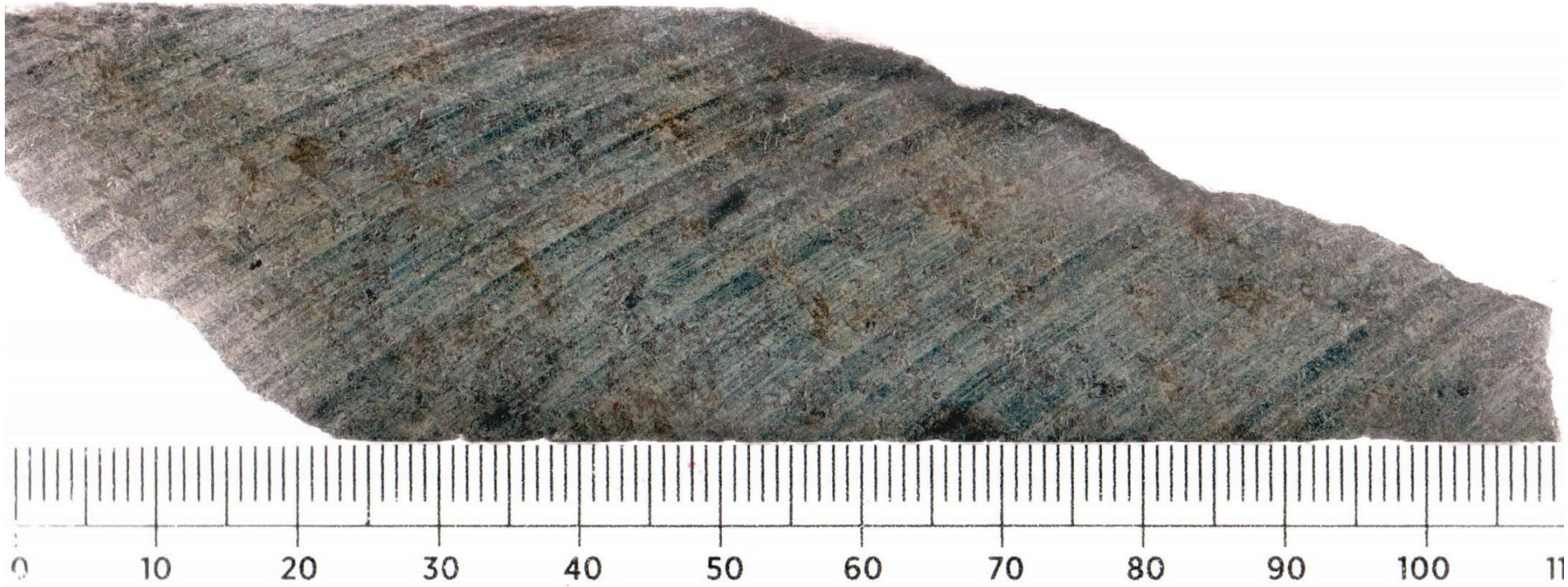

Figure 21 Photos of the drill core sample 2022440214 from drill hole DH 119114 of the Mount Arrowsmith region, New South Wales, Australia.

Sample ID	Prospect	Borehole Name	From (m)	To (m)	Note
2022440218	Mount Arrowsmith East	DH 119114	46.2	46.4	Mafic rocks and sulfides

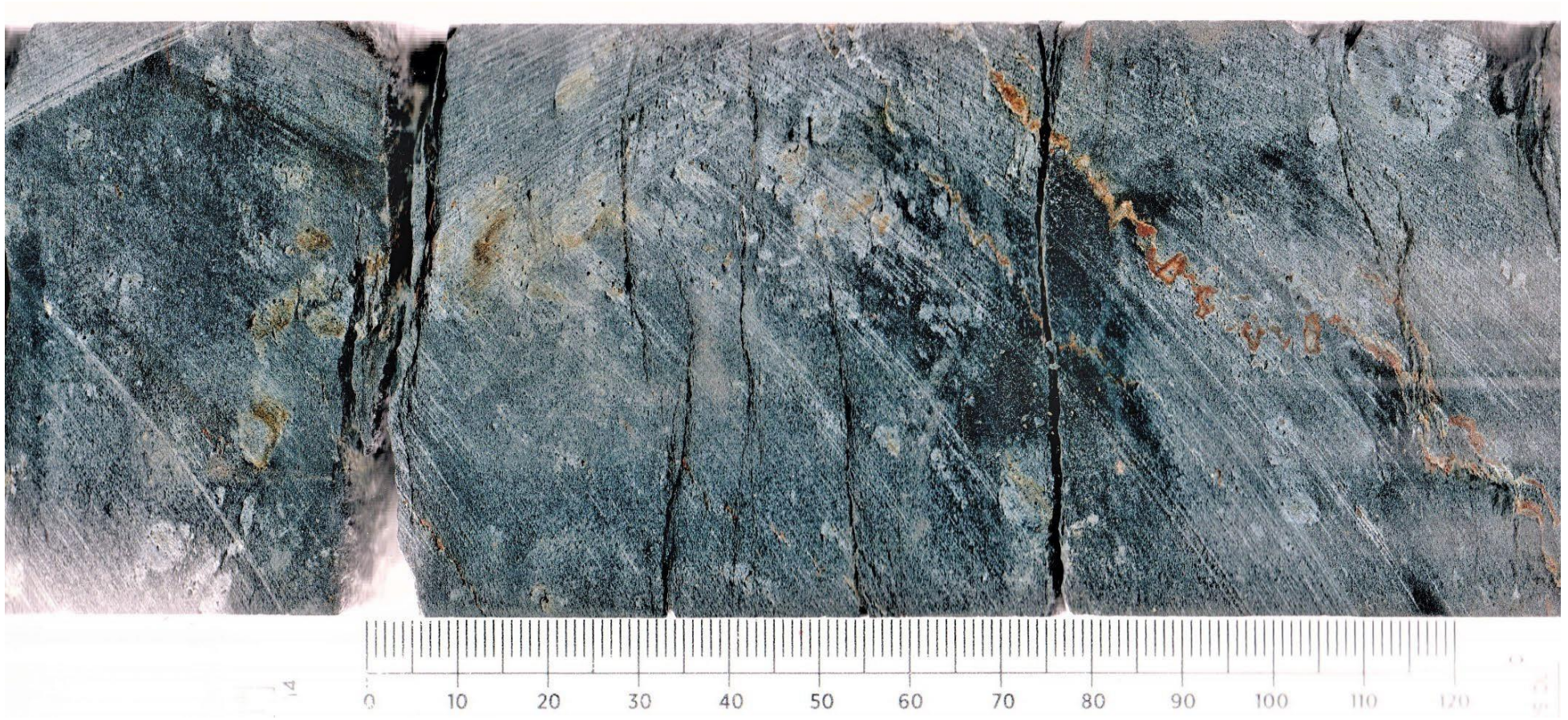

Figure 22 Photos of the drill core sample 2022440218 from drill hole DH 119114 of the Mount Arrowsmith region, New South Wales, Australia.

Sample ID	Prospect	Borehole Name	From (m)	To (m)	Note
2022440216	Mount Arrowsmith East	DH 119114	40.08	40.21	Mafic rocks and sulfides

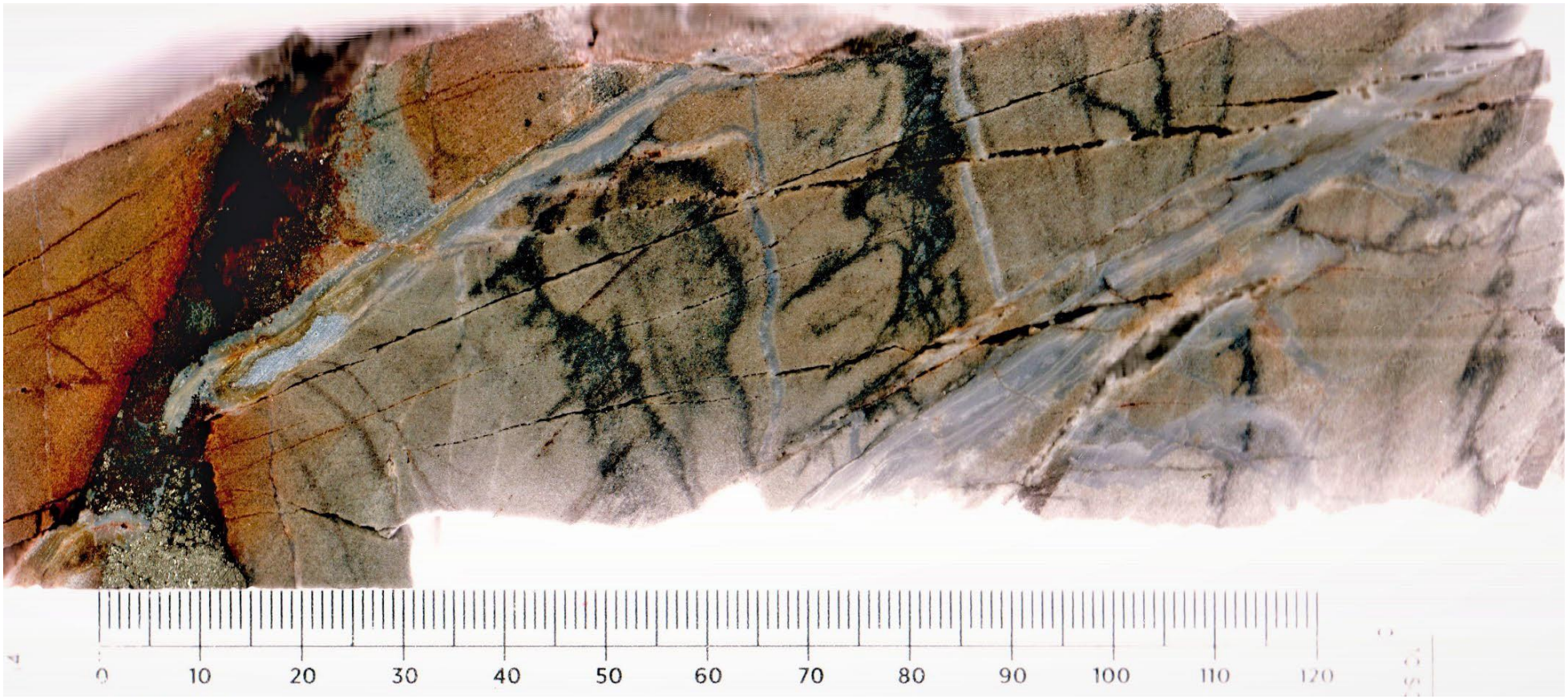

Figure 23 Photos of the drill core sample 2022440216 from drill hole DH 119114 of the Mount Arrowsmith region, New South Wales, Australia.

Sample ID	Prospect	Borehole Name	From (m)	To (m)	Note
2022440217	Mount Arrowsmith East	DH 119114	43.15	43.25	Mafic rocks and sulfides

Figure 24 Photos of the drill core sample 2022440217 from drill hole DH 119114 of the Mount Arrowsmith region, New South Wales, Australia.

S3.1 New Bendigo prospect

Warratta Inlier, New South Wales

Detailed image data: Appendix 10 (individual data file)

(A) Sample List

Sample No.	Sample ID	Borehole	From (m)	To (m)	Notes
8012551	2022440151	AWNB05	57.56	57.58	Sulfide ore and hydrothermal alteration
—	2022440158	AWNB05	—	—	Sulfide ore and hydrothermal alteration
—	2022440148	AWNB05	—	—	Sulfide ore and hydrothermal alteration
—	2022440157	AWNB05	—	—	Sulfide ore and hydrothermal alteration
—	2022440156	AWNB05	—	—	Sulfide ore and hydrothermal alteration
—	2022440150	AWNB05	—	—	Sulfide ore and hydrothermal alteration
—	2022440152	AWNB05	—	—	Sulfide ore and hydrothermal alteration
—	2022440153	AWNB05	—	—	Sulfide ore and hydrothermal alteration
—	2022440154	AWNB05	—	—	Sulfide ore and hydrothermal alteration

(B) Mineralisation Characteristics

Data Type	Mineral Assemblage
Hyperspectral SWIR	*Qtz, Chl, Car, Hem, Fsp, Apy, Cpy, Sph*
Hyperspectral TIR	*Qtz, Py, Car, Hem, Fsp, Apy, Cpy, Sph, Ab, Ap, Mnz, Kfsp, Chl, Bt*
Hyperspectral VNIR	*Gth, Hem*
Drill core specimen	*Py, Qtz (with Py–Qtz veins)*
Thin section	—
AMICS mineral map	*Qtz, Py, Cal, Apy, Chl, Ap, Ttn (AMICS)*

(C) Mineralogical Textures and Paragenesis

Category	Description
Texture	Pyrite–quartz vein hosted mineralisation. HyLogger hyperspectral data available for drill hole AWNB05.

Category	Description
Paragenesis	Pyrite and arsenopyrite form an early phase. Quartz–calcite veins with chlorite represent the main hydrothermal event. Titanite is an accessory phase.

(D) Supplementary Figure Reference

Supplementary Figures *include (1) downhole HyLogger hyperspectral image and summary of drill hole AWNB05; and (2) drill core photographs of samples 2022440151, 2022440158, 2022440148, 2022440157, 2022440156, 2022440150, 2022440152, 2022440153 and 2022440154; BSE image and AMICS mineral map of representative sulfide ore. AMICS mineral standard legend included.*

S3.1 The New Bendigo prospect, Warratta Inlier, New South Wales

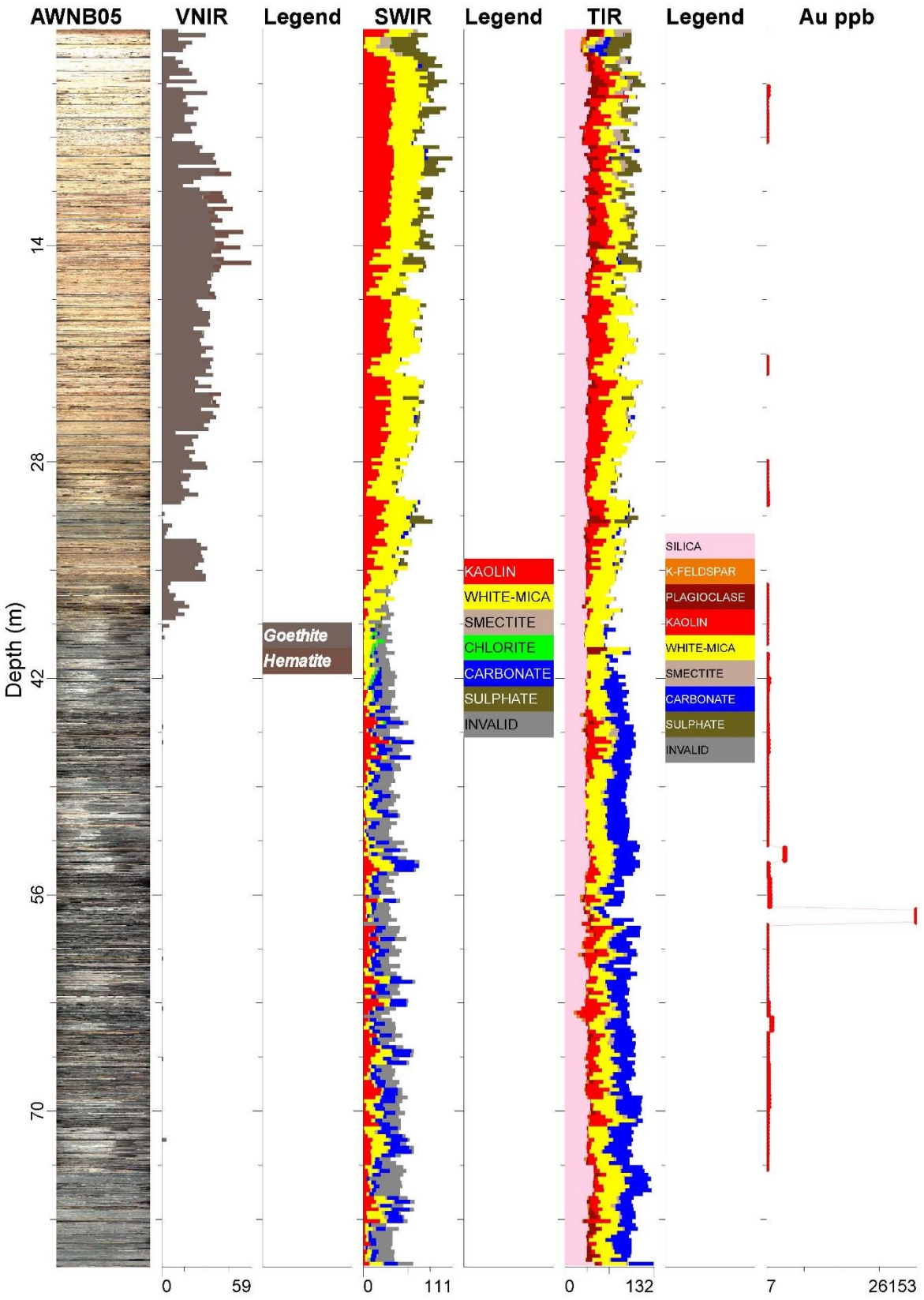

Figure 1 Downhole hylogger hyperspectral image of the hole AWNB05 of the New Bendigo prospect, Warratta Inlier, New South Wales, Australia

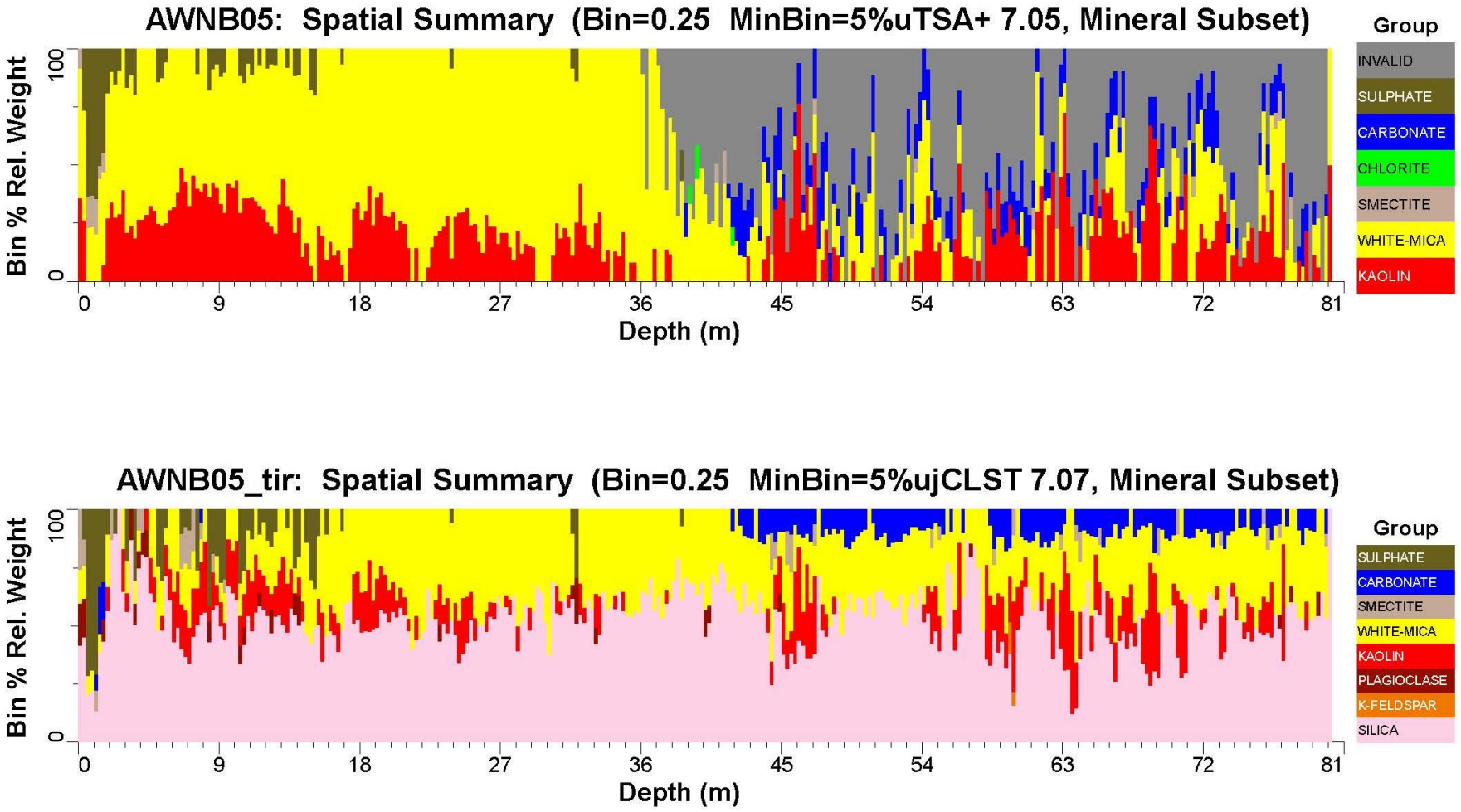

Figure 2 Summary of the hylogger hyperspectral image of the hole AWNB05 of the New Bendigo prospect, Warratta Inlier, New South Wales, Australia

Sample ID	Prospect	Borehole Name	From (m)	To (m)	Note
2022440151	New Bendigo	AWNB05	57.56	57.58	Sulfide ore and hydrothermal alteration

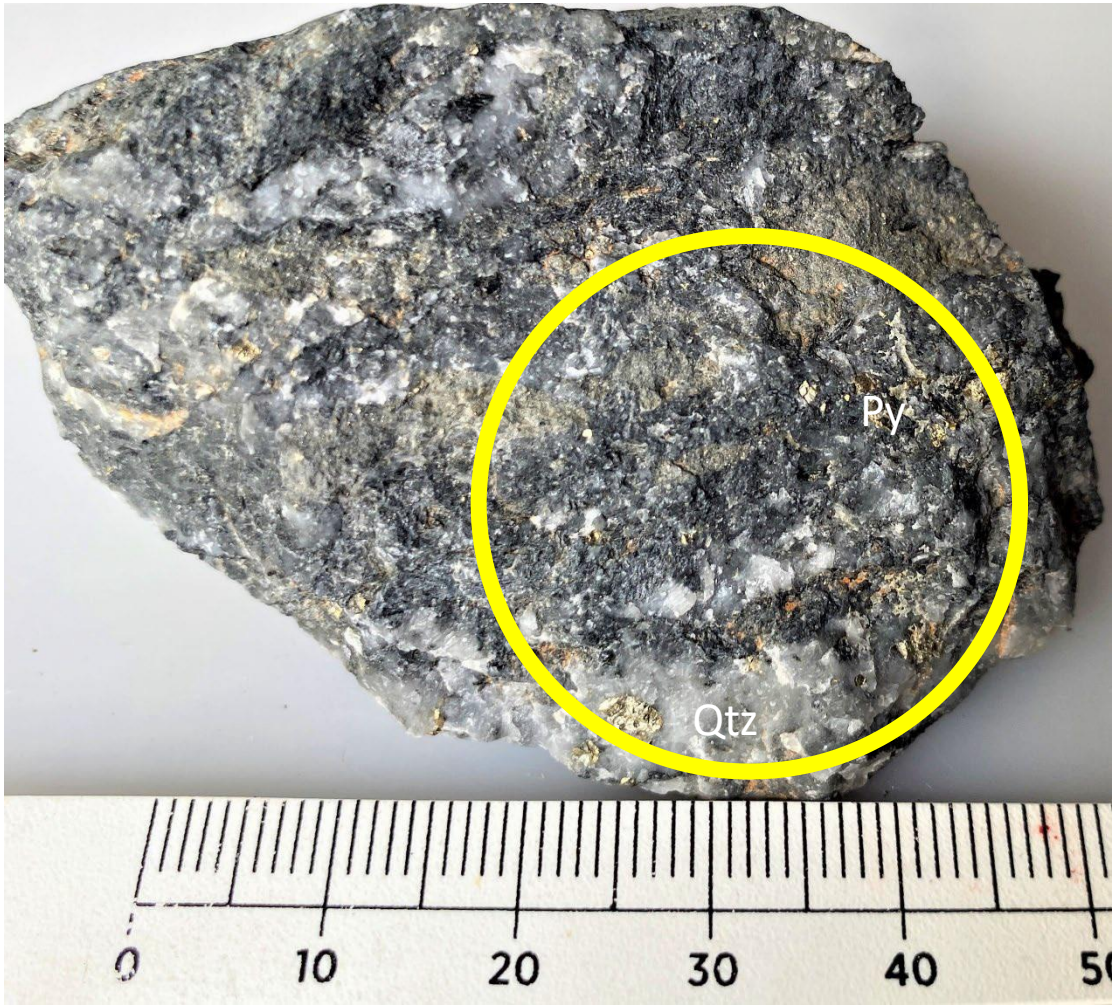

Figure 3 Photos of the drill core sample 2022440151 from drill hole AWNB05 of the New Bendigo prospect, Warratta Inlier, New South Wales, Australia. Py-pyrite; Qtz-quartz

Sample ID	Prospect	Borehole Name	From (m)	To (m)	Note
2022440151	New Bendigo	AWNB05	57.56	57.58	Sulfide ore and hydrothermal alteration

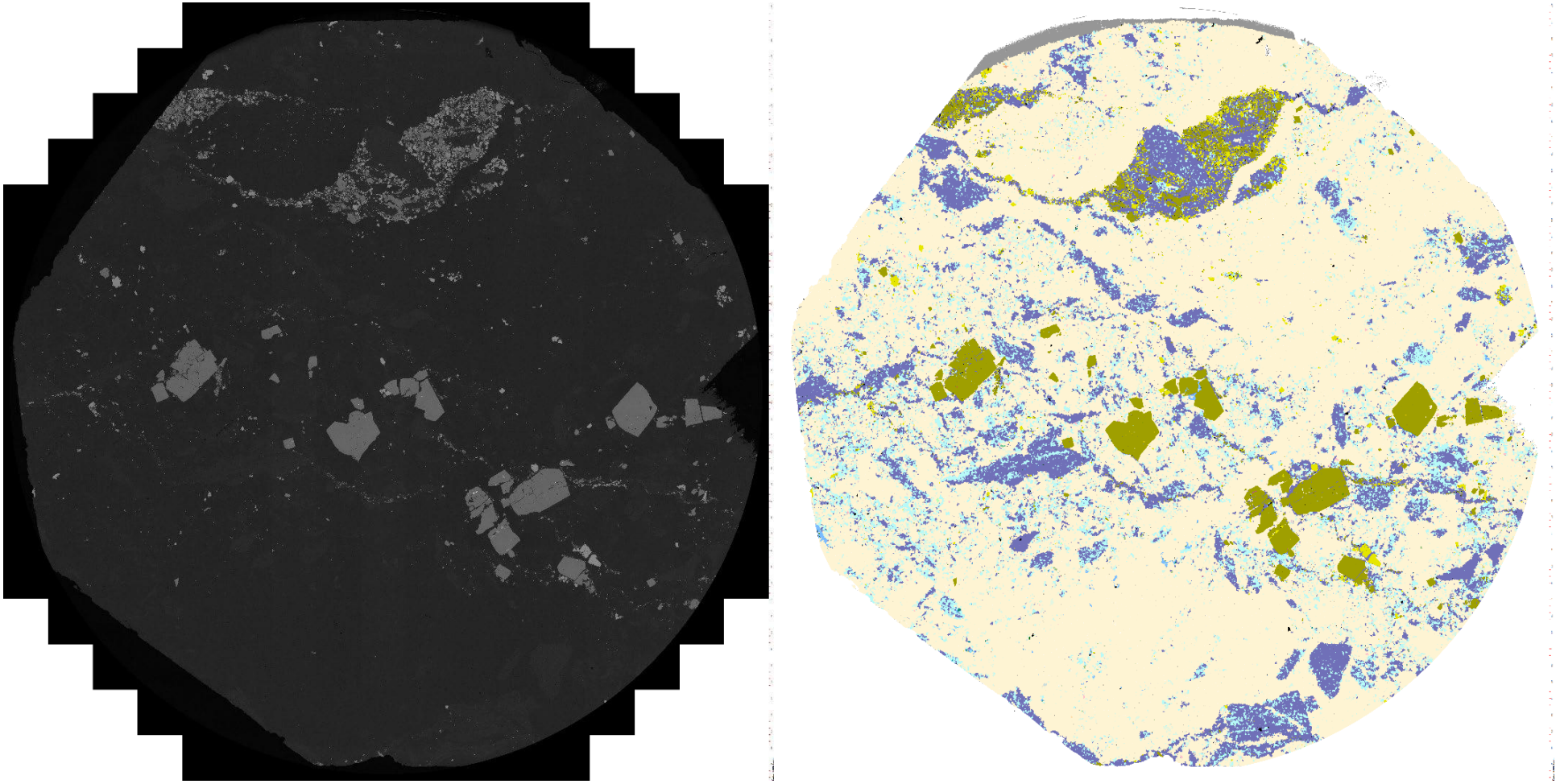

Figure 4 Backscattered electron (BSE) image (left) and Advanced Mineral Identification and Characterization System (AMICS) mineral map (right) of the sample 2022440151 from drill hole AWNB05 of the New Bendigo prospect, Warratta Inlier, New South Wales, Australia. See Figure 13 at the end of this document for the legend of minerals identified using Mineral Liberation Analysis (MLA) mapping.

Sample ID	Prospect	Borehole Name	From (m)	To (m)	Note
2022440158	New Bendigo	AWNB05	64.3	64.4	Sulfide ore and hydrothermal alteration

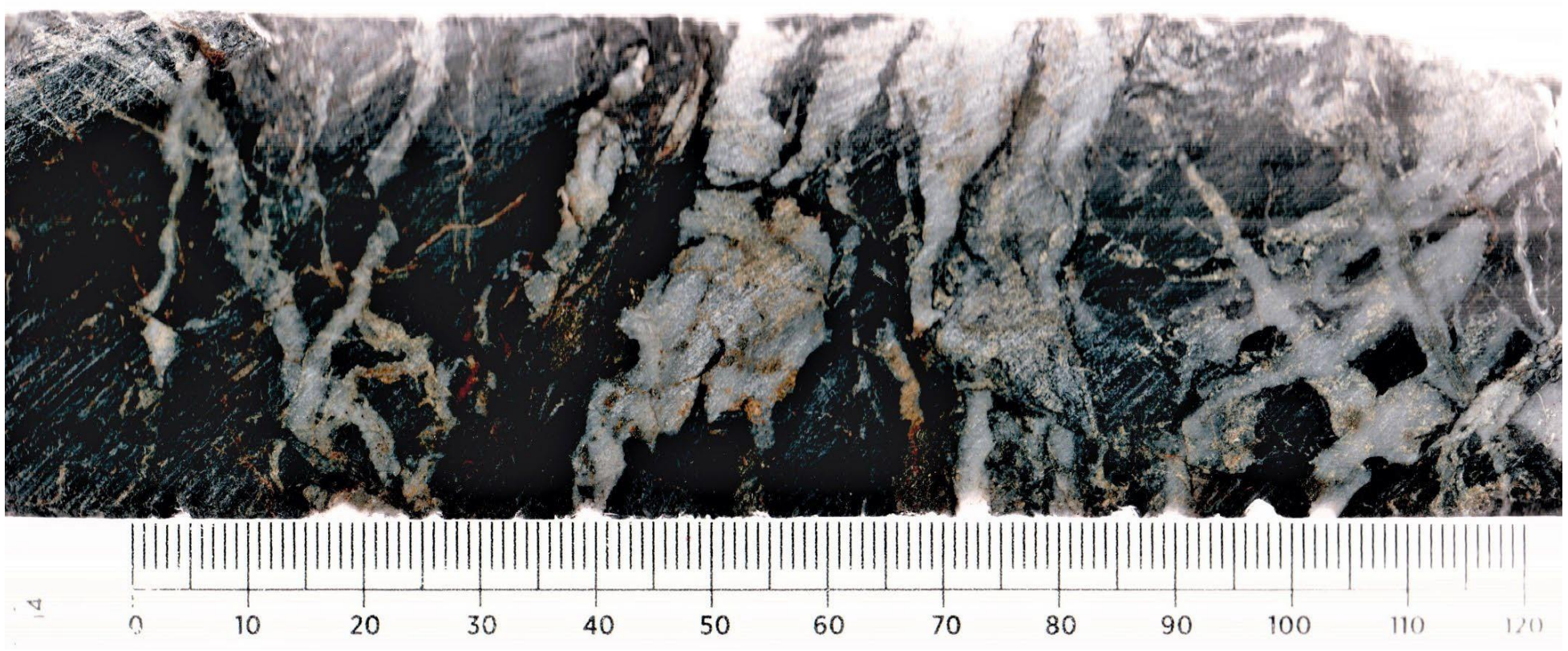

Figure 5 Photos of the drill core sample 2022440158 from drill hole AWNB05 of the New Bendigo prospect, Warratta Inlier, New South Wales, Australia.

Sample ID	Prospect	Borehole Name	From (m)	To (m)	Note
2022440148	New Bendigo	AWNB05	53.6	53.75	Sulfide ore and hydrothermal alteration

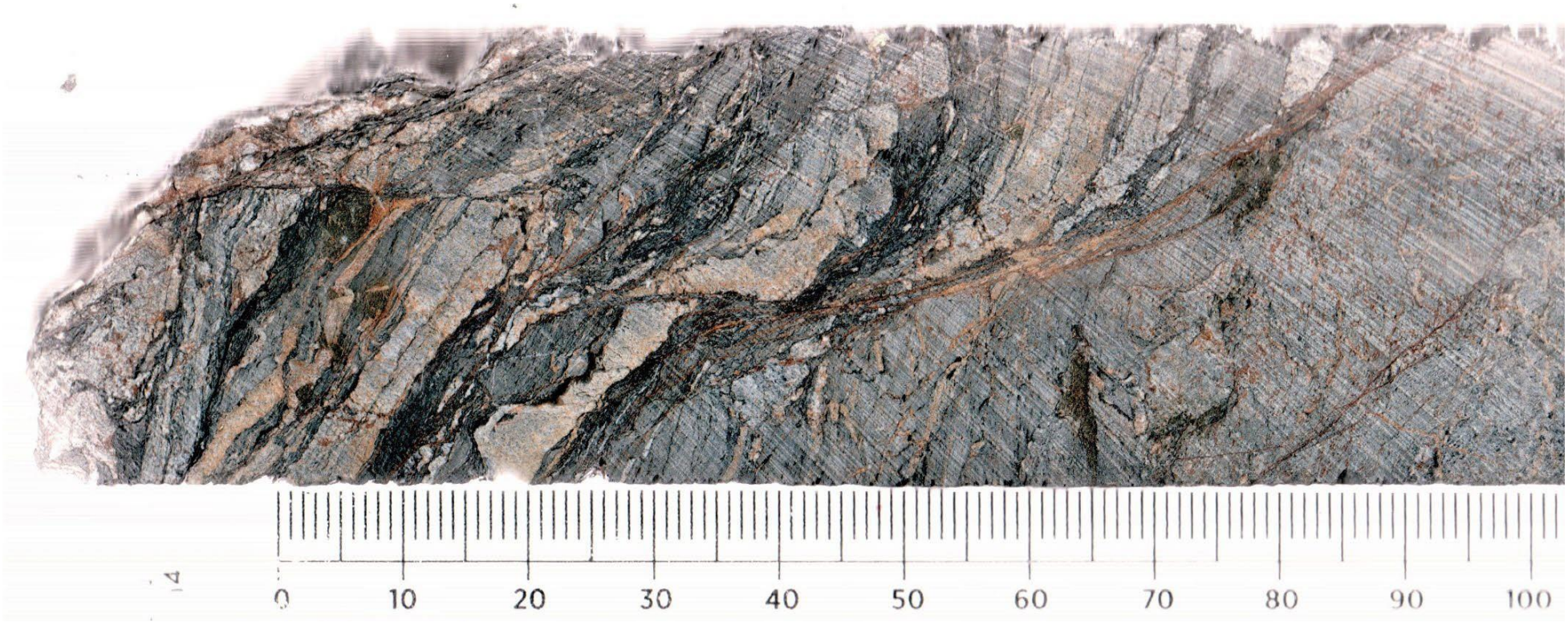

Figure 6 Photos of the drill core sample 2022440148 from drill hole AWNB05 of the New Bendigo prospect, Warratta Inlier, New South Wales, Australia.

Sample ID	Prospect	Borehole Name	From (m)	To (m)	Note
2022440157	New Bendigo	AWNB05	62.6	62.7	Sulfide ore and hydrothermal alteration

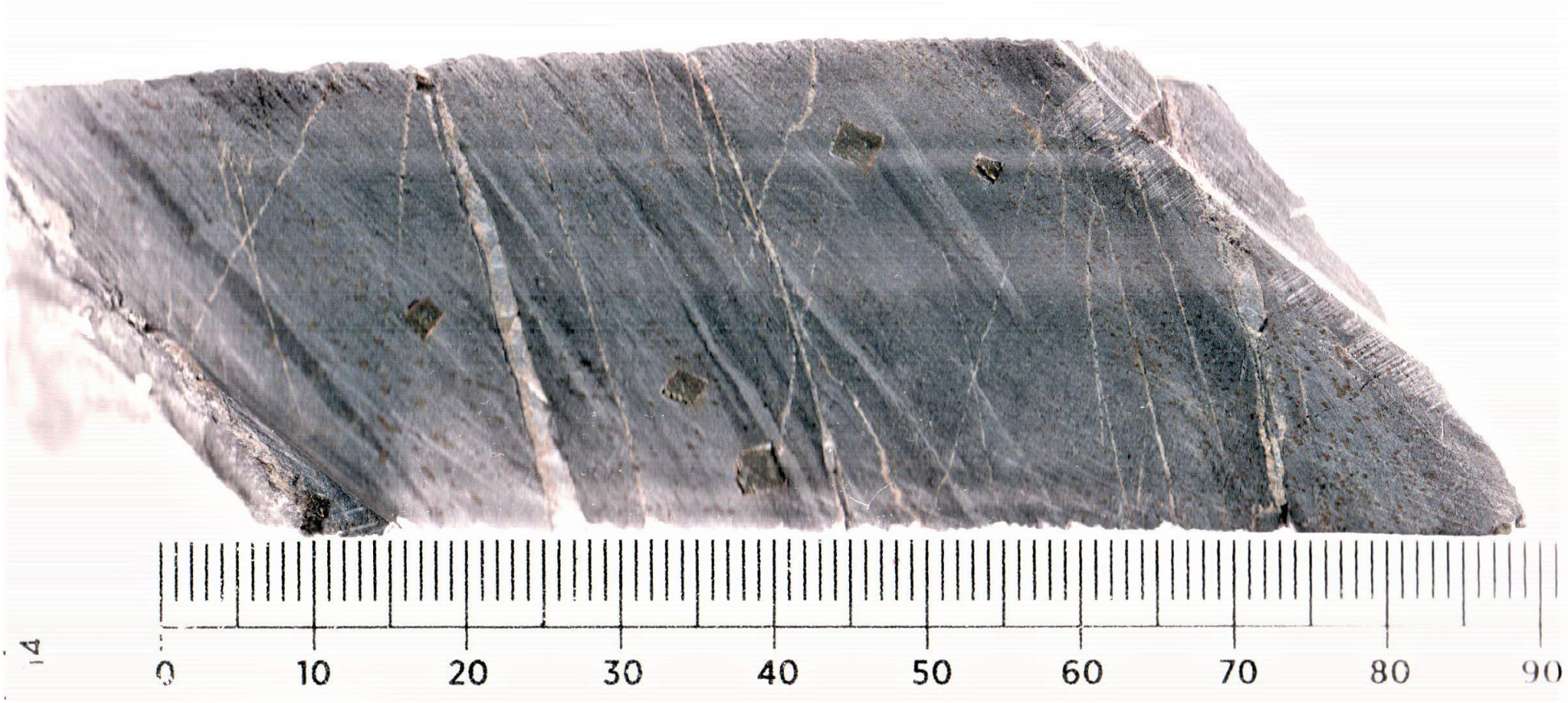

Figure 7 Photos of the drill core sample 2022440157 from drill hole AWNB05 of the New Bendigo prospect, Warratta Inlier, New South Wales, Australia.

Sample ID	Prospect	Borehole Name	From (m)	To (m)	Note
2022440156	New Bendigo	AWNB05	60.96	61.08	Sulfide ore and hydrothermal alteration

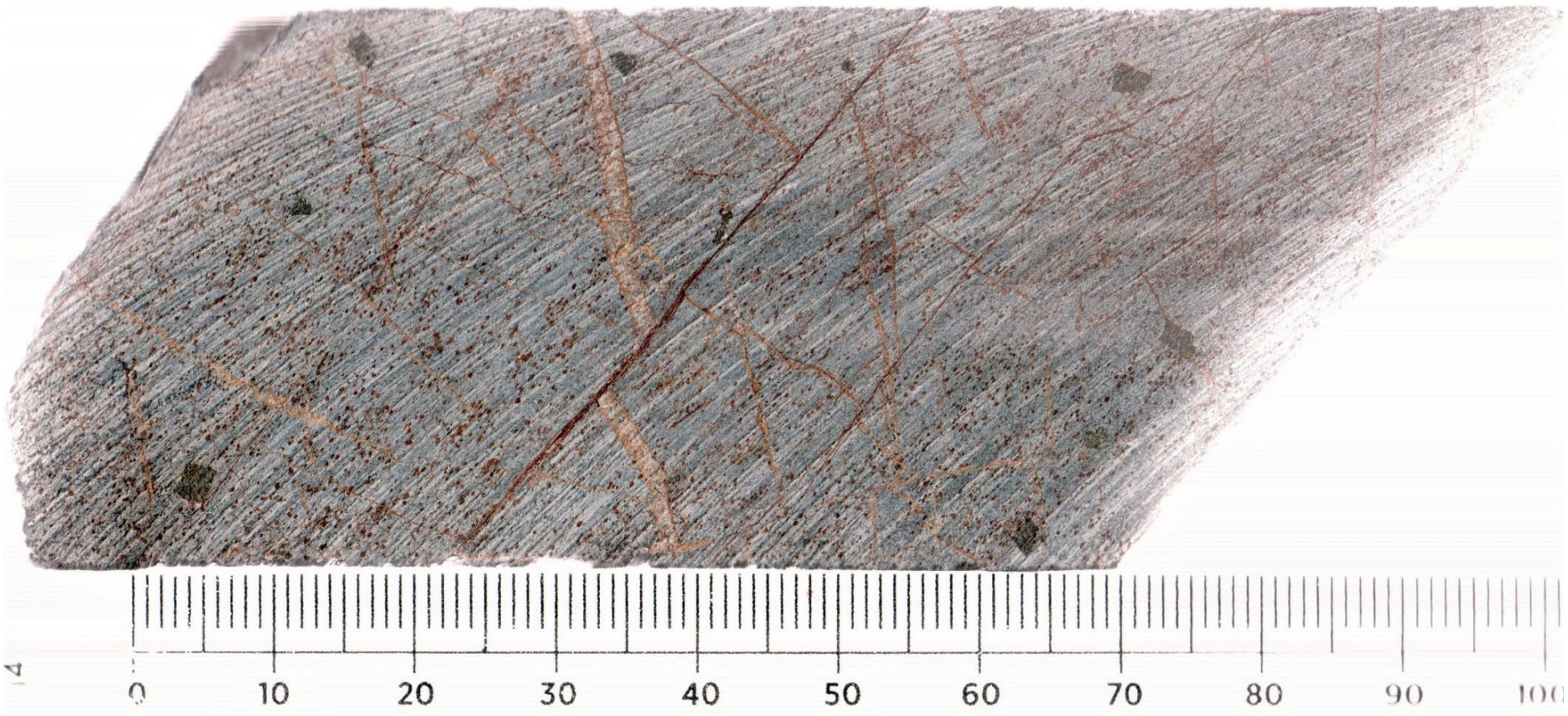

Figure 8 Photos of the drill core sample 2022440156 from drill hole AWNB05 of the New Bendigo prospect, Warratta Inlier, New South Wales, Australia.

Sample ID	Prospect	Borehole Name	From (m)	To (m)	Note
2022440150	New Bendigo	AWNB05	57.01	57.11	Sulfide ore and hydrothermal alteration

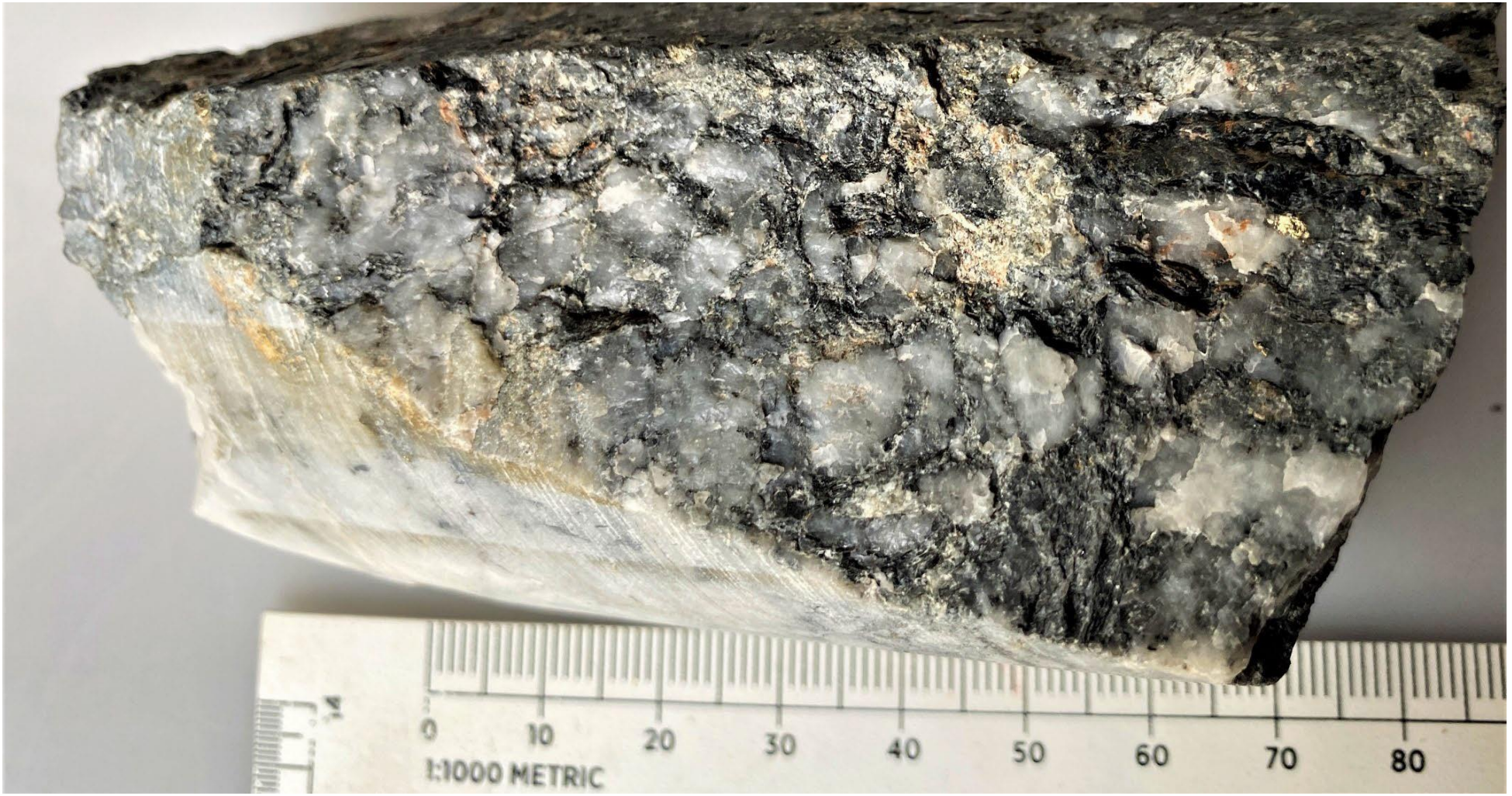

Figure 9 Photos of the drill core sample 2022440150 from drill hole AWNB05 of the New Bendigo prospect, Warratta Inlier, New South Wales, Australia.

Sample ID	Prospect	Borehole Name	From (m)	To (m)	Note
2022440152	New Bendigo	AWNB05	57.96	58.03	Sulfide ore and hydrothermal alteration

Figure 10 Photos of the drill core sample 2022440152 from drill hole AWNB05 of the New Bendigo prospect, Warratta Inlier, New South Wales, Australia.

Sample ID	Prospect	Borehole Name	From (m)	To (m)	Note
2022440153	New Bendigo	AWNB05	57.23	57.31	Sulfide ore and hydrothermal alteration

Figure 11 Photos of the drill core sample 2022440153 from drill hole AWNB05 of the New Bendigo prospect, Warratta Inlier, New South Wales, Australia.

Sample ID	Prospect	Borehole Name	From (m)	To (m)	Note
2022440154	New Bendigo	AWNB05	58.25	58.28	Sulfide ore and hydrothermal alteration

Figure 12 Photos of the drill core sample 2022440154 from drill hole AWNB05 of the New Bendigo prospect, Warratta Inlier, New South Wales, Australia.

S3.2 Pioneer prospect

Warratta Inlier, New South Wales

Detailed image data: Appendix 11 (individual data file)

(A) Sample List

Sample No.	Sample ID	Borehole	From (m)	To (m)	Notes
—	2022440133	AWPN01A	6.53	6.60	Sulfide ore and hydrothermal alteration
—	2022440141	AWPN02A	70.58	70.71	Sulfide ore and hydrothermal alteration
—	2022440143	AWPN02A	—	—	Sulfide ore and hydrothermal alteration
—	2022440144	AWPN02A	—	—	Sulfide ore and hydrothermal alteration
—	2022440140	AWPN01A	—	—	Sulfide ore and hydrothermal alteration
—	2022440142	AWPN01A	—	—	Sulfide ore and hydrothermal alteration
—	2022440134–2022440139	AWPN01A / AWPN02A	—	—	Sulfide ore and hydrothermal alteration

(B) Mineralisation Characteristics

Data Type	Mineral Assemblage
Hyperspectral SWIR	—
Hyperspectral TIR	—
Hyperspectral VNIR	—
Drill core specimen	*Qtz, Fsp, Chl, Py, Cpy*
Thin section	—
AMICS mineral map	*Qtz, Fsp, Chl, Py, Cpy, Ab, Ep, Cal, Kfsp, Bt, Ttn, Ap, Ser*

(C) Mineralogical Textures and Paragenesis

Category	Description
Texture	Disseminated and vein-hosted Py–Cpy mineralisation in quartz–feldspar–chlorite altered host rocks.
Paragenesis	Feldspar (albite + K-feldspar) represents early sodic–potassic alteration. Chlorite overprints feldspar alteration. Pyrite is associated with early feldspar stage; chalcopyrite is found in later epidote–calcite veins.

(D) Supplementary Figure Reference

Supplementary Figures *include drill core photographs of samples 2022440133, 2022440141, 2022440143, 2022440144, 2022440140, 2022440142 and 2022440134–2022440139; BSE images and AMICS mineral maps of Py–Cpy mineralisation. AMICS mineral standard legend included.*

S3.2 The Pioneer prospect, Warratta Inlier, New South Wales

Sample ID	Prospect	Borehole Name	From (m)	To (m)	Note
2022440133	Pioneer	AWPN01A	6.53	6.6	Sulfide ore and hydrothermal alteration

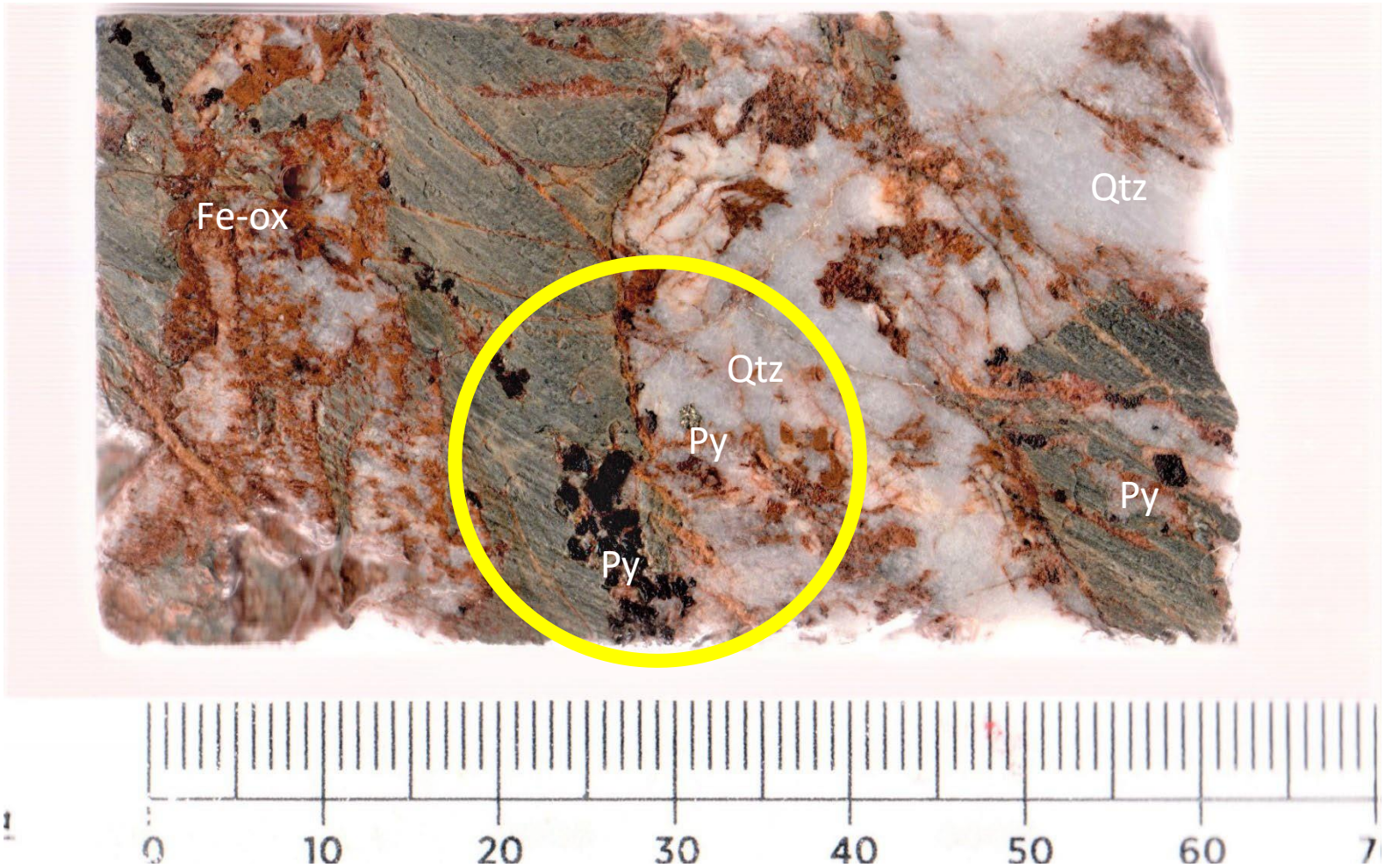

Figure 1 Photos of the drill core sample 2022440133 from drill hole AWPN01A of the Pioneer prospect, Warratta Inlier, New South Wales, Australia. Qtz-quartz; Py-pyrite; Fe-Ox-Fe oxides.

Sample ID	Prospect	Borehole Name	From (m)	To (m)	Note
2022440133	Pioneer	AWPN01A	6.53	6.6	Sulfide ore and hydrothermal alteration

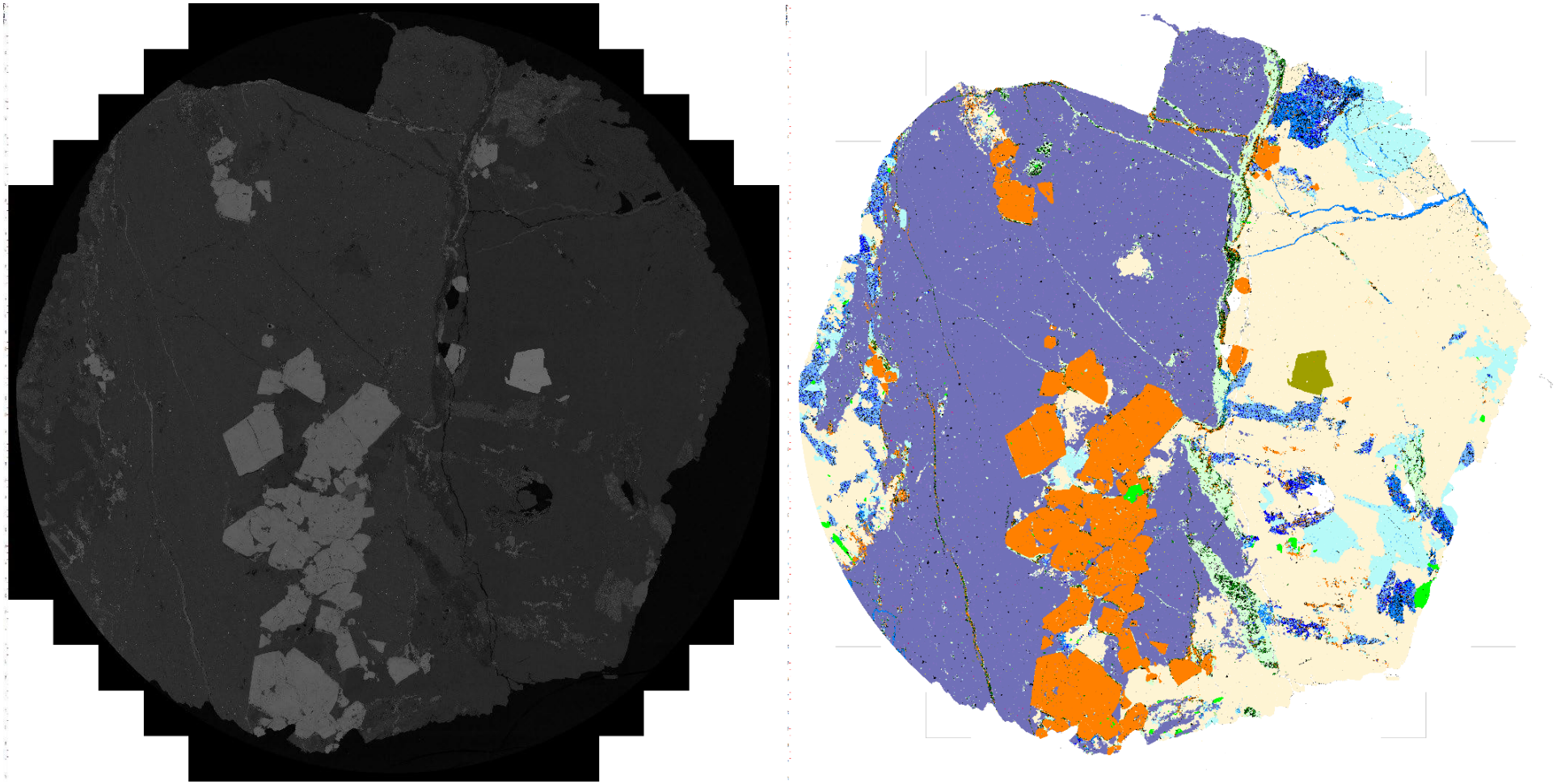

Figure 2 Backscattered electron (BSE) image (left) and Advanced Mineral Identification and Characterization System (AMICS) mineral map (right) of the sample 2022440133 from drill hole AWPN01A of the Pioneer prospect, Warratta Inlier, New South Wales, Australia. See Figure 17 at the end of this document for the legend of minerals identified using Mineral Liberation Analysis (MLA) mapping.

Sample ID	Prospect	Borehole Name	From (m)	To (m)	Note
2022440141	Pioneer	AWPN02A	70.58	70.71	Sulfide ore and hydrothermal alteration

Figure 3 Photos of the drill core sample 2022440141 from drill hole AWPN02A of the Pioneer prospect, Warratta Inlier, New South Wales, Australia.

Sample ID	Prospect	Borehole Name	From (m)	To (m)	Note
2022440141	Pioneer	AWPN02A	70.58	70.71	Sulfide ore and hydrothermal alteration

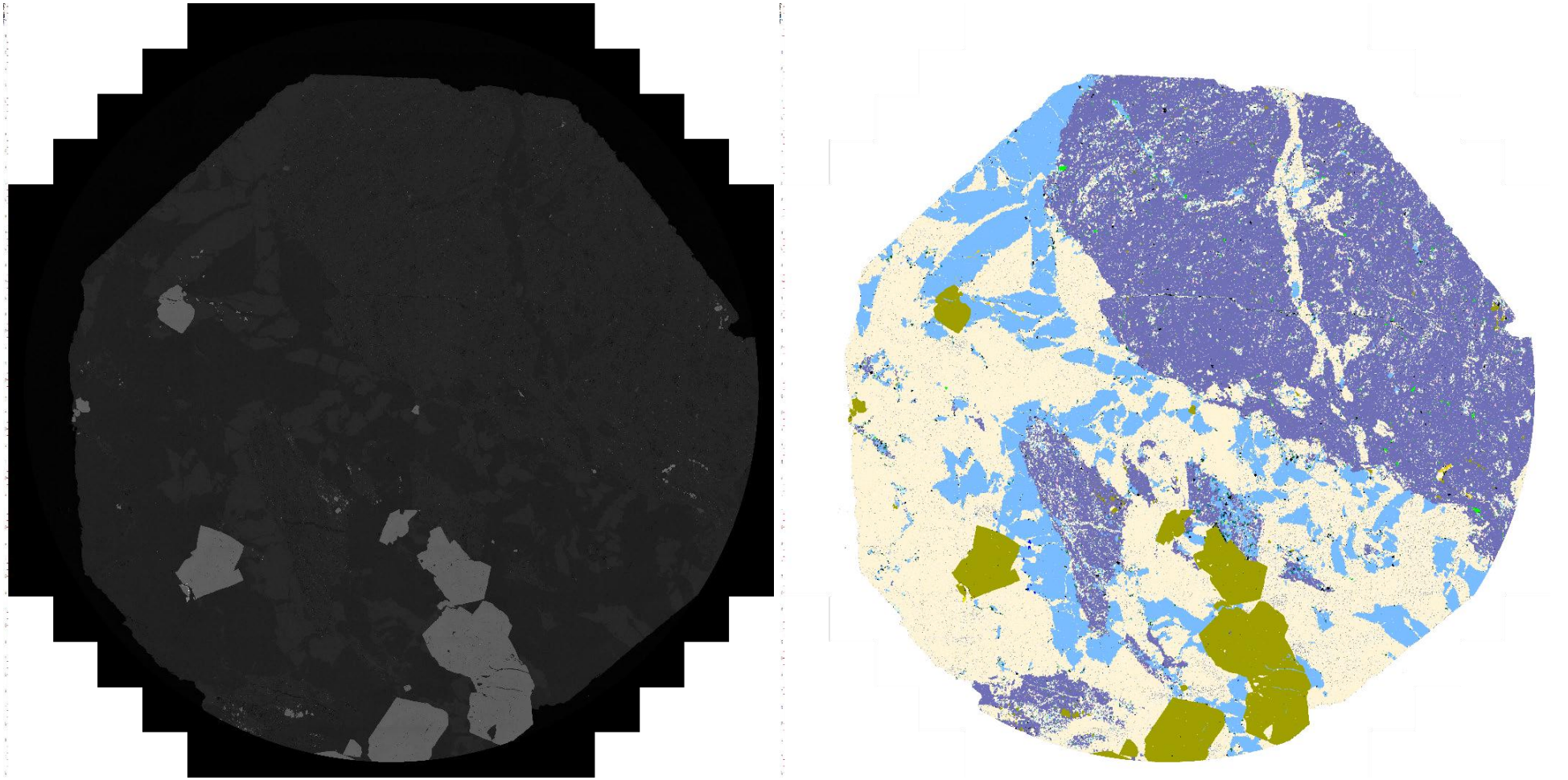

Figure 4 Backscattered electron (BSE) image (left) and Advanced Mineral Identification and Characterization System (AMICS) mineral map (right) of the sample 2022440141 from drill hole AWPN02A of the Pioneer prospect, Warratta Inlier, New South Wales, Australia. See Figure 17 at the end of this document for the legend of minerals identified using Mineral Liberation Analysis (MLA) mapping.

Sample ID	Prospect	Borehole Name	From (m)	To (m)	Note
2022440143	Pioneer	AWPN02A	71.52	71.58	Sulfide ore and hydrothermal alteration

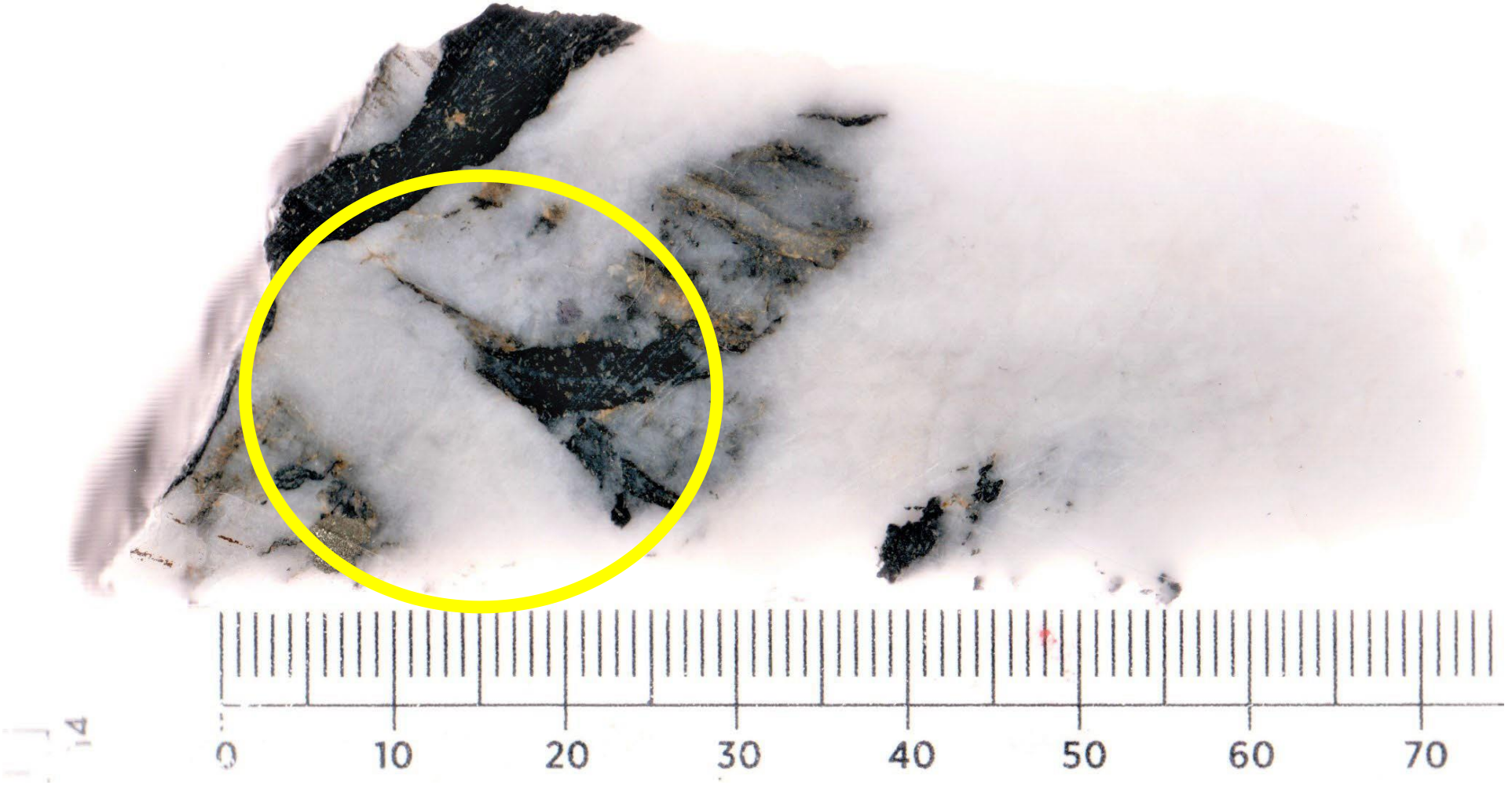

Figure 5 Photos of the drill core sample 2022440143 from drill hole AWPN02A of the Pioneer prospect, Warratta Inlier, New South Wales, Australia.

Sample ID	Prospect	Borehole Name	From (m)	To (m)	Note
2022440143	Pioneer	AWPN02A	71.52	71.58	Sulfide ore and hydrothermal alteration

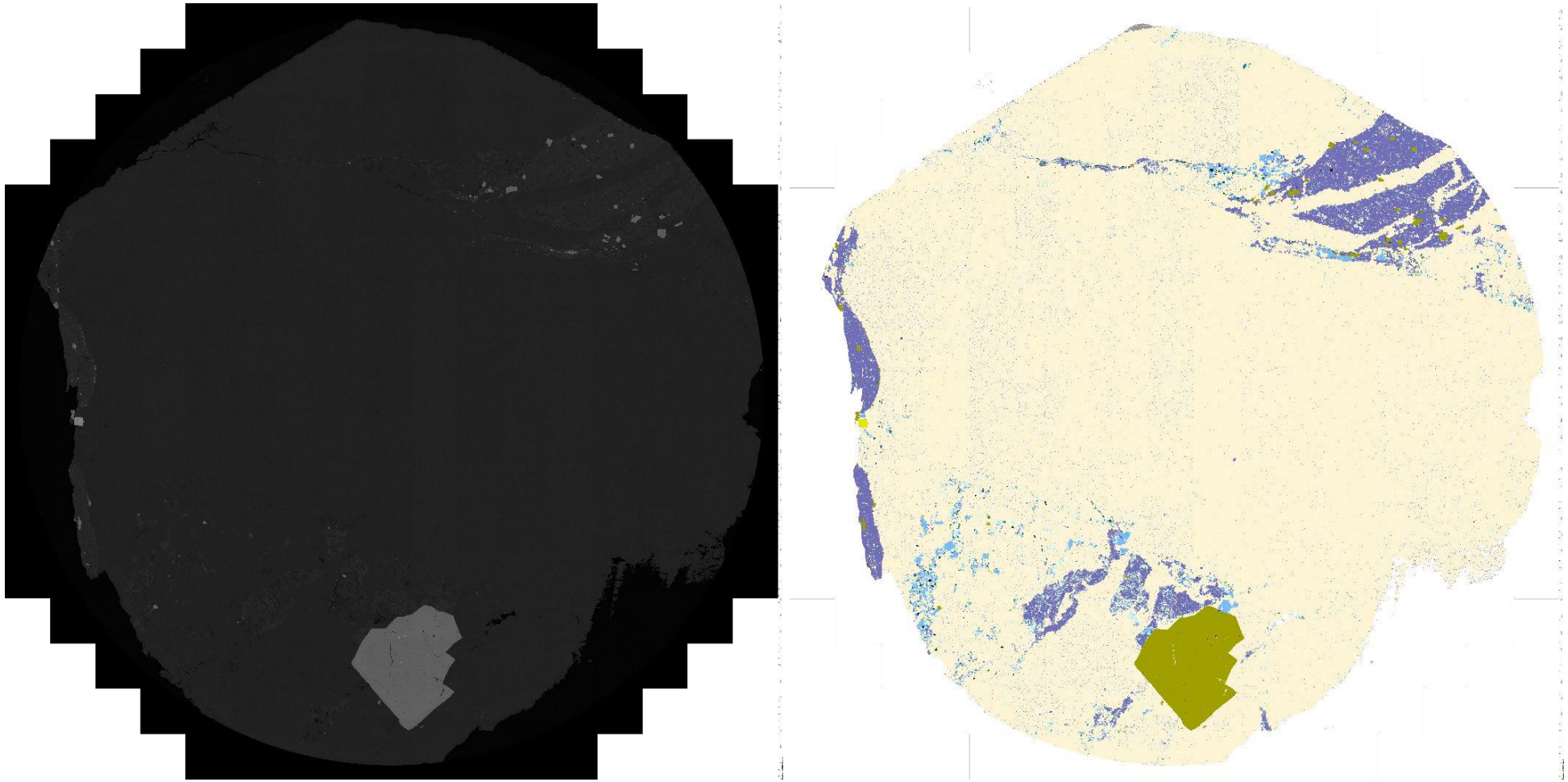

Figure 6 Backscattered electron (BSE) image (left) and Advanced Mineral Identification and Characterization System (AMICS) mineral map (right) of the sample 2022440143 from drill hole AWPN02A of the Pioneer prospect, Warratta Inlier, New South Wales, Australia. See Figure 17 at the end of this document for the legend of minerals identified using Mineral Liberation Analysis (MLA) mapping.

Sample ID	Prospect	Borehole Name	From (m)	To (m)	Note
2022440144	Pioneer	AWPN02A	71.73	71.79	Sulfide ore and hydrothermal alteration

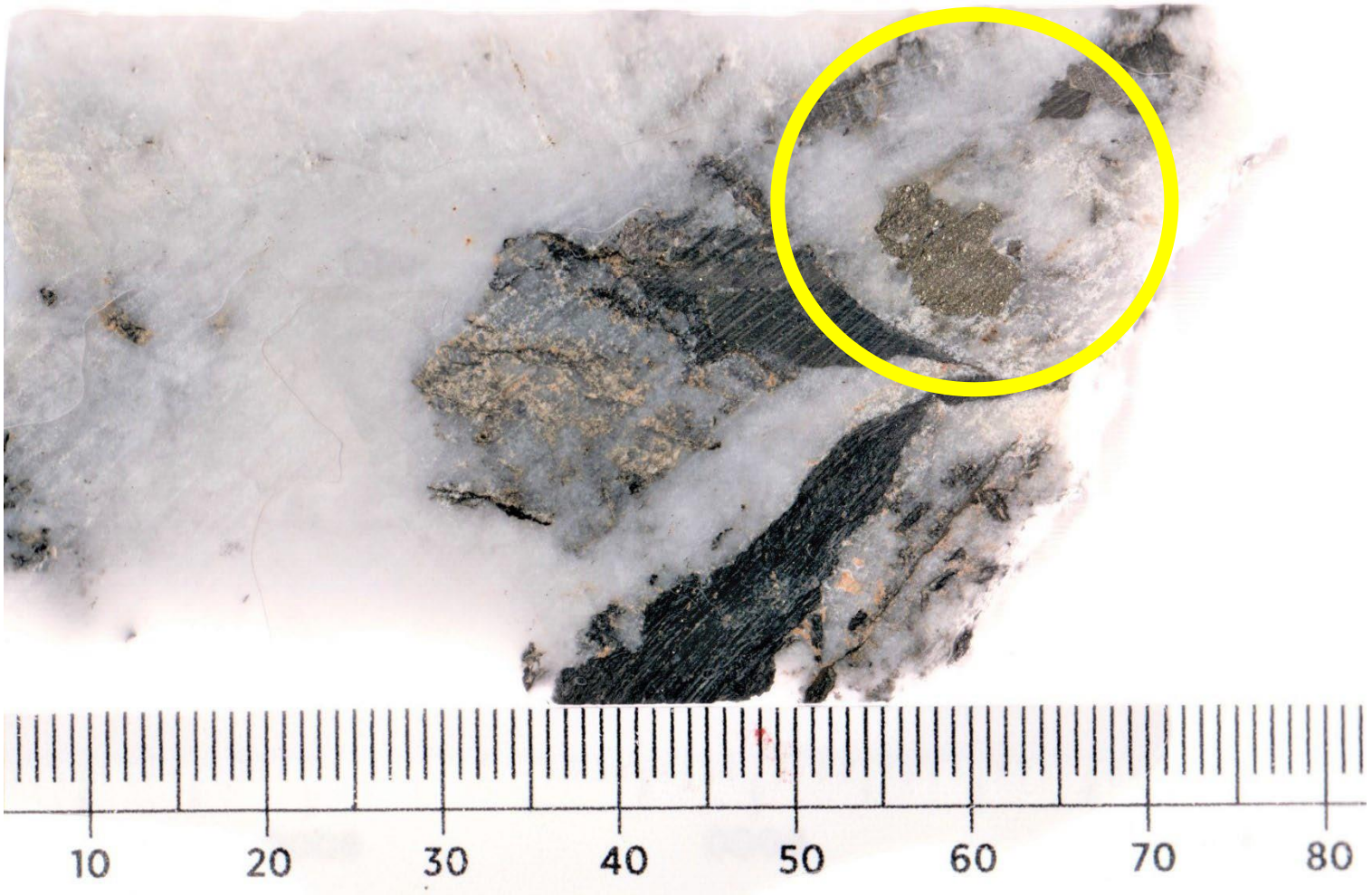

Figure 7 Photos of the drill core sample 2022440144 from drill hole AWPN02A of the Pioneer prospect, Warratta Inlier, New South Wales, Australia.

Sample ID	Prospect	Borehole Name	From (m)	To (m)	Note
2022440144	Pioneer	AWPN02A	71.73	71.79	Sulfide ore and hydrothermal alteration

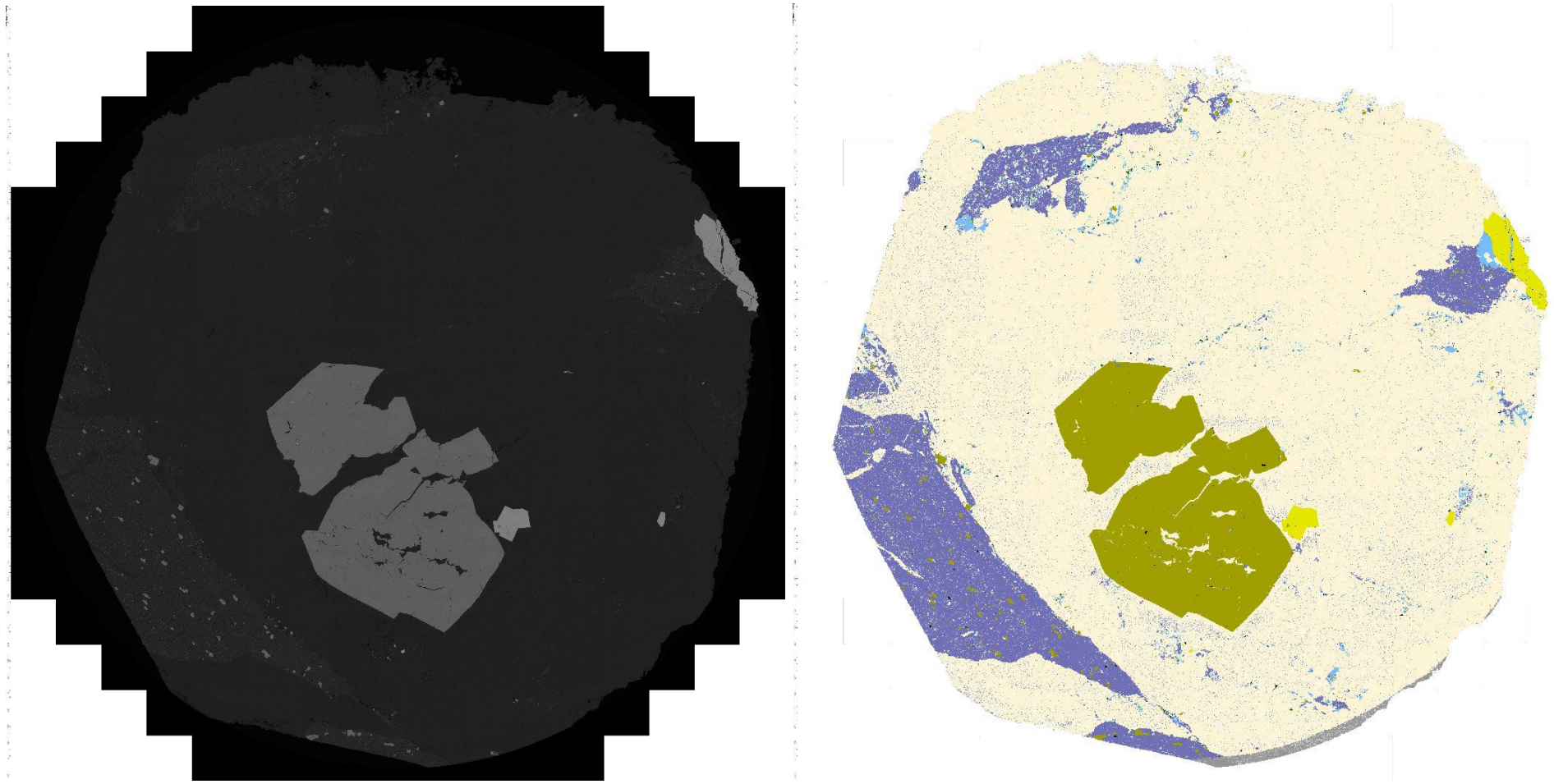

Figure 8 Backscattered electron (BSE) image (left) and Advanced Mineral Identification and Characterization System (AMICS) mineral map (right) of the sample 2022440144 from drill hole AWPN02A of the Pioneer prospect, Warratta Inlier, New South Wales, Australia. See Figure 17 at the end of this document for the legend of minerals identified using Mineral Liberation Analysis (MLA) mapping.

Sample ID	Prospect	Borehole Name	From (m)	To (m)	Note
2022440140	Pioneer	AWPN02A	70.4	70.55	Sulfide ore and hydrothermal alteration

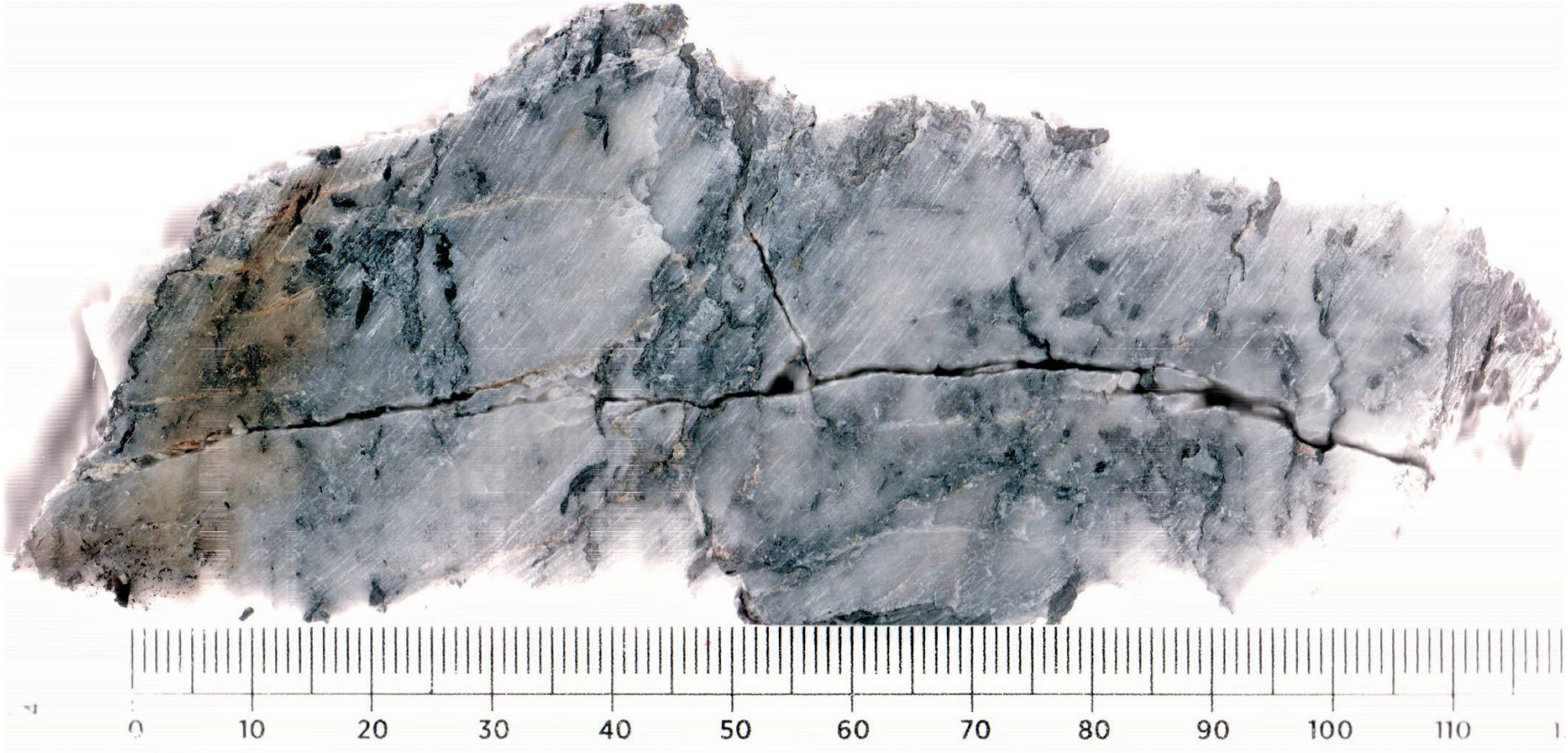

Figure 9 Photos of the drill core sample 2022440140 from drill hole AWPN02A of the Pioneer prospect, Warratta Inlier, New South Wales, Australia.

Sample ID	Prospect	Borehole Name	From (m)	To (m)	Note
2022440142	Pioneer	AWPN02A	71.18	71.25	Sulfide ore and hydrothermal alteration

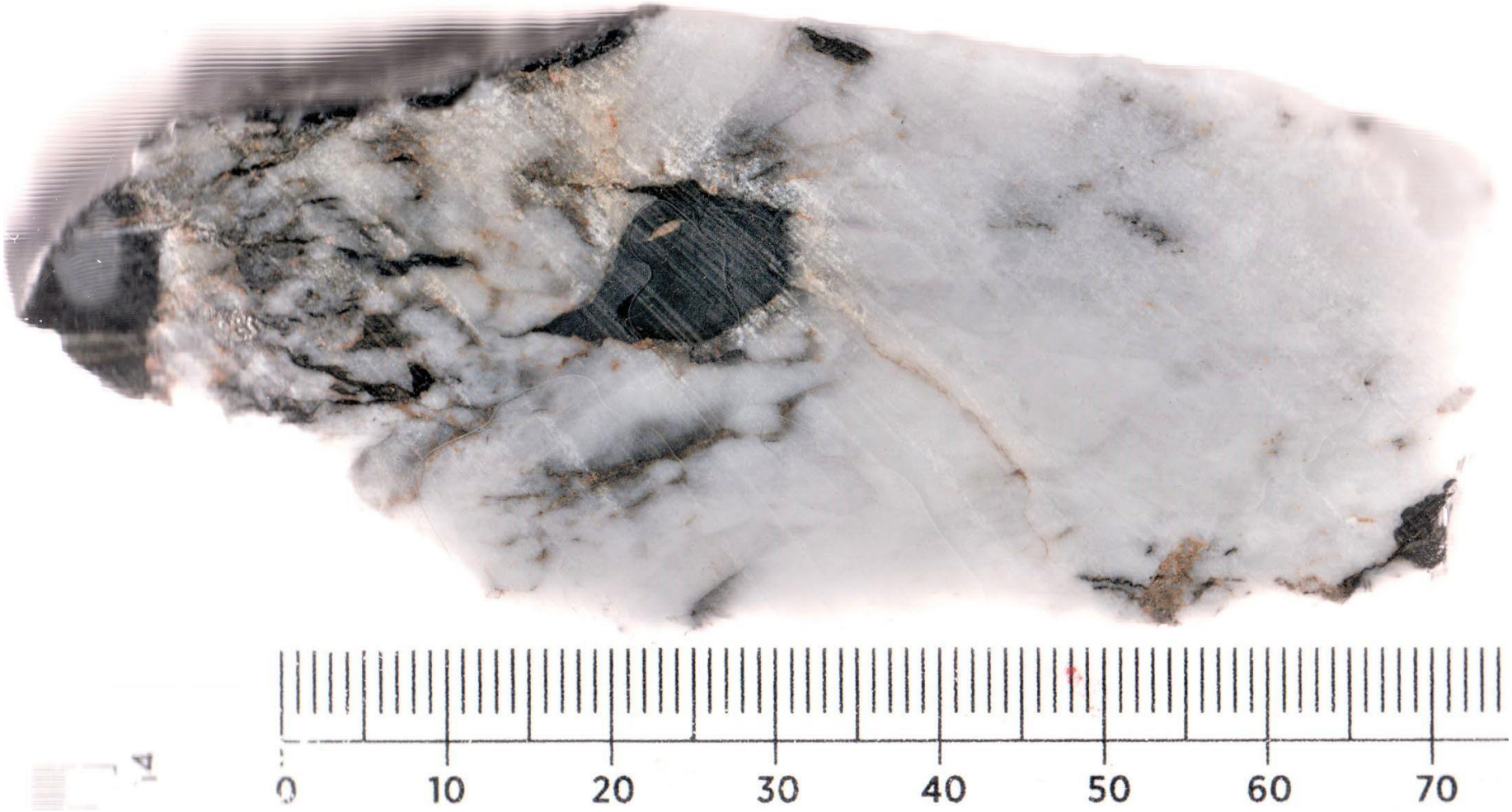

Figure 10 Photos of the drill core sample 2022440142 from drill hole AWPN02A of the Pioneer prospect, Warratta Inlier, New South Wales, Australia.

Sample ID	Prospect	Borehole Name	From (m)	To (m)	Note
2022440134	Pioneer	AWPN01A	10.3	10.5	Sulfide ore and hydrothermal alteration

Figure 11 Photos of the drill core sample 2022440134 from drill hole AWPN01A of the Pioneer prospect, Warratta Inlier, New South Wales, Australia.

Sample ID	Prospect	Borehole Name	From (m)	To (m)	Note
2022440135	Pioneer	AWPN01A	28.17	28.25	Sulfide ore and hydrothermal alteration

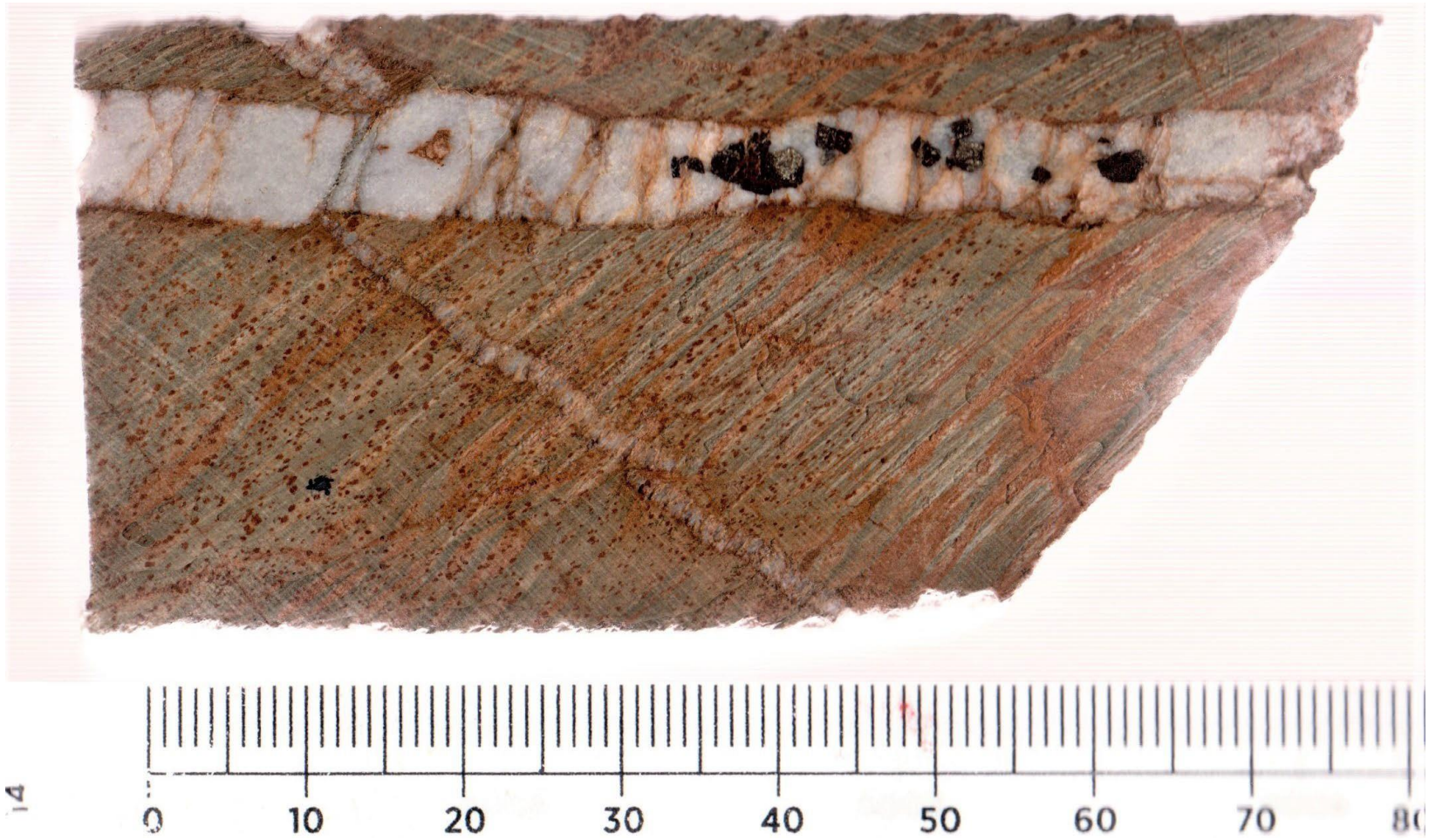

Figure 12 Photos of the drill core sample 2022440135 from drill hole AWPN01A of the Pioneer prospect, Warratta Inlier, New South Wales, Australia.

Sample ID	Prospect	Borehole Name	From (m)	To (m)	Note
2022440136	Pioneer	AWPN01A	29.32	29.45	Sulfide ore and hydrothermal alteration

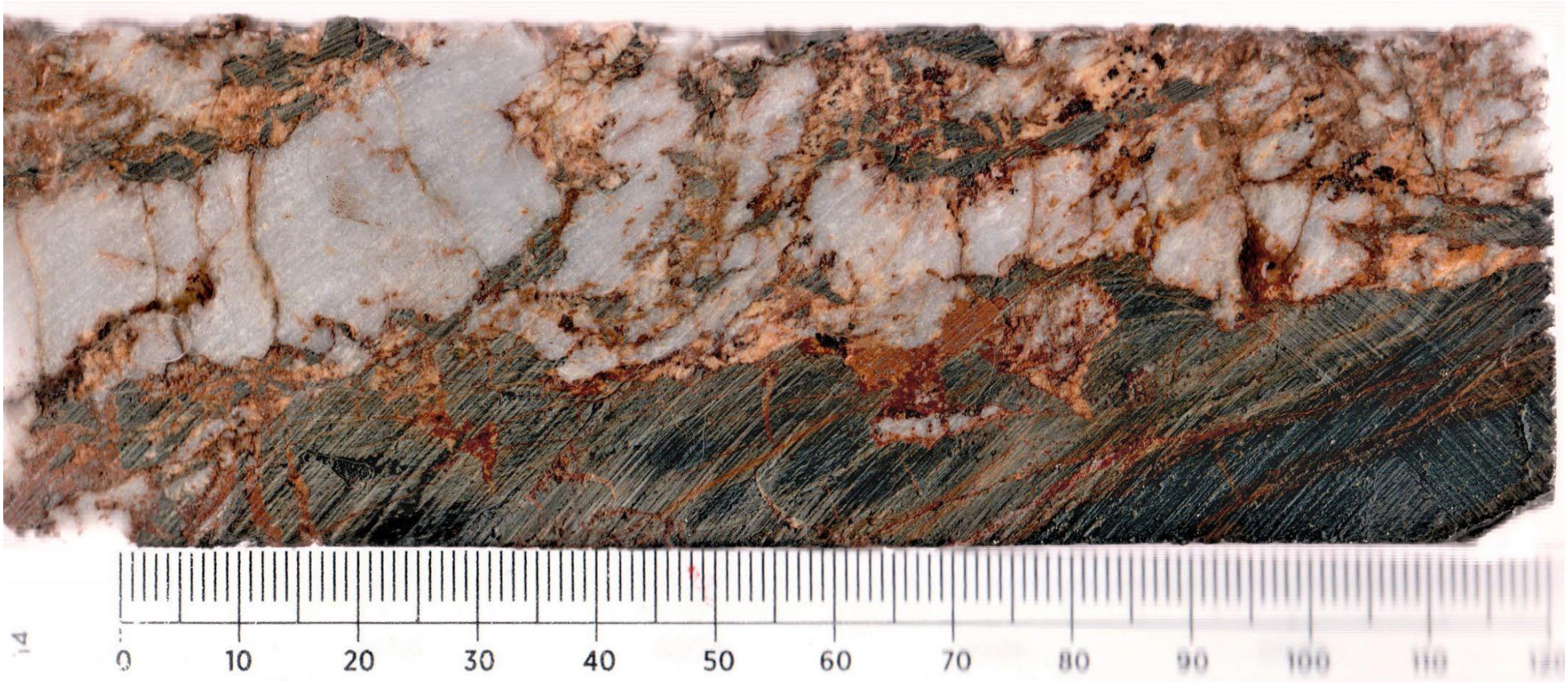

Figure 13 Photos of the drill core sample 2022440136 from drill hole AWPN01A of the Pioneer prospect, Warratta Inlier, New South Wales, Australia.

Sample ID	Prospect	Borehole Name	From (m)	To (m)	Note
2022440137	Pioneer	AWPN01A	110.21	110.35	Sulfide ore and hydrothermal alteration

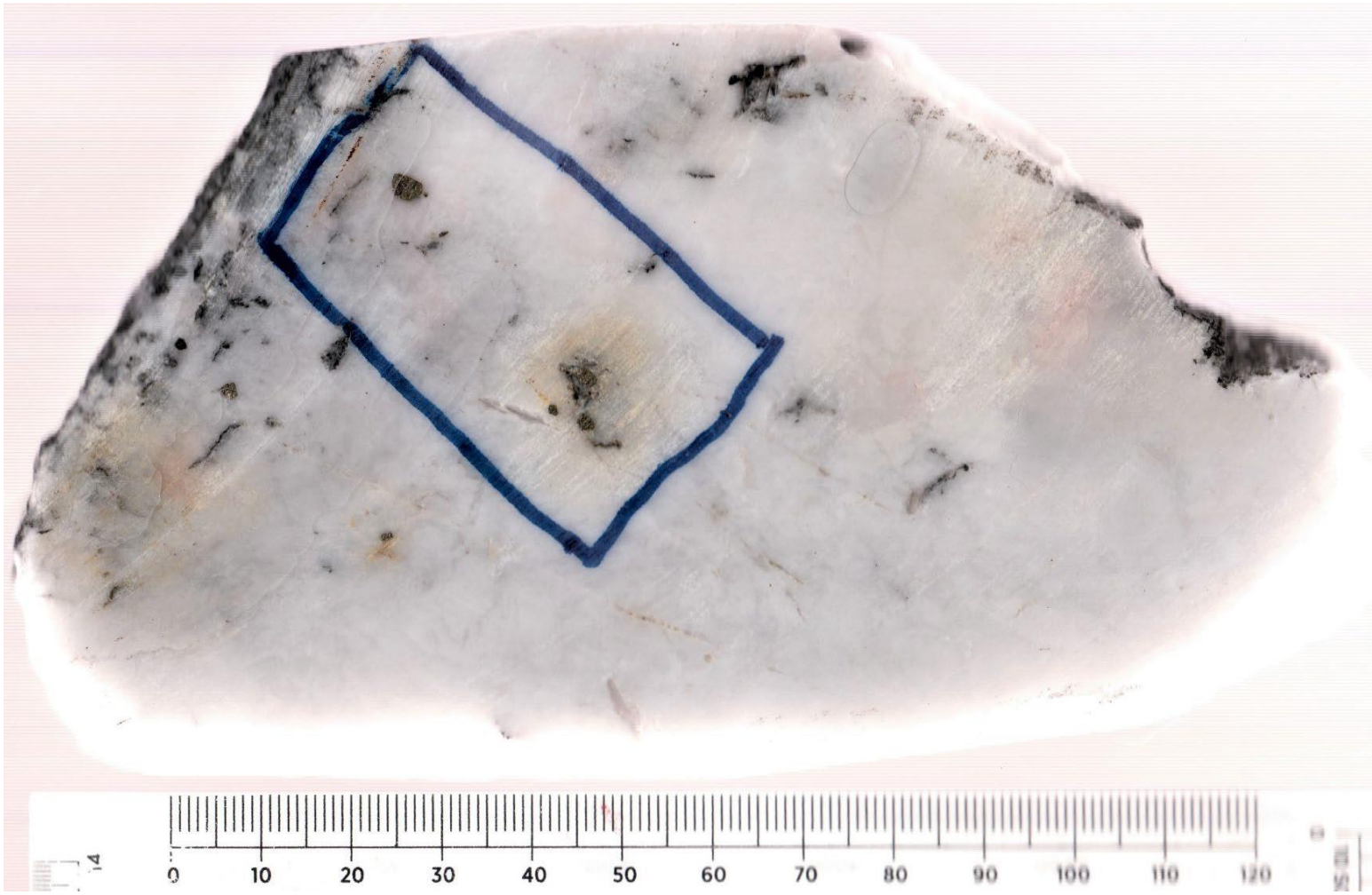

Figure 14 Photos of the drill core sample 2022440137 from drill hole AWPN01A of the Pioneer prospect, Warratta Inlier, New South Wales, Australia.

Sample ID	Prospect	Borehole Name	From (m)	To (m)	Note
2022440138	Pioneer	AWPN02A	16.2	16.3	Sulfide ore and hydrothermal alteration

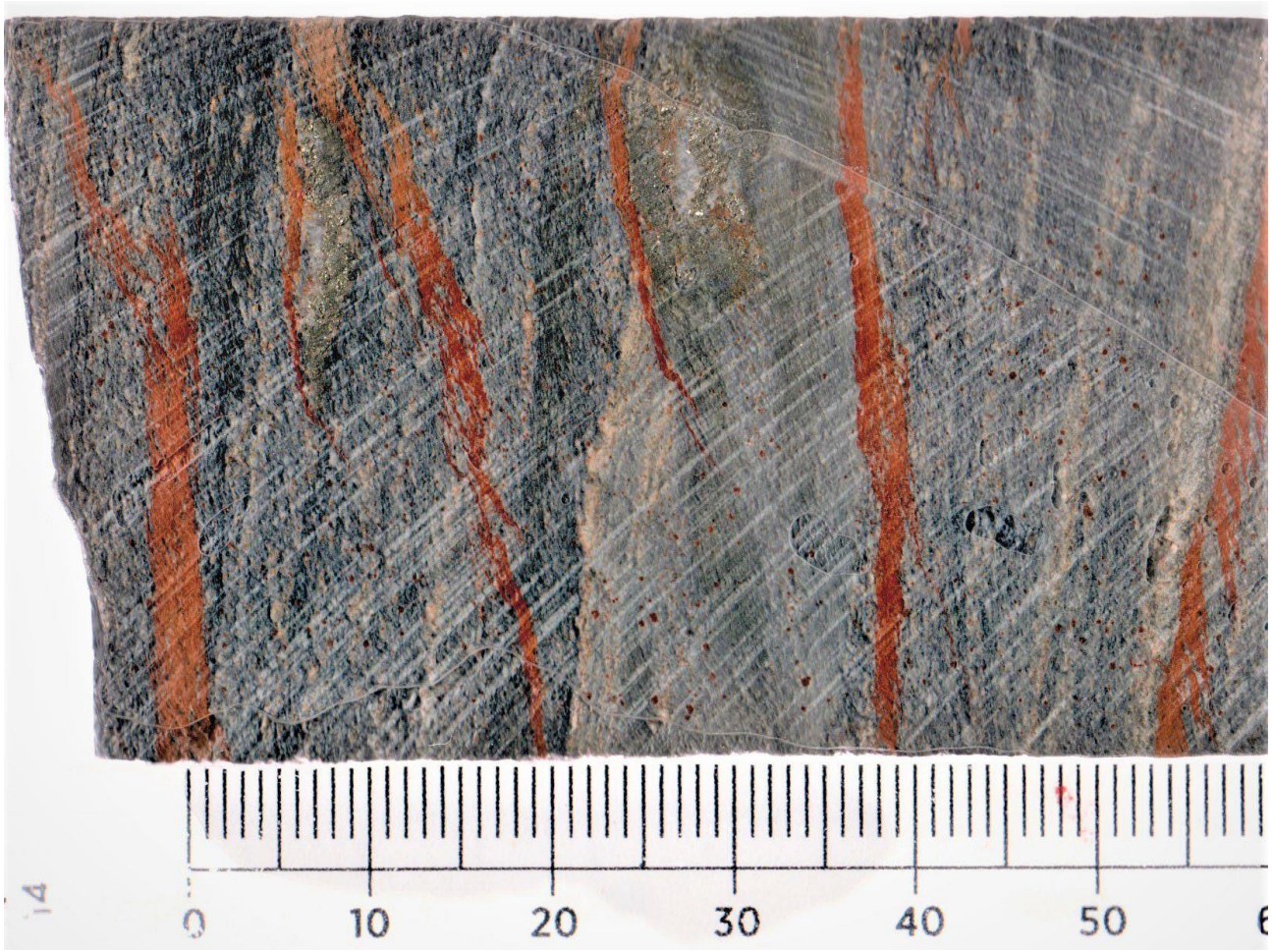

Figure 15 Photos of the drill core sample 2022440138 from drill hole AWPN02A of the Pioneer prospect, Warratta Inlier, New South Wales, Australia.

Sample ID	Prospect	Borehole Name	From (m)	To (m)	Note
2022440139	Pioneer	AWPN02A	38.25	38.4	Sulfide ore and hydrothermal alteration

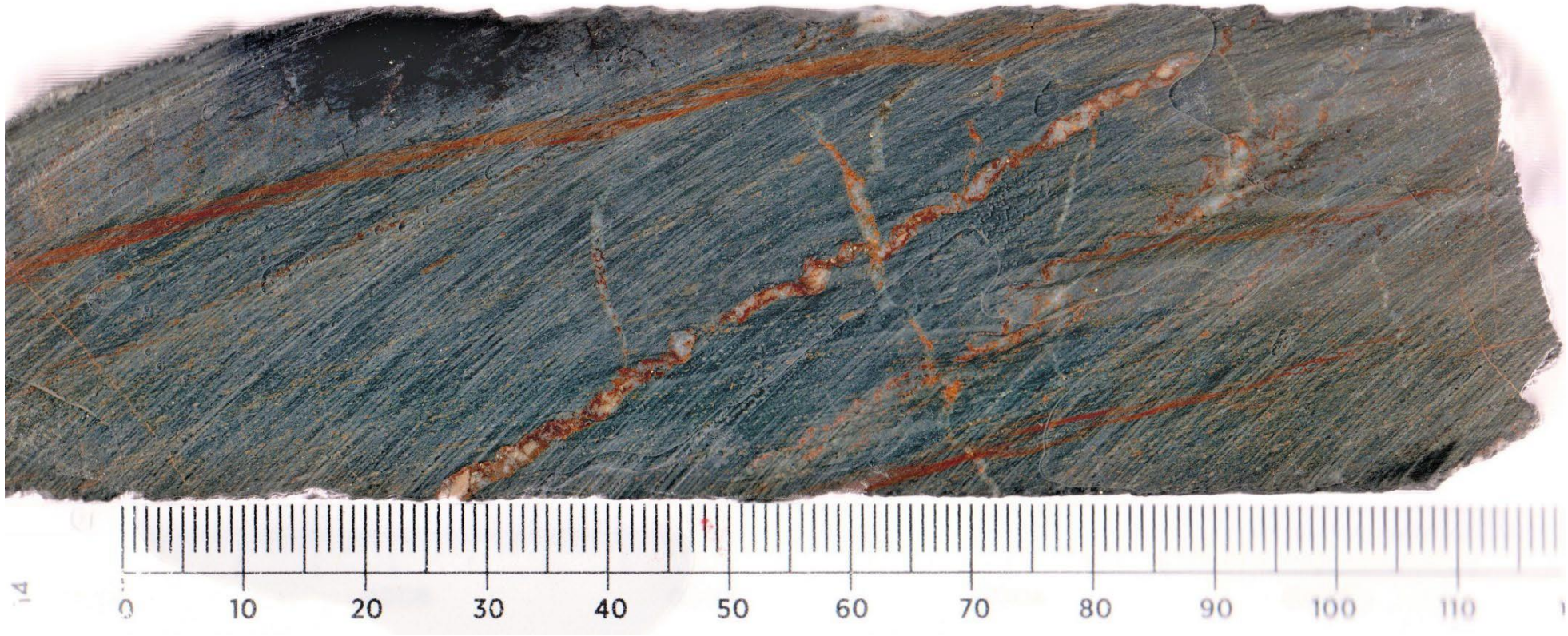

Figure 16 Photos of the drill core sample 2022440139 from drill hole AWPN02A of the Pioneer prospect, Warratta Inlier, New South Wales, Australia.

S3.3 Good Friday prospect

Warratta Inlier, New South Wales

Detailed image data: Appendix 12 (individual data file)

(A) Sample List

Sample No.	Sample ID	Borehole	From (m)	To (m)	Notes
—	2022440131	AWGF02	59.16	59.42	Sulfide ore and hydrothermal alteration
—	2022440132	AWGF02	61.52	61.76	Sulfide ore and hydrothermal alteration

(B) Mineralisation Characteristics

Data Type	Mineral Assemblage
Hyperspectral SWIR	—
Hyperspectral TIR	—
Hyperspectral VNIR	—
Drill core specimen	*Py, Qtz, Gn, Car*
Thin section	—
AMICS mineral map	*Py, Qtz, Gn, Car, Ap, Mnz, Cpy, Sph*

(C) Mineralogical Textures and Paragenesis

Category	Description
Texture	Galena-bearing sulfide mineralisation hosted in quartz–carbonate veins. Monazite is present as an accessory phase.
Paragenesis	Pyrite formed first, followed by galena. Carbonate veins represent the latest hydrothermal event, with minor apatite and monazite as accessories.

(D) Supplementary Figure Reference

Supplementary Figures *include drill core photographs of sulfide ore samples 2022440131 and 2022440132 from drill hole AWGF02, Good Friday prospect, Warratta Inlier, NSW.*

S3.3 The Good Friday prospect, Warratta Inlier, New South Wales

Sample ID	Prospect	Borehole Name	From (m)	To (m)	Note
2022440131	Good Friday	AWGF02	59.16	59.42	Sulfide ore and hydrothermal alteration

Figure 1 Photos of the drill core sample 2022440131 from drill hole AWGF02 of the Good Friday prospect, Warratta Inlier, New South Wales, Australia. Qtz-quartz; Ms-muscovite.

Sample ID	Prospect	Borehole Name	From (m)	To (m)	Note
2022440132	Good Friday	AWGF02	61.52	61.76	Sulfide ore and hydrothermal alteration

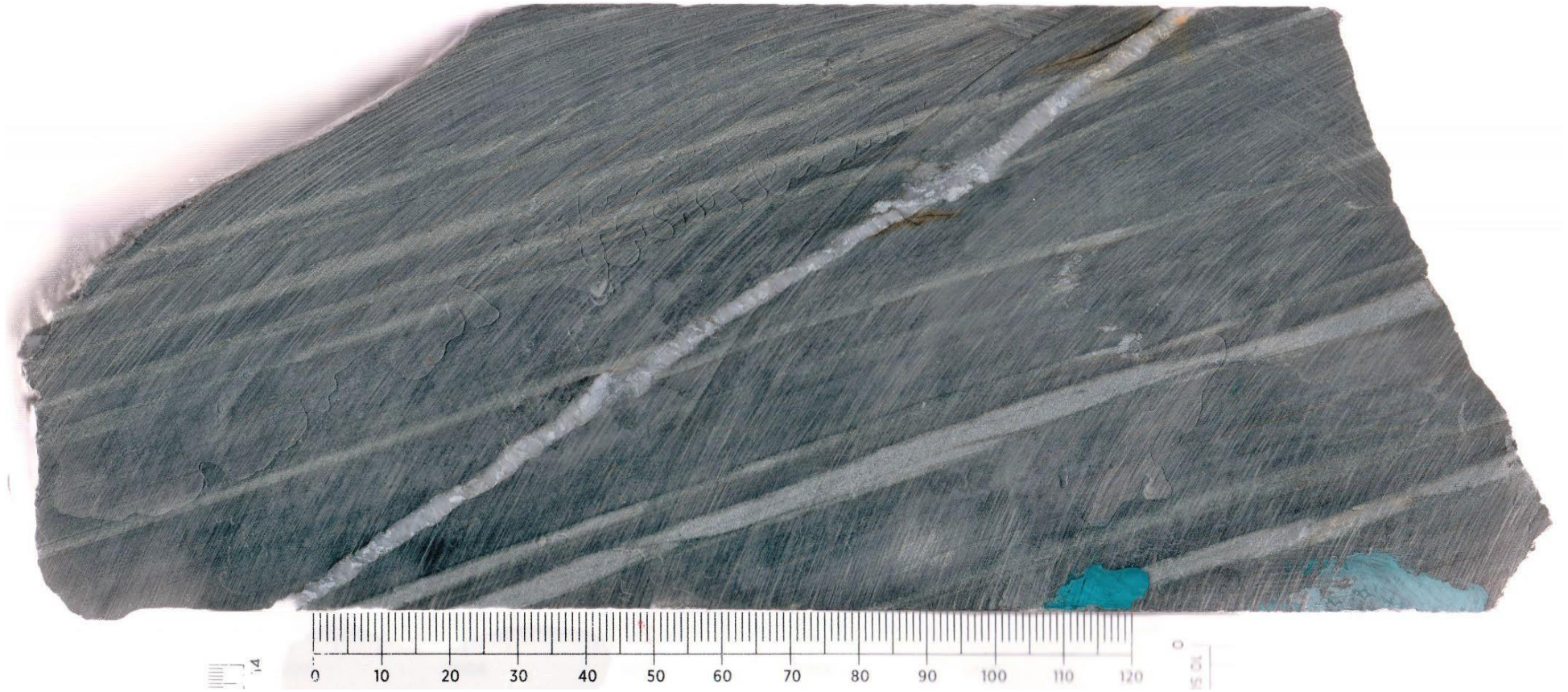

Figure 2 Photos of the drill core sample 2022440132 from drill hole AWGF02 of the Good Friday prospect, Warratta Inlier, New South Wales, Australia.

S4.1 Sherlock prospect

Kanmantoo–Glenelg River Zone, South Australia

(A) Sample List

Sample No.	Sample ID	Borehole	From (m)	To (m)	Notes
8012405	2022440045	EKB10CD001	116.70	116.90	Sulfide ore and hydrothermal alteration
8012406	2022440046	EKB10CD001	117.60	117.80	Sulfide ore and hydrothermal alteration
8012407	2022440047	EKB10CD001	150.10	150.30	Sulfide ore and hydrothermal alteration
8012408	2022440048	EKB10CD001	200.52	200.72	Sulfide ore and hydrothermal alteration

(B) Mineralisation Characteristics

Data Type	Mineral Assemblage
Hyperspectral SWIR	*Ms, Chl, Hbl, Bt, Act, Cal, Phl*
Hyperspectral TIR	*Qtz, Fsp, Amp, Px, Py, Cpy, Sph, Po, Ank, Gn, Ap, Kfsp, Ab, Ttn, Ank, Kln*
Hyperspectral VNIR	*Gth, Hem*
Drill core specimen	*Py, Cpy, Sph, Po, Cal, Chl*
Thin section	—
AMICS mineral map	*Qtz, Cal, Py, Apy, Sph, Cpy, Gn, Ser, Chl, Ab, Hem, Kfsp, Ttn, Ap, Bt*

(C) Mineralogical Textures and Paragenesis

Category	Description
Texture	Base-metal rich sulfide mineralisation (Cu–Zn–Pb–Au) in a calc-silicate / amphibolite host. Hornblende, biotite, actinolite and phlogopite characterise the amphibolite-facies metamorphic host.
Paragenesis	Pyrite and arsenopyrite formed early. Chalcopyrite–sphalerite–galena–pyrrhotite represent the main ore stage. Carbonate veins and late epidote–calcite overprint the ore assemblage.

(D) Supplementary Figure Reference

Supplementary Figures *include HyLogger hyperspectral images of EKB10CD001 and AMICS mineral maps of base-metal sulfide assemblage (Py–Apy–Cpy–Sph–Gn), Sherlock prospect, Kanmantoo–Glenelg River Zone, SA.*

S4.1 The Sherlock prospect, Tailem Bend region, South Australia

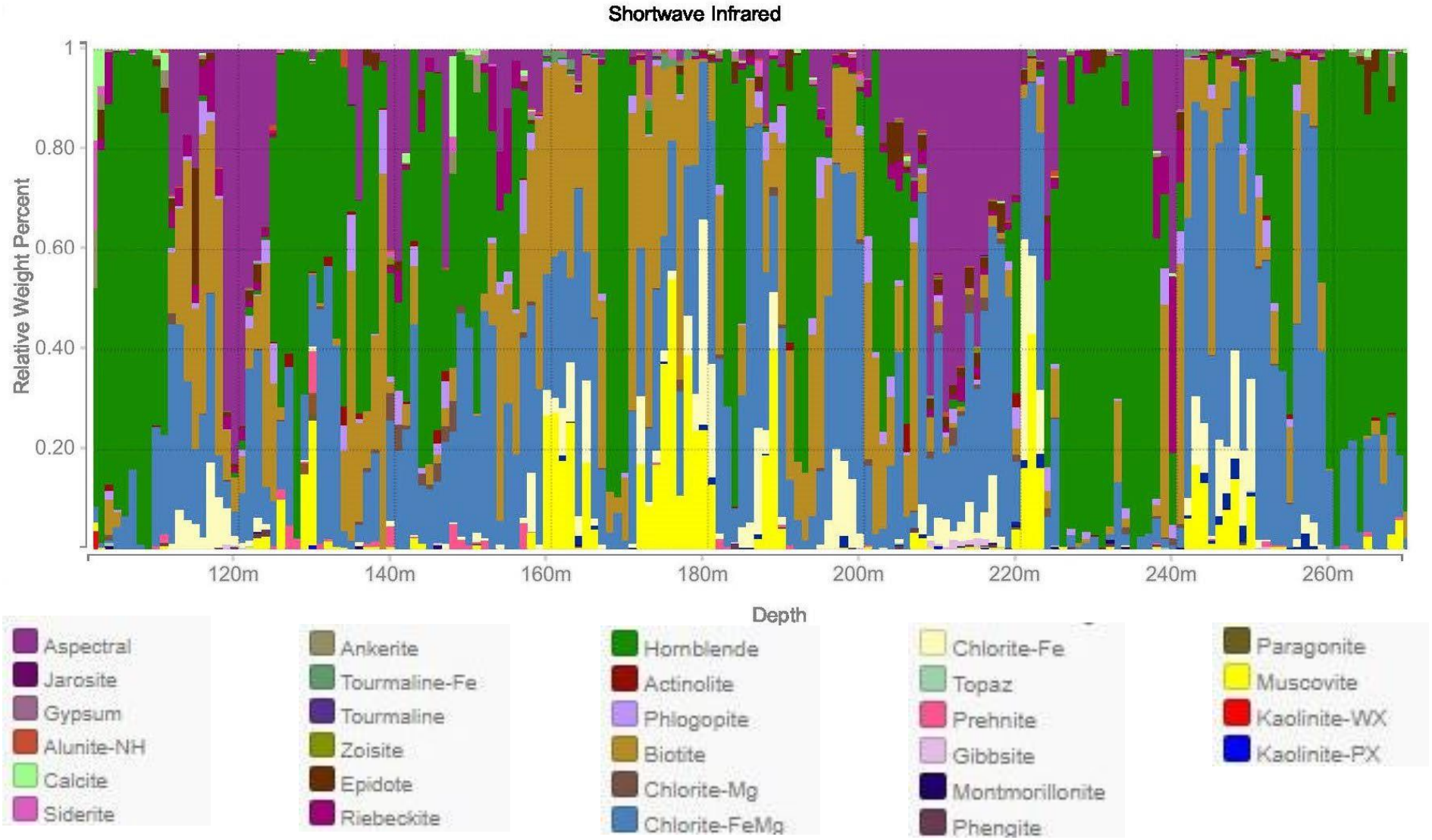

Figure 1 Summary of the shortwave infrared (SWIR) hylogger hyperspectral image of the hole SHR 26 of the Sherlock prospect, Tailem Bend region, South Australia, Australia

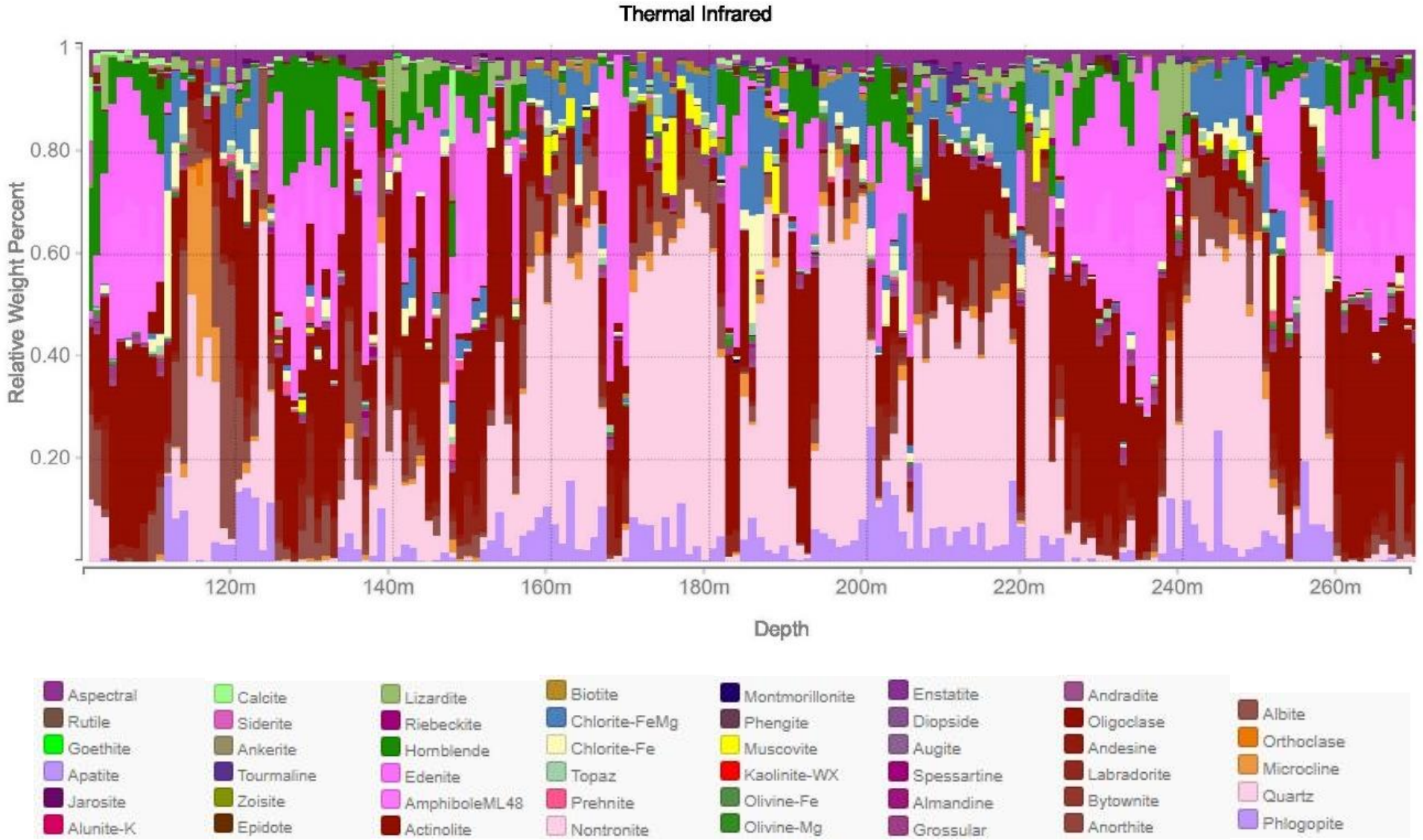

Figure 2 Summary of the thermal infrared (TIR) hylogger hyperspectral image of the hole SHR 26 of the Sherlock prospect, Tailem Bend region, South Australia, Australia

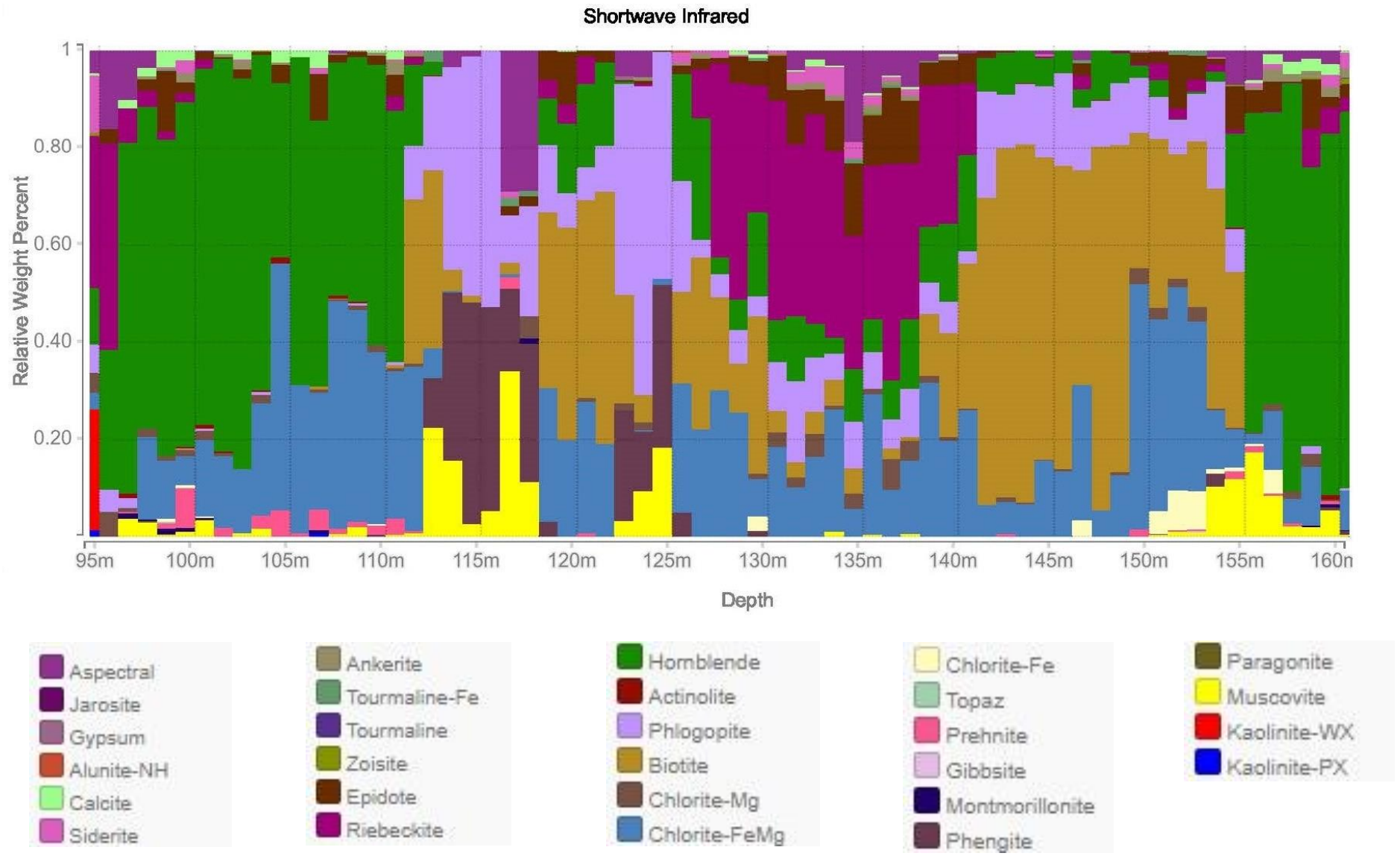

Figure 3 Summary of the shortwave infrared (SWIR) hylogger hyperspectral image of the hole SHR 34 of the Sherlock prospect, Tailem Bend region, South Australia, Australia

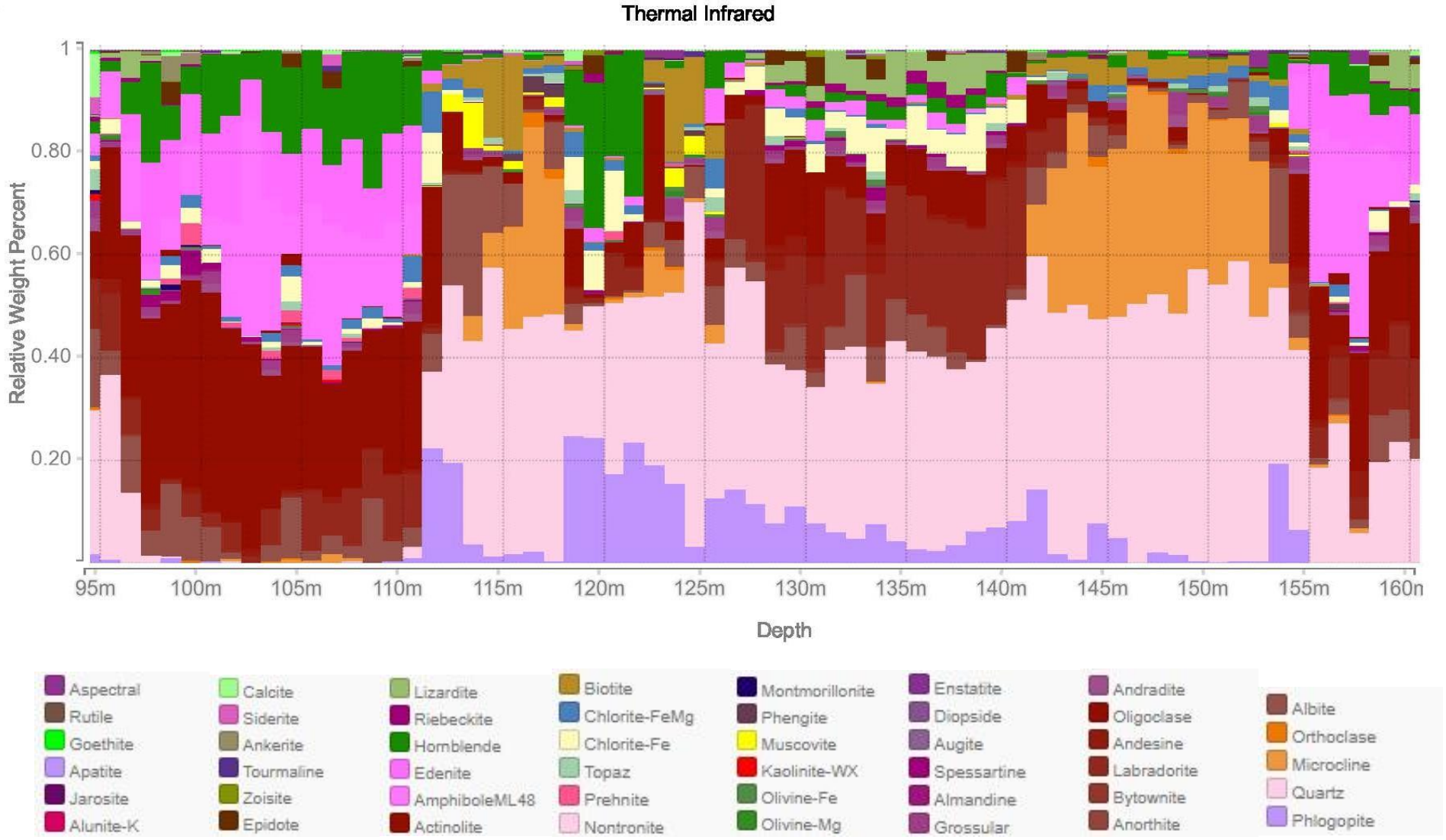

Figure 4 Summary of the thermal infrared (TIR) hylogger hyperspectral image of the hole SHR 34 of the Sherlock prospect, Tailem Bend region, South Australia, Australia

Sample ID	Prospect	Borehole Name	From (m)	To (m)	Note
4351206	Sherlock	SHR026	110.23	110.30	Sulfide ore and hydrothermal alteration

Figure 5 Photos of the drill core sample 4351206 from drill hole SHR026 of the Sherlock prospect, Tailem Bend region, South Australia, Australia. Py-pyrite; Sph-sphalerite; Cpy-chalcopyrite; Fsp-feldspar; Act-actinolite

Sample ID	Prospect	Borehole Name	From (m)	To (m)	Note
4351206	Sherlock	SHR026	110.23	110.30	Sulfide ore and hydrothermal alteration

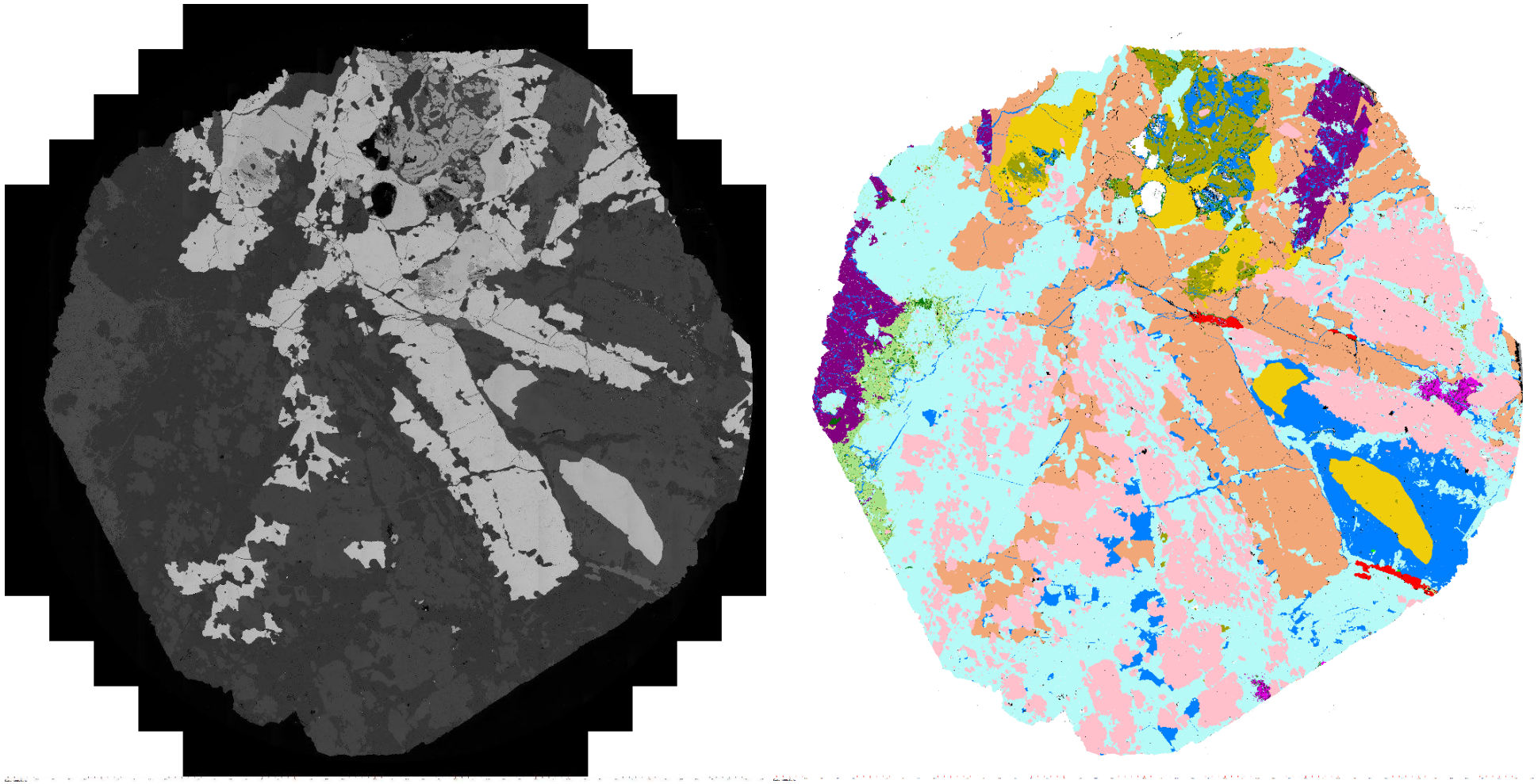

Figure 6 Backscattered electron (BSE) image (left) and Advanced Mineral Identification and Characterization System (AMICS) mineral map (right) of the sample 4351206 from drill hole SHR026 of the Sherlock prospect, Tailem Bend region, South Australia, Australia. See Figure 21 at the end of this document for the legend of minerals identified using Mineral Liberation Analysis (MLA) mapping.

Sample ID	Prospect	Borehole Name	From (m)	To (m)	Note
4351202	Sherlock	SHR034	135.55	135.69	Sulfide ore and hydrothermal alteration

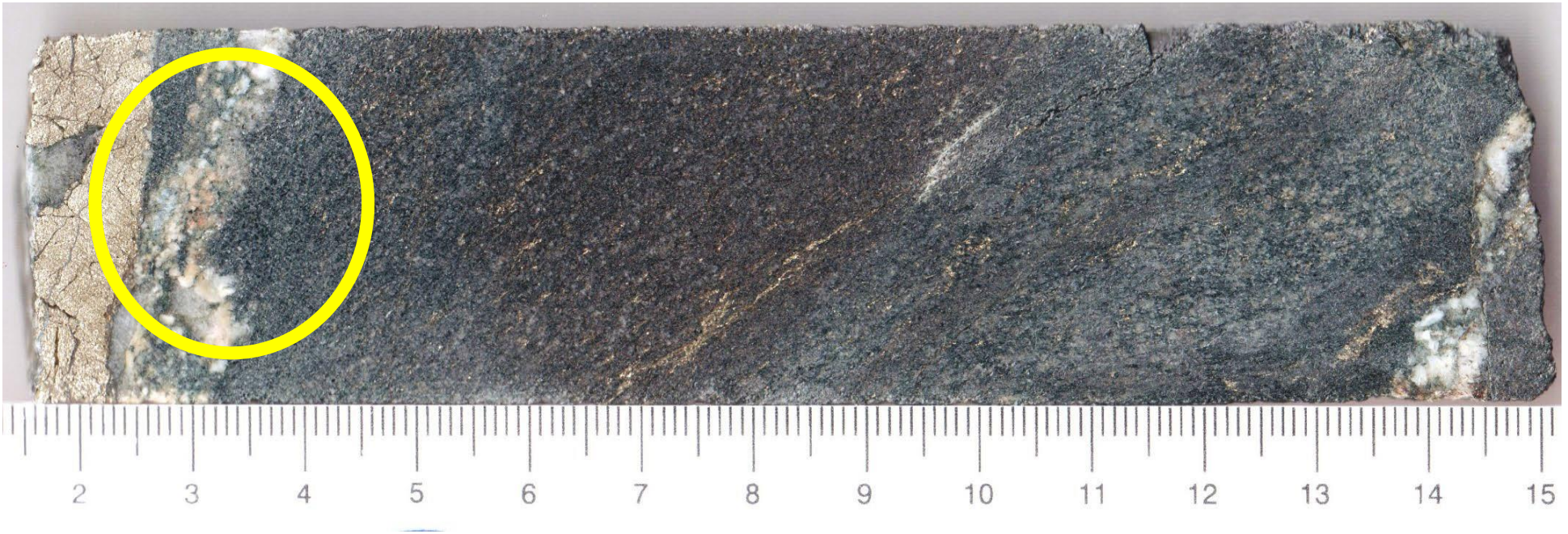

Figure 7 Photos of the drill core sample 4351202 from drill hole SHR034 of the Sherlock prospect, Tailem Bend region, South Australia, Australia.

Sample ID	Prospect	Borehole Name	From (m)	To (m)	Note
4351202	Sherlock	SHR034	135.55	135.69	Sulfide ore and hydrothermal alteration

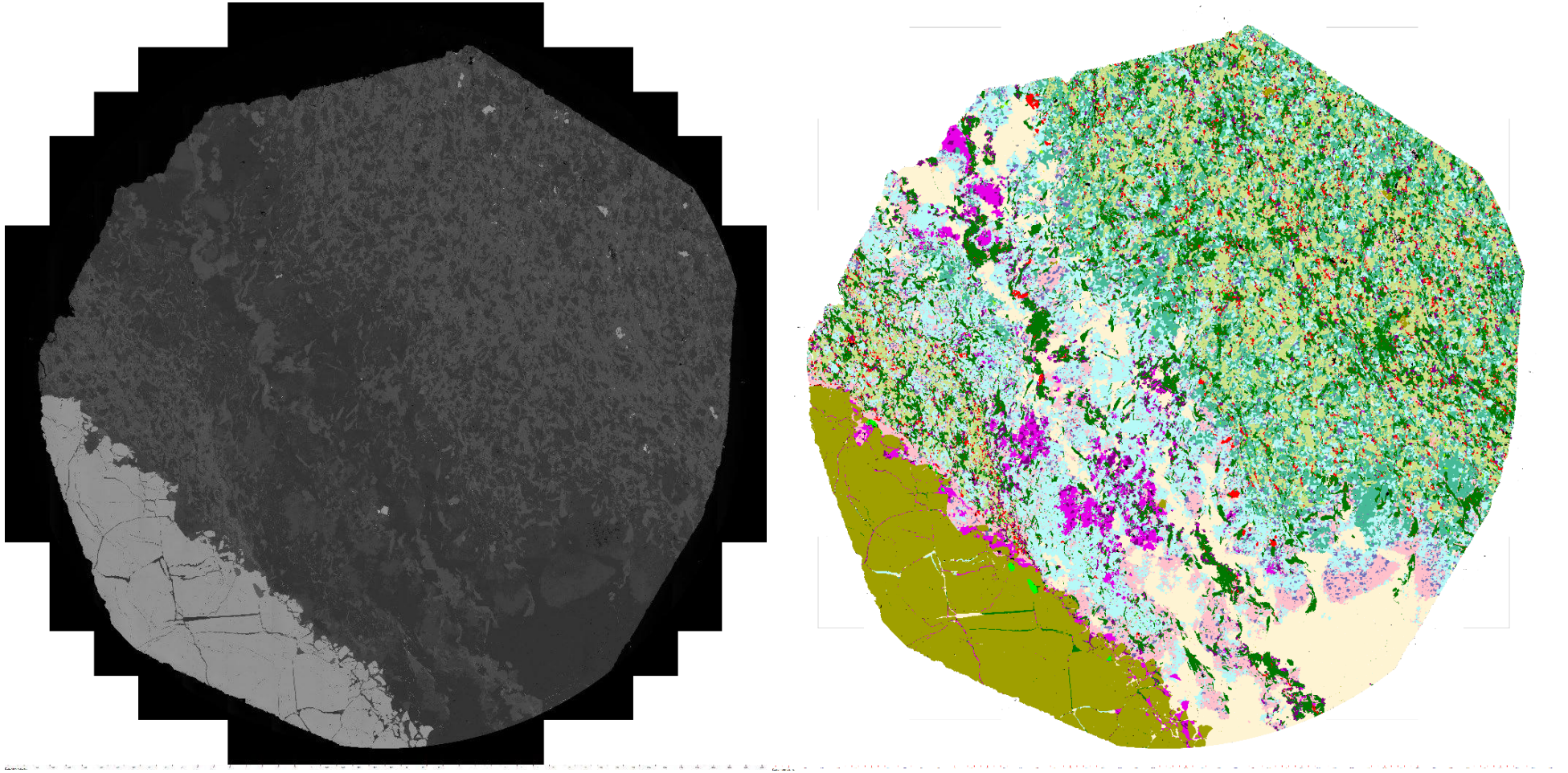

Figure 8 Backscattered electron (BSE) image (left) and Advanced Mineral Identification and Characterization System (AMICS) mineral map (right) of the sample 4351202 from drill hole SHR034 of the Sherlock prospect, Tailem Bend region, South Australia, Australia. See Figure 21 at the end of this document for the legend of minerals identified using Mineral Liberation Analysis (MLA) mapping.

Sample ID	Prospect	Borehole Name	From (m)	To (m)	Note
4351203	Sherlock	SHR034	156.16	156.36	Sulfide ore and hydrothermal alteration

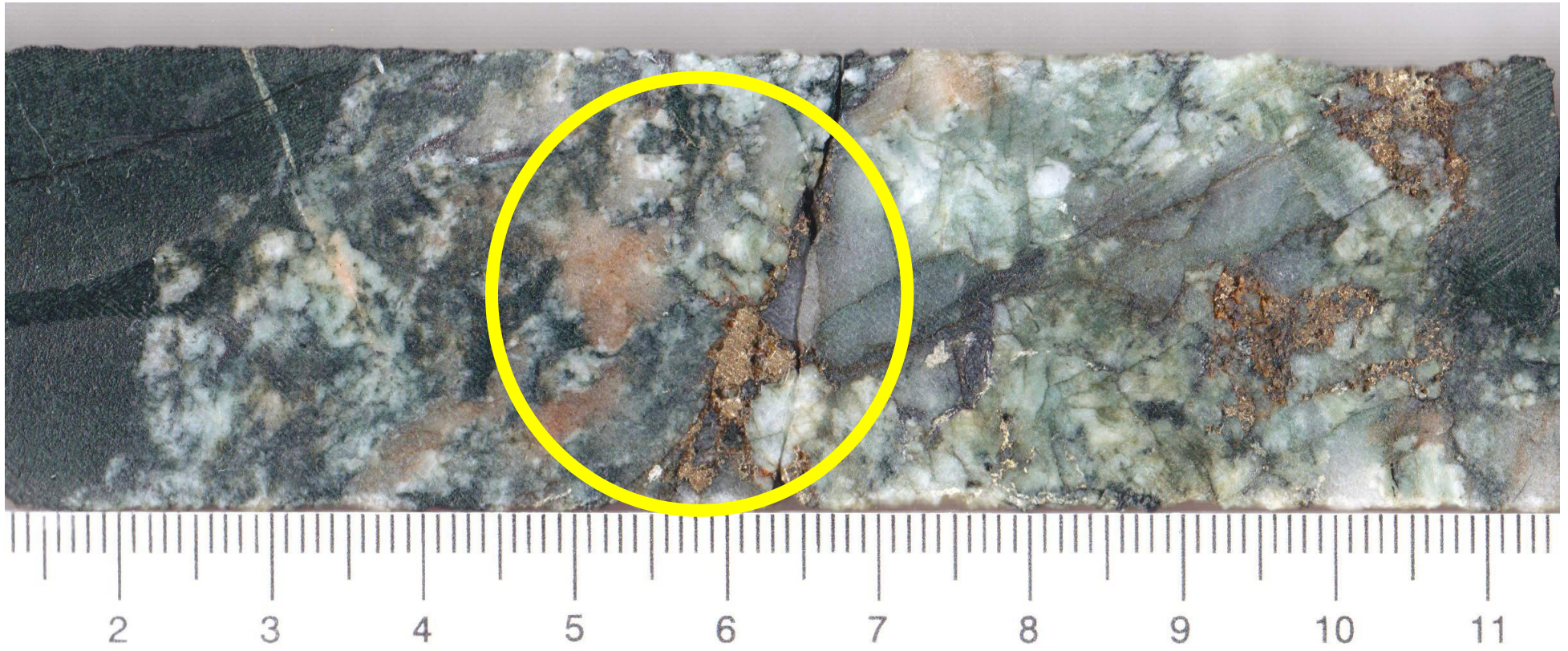

Figure 9 Photos of the drill core sample 4351203 from drill hole SHR034 of the Sherlock prospect, Tailem Bend region, South Australia, Australia.

Sample ID	Prospect	Borehole Name	From (m)	To (m)	Note
4351203	Sherlock	SHR034	156.16	156.36	Sulfide ore and hydrothermal alteration

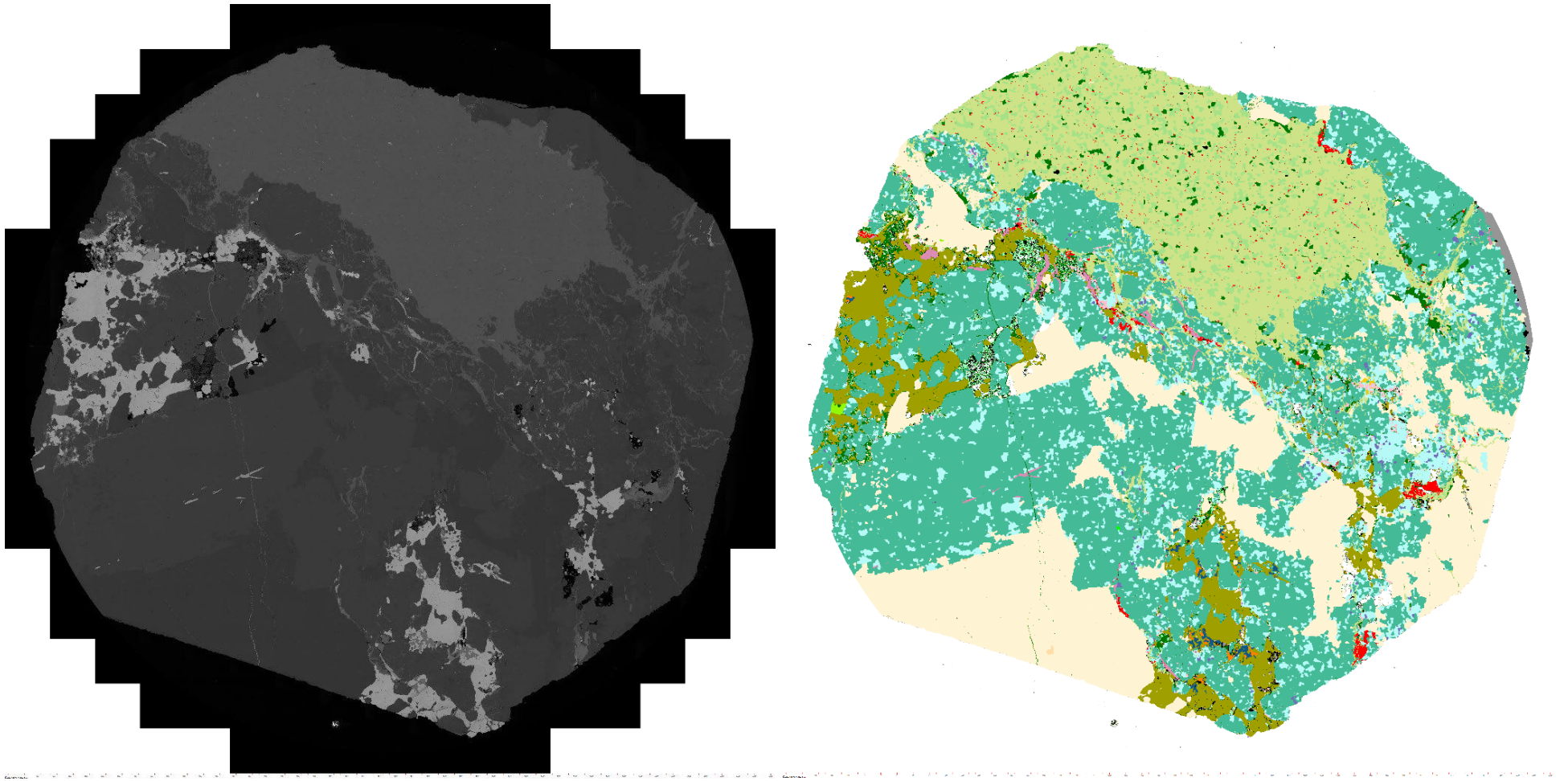

Figure 10 Backscattered electron (BSE) image (left) and Advanced Mineral Identification and Characterization System (AMICS) mineral map (right) of the sample 4351203 from drill hole SHR034 of the Sherlock prospect, Tailem Bend region, South Australia, Australia. See Figure 21 at the end of this document for the legend of minerals identified using Mineral Liberation Analysis (MLA) mapping.

Sample ID	Prospect	Borehole Name	From (m)	To (m)	Note
4351208	Sherlock	SHR026	187.73	187.89	Sulfide ore and hydrothermal alteration

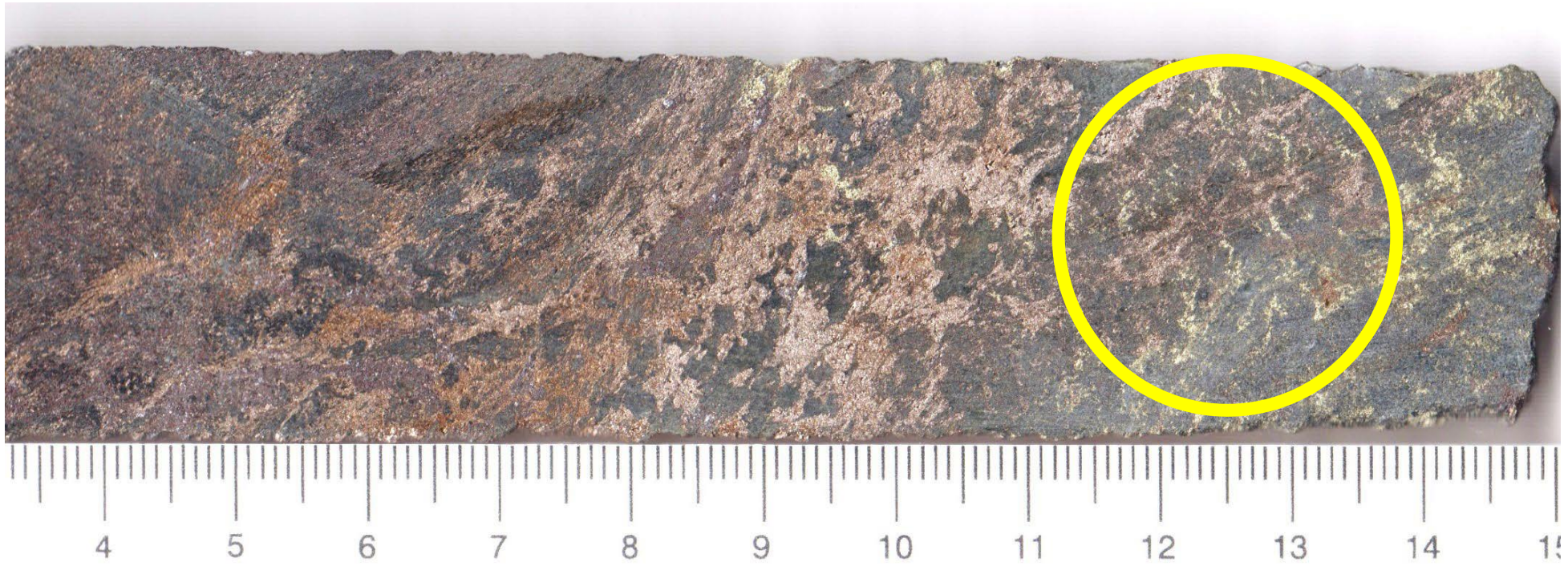

Figure 11 Photos of the drill core sample 4351208 from drill hole SHR026 of the Sherlock prospect, Tailem Bend region, South Australia, Australia.

Sample ID	Prospect	Borehole Name	From (m)	To (m)	Note
4351208	Sherlock	SHR026	187.73	187.89	Sulfide ore and hydrothermal alteration

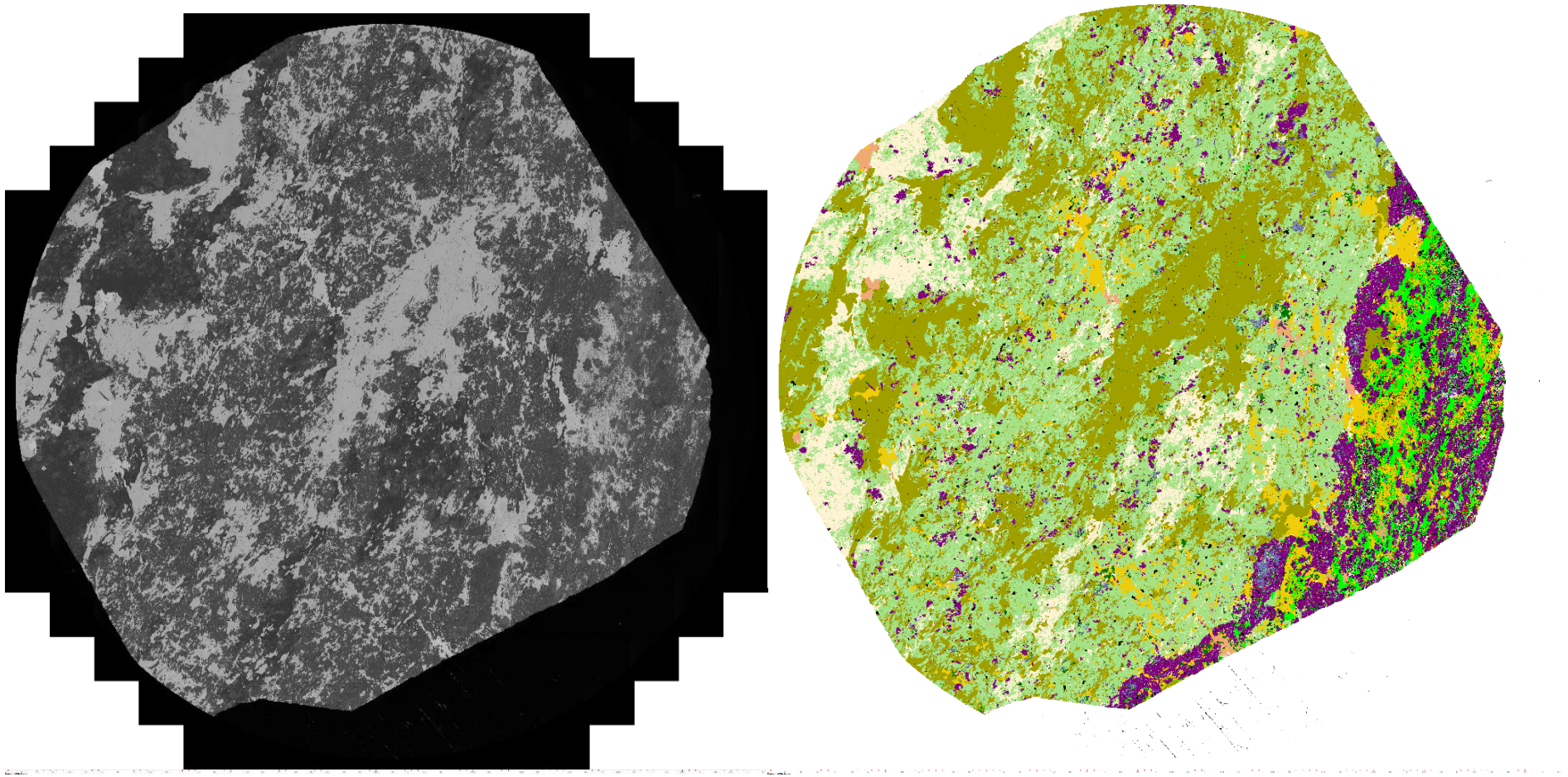

Figure 12 Backscattered electron (BSE) image (left) and Advanced Mineral Identification and Characterization System (AMICS) mineral map (right) of the sample 4351208 from drill hole SHR026 of the Sherlock prospect, Tailem Bend region, South Australia, Australia. See Figure 21 at the end of this document for the legend of minerals identified using Mineral Liberation Analysis (MLA) mapping.

Sample ID	Prospect	Borehole Name	From (m)	To (m)	Note
4351210	Sherlock	SHR008	91.86	92.09	Sulfide ore and hydrothermal alteration

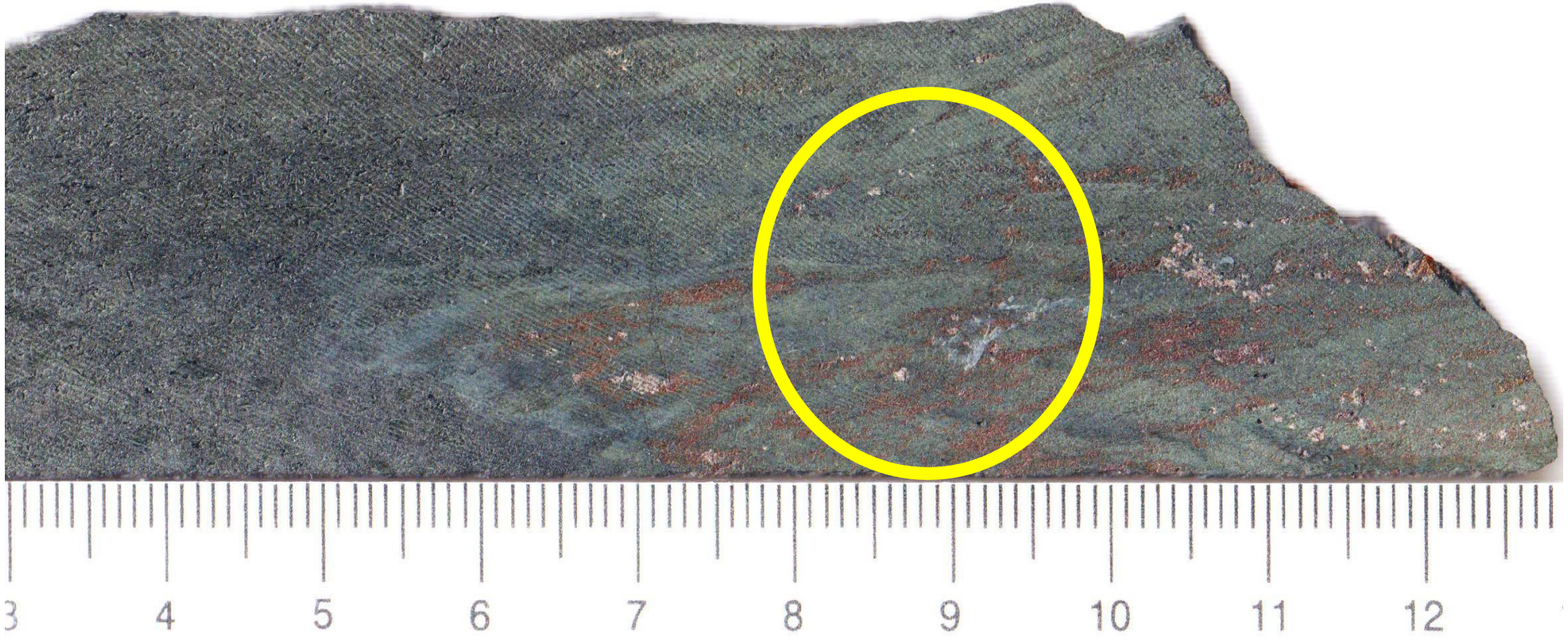

Figure 13 Photos of the drill core sample 4351210 from drill hole SHR008 of the Sherlock prospect, Tailem Bend region, South Australia, Australia.

Sample ID	Prospect	Borehole Name	From (m)	To (m)	Note
4351210	Sherlock	SHR008	91.86	92.09	Sulfide ore and hydrothermal alteration

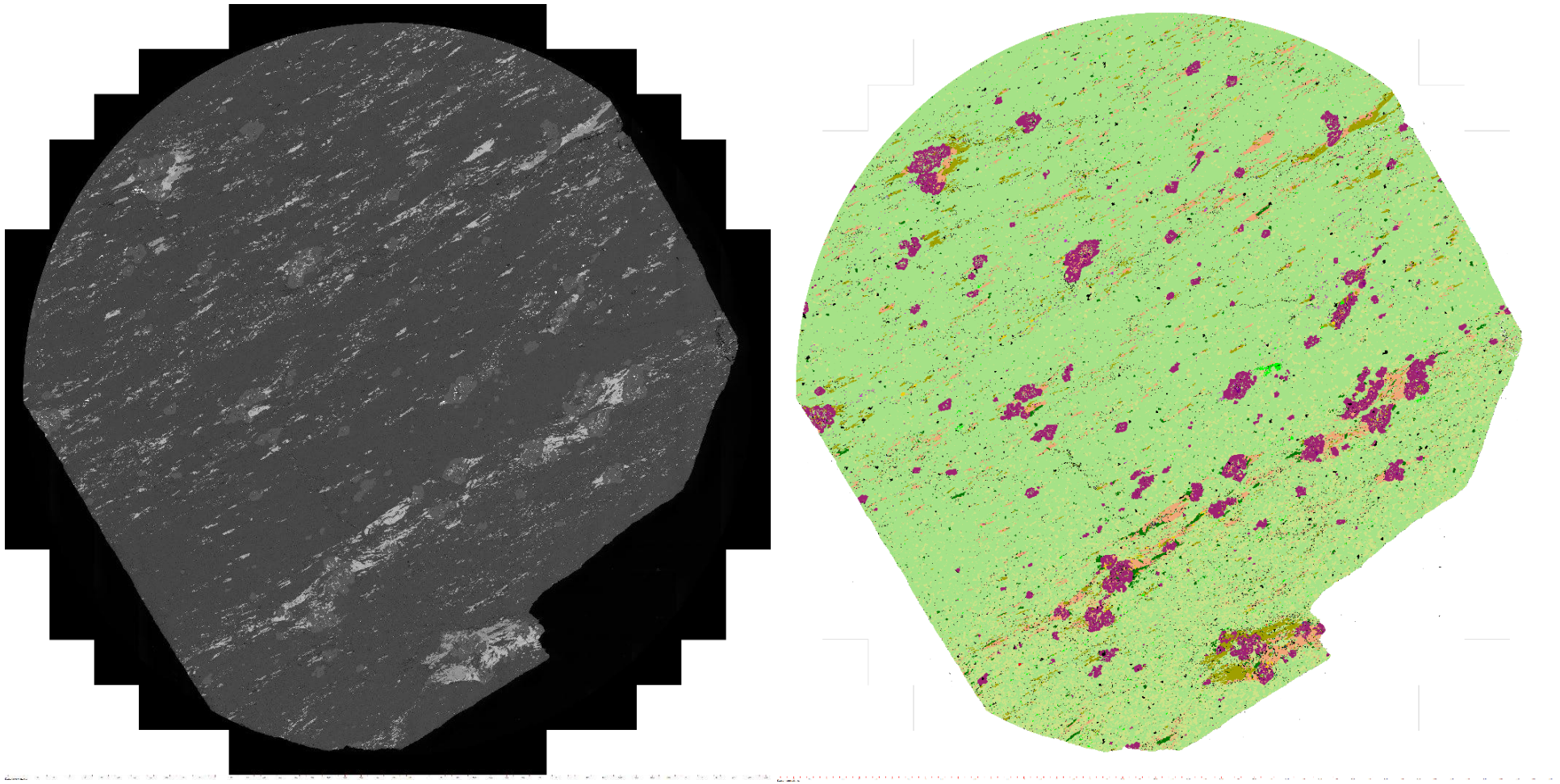

Figure 14 Backscattered electron (BSE) image (left) and Advanced Mineral Identification and Characterization System (AMICS) mineral map (right) of the sample 4351210 from drill hole SHR008 of the Sherlock prospect, Tailem Bend region, South Australia, Australia. See Figure 21 at the end of this document for the legend of minerals identified using Mineral Liberation Analysis (MLA) mapping.

Sample ID	Prospect	Borehole Name	From (m)	To (m)	Note
4351225	Sherlock	SHR026	205.20	205.35	Sulfide ore and hydrothermal alteration

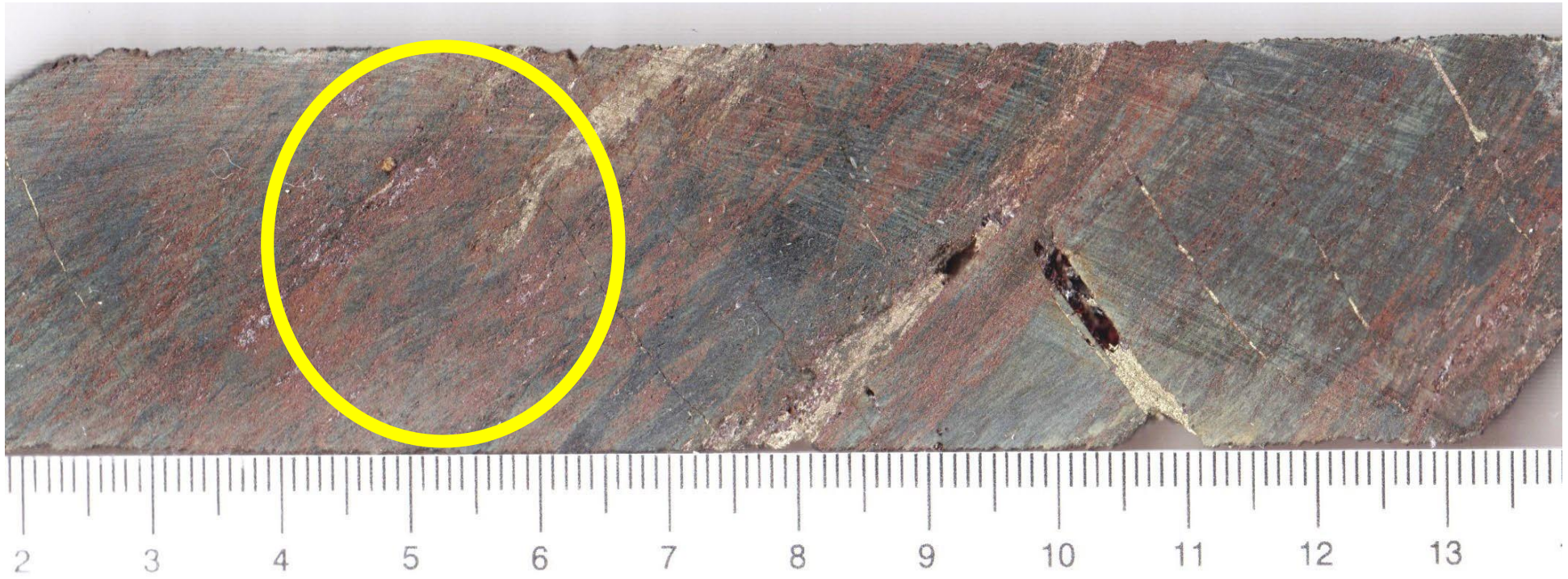

Figure 15 Photos of the drill core sample 4351225 from drill hole SHR026 of the Sherlock prospect, Tailem Bend region, South Australia, Australia.

Sample ID	Prospect	Borehole Name	From (m)	To (m)	Note
4351225	Sherlock	SHR026	205.20	205.35	Sulfide ore and hydrothermal alteration

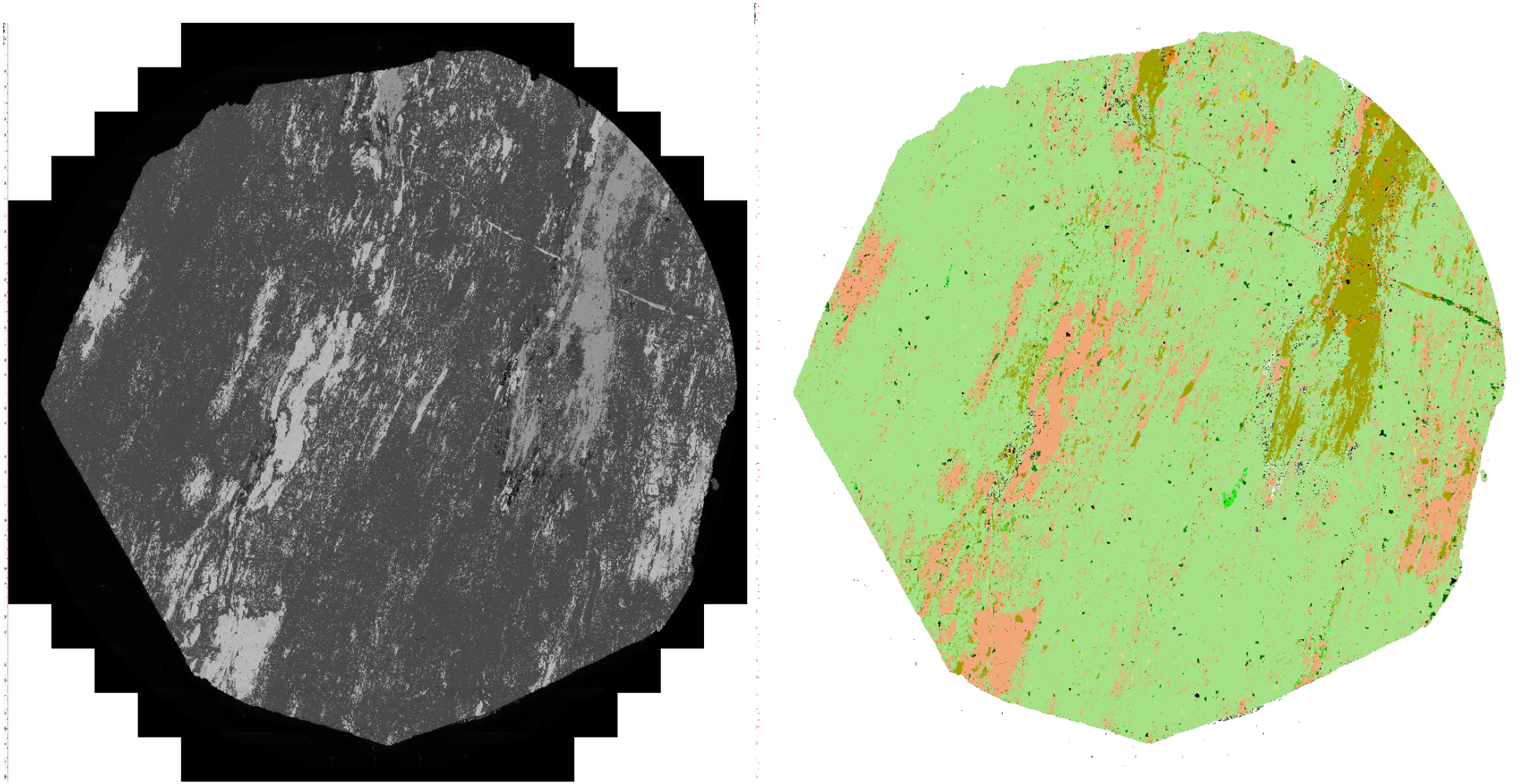

Figure 16 Backscattered electron (BSE) image (left) and Advanced Mineral Identification and Characterization System (AMICS) mineral map (right) of the sample 4351225 from drill hole SHR026 of the Sherlock prospect, Tailem Bend region, South Australia, Australia. See Figure 21 at the end of this document for the legend of minerals identified using Mineral Liberation Analysis (MLA) mapping.

Sample ID	Prospect	Borehole Name	From (m)	To (m)	Note
4351204	Sherlock	SHR026	110.32	110.45	Sulfide ore and hydrothermal alteration

Figure 17 Photos of the drill core sample 4351204 from drill hole SHR026 of the Sherlock prospect, Tailem Bend region, South Australia, Australia.

Sample ID	Prospect	Borehole Name	From (m)	To (m)	Note
4351205	Sherlock	SHR026	109.80	109.90	Sulfide ore and hydrothermal alteration

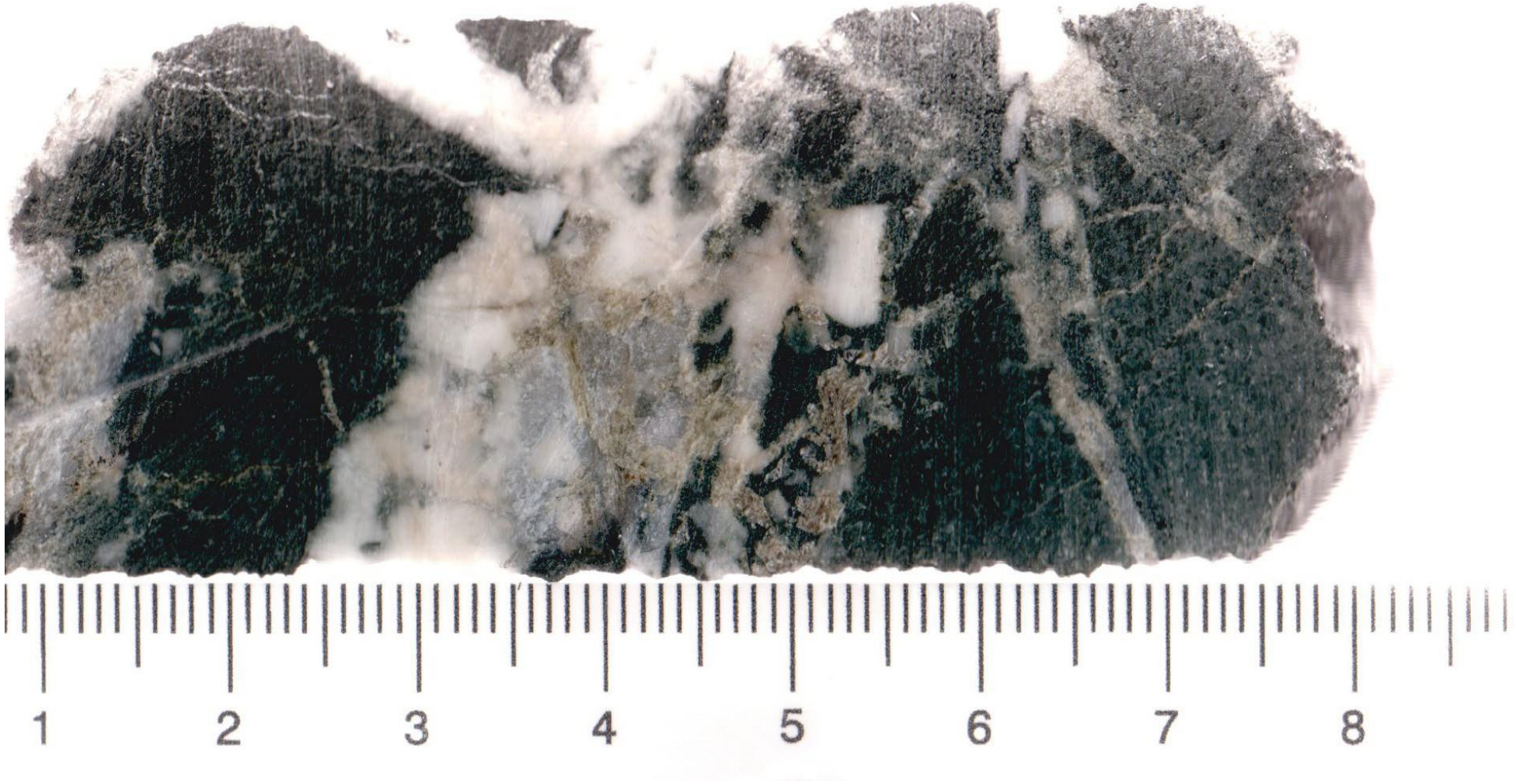

Figure 18 Photos of the drill core sample 4351205 from drill hole SHR026 of the Sherlock prospect, Tailem Bend region, South Australia, Australia.

Sample ID	Prospect	Borehole Name	From (m)	To (m)	Note
4351209	Sherlock	SHR026	219.75	219.95	Sulfide ore and hydrothermal alteration

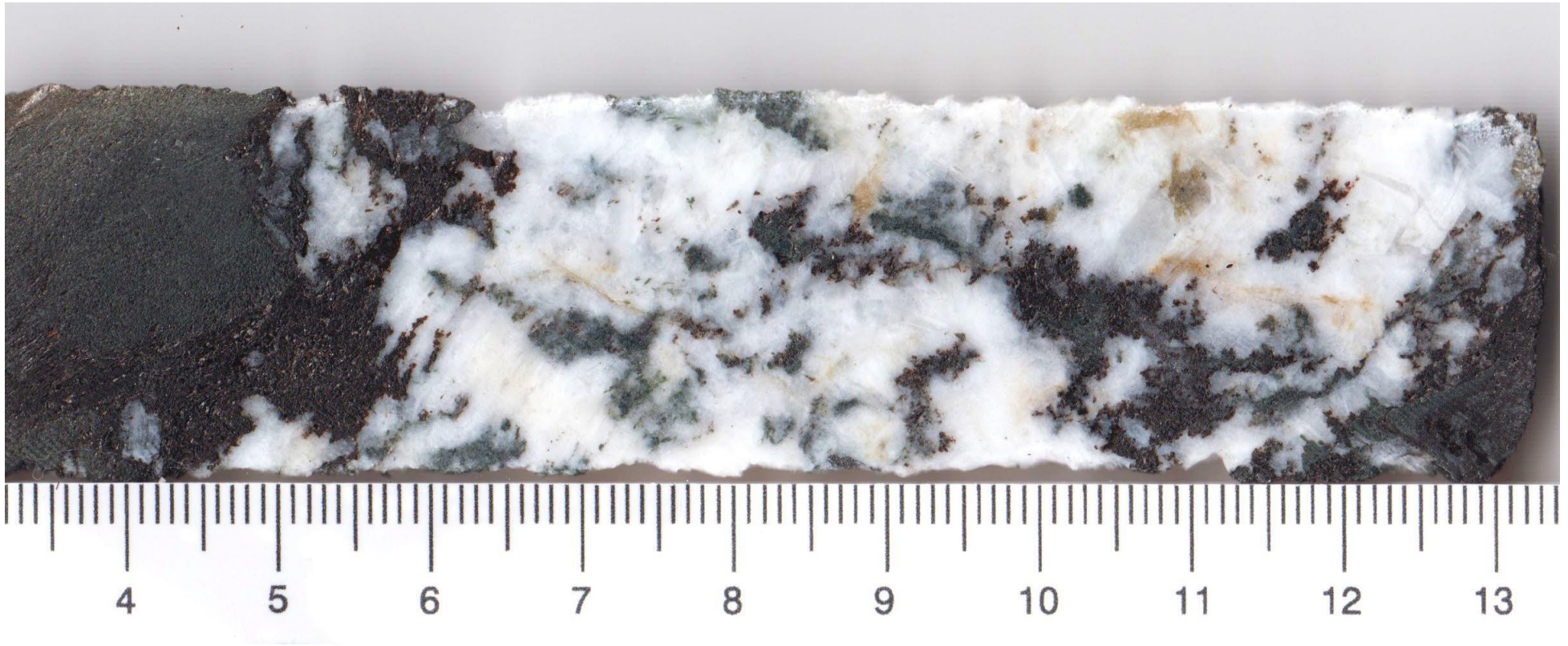

Figure 19 Photos of the drill core sample 4351209 from drill hole SHR026 of the Sherlock prospect, Tailem Bend region, South Australia, Australia.

Sample ID	Prospect	Borehole Name	From (m)	To (m)	Note
4351207	Sherlock	SHR026	147.52	147.65	Sulfide ore and hydrothermal alteration

Figure 20 Photos of the drill core sample 4351207 from drill hole SHR026 of the Sherlock prospect, Tailem Bend region, South Australia, Australia.

S4.2 Haylands prospect

Morgan Region, South Australia

Detailed image data: Appendix 14 (individual data file)

(A) Sample List

Sample No.	Sample ID	Borehole	From (m)	To (m)	Notes
4351174	4351174	DEL10ACD001	330.79	330.95	Sulfide ore and hydrothermal alteration
4351177	4351177	DEL10ACD001	—	—	Sulfide ore and hydrothermal alteration
4351178	4351178	DEL10ACD001	—	—	Sulfide ore and hydrothermal alteration
4351175	4351175	DEL10ACD001	—	—	Sulfide ore and hydrothermal alteration

(B) Mineralisation Characteristics

Data Type	Mineral Assemblage
Hyperspectral SWIR	*Ms, Chl, Car, Plag*
Hyperspectral TIR	*Qtz, Chl, Amp, Fsp*
Hyperspectral VNIR	*Gth*
Drill core specimen	*Py, Qtz, Chl, Cal, Cpy*
Thin section	—
AMICS mineral map	*Qtz, Py, Mo, Cpy, Ab, Ap, Hem, Cal, Ttn, Ep, Bt*

(C) Mineralogical Textures and Paragenesis

Category	Description
Texture	Molybdenite-bearing Cu–Py mineralisation in quartz–feldspar–chlorite altered host. Epidote–calcite veins crosscut the sulfide assemblage.
Paragenesis	Pyrite is associated with early albite–quartz alteration. Molybdenite and chalcopyrite form a later porphyry-style assemblage. Epidote–calcite veins represent the final hydrothermal stage.

(D) Supplementary Figure Reference

Supplementary Figure *include (1) downhole SWIR and TIR HyLogger hyperspectral image of drill hole DEL10ACD001, Haylands prospect, Morgan Region, SA; (2) Drill core photographs and BSE/AMICS mineral maps of Mo–Py–Cpy assemblage, samples 4351174, 4351177, 4351178 and 4351175. AMICS mineral standard legend included.*

S4.2 The Haylands prospect, Morgan region, South Australia

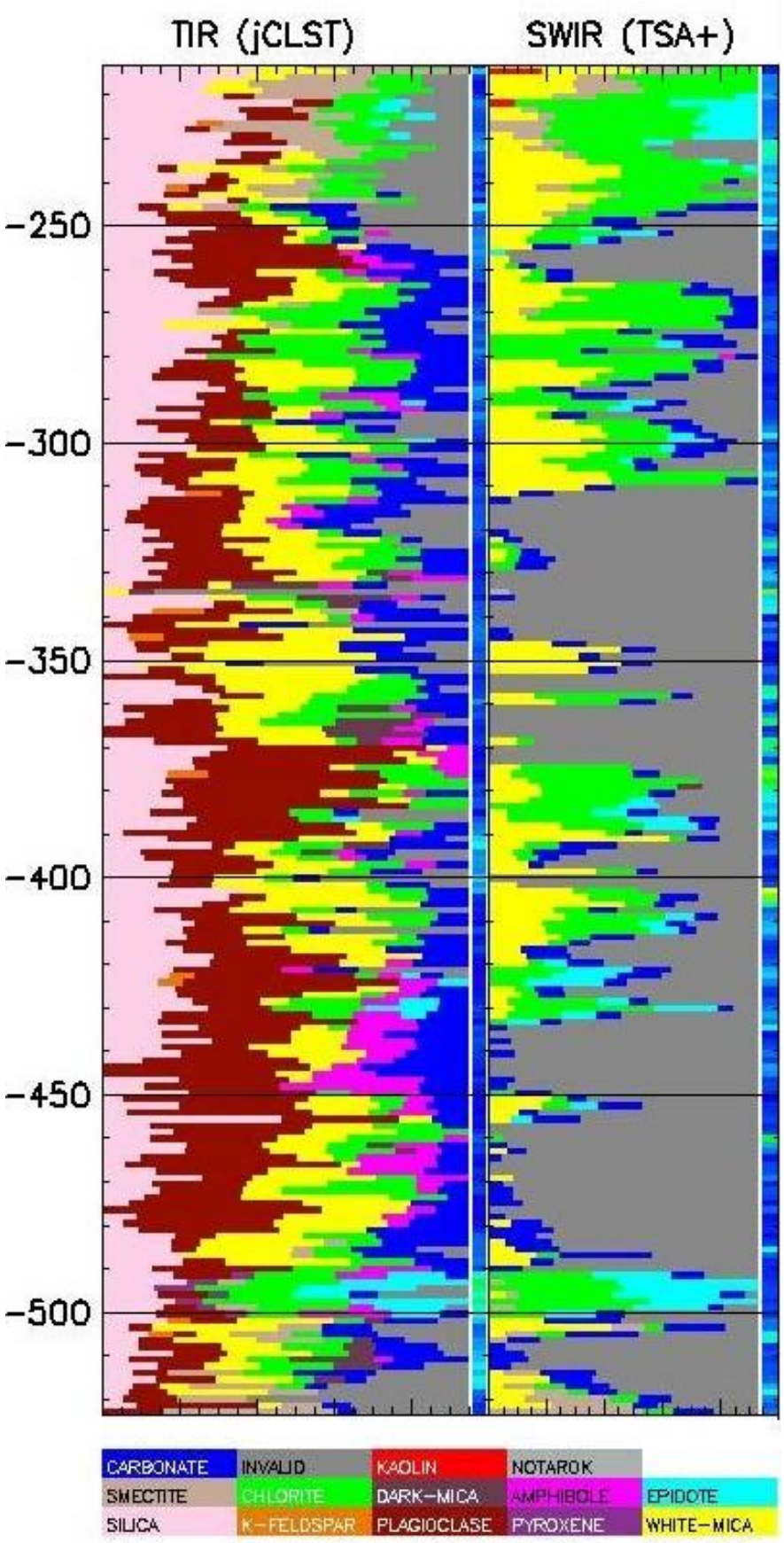

Figure 1 Downhole shortwave infrared (SWIR) and thermal infrared (TIR) hylogger hyperspectral image of the hole DEL10ACD00 1, Haylands prospect, Morgan region, South Australia, Australia

Sample ID	Prospect	Borehole Name	From (m)	To (m)	Note
4351174	Haylands	DEL10ACD001	330.79	330.95	Sulfide ore and hydrothermal alteration

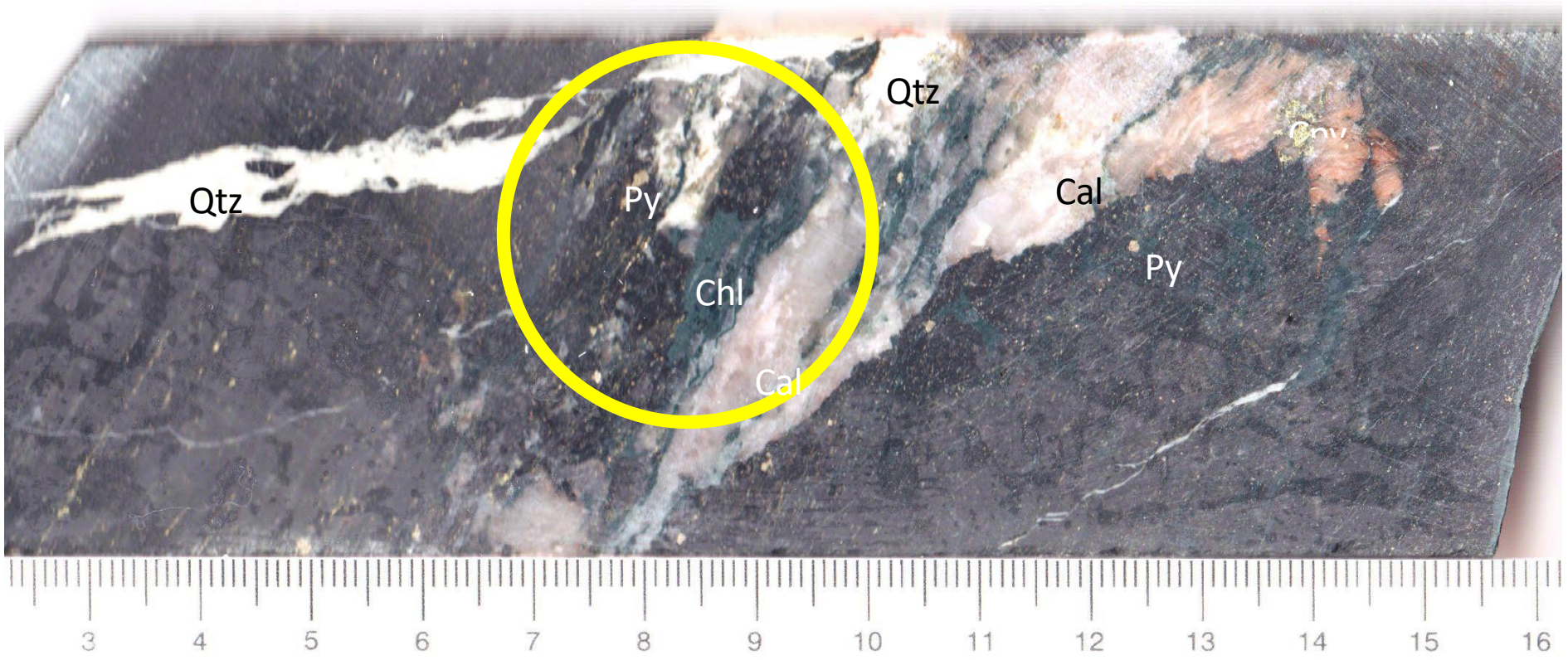

Figure 2 Photos of the drill core sample 4351174 from drill hole DEL10ACD00 1, Haylands prospect, Morgan region, South Australia, Australia. Py-pyrite; Qtz-quartz; Chl-chlorite; Cal-calcite; Cpy-chalcopyrite.

Sample ID	Prospect	Borehole Name	From (m)	To (m)	Note
4351174	Haylands	DEL10ACD001	330.79	330.95	Sulfide ore and hydrothermal alteration

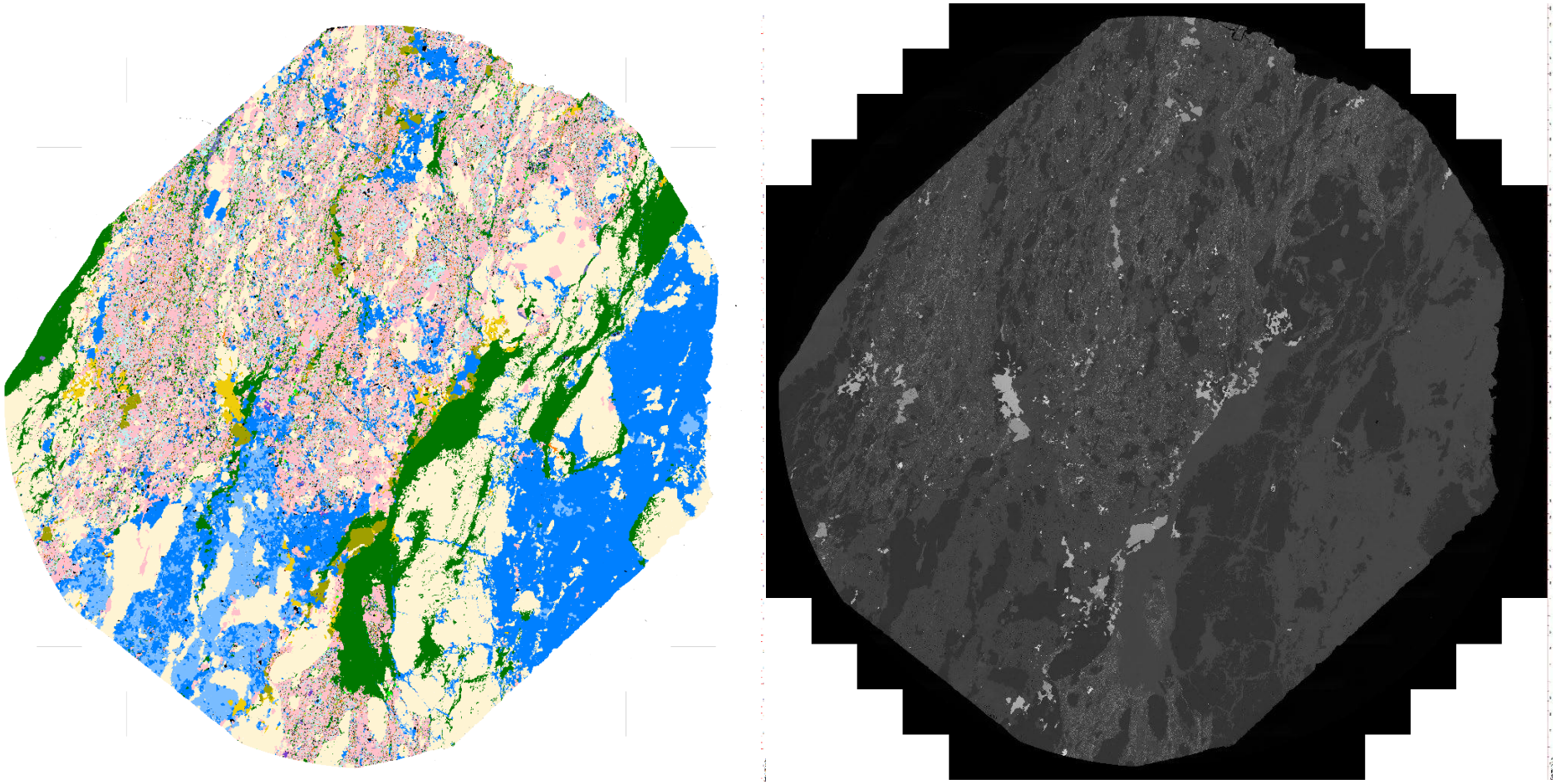

Figure 3 Backscattered electron (BSE) image (left) and Advanced Mineral Identification and Characterization System (AMICS) mineral map (right) of the sample 4351174 from drill hole DEL10ACD00 1, Haylands prospect, Morgan region, South Australia, Australia. See Figure 9 at the end of this document for the legend of minerals identified using Mineral Liberation Analysis (MLA) mapping.

Sample ID	Prospect	Borehole Name	From (m)	To (m)	Note
4351177	Haylands	DEL10ACD001	357.97	358.03	Sulfide ore and hydrothermal alteration

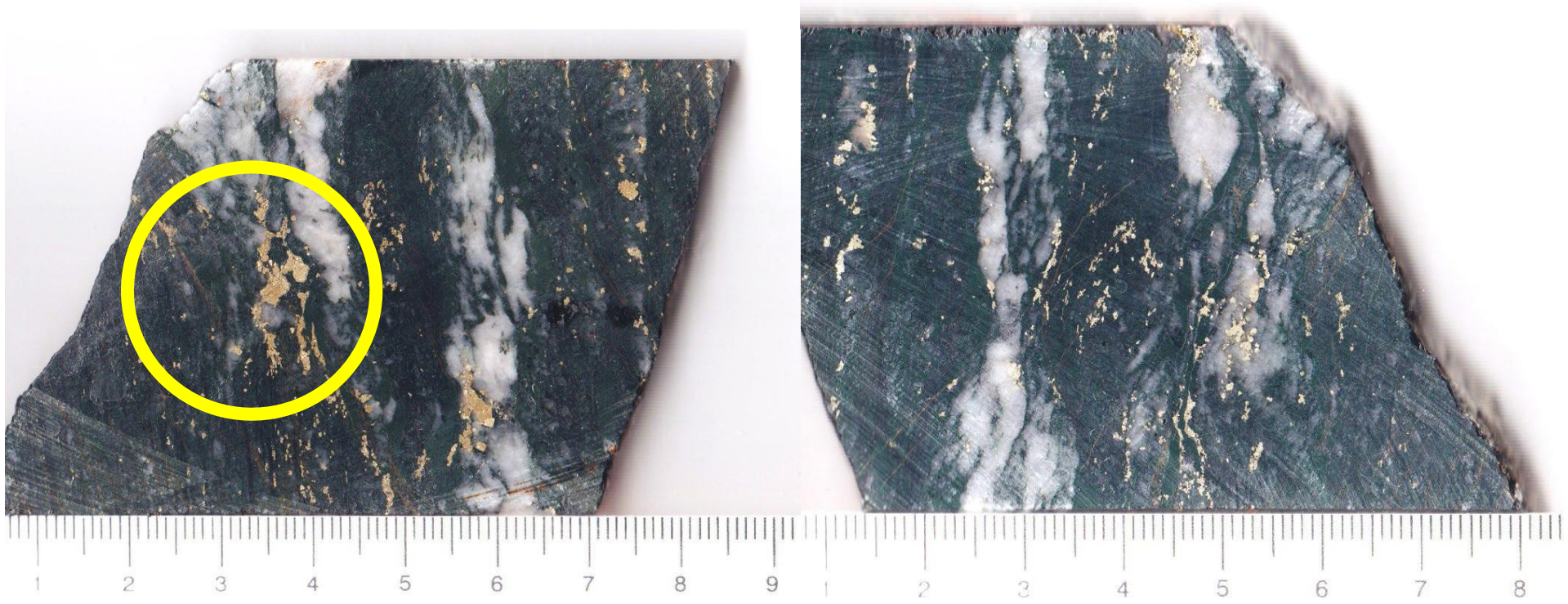

Figure 4 Photos of the drill core sample 4351177 from drill hole DEL10ACD00 1, Haylands prospect, Morgan region, South Australia, Australia.

Sample ID	Prospect	Borehole Name	From (m)	To (m)	Note
4351177	Haylands	DEL10ACD001	357.97	358.03	Sulfide ore and hydrothermal alteration

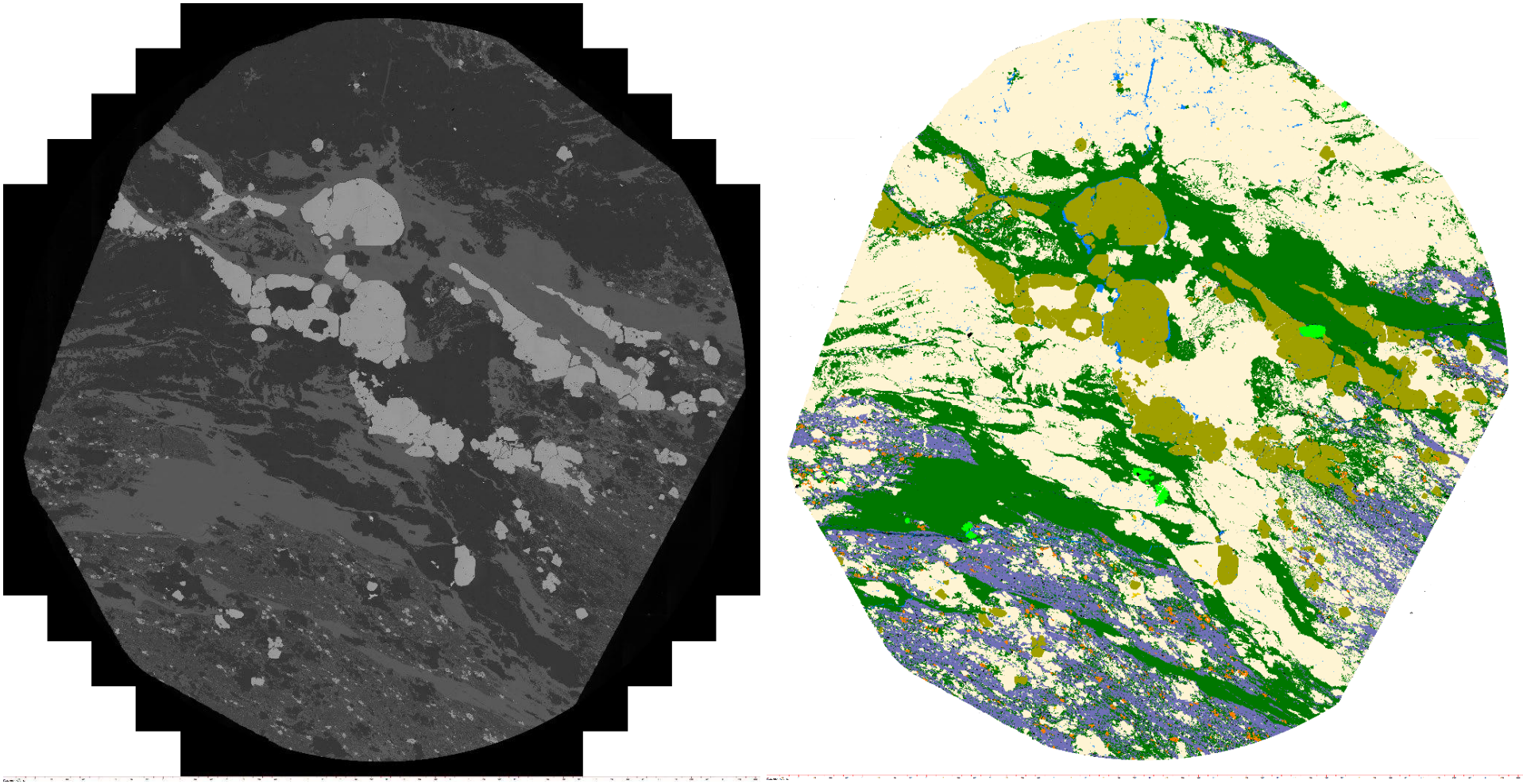

Figure 5 Backscattered electron (BSE) image (left) and Advanced Mineral Identification and Characterization System (AMICS) mineral map (right) of the sample 4351177 from drill hole DEL10ACD00 1, Haylands prospect, Morgan region, South Australia, Australia. See Figure 9 at the end of this document for the legend of minerals identified using Mineral Liberation Analysis (MLA) mapping.

Sample ID	Prospect	Borehole Name	From (m)	To (m)	Note
4351178	Haylands	DEL10ACD001	499.22	499.36	Sulfide ore and hydrothermal alteration

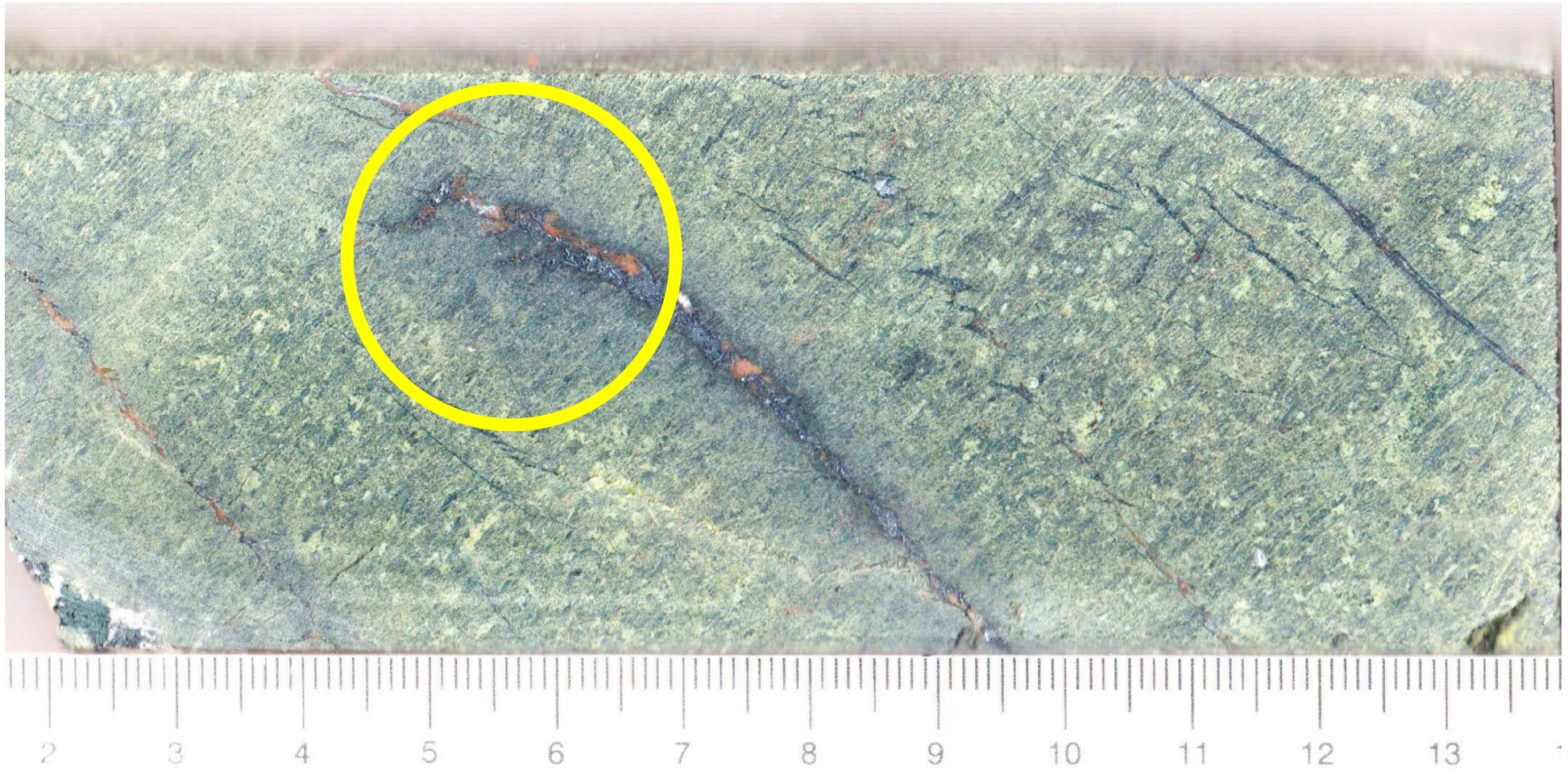

Figure 6 Photos of the drill core sample 4351178 from drill hole DEL10ACD001, Haylands prospect, Morgan region, South Australia, Australia.

Sample ID	Prospect	Borehole Name	From (m)	To (m)	Note
4351178	Haylands	DEL10ACD001	499.22	499.36	Sulfide ore and hydrothermal alteration

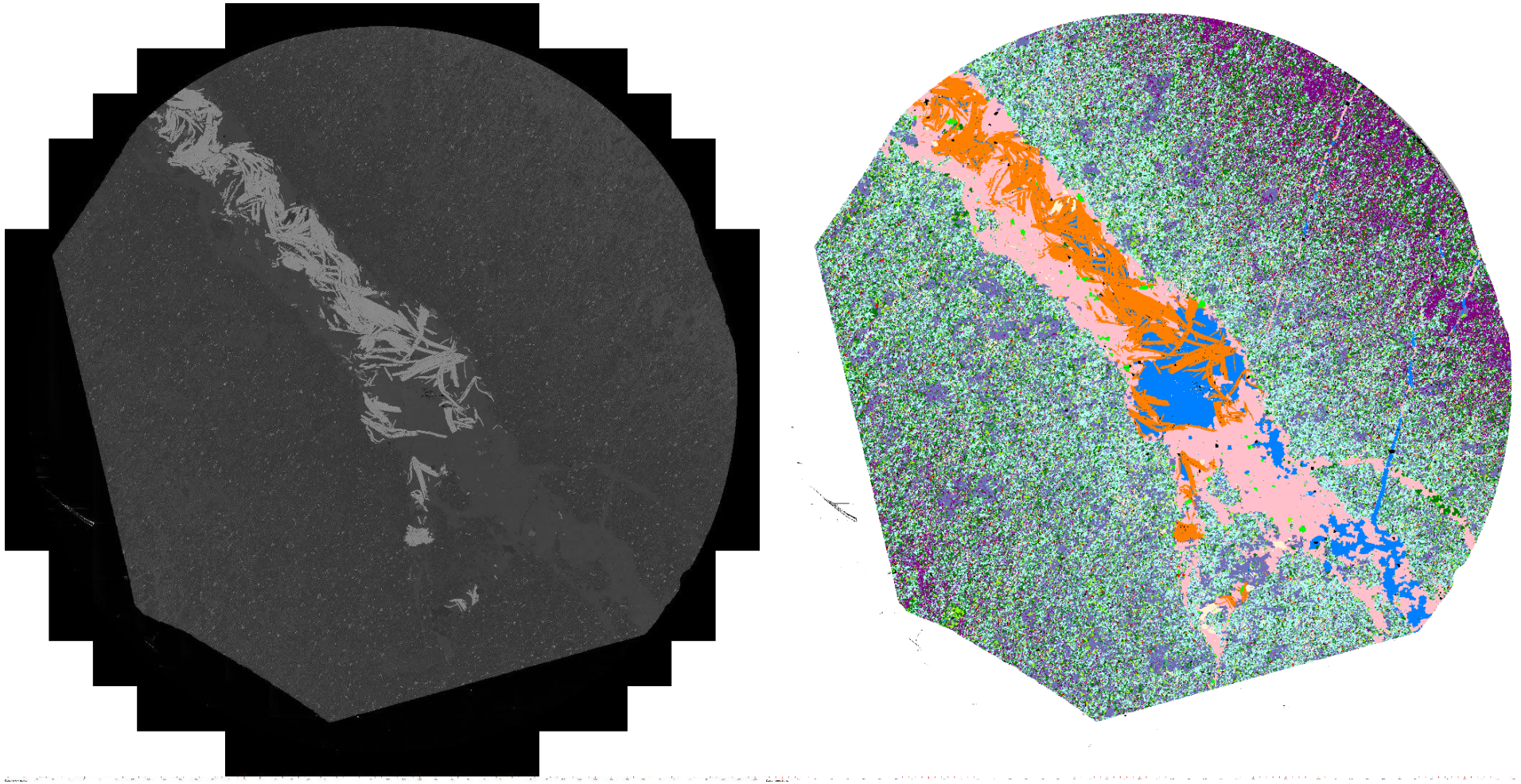

Figure 7 Backscattered electron (BSE) image (left) and Advanced Mineral Identification and Characterization System (AMICS) mineral map (right) of the sample 4351178 from drill hole DEL10ACD001, Haylands prospect, Morgan region, South Australia, Australia. See Figure 9 at the end of this document for the legend of minerals identified using Mineral Liberation Analysis (MLA) mapping.

Sample ID	Prospect	Borehole Name	From (m)	To (m)	Note
4351175	Haylands	DEL10ACD001	331.14	331.29	Sulfide ore and hydrothermal alteration

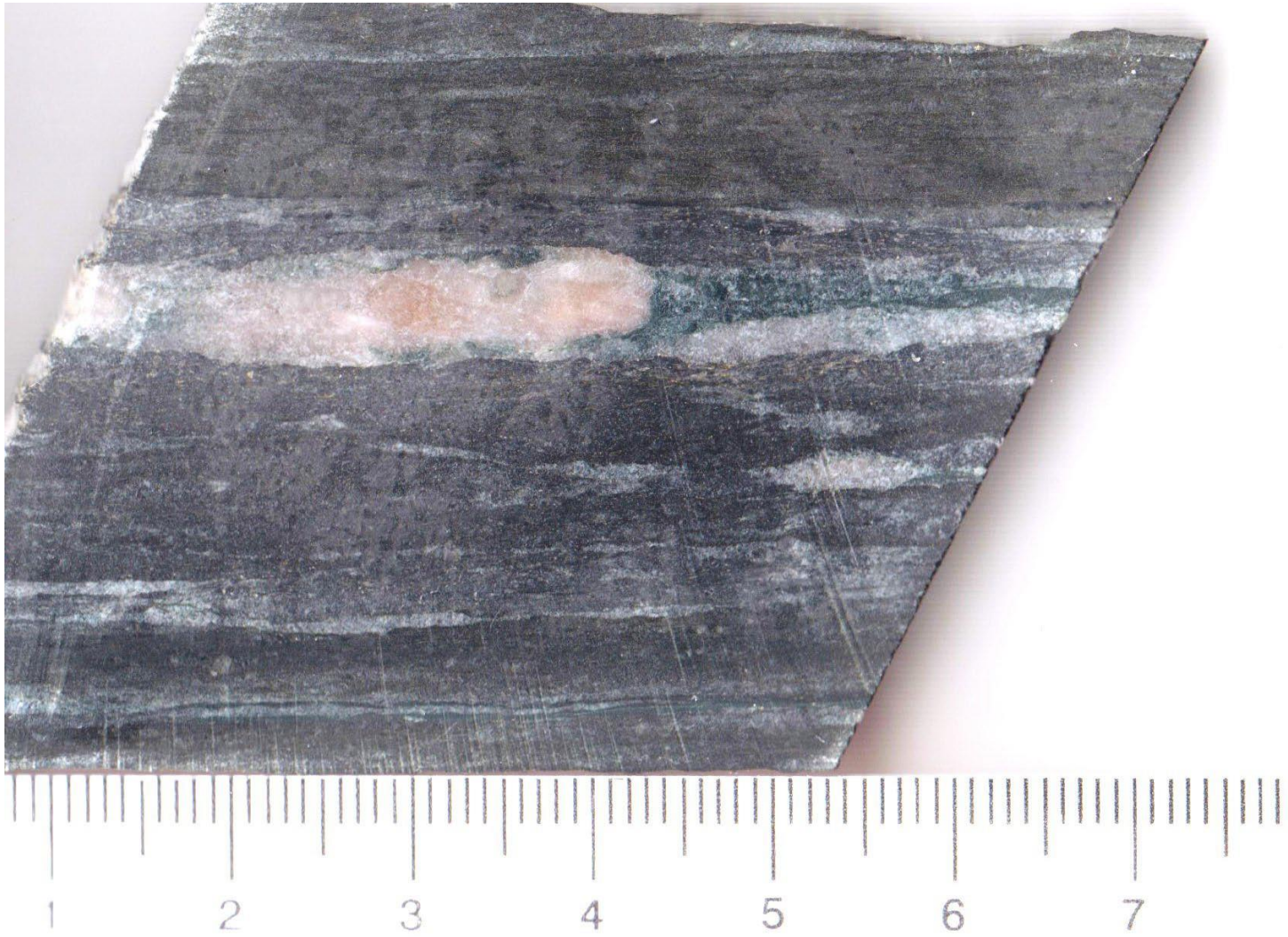

Figure 8 Photos of the drill core sample 4351175 from drill hole DEL10ACD001, Haylands prospect, Morgan region, South Australia, Australia.

S5.1 Eclipse prospect

Stavely Zone, Victoria

Detailed image data: Appendix 15 (individual data file)

(A) Sample List

Sample No.	Sample ID	Borehole	From (m)	To (m)	Notes
321889	321889	ED003	166.80	166.95	Sulfide ore and hydrothermal alteration
321893	321893	ED003	308.75	309.00	Sulfide ore and hydrothermal alteration
321888	321888	ED003	—	—	Sulfide ore and hydrothermal alteration
321890	321890	ED003	—	—	Sulfide ore and hydrothermal alteration
321891	321891	ED003	—	—	Sulfide ore and hydrothermal alteration
321892	321892	ED003	—	—	Sulfide ore and hydrothermal alteration
321894	321894	ED003	—	—	Sulfide ore and hydrothermal alteration

(B) Mineralisation Characteristics

Data Type	Mineral Assemblage
Hyperspectral SWIR	—
Hyperspectral TIR	—
Hyperspectral VNIR	—
Drill core specimen	*Qtz, Py, Cpy, Sph, Mgt, Hem, Apy*
Thin section	—
AMICS mineral map	*Qtz, Cpy, Py, Sph, Mgt, Hem, Apy, Chl, Bt, Ap, Cal*

(C) Mineralogical Textures and Paragenesis

Category	Description
Texture	Cu–Zn polymetallic sulfide (Cpy–Sph) with magnetite and arsenopyrite in a quartz–chlorite–biotite gangue. Two separate depth intervals sampled in ED003.
Paragenesis	Magnetite and arsenopyrite formed early. Pyrite–chalcopyrite–sphalerite form the main ore stage. Hematite and late calcite represent post-ore alteration.

(D) Supplementary Figure Reference

Supplementary Figures *include drill core photographs of samples 321889, 321893, 321888, 321890, 321891, 321892 and 321894 from ED003; BSE images and AMICS mineral maps of Cu–Zn polymetallic sulfide assemblage. AMICS mineral standard legend included.*

S5.1 The Eclipse prospect, Stavely region, Victoria

Sample ID	Prospect	Borehole Name	From (m)	To (m)	Note
321889	Eclipse	ED003	166.8	166.95	Sulfide ore and hydrothermal alteration

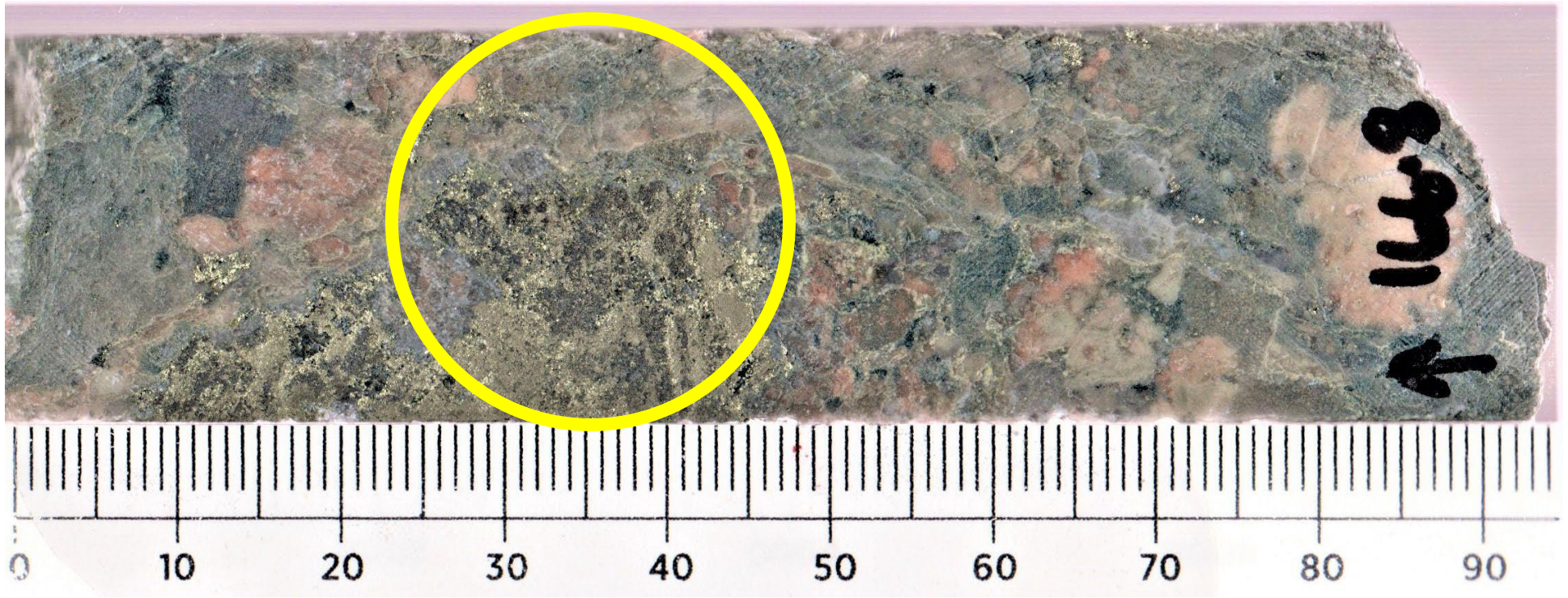

Figure 1 Photos of the drill core sample 321889 from drill hole ED003, Eclipse prospect, Stavely region, Victoria, Australia.

Sample ID	Prospect	Borehole Name	From (m)	To (m)	Note
321889	Eclipse	ED003	166.8	166.95	Sulfide ore and hydrothermal alteration

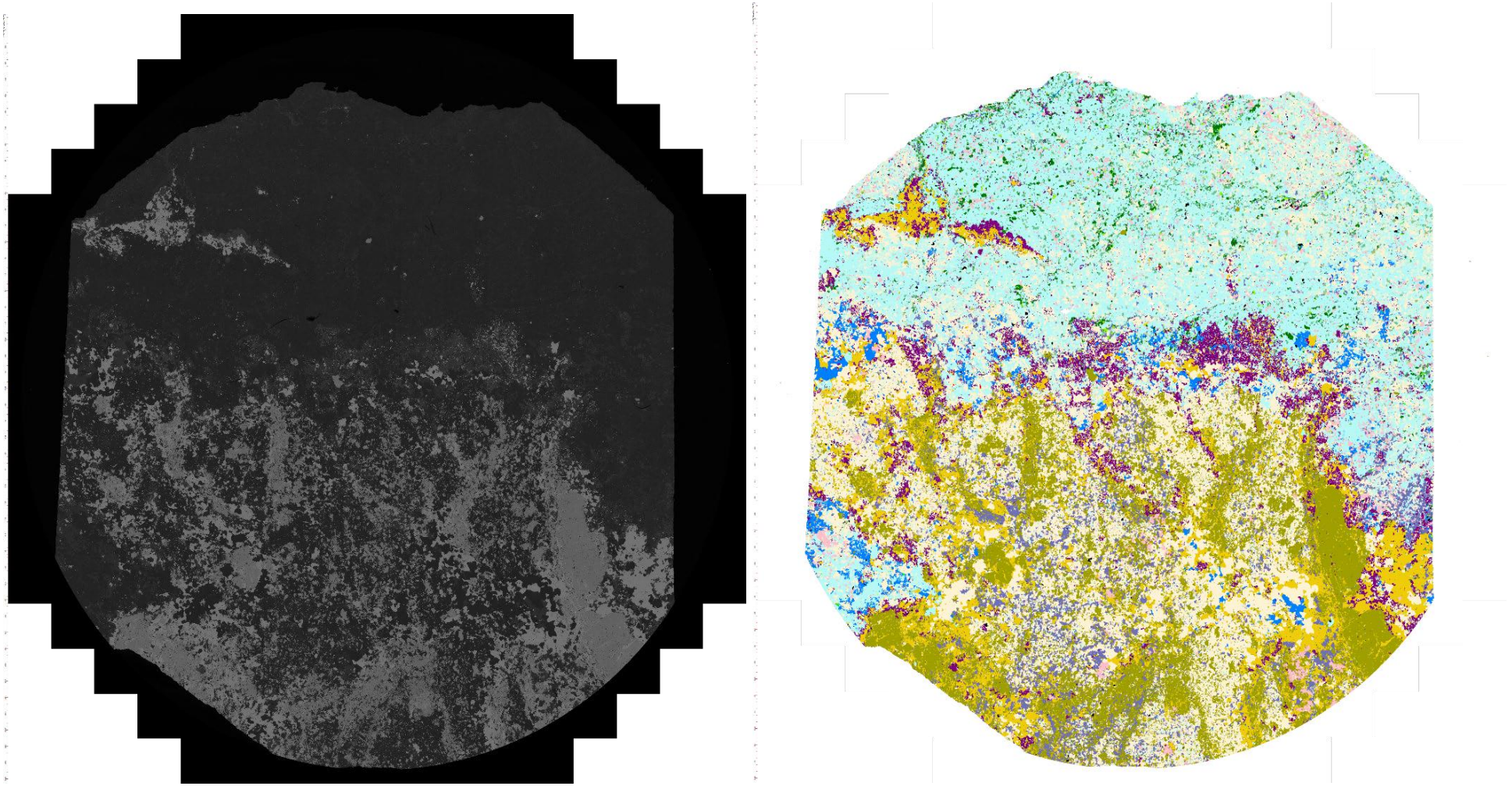

Figure 2 Backscattered electron (BSE) image (left) and Advanced Mineral Identification and Characterization System (AMICS) mineral map (right) of the sample 321889 from drill hole ED003, Eclipse prospect, Stavely region, Victoria, Australia. See Figure 10 at the end of this document for the legend of minerals identified using Mineral Liberation Analysis (MLA) mapping.

Sample ID	Prospect	Borehole Name	From (m)	To (m)	Note
321893	Eclipse	ED003	308.75	309	Sulfide ore and hydrothermal alteration

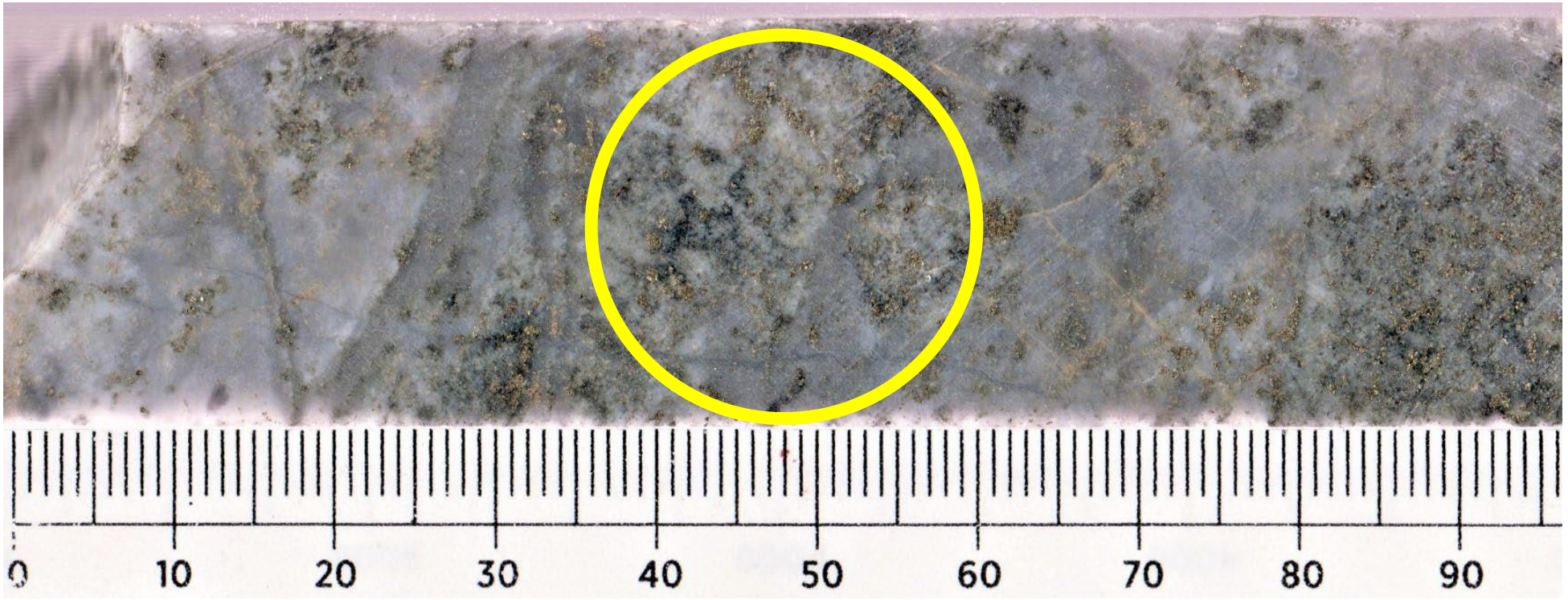

Figure 3 Photos of the drill core sample 321893 from drill hole ED003, Eclipse prospect, Stavely region, Victoria, Australia.

Sample ID	Prospect	Borehole Name	From (m)	To (m)	Note
321893	Eclipse	ED003	308.75	309	Sulfide ore and hydrothermal alteration

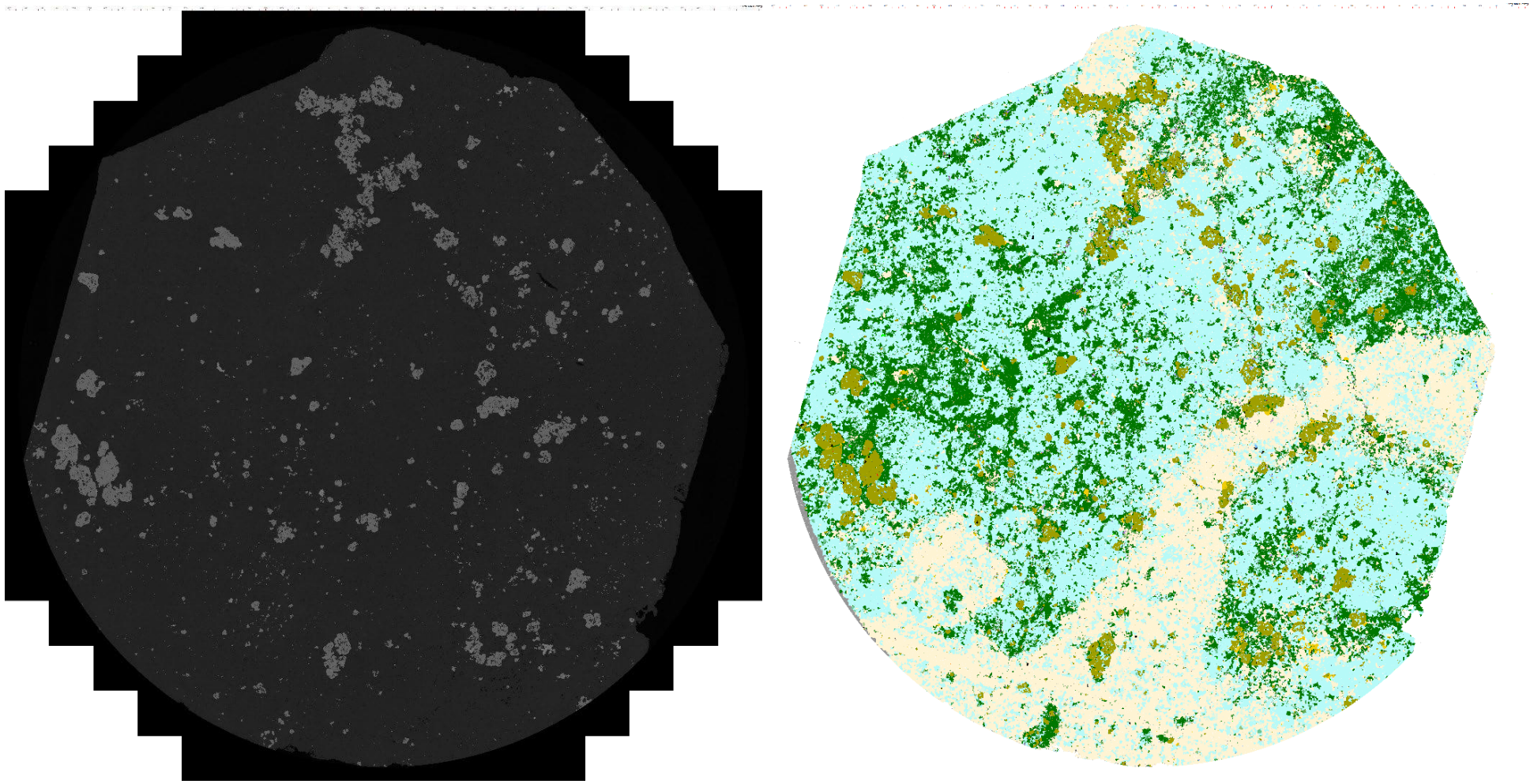

Figure 4 Backscattered electron (BSE) image (left) and Advanced Mineral Identification and Characterization System (AMICS) mineral map (right) of the sample 321893 from drill hole ED003, Eclipse prospect, Stavely region, Victoria, Australia. See Figure 10 at the end of this document for the legend of minerals identified using Mineral Liberation Analysis (MLA) mapping.

Sample ID	Prospect	Borehole Name	From (m)	To (m)	Note
321888	Eclipse	ED003	111.9	112.2	Sulfide ore and hydrothermal alteration

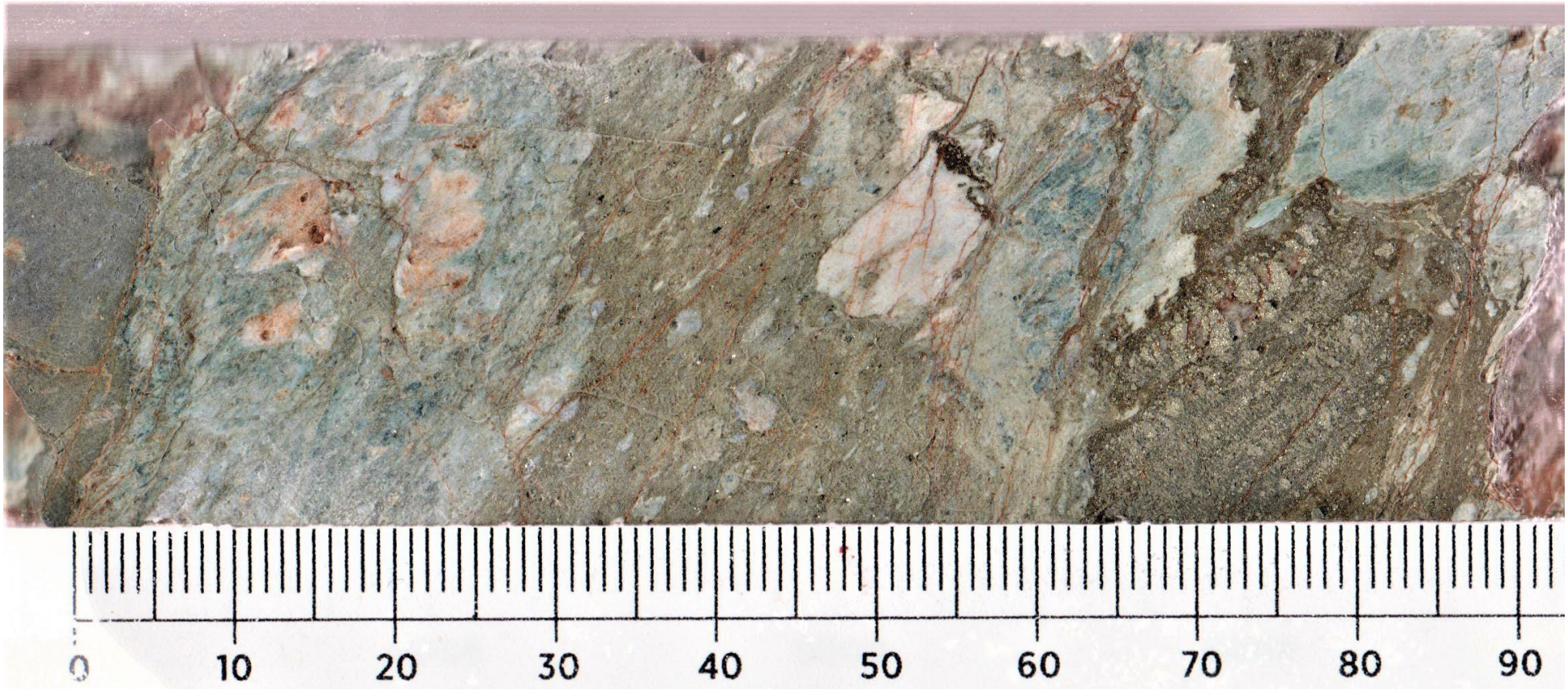

Figure 5 Photos of the drill core sample 321888 from drill hole ED003, Eclipse prospect, Stavely region, Victoria, Australia.

Sample ID	Prospect	Borehole Name	From (m)	To (m)	Note
321890	Eclipse	ED003	182.55	182.75	Sulfide ore and hydrothermal alteration

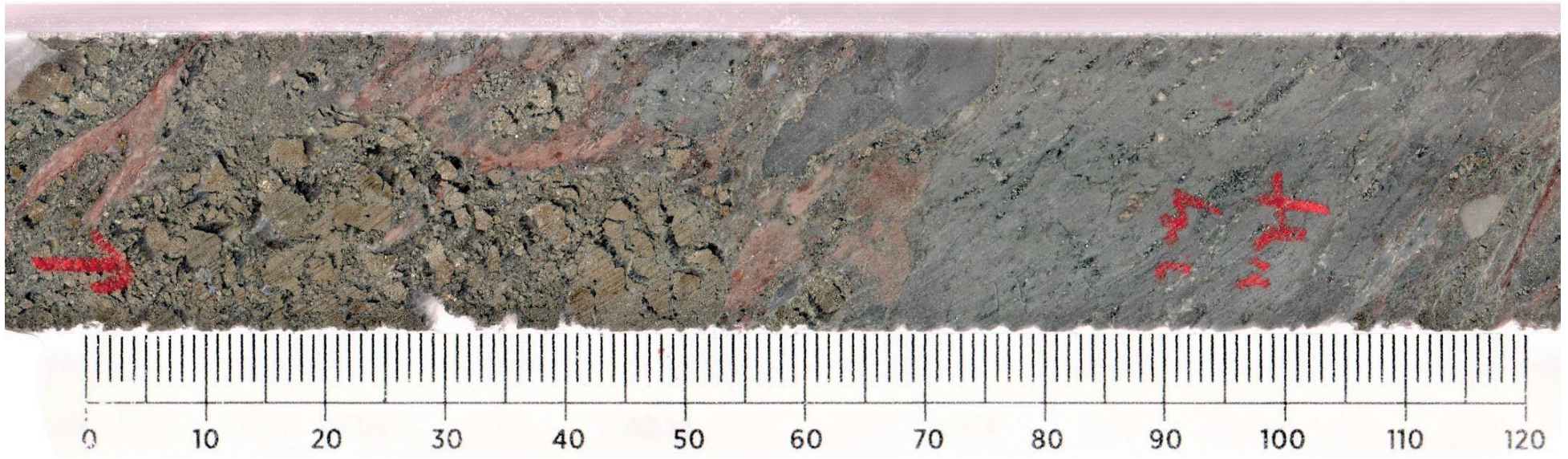

Figure 6 Photos of the drill core sample 321890 from drill hole ED003, Eclipse prospect, Stavely region, Victoria, Australia.

Sample ID	Prospect	Borehole Name	From (m)	To (m)	Note
321891	Eclipse	ED003	191.66	191.94	Sulfide ore and hydrothermal alteration

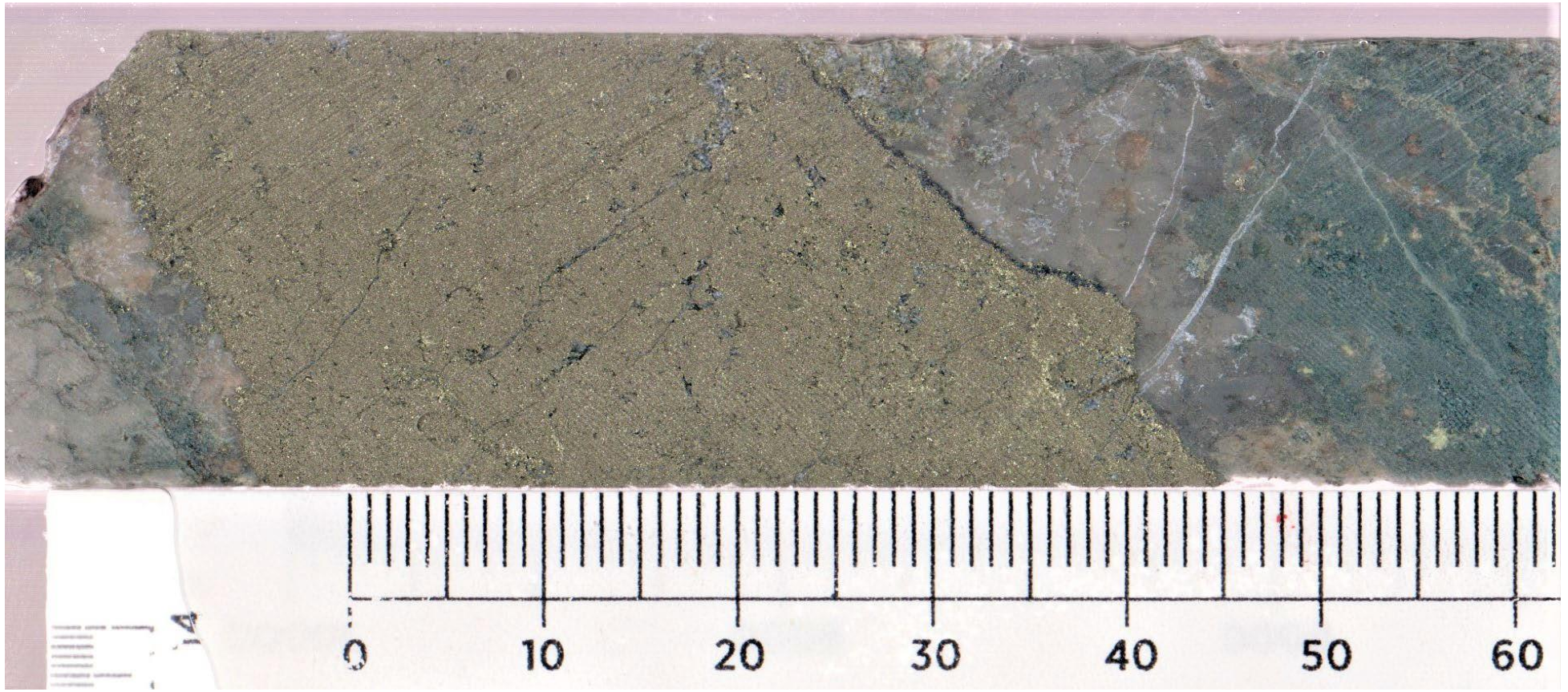

Figure 7 Photos of the drill core sample 321891 from drill hole ED003, Eclipse prospect, Stavely region, Victoria, Australia.

Sample ID	Prospect	Borehole Name	From (m)	To (m)	Note
321892	Eclipse	ED003	194.9	195.3	Sulfide ore and hydrothermal alteration

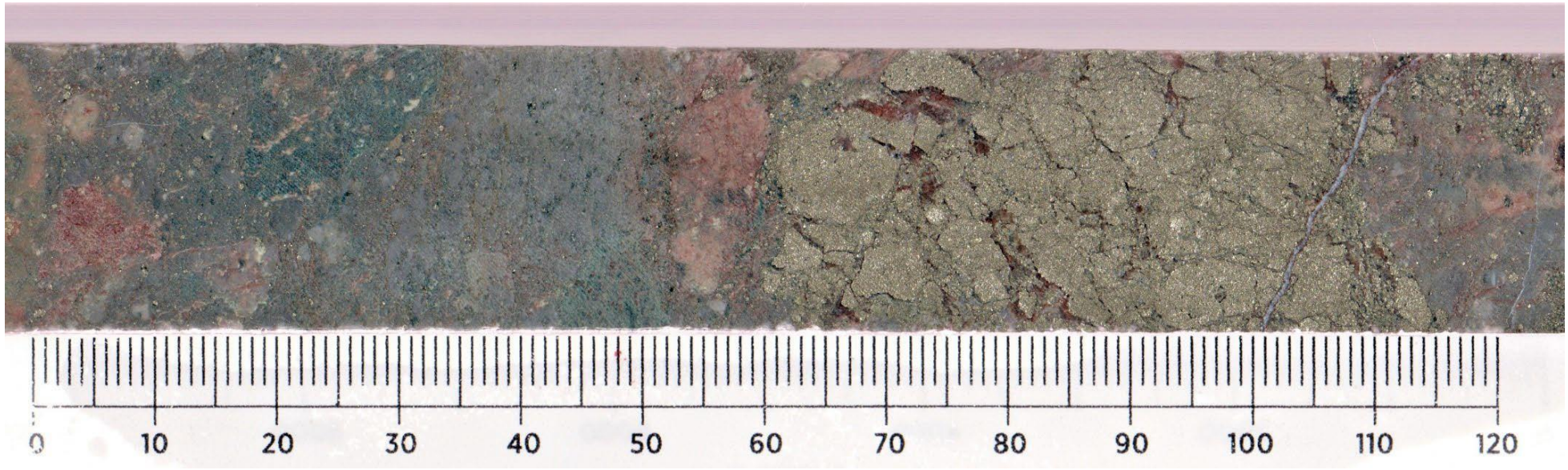

Figure 8 Photos of the drill core sample 321892 from drill hole ED003, Eclipse prospect, Stavely region, Victoria, Australia.

Sample ID	Prospect	Borehole Name	From (m)	To (m)	Note
321894	Eclipse	ED003	314	314.33	Sulfide ore and hydrothermal alteration

Figure 9 Photos of the drill core sample 321894 from drill hole ED003, Eclipse prospect, Stavely region, Victoria, Australia.

S5.2 Fiddlers Reef prospect

Stavely Zone, Victoria

Detailed image data: Appendix 16 (individual data file)

(A) Sample List

Sample No.	Sample ID	Borehole	From (m)	To (m)	Notes
321904	321904	YEHRIP01	33.06	33.13	Sulfide ore and hydrothermal alteration
321903	321903	YEHRIP01	30.00	30.10	Sulfide ore and hydrothermal alteration
321905	321905	YEHRIP01	—	—	Sulfide ore and hydrothermal alteration

(B) Mineralisation Characteristics

Data Type	Mineral Assemblage
Hyperspectral SWIR	—
Hyperspectral TIR	—
Hyperspectral VNIR	—
Drill core specimen	*Py, Qtz, Gn, Car, Ap, Mnz, Cpy, Sph*
Thin section	—
AMICS mineral map	*Py, Qtz, Gn, Car, Ap, Mnz, Cpy, Sph*

(C) Mineralogical Textures and Paragenesis

Category	Description
Texture	This prospect is notable for its exceptional sulfur isotope signature (see main text). Pb–Zn–Ag sulfide mineralisation with prominent galena–sphalerite, hosted in quartz–carbonate veins.
Paragenesis	Pyrite formed first. Galena and sphalerite formed together in a later hydrothermal event. Monazite, apatite and carbonate accompany the main ore stage.

(D) Supplementary Figure Reference

Supplementary Figures *include drill core photographs of samples 321904, 321903 and 321905 from YEHRIP01; BSE images and AMICS mineral maps of Pb–Zn–Ag sulfide assemblage (Py–Gn–Sph). AMICS mineral standard legend included.*

S5.2 The Fiddlers Reef prospect, Stavely region, Victoria

Sample ID	Prospect	Borehole Name	From (m)	To (m)	Note
321904	Fiddlers Reef	YEHRIP01	33.06	33.13	Sulfide ore and hydrothermal alteration

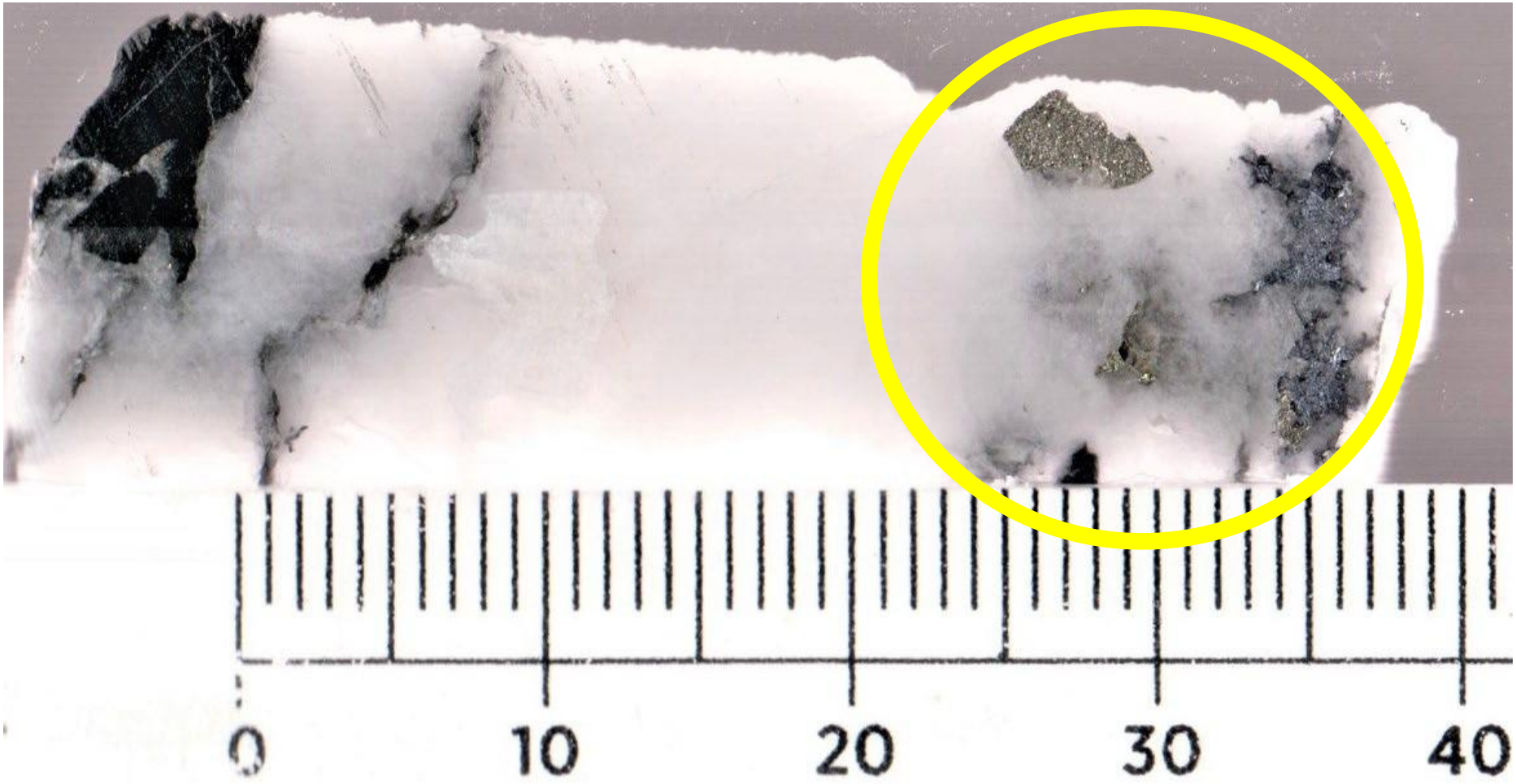

Figure 1 Photos of the drill core sample 321904 from drill hole YEHRIP01, Fiddlers Reef prospect, Stavely region, Victoria, Australia.

Sample ID	Prospect	Borehole Name	From (m)	To (m)	Note
321904	Fiddlers Reef	YEHRIP01	33.06	33.13	Sulfide ore and hydrothermal alteration

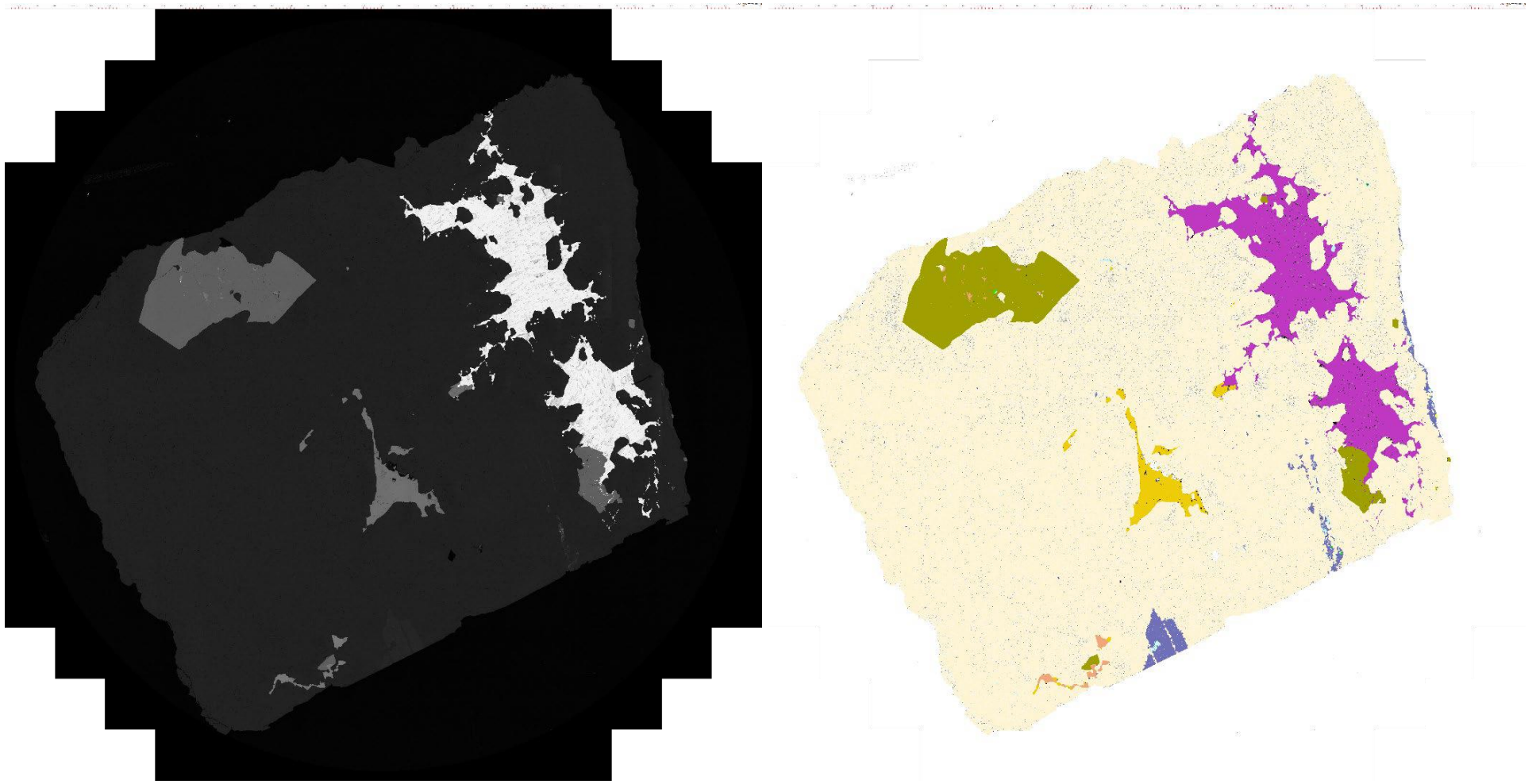

Figure 2 Backscattered electron (BSE) image (left) and Advanced Mineral Identification and Characterization System (AMICS) mineral map (right) of the sample 321904 from drill hole YEHRIP01, Fiddlers Reef prospect, Stavely region, Victoria, Australia. See Figure 7 at the end of this document for the legend of minerals identified using Mineral Liberation Analysis (MLA) mapping.

Sample ID	Prospect	Borehole Name	From (m)	To (m)	Note
321903	Fiddlers Reef	YEHRIP01	30.0	30.1	Sulfide ore and hydrothermal alteration

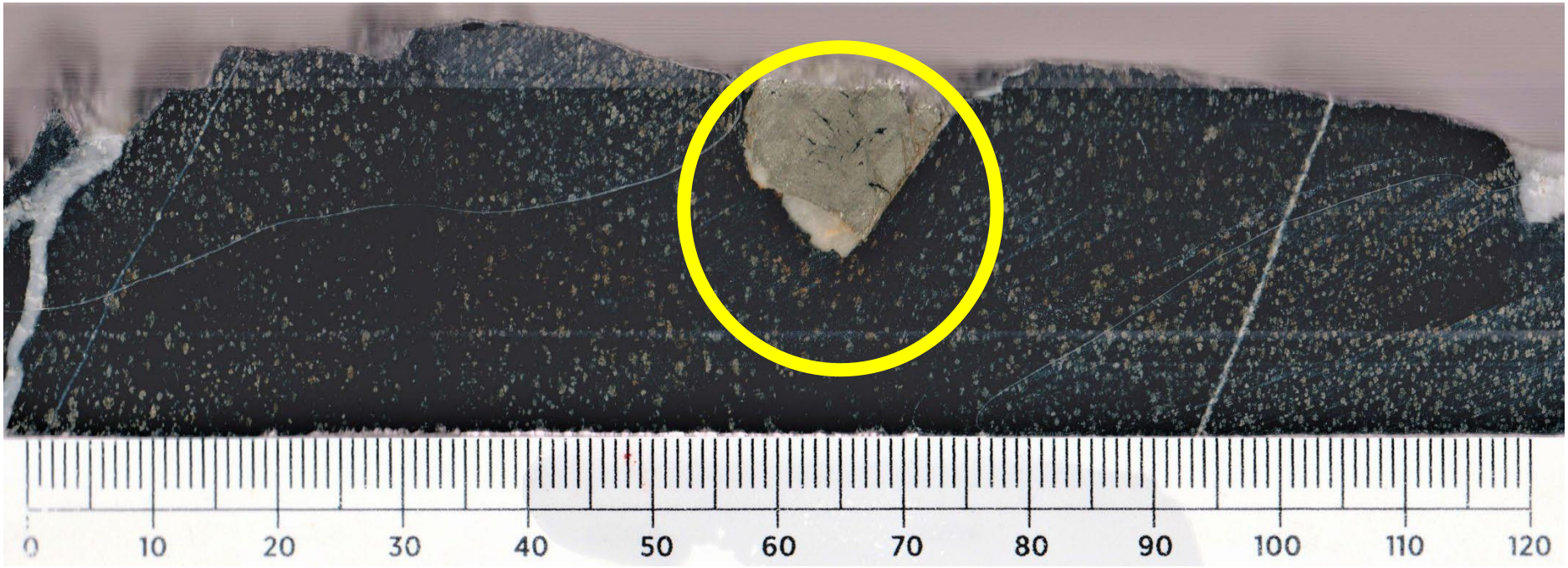

Figure 3 Photos of the drill core sample 321903 from drill hole YEHRIP01, Fiddlers Reef prospect, Stavely region, Victoria, Australia.

Sample ID	Prospect	Borehole Name	From (m)	To (m)	Note
321903	Fiddlers Reef	YEHRIP01	30.0	30.1	Sulfide ore and hydrothermal alteration

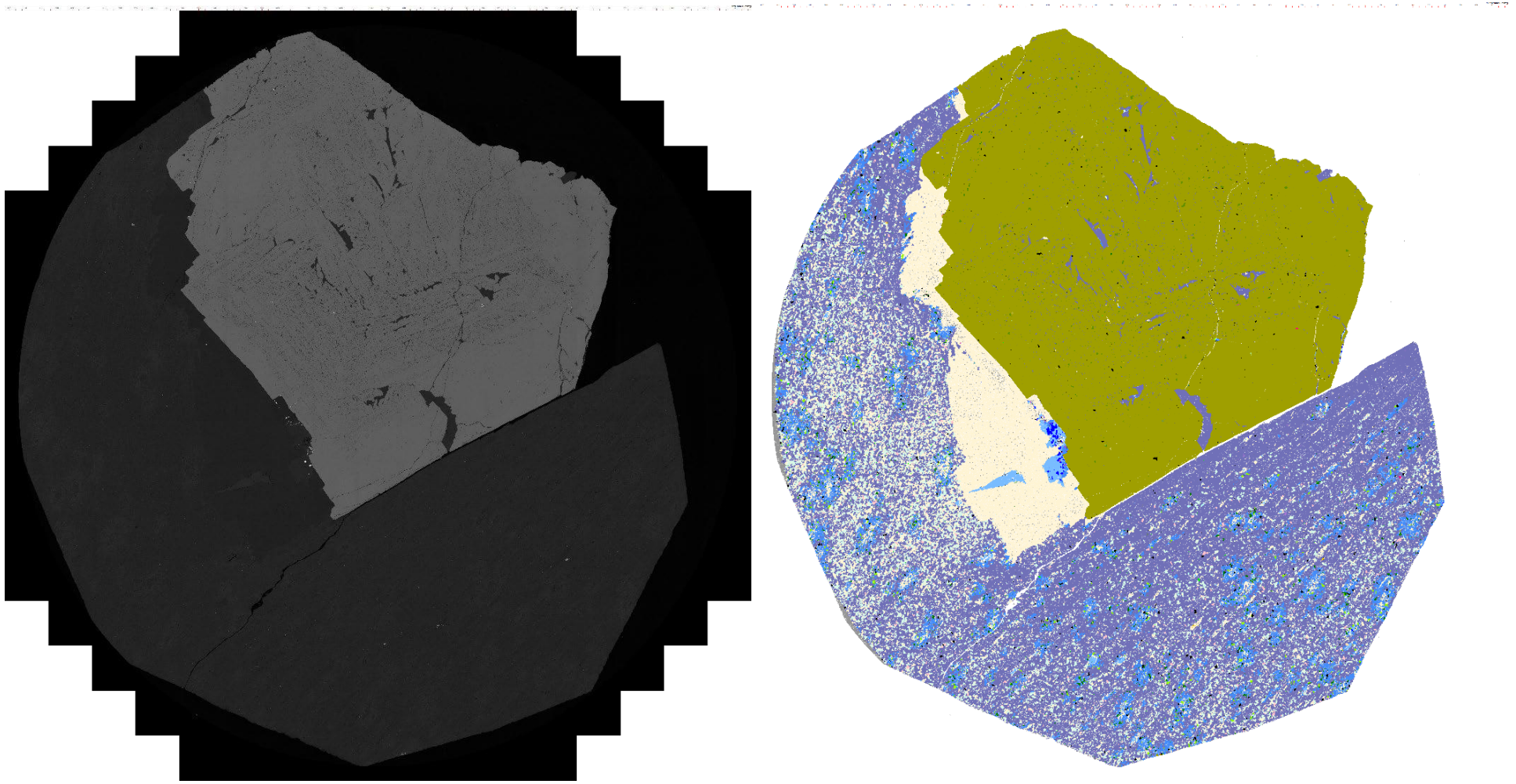

Figure 4 Backscattered electron (BSE) image (left) and Advanced Mineral Identification and Characterization System (AMICS) mineral map (right) of the sample 321903 from drill hole YEHRIP01, Fiddlers Reef prospect, Stavely region, Victoria, Australia. See Figure 7 at the end of this document for the legend of minerals identified using Mineral Liberation Analysis (MLA) mapping.

Sample ID	Prospect	Borehole Name	From (m)	To (m)	Note
321905	Fiddlers Reef	YEHRIP01	34.26	34.39	Sulfide ore and hydrothermal alteration

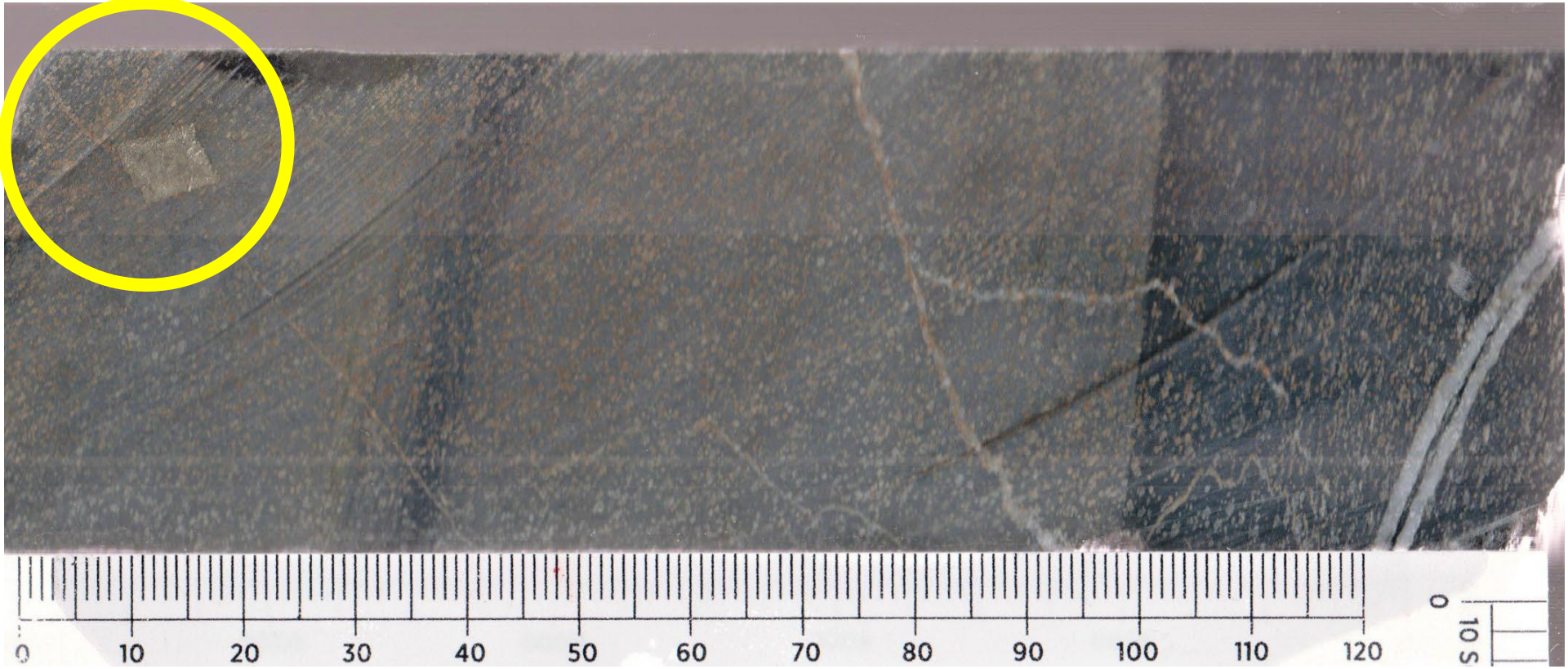

Figure 5 Photos of the drill core sample 321905 from drill hole YEHRIP01, Fiddlers Reef prospect, Stavely region, Victoria, Australia.

Sample ID	Prospect	Borehole Name	From (m)	To (m)	Note
321905	Fiddlers Reef	YEHRIP01	34.26	34.39	Sulfide ore and hydrothermal alteration

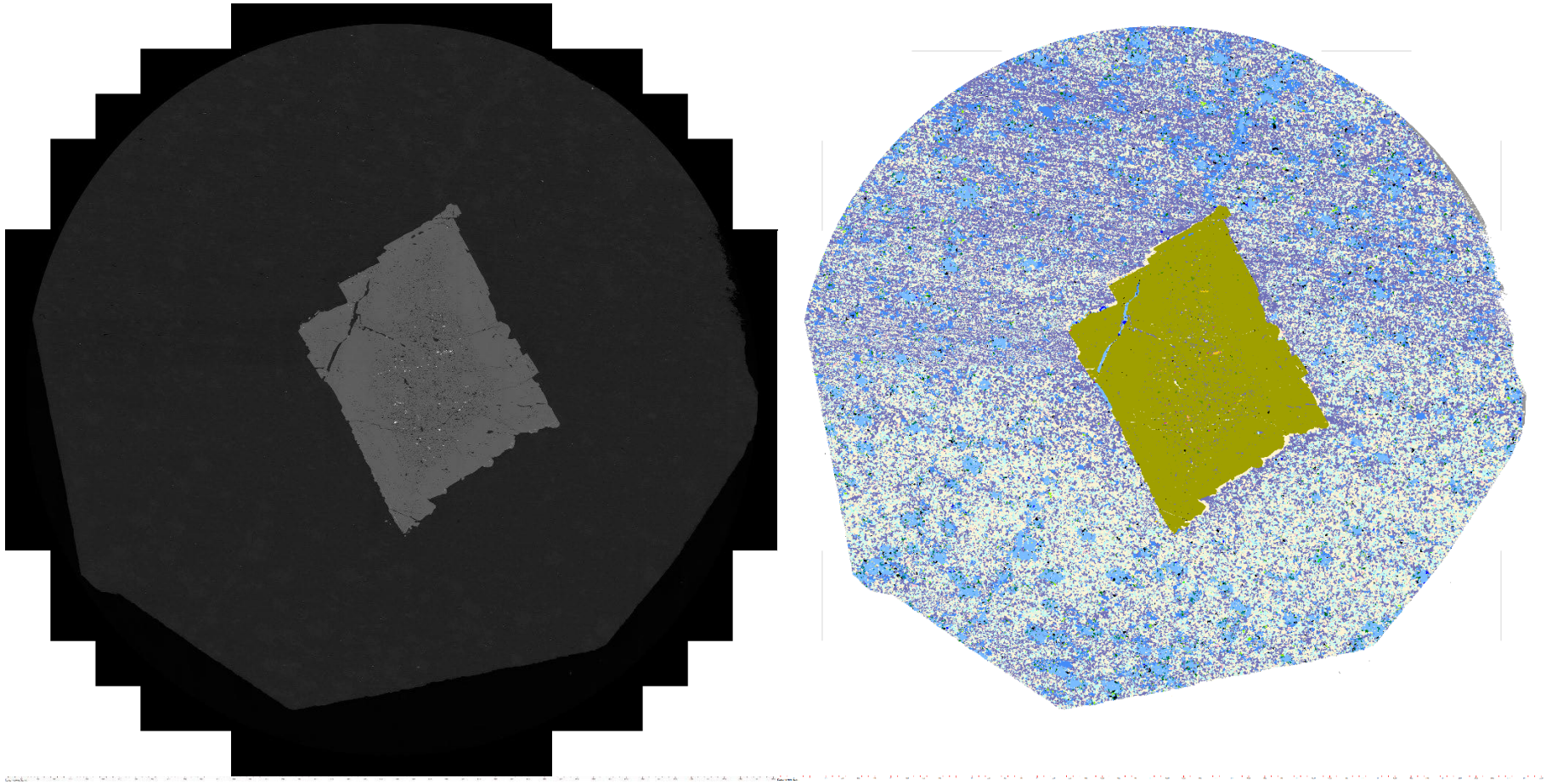

Figure 6 Backscattered electron (BSE) image (left) and Advanced Mineral Identification and Characterization System (AMICS) mineral map (right) of the sample 321905 from drill hole YEHRIP01, Fiddlers Reef prospect, Stavely region, Victoria, Australia. See Figure 7 at the end of this document for the legend of minerals identified using Mineral Liberation Analysis (MLA) mapping.

S5.3 Glenyle prospect

Stavely Zone, Victoria

Detailed image data: Appendix 17 (individual data file)

(A) Sample List

Sample No.	Sample ID	Borehole	From (m)	To (m)	Notes
2023440012	2023440012	GDD008	138.20	138.55	Sulfide ore and hydrothermal alteration
2023440005	2023440005	GDD003	266.40	266.71	Sulfide ore and hydrothermal alteration
2023440006	2023440006	GDD003	—	—	Sulfide ore and hydrothermal alteration
2023440007	2023440007	GDD003	—	—	Sulfide ore and hydrothermal alteration
2023440001–2023440004	2023440001–2023440004	GDD001	—	—	Sulfide ore and hydrothermal alteration
2023440009–2023440011	2023440009–2023440011	GDD005	—	—	Sulfide ore and hydrothermal alteration
2023440013–2023440014	2023440013–2023440014	GDD008	—	—	Sulfide ore and hydrothermal alteration

(B) Mineralisation Characteristics

Data Type	Mineral Assemblage
Hyperspectral SWIR	—
Hyperspectral TIR	—
Hyperspectral VNIR	—
Drill core specimen	*Py, Apy, Sph, Qtz, Cal, Chl*
Thin section	—
AMICS mineral map	*Qtz, Cal, Py, Apy, Sph, Cpy, Gn, Ser, Chl, Ab, Hem, Kfsp, Ttn, Ap, Bt*

(C) Mineralogical Textures and Paragenesis

Category	Description
Texture	Au-bearing Py–Apy–Sph sulfide mineralisation hosted in quartz–calcite–chlorite veins. Sampled across multiple drill holes (GDD001, GDD003, GDD005, GDD008).
Paragenesis	Arsenopyrite and pyrite formed in the early hydrothermal stage. Sphalerite, chalcopyrite and galena form the main ore assemblage. Carbonate, sericite and chlorite represent retrograde alteration.

(D) Supplementary Figure Reference

Supplementary Figures *include drill core photographs of samples 2023440012, 2023440005–2023440007, 2023440001–2023440004, 2023440009–2023440011 and 2023440013–2023440014; BSE image and AMICS mineral map of Py–Apy–Sph–Cpy–Gn assemblage. AMICS mineral standard legend included.*

S5.3 The Glenyle prospect, Stavely region, Victoria

Sample ID	Prospect	Borehole Name	From (m)	To (m)	Note
2023440012	Glenyle	GDD008	138.2	138.55	Sulfide ore and hydrothermal alteration

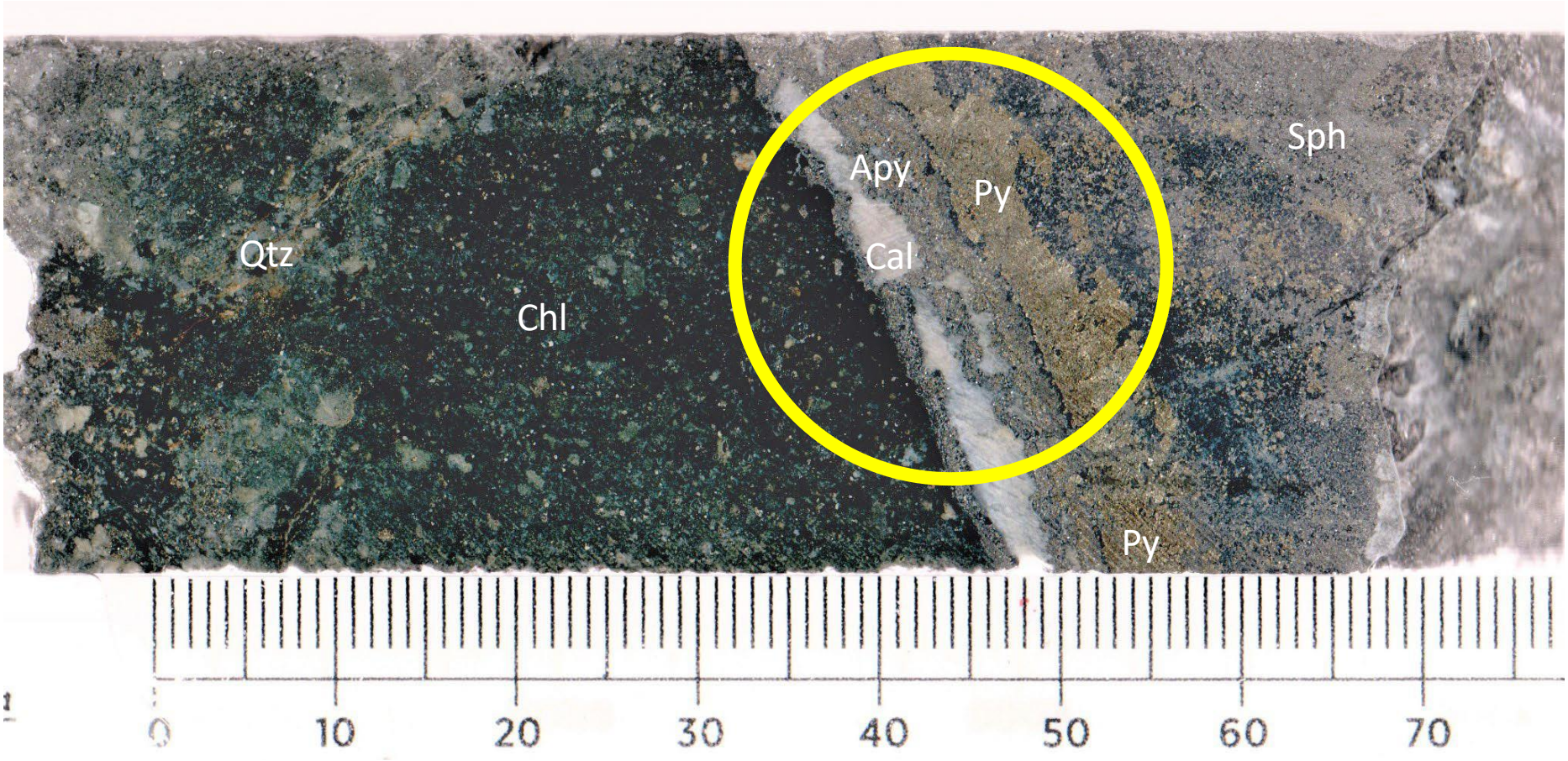

Figure 1 Photos of the drill core sample 2023440012 from drill hole GDD008, Glenyle prospect, Stavely region, Victoria, Australia. Py-pyrite; Apy-arsenopyrite; Sph-sphalerite; Qtz-quartz; Cal-calcite; Chl-chlorite.

Sample ID	Prospect	Borehole Name	From (m)	To (m)	Note
2023440012	Glenyle	GDD008	138.2	138.55	Sulfide ore and hydrothermal alteration

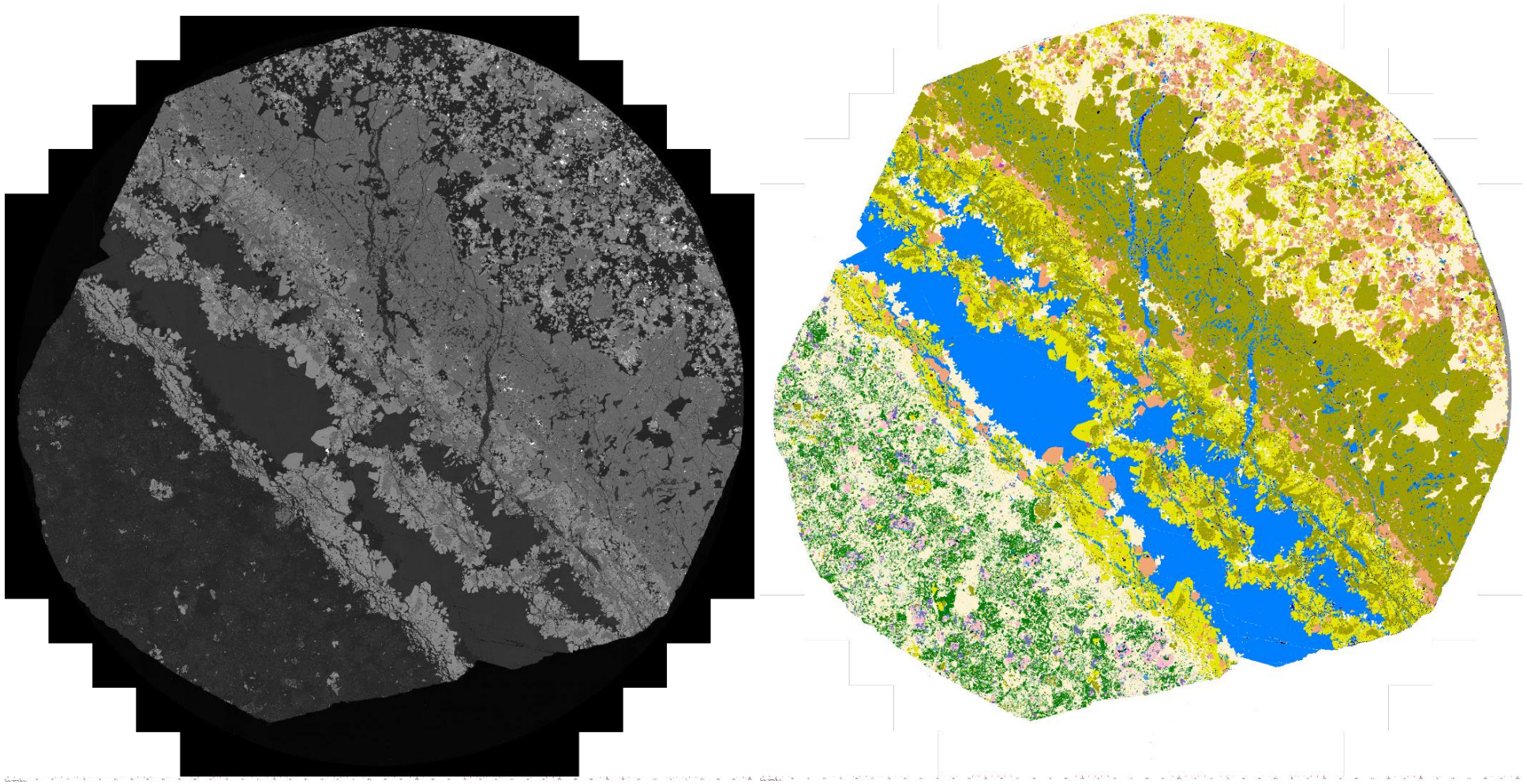

Figure 2 Backscattered electron (BSE) image (left) and Advanced Mineral Identification and Characterization System (AMICS) mineral map (right) of the sample 2023440012 from drill hole GDD008, Glenyle prospect, Stavely region, Victoria, Australia. See Figure 15 at the end of this document for the legend of minerals identified using Mineral Liberation Analysis (MLA) mapping.

Sample ID	Prospect	Borehole Name	From (m)	To (m)	Note
2023440005	Glenyle	GDD003	266.4	266.71	Sulfide ore and hydrothermal alteration

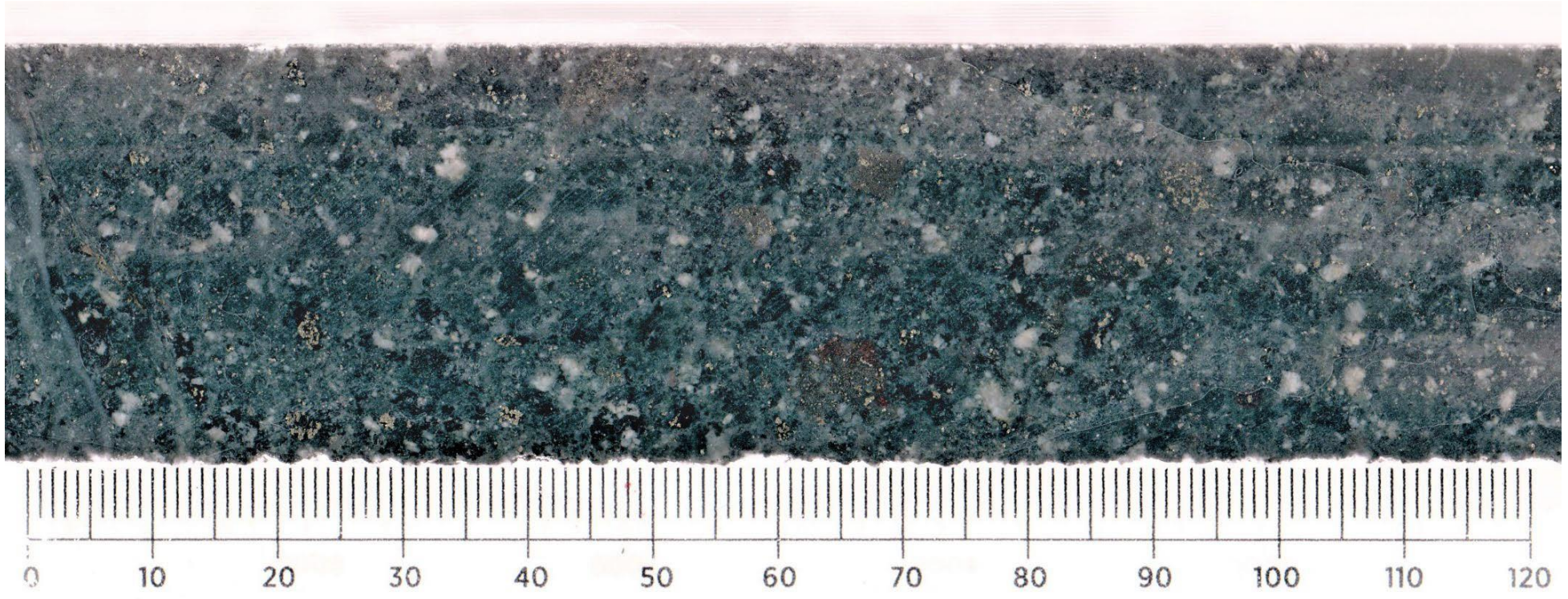

Figure 3 Photos of the drill core sample 2023440005 from drill hole GDD003, Glenyle prospect, Stavely region, Victoria, Australia.

Sample ID	Prospect	Borehole Name	From (m)	To (m)	Note
2023440006	Glenyle	GDD003	213.18	213.26	Sulfide ore and hydrothermal alteration

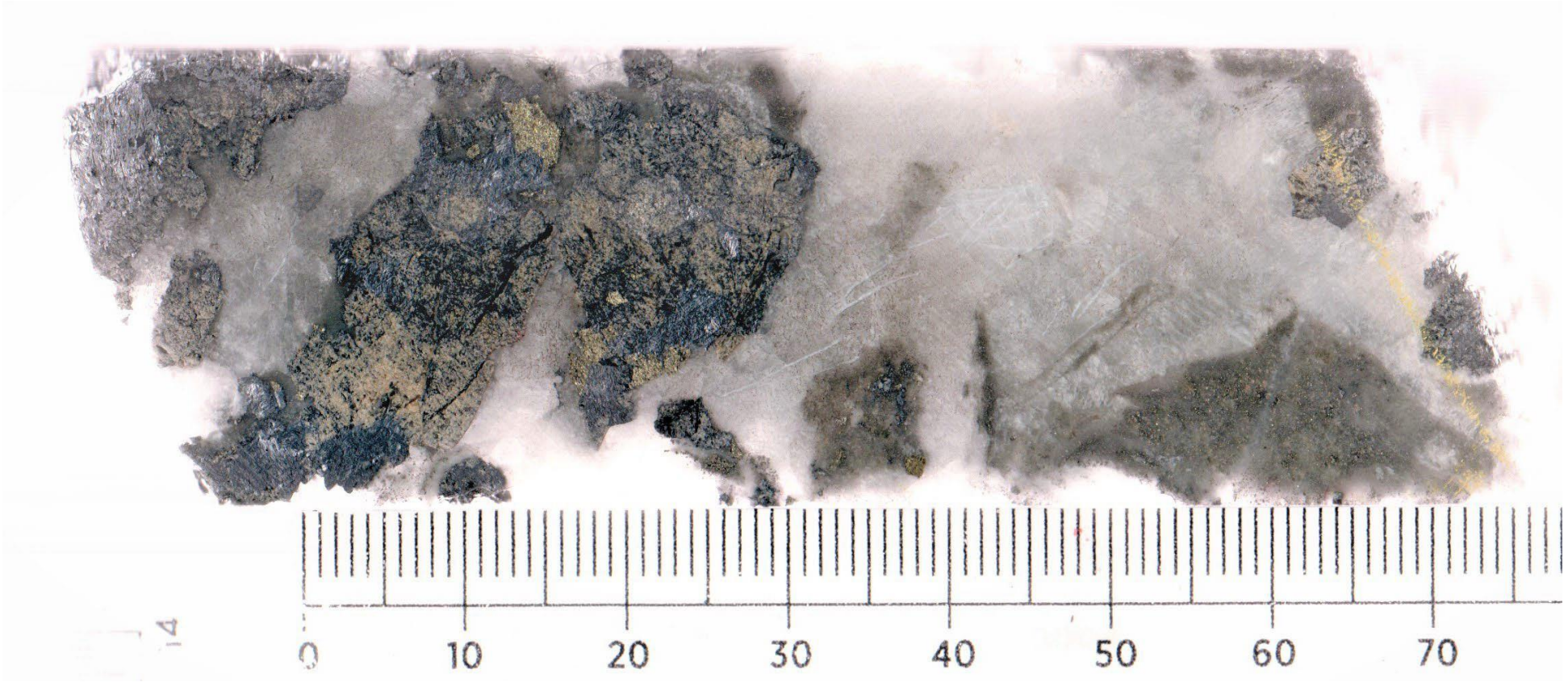

Figure 4 Photos of the drill core sample 2023440006 from drill hole GDD003, Glenyle prospect, Stavely region, Victoria, Australia.

Sample ID	Prospect	Borehole Name	From (m)	To (m)	Note
2023440007	Glenyle	GDD003	161.05	161.36	Sulfide ore and hydrothermal alteration

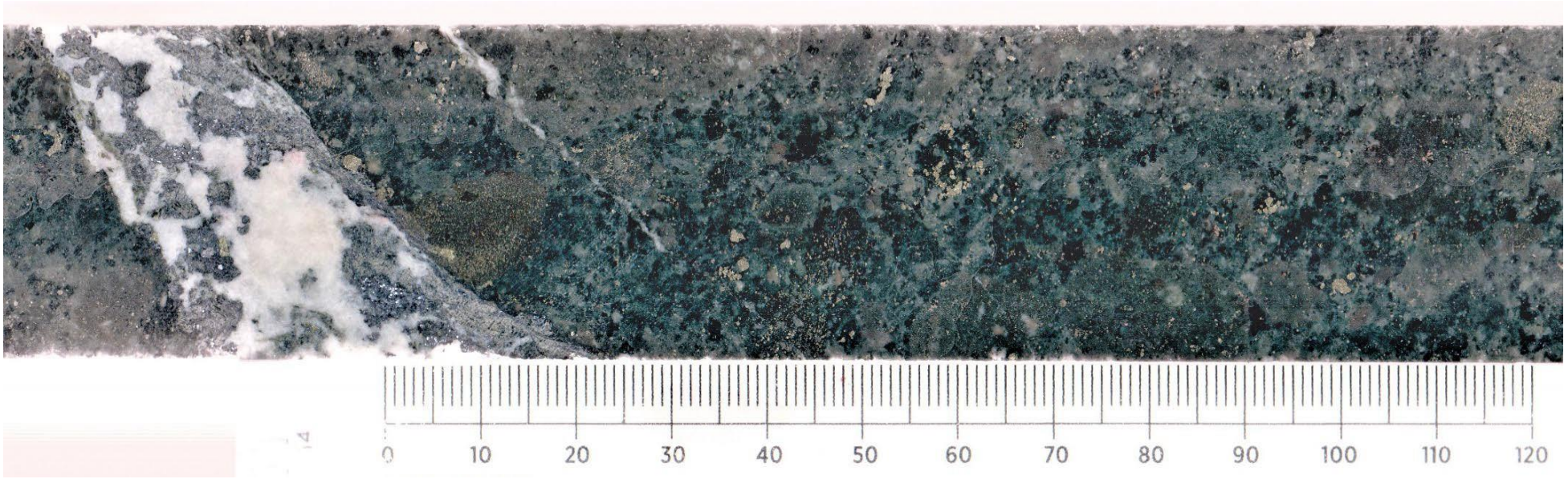

Figure 5 Photos of the drill core sample 2023440007 from drill hole GDD003, Glenyle prospect, Stavely region, Victoria, Australia.

Sample ID	Prospect	Borehole Name	From (m)	To (m)	Note
2023440001	Glenyle	GDD006	287.2	287.6	Sulfide ore and hydrothermal alteration

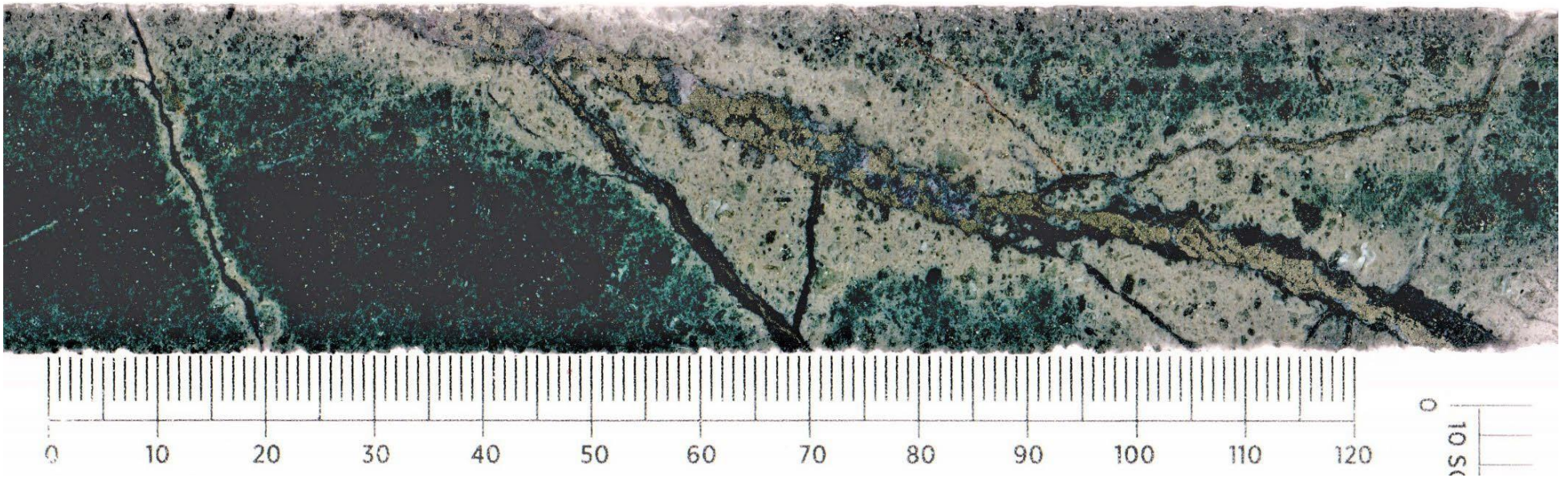

Figure 6 Photos of the drill core sample 2023440001 from drill hole GDD006, Glenyle prospect, Stavely region, Victoria, Australia.

Sample ID	Prospect	Borehole Name	From (m)	To (m)	Note
2023440002	Glenyle	GDD006	281.00	281.22	Sulfide ore and hydrothermal alteration

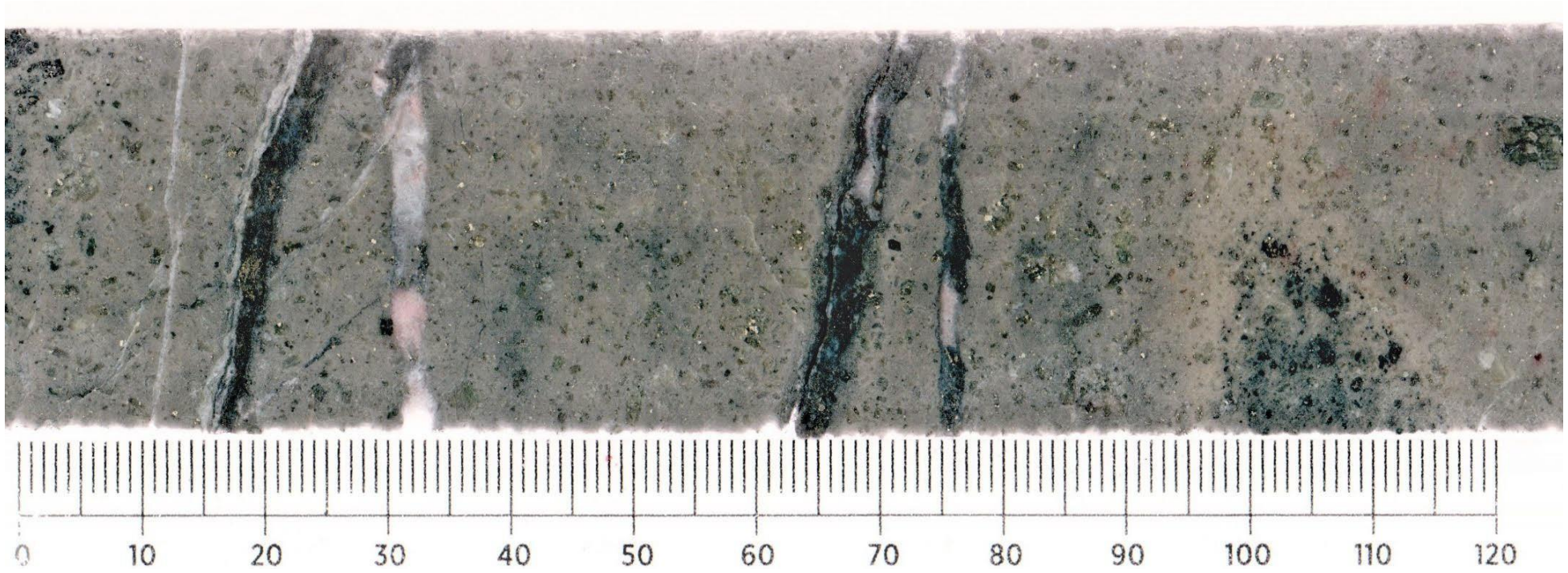

Figure 7 Photos of the drill core sample 2023440002 from drill hole GDD006, Glenyle prospect, Stavely region, Victoria, Australia.

Sample ID	Prospect	Borehole Name	From (m)	To (m)	Note
2023440003	Glenyle	GDD006	264.93	265.24	Sulfide ore and hydrothermal alteration

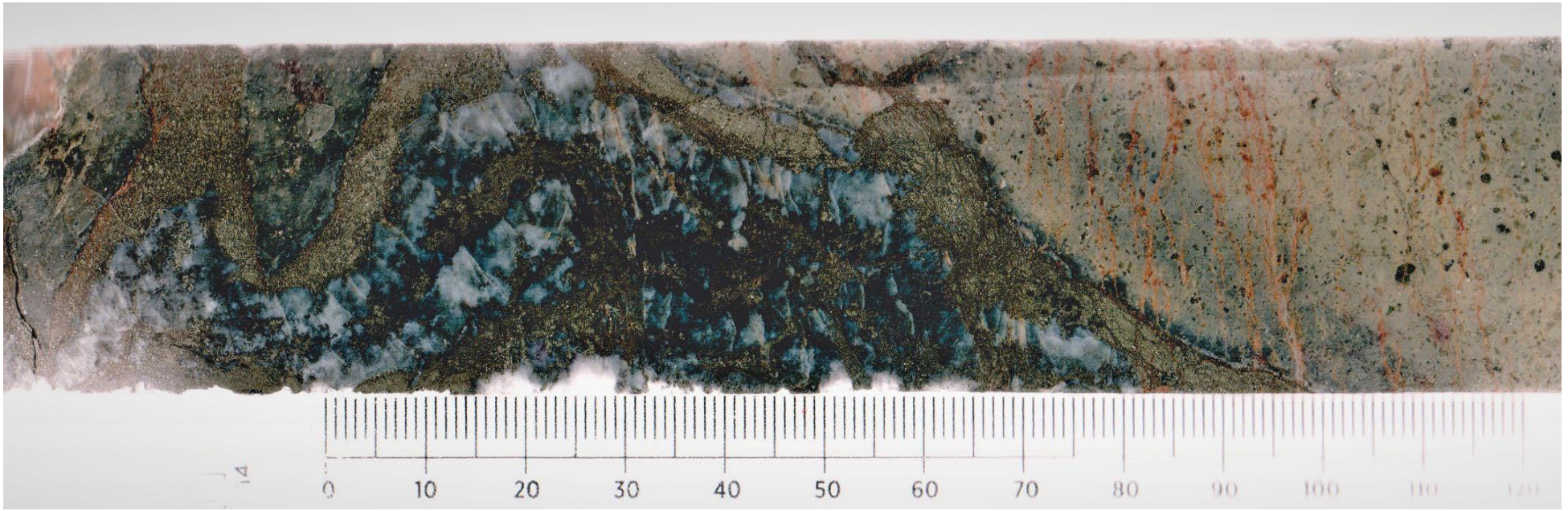

Figure 8 Photos of the drill core sample 2023440003 from drill hole GDD006, Glenyle prospect, Stavely region, Victoria, Australia.

Sample ID	Prospect	Borehole Name	From (m)	To (m)	Note
2023440004	Glenyle	GDD006	192.43	192.71	Sulfide ore and hydrothermal alteration

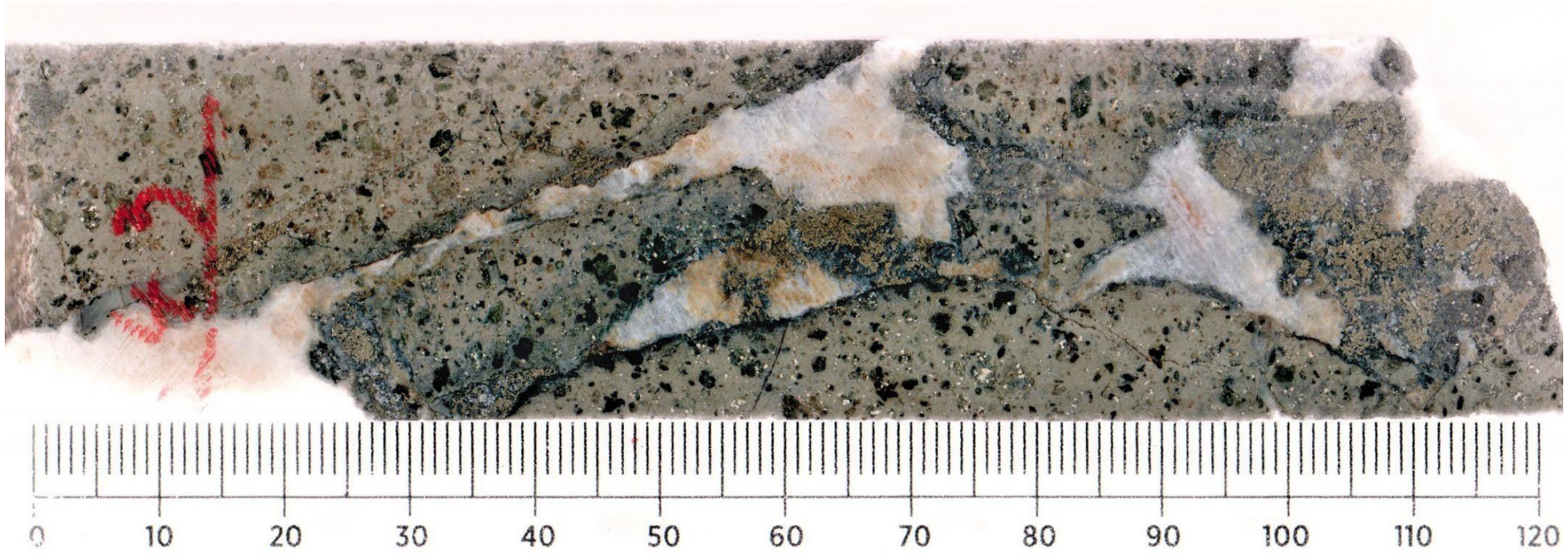

Figure 9 Photos of the drill core sample 2023440004 from drill hole GDD006, Glenyle prospect, Stavely region, Victoria, Australia.

Sample ID	Prospect	Borehole Name	From (m)	To (m)	Note
2023440013	Glenyle	GDD006	309.41	309.6	Sulfide ore and hydrothermal alteration

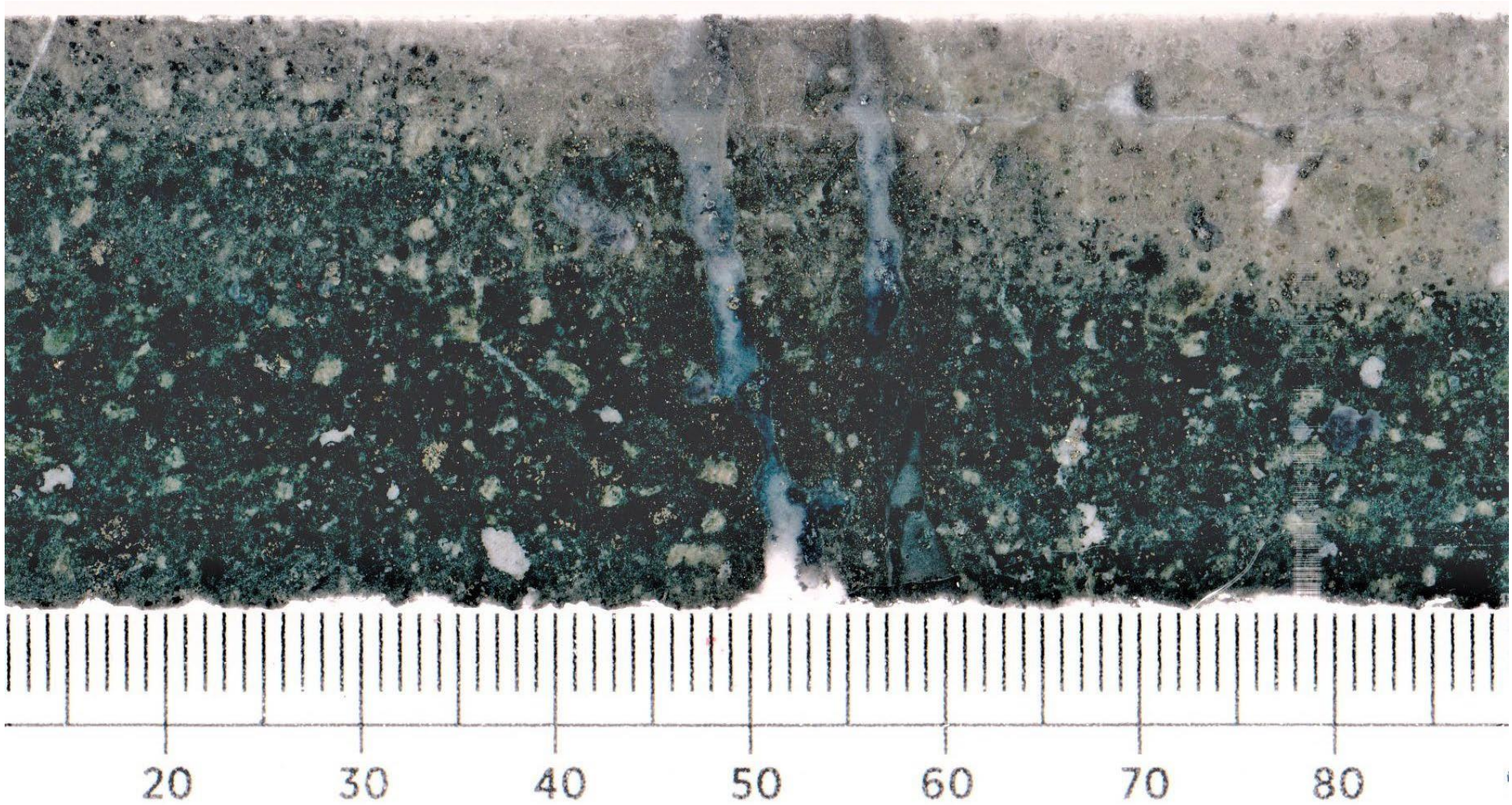

Figure 10 Photos of the drill core sample 2023440013 from drill hole GDD006, Glenyle prospect, Stavely region, Victoria, Australia.

Sample ID	Prospect	Borehole Name	From (m)	To (m)	Note
2023440014	Glenyle	GDD006	310.9	311.1	Sulfide ore and hydrothermal alteration

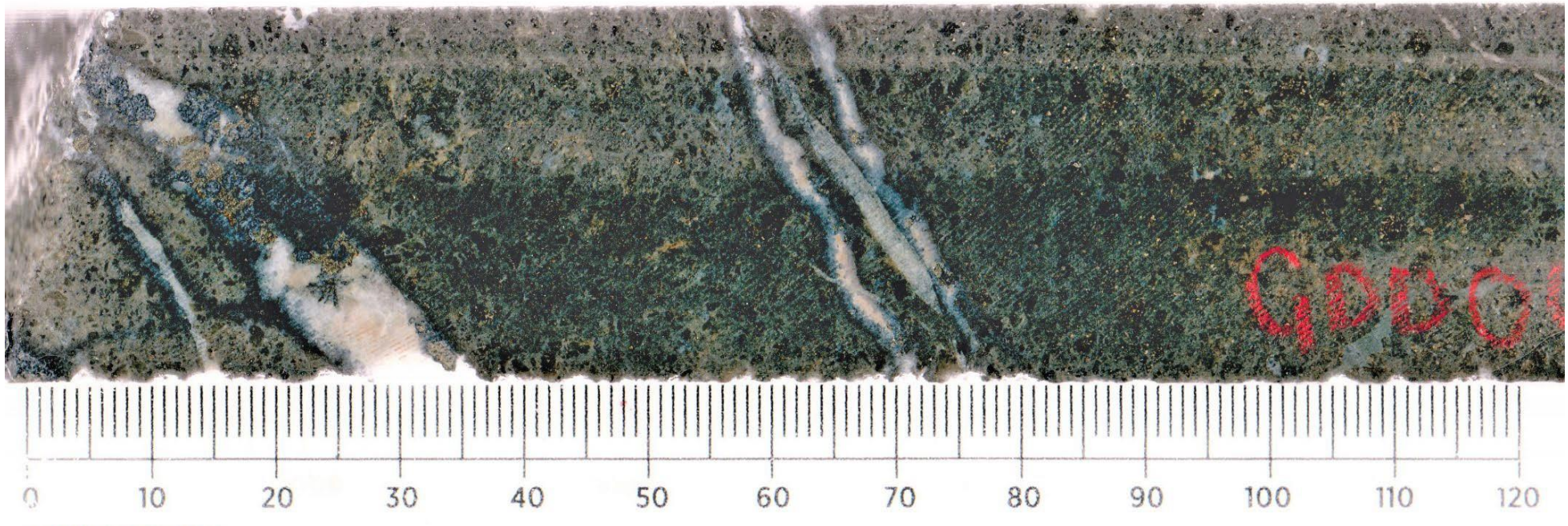

Figure 11 Photos of the drill core sample 2023440014 from drill hole GDD006, Glenyle prospect, Stavely region, Victoria, Australia.

Sample ID	Prospect	Borehole Name	From (m)	To (m)	Note
2023440009	Glenyle	GDD008	113.6	113.8	Sulfide ore and hydrothermal alteration

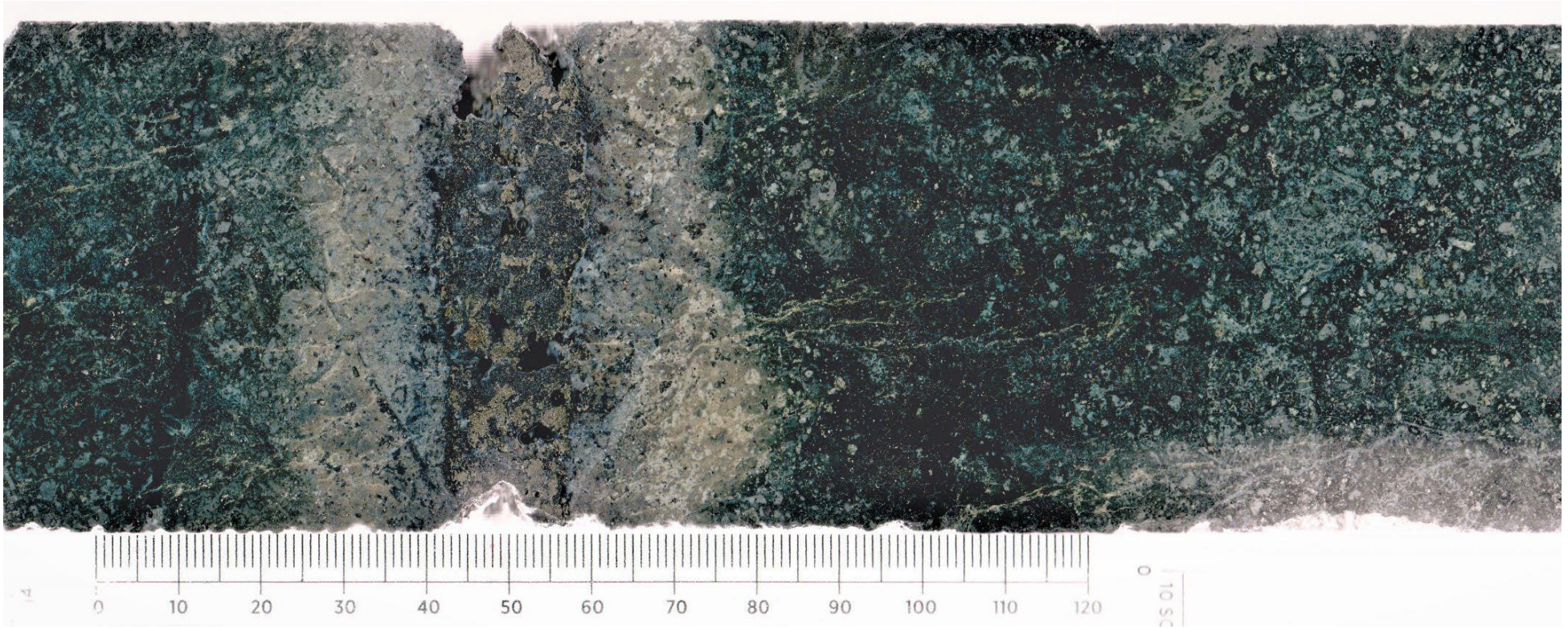

Figure 12 Photos of the drill core sample 2023440009 from drill hole GDD008, Glenyle prospect, Stavely region, Victoria, Australia.

Sample ID	Prospect	Borehole Name	From (m)	To (m)	Note
2023440010	Glenyle	GDD008	118.00	118.1	Sulfide ore and hydrothermal alteration

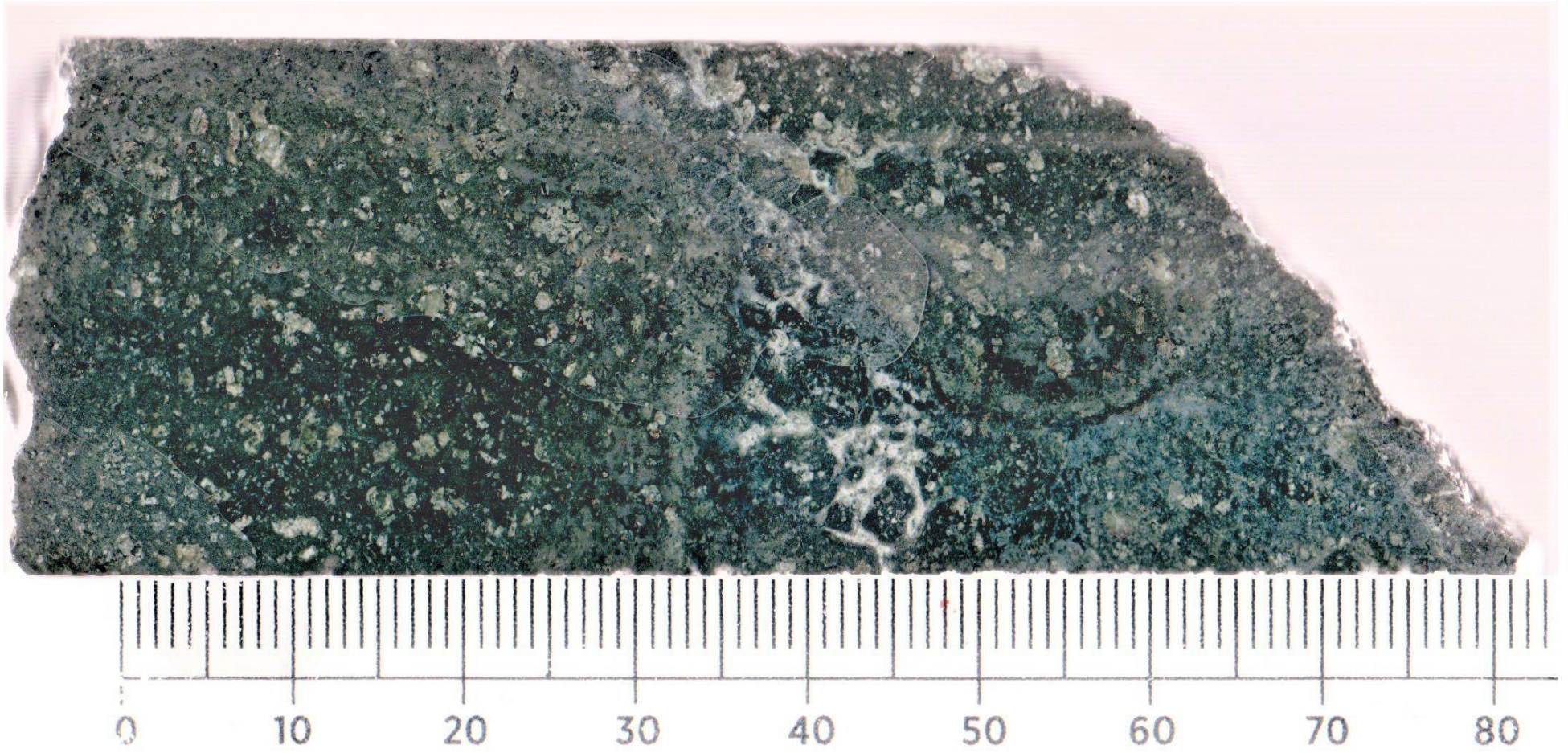

Figure 13 Photos of the drill core sample 2023440010 from drill hole GDD008, Glenyle prospect, Stavely region, Victoria, Australia.

Sample ID	Prospect	Borehole Name	From (m)	To (m)	Note
2023440011	Glenyle	GDD008	122.88	123.95	Sulfide ore and hydrothermal alteration

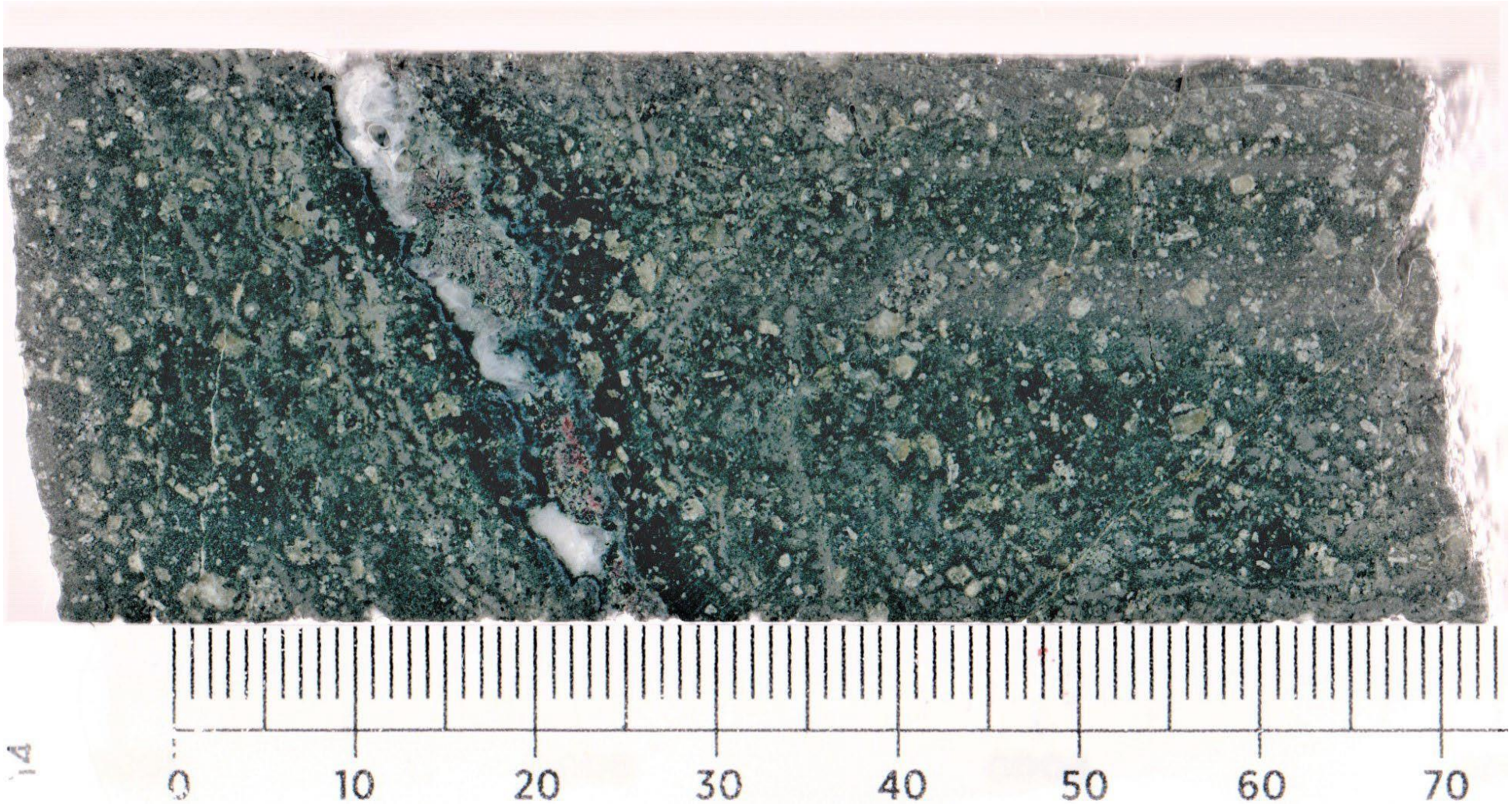

Figure 14 Photos of the drill core sample 2023440011 from drill hole GDD008, Glenyle prospect, Stavely region, Victoria, Australia.

S5.4 Mount Ararat prospect

Stawell Zone, Victoria

(A) Sample List

Sample No.	Sample ID	Borehole	From (m)	To (m)	Notes
321812	321812	DD90GR01	—	—	Sulfide ore and hydrothermal alteration
321813	321813	DD90GR01	—	—	Sulfide ore and hydrothermal alteration

(B) Mineralisation Characteristics

Data Type	Mineral Assemblage
Hyperspectral SWIR	—
Hyperspectral TIR	—
Hyperspectral VNIR	—
Drill core specimen	*Qtz, Fsp, Ms*
Thin section	—
AMICS mineral map	*Qtz, Fsp, Ms, Car, Hem*

(C) Mineralogical Textures and Paragenesis

Category	Description
Texture	Strongly altered felsic host with quartz–feldspar–muscovite assemblage and hematite staining.
Paragenesis	Muscovite and carbonate represent the main alteration phases. Hematite forms as a late oxidation product.

(D) Supplementary Figure Reference

Supplementary Figures *include drill core photographs and AMICS mineral maps of quartz–feldspar–muscovite altered host, Mount Ararat prospect, Stawell Zone, VIC.*

S5.4 The Mt Ararat prospect, Stavely region, Victoria

Sample ID	Prospect	Borehole Name	From (m)	To (m)	Note
322128	Mt Ararat	Mt Ararat 10	177.17	177.26	Massive sulfide ore

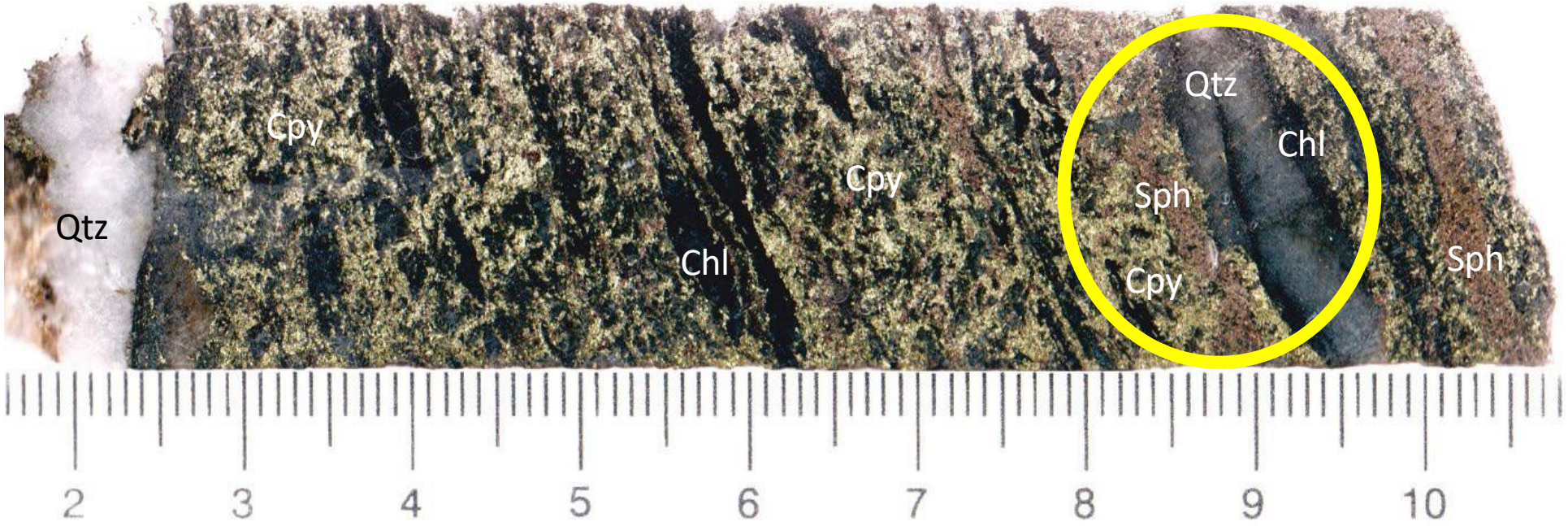

Figure 1 Photos of the drill core sample 322128 from drill hole Mt Ararat 10, Mt Ararat prospect, Stavely region, Victoria, Australia. Cpy-chalcopyrite; Qtz-quartz; Chl-chlorite; Sph-sphalerite.

Sample ID	Prospect	Borehole Name	From (m)	To (m)	Note
322128	Mt Ararat	Mt Ararat 10	177.17	177.26	Massive sulfide ore

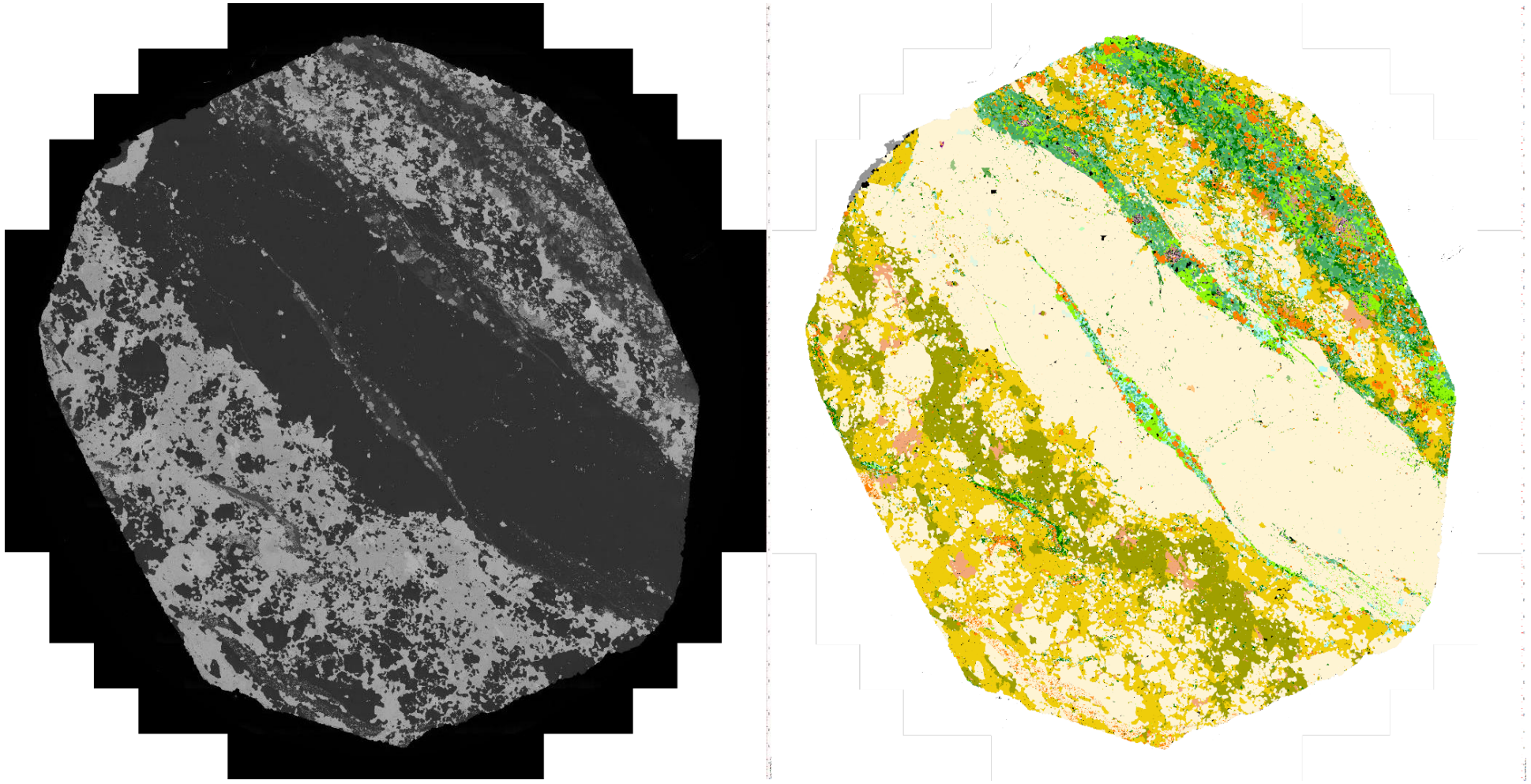

Figure 2 Backscattered electron (BSE) image (left) and Advanced Mineral Identification and Characterization System (AMICS) mineral map (right) of the sample 322128 from drill hole Mt Ararat 10, Mt Ararat prospect, Stavely region, Victoria, Australia. See Figure 11 at the end of this document for the legend of minerals identified using Mineral Liberation Analysis (MLA) mapping.

Sample ID	Prospect	Borehole Name	From (m)	To (m)	Note
322129	Mt Ararat	Mt Ararat 10	177.7	177.76	Massive sulfide ore

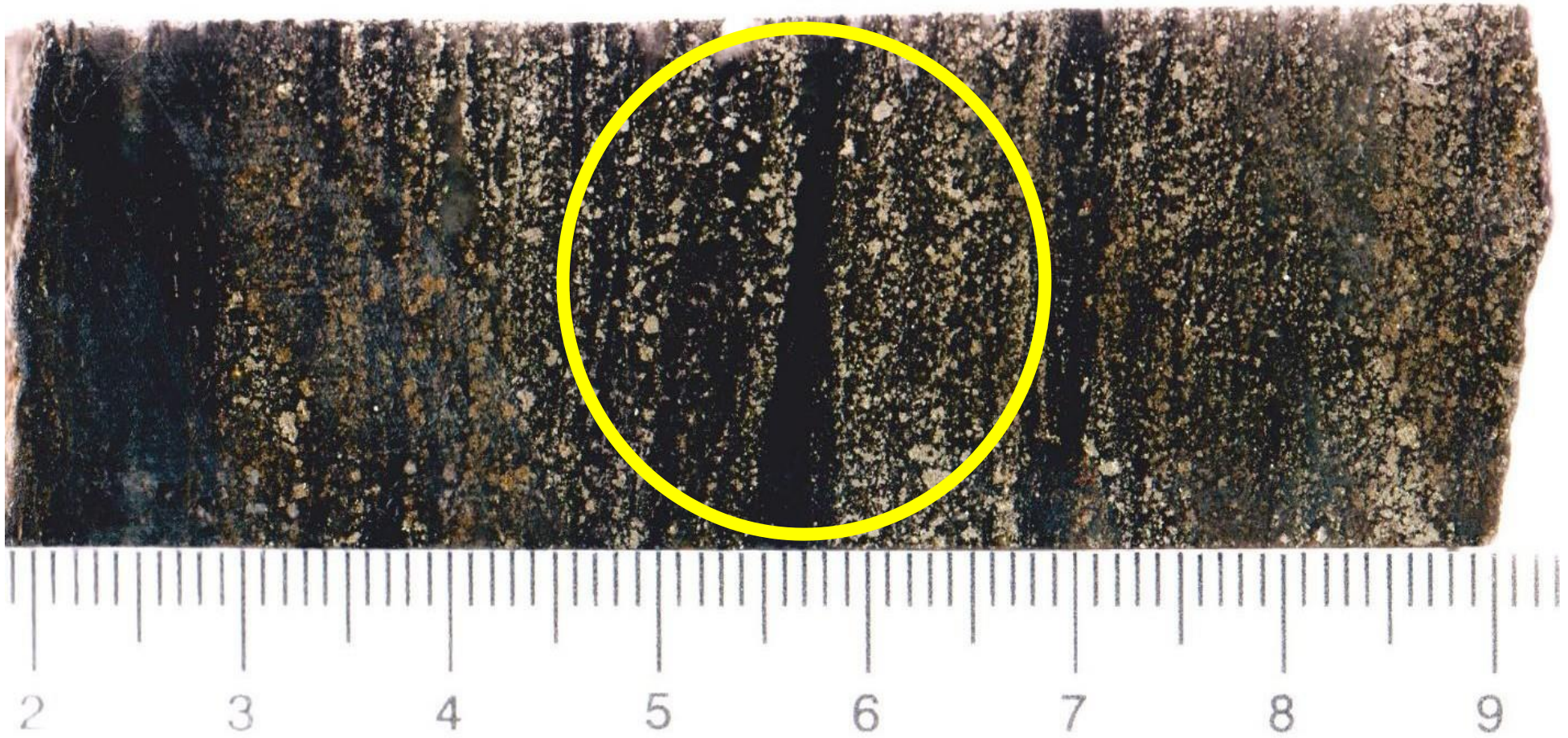

Figure 3 Photos of the drill core sample 322129 from drill hole Mt Ararat 10, Mt Ararat prospect, Stavely region, Victoria, Australia.

Sample ID	Prospect	Borehole Name	From (m)	To (m)	Note
322129	Mt Ararat	Mt Ararat 10	177.7	177.76	Massive sulfide ore

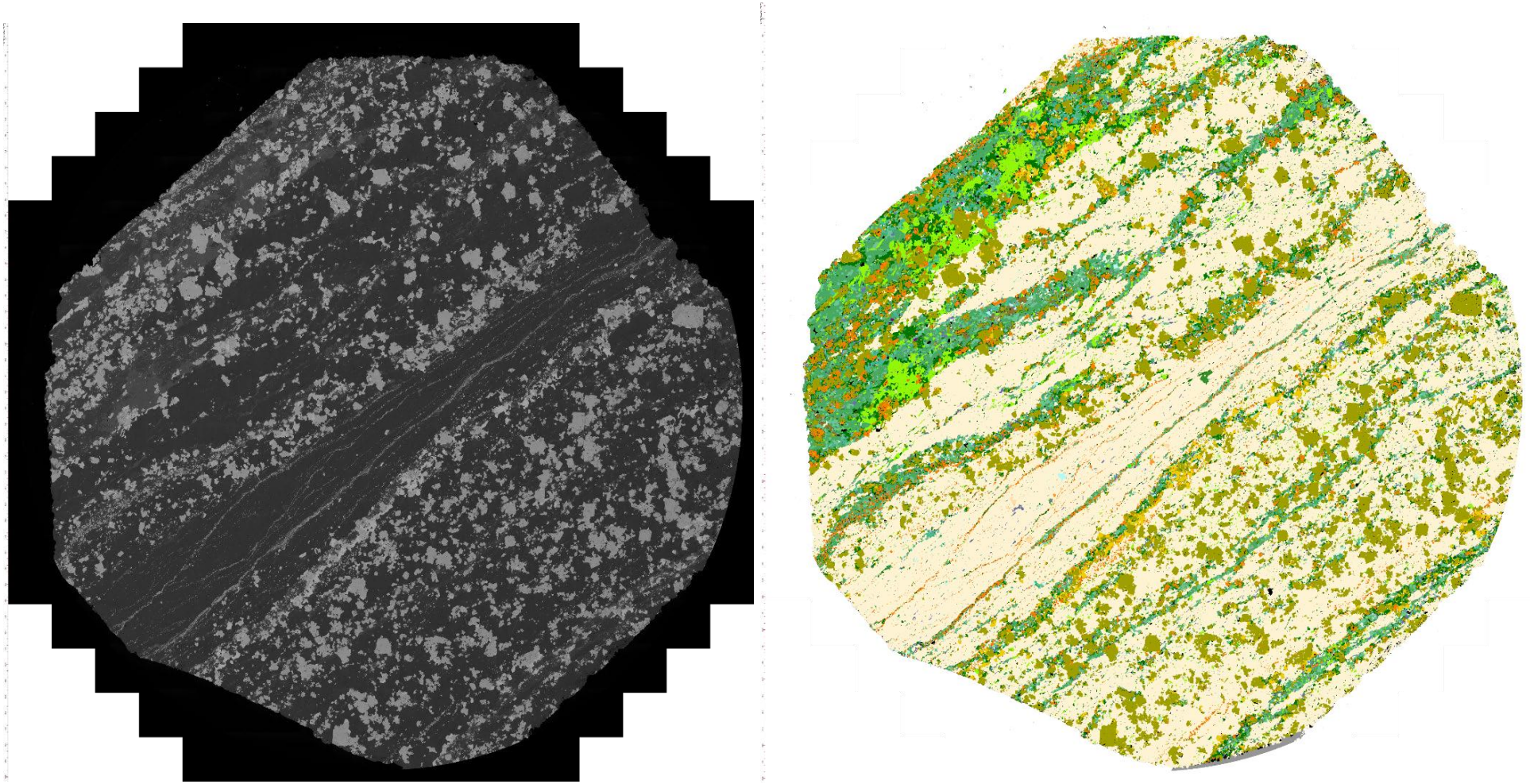

Figure 4 Backscattered electron (BSE) image (left) and Advanced Mineral Identification and Characterization System (AMICS) mineral map (right) of the sample 322129 from drill hole Mt Ararat 10, Mt Ararat prospect, Stavely region, Victoria, Australia. See Figure 11 at the end of this document for the legend of minerals identified using Mineral Liberation Analysis (MLA) mapping.

Sample ID	Prospect	Borehole Name	From (m)	To (m)	Note
322130	Mt Ararat	Mt Ararat 10	178.65	178.71	Massive sulfide ore

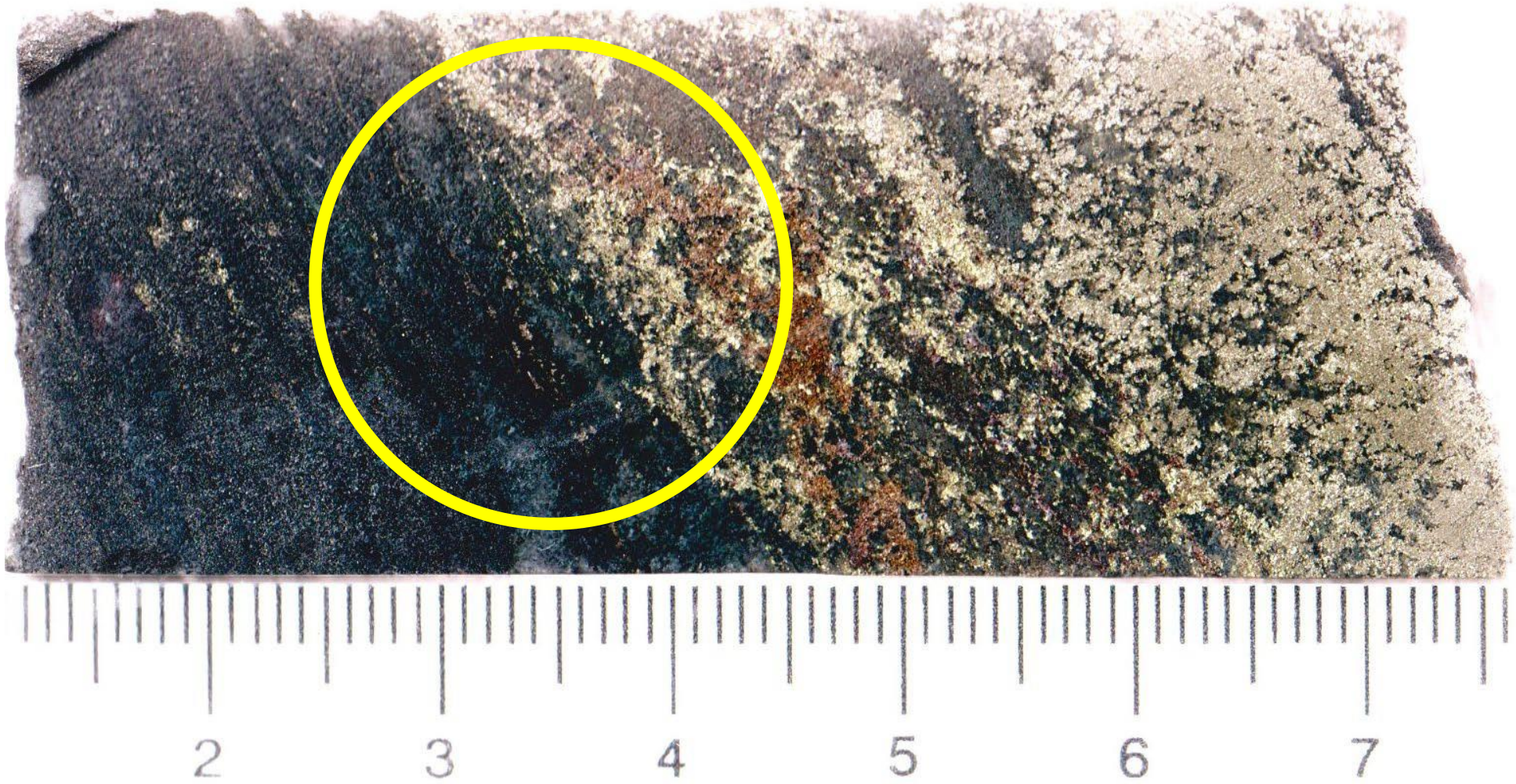

Figure 5 Photos of the drill core sample 322130 from drill hole Mt Ararat 10, Mt Ararat prospect, Stavely region, Victoria, Australia.

Sample ID	Prospect	Borehole Name	From (m)	To (m)	Note
322130	Mt Ararat	Mt Ararat 10	178.65	178.71	Massive sulfide ore

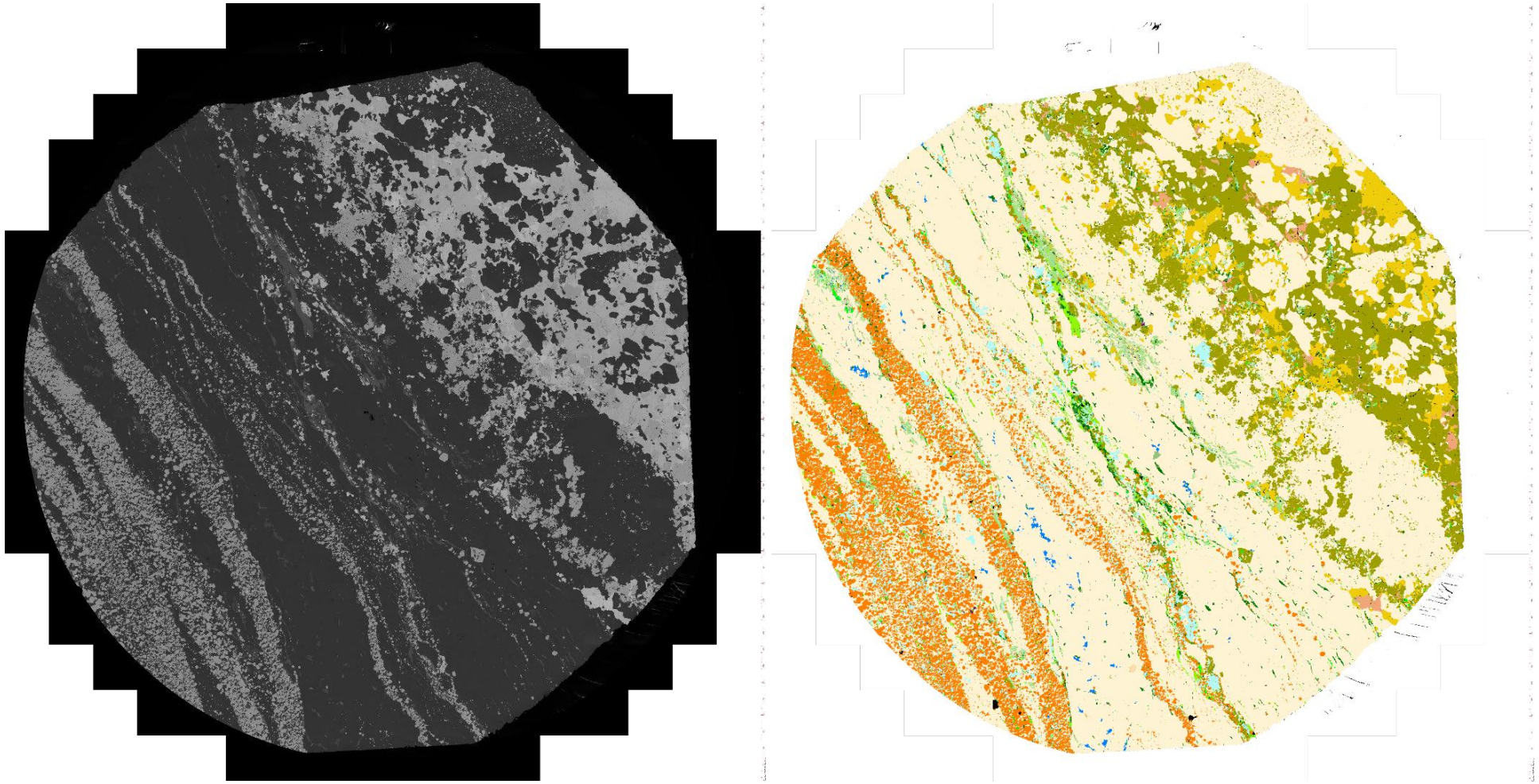

Figure 6 Backscattered electron (BSE) image (left) and Advanced Mineral Identification and Characterization System (AMICS) mineral map (right) of the sample 322130 from drill hole Mt Ararat 10, Mt Ararat prospect, Stavely region, Victoria, Australia. See Figure 11 at the end of this document for the legend of minerals identified using Mineral Liberation Analysis (MLA) mapping.

Sample ID	Prospect	Borehole Name	From (m)	To (m)	Note
322132	Mt Ararat	Mt Ararat 10	181.12	181.18	Massive sulfide ore

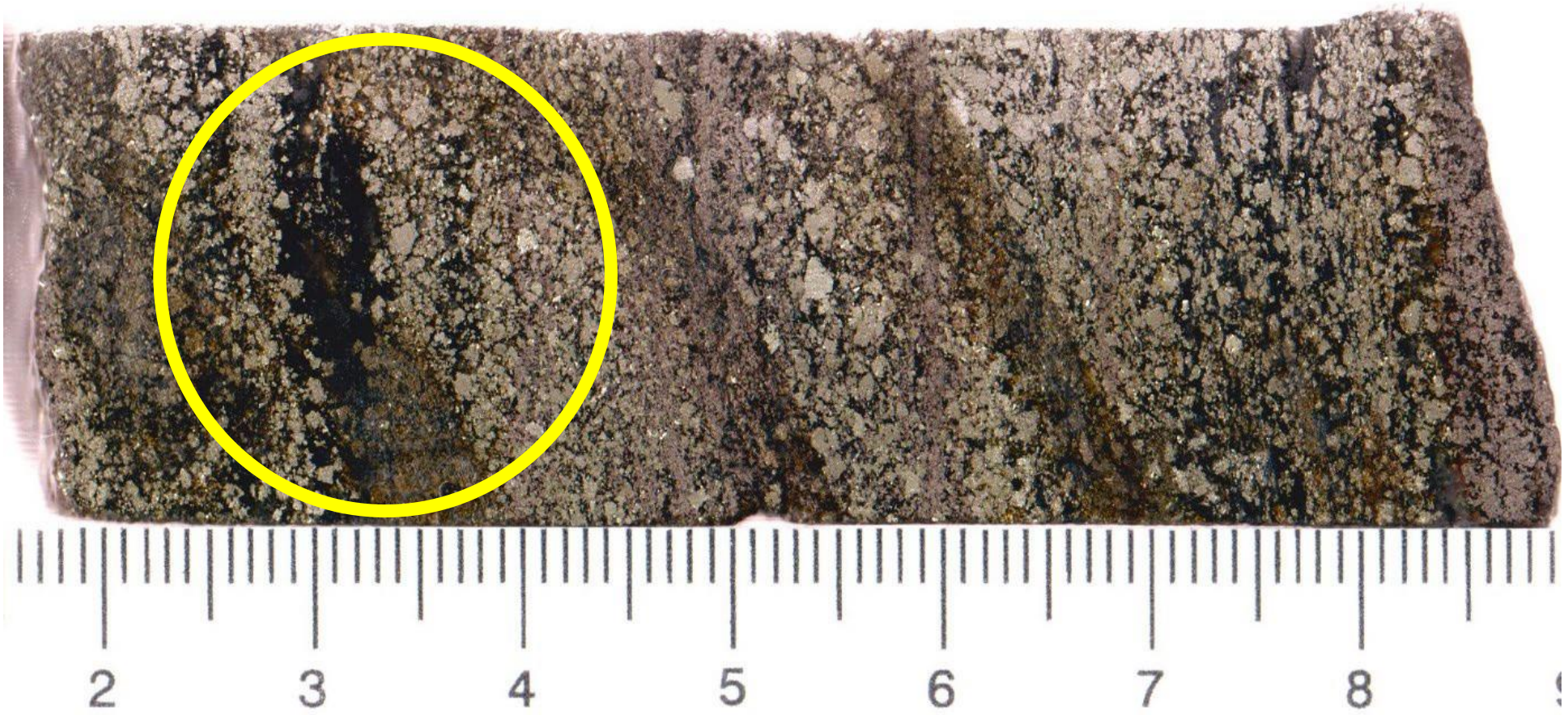

Figure 7 Photos of the drill core sample 322132 from drill hole Mt Ararat 10, Mt Ararat prospect, Stavely region, Victoria, Australia.

Sample ID	Prospect	Borehole Name	From (m)	To (m)	Note
322132	Mt Ararat	Mt Ararat 10	181.12	181.18	Massive sulfide ore

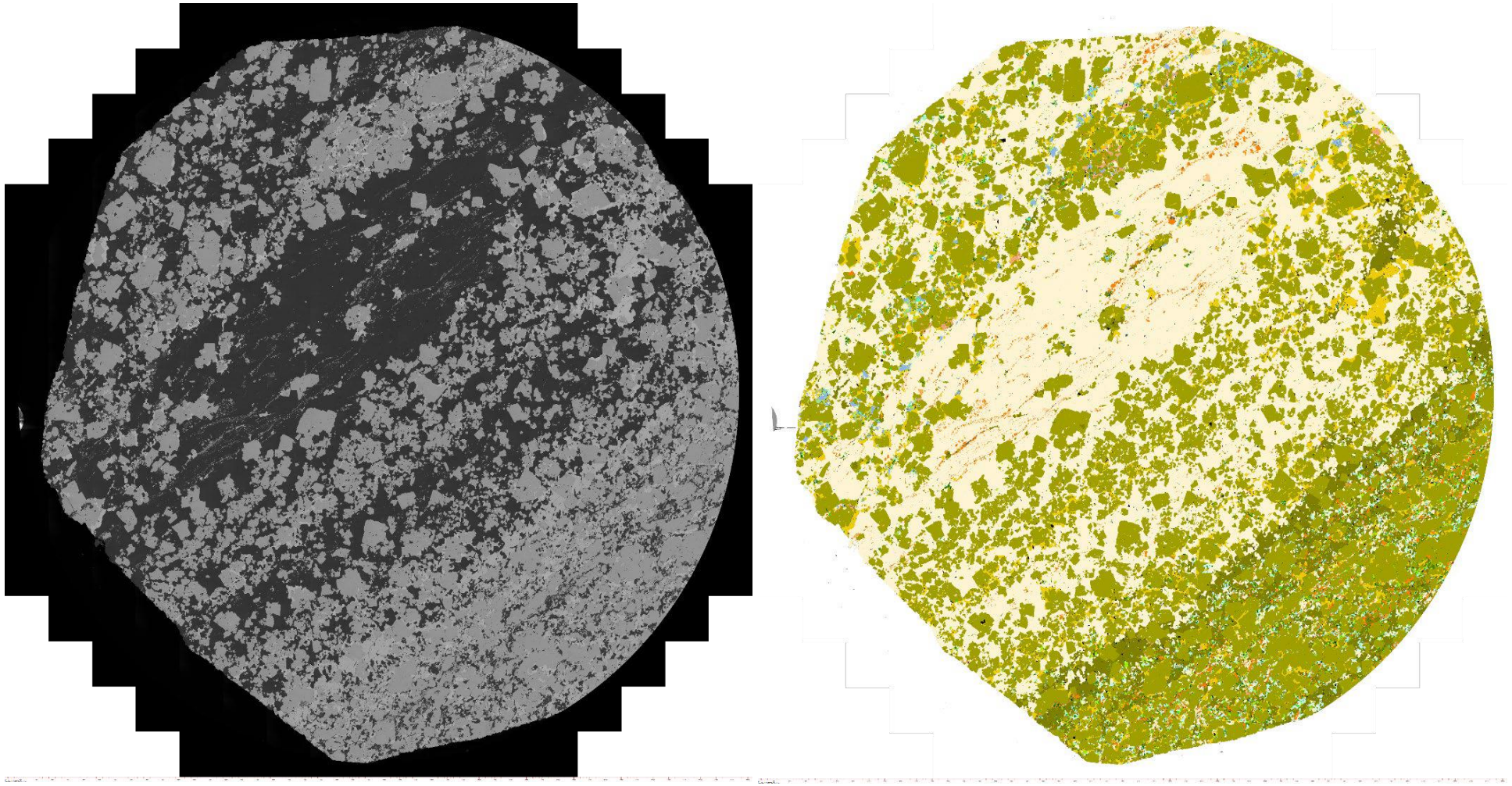

Figure 8 Backscattered electron (BSE) image (left) and Advanced Mineral Identification and Characterization System (AMICS) mineral map (right) of the sample 322132 from drill hole Mt Ararat 10, Mt Ararat prospect, Stavely region, Victoria, Australia. See Figure 11 at the end of this document for the legend of minerals identified using Mineral Liberation Analysis (MLA) mapping.

Sample ID	Prospect	Borehole Name	From (m)	To (m)	Note
322135	Mt Ararat	Mt Ararat 1	60.62	60.79	Massive sulfide ore

Figure 9 Photos of the drill core sample 322135 from drill hole Mt Ararat 1, Mt Ararat prospect, Stavely region, Victoria, Australia.

Sample ID	Prospect	Borehole Name	From (m)	To (m)	Note
322135	Mt Ararat	Mt Ararat 1	60.62	60.79	Massive sulfide ore

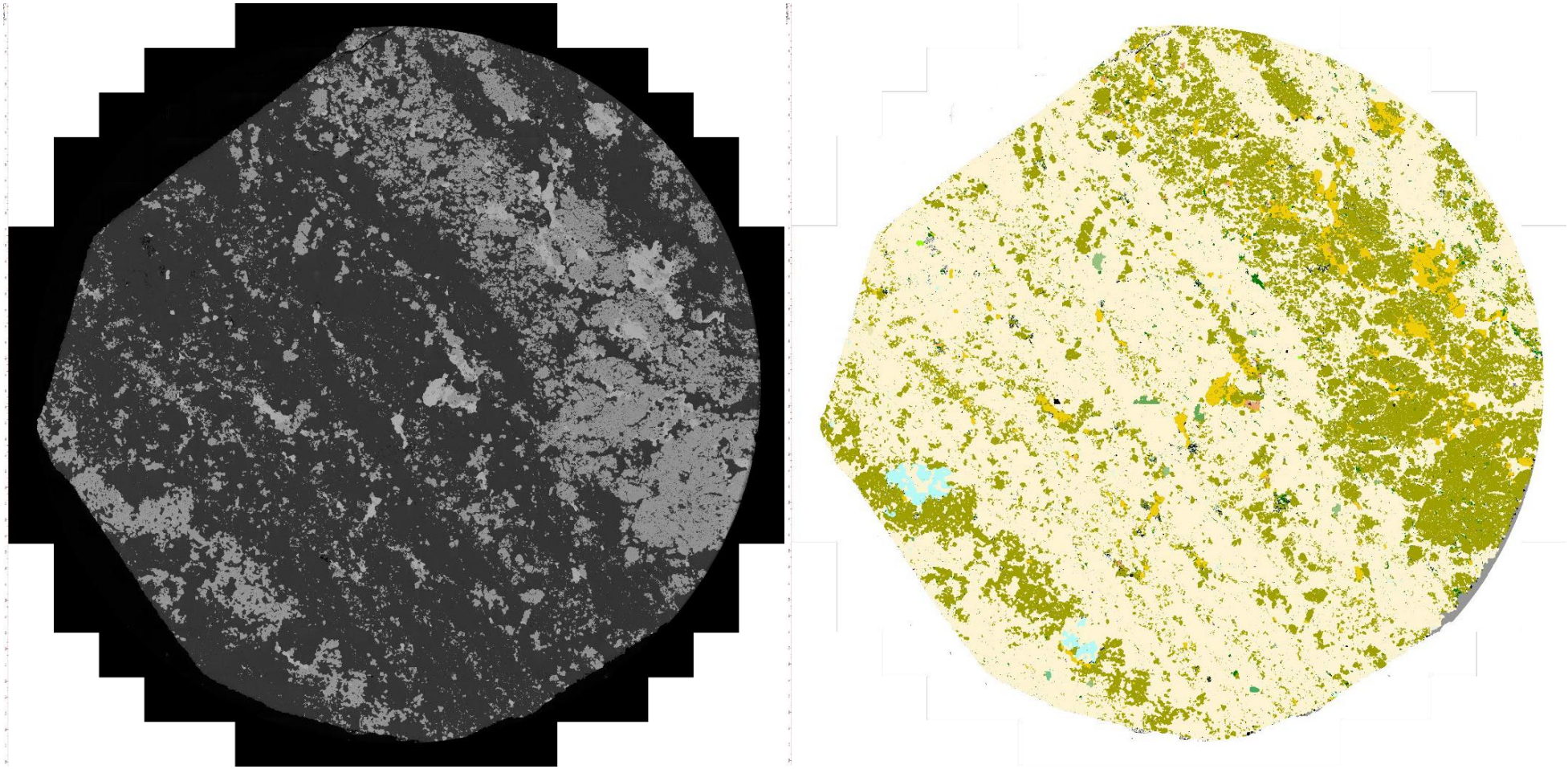

Figure 10 Backscattered electron (BSE) image (left) and Advanced Mineral Identification and Characterization System (AMICS) mineral map (right) of the sample 322135 from drill hole Mt Ararat 1, Mt Ararat prospect, Stavely region, Victoria, Australia. See Figure 11 at the end of this document for the legend of minerals identified using Mineral Liberation Analysis (MLA) mapping.

S5.5 Resolution (Irvine) prospect

Stavely Zone, Victoria

Detailed image data: Appendix 19 (individual data file)

(A) Sample List

Sample No.	Sample ID	Borehole	From (m)	To (m)	Notes
321916	321916	RD002	72.62	72.80	Sulfide ore and hydrothermal alteration
321915	321915	RD002	72.01	72.08	Sulfide ore and hydrothermal alteration
321917	321917	RD002	75.99	76.15	Sulfide ore and hydrothermal alteration

(B) Mineralisation Characteristics

Data Type	Mineral Assemblage
Hyperspectral SWIR	—
Hyperspectral TIR	—
Hyperspectral VNIR	—
Drill core specimen	*Apy, Py, Chl, Qtz, Fsp*
Thin section	—
AMICS mineral map	*Qtz, Apy, Py, Chl, Fsp, Hem, Ser, Cal*

(C) Mineralogical Textures and Paragenesis

Category	Description
Texture	Arsenopyrite-dominant sulfide mineralisation hosted in quartz–feldspar–chlorite with sericite alteration. Hematite occurs as an accessory phase.
Paragenesis	Arsenopyrite predates pyrite. Quartz–feldspar veining accompanies the main mineralisation stage. Sericite and calcite form a late retrograde overprint.

(D) Supplementary Figure Reference

Supplementary Figures *include drill core photographs of samples 321916, 321915 and 321917 from drill hole RD002, Resolution (Irvine) prospect, Stavely Zone, VIC.*

S5.5 The Resolution (Irvine) prospect, Stavely region, Victoria

Sample ID	Prospect	Borehole Name	From (m)	To (m)	Note
321916	Resolution / Irvine	RD002	72.62	72.8	Sulfide ore and hydrothermal alteration

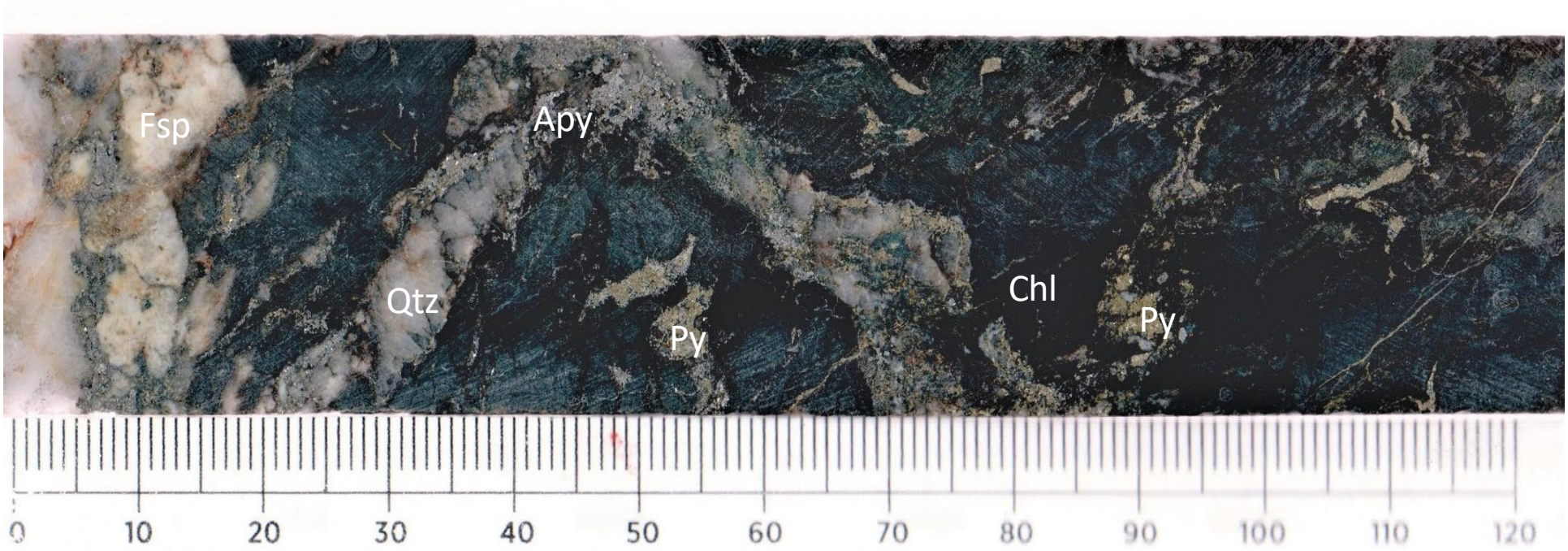

Figure 1 Photos of the drill core sample 321916 from drill hole RD002, Resolution / Irvine prospect, Stavely region, Victoria, Australia. Apy-arsenopyrite; Py-pyrite; Chl-chlorite; Qtz-quartz; Fsp-feldspar.

Sample ID	Prospect	Borehole Name	From (m)	To (m)	Note
321915	Resolution / Irvine	RD002	72.01	72.08	Sulfide ore and hydrothermal alteration

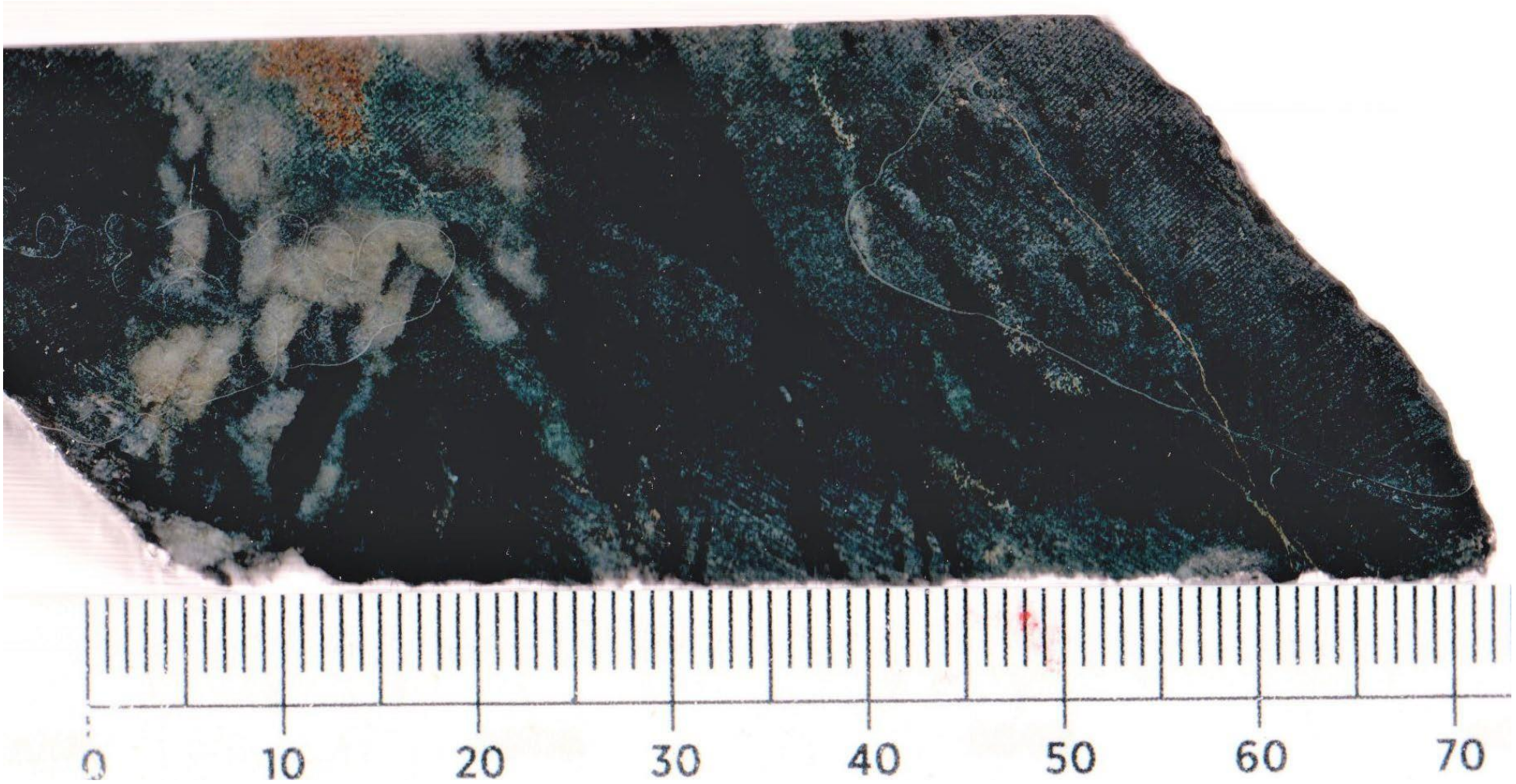

Figure 2 Photos of the drill core sample 321915 from drill hole RD002, Resolution / Irvine prospect, Stavely region, Victoria, Australia.

Sample ID	Prospect	Borehole Name	From (m)	To (m)	Note
321917	Resolution / Irvine	RD002	75.99	76.15	Sulfide ore and hydrothermal alteration

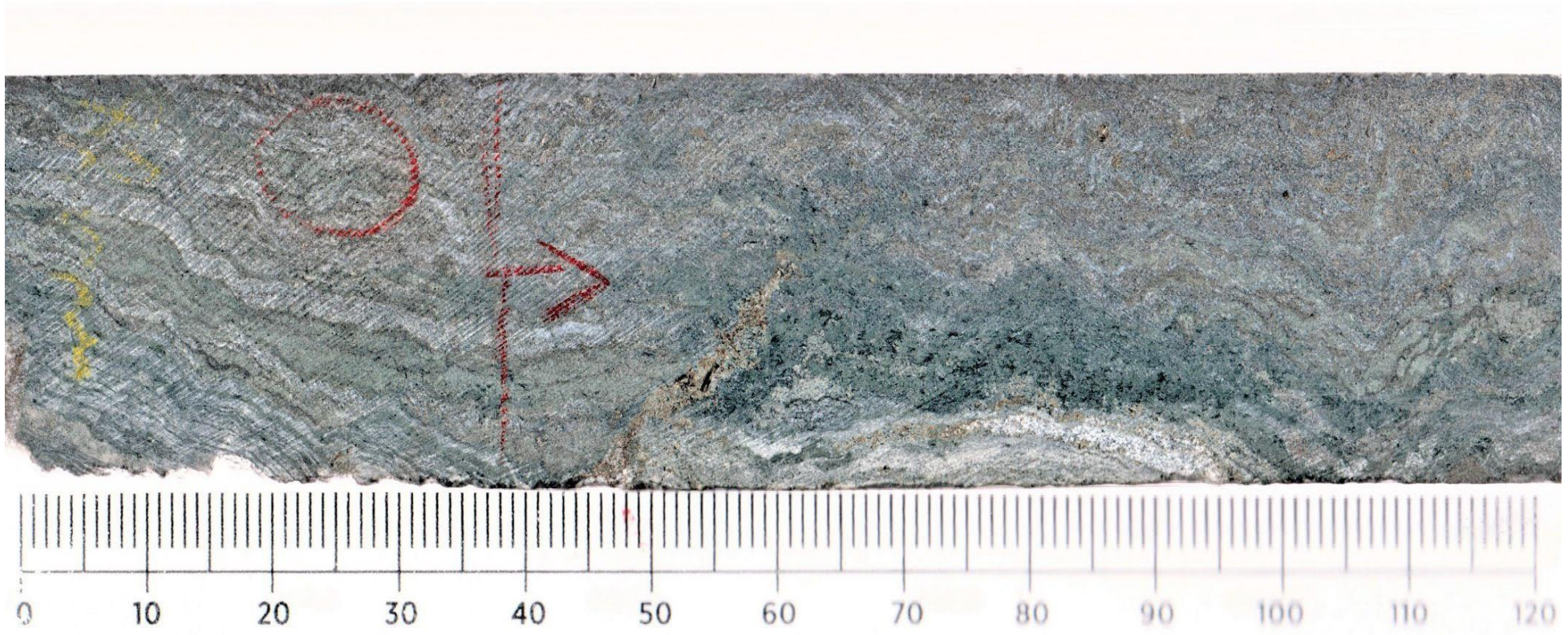

Figure 3 Photos of the drill core sample 321917 from drill hole RD002, Resolution / Irvine prospect, Stavely region, Victoria, Australia.

S5.6 Stawell (Wonga) prospect

Stawell Zone, Victoria

(A) Sample List

Sample No.	Sample ID	Borehole	From (m)	To (m)	Notes
8012644	321878	SSDD0001	112.10	112.25	Sulfide ore and hydrothermal alteration
8012645	321879	SSDD0001	117.19	117.37	Sulfide ore and hydrothermal alteration
8012646	321880	SSDD0001	126.58	126.78	Sulfide ore and hydrothermal alteration
8012647	321881	SSDD0001	128.10	128.28	Sulfide ore and hydrothermal alteration
8012648	321882	SSDD0001	131.80	132.00	Sulfide ore and hydrothermal alteration
8012649	321883	SSDD0001	132.75	133.00	Sulfide ore and hydrothermal alteration
8012650	321884	SSDD0001	144.45	144.65	Sulfide ore and hydrothermal alteration
8012651	321885	SSDD0001	162.82	162.98	Sulfide ore and hydrothermal alteration
8012652	321886	SSDD0001	178.26	178.42	Sulfide ore and hydrothermal alteration
8012653	321887	SSDD0001	184.82	185.02	Sulfide ore and hydrothermal alteration
9651891	2023440015	SSDD0001	199.53	199.83	Sulfide ore and hydrothermal alteration

(B) Mineralisation Characteristics

Data Type	Mineral Assemblage
Hyperspectral SWIR	—
Hyperspectral TIR	—
Hyperspectral VNIR	—
Drill core specimen	*Qtz, Apy, Py, Chl, Hem, Cal, Fsp*
Thin section	—
AMICS mineral map	*Kfsp, Ab, Chl, Ep, Car, Ttn, Ap, Mnz, Py, Apy, Lö*

(C) Mineralogical Textures and Paragenesis

Category	Description
Texture	Apart from quartz, alteration minerals include K-feldspar, albite, chlorite, epidote, carbonate, titanite, apatite and minor monazite. Metallic minerals are pyrite, arsenopyrite and löllingite.
Paragenesis	Löllingite is universally rimmed on arsenopyrite. The reaction $2Fe^{3+}AsS$ (arsenopyrite) → $Fe^{2+}As_2$ (löllingite) + $Fe^{2+}S$ (pyrrhotite) + $0.5S_2$ has been proposed for this assemblage (Tomkins & Mavrogenes 2001); however, pyrrhotite has not been identified in the current sample suite.

(D) Supplementary Figure Reference

Supplementary Figures *include drill core photographs and AMICS mineral maps of Apy–Py–Lö assemblage with K-feldspar–albite–chlorite–epidote alteration, Stawell (Wonga) prospect, SSDD0001. AMICS mineral standard legend included.*

S5.6 The Stawell (Wonga) prospect, Stavely region, Victoria

Sample ID	Prospect	Borehole Name	From (m)	To (m)	Note
2023440018	Stawell	SSDD0001	161.25	161.35	Sulfide ore and hydrothermal alteration

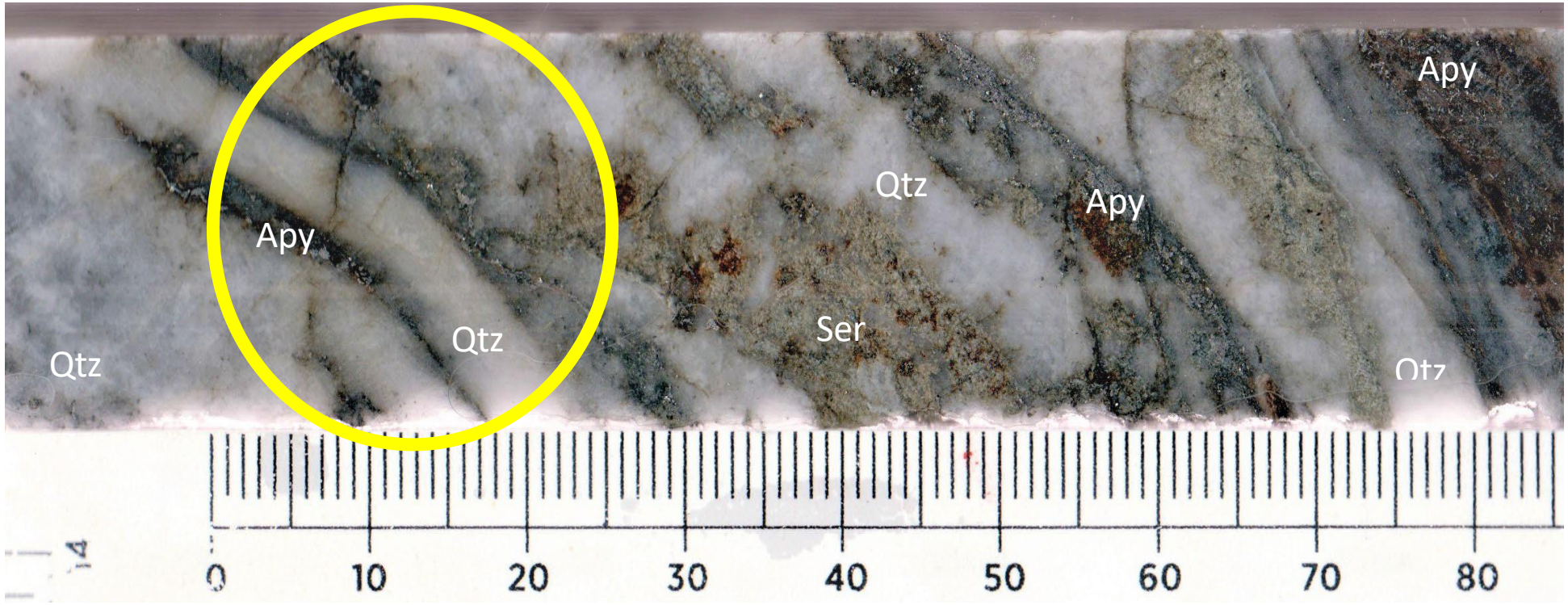

Figure 1 Photos of the drill core sample 2023440018 from drill hole SSDD0001, Stawell / Wonga prospect, Stavely region, Victoria, Australia. Apy-arsenopyrite; Qtz-quartz; Ser-sericite.

Sample ID	Prospect	Borehole Name	From (m)	To (m)	Note
2023440018	Stawell	SSDD0001	161.25	161.35	Sulfide ore and hydrothermal alteration

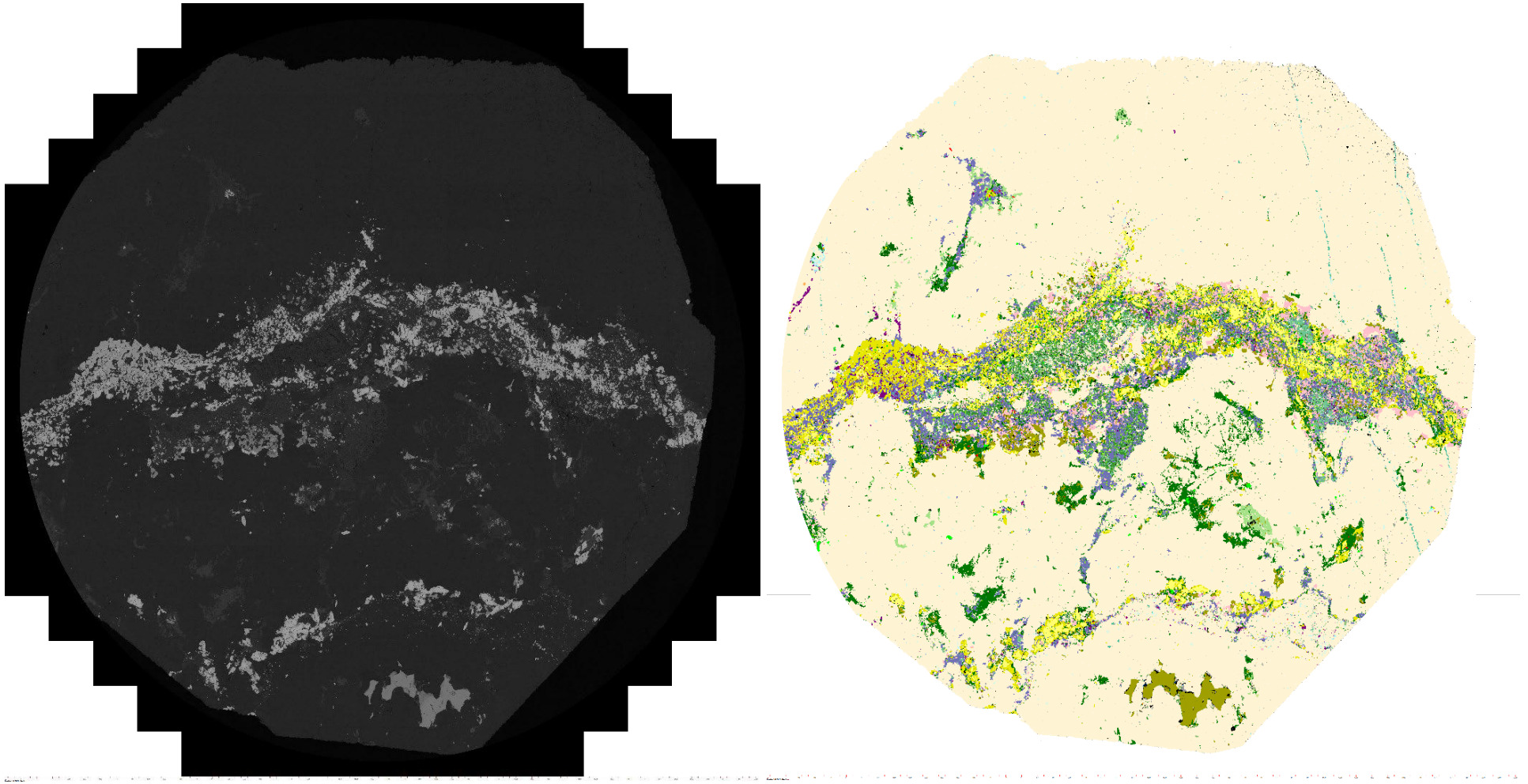

Figure 2 Backscattered electron (BSE) image (left) and Advanced Mineral Identification and Characterization System (AMICS) mineral map (right) of the sample 2023440018 from drill hole SSDD0001, Stawell / Wonga prospect, Stavely region, Victoria, Australia. See Figure 6 at the end of this document for the legend of minerals identified using Mineral Liberation Analysis (MLA) mapping.

Sample ID	Prospect	Borehole Name	From (m)	To (m)	Note
2023440015	Stawell	SSDD0001	199.53	199.83	Sulfide ore and hydrothermal alteration

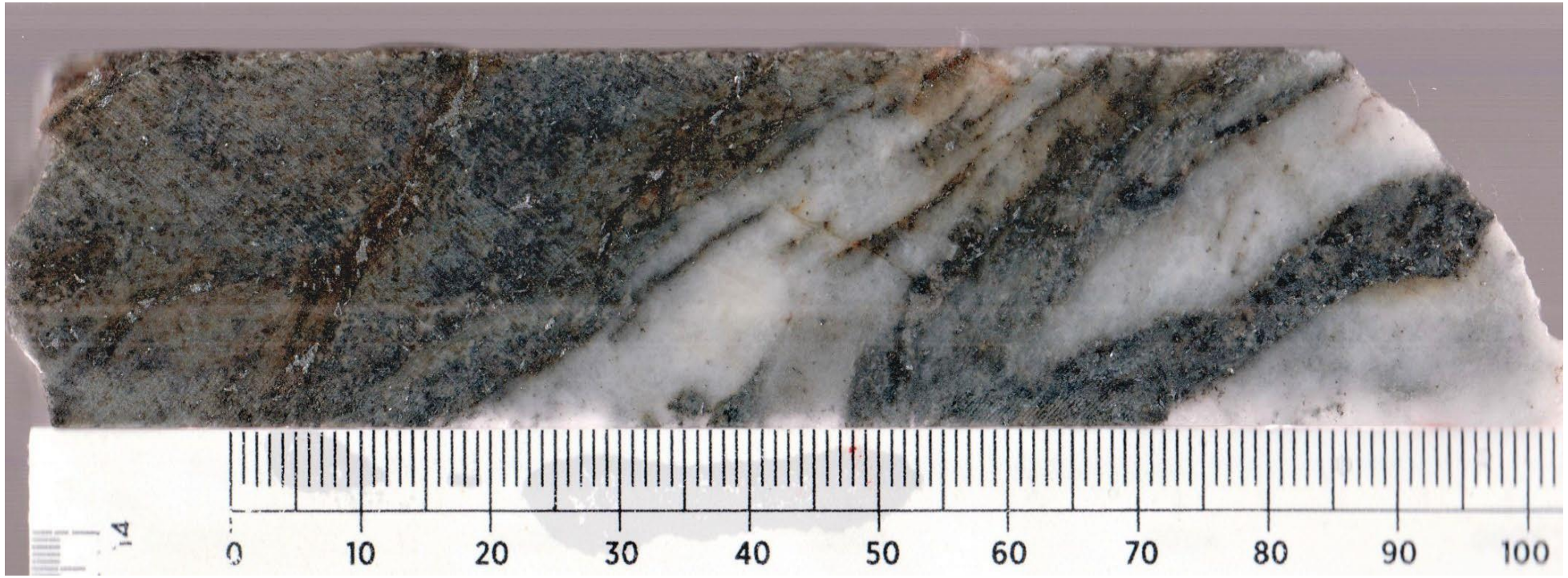

Figure 3 Photos of the drill core sample 2023440015 from drill hole SSDD0001, Stawell / Wonga prospect, Stavely region, Victoria, Australia.

Sample ID	Prospect	Borehole Name	From (m)	To (m)	Note
2023440016	Stawell	SSDD0001	187.4	187.7	Sulfide ore and hydrothermal alteration

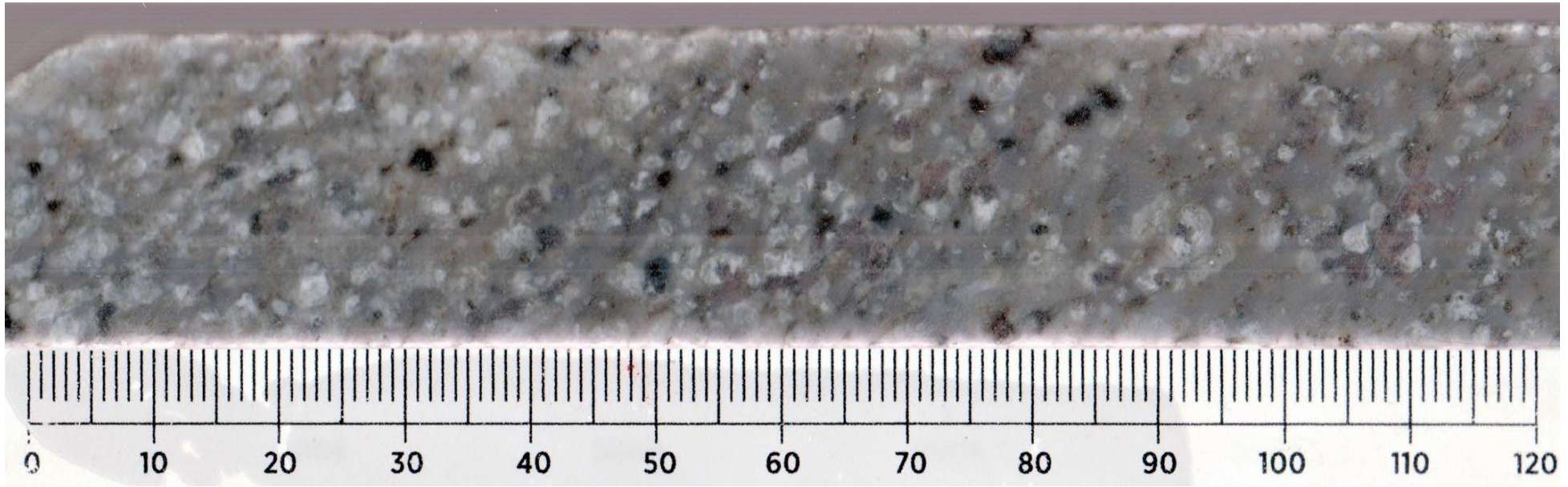

Figure 4 Photos of the drill core sample 2023440016 from drill hole SSDD0001, Stawell / Wonga prospect, Stavely region, Victoria, Australia.

Sample ID	Prospect	Borehole Name	From (m)	To (m)	Note
2023440017	Stawell	SSDD0001	165.15	165.25	Sulfide ore and hydrothermal alteration

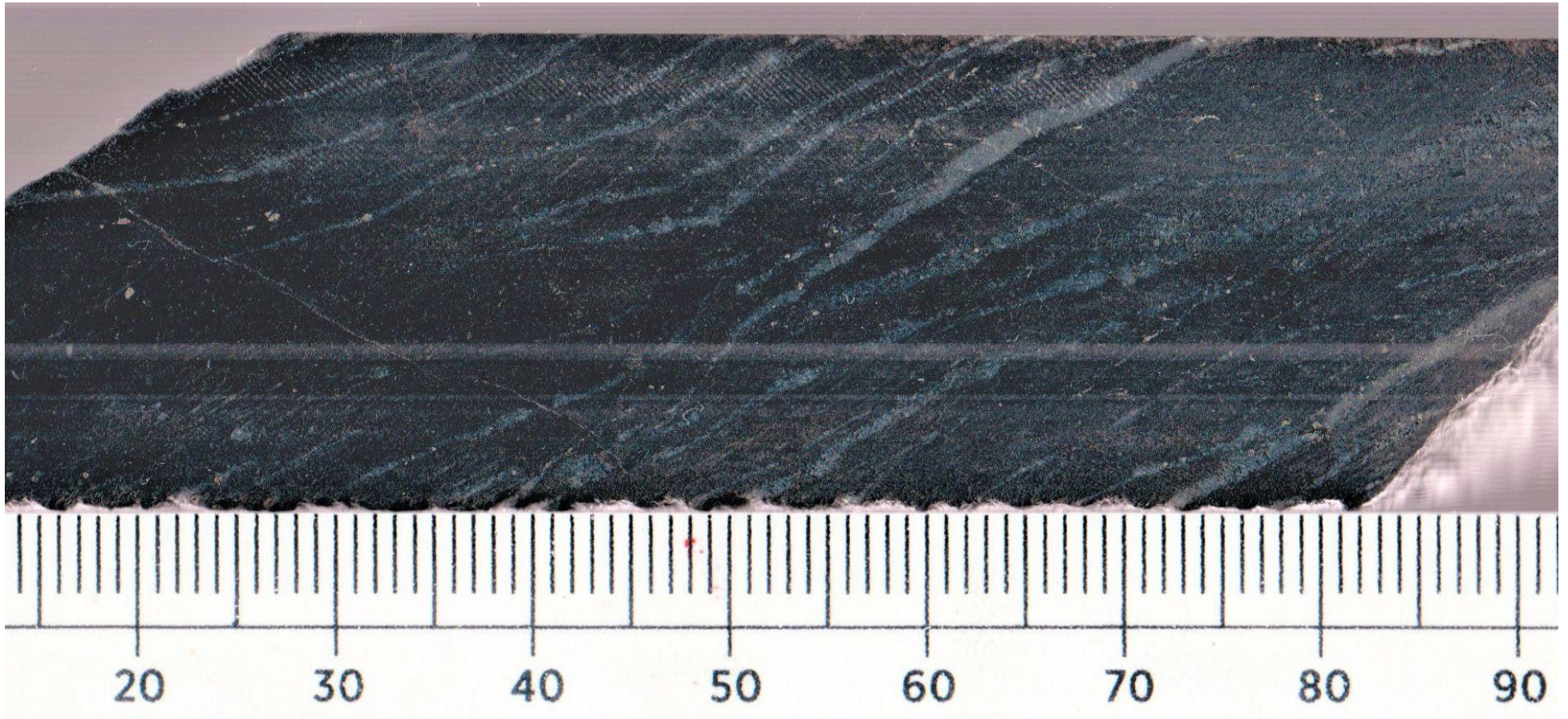

Figure 5 Photos of the drill core sample 2023440017 from drill hole SSDD0001, Stawell / Wonga prospect, Stavely region, Victoria, Australia.

S5.7 The Gerang Gerung and Balbeggie prospects, Stavely region, Victoria

Stavely Zone, Victoria

(A) Sample List

Sample No.	Sample ID	Borehole	From (m)	To (m)	Notes
8012657	321862	GG-01	282.05	282.22	Sulfide and hydrothermal alteration (Unnamed 1)
8012658	321863	GG-01	306.23	306.51	Sulfide ore and hydrothermal alteration (Unnamed 1)
8012659	321864	GG-01	308.03	308.35	Sulfide ore and hydrothermal alteration (Unnamed 1)
8012660	321865	GG-01	321.50	321.73	Sulfide ore and hydrothermal alteration (Unnamed 1)
8012661	321866	GG-01	324.13	324.29	Sulfide ore and hydrothermal alteration (Unnamed 1)
8012675	321921	SB1DH1	146.10	146.24	Sulfide ore and hydrothermal alteration (Unnamed 2)

(B) Mineralisation Characteristics

Data Type	Mineral Assemblage
Hyperspectral SWIR	—
Hyperspectral TIR	—
Hyperspectral VNIR	—
Drill core specimen	*Qtz, Py, Sph, Chl, Ep*
Thin section	—
AMICS mineral map	*Sph, Qtz, Chl, Ab, Py, Ep, Ttn, Ap, Cal, Cpy, Kfsp*

(C) Mineralogical Textures and Paragenesis

Category	Description
Texture	Abundant Zn-rich sulfides associated with strongly altered intermediate igneous rocks, overprinted by pervasive chlorite–epidote–quartz–albite alteration and crosscut by epidote–calcite–quartz veins.
Paragenesis	Sphalerite–galena–pyrite assemblage overprints the quartz–albite–chlorite alteration. Pyrite in sample 321921 displays a core–rim texture indicating multi-stage formation.

(D) Supplementary Figure Reference

Supplementary Figures *include drill core photographs and AMICS mineral maps of Zn-rich sulfide (Sph–Py–Cpy) assemblage in chlorite–epidote–albite altered intermediate igneous rocks, Unnamed Prospects 1 and 2, Stavely Zone, VIC.*

S5.7 The Gerang Gerung and Balbeggie prospects, Stavely region, Victoria

Sample ID	Prospect	Borehole Name	From (m)	To (m)	Note
321864	Gerang Gerung	GG-01	308.03	308.35	Sulfide ore and hydrothermal alteration

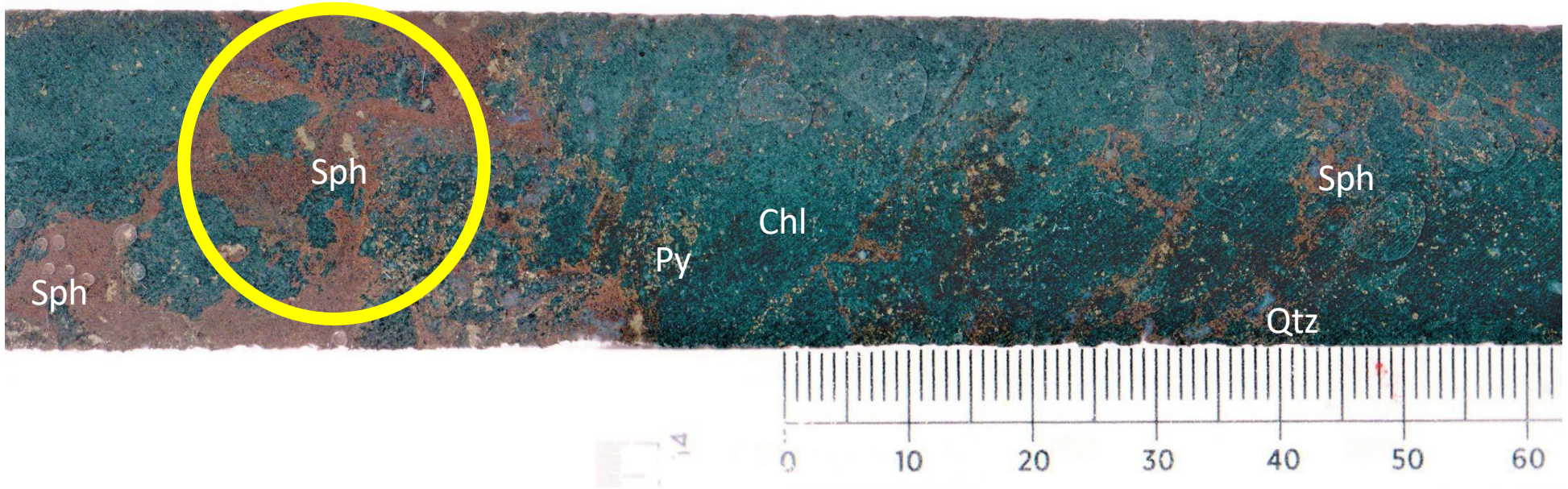

Figure 1 Photos of the drill core sample 321864 from drill hole GG-01, the Gerang Gerung prospect, Stavely region, Victoria, Australia. Py-pyrite; Sph-sphalerite; Chl-chlorite; Qtz-quartz.

Sample ID	Prospect	Borehole Name	From (m)	To (m)	Note
321864	Gerang Gerung	GG-01	308.03	308.35	Sulfide ore and hydrothermal alteration

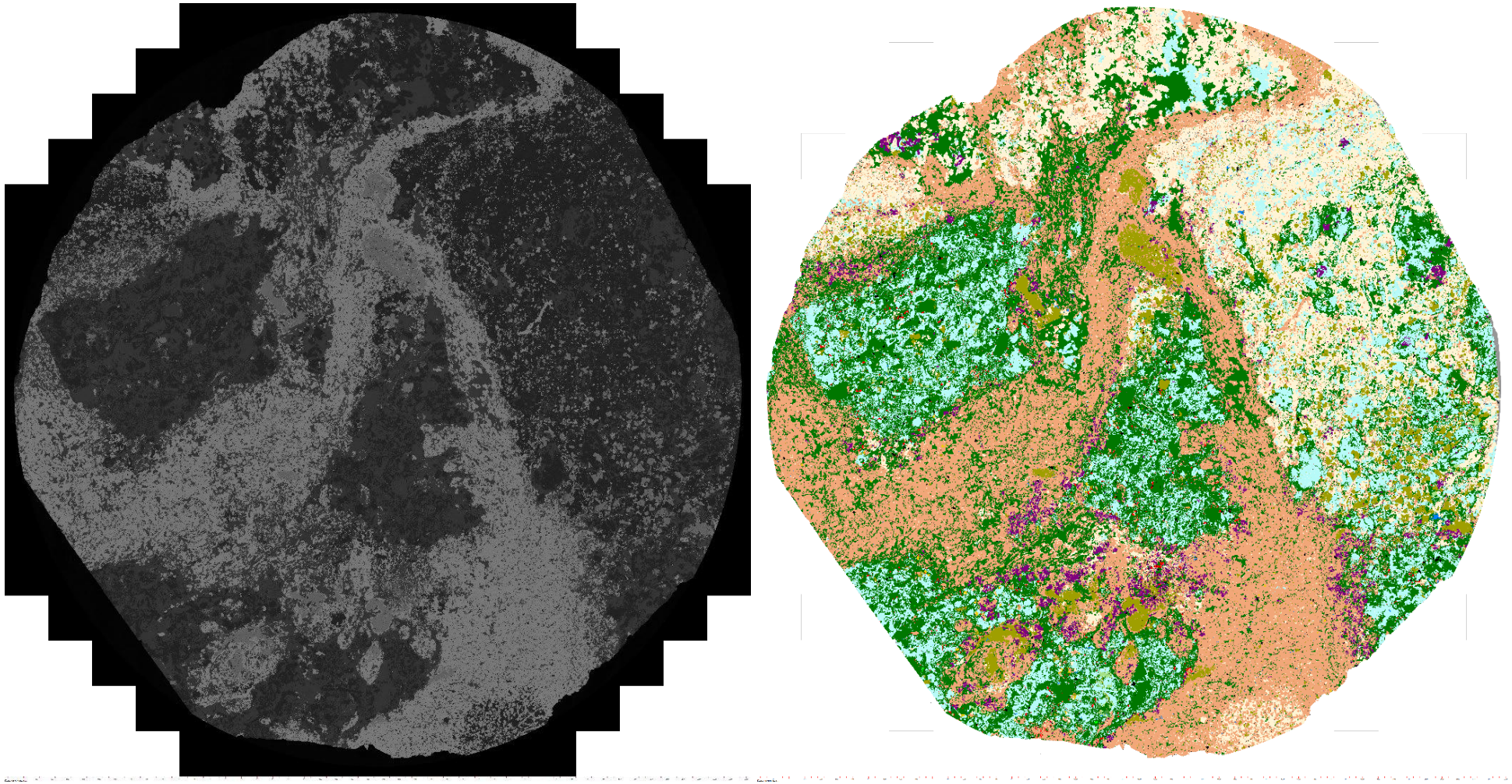

Figure 2 Backscattered electron (BSE) image (left) and Advanced Mineral Identification and Characterization System (AMICS) mineral map (right) of the sample 321864 from drill hole GG-01, the Gerang Gerung prospect, Stavely region, Victoria, Australia. See Figure 9 at the end of this document for the legend of minerals identified using Mineral Liberation Analysis (MLA) mapping.

Sample ID	Prospect	Borehole Name	From (m)	To (m)	Note
321921	Balbeggie	SB1DH1	146.10	146.24	Sulfide ore and hydrothermal alteration

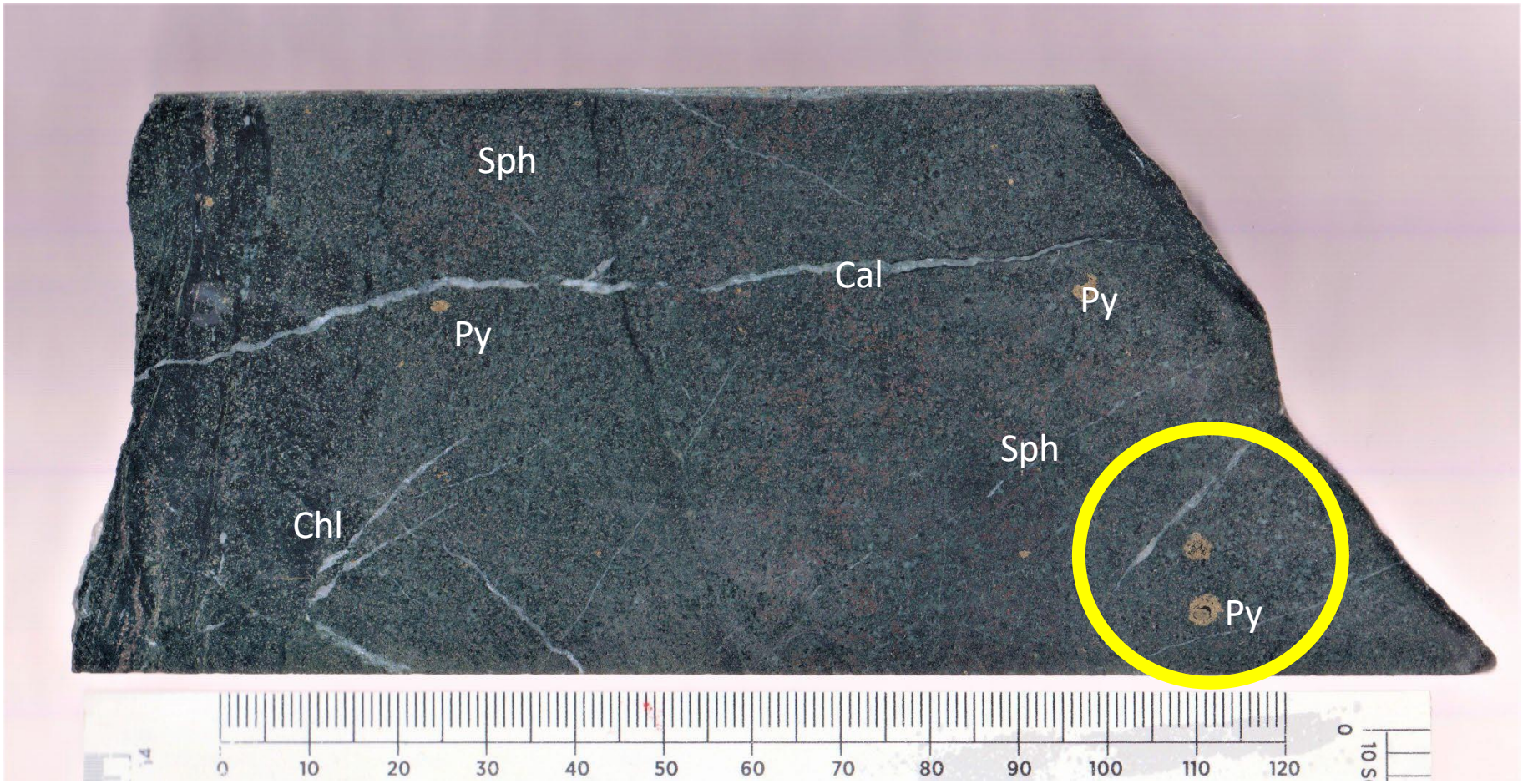

Figure 3 Photos of the drill core sample 321921 from drill hole SB1DH1, the Balbeggie prospect, Stavely region, Victoria, Australia. Py-pyrite; Sph-sphalerite; Chl-chlorite; Cal-calcite.

Sample ID	Prospect	Borehole Name	From (m)	To (m)	Note
321921	Balbeggie	SB1DH1	146.10	146.24	Sulfide ore and hydrothermal alteration

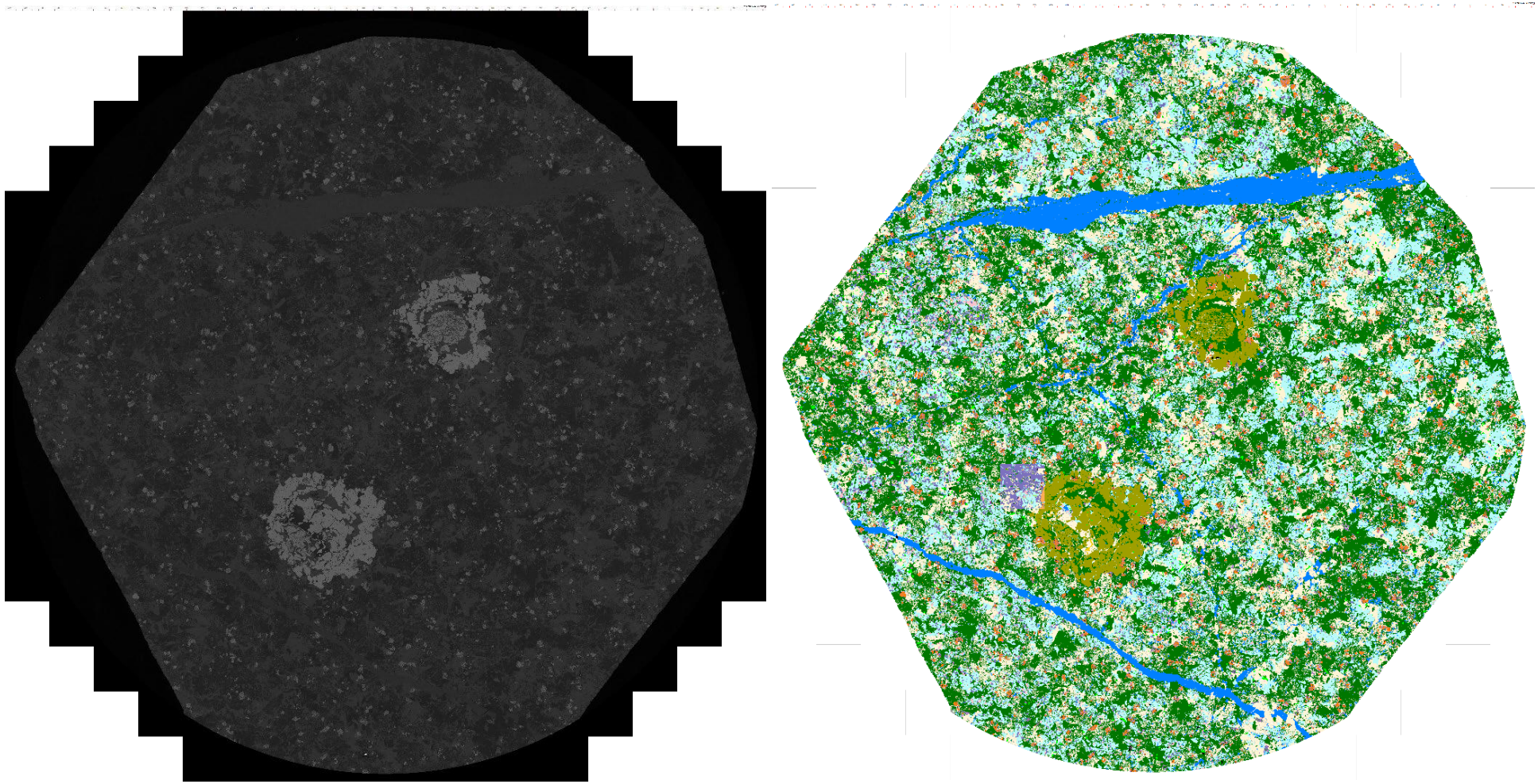

Figure 4 Backscattered electron (BSE) image (left) and Advanced Mineral Identification and Characterization System (AMICS) mineral map (right) of the sample 321921 from drill hole SB1DH1, the Balbeggie prospect, Stavely region, Victoria, Australia. See Figure 9 at the end of this document for the legend of minerals identified using Mineral Liberation Analysis (MLA) mapping.

Sample ID	Prospect	Borehole Name	From (m)	To (m)	Note
321862	Gerang Gerung	GG-01	282.05	282.22	Sulfide ore and hydrothermal alteration

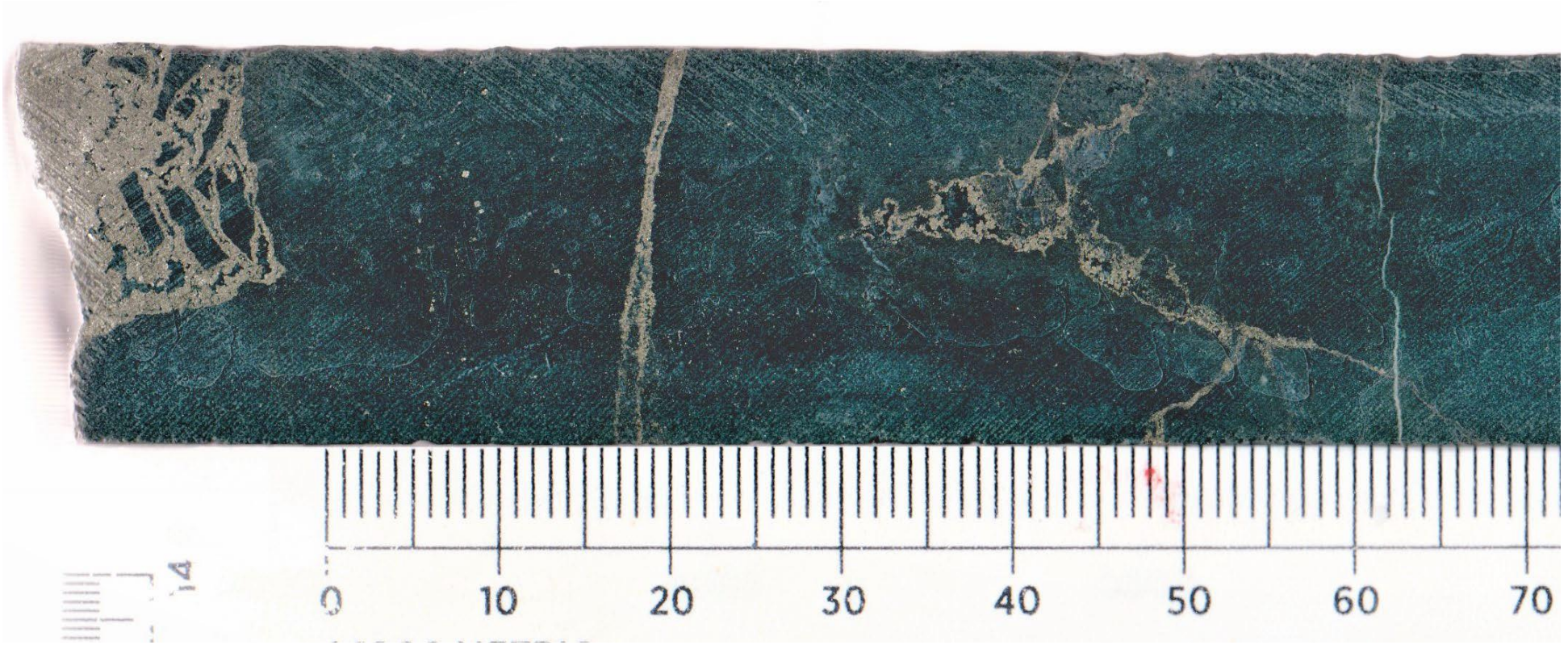

Figure 5 Photos of the drill core sample 321862 from drill hole GG-01, the Gerang Gerung prospect, Stavely region, Victoria, Australia.

Sample ID	Prospect	Borehole Name	From (m)	To (m)	Note
321863	Gerang Gerung	GG-01	306.23	306.51	Sulfide ore and hydrothermal alteration

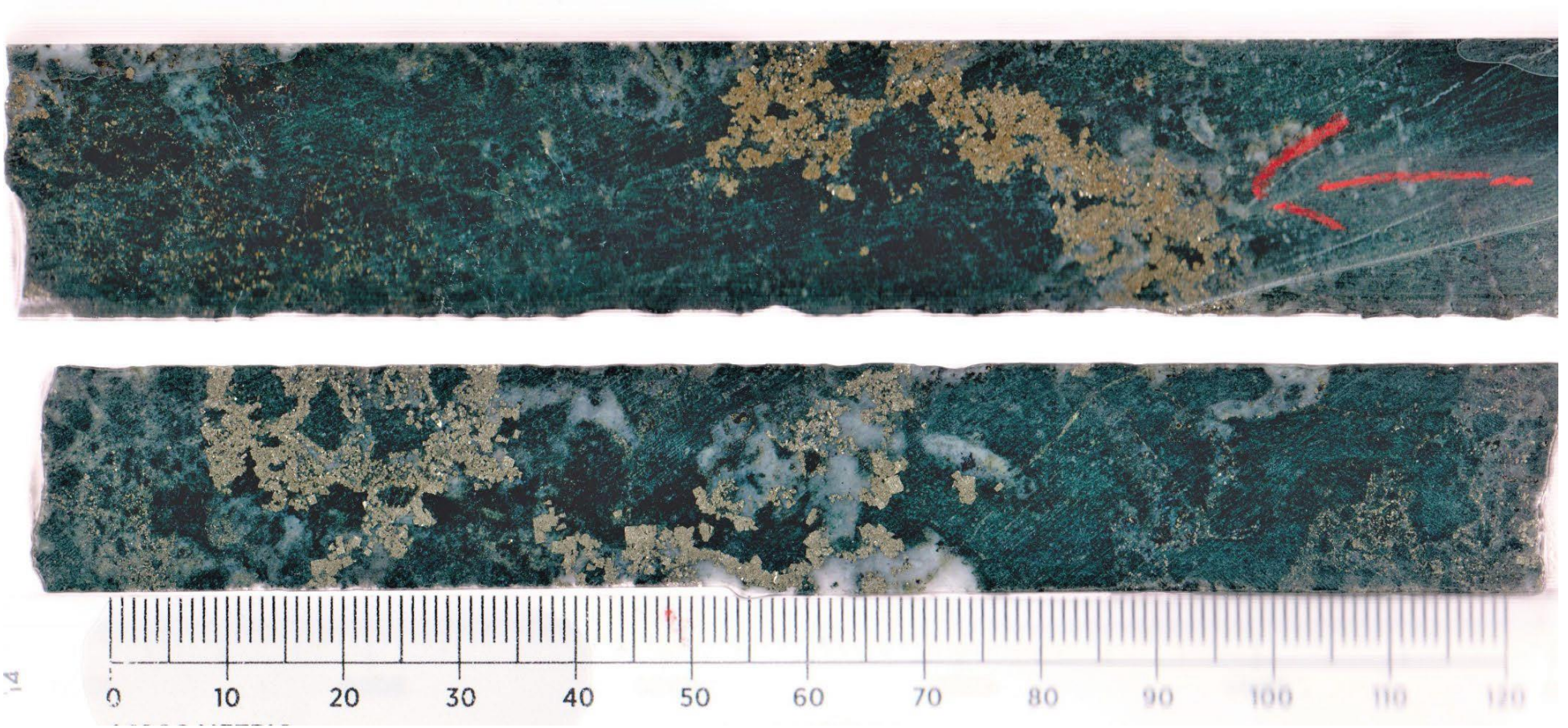

Figure 6 Photos of the drill core sample 321863 from drill hole GG-01, the Gerang Gerung prospect, Stavely region, Victoria, Australia.

Sample ID	Prospect	Borehole Name	From (m)	To (m)	Note
321865	Gerang Gerung	GG-01	321.50	321.73	Sulfide ore and hydrothermal alteration

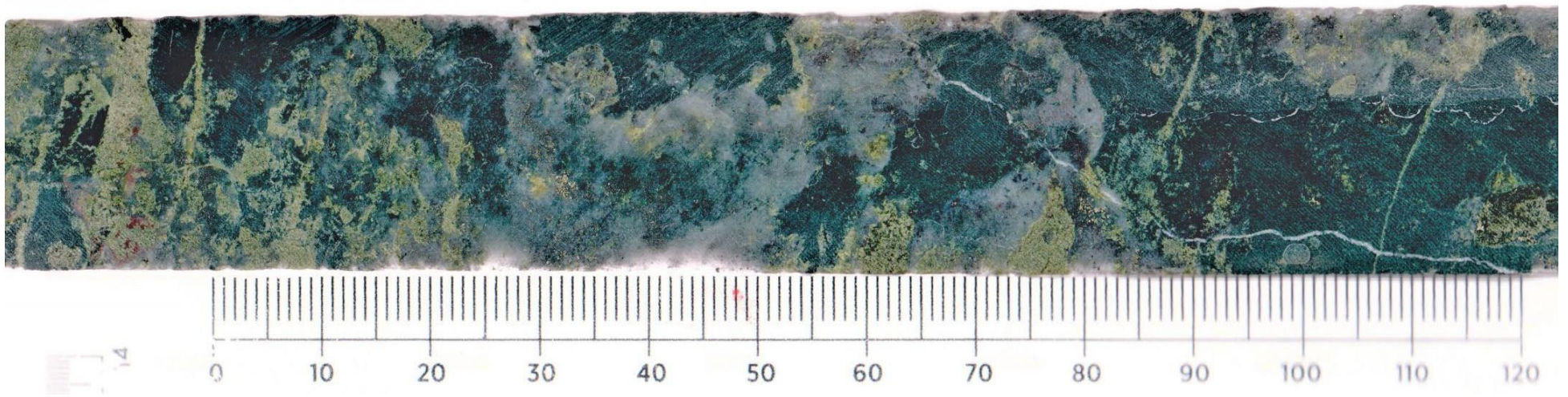

Figure 7 Photos of the drill core sample 321865 from drill hole GG-01, the Gerang Gerung prospect, Stavely region, Victoria, Australia.

Sample ID	Prospect	Borehole Name	From (m)	To (m)	Note
321866	Gerang Gerung	GG-01	324.13	324.29	Sulfide ore and hydrothermal alteration

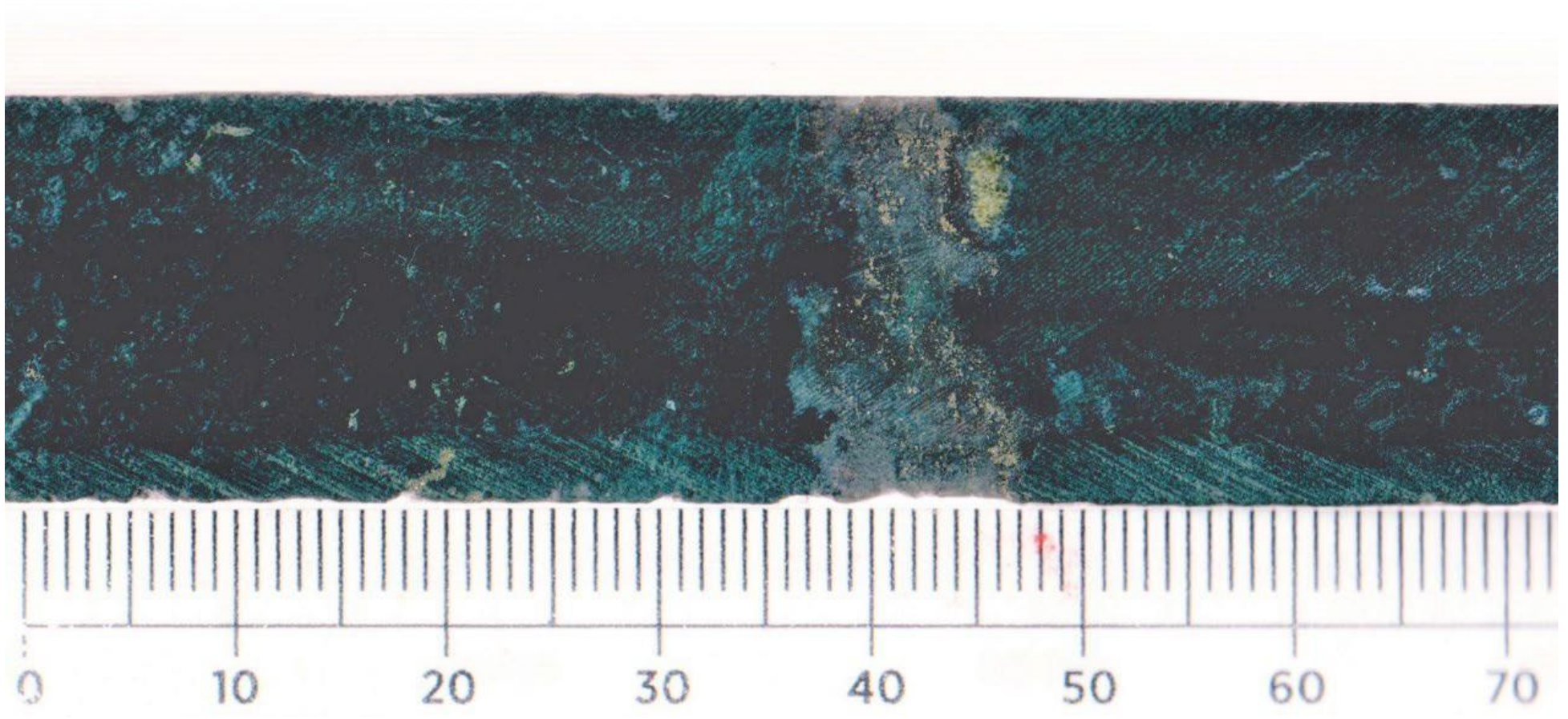

Figure 8 Photos of the drill core sample 321866 from drill hole GG-01, the Gerang Gerung prospect, Stavely region, Victoria, Australia.

Legend of the primary mineral standard of the Mineral Liberation Analysis (MLA) mineral map

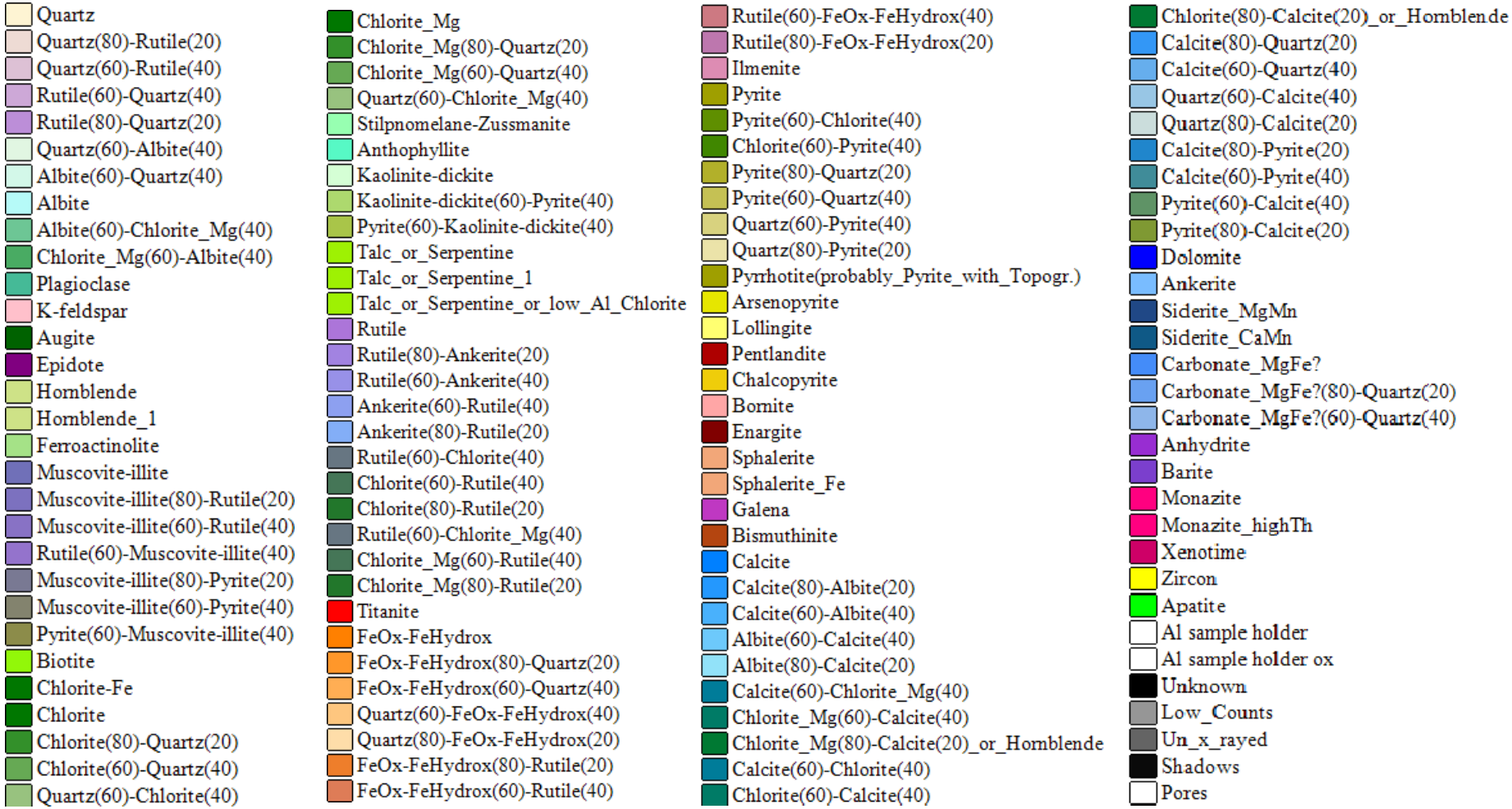

Mineral Abbreviation Legend

Abbreviations follow the conventions of Whitney & Evans (2010, American Mineralogist) and are used consistently throughout this Supplementary Appendix. Analytical method abbreviations are listed at the foot of the table.

Abbrev.	Mineral	Abbrev.	Mineral
Ab	Albite	Lö	Löllingite
Act	Actinolite	Mgt	Magnetite
Amp	Amphibole	Mnz	Monazite
An	Anorthite	Mo	Molybdenite
Ank	Ankerite	Ms	Muscovite
Ap	Apatite	Ol	Olivine
Apy	Arsenopyrite	Or	Orthoclase
Brt	Barite	Phl	Phlogopite
Bt	Biotite	Pl	Plagioclase
Cal	Calcite	Po	Pyrrhotite
Car	Carbonate (general)	Px	Pyroxene
Chl	Chlorite	Py	Pyrite
Cpy	Chalcopyrite	Qtz	Quartz
Di	Diopside	Ser	Sericite
Ed	Edenite	Sid	Siderite
Ep	Epidote	Sme	Smectite
Fsp	Feldspar (general)	Sph	Sphalerite
Gn	Galena	Srp	Serpentine
Grt	Garnet	Tlc	Talc
Gth	Goethite	Ttn	Titanite
Hbl	Hornblende	Tur	Tourmaline
Hem	Haematite	VNIR	Visible to near infrared
Kfsp	K-feldspar	Zrn	Zircon
Kln	Kaolinite		

Analytical Methods: SWIR — short-wave infrared; TIR — thermal infrared; VNIR — visible to near infrared; AMICS — Advanced Mineral Identification and Characterisation System (FEI/Thermo Fisher); MLA — Mineral Liberation Analysis (FEI).

Mineral systems	Deposits	Regions	States	Sample ID
Epithermal	Glenyle	Stavely Zone	Victoria	2023440012
IRGS	Stawell	Stawell Zone	Victoria	2023440018
Mafic-ultramafic magmatic	Mount Arrowsmith	Koonenberry Belt	New South Wales	2022440213
Mafic-ultramafic magmatic	Mount Arrowsmith	Koonenberry Belt	New South Wales	2022440202
Magmatic-hydrothermal	Thackaringa	Broken Hill	New South Wales	2023440366
Magmatic-hydrothermal	Thackaringa	Broken Hill	New South Wales	2023440367
Magmatic-hydrothermal	Gerang Gerung	Stavely	Victoria	321864
Magmatic-hydrothermal	Gerang Gerung	Stavely	Victoria	321864
Magmatic-hydrothermal	NDILLK09	Loch Lilly-Kars Belt	New South Wales	2620021
Magmatic-hydrothermal	NDIWMP02	Loch Lilly-Kars Belt	New South Wales	2620007
Porphyry	Wahratta	Loch Lilly-Kars Belt	New South Wales	2022330063
Porphyry	Wahratta	Loch Lilly-Kars Belt	New South Wales	2022330070
Porphyry	Quondong	Loch Lilly-Kars Belt	New South Wales	2022330094
Porphyry	Eclipse	Stavely Zone	Victoria	321889
Porphyry	Gerang Gerung	Stavely Zone	Victoria	321864
Porphyry	Eclipse	Wertago Region	New South Wales	2022440190
Porphyry	Bunker Hill	Wertago Region	New South Wales	2022440196
Porphyry	Eclipse	Wertago Region	New South Wales	2022440190
Skarn	Scropes Range	Loch Lilly-Kars Belt	New South Wales	2022330033
Skarn	Gerang Gerung	Stavely Zone	Victoria	321864
Skarn	Eaglehawk	Loch Lilly-Kars Belt	New South Wales	2022330048
Skarn	Eaglehawk	Loch Lilly-Kars Belt	New South Wales	2022330048
VHMS	Sherlock	Padthaway Ridge	South Australia	4351206
VHMS	Mt Ararat	Stawell Zone	Victoria	322128
VHMS	Mt Ararat	Stawell Zone	Victoria	322130

Age (Ma)	±2s (Ma)	Mineral	Isotopes	Method	Laboratory
500	27.0	Apatite	U-Pb	LA-ICP-MS	UniTasmania
399	12.0	Apatite	U-Pb	LA-ICP-MS	UniTasmania
589	11.0	Apatite	U-Pb	LA-ICP-MS	UniTasmania
580	21.0	Apatite	U-Pb	LA-ICP-MS	UniTasmania
511	27.0	Siderite	Lu-Hf	LA-ICP-MS	UniAdelaide
400	11.0	Muscovite	Rb-Sr	LA-ICP-MS	UniAdelaide
412	22.0	Titanite	U-Pb	LA-ICP-MS	UniTasmania
494	20.0	Titanite	U-Pb	LA-ICP-MS	UniTasmania
437	36.0	Titanite	U-Pb	LA-ICP-MS	UniTasmania
492	5.4	Titanite	U-Pb	LA-ICP-MS	UniTasmania
521	1.1	Sericite	Ar-Ar	Radiation and MC-MS	ANU
518	3.1	Titanite	U-Pb	SHRIMP	GA
499	8.0	Titanite	U-Pb	LA-ICP-MS	UniTasmania
446	24.0	Titanite	U-Pb	LA-ICP-MS	UniTasmania
412	22.0	Titanite	U-Pb	LA-ICP-MS	UniTasmania
412	38.0	Titanite	U-Pb	LA-ICP-MS	UniTasmania
407	10.0	Titanite	U-Pb	LA-ICP-MS	UniTasmania
435	19.0	Apatite	U-Pb	LA-ICP-MS	UniTasmania
498	16.0	Fluorite	Sm-Nd	ID-TIMS	UniMelbourne
494	20.0	Titanite	U-Pb	LA-ICP-MS	UniTasmania
421	4.0	Titanite	U-Pb	SHRIMP	GA
424	6.3	Titanite	U-Pb	SHRIMP	ANU
525	30.0	Titanite	U-Pb	LA-ICP-MS	UniTasmania
407	15.0	Apatite	U-Pb	LA-ICP-MS	UniTasmania
405	9.0	Apatite	U-Pb	LA-ICP-MS	UniTasmania

Sample number	Analysis ID	207 cor 206Pb/238U		207Pb/206Pb	
		age (Ma)	+/-1 ster	age (Ma)	+/-1 ster
2022330094	C23DEC04A0073	446.38	12.82	2664.84	47.83
2022330094	C23DEC04A0073	544.59	11.70	1822.70	44.21
2022330094	C23DEC04A0074	466.03	9.72	1808.39	47.23
2022330094	C23DEC04A0074	499.69	11.85	1541.04	75.77
2022330094	C23DEC04A0079	476.00	23.47	2577.73	80.78
2022330094	C23DEC04A0079	476.27	26.50	3112.28	71.48
2022330094	C23DEC04A0080	452.43	24.58	2876.94	83.37
2022330094	C23DEC04A0080	495.45	55.20	3736.51	110.60
2022330094	C23DEC04A0080	528.34	36.54	2100.43	149.71
2022330094	C23DEC04A0081	469.79	20.92	4236.85	20.58
2022330094	C23DEC04A0081	558.77	42.35	4403.38	27.09
2022330094	C23DEC04A0081	568.85	38.34	3884.10	52.87
2022330094	C23DEC04A0082	473.97	15.08	2538.92	59.26
2022330094	C23DEC04A0082	495.21	15.41	1283.69	100.68
2022330094	C23DEC04A0082	628.43	50.43	3913.78	58.67
2022330094	C23DEC04A0083	517.95	20.35	3396.60	45.19
2022330094	C23DEC04A0083	581.46	25.80	3592.68	41.17
2022330094	C23DEC04A0084	501.78	37.48	4161.64	41.26
2022330094	C23DEC04A0084	509.45	29.52	3703.33	53.83
2022330094	C23DEC04A0084	567.15	81.00	4611.48	35.09
2022330094	C23DEC04A0085	527.88	11.27	1683.54	50.00
2022330094	C23DEC04A0085	538.44	12.10	1947.35	38.75
2022330094	C23DEC04A0086	497.25	7.15	1137.84	19.85
2022330094	C23DEC04A0087	484.50	53.74	4230.87	47.79
2022330094	C23DEC04A0087	497.54	198.30	4954.54	16.71
2022330094	C23DEC04A0087	533.70	15.19	2712.92	49.58
2022330094	C23DEC04A0087	533.86	16.18	2779.41	50.63
2022330094	C23DEC04A0087	554.98	21.34	2995.55	56.01
2022330094	C23DEC04A0087	732.20	90.59	4734.66	16.37
2022330094	C23DEC04A0087	895.47	165.12	4833.75	19.42
2022330094	C23DEC04A0088	453.37	11.15	2369.56	39.89
2022330094	C23DEC04A0088	459.51	8.41	2014.73	35.85
2022330094	C23DEC04A0088	516.44	14.98	2186.84	56.14
2022330094	C23DEC04A0089	478.50	23.58	4429.57	15.97
2022330094	C23DEC04A0089	484.85	21.56	2660.43	96.26
2022330094	C23DEC04A0089	485.19	35.35	3920.60	41.41
2022330094	C23DEC04A0089	503.74	14.28	1309.80	80.54
2022330094	C23DEC04A0089	543.46	22.76	4165.71	20.98
2022330094	C23DEC04A0089	552.17	31.57	3575.96	59.83
2022330094	C23DEC04A0089	552.49	24.09	4068.29	25.11
2022330094	C23DEC04A0089	575.35	30.87	2848.69	98.17
2022330094	C23DEC04A0090	436.48	8.44	3317.45	17.41
2022330094	C23DEC04A0090	443.04	9.23	3309.10	18.90
2022330094	C23DEC04A0090	470.34	13.69	2890.98	41.35
2022330094	C23DEC04A0090	488.56	12.62	3158.64	28.73
2022330094	C23DEC04A0091	460.14	15.89	2648.54	51.47
2022330094	C23DEC04A0091	478.01	18.75	2655.67	63.93
2022330094	C23DEC04A0091	482.70	16.62	3266.76	40.40

2022330094	C23DEC04A0091	520.77	14.66	2668.95	43.14
2022330094	C23DEC04A0091	548.10	20.34	3226.15	42.80
2022330094	C23DEC04A0099	488.60	33.56	4343.65	28.25
2022330094	C23DEC04A0099	489.40	23.62	4023.74	29.78
2022330094	C23DEC04A0099	526.40	25.49	4100.73	26.52
2022330094	C23DEC04A0100	482.46	12.53	1986.62	53.42
2022330094	C23DEC04A0100	483.80	12.63	2008.36	51.49
2022330094	C23DEC04A0100	519.16	18.87	2005.95	78.45
2022330094	C23DEC04A0100	532.80	15.94	1757.03	57.61
2022330094	C23DEC04A0101	477.66	11.19	2575.42	35.50
2022330094	C23DEC04A0101	497.36	12.89	3140.42	32.22
2022330094	C23DEC04A0101	540.27	20.47	2600.38	70.90
2022330094	C23DEC04A0102	480.14	11.12	2664.13	32.55
2022330094	C23DEC04A0102	506.56	12.28	2436.38	41.22
2022330094	C23DEC04A0103	454.88	19.32	3109.91	52.48
2022330094	C23DEC04A0103	463.06	17.66	3438.72	39.13
2022330094	C23DEC04A0103	480.66	15.53	3406.86	33.11
2022330094	C23DEC04A0103	513.92	25.79	3553.11	44.47
2022330094	C23DEC04A0104	479.34	18.14	3372.63	40.31
2022330094	C23DEC04A0104	510.37	15.45	2422.47	52.65
2022330094	C23DEC04A0104	557.49	15.13	3078.40	34.78
2022330094	C23DEC04A0105	494.37	13.48	2262.69	52.61
2022330094	C23DEC04A0105	525.28	14.07	2817.28	37.30
2022330094	C23DEC04A0106	514.75	9.91	2847.98	23.14
2022330094	C23DEC04A0107	494.21	9.19	3080.08	20.57
2022330094	C23DEC04A0108	477.13	14.78	3146.68	34.93
2022330094	C23DEC04A0108	500.39	22.06	3396.76	50.75
2022330094	C23DEC04A0108	533.73	19.70	3623.93	33.00
2022330094	C23DEC04A0109	525.84	21.55	3323.75	53.10
2022330094	C23DEC04A0110	490.34	11.85	2622.18	33.22
2022330094	C23DEC04A0110	546.21	24.87	3058.21	59.69
2022330094	C23DEC04A0110	551.68	26.36	2998.64	67.81
2022330094	C23DEC04A0111	519.79	15.51	2681.02	43.57
2022330094	C23DEC04A0116	509.86	10.71	2754.19	27.51
2022330094	C23DEC04A0116	538.18	11.52	2135.75	38.56
2022330094	C23DEC04A0117	498.28	11.22	2345.72	37.41
2022330094	C23DEC04A0117	532.81	10.72	2312.93	31.62
2022330094	C23DEC04A0118	506.15	8.95	1826.87	28.81
2022440189	C23DEC04A0119	427.58	50.57	4201.08	65.66
2022440189	C23DEC04A0121	404.08	47.77	4424.30	48.30
2022440189	C23DEC04A0136	425.98	64.31	4442.44	58.38
2022440189	C23DEC04A0124	550.36	54.89	4444.32	40.27
2022440189	C23DEC04A0123	460.92	44.33	4508.68	34.95
2022440189	C23DEC04A0121	549.92	53.36	4543.39	34.99
2022440189	C23DEC04A0120	504.26	62.66	4560.11	43.36
2022440189	C23DEC04A0126	583.69	65.64	4608.61	37.60
2022440189	C23DEC04A0119	565.40	51.08	4609.68	29.45
2022440189	C23DEC04A0140	637.67	147.94	4610.48	81.04
2022440189	C23DEC04A0122	839.25	79.46	4627.35	34.17
2022440189	C23DEC04A0126	733.34	59.24	4628.95	27.68

2022440189	C23DEC04A0137	369.14	79.26	4630.63	62.38
2022440189	C23DEC04A0126	562.90	88.56	4642.41	50.70
2022440189	C23DEC04A0138	481.51	90.82	4642.90	56.92
2022440189	C23DEC04A0123	721.17	158.65	4683.38	72.31
2022440189	C23DEC04A0121	692.81	83.12	4693.79	37.39
2022440189	C23DEC04A0125	654.19	104.16	4711.51	48.50
2022440189	C23DEC04A0120	448.13	84.44	4736.43	46.73
2022440189	C23DEC04A0123	519.89	54.16	4767.56	24.54
2022440189	C23DEC04A0127	337.68	103.05	4798.70	60.13
2022440189	C23DEC04A0120	709.63	87.39	4800.46	32.21
2022440189	C23DEC04A0139	721.15	51.85	4846.59	16.71
2022440189	C23DEC04A0138	797.79	114.66	4857.64	36.21
2022440189	C23DEC04A0138	1420.82	138.11	4963.92	27.30
2022440196	C23DEC04A0162	428.06	38.60	2542.19	154.66
2022440196	C23DEC04A0162	399.90	17.47	3031.17	58.21
2022440196	C23DEC04A0141	446.32	20.39	3085.56	56.86
2022440196	C23DEC04A0162	418.49	16.10	3105.68	56.01
2022440196	C23DEC04A0174	392.03	13.89	3283.68	41.54
2022440196	C23DEC04A0163	399.63	14.90	3553.93	35.25
2022440196	C23DEC04A0163	436.63	17.75	3585.92	35.48
2022440196	C23DEC04A0174	398.74	13.65	3603.21	32.67
2022440196	C23DEC04A0142	537.86	65.93	3607.96	120.32
2022440196	C23DEC04A0177	398.11	35.88	3662.22	92.18
2022440196	C23DEC04A0143	379.69	45.76	3675.42	113.72
2022440196	C23DEC04A0176	413.60	29.90	3709.52	67.42
2022440196	C23DEC04A0163	419.53	29.68	3718.04	59.48
2022440196	C23DEC04A0176	466.47	46.33	3932.33	79.47
2022440196	C23DEC04A0174	415.83	26.44	3958.77	44.22
2022440196	C23DEC04A0142	360.28	67.87	3960.50	145.49
2022440196	C23DEC04A0174	414.54	14.44	4082.20	19.78
2022440196	C23DEC04A0176	562.00	53.75	4106.69	60.89
2022440196	C23DEC04A0143	397.25	41.86	4145.35	61.87
2022440196	C23DEC04A0177	312.69	44.45	4176.06	81.52
2022440196	C23DEC04A0175	433.09	29.64	4211.28	37.70
2022440196	C23DEC04A0176	414.76	74.66	4246.58	96.14
2022440196	C23DEC04A0142	360.84	61.16	4389.75	72.24
2022440196	C23DEC04A0175	477.41	40.69	4389.82	37.13
2022440196	C23DEC04A0181	552.29	199.47	4425.52	169.50
2022440196	C23DEC04A0148	950.57	323.07	4503.82	163.62
2022440196	C23DEC04A0153	408.15	35.13	4519.99	29.58
2022440196	C23DEC04A0180	456.29	115.40	4604.27	80.38
2022440196	C23DEC04A0164	535.70	113.74	4611.25	69.99
2022440196	C23DEC04A0157	617.27	63.72	4628.95	34.04
2022440196	C23DEC04A0177	400.52	98.62	4633.97	72.16
2022440196	C23DEC04A0160	976.57	277.85	4650.60	111.76
2022440196	C23DEC04A0154	761.45	127.61	4660.04	57.04
2022440196	C23DEC04A0180	669.31	102.59	4715.01	45.94
2022440196	C23DEC04A0157	603.52	69.20	4721.23	32.00
2022440196	C23DEC04A0158	1312.23	163.19	4756.90	46.25
2022440196	C23DEC04A0161	1493.47	172.99	4762.64	45.14

2022440196	C23DEC04A0154	431.14	63.34	4765.22	33.30
2022440196	C23DEC04A0153	380.06	96.86	4765.40	56.97
2022440196	C23DEC04A0156	390.62	59.47	4771.96	33.02
2022440196	C23DEC04A0161	1037.86	73.34	4780.30	22.17
2022440196	C23DEC04A0148	537.01	88.69	4803.73	38.82
2022440196	C23DEC04A0164			4805.50	106.80
2022440196	C23DEC04A0159	1589.12	244.98	4828.97	55.39
2022440196	C23DEC04A0175	359.45	101.69	4846.76	51.54
2022440196	C23DEC04A0179	1501.48	147.79	4863.35	32.94
2022440196	C23DEC04A0160	1023.68	102.23	4867.25	28.14
2022440196	C23DEC04A0175	747.93	91.32	4878.88	29.01
2022440196	C23DEC04A0160	650.79	268.98	4882.81	26.71
2022440196	C23DEC04A0175	453.23	169.05	4888.12	69.93
2022440196	C23DEC04A0148	339.13	89.92	4894.66	41.87
2022440196	C23DEC04A0154	570.21	127.25	4900.82	45.26
2022440196	C23DEC04A0173	1239.07	138.78	4916.84	32.51
2022440196	C23DEC04A0180	1221.54	224.27	4924.42	53.18
2022440196	C23DEC04A0165	1743.39	201.19	4924.74	34.15
2022440196	C23DEC04A0164	965.50	207.11	4931.53	52.58
2022440196	C23DEC04A0173	1678.07	263.55	4950.63	40.79
2022440196	C23DEC04A0158	569.34	241.99	4959.63	77.98
2022440196	C23DEC04A0159	619.80	141.22	4970.70	42.48
2022440196	C23DEC04A0165			4977.21	45.16
2022440196	C23DEC04A0165	1291.25	293.10	4981.06	62.22
2022440196	C23DEC04A0173	507.60	220.86	4990.68	70.17
2022440196	C23DEC04A0165	1193.18	305.37	4996.51	66.43
2022440196	C23DEC04A0157			5007.85	30.84
2022440196	C23DEC04A0155			5016.13	39.38
2022440196	C23DEC04A0156			5135.84	35.68
321864	C23DEC04A0034	388.08	24.03	4153.99	35.69
321864	C23DEC04A0049	413.08	38.70	3930.54	69.02
321864	C23DEC04A0044	428.50	39.75	4348.89	43.27
321864	C23DEC04A0048	429.22	17.62	4252.41	19.44
321864	C23DEC04A0034	448.78	24.96	4169.95	30.39
321864	C23DEC04A0071	461.15	28.87	4385.42	26.43
321864	C23DEC04A0049	465.90	28.13	4154.59	34.31
321864	C23DEC04A0063	467.86	45.06	4686.43	25.07
321864	C23DEC04A0033	473.92	46.79	4358.95	45.80
321864	C23DEC04A0071	475.46	39.58	4444.32	33.47
321864	C23DEC04A0046	483.12	16.75	4369.49	13.03
321864	C23DEC04A0072	483.34	17.32	4446.25	12.09
321864	C23DEC04A0036	484.18	36.83	4084.28	49.23
321864	C23DEC04A0037	484.98	27.24	4278.40	28.03
321864	C23DEC04A0053	487.27	38.05	4656.24	21.90
321864	C23DEC04A0042	495.35	12.35	3853.90	15.98
321864	C23DEC04A0064	502.22	44.40	4621.84	26.96
321864	C23DEC04A0044	514.16	28.49	4499.09	19.22
321864	C23DEC04A0037	514.85	18.35	4192.91	18.15
321864	C23DEC04A0048	515.03	39.35	4286.79	40.78
321864	C23DEC04A0054	515.62	49.03	4679.78	26.41

321864	C23DEC04A0063	517.31	51.52	4750.08	24.28
321864	C23DEC04A0037	519.49	31.43	4121.59	36.17
321864	C23DEC04A0036	521.22	22.45	4078.89	26.05
321864	C23DEC04A0048	521.66	41.42	4149.39	46.82
321864	C23DEC04A0047	528.42	13.71	3818.33	17.84
321864	C23DEC04A0034	529.76	22.82	4143.12	24.24
321864	C23DEC04A0047	530.70	27.30	3939.44	38.15
321864	C23DEC04A0044	534.02	30.58	4501.93	20.72
321864	C23DEC04A0036	540.49	32.94	4036.02	43.18
321864	C23DEC04A0050	551.72	66.19	4563.46	42.04
321864	C23DEC04A0069	555.96	79.17	4703.30	40.66
321864	C23DEC04A0032	559.15	51.24	4365.37	42.48
321864	C23DEC04A0063	569.53	53.62	4804.98	21.72
321864	C23DEC04A0031	571.26	31.65	4262.07	28.60
321864	C23DEC04A0035	573.12	24.97	4136.80	26.74
321864	C23DEC04A0064	582.39	48.99	4588.49	28.50
321864	C23DEC04A0053	597.51	44.27	4637.90	22.98
321864	C23DEC04A0043	610.97	35.73	4475.93	22.47
321864	C23DEC04A0068	613.10	50.21	4690.84	23.71
321864	C23DEC04A0069	616.29	61.76	4713.00	28.46
321864	C23DEC04A0051	637.23	43.43	4675.35	20.24
321864	C23DEC04A0067	638.21	81.77	4733.77	36.29
321864	C23DEC04A0053	638.44	49.51	4510.34	30.01
321864	C23DEC04A0070	645.94	57.30	4486.56	35.66
321864	C23DEC04A0045	683.97	43.31	4612.34	21.22
321864	C23DEC04A0051	694.36	58.21	4685.84	26.31
321864	C23DEC04A0052	697.95	155.05	4542.00	88.13
321864	C23DEC04A0062	702.10	63.66	4542.55	35.99
321864	C23DEC04A0054	714.63	69.04	4589.08	35.87
321864	C23DEC04A0068	751.89	65.27	4772.61	24.18
321864	C23DEC04A0045	762.63	43.55	4565.96	21.02
321864	C23DEC04A0066	785.64	86.34	4683.46	36.48
321864	C23DEC04A0063	808.61	42.36	4629.19	17.81
321864	C23DEC04A0070	860.40	67.69	4498.89	33.89
321864	C23DEC04A0065	962.54	91.70	4785.50	29.61
321864	C23DEC04A0065	963.07	89.23	4798.86	28.09
321889	C23DEC04A0027			5004.18	8.76
321889	C23DEC04A0027			5024.23	4.34
321889	C23DEC04A0027			5027.46	6.63
321889	C23DEC04A0015	445.05	31.60	4073.53	43.63
321889	C23DEC04A0013	479.64	60.72	4599.03	38.86
321889	C23DEC04A0015	479.81	29.03	4429.14	23.47
321889	C23DEC04A0017	486.48	27.10	4442.90	21.51
321889	C23DEC04A0015	491.15	26.13	4188.32	28.79
321889	C23DEC04A0030	645.73	27.83	4687.95	10.87
321889	C23DEC04A0028	678.17	96.69	4796.47	37.38
321889	C23DEC04A0013	713.91	56.04	4803.11	19.43
321889	C23DEC04A0028	746.53	82.31	4843.31	27.89
321889	C23DEC04A0013	795.29	69.02	4676.30	28.68
321889	C23DEC04A0013	896.28	147.19	4774.92	48.92

321889	C23DEC04A0016	908.64	116.76	4990.82	28.47
321889	C23DEC04A0028	939.14	102.77	4825.20	30.03
321889	C23DEC04A0025	1071.61	55.48	4917.07	12.48
321889	C23DEC04A0026	1423.51	70.10	4973.72	8.83
321889	C23DEC04A0025	1647.44	83.72	4962.70	12.12
321889	C23DEC04A0012	8854.34	856.94	4961.73	70.54
4351206	C23DEC04A0008	521.18	22.83	3874.87	32.96
4351206	C23DEC04A0008	661.97	52.51	3946.01	57.95
4351206	C23DEC04A0009	532.45	33.13	4063.32	40.38
4351206	C23DEC04A0009	632.02	51.24	4197.99	44.10
4351206	C23DEC04A0009	647.14	58.68	4268.43	48.95
4351206	C23DEC04A0007	507.45	29.85	4338.43	27.02
4351206	C23DEC04A0008	544.05	153.70	4570.12	101.62
4351206	C23DEC04A0010	1299.66	313.37	4768.62	88.35
4351206	C23DEC04A0010	737.09	180.86	4808.58	66.52
4351206	C23DEC04A0010	544.31	190.29	4911.22	68.56
4351206	C23DEC04A0006	1588.82	1504.35	4932.21	293.78
4351206	C23DEC04A0011	nil	nil	5023.51	72.23
4351206	C23DEC04A0005	nil	nil	5034.53	61.69

Sample ID	Analysis ID	U ppm	~Th ppm	~Th/U	204Pb/206Pb
2022330070	T76-1.1	93	86	0.92	2.92E-03
2022330070	T76-2.1	64	69	1.07	6.18E-03
2022330070	T76-3.1	35	37	1.07	5.22E-03
2022330070	T76-4.1	14	28	2.06	1.19E-02
2022330070	T76-5.1	32	52	1.63	5.28E-03
2022330070	T76-6.1	130	127	0.98	8.08E-03
2022330070	T76-7.1	34	59	1.74	7.34E-03
2022330070	T76-8.1	45	54	1.21	6.30E-03
2022330070	T76-8.2	29	56	1.97	8.02E-03
2022330070	T76-9.1	21	42	1.99	1.44E-02
2022330070	T76-10.1	25	52	2.12	7.91E-03
2022330070	T76-10.2	60	71	1.18	3.75E-03
2022330070	T76-11.1	59	63	1.08	6.20E-03
2022330070	T76-11.2	28	54	1.94	8.63E-03
2022330070	T76-11.3	24	54	2.23	1.05E-02
2022330070	T76-11.4	19	46	2.40	1.11E-02
2022330070	T76-12.1	25	47	1.89	8.45E-03
2022330070	T76-13.1	58	70	1.20	3.88E-03
2022330070	T76-14.1	19	53	2.82	2.26E-02
2022330070	T76-15.1	23	48	2.13	2.13E-02
2022330070	T76-15.2	18	42	2.34	2.19E-02
2022330070	T76-16.1	13	32	2.60	9.17E-03
2022330070	T76-17.1	66	71	1.07	4.33E-03
2022330070	T76-18.1	31	59	1.86	6.84E-03
2022330070	T76-18.2	11	29	2.75	2.02E-02
2022330070	T76-19.1	126	121	0.96	2.16E-03
2022330070	T76-19.2	30	41	1.35	8.80E-03

2022330070	T76-19.3	24	52	2.14	1.58E-02
2022330070	T76-19.4	59	74	1.27	6.07E-03
2022330070	T76-20.1	27	42	1.53	1.21E-02
2022330070	T76-21.1	45	57	1.25	6.47E-03
2022330070	T76-22.1	87	94	1.08	5.22E-03
2022330070	T76-23.1	20	46	2.35	9.49E-03
2022330070	T76-24.1	13	28	2.12	1.59E-02
2022330070	T76-25.1	51	55	1.08	4.17E-03
2022330070	T76-26.1	54	51	0.94	5.32E-03
2022330070	T76-27.1	59	71	1.20	4.75E-03
2022330070	T76-28.1	35	49	1.42	6.21E-03

Sample ID	**Analysis ID**	**U ppm**	**~Th ppm**	**~Th/U**	**204Pb/206Pb**
2022330048	T1-1	1649	167	0.10	1.00E-04
2022330048	T2-1	69	21	0.31	3.55E-03
2022330048	T3-1	25	21	0.84	2.86E-03
2022330048	T3-2	255	81	0.32	4.18E-04
2022330048	T3-3	82	28	0.34	2.99E-03
2022330048	T4-1	110	27	0.24	3.53E-03
2022330048	T5-1	56	93	1.65	9.47E-04
2022330048	T5-2	232	86	0.37	2.87E-03
2022330048	T13-3.1	15	40	2.59	2.00E-05
2022330048	T13-3.2	75	57	0.76	1.06E-02
2022330048	T13-3.3	197	110	0.56	5.21E-03
2022330048	T13-4.1	30	81	2.66	8.49E-04
2022330048	T13-4.2	96	157	1.63	2.38E-04
2022330048	T13-4.3	254	164	0.65	1.25E-03
2022330048	T13-5.1	68	62	0.91	1.47E-03
2022330048	T13-5.2	27	106	3.88	2.30E-03
2022330048	T13-6.1	119	87	0.73	2.42E-03
2022330048	T13-7.2	166	60	0.36	1.57E-03
2022330048	T13-7.3	17	3	0.18	4.23E-03
2022330048	T13-7.4	76	123	1.62	9.46E-03
2022330048	T13-7.5	52	118	2.28	3.94E-03
2022330048	T13-7.6	55	85	1.55	5.03E-03
2022330048	T14-1.1	12	35	3.03	5.26E-03
2022330048	T14-2.1	9	57	6.72	3.50E-03
2022330048	T14-3.1	64	90	1.40	8.36E-04
2022330048	T14-3.2	13	54	4.21	9.61E-03
2022330048	T14-3.3	25	28	1.12	5.46E-03
2022330048	T14-4.1	339	676	1.99	2.31E-03
2022330048	T14-5.1	753	216	0.29	2.59E-04
2022330048	T14-5.2	322	151	0.47	7.02E-04
2022330048	T14-5.3	195	88	0.45	1.05E-03
2022330048	T15-1.1	76	64	0.83	1.18E-03
2022330048	T15-2.1	58	83	1.43	8.30E-04
2022330048	T15-3.1	91	92	1.01	2.00E-05

2022330048	T15-3.2	33	75	2.30	1.21E-04
2022330048	T15-3.3	75	181	2.40	9.85E-03
2022330048	T15-3.4	43	98	2.25	1.93E-03

GA SHRIMP II data

	Spot Name	204 /206	% err	Total 207 /206	% err
202256532620007	1900-1.1	8.00E-04	33	0.0756	2.7
202256532620007	1900-1.2	2.20E-03	26	0.0864	7.7
202256532620007	1900-1.3	3.00E-03	26	0.0819	4
202256532620007	1900-1.4	2.70E-03	26	0.1025	10.4
202256532620007	1900-1.5	1.20E-03	33	0.0672	3.5
202256532620007	1900-1.6	-6.20E-04	41	0.066	3.2
202256532620007	1900-1.7	6.50E-05	22	0.0584	0.6
202256532620007	1900-1.8	5.60E-03	18	0.1305	6.2
202256532620007	1900-2.1	-1.90E-04	41	0.0565	1.8
202256532620007	1900-2.2	4.90E-04	71	0.0705	4.7
202256532620007	1900-2.3	2.20E-04	23	0.0585	1.8
202256532620007	~~1900-2.4~~	~~-2.70E-05~~	~~49~~	~~0.0587~~	~~0.8~~
202256532620007	1900-2.5	1.20E-03	30	0.0704	3
202256532620007	1900-2.6	1.60E-04	100	0.0602	4.1
202256532620007	1900-2.7	1.50E-04	71	0.0609	2.7
202256532620007	1900-2.8	-3.40E-04	58	0.0644	3.3
202256532620007	1900-2.9	1.20E-03	25	0.0614	2.7
202256532620007	1900-2.10	1.10E-03	30	0.0594	3.7
202256532620007	1900-2.11	8.80E-04	33	0.0626	5.1
202256532620007	1900-2.12	3.10E-04	41	0.0647	2.2
202256532620007	1900-2.13	5.30E-04	39	0.0581	4.6
202256532620007	1900-2.14	8.20E-04	32	0.0599	2.9
202256532620007	1900-2.15	1.60E-03	16	0.0709	6.8
202256532620007	1900-2.16	4.60E-04	35	0.0615	2.4
202256532620007	1900-2.17	1.00E-03	25	0.0642	2.5
202256532620007	1900-2.18	2.60E-04	58	0.0597	3
202256532620007	1900-2.19	4.10E-04	38	0.0598	2.4
202256532620007	1900-2.20	1.30E-04	71	0.0631	2.6
202256532620007	1900-2.21	8.10E-04	26	0.0668	2.3
202256532620007	1900-2.23	1.50E-03	25	0.0675	3
202256532620007	1900-2.24	6.60E-04	27	0.0618	2.2
202256532620007	1900-2.25	6.00E-04	45	0.0667	3.3
202256532620007	1900-2.26	1.50E-04	45	0.0588	1.8
202256532620007	1900-3.1	5.80E-05	71	0.0613	2.8
202256532620007	1900-3.2	6.80E-04	35	0.0628	3
202256532620007	1900-3.3	5.40E-04	25	0.0608	1.8
202256532620007	1900-3.4	----	---	0.0586	3.3
202256532620007	1900-3.5	5.30E-04	18	0.0667	2.4
202256532620007	1900-3.6	9.30E-05	38	0.0592	1.2

202256532620007	1900-3.7	5.90E-04	50	0.0714	3.6
202256532620007	1900-3.8	7.40E-05	23	0.0589	1
202256532620007	1900-3.9	-3.20E-05	35	0.0577	0.6
202256532620007	1900-3.10	-2.60E-05	100	0.0603	1.6
202256532620007	1900-3.11	2.90E-03	30	0.0698	4.8
202256532620011	1904-2.1	8.20E-03	16	0.1944	2.6
202256532620011	1904-2.2	4.50E-03	22	0.1763	4.7
202256532620011	1904-2.3	8.40E-03	16	0.1893	2.6
202256532620011	1904-2.4	4.60E-03	13	0.131	1.9
202256532620011	1904-2.5	8.50E-03	16	0.1958	2.5
202256532620011	1904-2.6	5.30E-03	26	0.1515	2.2
202256532620011	1904-2.7	8.20E-03	15	0.197	4
202256532620011	1904-1.1	2.70E-03	17	0.0882	2.3
202256532620011	1904-1.2	2.00E-03	19	0.0848	2
202256532620011	1904-1.3	8.20E-03	19	0.1562	3.6
202256532620011	1904-1.4	4.60E-03	16	0.1356	3.8
202256532620011	1904-1.5	8.90E-03	15	0.2107	2.4
202256532620011	1904-1.6	4.40E-03	21	0.1146	3.4
202256532620011	1904-1.7	2.00E-02	10	0.3744	4
202256532620011	1904-1.8	6.50E-03	17	0.162	2.6
202256532620011	1904-1.9	1.20E-02	14	0.2256	4.5
202256532620011	1904-3.1	7.00E-03	15	0.1638	2.3
202256532620011	1904-3.2	1.00E-02	15	0.1956	2.7
202256532620011	1904-3.3	7.80E-03	16	0.1929	4
202256532620011	1904-3.4	3.20E-03	12	0.1014	1.6
202256532620011	1904-3.5	8.00E-03	14	0.1703	2.5
202256532620011	1904-3.6	5.70E-03	21	0.2188	3.1
202256532620011	1904-3.7	9.30E-03	14	0.1814	2.6
202256532620011	1904-4.1	6.20E-03	17	0.1766	2.4
202256532620011	1904-4.2	3.30E-03	17	0.1233	2
202256532620011	1904-4.3	1.00E-02	15	0.2072	2.6
202256532620011	1904-4.4	5.90E-03	13	0.1334	2.1
202256532620011	1904-4.5	1.60E-03	20	0.0827	2.2
202256532620011	1904-4.6	6.80E-03	15	0.1349	2.5
202256532620011	1904-6.5	5.40E-03	18	0.1695	2.2
202256532620011	1904-6.6	4.80E-03	15	0.1268	2.3
202256532620011	1904-6.7	3.60E-03	16	0.1195	2.1
202256532620011	1904-6.8	6.90E-03	19	0.1482	3.5

206Pb/238U		207Pb/206Pb		207Pb/235U		208Pb/
ratio	+/-1 RSE	ratio	+/-1 RSE	ratio	+/-1 RSE	ratio
0.0847	2.4989	0.1813	5.7749	2.1312	5.1494	0.0411
0.0943	2.0810	0.1114	4.8734	1.4554	5.0206	0.0354
0.0803	1.9925	0.1105	5.1972	1.2539	5.1702	0.0284
0.0846	2.2123	0.0957	8.0586	1.1701	8.0760	0.0282
0.0893	4.4404	0.1721	9.6721	2.1204	9.6288	0.0359
0.0988	4.5538	0.2388	8.9773	3.3482	9.0379	0.0435
0.0891	4.5363	0.2063	10.2631	2.5664	9.3460	0.0299
0.1264	5.2535	0.3569	14.5481	6.3405	14.2814	0.0412
0.0937	6.4196	0.1302	17.0498	1.7016	15.7378	0.0318
0.1653	2.1609	0.4985	2.7910	11.4034	3.1588	0.1669
0.2352	3.5681	0.5584	3.7080	18.1736	5.0986	0.2292
0.1568	3.6914	0.3934	7.0222	8.5374	5.9891	0.2010
0.0884	2.7728	0.1681	7.0681	2.1305	7.6246	0.0295
0.0825	2.9884	0.0836	10.3378	0.9716	10.4259	0.0290
0.1766	4.7739	0.4013	7.8070	9.6859	7.9522	0.0475
0.1163	2.8108	0.2861	5.8033	4.6222	5.6350	0.0633
0.1402	3.1965	0.3248	5.3629	6.3494	6.3395	0.0775
0.1658	3.5543	0.4738	5.5734	10.8951	6.2728	0.1807
0.1282	3.5189	0.3492	7.0644	6.1436	6.5998	0.1069
0.3293	3.7689	0.6444	4.8560	29.8405	4.7542	0.2125
0.0904	2.0614	0.1033	5.4167	1.3108	5.7967	0.0307
0.0942	2.1959	0.1194	4.3357	1.5713	4.5531	0.0304
0.0823	1.4577	0.0776	1.9960	0.8874	2.7501	0.0300
0.1696	7.2740	0.4965	6.4801	11.9493	12.1904	0.0622
1.2418	2.9632	0.8187	2.3504	141.1948	3.3590	0.5474
0.1025	2.3994	0.1867	6.0134	2.6396	6.0315	0.0334
0.1037	2.5365	0.1944	6.1776	2.7879	5.5131	0.0354
0.1125	3.1249	0.2220	6.9656	3.4842	7.7371	0.0365
0.5736	7.1779	0.7019	2.2794	56.3111	8.6226	0.2180
1.0040	4.2442	0.7522	2.7160	105.3083	4.9327	0.3914
0.0826	2.3032	0.1521	4.6772	1.7426	4.7861	0.0293
0.0806	1.7410	0.1240	4.0431	1.3633	4.2531	0.0290
0.0924	2.7134	0.1368	6.4552	1.7536	6.3970	0.0312
0.2073	2.0452	0.5685	2.1891	16.2993	2.6738	0.0851
0.0921	3.3733	0.1808	11.6162	2.3043	11.5902	0.0328
0.1360	5.6724	0.4031	5.5124	7.4975	10.1626	0.0576
0.0841	2.7594	0.0847	8.3002	0.9967	8.2225	0.0280
0.1805	2.2769	0.4751	2.8348	11.9754	3.1186	0.0663
0.1321	3.6525	0.3213	7.7834	5.8823	8.4381	0.0462
0.1706	2.5207	0.4449	3.3734	10.4161	3.5707	0.0582
0.1134	4.1073	0.2028	12.0540	3.2351	14.0108	0.0371
0.0953	1.6372	0.2720	2.2223	3.5632	2.6831	0.0360
0.0966	1.7758	0.2705	2.4107	3.6169	2.8825	0.0364
0.0930	2.4923	0.2081	5.0959	2.6731	4.7525	0.0331
0.1025	2.1951	0.2459	3.6216	3.4931	3.5535	0.0379
0.0872	3.1322	0.1795	6.2040	2.1727	6.7478	0.0396
0.0907	3.4615	0.1803	7.7120	2.2627	7.4297	0.0365
0.1042	2.6960	0.2633	5.1373	3.8157	5.3703	0.0581

0.0993	2.5244	0.1818	5.2101	2.5027	5.6349	0.0366
0.1174	3.0308	0.2566	5.4248	4.1391	5.2911	0.0499
0.1913	2.8769	0.5361	3.8549	14.1582	4.0651	0.0906
0.1462	2.8099	0.4318	3.9899	8.7492	3.8913	0.0670
0.1661	2.8372	0.4547	3.5686	10.5258	3.7602	0.0763
0.0845	2.4667	0.1221	6.0049	1.4398	6.2353	0.0313
0.0849	2.4884	0.1236	5.8024	1.4514	5.7277	0.0342
0.0912	3.4224	0.1234	8.8386	1.5664	9.2660	0.0347
0.0917	2.9329	0.1075	6.3000	1.3744	6.3635	0.0362
0.0896	2.1472	0.1718	4.2492	2.1237	4.6449	0.0401
0.1040	2.1068	0.2431	4.0560	3.5155	4.4643	0.0523
0.1020	3.2408	0.1744	8.5070	2.4663	8.6848	0.0451
0.0913	2.1210	0.1812	3.9298	2.2901	4.3074	0.0330
0.0933	2.2267	0.1582	4.8659	2.0658	5.1945	0.0321
0.0942	3.5409	0.2385	6.5893	3.1338	6.2986	0.0339
0.1051	2.8884	0.2940	5.0406	4.2697	4.9115	0.0391
0.1081	2.5036	0.2880	4.2553	4.3335	4.7861	0.0467
0.1217	3.9000	0.3165	5.7762	5.3644	6.3318	0.0436
0.1067	2.9418	0.2817	5.1668	4.1422	5.0168	0.0490
0.0939	2.7774	0.1569	6.2063	2.0325	5.7421	0.0367
0.1151	2.2529	0.2338	4.3555	3.7207	4.7570	0.0531
0.0891	2.5168	0.1429	6.0998	1.7919	6.6857	0.0316
0.1027	2.3729	0.1989	4.5670	2.8045	4.9100	0.0443
0.1012	1.7537	0.2027	2.8408	2.8309	3.3650	0.0501
0.1018	1.6143	0.2341	2.5769	3.2912	3.1830	0.0410
0.0998	2.6404	0.2441	4.3991	3.4596	4.4372	0.0405
0.1123	3.1558	0.2861	6.5169	4.4835	7.2794	0.0389
0.1300	2.6297	0.3315	4.3074	6.0235	4.8990	0.0754
0.1156	2.8005	0.2731	6.7819	4.4372	6.7468	0.0468
0.0927	2.2436	0.1767	3.9943	2.3409	4.1390	0.0345
0.1122	3.7992	0.2309	7.4633	3.6370	7.2905	0.0429
0.1119	3.9413	0.2225	8.4356	3.4494	7.6780	0.0497
0.0993	2.7063	0.1831	5.2689	2.5256	5.0789	0.0380
0.0985	1.9172	0.1914	3.3486	2.5846	3.6764	0.0372
0.0959	2.0402	0.1328	4.4094	1.7221	4.5536	0.0336
0.0907	2.1114	0.1500	4.3754	1.8836	4.5272	0.0338
0.0968	1.9149	0.1471	3.6861	1.9473	4.1409	0.0355
0.0875	1.7464	0.1117	3.1780	1.3569	3.6719	0.0315
0.1407	5.7315	0.4866	8.8889	9.6502	7.8889	0.1628
0.1622	4.5114	0.5665	6.6197	12.9525	5.8137	0.1586
0.1732	7.0179	0.5736	8.0080	14.2240	6.6639	0.0964
0.2177	4.8261	0.5743	5.5250	17.2712	5.1778	0.2622
0.1990	3.5938	0.6003	4.8112	16.8896	4.8314	0.1918
0.2402	3.6872	0.6148	4.8251	20.3998	5.0963	0.2648
0.2274	4.2311	0.6219	5.9846	18.9885	5.5321	0.1823
0.2709	3.9802	0.6431	5.2026	24.2266	4.8626	0.2730
0.2644	3.2171	0.6436	4.0744	23.5101	3.9855	0.3478
0.2916	8.2473	0.6440	11.2130	26.2050	9.8602	0.1777
0.3691	4.1505	0.6515	4.7324	33.4599	4.8268	0.1201
0.3324	3.2053	0.6523	3.8342	29.9025	3.9127	0.3706

0.1914	4.8751	0.6530	8.6394	17.3581	8.0411	0.0606
0.2736	4.3137	0.6584	7.0262	24.9956	6.0117	0.3259
0.2416	5.8181	0.6586	7.8885	22.1209	6.9455	0.1664
0.3477	7.2407	0.6773	10.0419	32.8846	10.3671	0.3227
0.3411	4.1459	0.6823	5.1950	32.4549	5.5312	0.3487
0.3334	4.2153	0.6907	6.7447	32.1958	5.7738	0.3151
0.2592	4.9900	0.7028	6.5061	25.3304	5.8434	0.2790
0.3023	3.5452	0.7182	3.4221	29.8273	4.1876	0.3279
0.2325	6.7196	0.7340	8.3962	23.4742	7.4157	0.1484
0.3937	4.2891	0.7349	4.4985	39.9947	4.8252	0.3640
0.4217	2.3652	0.7590	2.3382	45.0108	2.8350	0.1706
0.4574	5.3022	0.7648	5.0696	48.9285	7.6576	0.4580
0.7766	3.8462	0.8241	3.8408	89.0114	4.2162	0.8397
0.0797	8.0619	0.1684	18.4522	1.8742	19.6837	0.1171
0.0812	3.6276	0.2270	7.2617	2.5438	7.2509	0.2823
0.0918	3.8481	0.2349	7.1249	3.0310	6.7748	0.3969
0.0864	2.8849	0.2379	7.0305	2.7631	6.9229	0.4781
0.0846	2.7266	0.2662	5.2892	3.1316	5.5495	0.4063
0.0939	2.7173	0.3167	4.5794	4.1438	4.8803	6.8445
0.1038	3.1115	0.3234	4.6189	4.6469	4.6227	2.1792
0.0955	2.3201	0.3270	4.2586	4.3257	4.4662	0.7333
0.1287	8.6023	0.3280	15.6888	5.8602	15.1015	0.4318
0.0975	5.0729	0.3399	12.0651	4.6129	9.0295	0.7570
0.0935	7.6354	0.3428	14.8970	4.4399	12.8894	0.3889
0.1033	4.4167	0.3506	8.8525	4.8538	8.4255	1.8263
0.1051	4.9407	0.3525	7.8146	5.2851	8.0387	2.2776
0.1292	4.8699	0.4062	10.5867	7.2556	9.4535	1.3688
0.1172	3.8193	0.4135	5.9004	6.6851	5.4742	0.8310
0.1020	8.2598	0.4139	19.4154	5.7907	15.0082	0.4063
0.1258	2.0354	0.4491	2.6593	7.8381	2.9671	0.9380
0.1710	5.2162	0.4566	8.1983	10.7739	7.3629	1.6014
0.1260	5.2692	0.4686	8.3485	8.2412	7.8147	0.7471
0.1025	5.8220	0.4784	11.0197	6.7954	9.0590	0.6780
0.1435	3.0970	0.4900	5.1061	9.7652	4.5562	0.1881
0.1416	7.7891	0.5018	13.0480	9.8929	13.3662	3.1112
0.1413	6.4245	0.5532	9.8825	11.0692	10.2766	0.6164
0.1823	3.6407	0.5533	5.0798	13.9692	5.1326	0.1478
0.2146	7.6373	0.5670	23.2312	16.8085	9.8951	0.6092
0.3659	11.8831	0.5983	22.5174	28.9946	17.9678	1.9773
0.1814	3.1033	0.6050	4.0744	15.2892	4.0951	2.5695
0.2204	8.1950	0.6412	11.1190	19.4527	9.7332	0.8646
0.2535	7.0736	0.6443	9.6845	22.4825	8.5031	3.2880
0.2899	3.5690	0.6523	4.7144	25.9172	4.3341	1.1102
0.2056	6.6722	0.6545	9.9967	18.8932	9.0426	4.8909
0.4247	10.3071	0.6621	15.4950	37.2674	12.2684	1.6743
0.3535	6.5530	0.6665	7.9122	32.5795	7.3528	2.9273
0.3406	5.0362	0.6924	6.3887	32.8142	6.6602	6.2106
0.3175	3.8391	0.6954	4.4525	30.5998	4.5194	1.2026
0.5860	5.6110	0.7129	6.4448	57.7788	6.3137	1.0768
0.6506	5.3452	0.7157	6.2929	64.6367	6.2126	2.6520

0.2629	4.1322	0.7170	4.6431	26.4549	4.4453	2.6720
0.2396	4.8778	0.7171	7.9418	23.3941	5.8143	3.3450
0.2471	3.6623	0.7204	4.6049	24.5249	4.3344	2.0850
0.5040	2.9551	0.7246	3.0930	50.2761	3.5180	2.6329
0.3255	4.1588	0.7366	5.4216	33.2043	5.0892	4.0858
2.4154	23.5815	0.7375	14.9169	250.5384	59.1456	10.4515
0.7279	7.4257	0.7497	7.7454	78.6314	8.1182	2.7679
0.2647	5.1809	0.7590	7.2122	27.8039	6.5445	0.1714
0.7203	4.4786	0.7679	4.6135	76.1823	4.9764	4.6373
0.5473	3.7565	0.7700	3.9416	58.0671	4.2270	2.9720
0.4501	3.7125	0.7763	4.0655	48.5101	4.2195	0.3082
1.1608	4.3052	0.7784	3.7438	124.7900	4.7181	9.9351
0.3309	6.5008	0.7814	9.8050	36.3861	8.1257	0.2709
0.2787	4.5660	0.7849	5.8718	27.5150	5.8703	2.8098
0.3900	5.2971	0.7883	6.3490	42.6173	5.9001	3.8590
0.6603	4.3077	0.7973	4.5636	73.3914	4.7585	10.3231
0.6593	6.7304	0.8015	7.4686	72.0710	7.2761	7.6248
0.9219	4.8072	0.8017	4.7966	103.7319	5.2201	13.6579
0.5669	9.0691	0.8055	7.3868	63.8658	8.6797	3.8845
0.9654	6.8748	0.8164	5.7351	109.2975	5.7326	6.7532
0.4261	8.6160	0.8216	10.9682	48.9710	9.2910	0.9872
0.4552	5.1668	0.8280	5.9787	53.0660	5.7491	3.7484
1.2461	7.7661	0.8318	6.3573	142.4011	7.0942	14.8866
0.7357	7.4674	0.8341	8.7602	86.5916	8.8568	11.8345
0.4197	7.8751	0.8397	9.8842	49.7132	9.5742	10.2196
0.7082	7.6438	0.8432	9.3588	82.8676	8.2084	15.1511
2.5531	6.6295	0.8500	4.3471	300.7371	6.8969	16.4479
1.6729	7.5602	0.8549	5.5536	197.8849	9.8783	4.0001
2.7237	7.9311	0.9304	5.0566	353.4074	8.1216	15.8692
0.1240	2.9686	0.4713	4.8180	8.1089	5.3974	1.3819
0.1146	5.4691	0.4058	9.1930	6.3502	6.9080	0.6645
0.1592	3.4975	0.5380	5.9062	11.8779	5.5861	1.9950
0.1469	2.1088	0.5038	2.6395	10.3383	3.0674	2.8766
0.1440	3.0555	0.4764	4.1063	9.5130	4.6558	1.9402
0.1760	2.8054	0.5516	3.6146	13.1230	3.9518	1.4938
0.1477	3.2750	0.4715	4.6326	9.7074	5.0125	0.8106
0.2499	3.5755	0.6788	3.4813	23.5723	3.8089	2.9105
0.1761	4.0190	0.5417	6.2551	13.1887	5.5199	1.8744
0.1913	3.3408	0.5743	4.5925	15.2986	4.3356	2.0838
0.1809	1.8126	0.5456	1.7805	13.8173	2.6796	1.8048
0.1945	1.6850	0.5751	1.6588	15.6817	2.3393	1.6797
0.1462	3.9454	0.4497	6.6192	9.0836	6.0372	2.3697
0.1681	2.6241	0.5128	3.8105	11.9814	3.5846	1.5908
0.2481	2.5719	0.6647	3.0378	22.9298	3.2239	1.6180
0.1317	1.8202	0.3856	2.1185	7.0632	2.5983	1.4789
0.2435	3.0822	0.6490	3.7326	22.0714	3.7318	1.8606
0.2166	2.5908	0.5963	2.6442	17.9167	2.8892	2.9521
0.1667	2.0250	0.4839	2.4559	11.1656	2.8481	0.9513
0.1789	2.7978	0.5157	5.5477	12.8848	5.6184	2.2557
0.2673	3.2567	0.6757	3.6665	24.9825	3.6498	2.8882

0.2940	3.2687	0.7095	3.3822	28.8997	3.8662	3.2875
0.1602	3.4166	0.4612	4.8736	10.2811	4.4940	0.9140
0.1564	2.5675	0.4481	3.5010	10.0060	3.4237	2.1584
0.1638	4.3386	0.4699	6.3189	10.5639	4.7845	2.7617
0.1379	1.8965	0.3766	2.3588	7.2235	2.9017	1.5131
0.1655	2.4880	0.4679	3.2699	10.7555	3.4045	1.8435
0.1470	3.0350	0.4082	5.0849	8.3325	5.3976	1.6522
0.2244	2.3868	0.5975	2.8517	18.4423	3.1100	2.7273
0.1578	3.0421	0.4354	5.7889	9.4988	5.8530	2.1225
0.2461	4.6376	0.6234	5.8032	21.5281	5.3345	2.4414
0.2918	4.0426	0.6868	5.6513	27.8040	5.0061	2.2672
0.2057	4.2494	0.5441	5.8038	15.5222	5.2693	1.8328
0.3397	2.7324	0.7372	3.0338	34.8026	3.2433	3.5860
0.1931	2.8378	0.5071	3.8855	13.7349	3.8701	1.8977
0.1775	2.1835	0.4659	3.6070	11.5890	4.0450	3.0663
0.2645	3.1148	0.6342	3.9395	23.3571	3.8786	2.0608
0.2854	2.7173	0.6563	3.1842	26.2130	3.6099	1.2959
0.2456	2.7991	0.5869	3.0883	19.9620	4.0563	3.1387
0.3097	2.8279	0.6809	3.2942	29.3090	3.4628	1.9748
0.3193	3.3580	0.6914	3.9576	30.6654	3.8940	2.4868
0.3133	2.3968	0.6736	2.8093	29.1263	3.0197	2.3331
0.3362	4.0517	0.7015	5.0519	32.7598	5.3394	2.0916
0.2635	3.3586	0.6010	4.1315	22.0311	3.5025	1.7136
0.2602	4.0298	0.5912	4.9033	21.2988	5.6673	1.2800
0.3091	2.4934	0.6448	2.9367	27.7845	3.1512	3.3246
0.3387	2.6481	0.6785	3.6545	31.9494	3.4895	2.4094
0.2928	8.7760	0.6142	12.1521	25.3689	10.7153	2.3135
0.2944	3.2375	0.6145	4.9626	25.2179	4.1135	0.8078
0.3126	3.4712	0.6345	4.9584	27.6147	5.1012	2.6011
0.3967	2.9546	0.7207	3.3718	39.6078	3.5376	2.6282
0.3223	2.5110	0.6245	2.9018	28.0782	3.3182	3.4970
0.3712	4.0727	0.6774	5.0656	34.6356	4.8544	3.4400
0.3591	2.1911	0.6524	2.4661	32.5177	3.0147	3.6764
0.3353	3.7709	0.5962	4.6627	27.5993	4.6880	2.5009
0.4800	3.5071	0.7272	4.1325	48.4086	4.1178	5.0763
0.4870	3.4629	0.7341	3.9221	49.6793	4.0364	3.5885
2.9759	2.3185	0.8478	1.2343	350.6585	2.7260	21.8333
5.4085	2.1769	0.8598	0.6120	647.3058	2.6315	41.3076
3.7731	2.7649	0.8618	0.9355	450.7663	3.1645	34.1795
0.1340	4.1494	0.4465	5.8620	8.2967	5.4296	1.5063
0.2282	5.4958	0.6389	5.3733	20.2976	5.7897	2.8246
0.1900	2.8747	0.5684	3.2180	15.0101	3.9661	2.5805
0.1950	2.4100	0.5738	2.9513	15.6170	3.3672	2.8921
0.1589	2.9039	0.4824	3.8951	10.6522	4.2471	1.8573
0.3211	1.8013	0.6795	1.5097	30.3686	2.4840	8.6929
0.3795	4.4353	0.7328	5.2189	38.6637	5.0858	2.2279
0.3966	3.0747	0.7362	2.7139	40.2688	3.6602	5.4104
0.4298	3.1783	0.7572	3.9021	45.2914	4.3395	1.9985
0.3718	3.4407	0.6740	3.9808	34.8500	4.1772	4.0345
0.4510	7.3912	0.7219	6.8238	44.6051	6.3827	6.5229

0.5877	3.6184	0.8398	4.0099	67.8695	4.0340	4.2531
0.4923	5.2098	0.7477	4.1982	50.8701	5.6506	1.9623
0.5972	2.1417	0.7974	1.7527	66.6297	2.6912	4.7136
0.7887	3.6571	0.8298	1.2433	92.2074	3.9809	6.2156
0.9494	2.0687	0.8234	1.7048	109.1025	2.5310	7.4101
2.0724	12.0095	0.8228	9.9227	239.8223	16.5273	6.8938
0.1398	2.8370	0.3910	4.3746	7.5571	4.2850	31.5162
0.1827	5.1797	0.4100	7.7264	10.5412	7.1165	52.1094
0.1581	3.5331	0.4434	5.4226	9.7290	5.0787	40.7528
0.2026	4.9830	0.4856	5.9693	13.5992	5.5688	26.0568
0.2176	4.6276	0.5093	6.6513	14.9567	6.1473	20.6897
0.1841	2.7615	0.5342	3.6862	13.8080	3.6992	30.8203
0.2451	8.6937	0.6263	14.0324	21.9890	10.4821	49.9462
0.5881	10.8670	0.7187	12.3195	58.5283	12.0426	< DL
0.4083	7.5896	0.7390	9.2929	44.4350	8.4835	< DL
0.3849	7.3214	0.7941	9.6229	43.5331	8.6763	62.4689
0.8230	39.1963	0.8059	41.2733	92.2751	37.3592	1.6116
10.3856	21.4216	0.8594	10.1894	1238.1834	27.0253	< DL
11.7397	17.6615	0.8661	8.7059	1424.9691	19.6702	< DL

±	f206%					Radiogenic - 2
		208Pb/206Pb	±	206Pb/238U	±	207Pb/235U
3.35E-04	5.3	0.309	0.015	0.0698	0.0021	0.62
5.50E-04	11.2	0.308	0.025	0.0626	0.0026	0.34
7.63E-04	9.5	0.338	0.034	0.0668	0.0038	0.55
1.58E-03	21.7	0.711	0.083	0.0674	0.0075	0.78
1.04E-03	9.6	0.511	0.048	0.0696	0.0037	0.63
6.98E-04	14.7	0.272	0.033	0.0675	0.0021	0.49
1.05E-03	13.3	0.571	0.048	0.0672	0.0029	0.54
6.69E-04	11.4	0.378	0.032	0.0686	0.0032	0.64
1.48E-03	14.6	0.682	0.073	0.0703	0.0038	0.71
1.68E-03	26.1	0.481	0.082	0.0584	0.0043	-
1.52E-03	14.4	0.707	0.071	0.0726	0.0042	1.03
5.69E-04	6.8	0.382	0.025	0.0684	0.0020	0.56
6.29E-04	11.2	0.328	0.029	0.0689	0.0022	0.51
1.20E-03	15.7	0.565	0.054	0.0674	0.0029	0.29
1.47E-03	19.0	0.606	0.076	0.0599	0.0029	-
1.99E-03	20.1	0.816	0.095	0.0641	0.0051	0.66
1.43E-03	15.3	0.543	0.067	0.0695	0.0037	0.42
6.90E-04	7.0	0.371	0.029	0.0701	0.0020	0.60
2.49E-03	41.0	0.758	0.137	0.0677	0.0061	0.08
2.74E-03	38.6	0.619	0.176	0.0617	0.0060	-
1.73E-03	39.8	0.679	0.097	0.0653	0.0049	-
2.40E-03	16.6	0.774	0.114	0.0687	0.0053	0.48
5.93E-04	7.8	0.337	0.025	0.0686	0.0027	0.49
1.19E-03	12.4	0.600	0.056	0.0702	0.0044	0.68
4.32E-03	36.7	0.741	0.228	0.0620	0.0094	-
2.79E-04	3.9	0.324	0.014	0.0688	0.0013	0.65
2.06E-03	16.0	0.444	0.100	0.0635	0.0034	0.70

1.90E-03	28.6	0.621	0.143	0.0623	0.0038	-
7.85E-04	11.0	0.338	0.038	0.0665	0.0025	0.36
2.37E-03	21.9	0.659	0.387	0.0802	0.0107	1.45
6.68E-04	11.7	0.403	0.029	0.0676	0.0021	0.58
1.04E-03	9.5	0.387	0.045	0.0691	0.0025	0.84
1.43E-03	17.2	0.786	0.075	0.0677	0.0034	0.60
2.47E-03	28.9	0.432	0.116	0.0613	0.0052	-
5.40E-04	7.6	0.366	0.023	0.0713	0.0020	0.64
8.05E-04	9.6	0.268	0.034	0.0659	0.0032	0.46
9.42E-04	8.6	0.360	0.040	0.0669	0.0033	0.45
1.04E-03	11.3	0.454	0.045	0.0693	0.0049	0.53

±	f206%					Radiogenic - 2
		208Pb/206Pb	±	206Pb/238U	±	207Pb/235U
1.96E-05	0.18	0.035	0.001	0.0837	0.0008	0.67
4.58E-04	6.39	0.261	0.020	0.0714	0.0028	0.48
7.85E-04	5.15	0.289	0.033	0.0838	0.0072	0.79
9.42E-05	0.75	0.149	0.005	0.0843	0.0021	0.68
3.63E-04	5.38	0.180	0.015	0.0830	0.0021	0.71
7.06E-04	6.35	0.180	0.028	0.0754	0.0023	0.63
3.19E-04	1.70	0.519	0.017	0.0840	0.0025	0.70
3.68E-04	5.16	0.233	0.015	0.0632	0.0021	0.49
2.00E-05	0.04	0.793	0.024	0.0853	0.0056	0.91
7.18E-04	19.11	1.175	0.041	0.0629	0.0029	0.38
5.39E-04	9.37	0.532	0.044	0.0896	0.0023	0.68
2.86E-04	1.53	0.869	0.021	0.0831	0.0050	0.73
9.19E-05	0.43	0.529	0.008	0.0848	0.0031	0.71
1.89E-04	2.25	0.195	0.010	0.0838	0.0027	0.65
3.67E-04	2.64	0.353	0.017	0.0780	0.0021	0.60
4.96E-04	4.13	1.277	0.032	0.0794	0.0059	0.57
4.05E-04	4.35	0.259	0.017	0.0820	0.0018	0.68
1.92E-04	2.82	0.200	0.009	0.0767	0.0022	0.60
8.27E-04	7.60	0.045	0.034	0.0797	0.0044	0.58
5.68E-04	17.00	0.517	0.026	0.0811	0.0038	0.61
1.00E-03	7.09	0.825	0.058	0.0798	0.0032	0.50
6.79E-04	9.03	0.532	0.034	0.0600	0.0029	0.32
1.18E-03	9.44	0.964	0.070	0.0884	0.0058	0.89
1.09E-03	6.29	2.010	0.085	0.0818	0.0070	0.49
2.05E-04	1.50	0.440	0.012	0.0826	0.0036	0.69
1.47E-03	17.26	1.485	0.102	0.0796	0.0052	0.15
8.79E-04	9.82	0.424	0.041	0.0840	0.0059	0.94
2.14E-04	4.15	0.620	0.010	0.0844	0.0011	0.72
3.18E-05	0.47	0.084	0.002	0.0855	0.0012	0.67
8.16E-05	1.26	0.136	0.004	0.0851	0.0015	0.62
1.39E-04	1.90	0.134	0.007	0.0834	0.0014	0.62
2.45E-04	2.13	0.349	0.012	0.0795	0.0021	0.60
1.86E-04	1.49	0.572	0.014	0.0829	0.0022	0.73
2.00E-05	0.04	0.340	0.008	0.0823	0.0019	0.70

5.70E-05	0.22	0.849	0.017	0.0831	0.0033	0.79
6.50E-04	17.71	0.711	0.031	0.0772	0.0021	0.39
6.05E-04	3.47	1.224	0.060	0.0998	0.0035	1.07

Total 208 /206	**% err**	**7-corr %com 206**	**7-corr 208Pb* /206Pb***	**% err**	**ppm U**	**ppm Th**
1.12	2.1	2.24	1.1	2.2	34	104
1.93	2.3	3.65	1.93	2.4	22	106
1.7	2.8	2.98	1.69	2.9	15	69
0.86	2.5	5.46	0.79	3.7	30	66
0.67	3.2	1.1	0.66	3.4	26	49
1.06	4.6	1.02	1.04	4.7	30	84
0.23	0.8	0.09	0.23	1.3	984	601
1.21	2.5	8.99	1.13	3.1	25	74
0.34	2.1	-0.18	0.35	2.2	89	86
0.78	4.2	1.58	0.75	4.5	13	31
0.21	1.6	0.05	0.21	2.1	226	132
~~0.27~~	~~1.1~~	~~0.08~~	~~0.27~~	~~1.3~~	~~379~~	~~286~~
0.94	2.5	1.55	0.93	2.6	30	77
0.87	3.2	0.31	0.86	3.3	20	47
0.37	3.1	0.38	0.36	3.4	40	39
0.73	2.9	0.85	0.72	3	33	68
0.93	2.1	0.48	0.92	2.2	42	107
1.79	1.9	0.22	1.79	1.9	33	163
0.49	3.1	0.58	0.48	3.6	32	45
0.72	2	0.88	0.7	2	57	115
1.01	2.1	0.01	1.01	2.1	37	109
0.81	2.3	0.25	0.8	2.4	44	98
0.29	5.2	1.65	0.26	7.3	152	114
0.37	6.2	0.5	0.36	6.5	49	51
0.78	2.1	0.84	0.77	2.2	48	103
0.94	2.3	0.25	0.94	2.3	40	104
0.58	2.3	0.33	0.58	2.4	58	90
0.56	2.4	0.71	0.55	2.6	46	69
0.81	5.5	1.14	0.79	5.7	53	115
0.63	2.9	1.31	0.61	3.1	35	59
0.4	2.4	0.49	0.39	2.6	69	73
0.55	3.3	1.17	0.54	3.5	28	41
0.09	3.9	0.12	0.09	5.5	117	30
0.7	1.5	0.46	0.7	1.6	118	222
2.06	1.8	0.7	2.06	1.8	35	192
2.54	1	0.38	2.54	1	86	596
2.97	1	0.12	2.97	1	86	700
2.59	1.8	1.07	2.6	1.8	263	1920
1.65	0.7	0.2	1.65	0.7	298	1341

0.92	3	1.73	0.9	3.1	23	57
0.09	14.7	0.12	0.09	15.6	738	140
0.11	2.2	-0.06	0.11	2.8	746	238
0.45	4.3	0.36	0.44	4.4	121	151
1.27	3.5	1.48	1.26	3.7	12	45
0.91	3.3	17.26	0.66	5.7	22	38
0.84	3	14.94	0.62	5.6	26	45
0.87	3.1	16.62	0.63	5.4	25	44
0.54	2.5	9.36	0.38	4.2	56	57
0.9	3.1	17.38	0.65	5.4	22	42
0.67	2.8	11.95	0.47	4.8	41	52
0.84	3.1	17.48	0.57	6.4	22	36
0.29	3.1	4.04	0.21	5	65	38
0.37	2.6	3.66	0.31	3.6	63	53
0.98	3.5	12.44	0.82	5	16	38
0.69	2.8	9.93	0.53	4.5	36	52
0.96	3	19.37	0.68	5.5	22	41
0.69	3.8	7.34	0.57	5.1	19	27
1.36	2.9	39.45	0.88	8.6	19	46
0.92	3.1	13.26	0.74	4.5	23	45
1.05	3.2	20.94	0.77	6.2	16	36
0.82	2.8	13.41	0.63	4.5	30	52
0.98	3.2	17.35	0.74	5.3	21	41
0.95	3.2	17	0.71	5.6	22	42
0.47	2.1	5.62	0.38	3.1	94	98
0.93	2.9	14.29	0.73	4.5	26	53
1.4	3.4	20.25	1.23	5	13	40
0.87	3.1	15.48	0.65	5.2	23	42
0.79	3	15.1	0.56	5.3	32	48
0.55	2.6	8.42	0.41	4.1	49	53
1.02	3.2	18.82	0.77	5.4	21	42
0.63	2.6	9.69	0.47	4.1	49	59
0.37	2.9	3.37	0.31	3.9	61	50
0.64	8.8	9.96	0.48	13.2	35	51
0.7	2.9	14.15	0.47	5.4	33	43
0.78	2.6	8.87	0.66	3.5	38	67
0.5	2.8	7.97	0.36	4.5	46	48
0.82	6.6	11.56	0.65	9.6	14	28

/232Th	238U/206Pb		207Pb/206Pb		common Pb	206Pb
+/-1 RSE	ratio	+/-1 std err	ratio	+/-1 std err	at age of zirc	age (Ma)
6.2140	11.8015	0.2949	0.1813	0.0105	0.8713	524.32
6.1043	10.6043	0.2207	0.1114	0.0054	0.8713	580.93
5.3432	12.4515	0.2481	0.1105	0.0057	0.8713	497.98
5.6280	11.8214	0.2615	0.0957	0.0077	0.8713	523.48
7.9061	11.1997	0.4973	0.1721	0.0166	0.8713	551.33
10.5624	10.1240	0.4610	0.2388	0.0214	0.8713	607.23
6.4616	11.2180	0.5089	0.2063	0.0212	0.8713	550.46
7.1589	7.9090	0.4155	0.3569	0.0519	0.8713	767.52
7.3917	10.6683	0.6849	0.1302	0.0222	0.8713	577.59
5.5382	6.0510	0.1308	0.4985	0.0139	0.8713	985.95
6.1685	4.2523	0.1517	0.5584	0.0207	0.8713	1361.53
9.1215	6.3772	0.2354	0.3934	0.0276	0.8713	939.01
5.5077	11.3122	0.3137	0.1681	0.0119	0.8713	546.07
5.4925	12.1159	0.3621	0.0836	0.0086	0.8713	511.24
6.6468	5.6629	0.2703	0.4013	0.0313	0.8713	1048.32
6.4193	8.5968	0.2416	0.2861	0.0166	0.8713	709.36
6.5319	7.1308	0.2279	0.3248	0.0174	0.8713	846.00
8.0933	6.0322	0.2144	0.4738	0.0264	0.8713	988.79
8.6399	7.8015	0.2745	0.3492	0.0247	0.8713	777.48
6.9150	3.0367	0.1145	0.6444	0.0313	0.8713	1834.99
5.2417	11.0659	0.2281	0.1033	0.0056	0.8713	557.71
5.1845	10.6156	0.2331	0.1194	0.0052	0.8713	580.34
5.0381	12.1566	0.1772	0.0776	0.0015	0.8713	509.60
8.1805	5.8950	0.4288	0.4965	0.0322	0.8713	1010.11
5.4894	0.8053	0.0239	0.8187	0.0192	0.8713	5204.13
5.9597	9.7540	0.2340	0.1867	0.0112	0.8713	629.17
5.7669	9.6413	0.2445	0.1944	0.0120	0.8713	636.17
5.6864	8.8865	0.2777	0.2220	0.0155	0.8713	687.43
8.5092	1.7432	0.1251	0.7019	0.0160	0.8713	2922.76
7.4690	0.9960	0.0423	0.7522	0.0204	0.8713	4481.28
5.4536	12.1075	0.2789	0.1521	0.0071	0.8713	511.58
5.2094	12.4084	0.2160	0.1240	0.0050	0.8713	499.65
5.8204	10.8231	0.2937	0.1368	0.0088	0.8713	569.69
5.6853	4.8230	0.0986	0.5685	0.0124	0.8713	1214.62
6.1902	10.8528	0.3661	0.1808	0.0210	0.8713	568.19
6.9305	7.3540	0.4171	0.4031	0.0222	0.8713	821.89
6.4004	11.8889	0.3281	0.0847	0.0070	0.8713	520.62
5.7192	5.5406	0.1262	0.4751	0.0135	0.8713	1069.62
6.0981	7.5674	0.2764	0.3213	0.0250	0.8713	800.09
5.8519	5.8628	0.1478	0.4449	0.0150	0.8713	1015.24
6.6823	8.8182	0.3622	0.2028	0.0244	0.8713	692.48
5.1076	10.4879	0.1717	0.2720	0.0060	0.8713	587.09
5.1949	10.3543	0.1839	0.2705	0.0065	0.8713	594.33
5.5701	10.7526	0.2680	0.2081	0.0106	0.8713	573.26
5.3242	9.7533	0.2141	0.2459	0.0089	0.8713	629.22
7.2640	11.4704	0.3593	0.1795	0.0111	0.8713	538.84
7.5395	11.0200	0.3815	0.1803	0.0139	0.8713	559.94
6.2626	9.5995	0.2588	0.2633	0.0135	0.8713	638.81

6.7995	10.0738	0.2543	0.1818	0.0095	0.8713	610.11
8.1131	8.5214	0.2583	0.2566	0.0139	0.8713	715.30
6.0715	5.2271	0.1504	0.5361	0.0207	0.8713	1128.47
6.1569	6.8418	0.1922	0.4318	0.0172	0.8713	879.40
6.2336	6.0190	0.1708	0.4547	0.0162	0.8713	990.80
6.8680	11.8361	0.2920	0.1221	0.0073	0.8713	522.85
5.8917	11.7789	0.2931	0.1236	0.0072	0.8713	525.29
7.6521	10.9610	0.3751	0.1234	0.0109	0.8713	562.82
6.2358	10.9010	0.3197	0.1075	0.0068	0.8713	565.79
6.1933	11.1637	0.2397	0.1718	0.0073	0.8713	553.03
6.0542	9.6198	0.2027	0.2431	0.0099	0.8713	637.53
6.8322	9.8049	0.3178	0.1744	0.0148	0.8713	626.06
5.3281	10.9553	0.2324	0.1812	0.0071	0.8713	563.10
5.2938	10.7173	0.2386	0.1582	0.0077	0.8713	575.06
6.1916	10.6168	0.3759	0.2385	0.0157	0.8713	580.27
5.9106	9.5110	0.2747	0.2940	0.0148	0.8713	644.47
6.2367	9.2498	0.2316	0.2880	0.0123	0.8713	661.76
6.4764	8.2152	0.3204	0.3165	0.0183	0.8713	740.49
6.3583	9.3755	0.2758	0.2817	0.0146	0.8713	653.33
6.7842	10.6547	0.2959	0.1569	0.0097	0.8713	578.30
5.7034	8.6849	0.1957	0.2338	0.0102	0.8713	702.54
5.9377	11.2234	0.2825	0.1429	0.0087	0.8713	550.21
5.6604	9.7367	0.2310	0.1989	0.0091	0.8713	630.23
5.3780	9.8850	0.1734	0.2027	0.0058	0.8713	621.23
5.1528	9.8219	0.1586	0.2341	0.0060	0.8713	625.03
5.9622	10.0219	0.2646	0.2441	0.0107	0.8713	613.13
6.7828	8.9054	0.2810	0.2861	0.0186	0.8713	686.04
6.0684	7.6902	0.2022	0.3315	0.0143	0.8713	788.06
6.7667	8.6533	0.2423	0.2731	0.0185	0.8713	704.97
5.5665	10.7925	0.2421	0.1767	0.0071	0.8713	571.23
6.9292	8.9098	0.3385	0.2309	0.0172	0.8713	685.72
8.0954	8.9351	0.3522	0.2225	0.0188	0.8713	683.88
6.0603	10.0737	0.2726	0.1831	0.0096	0.8713	610.12
5.3618	10.1507	0.1946	0.1914	0.0064	0.8713	605.70
5.6053	10.4312	0.2128	0.1328	0.0059	0.8713	590.14
5.5589	11.0251	0.2328	0.1500	0.0066	0.8713	559.69
5.3476	10.3348	0.1979	0.1471	0.0054	0.8713	595.40
5.1667	11.4259	0.1995	0.1117	0.0035	0.8713	540.86
9.0198	7.1053	0.4072	0.4866	0.0433	0.8634	848.84
7.6808	6.1670	0.2782	0.5665	0.0375	0.8634	968.74
8.4308	5.7744	0.4052	0.5736	0.0459	0.8634	1029.60
7.2318	4.5937	0.2217	0.5743	0.0317	0.8634	1269.66
6.4633	5.0244	0.1806	0.6003	0.0289	0.8634	1170.10
6.7488	4.1628	0.1535	0.6148	0.0297	0.8634	1387.86
7.8890	4.3968	0.1860	0.6219	0.0372	0.8634	1321.05
7.2470	3.6909	0.1469	0.6431	0.0335	0.8634	1545.55
6.6374	3.7829	0.1217	0.6436	0.0262	0.8634	1512.06
14.1186	3.4295	0.2828	0.6440	0.0722	0.8634	1649.47
6.5004	2.7093	0.1124	0.6515	0.0308	0.8634	2025.19
6.6625	3.0086	0.0964	0.6523	0.0250	0.8634	1849.93

8.6903	5.2251	0.2547	0.6530	0.0564	0.8634	1128.87
7.0640	3.6555	0.1577	0.6584	0.0463	0.8634	1558.84
8.2696	4.1393	0.2408	0.6586	0.0520	0.8634	1394.95
10.8016	2.8764	0.2083	0.6773	0.0680	0.8634	1923.37
7.8936	2.9316	0.1215	0.6823	0.0354	0.8634	1892.02
7.1033	2.9995	0.1264	0.6907	0.0466	0.8634	1854.78
7.5145	3.8579	0.1925	0.7028	0.0457	0.8634	1485.80
6.3818	3.3078	0.1173	0.7182	0.0246	0.8634	1702.80
8.8187	4.3012	0.2890	0.7340	0.0616	0.8634	1347.55
6.8168	2.5401	0.1089	0.7349	0.0331	0.8634	2139.92
5.4616	2.3715	0.0561	0.7590	0.0177	0.8634	2268.04
9.9114	2.1863	0.1159	0.7648	0.0388	0.8634	2428.02
6.3701	1.2877	0.0495	0.8241	0.0317	0.8634	3704.59
30.9614	12.5422	1.0111	0.1684	0.0311	0.8645	494.51
12.1975	12.3226	0.4470	0.2270	0.0165	0.8645	502.99
29.5742	10.8990	0.4194	0.2349	0.0167	0.8645	565.89
8.4536	11.5757	0.3339	0.2379	0.0167	0.8645	534.14
8.5869	11.8165	0.3222	0.2662	0.0141	0.8645	523.68
27.0211	10.6452	0.2893	0.3167	0.0145	0.8645	578.79
12.8430	9.6343	0.2998	0.3234	0.0149	0.8645	636.61
6.8311	10.4765	0.2431	0.3270	0.0139	0.8645	587.70
47.9134	7.7686	0.6683	0.3280	0.0515	0.8645	780.58
12.2724	10.2539	0.5202	0.3399	0.0410	0.8645	599.88
16.7127	10.6895	0.8162	0.3428	0.0511	0.8645	576.49
17.5500	9.6826	0.4276	0.3506	0.0310	0.8645	633.59
14.2101	9.5129	0.4700	0.3525	0.0276	0.8645	644.34
18.3486	7.7408	0.3770	0.4062	0.0430	0.8645	783.22
9.1040	8.5337	0.3259	0.4135	0.0244	0.8645	714.33
17.7819	9.8048	0.8099	0.4139	0.0804	0.8645	626.07
6.1136	7.9479	0.1618	0.4491	0.0119	0.8645	763.97
12.3949	5.8493	0.3051	0.4566	0.0374	0.8645	1017.40
10.0621	7.9343	0.4181	0.4686	0.0391	0.8645	765.21
13.3685	9.7569	0.5680	0.4784	0.0527	0.8645	629.00
6.7416	6.9666	0.2158	0.4900	0.0250	0.8645	864.66
18.3804	7.0608	0.5500	0.5018	0.0655	0.8645	853.86
13.3984	7.0765	0.4546	0.5532	0.0547	0.8645	852.08
6.7456	5.4855	0.1997	0.5533	0.0281	0.8645	1079.53
36.2996	4.6604	0.3559	0.5670	0.1317	0.8645	1253.14
64.1252	2.7332	0.3248	0.5983	0.1347	0.8645	2009.94
8.4857	5.5138	0.1711	0.6050	0.0246	0.8645	1074.41
87.2434	4.5378	0.3719	0.6412	0.0713	0.8645	1283.83
1382.8155	3.9453	0.2791	0.6443	0.0624	0.8645	1456.33
7.3604	3.4495	0.1231	0.6523	0.0307	0.8645	1641.02
39.6568	4.8632	0.3245	0.6545	0.0654	0.8645	1205.47
16.4559	2.3544	0.2427	0.6621	0.1026	0.8645	2281.93
16.9243	2.8285	0.1853	0.6665	0.0527	0.8645	1951.51
19.9457	2.9364	0.1479	0.6924	0.0442	0.8645	1889.33
7.1797	3.1493	0.1209	0.6954	0.0310	0.8645	1777.68
8.5190	1.7065	0.0957	0.7129	0.0459	0.8645	2973.21
10.8429	1.5370	0.0822	0.7157	0.0450	0.8645	3230.62

10.6277	3.8043	0.1572	0.7170	0.0333	0.8645	1504.47
12.8092	4.1738	0.2036	0.7171	0.0570	0.8645	1384.57
8.2821	4.0473	0.1482	0.7204	0.0332	0.8645	1423.39
6.9287	1.9841	0.0586	0.7246	0.0224	0.8645	2630.98
12.2901	3.0722	0.1278	0.7366	0.0399	0.8645	1816.52
40.3267	0.4140	0.0976	0.7375	0.1100	0.8645	7918.03
408.2690	1.3739	0.1020	0.7497	0.0581	0.8645	3525.49
7.5056	3.7784	0.1958	0.7590	0.0547	0.8645	1513.66
33.8527	1.3883	0.0622	0.7679	0.0354	0.8645	3497.27
8.7573	1.8272	0.0686	0.7700	0.0304	0.8645	2813.83
6.3200	2.2218	0.0825	0.7763	0.0316	0.8645	2395.64
15.5531	0.8615	0.0371	0.7784	0.0291	0.8645	4966.84
8.1577	3.0225	0.1965	0.7814	0.0766	0.8645	1842.53
25.6853	3.5883	0.1638	0.7849	0.0461	0.8645	1584.75
12.9086	2.5638	0.1358	0.7883	0.0501	0.8645	2123.03
48.3412	1.5144	0.0652	0.7973	0.0364	0.8645	3268.51
16.7734	1.5167	0.1021	0.8015	0.0599	0.8645	3264.49
113.7783	1.0847	0.0521	0.8017	0.0385	0.8645	4211.51
128.3135	1.7641	0.1600	0.8055	0.0595	0.8645	2894.90
11.6671	1.0359	0.0712	0.8164	0.0468	0.8645	4355.68
13.1373	2.3469	0.2022	0.8216	0.0901	0.8645	2288.06
14.3794	2.1967	0.1135	0.8280	0.0495	0.8645	2418.48
83.2041	0.8025	0.0623	0.8318	0.0529	0.8645	5216.32
41.7141	1.3593	0.1015	0.8341	0.0731	0.8645	3554.45
56.6342	2.3825	0.1876	0.8397	0.0830	0.8645	2259.27
55.5538	1.4121	0.1079	0.8432	0.0789	0.8645	3451.48
23.3226	0.3917	0.0260	0.8500	0.0369	0.8645	8172.91
202.5970	0.5978	0.0452	0.8549	0.0475	0.8645	6337.94
69.5149	0.3671	0.0291	0.9304	0.0470	0.8645	8475.22
8.9098	8.0637	0.2394	0.4713	0.0227	0.8634	753.62
14.8775	8.7230	0.4771	0.4058	0.0373	0.8645	699.64
8.9141	6.2823	0.2197	0.5380	0.0318	0.8645	952.20
6.7366	6.8059	0.1435	0.5038	0.0133	0.8645	883.74
9.0675	6.9423	0.2121	0.4764	0.0196	0.8645	867.50
7.4075	5.6830	0.1594	0.5516	0.0199	0.8645	1044.89
7.6597	6.7724	0.2218	0.4715	0.0218	0.8645	887.83
7.7714	4.0018	0.1431	0.6788	0.0236	0.8645	1437.91
11.1244	5.6784	0.2282	0.5417	0.0339	0.8693	1045.67
8.4253	5.2265	0.1746	0.5743	0.0264	0.8693	1128.59
5.7087	5.5279	0.1002	0.5456	0.0097	0.8693	1071.90
5.4426	5.1411	0.0866	0.5751	0.0095	0.8693	1145.76
11.0499	6.8383	0.2698	0.4497	0.0298	0.8693	879.82
8.1316	5.9491	0.1561	0.5128	0.0195	0.8693	1001.59
6.4187	4.0314	0.1037	0.6647	0.0202	0.8693	1428.42
5.8402	7.5955	0.1383	0.3856	0.0082	0.8693	797.31
7.3134	4.1060	0.1266	0.6490	0.0242	0.8693	1405.11
7.2848	4.6178	0.1196	0.5963	0.0158	0.8693	1263.64
6.3270	5.9996	0.1215	0.4839	0.0119	0.8693	993.79
15.1929	5.5900	0.1564	0.5157	0.0286	0.8693	1060.91
7.7879	3.7418	0.1219	0.6757	0.0248	0.8693	1526.84

8.3623	3.4009	0.1112	0.7095	0.0240	0.8693	1661.67
9.3928	6.2435	0.2133	0.4612	0.0225	0.8693	957.71
7.3973	6.3941	0.1642	0.4481	0.0157	0.8693	936.70
12.4032	6.1059	0.2649	0.4699	0.0297	0.8693	977.73
6.0082	7.2501	0.1375	0.3766	0.0089	0.8693	832.94
6.8998	6.0427	0.1503	0.4679	0.0153	0.8693	987.21
8.8063	6.8030	0.2065	0.4082	0.0208	0.8693	884.09
6.9273	4.4563	0.1064	0.5975	0.0170	0.8693	1305.08
8.8002	6.3365	0.1928	0.4354	0.0252	0.8693	944.63
10.3528	4.0629	0.1884	0.6234	0.0362	0.8693	1418.50
11.2684	3.4267	0.1385	0.6868	0.0388	0.8693	1650.63
8.5123	4.8617	0.2066	0.5441	0.0316	0.8693	1205.82
7.2289	2.9436	0.0804	0.7372	0.0224	0.8693	1885.31
7.6284	5.1781	0.1469	0.5071	0.0197	0.8693	1138.26
7.5373	5.6327	0.1230	0.4659	0.0168	0.8693	1053.49
8.2192	3.7807	0.1178	0.6342	0.0250	0.8693	1512.83
6.7959	3.5044	0.0952	0.6563	0.0209	0.8693	1618.27
7.5765	4.0713	0.1140	0.5869	0.0181	0.8693	1415.86
6.7981	3.2290	0.0913	0.6809	0.0224	0.8693	1739.20
7.7503	3.1316	0.1052	0.6914	0.0274	0.8693	1786.43
6.4651	3.1920	0.0765	0.6736	0.0189	0.8693	1756.86
9.3735	2.9748	0.1205	0.7015	0.0354	0.8693	1868.15
6.9313	3.7946	0.1274	0.6010	0.0248	0.8693	1507.90
9.8126	3.8428	0.1549	0.5912	0.0290	0.8693	1490.99
8.0815	3.2354	0.0807	0.6448	0.0189	0.8693	1736.17
6.7142	2.9529	0.0782	0.6785	0.0248	0.8693	1880.19
18.4266	3.4155	0.2997	0.6142	0.0746	0.8693	1655.43
6.9231	3.3969	0.1100	0.6145	0.0305	0.8693	1663.41
8.5882	3.1985	0.1110	0.6345	0.0315	0.8693	1753.72
7.0887	2.5210	0.0745	0.7207	0.0243	0.8693	2153.68
7.4963	3.1032	0.0779	0.6245	0.0181	0.8693	1800.72
10.4266	2.6943	0.1097	0.6774	0.0343	0.8693	2034.85
6.4020	2.7847	0.0610	0.6524	0.0161	0.8693	1977.91
9.3371	2.9825	0.1125	0.5962	0.0278	0.8693	1863.96
11.3677	2.0833	0.0731	0.7272	0.0301	0.8693	2527.25
8.4077	2.0533	0.0711	0.7341	0.0288	0.8693	2557.77
7.2435	0.3360	0.0078	0.8478	0.0105	0.8645	8897.73
6.1855	0.1849	0.0040	0.8598	0.0053	0.8645	11975.02
6.2909	0.2650	0.0073	0.8618	0.0081	0.8645	10075.76
9.7430	7.4645	0.3097	0.4465	0.0262	0.8645	810.46
10.4434	4.3822	0.2408	0.6389	0.0343	0.8645	1325.02
7.4903	5.2618	0.1513	0.5684	0.0183	0.8645	1121.63
7.1998	5.1286	0.1236	0.5738	0.0169	0.8645	1148.32
9.7408	6.2920	0.1827	0.4824	0.0188	0.8645	950.83
6.4091	3.1139	0.0561	0.6795	0.0103	0.8645	1795.27
9.7613	2.6350	0.1169	0.7328	0.0382	0.8645	2074.01
9.1949	2.5212	0.0775	0.7362	0.0200	0.8645	2153.53
7.8079	2.3266	0.0739	0.7572	0.0295	0.8645	2304.84
9.0245	2.6893	0.0925	0.6740	0.0268	0.8645	2038.05
16.2252	2.2173	0.1639	0.7219	0.0493	0.8645	2399.65

8.3631	1.7017	0.0616	0.8398	0.0337	0.8645	2979.94
7.7371	2.0312	0.1058	0.7477	0.0314	0.8645	2580.73
5.9727	1.6745	0.0359	0.7974	0.0140	0.8645	3018.49
6.5845	1.2679	0.0464	0.8298	0.0103	0.8645	3748.45
6.3456	1.0533	0.0218	0.8234	0.0140	0.8645	4303.14
123.3381	0.4825	0.0579	0.8228	0.0816	0.8645	7235.87
24.0641	7.1542	0.2030	0.3910	0.0171	0.8715	843.41
54.8488	5.4749	0.2836	0.4100	0.0317	0.9155	1081.44
31.8963	6.3248	0.2235	0.4434	0.0240	0.9043	946.25
31.6614	4.9351	0.2459	0.4856	0.0290	0.9248	1189.43
29.1189	4.5956	0.2127	0.5093	0.0339	0.9318	1269.19
19.2913	5.4315	0.1500	0.5342	0.0197	0.9162	1089.40
87.9796	4.0807	0.3548	0.6263	0.0879	0.9448	1412.91
105.0964	1.7005	0.1848	0.7187	0.0885	1.1073	2981.52
85.8072	2.4493	0.1859	0.7390	0.0687	1.0239	2207.02
52.1698	2.5979	0.1902	0.7941	0.0764	1.0125	2099.23
118.0800	1.2150	0.4762	0.8059	0.3326	1.1699	3871.08
111.2464	0.0963	0.0206	0.8594	0.0876	4358.8654	15679.92
255.5497	0.0852	0.0150	0.8661	0.0754	7669.7763	16404.34

04Pb corrected					**Tota**	
±	**238U/206Pb**	**±**	**207Pb/206Pb**	**±**	**238U/206Pb**	**±**
0.06	14.32	0.45	0.0639	0.0060	13.56	0.42
0.09	15.97	0.62	0.0389	0.0097	14.18	0.53
0.13	14.98	0.91	0.0598	0.0133	13.56	0.79
0.29	14.84	1.74	0.0840	0.0295	11.63	1.29
0.18	14.36	0.82	0.0659	0.0187	12.98	0.69
0.13	14.81	0.47	0.0523	0.0140	12.63	0.35
0.17	14.88	0.70	0.0584	0.0188	12.90	0.53
0.12	14.58	0.70	0.0676	0.0123	12.91	0.60
0.25	14.23	0.81	0.0731	0.0261	12.16	0.57
-	17.13	1.33	-	-	12.66	0.83
0.29	13.77	0.87	0.1028	0.0289	11.79	0.63
0.11	14.62	0.44	0.0591	0.0112	13.62	0.38
0.10	14.52	0.49	0.0539	0.0110	12.89	0.40
0.21	14.85	0.70	0.0316	0.0233	12.52	0.49
-	16.69	0.90	-	-	13.52	0.56
0.32	15.60	1.41	0.0746	0.0375	12.47	0.95
0.23	14.39	0.81	0.0443	0.0248	12.19	0.56
0.11	14.26	0.44	0.0625	0.0117	13.26	0.37
0.52	14.76	1.46	0.0090	0.0583	8.70	0.50
-	16.20	1.72	-	-	9.95	0.64
-	15.31	1.25	-	-	9.22	0.56
0.40	14.55	1.20	0.0507	0.0433	12.13	0.76
0.10	14.58	0.62	0.0518	0.0103	13.44	0.54
0.20	14.24	0.98	0.0701	0.0210	12.47	0.79
-	16.13	2.72	-	-	10.22	1.08
0.06	14.54	0.28	0.0681	0.0067	13.97	0.26
0.32	15.74	0.93	0.0794	0.0374	13.22	0.48

-	16.05	1.09	-	-	11.46	0.52
0.12	15.05	0.61	0.0388	0.0134	13.39	0.50
1.49	12.47	1.83	0.1313	0.1380	9.74	1.31
0.11	14.80	0.50	0.0621	0.0117	13.06	0.40
0.21	14.47	0.55	0.0878	0.0222	13.10	0.41
0.24	14.78	0.82	0.0644	0.0264	12.23	0.55
-	16.31	1.29	-	-	11.60	0.58
0.10	14.03	0.42	0.0649	0.0105	12.97	0.36
0.13	15.18	0.79	0.0508	0.0140	13.71	0.67
0.15	14.94	0.81	0.0491	0.0163	13.65	0.69
0.18	14.42	1.11	0.0553	0.0183	12.80	0.94

04Pb corrected						**Tota**
±	**238U/206Pb**	**±**	**207Pb/206Pb**	**±**	**238U/206Pb**	**±**
0.01	11.94	0.12	0.0578	0.0005	11.92	0.12
0.08	14.01	0.56	0.0493	0.0082	13.12	0.51
0.17	11.94	1.12	0.0688	0.0137	11.32	1.04
0.03	11.87	0.32	0.0588	0.0018	11.78	0.31
0.07	12.05	0.32	0.0620	0.0064	11.40	0.29
0.13	13.26	0.38	0.0609	0.0116	12.42	0.31
0.07	11.91	0.35	0.0602	0.0054	11.71	0.34
0.07	15.82	0.33	0.0560	0.0063	15.00	0.31
0.09	11.72	0.82	0.0771	0.0056	11.71	0.82
0.12	15.90	0.82	0.0437	0.0143	12.86	0.62
0.14	11.16	0.31	0.0553	0.0117	10.11	0.26
0.09	12.03	0.76	0.0637	0.0061	11.84	0.75
0.04	11.79	0.45	0.0607	0.0021	11.74	0.44
0.05	11.93	0.41	0.0561	0.0035	11.67	0.40
0.07	12.81	0.36	0.0559	0.0062	12.48	0.34
0.12	12.60	0.99	0.0517	0.0104	12.08	0.94
0.08	12.20	0.28	0.0606	0.0069	11.67	0.26
0.04	13.04	0.38	0.0569	0.0034	12.68	0.37
0.18	12.54	0.69	0.0524	0.0160	11.59	0.61
0.13	12.33	0.52	0.0545	0.0108	10.23	0.41
0.18	12.54	0.55	0.0452	0.0169	11.65	0.45
0.13	16.67	0.45	0.0386	0.0118	15.16	0.38
0.27	11.32	0.79	0.0733	0.0215	10.25	0.67
0.23	12.23	1.11	0.0433	0.0203	11.46	1.01
0.05	12.10	0.58	0.0607	0.0038	11.92	0.56
0.29	12.56	0.92	0.0137	0.0274	10.39	0.67
0.19	11.91	0.91	0.0810	0.0154	10.74	0.80
0.05	11.84	0.16	0.0618	0.0040	11.35	0.15
0.02	11.69	0.17	0.0569	0.0010	11.64	0.17
0.02	11.75	0.22	0.0527	0.0015	11.60	0.22
0.04	11.99	0.22	0.0540	0.0033	11.76	0.21
0.05	12.58	0.33	0.0551	0.0044	12.31	0.32
0.05	12.06	0.35	0.0642	0.0044	11.88	0.34
0.03	12.14	0.31	0.0618	0.0016	12.14	0.31

0.06	12.03	0.53	0.0688	0.0040	12.01	0.53
0.13	12.96	0.33	0.0366	0.0121	10.67	0.23
0.15	10.02	0.39	0.0779	0.0107	9.67	0.36

232Th /238U	% err	Total 206Pb /238U	% err	Age S-K com Pb	C-Pb 206 /204	C-Pb 207 /206
3.18	1.2	0.0833	1.8	505	17.91	0.87
5.09	1.4	0.0807	2.2	483	17.95	0.868
4.78	1.7	0.0864	4	519	17.89	0.871
2.29	2.1	0.0908	1.9	531	17.87	0.872
1.97	1.5	0.0883	3.4	540	17.85	0.873
2.87	1.3	0.0842	1.9	516	17.89	0.871
0.63	1.4	0.0834	1.7	516	17.89	0.871
3.06	1.4	0.0901	2	508	17.9	0.87
1	0.9	0.085	1.4	527	17.87	0.872
2.37	3.5	0.0847	2.7	516	17.89	0.871
0.6	0.6	0.0863	1.1	533	17.86	0.872
~~0.78~~	~~1.3~~	~~0.0858~~	~~1.3~~	~~530~~	~~17.87~~	~~0.872~~
2.63	1.3	0.0852	1.9	519	17.89	0.871
2.41	1.6	0.0838	2.3	517	17.89	0.871
1	1.3	0.085	1.7	524	17.88	0.871
2.15	1.3	0.0834	2	512	17.9	0.871
2.63	1.1	0.0829	1.7	511	17.9	0.871
5.06	1.2	0.0836	1.9	517	17.89	0.871
1.45	1.3	0.0851	2.9	524	17.88	0.871
2.09	0.9	0.0836	1.5	513	17.9	0.871
3.02	1.8	0.0857	1.8	530	17.87	0.872
2.28	1.1	0.0849	2.5	524	17.88	0.872
0.78	0.7	0.084	1.2	512	17.9	0.871
1.09	5.5	0.0829	1.6	511	17.9	0.871
2.21	1	0.0822	1.6	505	17.91	0.87
2.7	1.8	0.0839	1.8	518	17.89	0.871
1.6	1	0.0807	1.6	499	17.92	0.87
1.55	1.1	0.0822	1.6	506	17.91	0.87
2.24	1	0.0833	2.1	510	17.9	0.87
1.75	3.4	0.0793	1.9	486	17.94	0.869
1.08	1	0.085	1.5	524	17.88	0.871
1.49	1.5	0.0814	2	499	17.92	0.87
0.26	1.2	0.0845	1.3	522	17.88	0.871
1.95	0.7	0.0834	1.3	514	17.89	0.871
5.68	1.1	0.0805	2.6	495	17.93	0.869
7.15	0.7	0.0843	1.4	520	17.89	0.871
8.37	0.7	0.0836	1.4	517	17.89	0.871
7.55	0.7	0.0861	2.3	527	17.87	0.872
4.64	1.4	0.083	1.2	513	17.9	0.871

2.6	1.5	0.0828	2.2	504	17.91	0.87
0.2	0.5	0.0848	1.9	524	17.88	0.872
0.33	0.8	0.0866	1.3	535	17.86	0.872
1.29	1.8	0.0824	1.3	509	17.9	0.87
3.74	2	0.0854	2.8	521	17.88	0.871
1.82	1.68	0.079	2.3	409	18.06	0.863
1.79	1.51	0.081	2.1	427	18.04	0.865
1.83	1.57	0.079	2.2	411	18.06	0.863
1.04	1.1	0.075	1.6	423	18.04	0.864
1.97	1.55	0.082	2.2	420	18.05	0.864
1.32	1.26	0.075	2.7	410	18.06	0.863
1.68	1.63	0.084	2.2	434	18.03	0.865
0.61	2.88	0.072	1.5	431	18.03	0.865
0.86	1.03	0.07	1.5	420	18.05	0.864
2.54	1.81	0.079	2.5	430	18.03	0.865
1.52	1.27	0.075	1.8	424	18.04	0.864
1.91	1.59	0.077	2.2	387	18.1	0.862
1.53	1.71	0.073	2.4	422	18.04	0.864
2.54	1.86	0.112	2.4	423	18.04	0.864
2.03	1.5	0.075	2.1	406	18.07	0.863
2.3	1.78	0.092	2.4	452	18	0.866
1.78	1.4	0.079	2	427	18.04	0.864
2.03	1.72	0.082	2.3	422	18.04	0.864
2	1.64	0.082	2.2	427	18.04	0.864
1.08	0.88	0.076	2	447	18	0.866
2.06	1.42	0.076	3.6	405	18.07	0.863
3.33	1.92	0.084	2.7	416	18.05	0.864
1.88	1.63	0.086	2.2	452	18	0.866
1.56	1.46	0.075	2.1	398	18.08	0.862
1.13	1.15	0.074	2.3	422	18.04	0.864
2.09	1.71	0.082	2.4	414	18.06	0.864
1.26	1.17	0.074	1.7	415	18.06	0.864
0.85	1.12	0.072	1.6	431	18.03	0.865
1.51	1.31	0.069	5.1	391	18.09	0.862
1.37	2.46	0.078	1.9	417	18.05	0.864
1.83	1.18	0.073	1.8	417	18.05	0.864
1.07	1.2	0.072	1.7	415	18.05	0.864
2.03	1.92	0.073	2.7	406	18.07	0.863

/238U	208Pb/232Th	
+/-1 ster	age (Ma)	+/-1 ster
13.10	814.57	50.62
12.09	702.17	42.86
9.92	565.95	30.24
11.58	561.29	31.59
24.48	712.82	56.36
27.65	860.64	90.90
24.97	595.86	38.50
40.32	815.62	58.39
37.08	632.44	46.75
21.31	3120.60	172.83
48.58	4171.80	257.34
34.66	3702.34	337.71
15.14	588.14	32.39
15.28	577.25	31.71
50.05	937.20	62.29
19.94	1239.97	79.60
27.04	1508.92	98.56
35.14	3357.46	271.73
27.36	2053.25	177.40
69.16	3894.24	269.29
11.50	612.13	32.09
12.74	604.51	31.34
7.43	596.60	30.06
73.48	1220.35	99.83
154.21	8824.02	484.39
15.10	664.71	39.61
16.14	702.26	40.50
21.48	725.43	41.25
209.79	3986.81	339.24
190.20	6676.21	498.64
11.78	584.03	31.85
8.70	577.05	30.06
15.46	620.04	36.09
24.84	1651.66	93.90
19.17	652.68	40.40
46.62	1131.05	78.39
14.37	558.64	35.76
24.35	1298.11	74.24
29.22	912.35	55.64
25.59	1142.60	66.86
28.44	736.45	49.21
9.61	714.80	36.51
10.55	723.44	37.58
14.29	659.08	36.71
13.81	751.02	39.99
16.88	784.99	57.02
19.38	725.50	54.70
17.22	1142.24	71.53

15.40	727.37	49.46
21.68	984.76	79.89
32.46	1752.40	106.40
24.71	1309.97	80.65
28.11	1486.40	92.66
12.90	623.47	42.82
13.07	679.39	40.03
19.26	690.15	52.81
16.59	719.23	44.85
11.87	793.92	49.17
13.43	1030.42	62.38
20.29	891.27	60.89
11.94	655.98	34.95
12.81	639.25	33.84
20.55	673.33	41.69
18.61	774.29	45.77
16.57	921.96	57.50
28.88	861.89	55.82
19.22	966.78	61.47
16.06	727.54	49.36
15.83	1045.37	59.62
13.85	628.27	37.30
14.95	876.97	49.64
10.89	987.26	53.10
10.09	812.28	41.86
16.19	801.55	47.79
21.65	771.35	52.32
20.72	1468.35	89.11
19.74	923.50	62.49
12.82	686.04	38.19
26.05	848.92	58.82
26.95	979.59	79.30
16.51	753.74	45.68
11.61	738.89	39.62
12.04	667.01	37.39
11.82	670.91	37.30
11.40	705.02	37.70
9.45	626.14	32.35
48.65	3048.99	275.01
43.70	2975.09	228.51
72.26	1859.77	156.79
61.27	4706.56	340.37
42.05	3546.32	229.21
51.17	4748.87	320.49
55.90	3384.53	267.01
61.52	4878.16	353.52
48.64	6032.18	400.38
136.04	3306.68	466.86
84.05	2291.68	148.97
59.30	6371.74	424.52

55.03	1189.64	103.38
67.24	5701.39	402.75
81.16	3110.48	257.22
139.27	5652.87	610.60
78.44	6046.38	477.27
78.19	5536.54	393.28
74.14	4973.34	373.72
60.37	5732.26	365.82
90.55	2796.56	246.62
91.78	6274.30	427.71
53.64	3183.59	173.88
128.74	7621.77	755.42
142.49	12321.41	784.89
39.87	2238.78	693.16
18.25	5025.82	613.03
21.78	6756.69	1998.23
15.41	7898.05	667.67
14.28	6890.99	591.72
15.73	41633.35	11249.77
19.81	23378.17	3002.47
13.64	11117.31	759.44
67.15	7254.34	3475.80
30.43	11392.10	1398.08
44.02	6639.27	1109.60
27.98	20999.76	3685.46
31.83	23994.12	3409.59
38.14	17430.41	3198.23
27.28	12225.27	1112.99
51.71	6892.00	1225.53
15.55	13373.73	817.62
53.07	19323.80	2395.17
40.32	11277.56	1134.76
36.62	10462.28	1398.65
26.78	3484.41	234.90
66.51	28574.20	5252.05
54.74	9705.57	1300.39
39.30	2785.91	187.93
95.71	9615.28	3490.31
238.84	22051.81	14140.76
33.34	25718.81	2182.42
105.21	12593.52	10987.02
103.01	29425.29	406897.51
58.57	15094.52	1111.02
80.43	35844.56	14214.81
235.20	19882.82	3271.90
127.88	27649.31	4679.46
95.15	39930.35	7964.39
68.25	15960.40	1145.92
166.83	14771.27	1258.37
172.68	26180.61	2838.74

62.17	26290.96	2794.12
67.54	29692.18	3803.33
52.13	22769.96	1885.83
77.75	26074.53	1806.61
75.55	32874.35	4040.29
1867.19	49279.86	19872.95
261.79	26811.85	109464.45
78.42	3197.47	239.99
156.63	34954.96	11833.19
105.70	27877.94	2441.36
88.94	5430.34	343.20
213.83	48347.20	7519.50
119.78	4845.04	395.25
72.36	27035.65	6944.19
112.46	31952.06	4124.56
140.80	49052.02	23712.35
219.71	43550.06	7304.83
202.46	54269.45	61746.83
262.54	32058.11	41134.89
299.44	41396.86	4829.80
197.14	13880.49	1823.52
124.96	31486.79	4527.62
405.11	55896.44	46508.12
265.42	51584.33	21517.96
177.92	48866.28	27675.02
263.82	56230.18	31238.01
541.83	57791.16	13478.40
479.16	32530.87	65906.57
672.18	57109.41	39699.54
22.37	17541.81	1562.94
38.26	10298.41	1532.15
33.30	22171.96	1976.44
18.64	27386.69	1844.93
26.51	21798.29	1976.55
29.31	18470.36	1368.18
29.08	11998.69	919.07
51.41	27562.73	2142.02
42.03	21341.17	2374.09
37.70	22762.14	1917.78
19.43	20845.84	1190.02
19.31	19923.25	1084.35
34.71	24554.30	2713.24
26.28	19241.67	1564.65
36.74	19452.78	1248.61
14.51	18349.31	1071.64
43.31	21243.38	1553.62
32.74	27776.60	2023.46
20.12	13512.18	854.91
29.68	23858.37	3624.78
49.72	27447.18	2137.56

54.32	29423.19	2460.46
32.72	13121.83	1232.51
24.05	23245.17	1719.51
42.42	26778.33	3321.36
15.80	18626.18	1119.11
24.56	21122.41	1457.41
26.83	19715.09	1736.17
31.15	26592.67	1842.15
28.74	23014.61	2025.33
65.78	24979.63	2586.09
66.73	23929.99	2696.52
51.24	21046.08	1791.50
51.51	30783.40	2225.29
32.30	21504.19	1640.43
23.00	28352.40	2137.01
47.12	22611.03	1858.44
43.97	16799.12	1141.66
39.63	28708.99	2175.14
49.18	22035.19	1497.97
59.99	25244.51	1956.52
42.11	24333.48	1573.18
75.69	22813.58	2138.44
50.64	20177.04	1398.54
60.08	16658.11	1634.59
43.29	29597.18	2391.89
49.79	24791.05	1664.51
145.28	24214.12	4461.84
53.85	11967.61	828.53
60.88	25896.54	2224.05
63.63	26048.05	1846.47
45.22	30387.06	2277.92
82.87	30129.31	3141.45
43.34	31178.10	1996.01
70.29	25326.10	2364.72
88.63	36470.87	4145.89
88.57	30794.60	2589.12
206.30	63228.30	4579.92
260.68	75694.10	4682.04
278.58	71964.92	4527.24
33.63	18570.83	1809.36
72.82	27113.79	2831.61
32.24	25780.73	1931.07
27.67	27467.48	1977.60
27.61	21220.34	2067.03
32.34	45909.90	2942.42
91.99	23685.12	2311.96
66.21	37552.65	3452.94
73.25	22195.58	1733.01
70.12	32669.18	2948.23
177.36	40787.30	6617.82

107.83	33528.46	2804.02
134.45	21949.77	1698.28
64.65	35226.96	2104.00
137.08	39944.31	2630.15
89.02	43040.56	2731.20
868.99	41760.15	51506.17
23.93	70373.72	16934.81
56.02	80290.13	44038.20
33.43	75427.32	24058.55
59.27	66658.66	21105.08
58.73	62189.75	18108.96
30.08	69936.40	13491.61
122.84	79449.64	69899.45
324.00	nil	nil
167.50	nil	nil
153.69	83891.88	43766.19
1517.32	19402.74	22910.75
3358.90	nil	nil
2897.25	nil	nil

l Pb		**Rediogenic 207Pb corr.**				
207Pb/206Pb	**±**	**206Pb/238U**	**±**	**206/238 (4)**	**±**	**207/235 (4)**
0.1062	0.0025	0.0690	0.0020	435	13	487
0.1312	0.0031	0.0638	0.0026	392	16	294
0.1357	0.0042	0.0663	0.0036	417	23	445
0.2525	0.0092	0.0649	0.0069	420	45	586
0.1422	0.0074	0.0687	0.0035	434	22	498
0.1710	0.0076	0.0677	0.0020	421	12	403
0.1654	0.0065	0.0669	0.0026	419	17	439
0.1583	0.0051	0.0675	0.0030	428	19	502
0.1878	0.0067	0.0687	0.0031	438	23	543
0.1950	0.0116	0.0653	0.0042	366	26	-
0.2117	0.0127	0.0683	0.0036	452	25	718
0.1137	0.0063	0.0680	0.0019	427	12	450
0.1448	0.0035	0.0689	0.0020	429	13	420
0.1616	0.0111	0.0693	0.0027	420	18	261
0.1550	0.0095	0.0648	0.0026	375	18	-
0.2328	0.0134	0.0625	0.0044	400	31	514
0.1697	0.0051	0.0704	0.0031	433	22	359
0.1188	0.0031	0.0694	0.0018	437	12	480
0.3589	0.0287	0.0716	0.0054	423	36	82
0.3208	0.0338	0.0674	0.0056	386	36	-
0.3421	0.0106	0.0699	0.0041	408	29	-
0.1856	0.0133	0.0691	0.0042	429	32	398
0.1153	0.0036	0.0688	0.0026	428	16	405
0.1683	0.0065	0.0689	0.0041	437	27	526
0.2969	0.0357	0.0685	0.0077	388	57	-
0.0992	0.0050	0.0676	0.0013	429	8	506
0.2044	0.0126	0.0616	0.0023	397	21	536

0.2230	0.0075	0.0691	0.0029	390	23	-
0.1295	0.0033	0.0678	0.0023	415	15	309
0.2912	0.1313	0.0726	0.0182	497	63	910
0.1560	0.0035	0.0669	0.0020	421	13	464
0.1611	0.0140	0.0663	0.0023	431	15	617
0.2017	0.0093	0.0668	0.0029	422	21	478
0.2177	0.0074	0.0688	0.0038	384	31	-
0.1251	0.0057	0.0704	0.0019	444	12	501
0.1290	0.0045	0.0662	0.0030	411	19	385
0.1191	0.0052	0.0674	0.0032	418	20	380
0.1461	0.0060	0.0693	0.0047	432	30	431

l Pb		**Rediogenic 207Pb corr.**				
207Pb/206Pb	**±**	**206Pb/238U**	**±**	**206/238 (4)**	**±**	**207/235 (4)**
0.0592	0.0004	0.0837	0.0008	518.4	4.8	518.8
0.1016	0.0036	0.0721	0.0028	444.4	16.8	401.3
0.1100	0.0053	0.0826	0.0070	518.6	42.8	593.8
0.0649	0.0010	0.0841	0.0021	521.6	12.5	528.9
0.1055	0.0025	0.0825	0.0020	514.1	12.2	544.8
0.1123	0.0021	0.0751	0.0021	468.7	13.8	498.2
0.0740	0.0021	0.0837	0.0024	519.8	14.8	536.9
0.0980	0.0021	0.0633	0.0021	395.2	12.8	403.5
0.0774	0.0056	0.0833	0.0055	527.9	33.3	655.7
0.2015	0.0070	0.0639	0.0028	393.1	17.4	325.9
0.1316	0.0077	0.0898	0.0023	553.3	13.7	529.1
0.0760	0.0042	0.0825	0.0049	514.9	29.6	556.9
0.0642	0.0015	0.0845	0.0030	524.9	18.2	544.6
0.0744	0.0018	0.0839	0.0027	518.7	16.0	507.5
0.0774	0.0020	0.0782	0.0020	484.4	12.4	478.2
0.0854	0.0068	0.0799	0.0059	492.5	35.2	455.3
0.0958	0.0023	0.0816	0.0017	507.8	10.7	529.7
0.0798	0.0015	0.0767	0.0022	476.2	13.3	478.0
0.1145	0.0086	0.0802	0.0043	494.6	25.9	462.1
0.1930	0.0046	0.0814	0.0037	502.8	22.3	483.2
0.1036	0.0047	0.0809	0.0029	494.7	19.1	409.4
0.1137	0.0039	0.0614	0.0028	375.6	17.6	281.5
0.1485	0.0092	0.0866	0.0055	545.9	34.4	648.0
0.0953	0.0102	0.0831	0.0070	506.6	41.5	403.8
0.0729	0.0020	0.0823	0.0036	511.8	21.4	533.9
0.1614	0.0107	0.0839	0.0050	493.9	31.2	142.7
0.1584	0.0051	0.0815	0.0056	519.9	35.1	671.9
0.0953	0.0021	0.0840	0.0011	522.5	6.7	550.2
0.0607	0.0009	0.0856	0.0012	529.1	7.1	521.5
0.0630	0.0009	0.0856	0.0015	526.7	9.0	489.3
0.0694	0.0024	0.0838	0.0014	516.6	8.2	490.4
0.0724	0.0020	0.0797	0.0020	493.2	12.3	479.8
0.0763	0.0033	0.0822	0.0022	513.7	13.2	559.3
0.0621	0.0015	0.0819	0.0019	510.1	11.5	539.9

0.0706	0.0039	0.0819	0.0033	514.6	19.8	590.3
0.1841	0.0045	0.0791	0.0019	479.2	12.6	333.7
0.1054	0.0047	0.0973	0.0033	613.4	20.4	739.6

C-Pb 208 /206	207corr 206Pb /238U Age	1s err	Fe-corr 207corr 206Pb /238U Age	1s err	7corr 206* /238	% err
2.105	505	9	508	10	0.0815	1.8
2.103	~~483~~	~~11~~	487	12	0.0777	2.4
2.106	519	20	521	21	0.0838	4.1
2.107	531	12	535	13	0.0859	2.4
2.108	540	18	546	19	0.0874	3.5
2.106	516	10	521	11	0.0834	2
2.106	516	8	506	10	0.0834	1.7
2.105	508	11	513	12	0.082	2.3
2.107	527	7	530	9	0.0852	1.4
2.106	516	14	512	15	0.0834	2.8
2.107	533	6	527	8	0.0863	1.2
~~2.107~~	~~530~~	~~7~~			~~0.0857~~	~~1.4~~
2.106	519	10	523	11	0.0839	2
2.106	517	12	524	13	0.0835	2.3
2.106	524	9	527	10	0.0847	1.8
2.105	512	10	517	11	0.0827	2
2.105	511	9	515	10	0.0825	1.8
2.106	517	10	520	11	0.0834	1.9
2.106	524	15	529	16	0.0846	3
2.105	513	8	518	9	0.0828	1.6
2.107	530	9	534	11	0.0857	1.8
2.106	524	13	528	14	0.0847	2.5
2.105	512	7	514	9	0.0827	1.4
2.105	511	8	514	9	0.0825	1.6
2.105	505	8	509	10	0.0815	1.7
2.106	518	9	522	11	0.0837	1.8
2.104	499	8	504	9	0.0804	1.6
2.105	506	8	512	10	0.0816	1.7
2.105	510	11	514	12	0.0823	2.2
2.103	~~486~~	~~9~~	490	10	0.0783	1.9
2.106	524	8	527	9	0.0846	1.5
2.104	499	10	503	11	0.0804	2.1
2.106	522	7	523	9	0.0844	1.4
2.106	514	7	521	8	0.0831	1.4
2.104	495	13	504	14	0.0799	2.7
2.106	520	7	526	9	0.084	1.4
2.106	517	7	524	9	0.0835	1.4
2.107	527	12	529	13	0.0852	2.3
2.105	513	6	518	8	0.0829	1.2

2.105	504	11	505	12	0.0813	2.2
2.106	524	10	520	11	0.0847	2
2.107	535	7	524	8	0.0866	1.3
2.105	509	6	512	8	0.0821	1.3
2.106	521	14	523	15	0.0841	2.9
2.097	409	10	406	10	0.0656	2.4
2.098	427	10	423	11	0.0686	2.5
2.097	411	9	406	10	0.0659	2.3
2.098	423	7	419	8	0.0679	1.7
2.097	420	9	421	10	0.0674	2.3
2.097	410	11	406	12	0.0656	2.7
2.099	434	10	431	11	0.0696	2.5
2.098	431	7	430	8	0.0691	1.6
2.097	420	6	418	8	0.0673	1.6
2.098	430	11	430	12	0.069	2.7
2.098	424	8	427	9	0.068	2
2.095	387	9	~~387~~	~~10~~	0.0618	2.4
2.098	422	10	424	11	0.0677	2.5
2.098	423	16	430	17	0.0679	4
2.096	406	9	410	10	0.065	2.3
2.1	452	13	~~454~~	~~14~~	0.0726	2.9
2.098	427	9	428	10	0.0685	2.1
2.098	422	10	422	11	0.0677	2.5
2.098	427	11	428	11	0.0684	2.5
2.1	447	9	445	10	0.0719	2.1
2.096	405	15	407	15	0.0649	3.7
2.097	416	12	421	13	0.0666	2.9
2.1	452	10	447	11	0.0727	2.3
2.096	398	8	398	9	0.0636	2.2
2.098	422	10	422	11	0.0676	2.4
2.097	414	10	419	11	0.0664	2.5
2.097	415	7	416	8	0.0665	1.8
2.098	431	7	428	8	0.0691	1.6
2.095	391	20	395	20	0.0625	5.2
2.097	417	8	417	9	0.0668	2.1
2.097	417	8	421	9	0.0668	1.9
2.097	415	7	416	8	0.0666	1.8
2.096	406	11	409	12	0.065	2.8

Dates (Ma)				
±	207/206 (4)	±	206/238 (7)	±
38	738	187	430.3	12.2
66	-	-	399.0	15.6
79	596	420	414.1	21.9
153	1293	564	405.4	41.6
106	803	503	428.2	20.8
86	299	517	422.6	11.8
107	545	582	417.4	15.6
72	856	338	421.1	18.2
140	1017	592	428.0	18.6
-	-	-	407.5	25.5
136	1675	445	425.9	21.7
66	571	366	424.3	11.4
68	367	404	429.7	12.2
153	-	-	431.8	16.3
-	-	-	404.6	15.5
180	1058	776	390.9	26.6
155	-	-	438.4	18.7
69	691	356	432.8	11.0
396	-	-	445.7	32.2
-	-	-	420.3	33.8
-	-	-	435.3	24.5
244	227	1281	430.6	25.5
65	277	401	429.1	15.8
116	931	517	429.4	24.4
-	-	-	427.2	46.2
39	872	192	422.0	7.5
175	1182	726	385.3	14.1

-	-	-	430.5	17.6
87	-	-	422.7	14.1
482	2115	1187	451.5	108.5
68	678	358	417.7	11.8
111	1378	421	413.7	14.1
142	755	688	417.1	17.3
-	-	-	429.1	22.6
62	771	308	438.3	11.4
85	232	536	413.3	18.3
99	153	635	420.5	19.0
111	424	606	431.9	28.5

Dates (Ma)				
±	**207/206 (4)**	**±**	**206/238 (7)**	**±**
5.4	521	18	518.1	4.8
56.4	161	350	448.6	16.7
94.2	893	365	511.4	41.8
16.6	561	64	520.6	12.5
43.3	675	205	511.2	11.8
77.2	636	365	466.7	12.3
40.5	610	184	518.0	14.5
48.4	451	231	395.8	12.5
48.1	1124	138	515.5	32.7
85.1	-	-	399.4	17.1
82.3	426	413	554.6	13.6
49.1	732	192	511.0	29.4
21.8	628	73	522.7	18.0
28.4	458	133	519.4	16.0
42.4	448	227	485.2	12.0
77.3	272	407	495.7	35.4
46.4	625	228	505.8	10.1
26.0	487	126	476.4	13.3
110.4	304	577	497.4	25.5
80.9	391	392	504.4	21.8
116.7	-	-	501.8	17.4
96.9	-	-	384.0	16.9
134.5	1022	502	535.6	32.4
146.7	-	-	514.9	41.4
31.9	629	129	509.7	21.3
226.1	-	-	519.3	29.9
95.4	1222	334	505.2	33.4
28.0	666	133	519.7	6.5
9.7	488	39	529.3	7.1
13.7	318	65	529.5	9.0
23.8	370	130	518.5	8.3
32.3	416	167	494.4	12.2
31.5	750	139	509.4	13.2
14.9	668	53	507.3	11.5

31.8	893	115	507.5	19.8
93.9	-	-	490.8	11.3
70.9	1143	252	598.6	19.3

Comments

excluded (incorrect peak autocentre)

excluded (young outlier)

excluded (old outlier)

Sample number	Analysis ID	207 cor 206Pb/238U		206Pb/238U		207Pb/206Pb		207Pb
		age (Ma)	+/-1 ster	ratio	+/-1 RSE	ratio	+/-1 RSE	ratio
2022440202	C23OCT04B0128	548	14	0.133	1.9	0.3288	3.0	5.98
2022440202	C23OCT04B0122	568	12	0.142	1.6	0.3462	2.0	6.77
2022440202	C23OCT04B0123	563	38	0.157	4.2	0.4019	6.4	8.72
2022440202	C23OCT04B0128	602	12	0.137	1.6	0.2935	2.6	5.55
2022440202	C23OCT04B0128	617	28	0.187	2.7	0.4383	3.7	11.33
2022440202	C23OCT04B0123	610	45	0.236	3.3	0.5330	4.3	17.31
2022440202	C23OCT04B0123	633	137	0.306	7.5	0.6008	9.5	25.34
2022440202	C23OCT04B0125	449	67	0.421	2.5	0.7348	2.6	42.52
2022440202	C23OCT04B0124	568	25	0.364	1.2	0.6689	0.7	33.52
2022440202	C23OCT04B0127	372	124	0.531	3.9	0.7835	3.8	57.43
2022440202	C23OCT04B0127	525	76	0.503	2.4	0.7376	2.5	51.04
2022440202	C23OCT04B0123	757	196	0.421	8.1	0.6355	9.6	37.19
2022440202	C23OCT04B0125	596	100	0.597	2.8	0.7433	2.8	61.04
2022440202	C23OCT04B0125	648	61	0.594	1.8	0.7307	1.5	59.84
2022440202	C23OCT04B0127	598	142	0.637	3.6	0.7510	3.8	66.38
2022440202	C23OCT04B0126	564	108	0.660	2.7	0.7623	2.7	69.01
2022440202	C23OCT04B0126	205	162	1.014	2.6	0.8492	2.2	118.44
2022440202	C23OCT04B0126	576	188	0.824	3.7	0.7829	3.8	89.64
2022440213	C23OCT04B0164	218	16	0.103	2.8	0.5998	3.0	8.48
2022440213	C23OCT04B0164	229	15	0.066	3.2	0.4224	6.3	3.82
2022440213	C23OCT04B0147	533	12	0.166	1.4	0.4520	1.4	10.35
2022440213	C23OCT04B0132	471	42	0.233	3.1	0.6094	3.6	19.51
2022440213	C23OCT04B0131	450	95	0.443	3.3	0.7418	3.7	45.16
2022440213	C23OCT04B0154	500	70	0.391	2.8	0.7068	3.1	38.07
2022440213	C23OCT04B0148	536	29	0.125	4.4	0.3075	6.3	5.26
2022440213	C23OCT04B0152	548	23	0.115	3.7	0.2451	6.1	3.89
2022440213	C23OCT04B0153	551	35	0.206	2.9	0.5212	3.9	14.78
2022440213	C23OCT04B0131	552	99	0.700	2.4	0.7711	2.2	74.34
2022440213	C23OCT04B0153	553	39	0.230	3.0	0.5575	3.6	17.63
2022440213	C23OCT04B0150	565	8	0.138	1.2	0.3352	0.8	6.38
2022440213	C23OCT04B0146	565	34	0.133	4.6	0.3134	7.6	5.74
2022440213	C23OCT04B0145	568	11	0.116	1.7	0.2282	3.0	3.65
2022440213	C23OCT04B0148	571	16	0.141	2.1	0.3393	3.0	6.59
2022440213	C23OCT04B0146	572	34	0.209	2.9	0.5125	3.6	14.68
2022440213	C23OCT04B0149	572	15	0.117	2.2	0.2262	4.1	3.64
2022440213	C23OCT04B0155	574	11	0.114	1.7	0.2104	2.6	3.31
2022440213	C23OCT04B0129	577	53	0.430	2.0	0.6975	2.0	41.28
2022440213	C23OCT04B0144	578	12	0.118	1.8	0.2276	3.2	3.70
2022440213	C23OCT04B0133	583	24	0.145	3.0	0.3420	4.6	6.83
2022440213	C23OCT04B0152	584	79	0.430	3.8	0.6954	3.3	41.01
2022440213	C23OCT04B0135	586	13	0.132	1.9	0.2860	2.7	5.19
2022440213	C23OCT04B0147	588	16	0.176	1.7	0.4322	2.1	10.46
2022440213	C23OCT04B0152	588	90	0.438	7.6	0.6977	3.3	41.85
2022440213	C23OCT04B0132	589	138	0.437	4.5	0.6968	6.0	41.80
2022440213	C23OCT04B0134	595	56	0.245	4.2	0.5537	4.9	18.74
2022440213	C23OCT04B0167	595	21	0.147	2.4	0.3396	4.3	6.88
2022440213	C23OCT04B0146	595	30	0.172	3.2	0.4175	4.5	9.93
2022440213	C23OCT04B0150	598	13	0.180	1.4	0.4360	1.4	10.84

2022440213	C23OCT04B0162	602	19	0.238	1.5	0.5400	1.5	17.69
2022440213	C23OCT04B0163	604	25	0.134	3.3	0.2792	5.9	5.17
2022440213	C23OCT04B0161	605	16	0.156	1.9	0.3609	2.4	7.75
2022440213	C23OCT04B0133	606	24	0.131	3.2	0.2630	5.6	4.75
2022440213	C23OCT04B0143	607	16	0.125	2.2	0.2306	3.9	3.97
2022440213	C23OCT04B0147	608	14	0.151	1.9	0.3406	1.9	7.07
2022440213	C23OCT04B0151	612	21	0.194	1.9	0.4568	2.4	12.22
2022440213	C23OCT04B0150	615	14	0.158	1.7	0.3586	2.0	7.79
2022440213	C23OCT04B0130	620	39	0.295	2.2	0.5963	2.6	24.20
2022440213	C23OCT04B0146	623	43	0.235	2.8	0.5235	4.2	17.02
2022440213	C23OCT04B0165	623	13	0.124	1.9	0.2105	3.2	3.61
2022440213	C23OCT04B0134	637	22	0.139	2.9	0.2660	4.8	5.08
2022440213	C23OCT04B0156	637	17	0.136	2.1	0.2557	3.9	4.81
2022440213	C23OCT04B0132	650	36	0.182	3.3	0.4021	5.3	10.09
2022440213	C23OCT04B0129	656	30	0.239	2.4	0.5106	2.7	16.81
2022440213	C23OCT04B0151	656	26	0.237	2.1	0.5070	2.3	16.53
2022440213	C23OCT04B0153	661	56	0.202	4.9	0.4418	7.1	12.27
2022440213	C23OCT04B0166	662	26	0.179	2.9	0.3844	3.4	9.50
2022440213	C23OCT04B0154	668	89	0.544	2.8	0.7121	2.9	53.18
2022440213	C23OCT04B0153	676	83	0.145	9.2	0.2549	20.8	5.09
2022440213	C23OCT04B0151	693	39	0.327	2.2	0.5937	2.3	26.77
2022440213	C23OCT04B0131	695	92	0.364	4.6	0.6212	5.1	31.04
2022440213	C23OCT04B0163	763	96	0.537	3.1	0.6857	3.3	50.72
2023440012	C23OCT04B0263			14.985	1.7	0.8735	0.6	1813.26
2023440012	C23OCT04B0270	461	358	2.699	6.4	0.8474	1.7	318.40
2023440012	C23OCT04B0270	86	607	4.365	5.0	0.8672	1.7	525.88
2023440012	C23OCT04B0270	131	728	6.928	2.9	0.8673	1.1	827.49
2023440012	C23OCT04B0265	326	101	0.249	6.7	0.6997	7.4	23.97
2023440012	C23OCT04B0264	453	50	0.219	3.7	0.5988	4.7	18.06
2023440012	C23OCT04B0273	492	29	0.206	2.3	0.5573	2.9	15.83
2023440012	C23OCT04B0268	468	41	0.254	2.6	0.6284	3.1	22.01
2023440012	C23OCT04B0271	503	37	0.234	2.6	0.5883	3.2	18.99
2023440012	C23OCT04B0264	511	92	0.229	5.0	0.5776	8.9	18.18
2023440012	C23OCT04B0272	479	36	0.268	2.2	0.6360	2.5	23.52
2023440012	C23OCT04B0269	458	58	0.285	3.1	0.6594	3.8	25.92
2023440012	C23OCT04B0266	551	38	0.247	2.6	0.5765	3.2	19.63
2023440012	C23OCT04B0267	521	59	0.432	2.3	0.7118	2.3	42.39
2023440012	C23OCT04B0264	553	117	0.491	3.5	0.7218	4.2	48.74
2023440012	C23OCT04B0265	469	116	0.673	2.5	0.7785	2.7	72.26
2023440012	C23OCT04B0269	537	172	0.855	4.0	0.7872	3.2	92.77
2023440012	C23OCT04B0269	586	259	1.537	3.8	0.8195	2.5	173.30
2023440012	C23OCT04B0263	345	286	1.662	6.1	0.8427	2.4	192.05
2023440012	C23OCT04B0263	281	459	3.045	3.6	0.8578	2.0	359.27
2023440012	C23OCT04B0270	999	333	2.585	2.8	0.8180	1.8	291.12
202344018	C23OCT04B0306	n/a	n/a	2.195	3.4	0.8749	2.3	265.99
202344018	C23OCT04B0289	n/a	n/a	1.118	2.8	0.8755	2.1	134.59
202344018	C23OCT04B0294	n/a	n/a	1.563	2.7	0.8691	2.0	187.17
202344018	C23OCT04B0315	285	93	0.533	2.6	0.7945	2.6	58.42
202344018	C23OCT04B0308	287	121	1.096	2.0	0.8296	1.3	125.38
202344018	C23OCT04B0296	305	33	0.227	3.4	0.6903	2.4	21.41

202344018	C23OCT04B0308	319	185	1.191	2.9	0.8288	2.2	137.45
202344018	C23OCT04B0289	328	99	0.611	2.5	0.7941	2.4	66.84
202344018	C23OCT04B0304	355	119	0.879	2.4	0.8111	1.9	98.44
202344018	C23OCT04B0311	362	36	0.390	1.6	0.7435	1.1	40.03
202344018	C23OCT04B0295	368	48	0.284	4.3	0.6959	2.8	27.27
202344018	C23OCT04B0306	369	64	0.632	1.8	0.7878	1.2	68.68
202344018	C23OCT04B0290	380	48	0.461	1.8	0.7566	1.4	47.97
202344018	C23OCT04B0289	382	96	0.842	2.5	0.8046	1.5	93.17
202344018	C23OCT04B0307	387	14	0.183	1.4	0.5907	1.1	14.95
202344018	C23OCT04B0291	387	18	0.186	1.5	0.5937	1.7	15.19
202344018	C23OCT04B0291	390	12	0.172	1.4	0.5695	1.0	13.47
202344018	C23OCT04B0288	392	25	0.276	1.7	0.6794	1.3	25.82
202344018	C23OCT04B0315	392	87	0.475	3.3	0.7564	2.9	49.55
202344018	C23OCT04B0289	392	141	1.200	1.9	0.8210	1.5	135.87
202344018	C23OCT04B0288	393	101	0.635	3.0	0.7833	2.4	68.68
202344018	C23OCT04B0292	394	18	0.197	2.2	0.6050	1.3	16.50
202344018	C23OCT04B0305	396	62	0.455	4.2	0.7507	2.0	46.90
202344018	C23OCT04B0287	397	21	0.228	1.5	0.6384	1.4	20.09
202344018	C23OCT04B0313	398	8	0.130	1.2	0.4682	0.9	8.41
202344018	C23OCT04B0309	400	30	0.284	1.8	0.6812	1.6	26.73
202344018	C23OCT04B0285	402	34	0.405	1.4	0.7348	1.0	41.11
202344018	C23OCT04B0292	404	55	0.441	1.9	0.7447	1.8	45.33
202344018	C23OCT04B0286	405	79	0.905	1.5	0.8052	0.8	100.43
202344018	C23OCT04B0288	410	11	0.138	1.4	0.4773	1.5	9.07
202344018	C23OCT04B0305	411	114	1.313	2.2	0.8227	0.8	148.72
202344018	C23OCT04B0290	416	42	0.368	2.1	0.7170	1.7	36.39
202344018	C23OCT04B0294	421	246	1.403	2.4	0.8244	2.6	159.45
202344018	C23OCT04B0287	425	28	0.273	1.6	0.6614	1.6	24.84
202344018	C23OCT04B0294	435	132	1.224	1.9	0.8171	1.3	138.06
202344018	C23OCT04B0310	439	35	0.431	1.4	0.7313	0.9	43.49
202344018	C23OCT04B0305	446	145	1.416	1.8	0.8224	1.2	160.46
202344018	C23OCT04B0290	453	32	0.296	2.2	0.6649	1.7	27.10
202344018	C23OCT04B0307	455	24	0.205	1.9	0.5756	2.2	16.28
202344018	C23OCT04B0296	468	34	0.326	1.8	0.6772	1.6	30.47
202344018	C23OCT04B0286	545	101	0.545	3.0	0.7331	3.1	55.86
202344018	C23OCT04B0314	582	112	1.322	1.5	0.8058	0.8	147.01
202344018	C23OCT04B0312	1001	67	0.369	2.8	0.5037	4.4	25.77
322128	C23OCT04B0211	171	137	1.535	1.3	0.8490	0.7	179.76
322128	C23OCT04B0214	268	107	1.045	1.8	0.8303	1.1	119.74
322128	C23OCT04B0212	292	91	0.989	1.3	0.8253	0.9	112.51
322128	C23OCT04B0212	339	98	0.794	2.1	0.8082	1.6	88.12
322128	C23OCT04B0226	343	47	0.395	1.8	0.7513	1.7	40.87
322128	C23OCT04B0227	346	48	0.458	1.5	0.7659	1.4	48.39
322128	C23OCT04B0214	352	65	0.590	1.9	0.7861	1.4	63.80
322128	C23OCT04B0223	356	41	0.405	1.7	0.7497	1.3	41.80
322128	C23OCT04B0226	370	26	0.306	1.5	0.7074	1.0	29.88
322128	C23OCT04B0227	372	45	0.493	1.4	0.7658	1.1	52.04
322128	C23OCT04B0226	373	59	0.529	2.4	0.7721	1.5	56.27
322128	C23OCT04B0223	376	50	0.337	2.7	0.7189	2.4	33.26
322128	C23OCT04B0213	382	43	0.473	1.6	0.7589	1.1	49.45

322128	C23OCT04B0212	383	101	0.957	1.9	0.8116	1.3	106.79
322128	C23OCT04B0215	383	17	0.194	1.5	0.6078	1.4	16.24
322128	C23OCT04B0215	390	15	0.202	1.2	0.6133	1.0	17.06
322128	C23OCT04B0223	398	38	0.311	1.8	0.6976	2.0	29.86
322128	C23OCT04B0226	402	34	0.365	1.7	0.7207	1.2	36.30
322128	C23OCT04B0227	404	53	0.519	1.4	0.7626	1.3	54.51
322128	C23OCT04B0225	405	15	0.193	1.5	0.5921	1.1	15.77
322128	C23OCT04B0212	408	94	0.856	1.7	0.8016	1.4	94.53
322128	C23OCT04B0225	408	22	0.215	1.5	0.6174	1.7	18.30
322128	C23OCT04B0224	409	53	0.580	1.4	0.7719	1.0	61.69
322128	C23OCT04B0223	416	44	0.440	1.7	0.7409	1.4	45.03
322128	C23OCT04B0227	420	48	0.438	1.7	0.7390	1.5	44.57
322130	C23OCT04B0250	n/a	n/a	18.389	1.7	0.8733	0.5	2212.27
322130	C23OCT04B0250	n/a	n/a	13.266	2.0	0.8728	0.5	1599.80
322130	C23OCT04B0253	218	275	3.178	2.1	0.8545	0.6	374.32
322130	C23OCT04B0232	284	144	1.248	1.9	0.8340	1.4	143.92
322130	C23OCT04B0247	300	131	1.476	2.2	0.8370	0.8	171.87
322130	C23OCT04B0231	302	58	0.618	1.6	0.8004	1.0	68.16
322130	C23OCT04B0232	307	135	1.473	1.6	0.8364	0.9	169.67
322130	C23OCT04B0244	315	99	1.169	1.4	0.8285	0.7	133.78
322130	C23OCT04B0247	324	117	1.120	2.9	0.8260	1.2	127.20
322130	C23OCT04B0252	330	58	0.674	1.3	0.8002	0.8	74.41
322130	C23OCT04B0255	330	146	1.524	1.4	0.8353	1.0	176.35
322130	C23OCT04B0249	343	69	0.836	1.2	0.8103	0.7	93.48
322130	C23OCT04B0252	363	46	0.548	1.7	0.7778	0.8	58.65
322130	C23OCT04B0249	366	92	0.972	1.9	0.8146	1.0	109.23
322130	C23OCT04B0233	368	19	0.200	1.9	0.6258	1.5	17.35
322130	C23OCT04B0249	368	55	0.708	1.1	0.7961	0.6	77.63
322130	C23OCT04B0254	369	29	0.357	2.2	0.7298	0.9	36.16
322130	C23OCT04B0254	373	42	0.561	1.7	0.7773	0.5	60.17
322130	C23OCT04B0249	375	45	0.537	1.8	0.7730	0.8	57.21
322130	C23OCT04B0251	382	71	0.967	1.1	0.8122	0.3	108.29
322130	C23OCT04B0243	382	13	0.209	1.1	0.6266	0.4	18.03
322130	C23OCT04B0229	384	50	0.629	1.4	0.7844	0.7	68.03
322130	C23OCT04B0229	385	30	0.420	1.5	0.7446	0.4	43.04
322130	C23OCT04B0242	389	82	1.069	1.1	0.8163	0.4	120.42
322130	C23OCT04B0252	389	35	0.478	1.4	0.7581	0.5	49.95
322130	C23OCT04B0241	389	31	0.424	1.2	0.7445	0.6	43.44
322130	C23OCT04B0243	390	13	0.198	1.1	0.6084	0.6	16.59
322130	C23OCT04B0230	394	85	1.080	1.3	0.8160	0.5	121.55
322130	C23OCT04B0241	395	36	0.493	1.1	0.7594	0.5	51.54
322130	C23OCT04B0231	396	60	0.769	1.2	0.7966	0.6	84.58
322130	C23OCT04B0234	398	95	1.133	1.7	0.8179	0.7	127.48
322130	C23OCT04B0245	399	19	0.213	1.4	0.6210	1.4	18.29
322130	C23OCT04B0236	399	27	0.347	1.3	0.7145	0.8	34.19
322130	C23OCT04B0255	399	92	1.074	2.0	0.8151	0.8	121.04
322130	C23OCT04B0243	400	14	0.224	1.1	0.6318	0.4	19.50
322130	C23OCT04B0252	405	45	0.574	2.8	0.7720	0.6	60.96
322130	C23OCT04B0235	405	39	0.519	1.3	0.7623	0.6	54.57
322130	C23OCT04B0255	405	84	0.785	7.0	0.7964	1.2	85.40

322130	C23OCT04B0242	406	31	0.419	1.4	0.7381	0.6	42.76
322130	C23OCT04B0246	406	43	0.589	1.1	0.7741	0.5	62.92
322130	C23OCT04B0246	407	72	0.892	1.2	0.8042	0.6	98.88
322130	C23OCT04B0254	407	24	0.275	2.3	0.6716	1.1	25.39
322130	C23OCT04B0235	408	28	0.379	1.3	0.7237	0.7	37.81
322130	C23OCT04B0234	414	192	2.278	2.2	0.8398	0.6	264.14
322130	C23OCT04B0236	415	34	0.416	2.1	0.7342	0.8	42.16
322130	C23OCT04B0236	417	15	0.239	1.3	0.6374	0.5	21.04
322130	C23OCT04B0254	418	33	0.422	2.0	0.7349	0.7	42.63
322130	C23OCT04B0244	419	327	3.653	2.0	0.8484	0.8	427.70
322130	C23OCT04B0245	419	17	0.251	1.1	0.6472	0.7	22.41
322130	C23OCT04B0235	421	31	0.422	1.2	0.7341	0.6	42.76
322130	C23OCT04B0233	422	46	0.534	1.4	0.7611	1.0	56.09
322130	C23OCT04B0234	422	62	0.749	2.2	0.7902	0.7	81.38
322130	C23OCT04B0230	425	138	1.691	1.3	0.8307	0.6	193.52
322130	C23OCT04B0236	425	16	0.252	1.2	0.6445	0.5	22.35
322130	C23OCT04B0230	425	80	1.025	1.1	0.8095	0.5	114.28
322130	C23OCT04B0228	430	36	0.490	1.2	0.7495	0.6	50.65
322130	C23OCT04B0241	430	54	0.570	2.1	0.7654	1.1	60.13
322130	C23OCT04B0231	432	37	0.388	2.5	0.7189	1.2	38.67
322130	C23OCT04B0233	435	36	0.482	1.4	0.7463	0.6	49.55
322130	C23OCT04B0255	439	32	0.394	2.6	0.7188	0.8	39.03
322130	C23OCT04B0229	440	41	0.510	1.9	0.7513	0.8	52.83
322130	C23OCT04B0244	445	148	1.793	2.0	0.8311	0.6	204.68
322130	C23OCT04B0254	446	50	0.646	1.4	0.7736	0.6	68.95
322130	C23OCT04B0247	446	223	2.277	1.6	0.8378	1.0	263.81
322130	C23OCT04B0253	448	226	2.800	1.3	0.8425	0.5	325.06
322130	C23OCT04B0232	453	241	2.798	1.4	0.8423	0.7	324.44
322130	C23OCT04B0255	477	83	0.796	6.5	0.7855	1.2	87.08
322130	C23OCT04B0248	519	132	1.391	1.4	0.8147	1.0	155.91
322130	C23OCT04B0248	524	124	1.513	1.3	0.8182	0.7	170.64
322130	C23OCT04B0253	598	289	3.259	1.4	0.8393	0.8	377.41
322130	C23OCT04B0250	940	937	11.234	2.8	0.8522	0.7	1316.19
2022440190	C23OCT04B0169			6.829	12.9	0.8899	5.8	837.22
2022440190	C23OCT04B0170			6.453	14.1	0.7934	7.4	699.40
2022440190	C23OCT04B0171			10.900	20.4	0.9172	7.9	1431.18
2022440190	C23OCT04B0172			7.318	18.0	0.8790	7.7	886.60
2022440190	C23OCT04B0185			13.889	29.5	0.8611	14.7	1613.79
2022440190	C23OCT04B0184	406	16	0.137	2.0	0.4801	2.7	9.06
2022440190	C23OCT04B0168	388	62	0.175	5.4	0.5776	7.6	13.87
2022440190	C23OCT04B0174	425	15	0.132	2.1	0.4459	2.6	8.08
2022440190	C23OCT04B0175	424	31	0.170	3.0	0.5417	4.0	12.71
2022440190	C23OCT04B0173	435	30	0.159	3.1	0.5103	4.2	11.19
2022440190	C23OCT04B0172	445	27	0.184	3.0	0.5519	2.9	14.02
2022440190	C23OCT04B0170	468	49	0.175	4.1	0.5172	6.5	12.49
2022440190	C23OCT04B0185	490	37	0.163	4.2	0.4727	5.4	10.55
2022440190	C23OCT04B0186	538	44	0.189	3.9	0.4941	5.5	12.94
2022440190	C23OCT04B0173	546	39	0.188	3.4	0.4865	5.0	12.64
2022440190	C23OCT04B0171			0.557	7.9	0.8602	8.5	66.59
2022440190	C23OCT04B0168			7.226	10.3	0.8543	5.2	848.75

)/235U	208Pb/232Th		238U/206Pb		207Pb/206Pb		common Pb	206Pb/238U	
+/-1 RSE	ratio	+/-1 RSE	ratio	+/-1 std err	ratio	+/-1 std err	at age of zirc	age	+/-1 ster
3.3	0.0702	3.6	7.546	0.144	0.329	0.010	0.875	802	15
2.3	0.0507	2.4	7.038	0.113	0.346	0.007	0.875	856	14
6.8	0.0505	5.2	6.356	0.266	0.402	0.026	0.875	942	39
3.1	0.0501	2.8	7.285	0.115	0.293	0.007	0.875	829	13
4.1	0.0750	5.2	5.337	0.143	0.438	0.016	0.875	1107	30
3.7	0.0876	3.9	4.233	0.138	0.533	0.023	0.875	1367	45
8.2	0.1172	11.4	3.269	0.246	0.601	0.057	0.875	1720	129
2.5	0.1768	4.5	2.377	0.059	0.735	0.019	0.875	2264	56
1.2	0.8005	2.1	2.748	0.034	0.669	0.005	0.875	2001	25
4.4	0.2112	5.0	1.884	0.074	0.784	0.030	0.875	2745	107
2.6	0.1974	2.9	1.987	0.048	0.738	0.018	0.875	2628	64
8.5	0.1565	10.5	2.376	0.192	0.636	0.061	0.875	2265	183
2.8	0.2673	4.1	1.675	0.047	0.743	0.021	0.875	3018	84
1.8	0.2901	2.6	1.682	0.030	0.731	0.011	0.875	3007	53
3.7	0.2523	4.4	1.570	0.057	0.751	0.029	0.875	3177	115
2.8	0.2327	3.0	1.516	0.041	0.762	0.020	0.875	3266	88
2.5	0.3537	3.0	0.986	0.026	0.849	0.019	0.875	4514	119
3.8	0.3031	5.2	1.213	0.045	0.783	0.030	0.875	3876	144
2.8	0.0282	3.9	9.724	0.271	0.600	0.018	0.875	631	18
6.6	0.0212	4.6	15.199	0.491	0.422	0.027	0.875	411	13
1.6	0.0548	2.2	6.015	0.083	0.452	0.006	0.875	991	14
2.9	0.0718	3.2	4.289	0.132	0.609	0.022	0.875	1351	41
3.6	0.1867	4.1	2.257	0.076	0.742	0.027	0.875	2364	79
3.3	0.1385	3.7	2.558	0.073	0.707	0.022	0.875	2127	60
5.7	0.0425	4.3	8.019	0.352	0.307	0.019	0.875	758	33
5.5	0.0349	5.2	8.695	0.320	0.245	0.015	0.875	702	26
3.8	0.0754	3.7	4.859	0.142	0.521	0.020	0.875	1207	35
2.8	0.2934	3.2	1.428	0.034	0.771	0.017	0.875	3421	81
3.2	0.0916	3.7	4.348	0.130	0.557	0.020	0.875	1334	40
1.4	0.1166	2.7	7.230	0.089	0.335	0.003	0.875	835	10
6.7	0.0433	6.4	7.516	0.343	0.313	0.024	0.875	805	37
3.0	0.0397	2.6	8.606	0.151	0.228	0.007	0.875	709	12
2.9	0.0433	2.8	7.087	0.146	0.339	0.010	0.875	851	18
3.1	0.0716	3.8	4.794	0.140	0.512	0.018	0.875	1221	36
3.7	0.0329	3.1	8.571	0.189	0.226	0.009	0.875	711	16
2.7	0.0389	2.4	8.748	0.147	0.210	0.005	0.875	698	12
2.1	0.1799	3.0	2.328	0.047	0.698	0.014	0.875	2304	47
3.0	0.0377	2.6	8.461	0.153	0.228	0.007	0.875	720	13
4.2	0.0348	3.8	6.905	0.205	0.342	0.016	0.875	872	26
4.9	0.1877	4.6	2.327	0.087	0.695	0.023	0.875	2305	86
2.6	0.0427	2.6	7.593	0.142	0.286	0.008	0.875	798	15
2.3	0.0593	2.3	5.693	0.100	0.432	0.009	0.875	1043	18
8.4	0.2037	9.2	2.281	0.174	0.698	0.023	0.875	2344	179
5.6	0.1259	4.8	2.287	0.103	0.697	0.042	0.875	2338	106
4.9	0.0833	4.8	4.082	0.172	0.554	0.027	0.875	1412	59
4.8	0.0427	3.8	6.794	0.160	0.340	0.015	0.875	885	21
4.4	0.0568	4.6	5.805	0.183	0.418	0.019	0.875	1025	32
1.6	0.1813	2.7	5.544	0.075	0.436	0.006	0.875	1069	15

1.7	0.0981	2.3	4.205	0.061	0.540	0.008	0.875	1375	20
5.0	0.0417	4.6	7.441	0.245	0.279	0.016	0.875	813	27
2.7	0.0483	2.5	6.411	0.124	0.361	0.009	0.875	934	18
5.1	0.0340	4.2	7.617	0.248	0.263	0.015	0.875	795	26
3.6	0.0403	3.2	8.004	0.178	0.231	0.009	0.875	759	17
2.5	0.0479	2.2	6.630	0.125	0.341	0.006	0.875	906	17
2.4	0.0810	2.7	5.155	0.100	0.457	0.011	0.875	1143	22
3.2	0.0931	3.1	6.330	0.107	0.359	0.007	0.875	946	16
2.5	0.0959	3.2	3.391	0.076	0.596	0.015	0.875	1666	37
4.2	0.0865	4.2	4.257	0.120	0.523	0.022	0.875	1360	38
3.0	0.0360	2.8	8.039	0.150	0.210	0.007	0.875	756	14
4.3	0.0385	3.6	7.210	0.210	0.266	0.013	0.875	837	24
3.8	0.0432	3.2	7.328	0.156	0.256	0.010	0.875	825	18
5.0	0.0674	5.2	5.483	0.178	0.402	0.021	0.875	1080	35
2.8	0.0887	3.5	4.184	0.098	0.511	0.014	0.875	1382	32
2.5	0.0962	2.8	4.223	0.090	0.507	0.012	0.875	1370	29
7.4	0.0716	7.7	4.939	0.243	0.442	0.031	0.875	1189	59
4.3	0.0545	3.7	5.579	0.161	0.384	0.013	0.875	1063	31
2.9	0.2014	3.3	1.839	0.051	0.712	0.020	0.875	2799	77
14.3	0.0508	11.3	6.900	0.636	0.255	0.053	0.875	873	80
3.2	0.1443	3.0	3.057	0.069	0.594	0.014	0.875	1825	41
4.6	0.1380	5.1	2.747	0.126	0.621	0.032	0.875	2001	91
3.2	0.2091	3.9	1.863	0.058	0.686	0.023	0.875	2770	86
1.8	4.4854	2.2	0.067	0.001	0.874	0.005	0.870	17867	307
7.0	0.8506	3.3	0.371	0.024	0.847	0.015	0.870	8432	542
5.0	0.9558	4.6	0.229	0.011	0.867	0.015	0.870	10830	537
2.7	1.5356	3.2	0.144	0.004	0.867	0.009	0.870	13347	391
6.2	0.0897	5.7	4.012	0.267	0.700	0.052	0.870	1435	95
4.0	0.0686	4.2	4.574	0.168	0.599	0.028	0.870	1275	47
2.6	0.0623	2.9	4.852	0.113	0.557	0.016	0.870	1208	28
2.8	0.0885	3.1	3.937	0.102	0.628	0.020	0.870	1459	38
2.8	0.0807	3.3	4.268	0.110	0.588	0.019	0.870	1357	35
6.3	0.0714	5.4	4.363	0.216	0.578	0.052	0.870	1330	66
2.3	0.0834	2.7	3.729	0.081	0.636	0.016	0.870	1531	33
3.7	0.0934	3.7	3.508	0.110	0.659	0.025	0.870	1617	51
2.9	0.0811	3.5	4.053	0.105	0.577	0.018	0.870	1422	37
2.4	0.1360	2.7	2.314	0.052	0.712	0.016	0.870	2316	52
4.0	0.1376	4.5	2.036	0.071	0.722	0.030	0.870	2575	90
2.6	0.2243	3.2	1.486	0.037	0.779	0.021	0.870	3317	82
4.0	0.3856	4.9	1.170	0.046	0.787	0.025	0.870	3982	158
3.3	0.8516	4.0	0.651	0.025	0.820	0.021	0.870	6000	230
6.4	0.6770	5.3	0.602	0.037	0.843	0.021	0.870	6311	384
3.6	1.1016	5.1	0.328	0.012	0.858	0.017	0.870	9008	328
2.7	0.5826	2.7	0.387	0.011	0.818	0.015	0.870	8231	233
3.4	0.6980	3.1	0.456	0.015	0.875	0.020	0.863	7488	253
3.4	0.2563	12.8	0.895	0.025	0.876	0.018	0.863	4837	137
2.6	2.2291	5.1	0.640	0.017	0.869	0.017	0.863	6068	161
2.6	0.0402	3.7	1.877	0.048	0.794	0.021	0.863	2753	71
1.8	0.2831	4.5	0.912	0.018	0.830	0.011	0.863	4772	94
3.6	0.0247	2.4	4.405	0.150	0.690	0.017	0.863	1319	45

3.0	0.1274	5.7	0.840	0.024	0.829	0.018	0.863	5056	146
2.6	0.0590	3.1	1.635	0.041	0.794	0.019	0.863	3076	78
2.2	0.1388	10.2	1.138	0.027	0.811	0.015	0.863	4065	96
1.6	0.0436	2.6	2.562	0.041	0.744	0.008	0.863	2125	34
3.8	0.0184	7.9	3.516	0.150	0.696	0.020	0.863	1614	69
2.1	0.2435	3.3	1.582	0.028	0.788	0.010	0.863	3158	56
1.9	0.0551	5.0	2.169	0.040	0.757	0.010	0.863	2444	45
2.4	0.1117	4.9	1.188	0.029	0.805	0.012	0.863	3937	97
1.6	0.0322	2.3	5.452	0.077	0.591	0.007	0.863	1086	15
1.8	0.1864	7.3	5.390	0.081	0.594	0.010	0.863	1097	16
1.5	0.2163	3.3	5.823	0.081	0.569	0.006	0.863	1022	14
1.9	0.0569	3.1	3.629	0.063	0.679	0.009	0.863	1569	27
2.8	0.0351	4.4	2.106	0.070	0.756	0.022	0.863	2505	83
1.9	0.2535	4.6	0.833	0.016	0.821	0.012	0.863	5084	98
3.0	0.1367	5.6	1.574	0.048	0.783	0.019	0.863	3171	96
2.2	0.0602	3.5	5.065	0.114	0.605	0.008	0.863	1162	26
4.6	0.1225	4.1	2.198	0.092	0.751	0.015	0.863	2417	101
1.9	0.0462	2.8	4.383	0.064	0.638	0.009	0.863	1325	19
1.3	0.4087	2.5	7.679	0.090	0.468	0.004	0.863	789	9
1.9	0.0343	4.9	3.518	0.063	0.681	0.011	0.863	1613	29
1.4	0.1329	2.6	2.468	0.034	0.735	0.007	0.863	2193	30
1.9	0.0640	3.5	2.266	0.044	0.745	0.014	0.863	2356	45
1.6	0.2318	3.1	1.105	0.016	0.805	0.007	0.863	4153	61
1.9	0.0233	2.0	7.272	0.103	0.477	0.007	0.863	831	12
2.4	0.2738	2.7	0.762	0.017	0.823	0.006	0.863	5404	120
2.0	0.0597	4.2	2.717	0.056	0.717	0.012	0.863	2020	42
2.4	0.2187	14.3	0.713	0.017	0.824	0.021	0.863	5653	137
1.9	0.0430	3.7	3.663	0.060	0.661	0.011	0.863	1556	26
2.0	0.4152	9.6	0.817	0.016	0.817	0.011	0.863	5151	99
1.5	0.0640	2.5	2.320	0.032	0.731	0.007	0.863	2311	32
1.9	0.5546	6.9	0.706	0.013	0.822	0.010	0.863	5686	101
2.0	0.0450	3.6	3.375	0.073	0.665	0.011	0.863	1673	36
2.1	0.0340	3.0	4.873	0.095	0.576	0.013	0.863	1203	23
2.1	0.0326	2.7	3.063	0.057	0.677	0.011	0.863	1821	34
3.1	0.0634	4.9	1.833	0.055	0.733	0.023	0.863	2806	84
1.6	0.1213	2.9	0.756	0.012	0.806	0.006	0.863	5431	83
2.9	0.0385	4.5	2.707	0.076	0.504	0.022	0.863	2026	57
1.3	229.9	8.6	0.651	0.008	0.849	0.006	0.863	5997	78
2.0	275.7	14.3	0.957	0.017	0.830	0.009	0.863	4612	83
1.4	181.1	8.8	1.011	0.013	0.825	0.007	0.863	4432	57
1.8	234.7	20.6	1.259	0.026	0.808	0.013	0.863	3768	78
1.9	76.5	15.3	2.533	0.045	0.751	0.013	0.863	2145	38
1.6	163.7	14.6	2.182	0.033	0.766	0.010	0.863	2432	37
2.4	215.1	17.7	1.696	0.033	0.786	0.011	0.863	2988	57
1.8	102.0	10.9	2.470	0.042	0.750	0.010	0.863	2191	37
1.8	26.3	4.8	3.265	0.049	0.707	0.007	0.863	1722	26
1.4	217.2	13.0	2.028	0.029	0.766	0.008	0.863	2584	37
2.1	65.6	12.1	1.892	0.046	0.772	0.012	0.863	2736	66
1.9	97.4	59.7	2.972	0.081	0.719	0.018	0.863	1870	51
1.7	140.9	10.7	2.115	0.033	0.759	0.008	0.863	2496	39

1.9	290.4	17.9	1.044	0.020	0.812	0.010	0.863	4330	84
1.7	47.4	8.4	5.155	0.076	0.608	0.008	0.863	1143	17
1.3	50.1	8.8	4.957	0.061	0.613	0.006	0.863	1185	14
1.9	69.6	41.2	3.213	0.057	0.698	0.014	0.863	1747	31
2.1	38.3	12.5	2.738	0.047	0.721	0.009	0.863	2007	34
1.5	168.7	12.4	1.927	0.027	0.763	0.010	0.863	2695	38
1.6	47.1	10.2	5.174	0.079	0.592	0.007	0.863	1139	17
1.8	222.9	48.9	1.168	0.020	0.802	0.011	0.863	3987	69
2.0	60.0	45.0	4.652	0.070	0.617	0.011	0.863	1255	19
1.5	169.2	11.2	1.724	0.024	0.772	0.008	0.863	2948	41
1.7	128.6	10.7	2.272	0.038	0.741	0.010	0.863	2351	40
1.7	184.1	18.0	2.281	0.038	0.739	0.011	0.863	2343	39
1.9	125.0381	4.0	0.054	0.001	0.873	0.004	0.863	19112	328
2.1	81.8456	4.8	0.075	0.001	0.873	0.005	0.863	17134	341
2.1	77.8541	4.7	0.315	0.007	0.854	0.005	0.863	9217	196
2.3	91.2352	8.3	0.801	0.015	0.834	0.012	0.863	5222	99
2.3	31.5104	4.5	0.678	0.015	0.837	0.006	0.863	5844	129
1.5	14.5346	3.9	1.618	0.026	0.800	0.008	0.863	3102	51
1.5	105.1828	7.7	0.679	0.011	0.836	0.007	0.863	5837	94
1.3	34.8868	3.5	0.856	0.012	0.829	0.005	0.863	4991	68
3.1	26.1288	4.6	0.893	0.026	0.826	0.010	0.863	4845	142
1.4	14.0009	3.4	1.483	0.020	0.800	0.006	0.863	3323	45
1.4	29.7234	3.9	0.656	0.009	0.835	0.008	0.863	5968	84
1.3	14.8286	2.7	1.196	0.014	0.810	0.005	0.863	3918	46
1.8	10.7371	3.2	1.824	0.031	0.778	0.006	0.863	2817	48
1.9	16.5476	3.6	1.028	0.020	0.815	0.008	0.863	4379	84
2.3	3.6065	4.0	5.001	0.093	0.626	0.009	0.863	1175	22
1.3	12.7385	2.5	1.413	0.016	0.796	0.004	0.863	3450	39
2.4	5.5866	2.8	2.801	0.061	0.730	0.006	0.863	1968	43
1.8	10.4645	2.7	1.782	0.030	0.777	0.004	0.863	2871	48
1.9	9.1956	2.8	1.861	0.034	0.773	0.006	0.863	2773	50
1.2	15.5042	2.0	1.034	0.011	0.812	0.003	0.863	4362	48
1.2	2.4092	2.0	4.787	0.054	0.627	0.003	0.863	1223	14
1.6	13.2837	3.3	1.590	0.023	0.784	0.005	0.863	3146	45
1.6	8.7536	2.2	2.384	0.035	0.745	0.003	0.863	2258	33
1.2	24.8396	2.5	0.935	0.011	0.816	0.004	0.863	4688	53
1.4	8.5714	2.3	2.091	0.030	0.758	0.004	0.863	2519	36
1.2	8.3005	2.4	2.361	0.028	0.745	0.004	0.863	2276	27
1.3	2.2043	2.1	5.050	0.055	0.608	0.004	0.863	1165	13
1.4	28.6178	3.1	0.926	0.012	0.816	0.004	0.863	4720	61
1.2	9.3823	2.4	2.030	0.022	0.759	0.004	0.863	2582	28
1.2	17.3682	2.5	1.301	0.016	0.797	0.004	0.863	3675	44
1.9	29.5342	4.6	0.882	0.015	0.818	0.006	0.863	4884	81
1.9	4.5928	3.8	4.693	0.066	0.621	0.009	0.863	1245	18
1.5	7.2565	4.0	2.880	0.038	0.715	0.006	0.863	1921	25
1.9	20.5002	3.4	0.931	0.019	0.815	0.006	0.863	4703	96
1.2	2.6318	1.9	4.468	0.049	0.632	0.002	0.863	1302	14
3.0	10.6724	3.8	1.743	0.049	0.772	0.005	0.863	2923	82
1.2	12.8945	2.6	1.927	0.024	0.762	0.004	0.863	2695	34
7.5	12.7636	8.1	1.273	0.089	0.796	0.010	0.863	3737	262

1.6	8.6570	3.4	2.385	0.034	0.738	0.005	0.863	2258	33
1.2	11.5567	2.2	1.697	0.019	0.774	0.004	0.863	2987	34
1.3	19.9579	2.9	1.121	0.013	0.804	0.005	0.863	4110	49
1.9	3.8542	2.7	3.635	0.083	0.672	0.008	0.863	1566	36
1.5	8.4446	2.6	2.639	0.034	0.724	0.005	0.863	2071	27
2.3	72.2650	4.2	0.439	0.010	0.840	0.005	0.863	7654	167
2.0	9.4990	3.4	2.404	0.051	0.734	0.006	0.863	2242	48
1.4	6.5080	2.2	4.178	0.054	0.637	0.003	0.863	1383	18
2.0	6.9608	3.0	2.371	0.046	0.735	0.005	0.863	2268	44
2.1	174.3431	10.0	0.274	0.006	0.848	0.007	0.863	9911	201
1.2	6.0111	2.3	3.979	0.045	0.647	0.004	0.863	1445	16
1.4	9.3653	2.3	2.368	0.030	0.734	0.004	0.863	2271	28
1.7	13.0703	2.8	1.872	0.026	0.761	0.007	0.863	2760	38
2.5	20.7788	3.9	1.335	0.029	0.790	0.006	0.863	3604	79
1.5	38.5466	3.5	0.591	0.007	0.831	0.005	0.863	6382	80
1.4	5.9662	2.2	3.975	0.046	0.645	0.003	0.863	1447	17
1.2	25.7561	2.7	0.976	0.011	0.810	0.004	0.863	4548	51
1.2	11.1807	2.5	2.042	0.024	0.749	0.005	0.863	2569	31
2.3	11.0809	3.4	1.754	0.037	0.765	0.009	0.863	2908	62
2.8	7.7937	3.8	2.578	0.065	0.719	0.009	0.863	2113	53
1.5	12.1665	2.7	2.075	0.028	0.746	0.005	0.863	2535	34
2.9	5.7758	5.0	2.540	0.066	0.719	0.006	0.863	2140	56
2.2	10.6630	3.8	1.961	0.038	0.751	0.006	0.863	2656	51
2.2	49.4627	5.6	0.558	0.011	0.831	0.005	0.863	6622	132
1.4	11.5591	2.8	1.549	0.022	0.774	0.005	0.863	3211	46
1.7	45.7337	5.6	0.439	0.007	0.838	0.009	0.863	7651	126
1.4	65.6236	3.8	0.357	0.004	0.843	0.004	0.863	8606	108
1.5	226.1528	8.3	0.357	0.005	0.842	0.006	0.863	8602	121
6.8	14.7494	7.7	1.256	0.082	0.785	0.009	0.863	3776	247
1.5	23.1887	5.0	0.719	0.010	0.815	0.008	0.863	5620	81
1.4	27.5136	3.4	0.661	0.008	0.818	0.005	0.863	5941	75
1.5	64.6403	5.6	0.307	0.004	0.839	0.007	0.863	9341	131
2.9	71.4750	6.3	0.089	0.003	0.852	0.006	0.863	16143	456
12.8	0.1310	5.1	0.146	0.019	0.890	0.052	0.865	13266	1716
14.0	0.1181	9.1	0.155	0.022	0.793	0.059	0.865	12948	1820
21.0	0.0627	5.7	0.092	0.019	0.917	0.072	0.865	15965	3263
20.2	0.1538	9.4	0.137	0.025	0.879	0.068	0.865	13656	2453
28.6	0.1284	7.7	0.072	0.021	0.861	0.126	0.865	17409	5131
2.4	0.0629	2.9	7.302	0.149	0.480	0.013	0.865	827	17
6.1	0.0334	5.2	5.726	0.311	0.578	0.044	0.865	1038	56
2.8	0.0667	3.4	7.600	0.157	0.446	0.012	0.865	797	16
3.6	0.0476	3.5	5.880	0.176	0.542	0.022	0.865	1013	30
3.5	0.0725	4.0	6.281	0.192	0.510	0.021	0.865	952	29
3.4	0.0427	2.7	5.423	0.160	0.552	0.016	0.865	1091	32
6.8	0.0457	5.3	5.713	0.237	0.517	0.034	0.865	1040	43
5.7	0.0332	4.5	6.149	0.258	0.473	0.025	0.865	971	41
4.6	0.0880	6.5	5.279	0.206	0.494	0.027	0.865	1118	44
4.5	0.0759	4.7	5.312	0.181	0.486	0.024	0.865	1112	38
7.7	0.0646	5.9	1.796	0.143	0.860	0.073	0.865	2854	227
10.2	0.1316	4.6	0.138	0.014	0.854	0.044	0.865	13585	1394

208Pb/232Th	
age	+/-1 ster
1371	50
1000	24
995	52
989	28
1462	76
1696	66
2239	255
3290	146
11886	255
3873	195
3642	105
2940	309
4788	197
5149	133
4548	199
4229	128
6121	185
5352	279
562	22
423	20
1078	24
1402	45
3460	142
2622	96
842	36
694	36
1470	54
5199	165
1772	66
2229	60
858	55
787	21
857	24
1398	52
654	20
771	19
3343	101
747	20
692	26
3476	161
845	22
1165	27
3747	346
2398	116
1618	78
845	32
1117	51
3368	90

1892	44
825	38
953	24
675	28
799	26
945	21
1574	43
1798	56
1851	60
1676	70
714	20
763	28
855	27
1318	68
1717	60
1857	53
1398	107
1073	39
3708	121
1002	113
2724	83
2613	132
3838	148
34403	745
12441	405
13558	620
18806	604
1736	99
1341	56
1221	35
1715	54
1568	52
1395	75
1619	45
1805	67
1577	55
2578	69
2606	117
4090	131
6591	324
12451	495
10450	557
15012	769
9279	252
10701	334
4612	588
23693	1209
797	29
5039	228
493	12

2423	138
1159	36
2627	269
862	22
369	29
4404	147
1085	54
2141	105
641	15
3456	253
3958	130
1118	34
697	31
4567	210
2590	144
1181	41
2335	95
913	26
6926	171
681	33
2522	67
1254	44
4214	129
466	9
4891	132
1173	49
3998	573
852	31
7020	676
1253	31
8918	614
890	32
675	20
647	17
1243	60
2314	66
763	34
109992	9406
113649	16305
105194	9217
110413	22700
87942	13489
103164	15026
108655	19245
93671	10203
66876	3225
108847	14115
84851	10245
92759	55354
100151	10749

114701	20546
78419	6572
79499	6997
86032	35444
74192	9268
103774	12851
78286	7995
109374	53506
83082	37355
103832	11633
98326	10534
105521	18957
97758	3870
89277	4245
88279	4157
91447	7548
70370	3158
55444	2140
94293	7256
72367	2514
66712	3091
54737	1852
69227	2724
55823	1517
49778	1617
57906	2104
30874	1231
52960	1342
38101	1081
49303	1336
46932	1335
56667	1139
24790	505
53747	1769
46036	1018
65728	1644
45655	1044
45075	1064
23537	496
68487	2155
47299	1156
58830	1483
69102	3200
34795	1316
42668	1714
62012	2108
26069	487
49666	1870
53188	1375
52997	4295

45835	1538
51142	1147
61496	1770
31932	869
45385	1183
86793	3645
47525	1607
40747	914
41931	1258
104431	10464
39363	892
47266	1074
53442	1512
62273	2413
74330	2582
39233	860
66433	1813
50528	1269
50361	1688
43942	1653
52101	1387
38673	1932
49650	1904
79257	4467
51146	1435
77705	4351
84872	3238
109664	9105
55721	4301
64394	3202
67719	2270
84572	4753
86574	5413
2489	128
2256	204
1230	70
2892	273
2442	187
1234	36
664	34
1305	44
941	32
1414	56
845	22
903	47
660	29
1705	110
1478	69
1265	75
2499	115

Sample ID	Temperature (°C)	36Ar(mol)	±err%	37Ar(mol)	±err%	38Ar(mol)	±err%	39Ar(mol)
2022330063	450	2.31E-16	0.63	2.51E-16	13.34	9.12E-17	1.43	2.44E-15
2022330063	480	2.70E-16	0.56	3.46E-16	9.77	1.54E-16	0.97	6.98E-15
2022330063	510	3.20E-16	0.45	5.64E-16	6.75	2.64E-16	0.61	1.55E-14
2022330063	540	3.52E-16	0.40	6.51E-16	4.01	3.75E-16	0.43	2.50E-14
2022330063	570	3.72E-16	0.37	8.49E-16	2.93	5.32E-16	0.36	3.89E-14
2022330063	600	3.85E-16	0.40	1.09E-15	2.29	7.71E-16	0.26	6.02E-14
2022330063	630	4.00E-16	0.43	1.42E-15	2.00	1.09E-15	0.23	8.80E-14
2022330063	660	4.35E-16	0.39	1.98E-15	1.75	1.48E-15	0.20	1.23E-13
2022330063	690	4.54E-16	0.36	2.34E-15	1.68	1.70E-15	0.20	1.42E-13
2022330063	720	4.24E-16	0.37	2.26E-15	1.22	1.48E-15	0.22	1.23E-13
2022330063	750	3.51E-16	0.40	1.92E-15	2.28	9.86E-16	0.28	7.91E-14
2022330063	780	2.75E-16	0.45	1.50E-15	3.02	5.12E-16	0.44	3.73E-14
2022330063	810	2.64E-16	0.61	1.38E-15	3.62	3.35E-16	0.77	2.10E-14
2022330063	840	2.64E-16	0.50	1.25E-15	3.33	2.78E-16	0.66	1.56E-14
2022330063	870	2.12E-16	0.63	1.14E-15	3.58	2.85E-16	0.69	1.78E-14
2022330063	900	2.78E-16	0.48	1.55E-15	2.65	6.53E-16	0.44	4.96E-14
2022330063	930	3.03E-16	0.46	2.05E-15	1.94	1.06E-15	0.28	8.59E-14
2022330063	960	2.60E-16	0.49	2.25E-15	1.99	1.04E-15	0.36	8.37E-14
2022330063	990	3.00E-16	0.43	3.02E-15	1.97	1.08E-15	0.38	8.47E-14
2022330063	1020	2.89E-16	0.46	3.01E-15	1.63	9.16E-16	0.40	7.13E-14
2022330063	1050	2.88E-16	0.47	3.29E-15	1.16	9.82E-16	0.34	7.85E-14
2022330063	1080	3.02E-16	0.44	3.61E-15	0.95	1.05E-15	0.28	8.53E-14
2022330063	1110	2.96E-16	0.45	3.61E-15	1.00	8.27E-16	0.31	6.54E-14
2022330063	1140	2.89E-16	0.49	3.70E-15	0.86	5.27E-16	0.41	3.85E-14
2022330063	1170	2.84E-16	0.52	4.03E-15	0.91	3.43E-16	0.57	2.19E-14
2022330063	1200	2.78E-16	0.49	4.18E-15	1.08	2.76E-16	0.64	1.62E-14
2022330063	1250	3.05E-16	0.52	7.31E-15	0.44	3.49E-16	0.63	2.24E-14
2022330063	1300	2.66E-16	0.50	7.75E-15	0.44	3.00E-16	0.59	1.92E-14
2022330063	1350	3.28E-16	0.47	8.22E-15	0.41	2.67E-16	0.60	1.52E-14
2022330063	1450	5.09E-16	0.38	4.33E-15	0.75	3.20E-16	0.60	1.63E-14

±err%	40Ar(mol)	±err%	*40Ar%	±err%	*40Ar/39ArK	±err%	Cum39	Age (Ma)	±err (Ma)
0.09	3.74E-13	0.16	81.55	0.65	124.99	0.33	0.16	539.50	± 2.149
0.05	9.11E-13	0.16	91.13	0.58	118.85	0.23	0.61	516.44	± 1.866
0.04	1.89E-12	0.16	94.92	0.47	115.65	0.19	1.61	504.32	± 1.769
0.03	3.12E-12	0.16	96.63	0.44	120.74	0.18	3.22	523.60	± 1.811
0.03	5.05E-12	0.16	97.80	0.41	127.06	0.18	5.73	547.21	± 1.872
0.02	7.83E-12	0.16	98.53	0.43	128.09	0.17	9.61	551.05	± 1.878
0.02	1.12E-11	0.16	98.93	0.46	126.19	0.17	15.29	544.00	± 1.854
0.02	1.54E-11	0.16	99.15	0.42	124.58	0.17	23.22	537.99	± 1.834
0.02	1.77E-11	0.16	99.23	0.39	123.72	0.17	32.38	534.78	± 1.822
0.02	1.52E-11	0.16	99.16	0.40	122.98	0.17	40.31	532.00	± 1.814
0.02	9.75E-12	0.16	98.92	0.43	121.92	0.17	45.41	528.02	± 1.805
0.03	4.57E-12	0.16	98.20	0.47	120.10	0.18	47.82	521.17	± 1.794
0.05	2.54E-12	0.16	96.90	0.63	117.14	0.19	49.18	509.98	± 1.784
0.06	1.87E-12	0.16	95.78	0.53	115.14	0.20	50.19	502.36	± 1.767
0.05	2.15E-12	0.16	97.05	0.65	117.38	0.19	51.33	510.87	± 1.783
0.03	6.02E-12	0.16	98.61	0.51	119.64	0.18	54.54	519.42	± 1.787
0.03	1.04E-11	0.16	99.13	0.49	120.17	0.17	60.08	521.45	± 1.786
0.03	1.02E-11	0.16	99.23	0.51	120.48	0.17	65.48	522.58	± 1.79
0.03	1.02E-11	0.16	99.12	0.46	119.80	0.17	70.95	520.06	± 1.784
0.03	8.62E-12	0.16	98.99	0.49	119.66	0.17	75.55	519.52	± 1.783
0.03	9.51E-12	0.16	99.09	0.50	120.12	0.17	80.61	521.25	± 1.786
0.03	1.03E-11	0.16	99.12	0.47	120.21	0.17	86.12	521.57	± 1.785
0.03	7.95E-12	0.16	98.88	0.48	120.17	0.17	90.34	521.42	± 1.788
0.04	4.69E-12	0.16	98.16	0.52	119.61	0.18	92.82	519.31	± 1.79
0.05	2.68E-12	0.16	96.83	0.55	118.12	0.19	94.24	513.69	± 1.787
0.05	1.99E-12	0.16	95.82	0.52	117.59	0.19	95.28	511.68	± 1.791
0.04	2.74E-12	0.16	96.69	0.54	118.61	0.19	96.72	515.54	± 1.793
0.04	2.38E-12	0.16	96.66	0.52	119.59	0.19	97.96	519.24	± 1.803
0.05	1.92E-12	0.16	94.91	0.50	119.70	0.20	98.95	519.67	± 1.821
0.05	2.14E-12	0.16	92.90	0.41	121.50	0.20	100.00	526.45	± 1.847

Ca/K	Cl/K	Corrected36	±err%	Corrected39	±err%	Corrected40	±err%
0.20	0.11	2.31E-16	0.66	2.44E-15	0.09	3.74E-13	0.16
0.09	0.05	2.70E-16	0.61	6.98E-15	0.05	9.11E-13	0.16
0.07	0.03	3.20E-16	0.50	1.55E-14	0.04	1.89E-12	0.16
0.05	0.02	3.52E-16	0.45	2.50E-14	0.03	3.12E-12	0.16
0.04	0.01	3.72E-16	0.43	3.89E-14	0.03	5.05E-12	0.16
0.03	0.01	3.84E-16	0.46	6.02E-14	0.03	7.83E-12	0.16
0.03	0.01	4.00E-16	0.51	8.80E-14	0.02	1.12E-11	0.16
0.03	0.00	4.35E-16	0.47	1.23E-13	0.02	1.54E-11	0.16
0.03	0.00	4.53E-16	0.45	1.42E-13	0.02	1.77E-11	0.16
0.03	0.01	4.24E-16	0.43	1.23E-13	0.02	1.52E-11	0.16
0.05	0.01	3.50E-16	0.49	7.91E-14	0.03	9.75E-12	0.16
0.08	0.02	2.74E-16	0.52	3.73E-14	0.03	4.57E-12	0.16
0.13	0.03	2.63E-16	0.66	2.10E-14	0.05	2.54E-12	0.16
0.15	0.04	2.64E-16	0.54	1.56E-14	0.06	1.87E-12	0.16
0.12	0.03	2.12E-16	0.68	1.78E-14	0.05	2.15E-12	0.16
0.06	0.01	2.78E-16	0.56	4.96E-14	0.04	6.02E-12	0.17
0.05	0.01	3.03E-16	0.56	8.59E-14	0.03	1.04E-11	0.16
0.05	0.01	2.59E-16	0.60	8.37E-14	0.03	1.02E-11	0.16
0.07	0.01	3.00E-16	0.53	8.47E-14	0.04	1.02E-11	0.16
0.08	0.01	2.88E-16	0.53	7.13E-14	0.03	8.61E-12	0.16
0.08	0.01	2.87E-16	0.52	7.85E-14	0.03	9.51E-12	0.16
0.08	0.01	3.01E-16	0.49	8.53E-14	0.03	1.03E-11	0.16
0.11	0.01	2.96E-16	0.49	6.54E-14	0.03	7.95E-12	0.16
0.18	0.02	2.89E-16	0.52	3.85E-14	0.04	4.69E-12	0.16
0.35	0.03	2.83E-16	0.54	2.19E-14	0.05	2.68E-12	0.16
0.49	0.03	2.77E-16	0.50	1.62E-14	0.05	1.98E-12	0.16
0.62	0.03	3.04E-16	0.52	2.23E-14	0.04	2.74E-12	0.16
0.77	0.02	2.65E-16	0.50	1.92E-14	0.04	2.38E-12	0.16
1.03	0.03	3.26E-16	0.48	1.52E-14	0.05	1.92E-12	0.16
0.50	0.03	5.08E-16	0.39	1.63E-14	0.05	2.14E-12	0.17

Sample number	Analysis ID	Spot Size (µm)	Start (s)	End (s)	Time (s)	Concentration (ppm	
						23Na	24Mg
2023440367	GA-musc - 01	64	40.27	68.87	28.60	4922.22	4760.91
2023440367	GA-musc - 02	64	39.00	68.87	29.86	4155.42	5958.86
2023440367	GA-musc - 03	64	39.00	68.87	29.86	4855.25	4533.75
2023440367	GA-musc - 04	64	39.00	68.87	29.86	586.41	6890.38
2023440367	GA-musc - 05	64	39.00	68.87	29.86	2646.90	5521.29
2023440367	GA-musc - 06	64	39.00	68.87	29.86	4347.23	5420.51
2023440367	GA-musc - 07	64	39.00	68.87	29.86	4548.64	5285.88
2023440367	GA-musc - 08	64	39.00	68.87	29.86	4992.58	4290.25
2023440367	GA-musc - 09	64	39.00	68.87	29.86	4605.03	5078.96
2023440367	GA-musc - 10	64	45.15	68.87	23.72	4712.39	4691.39
2023440367	GA-musc - 12	64	41.30	68.87	27.57	4659.16	4747.93
2023440367	GA-musc - 13	64	39.00	68.87	29.86	4979.81	4659.57
2023440367	GA-musc - 14	64	39.00	68.87	29.86	4490.47	5032.27
2023440367	GA-musc - 15	64	39.00	68.87	29.86	4589.53	4432.71
2023440367	GA-musc - 16	64	39.00	68.87	29.86	2238.89	8013.59
2023440367	GA-musc - 17	64	39.00	68.87	29.86	609.80	7286.88
2023440367	GA-musc - 18	64	52.93	68.87	15.94	200.09	47068.14
2023440367	GA-musc - 19	64	39.00	68.87	29.86	5083.08	4311.51
2023440367	GA-musc - 20	64	39.00	68.87	29.86	4311.29	5396.11
2023440367	GA-musc - 21	64	39.00	68.87	29.86	4222.65	6668.93
2023440367	GA-musc - 22	64	48.17	68.87	20.70	4306.68	5235.79
2023440367	GA-musc - 23	64	47.66	68.87	21.21	3217.64	6392.14
2023440367	GA-musc - 24	64	51.24	68.87	17.63	2808.67	7921.92
2023440367	GA-musc - 25	64	47.20	68.87	21.66	3830.26	6195.49
2023440367	GA-musc - 26	64	39.00	68.87	29.86	4915.67	4780.34
2023440367	GA-musc - 27	64	39.00	68.87	29.86	4955.09	4532.17
2023440367	GA-musc - 28	64	39.00	62.29	23.28	4924.42	4435.14
2023440367	GA-musc - 29	64	39.00	60.34	21.34	4044.61	4781.94
2023440367	GA-musc - 30	64	39.00	68.87	29.86	4785.88	4478.54
2023440367	GA-musc - 31	64	39.00	68.87	29.86	3927.94	5517.10
2023440367	GA-musc - 32	64	39.00	57.41	18.41	4842.65	4412.39
2023440367	GA-musc - 33	64	53.64	68.87	15.23	3817.39	7987.56
2023440367	GA-musc - 34	64	50.68	68.87	18.19	4915.10	4378.34
2023440367	GA-musc - 35	64	39.00	68.87	29.86	4971.16	4308.03
2023440367	GA-musc - 36	64	39.00	68.87	29.86	4508.23	5022.92
2023440367	GA-musc - 37	64	39.00	68.87	29.86	4417.96	4988.98
2023440367	GA-musc - 38	64	39.00	68.87	29.86	5056.46	4399.84
2023440367	GA-musc - 39	64	39.00	68.87	29.86	3893.75	5943.96
2023440367	GA-musc - 40	64	39.00	68.87	29.86	5005.10	4555.47
2023440367	GA-musc - 41	64	39.00	59.50	20.50	4395.56	4939.62
2023440367	GA-musc - 42	64	39.00	68.87	29.86	4217.38	6081.34
2023440367	GA-musc - 43	64	39.00	68.87	29.86	4286.76	5698.22
2023440367	GA-musc - 44	64	39.00	68.87	29.86	4455.88	5441.29
2023440367	GA-musc - 45	64	39.00	68.87	29.86	3866.39	6225.50
2023440367	GA-musc - 46	64	39.00	68.87	29.86	4586.33	4683.79
2023440367	GA-musc - 47	64	39.00	68.87	29.86	4350.22	5738.52
2023440367	GA-musc - 48	64	43.67	68.87	25.19	3957.59	6370.09
2023440367	GA-musc - 49	64	39.00	68.87	29.86	4555.90	5164.77

2023440367	GA-musc - 50	64	39.00	68.87	29.86	4745.35	4710.01

ı)								
27Al	**29Si->44**	**31P->47**	**39K**	**43Ca->59**	**48Ti->80**	**55Mn**	**56Fe->72**	**85Rb**
215051.96	200719.11	17.89	106148.24	9.66	4291.66	55.56	10831.00	432.96
210215.64	202483.97	15.76	105188.32	5.15	7329.78	48.37	11099.24	564.47
213380.93	199300.27	21.31	106276.03	12.16	4421.50	52.40	15725.20	425.25
194917.81	216443.61	5.20	100643.79	477.86	14427.86	34.40	7346.95	699.35
178251.03	213884.95	15.02	92953.15	146.86	40191.16	51.35	9623.45	560.84
210360.94	202109.19	13.25	108070.60	26.03	5800.94	47.27	11301.97	550.47
210863.83	201900.09	23.02	108275.98	14.70	5112.38	52.92	11581.70	534.65
216020.94	200837.65	20.73	106451.57	7.11	4036.12	42.90	9807.30	434.40
212917.84	201853.57	23.11	108168.78	19.74	3838.48	46.66	10639.50	505.88
212240.25	202384.21	16.48	109088.59	8.61	3941.11	45.31	10196.85	473.78
212941.71	202357.08	20.75	108244.86	<3.410	3827.53	44.85	10135.19	471.47
215888.91	200226.84	11.85	107569.40	11.56	3456.26	50.71	10269.19	427.10
211266.61	199463.60	25.12	106167.27	14.55	10538.48	50.18	10361.89	483.50
215713.32	200434.01	19.26	108208.27	18.54	4010.90	41.13	9537.27	456.79
198148.70	212794.80	7.71	108321.01	37.46	4080.21	42.11	12168.33	799.26
189874.11	220281.11	10.64	103838.97	381.23	11348.44	51.53	8865.25	793.63
12442.77	18547.43	3.10	6964.78	2363.59	1862.14	30656.15	624942.12	61.27
214386.94	200822.31	23.32	108018.58	<0.730	4556.43	44.91	9968.32	438.03
210438.33	202645.28	19.62	108817.09	2.53	4554.25	52.12	11326.97	528.85
205524.91	196699.42	20.37	104425.92	498.43	4398.77	1188.80	29547.00	492.35
210733.06	203506.42	16.06	108810.64	27.59	4081.13	43.51	10281.43	529.42
205683.04	207119.77	13.29	110742.18	135.84	2813.97	48.20	10961.13	671.22
195614.72	209473.80	12.01	107405.52	21.09	11736.94	49.85	11796.55	780.40
205640.40	205646.86	16.13	107894.00	43.52	6374.98	48.80	11237.23	616.78
215709.42	199662.94	27.90	106770.90	12.90	4637.19	54.26	10545.90	445.35
214825.40	200349.43	22.96	107537.95	6.89	4565.90	49.35	10375.89	444.15
215230.94	200066.17	20.08	108148.04	<0.575	4457.50	44.69	9999.48	445.99
203278.07	199296.70	17.36	103651.57	75.14	22639.94	53.99	9588.38	508.78
214230.60	201389.61	14.88	107976.75	2.81	3972.25	44.78	10147.15	447.98
210395.03	204190.81	19.05	108675.48	13.00	3649.89	41.73	10346.00	567.39
213926.23	201103.50	24.00	108103.88	<0.649	4736.16	42.89	9976.80	454.87
199430.33	200846.50	25.16	105393.29	612.95	3176.53	1022.47	30942.81	613.44
211722.10	202872.67	21.21	108938.17	5.05	4270.29	45.38	10059.26	453.61
213808.97	201995.58	23.10	107386.35	6.06	4345.19	45.84	9846.11	437.69
212247.42	201906.61	22.61	109094.40	74.08	4045.16	45.87	10515.96	508.24
213695.79	201377.15	21.30	107931.83	9.07	4019.96	44.10	10596.12	515.48
214203.80	201164.22	25.93	107594.75	37.54	4493.34	50.34	10004.94	440.45
209950.36	204061.08	13.51	108402.47	5.17	3570.27	45.40	11050.13	599.51
214566.75	200376.91	23.91	107933.26	<1.251	4453.23	51.07	10417.24	434.33
214073.74	201272.66	19.32	107986.83	3.69	3872.92	44.38	10446.56	521.79
208925.26	204412.49	15.07	108291.14	17.55	3745.65	47.47	11322.75	586.68
210400.79	203339.99	19.36	108347.32	13.03	3732.52	47.63	11323.79	576.45
210420.32	202917.27	24.86	108731.71	13.05	4337.34	47.25	11017.88	552.66
208369.33	204580.71	14.17	108334.56	15.90	3925.18	43.12	11723.79	645.34
211883.68	202577.42	19.78	108250.74	24.11	4832.50	46.00	10138.57	476.74
210123.00	203524.27	20.49	108405.13	9.52	4152.60	48.48	10731.94	550.20
207629.52	205637.38	18.79	108074.78	30.82	3855.66	44.82	11109.19	614.79
211969.19	201948.79	24.04	108612.79	9.83	4367.08	50.24	10723.20	495.47

213952.26	201640.87	29.22	106540.62	9.32	4614.81	47.28	10347.73	461.97

86Sr->102	87Sr->104	88Sr->104	89Y->105	90Zr->122	93Nb->125	139La->155	140Ce->156
50.60	66.18	50.13	0.01	1.62	25.35	0.00	<0.001
40.39	58.68	40.26	6.72	2.54	30.82	3.73	6.64
47.64	62.37	47.38	0.03	1.97	25.46	0.01	0.02
7.78	23.39	7.47	10.93	19.50	32.00	7.16	13.29
33.22	49.37	32.99	37.56	11.87	162.40	23.46	42.37
45.29	63.25	44.97	0.76	3.18	25.49	0.52	1.02
43.49	59.21	42.91	0.37	2.12	27.68	0.37	0.74
46.49	62.03	46.43	0.01	2.30	24.60	<0.001	<0.002
42.77	59.28	41.95	0.02	1.82	21.61	<0.001	<0.002
42.73	57.33	42.29	0.03	2.33	22.41	<0.001	<0.002
43.14	58.12	43.15	0.02	1.92	22.70	0.00	0.00
48.60	63.91	48.72	0.03	1.05	22.15	0.01	0.01
43.02	58.75	42.46	2.42	4.18	59.23	1.49	2.71
42.70	58.23	42.20	0.02	2.83	23.03	0.00	<0.001
20.93	41.08	20.74	0.89	6.79	13.23	0.53	0.95
5.29	22.23	5.39	5.38	26.66	29.67	3.36	6.23
2.66	4.47	2.73	6.09	1.83	5.24	1.19	2.18
44.32	58.98	44.10	0.01	1.98	26.62	<0.001	0.01
41.36	58.66	41.43	0.24	2.87	21.22	0.18	0.27
39.35	53.79	38.61	0.43	3.45	23.04	0.21	0.40
42.00	58.48	41.80	0.03	2.74	20.98	0.01	0.01
29.71	48.08	30.03	0.05	3.76	13.20	0.01	0.01
28.99	49.62	28.57	9.09	5.61	40.69	5.44	10.00
35.15	53.38	35.38	3.41	3.18	26.26	1.95	3.56
46.70	61.77	46.27	0.02	1.78	27.27	0.01	0.02
47.35	62.66	46.96	0.02	1.82	27.06	0.00	<0.001
45.62	59.70	45.00	0.02	1.93	24.52	0.01	<0.001
43.83	59.98	43.48	30.56	21.62	74.49	17.51	30.60
49.37	65.84	49.33	0.11	2.27	21.25	0.04	0.08
37.12	54.39	37.45	0.19	6.71	17.10	0.11	0.27
42.49	56.22	41.50	0.14	1.79	25.72	0.08	0.12
35.48	52.23	35.38	0.35	5.91	17.99	0.18	0.30
43.29	57.99	42.85	0.02	1.58	26.35	<0.001	<0.001
44.70	59.73	44.41	0.02	2.22	26.59	<0.001	0.01
40.72	56.47	40.39	0.03	3.02	22.68	0.04	0.08
41.26	57.65	40.89	0.01	3.24	22.72	0.00	<0.003
45.61	59.94	45.01	0.09	3.66	25.85	0.04	0.10
35.57	53.23	35.67	0.02	4.10	19.07	0.01	0.02
47.01	62.87	47.16	0.01	1.88	26.28	<0.000	<0.002
40.50	56.69	39.93	0.06	3.95	21.57	0.02	0.01
37.25	54.24	36.96	0.02	2.04	20.69	0.00	0.00
40.04	57.41	39.63	0.03	4.38	20.39	0.01	0.00
39.06	56.07	39.28	0.04	4.16	22.82	0.00	0.02
33.88	52.72	33.86	0.29	6.70	20.08	0.35	0.28
41.94	56.74	41.80	0.21	3.39	25.64	0.16	0.33
39.97	56.68	39.72	0.03	2.29	22.50	0.01	0.00
34.85	53.59	35.48	0.02	3.40	19.15	0.00	0.01
43.88	59.51	43.56	0.02	2.14	24.08	<0.001	0.00

45.69	61.30	45.38	0.02	2.06	26.22	<0.001	0.00

141Pr->157	146Nd->162	147Sm->163	151Eu->167	157Gd->173	159Tb->175	163Dy->179
0.00	<0.002	<0.001	0.37	<0.001	<0.000	<0.000
0.73	2.35	0.60	0.52	0.83	0.18	1.40
0.00	0.00	0.01	0.35	<0.001	<0.000	<0.000
1.50	5.37	1.60	0.52	1.84	0.37	2.79
4.56	16.05	3.78	1.56	5.77	1.17	9.12
0.13	0.41	0.12	0.33	0.20	0.03	0.21
0.08	0.25	0.10	0.31	0.07	0.01	0.06
0.00	0.01	<0.001	0.28	<0.001	0.00	<0.000
<0.000	<0.001	<0.001	0.29	<0.001	<0.000	0.00
<0.000	0.01	0.01	0.29	<0.002	0.00	0.01
<0.000	<0.001	<0.001	0.29	<0.002	<0.000	0.01
<0.000	0.01	0.01	0.35	<0.002	<0.000	<0.000
0.33	1.35	0.37	0.40	0.44	0.11	0.60
<0.000	<0.001	<0.001	0.28	<0.002	<0.000	<0.000
0.13	0.39	0.14	0.14	0.17	0.04	0.22
0.68	2.49	0.66	0.26	1.06	0.18	1.51
0.23	1.08	0.37	0.25	0.49	0.14	1.17
0.00	<0.005	<0.001	0.25	<0.000	<0.000	0.00
0.03	0.12	0.02	0.26	0.03	0.01	0.06
0.05	0.14	0.04	0.28	0.03	0.01	0.09
0.00	<0.003	<0.001	0.20	<0.000	<0.000	<0.001
0.00	0.00	0.01	0.17	<0.000	0.00	0.00
1.08	3.78	0.90	0.47	1.23	0.33	2.37
0.38	1.36	0.34	0.37	0.58	0.10	0.86
<0.001	<0.001	0.01	0.34	<0.000	0.00	0.00
<0.001	<0.001	<0.001	0.33	<0.000	<0.000	<0.001
<0.001	<0.001	<0.004	0.29	<0.000	<0.000	<0.001
3.76	11.57	2.57	1.20	3.94	0.82	7.18
0.00	0.01	<0.001	0.27	0.01	<0.000	0.00
0.04	0.05	0.02	0.23	0.04	0.01	0.04
0.02	0.04	0.02	0.27	0.03	0.01	0.03
0.05	0.14	0.01	0.22	0.01	0.00	0.06
<0.001	<0.001	<0.001	0.29	<0.000	<0.000	<0.000
<0.001	0.01	0.01	0.30	<0.000	<0.000	<0.000
0.01	0.02	<0.001	0.22	<0.000	0.00	<0.000
0.00	<0.001	<0.001	0.30	<0.000	<0.001	<0.000
0.02	0.04	0.00	0.30	0.02	<0.001	0.02
0.00	0.01	<0.001	0.21	<0.000	<0.001	<0.000
<0.001	0.01	0.01	0.33	<0.000	<0.000	<0.000
0.00	0.02	<0.002	0.26	0.01	<0.000	0.02
0.00	<0.001	<0.002	0.23	<0.000	0.00	0.01
0.00	0.01	0.00	0.30	<0.000	<0.000	0.00
0.00	0.01	<0.002	0.28	0.01	<0.000	<0.003
0.04	0.13	0.00	0.21	0.08	0.01	0.09
0.03	0.09	0.02	0.29	0.01	0.01	0.03
0.00	<0.001	<0.002	0.26	<0.000	<0.000	<0.002
0.00	0.01	<0.002	0.24	<0.004	<0.000	<0.002
<0.000	<0.001	<0.002	0.33	<0.004	<0.000	<0.002

0.00	<0.001	<0.002	0.33	<0.006	0.00	<0.001

							Uncorrected Ratio	
165Ho->181	166Er->182	169Tm->185	172Yb->188	175Lu->191	232Th->264	238U	85Rb/87Sr	2s
<0.000	0.00	<0.001	0.04	0.01	<0.001	<0.000	26.00	0.34
0.34	1.09	0.14	0.90	0.15	5.06	0.89	38.25	0.50
<0.000	0.00	<0.000	0.02	0.01	0.02	0.09	27.13	0.38
0.57	2.10	0.30	2.11	0.26	16.82	5.04	119.07	2.27
2.00	6.52	0.95	6.37	0.90	31.83	7.86	45.27	0.99
0.04	0.19	0.02	0.12	0.02	1.21	0.38	34.64	0.46
0.02	0.08	0.01	0.05	0.03	0.47	0.14	35.92	0.50
<0.000	0.00	<0.001	0.01	0.01	0.00	0.02	27.87	0.41
<0.000	<0.000	<0.000	0.02	0.00	0.04	0.02	33.95	0.47
<0.000	<0.000	0.00	0.01	0.00	0.01	0.02	32.73	0.49
<0.000	0.00	0.00	0.01	0.01	0.02	0.02	32.22	0.46
0.00	0.01	<0.000	0.03	0.01	0.04	0.02	26.58	0.36
0.16	0.43	0.06	0.54	0.06	5.65	1.13	32.76	0.46
0.00	0.01	<0.000	0.02	0.01	0.01	0.03	31.25	0.50
0.03	0.14	0.04	0.11	0.03	1.35	0.55	77.48	2.41
0.29	1.02	0.15	1.13	0.12	8.42	5.77	142.17	2.78
0.27	0.89	0.16	1.37	0.24	2.74	0.67	54.02	2.66
<0.000	0.00	0.00	0.01	0.01	<0.000	<0.000	29.59	0.39
0.02	0.05	0.01	0.08	0.01	0.56	0.17	35.90	1.66
0.02	0.06	0.01	0.17	0.02	1.69	0.26	36.47	0.50
0.00	<0.000	<0.000	0.01	0.00	0.07	0.05	35.79	0.53
<0.000	0.00	0.00	0.01	0.01	0.10	0.10	55.24	1.72
0.55	1.65	0.22	1.64	0.23	9.81	1.82	62.14	2.42
0.19	0.48	0.08	0.49	0.07	2.88	0.72	45.74	0.79
0.00	0.00	0.00	0.03	0.01	0.00	0.00	28.71	0.36
<0.001	<0.000	<0.000	0.01	0.00	<0.000	<0.001	28.26	0.37
0.00	<0.000	<0.000	0.05	0.00	0.03	0.01	29.91	0.50
1.54	4.78	0.69	4.67	0.68	24.85	5.57	34.01	0.55
0.00	0.02	0.00	0.00	0.01	0.07	0.07	27.11	0.78
0.01	0.02	0.01	0.04	0.00	0.34	0.25	41.52	0.55
0.00	0.02	0.00	0.05	<0.001	0.11	0.04	32.50	0.97
0.01	0.05	0.01	0.13	0.02	1.69	0.36	46.28	1.81
<0.000	<0.000	<0.000	0.01	0.00	0.00	0.02	30.89	0.50
<0.000	<0.000	<0.000	0.00	0.01	0.01	0.00	29.22	0.37
<0.001	<0.003	<0.002	0.03	0.00	0.05	0.03	35.86	1.05
<0.001	0.00	0.00	0.03	0.01	0.02	0.03	35.66	1.34
0.00	0.01	0.00	0.04	0.01	0.30	0.16	29.27	0.37
0.00	<0.000	0.00	0.01	<0.000	0.09	0.06	44.89	1.55
<0.000	<0.000	0.00	0.02	0.01	<0.000	<0.001	27.55	0.37
0.00	<0.001	<0.000	<0.001	0.01	0.06	0.06	36.94	1.02
0.00	0.01	0.00	0.01	0.00	0.02	0.02	43.12	0.60
0.00	0.00	0.00	0.01	0.00	0.05	0.06	40.06	0.53
<0.000	0.00	0.00	0.03	0.01	0.03	0.03	39.29	0.82
0.01	0.06	0.01	0.11	0.01	0.40	0.16	48.78	1.52
0.00	0.04	0.01	0.05	0.01	0.57	0.26	33.50	0.59
0.00	0.01	<0.000	0.02	0.00	0.05	0.04	38.72	0.55
<0.000	<0.001	<0.000	0.03	0.00	0.08	0.08	45.60	0.77
<0.000	0.00	0.00	0.02	0.01	0.01	0.02	33.18	0.95

<0.000	0.00	0.00	0.02	0.01	0.01	0.00	30.08	0.38

ɔs			Corrrected to Entire Creek				
86Sr/87Sr	2s	Rho	85Rb/87Sr	2s	86Sr/87Sr	2s	Rho
1.08	0.02	0.62	24.57	0.33	1.08	0.02	0.62
0.97	0.02	0.55	36.15	0.47	0.97	0.02	0.55
1.08	0.02	0.50	25.64	0.36	1.08	0.02	0.50
0.47	0.01	0.50	112.53	2.14	0.47	0.01	0.50
0.95	0.02	0.11	42.78	0.94	0.95	0.02	0.11
1.01	0.02	0.49	32.74	0.43	1.01	0.02	0.49
1.03	0.02	0.38	33.95	0.48	1.03	0.02	0.38
1.05	0.02	0.51	26.34	0.39	1.05	0.02	0.51
1.01	0.02	0.64	32.09	0.45	1.01	0.02	0.64
1.05	0.02	0.58	30.93	0.47	1.05	0.02	0.58
1.04	0.02	0.44	30.45	0.43	1.04	0.02	0.44
1.07	0.02	0.58	25.12	0.34	1.07	0.02	0.58
1.03	0.02	0.57	30.96	0.43	1.03	0.02	0.57
1.03	0.02	0.49	29.53	0.47	1.03	0.02	0.49
0.72	0.03	-0.65	73.23	2.28	0.72	0.03	-0.65
0.34	0.02	-0.12	134.37	2.63	0.34	0.02	-0.12
0.84	0.06	0.40	51.05	2.51	0.84	0.06	0.40
1.06	0.02	0.57	27.96	0.37	1.06	0.02	0.57
0.99	0.02	-0.58	33.93	1.57	0.99	0.02	-0.58
1.03	0.02	0.50	34.47	0.47	1.03	0.02	0.50
1.01	0.02	0.65	33.82	0.50	1.01	0.02	0.65
0.87	0.02	-0.31	52.21	1.63	0.87	0.02	-0.31
0.82	0.03	-0.45	58.73	2.29	0.82	0.03	-0.45
0.93	0.02	0.29	43.23	0.75	0.93	0.02	0.29
1.06	0.02	0.51	27.13	0.34	1.06	0.02	0.51
1.06	0.02	0.42	26.70	0.35	1.06	0.02	0.42
1.08	0.02	0.46	28.26	0.47	1.08	0.02	0.46
1.03	0.02	0.02	32.15	0.52	1.03	0.02	0.02
1.06	0.02	0.03	25.63	0.74	1.06	0.02	0.03
0.96	0.02	0.43	39.24	0.52	0.96	0.02	0.43
1.06	0.02	-0.02	30.71	0.91	1.06	0.02	-0.02
0.96	0.02	-0.15	43.74	1.71	0.96	0.02	-0.15
1.05	0.02	0.52	29.19	0.47	1.05	0.02	0.52
1.05	0.02	0.52	27.61	0.35	1.05	0.02	0.52
1.02	0.02	0.02	33.89	0.99	1.02	0.02	0.02
1.01	0.02	-0.30	33.70	1.27	1.01	0.02	-0.30
1.07	0.02	0.49	27.67	0.35	1.07	0.02	0.49
0.94	0.02	-0.27	42.42	1.47	0.94	0.02	-0.27
1.05	0.02	0.48	26.03	0.35	1.05	0.02	0.48
1.01	0.02	-0.04	34.91	0.96	1.01	0.02	-0.04
0.97	0.02	0.62	40.75	0.57	0.97	0.02	0.62
0.98	0.02	0.58	37.86	0.51	0.98	0.02	0.58
0.98	0.02	-0.04	37.14	0.78	0.98	0.02	-0.04
0.90	0.02	-0.27	46.11	1.44	0.90	0.02	-0.27
1.04	0.02	0.39	31.66	0.56	1.04	0.02	0.39
0.99	0.02	0.33	36.60	0.52	0.99	0.02	0.33
0.92	0.02	0.18	43.10	0.73	0.92	0.02	0.18
1.04	0.02	-0.27	31.36	0.89	1.04	0.02	-0.27

1.05	0.02	0.43	28.42	0.36	1.05	0.02	0.43

Sample number	Analysis ID	Spot Size (µm)	Start (s)	End (s)	Time (s)	CO3 (calc)	27Al
2023440366	GA-siderite - 1	257	45.62	67.60	21.98	519001	18.58
2023440366	GA-siderite - 10	257	48.41	67.60	19.19	519147	39.37
2023440366	GA-siderite - 11	257	42.98	67.60	24.62	519485	9.12
2023440366	GA-siderite - 12	257	48.59	67.60	19.01	518976	7.34
2023440366	GA-siderite - 13	257	41.21	67.60	26.39	518556	24.04
2023440366	GA-siderite - 14	257	36.28	67.60	31.32	519451	11.67
2023440366	GA-siderite - 15	257	46.39	67.60	21.21	518798	7.39
2023440366	GA-siderite - 16	257	43.75	67.60	23.85	518651	11.78
2023440366	GA-siderite - 17	257	50.41	67.60	17.19	519369	21.06
2023440366	GA-siderite - 18	257	36.28	53.33	17.05	519241	10.10
2023440366	GA-siderite - 19	257	48.64	67.60	18.96	518900	11.96
2023440366	GA-siderite - 2	257	47.96	67.60	19.64	519593	16.32
2023440366	GA-siderite - 20	257	45.14	67.60	22.46	519458	11.78
2023440366	GA-siderite - 21	257	45.83	67.60	21.77	519276	12.99
2023440366	GA-siderite - 22	257	46.46	67.60	21.14	518431	9.36
2023440366	GA-siderite - 23	257	42.07	67.60	25.53	519552	12.24
2023440366	GA-siderite - 24	257	43.02	67.60	24.58	519442	9.56
2023440366	GA-siderite - 25	257	44.11	67.60	23.49	518940	11.46
2023440366	GA-siderite - 26	257	42.70	67.60	24.90	518793	10.19
2023440366	GA-siderite - 27	257	39.08	67.60	28.52	518757	9.96
2023440366	GA-siderite - 28	257	40.67	67.60	26.93	518690	9.58
2023440366	GA-siderite - 29	257	41.67	67.60	25.93	519094	11.77
2023440366	GA-siderite - 3	257	42.39	67.60	25.21	519498	11.27
2023440366	GA-siderite - 30	257	47.43	67.60	20.17	518802	7.01
2023440366	GA-siderite - 31	257	41.35	63.95	22.61	518874	10.79
2023440366	GA-siderite - 32	257	36.28	67.60	31.32	518618	73.99
2023440366	GA-siderite - 33	257	45.00	67.60	22.60	518761	6.52
2023440366	GA-siderite - 34	257	42.12	67.60	25.48	518739	8.12
2023440366	GA-siderite - 35	257	44.24	67.60	23.36	518708	10.54
2023440366	GA-siderite - 36	257	52.80	67.60	14.80	518690	17.64
2023440366	GA-siderite - 37	257	49.38	67.60	18.22	518552	5.64
2023440366	GA-siderite - 38	257	46.78	67.60	20.82	518673	4.94
2023440366	GA-siderite - 39	257	43.70	66.39	22.69	519295	113.03
2023440366	GA-siderite - 4	257	46.28	67.60	21.32	519527	13.81
2023440366	GA-siderite - 40	257	43.68	67.60	23.92	518879	9.57
2023440366	GA-siderite - 5	257	36.28	61.32	25.04	519137	18.44
2023440366	GA-siderite - 6	257	41.71	67.60	25.89	518873	15.31
2023440366	GA-siderite - 7	257	47.73	67.60	19.87	519305	15.51
2023440366	GA-siderite - 8	257	52.50	67.60	15.10	519063	11.30
2023440366	GA-siderite - 9	257	48.75	67.60	18.85	519288	61.59

Concentration (ppm)												
43Ca	**47Ti**	**57Fe**	**88Sr**	**89Y**	**90Zr**	**140Ce**	**146Nd**	**147Sm**	**172Yb**	**175Lu**	**176Hf**	**177Hf**
4939	11.33	475982	1.62	35.71	0.005	1.18	1.28	1.05	5.40	0.81	0.004	0.001
5572	1.70	475187	0.81	44.93	0.014	0.50	0.86	1.04	3.81	0.52	0.003	0.001
7406	1.40	473032	4.09	49.89	0.015	1.44	1.84	1.52	6.33	0.86	0.004	0.001
4907	1.27	476062	3.10	35.08	0.019	0.91	1.21	0.96	3.45	0.42	0.003	0.001
2749	1.32	478647	0.21	19.18	0.000	0.10	0.20	0.27	2.16	0.31	0.001	0.000
7218	1.07	473254	1.70	52.32	1.690	1.01	1.57	1.43	2.90	0.35	0.030	0.027
4041	1.00	477106	4.91	32.22	0.004	0.80	1.03	0.91	5.60	0.83	0.005	0.000
3283	1.39	478019	3.34	25.09	0.011	0.38	0.61	0.66	2.82	0.42	0.002	0.000
6773	1.16	473771	1.39	49.48	0.006	0.75	1.25	1.34	7.76	1.26	0.005	0.000
6190	2.27	474503	0.85	44.78	0.285	0.70	1.10	1.12	3.29	0.45	0.032	0.028
4506	1.20	476542	0.99	32.50	0.004	0.30	0.61	0.72	2.44	0.32	0.002	0.000
7888	1.49	472446	0.70	47.55	0.004	0.42	0.75	0.93	3.75	0.51	0.002	0.000
7253	1.18	473214	2.02	52.63	0.001	0.69	1.32	1.42	3.39	0.44	0.002	0.000
6352	0.96	474298	2.53	49.83	0.007	0.87	1.42	1.33	2.84	0.35	0.003	0.000
2213	1.57	479325	1.39	16.92	0.009	0.15	0.27	0.34	0.94	0.12	0.001	0.000
7712	0.85	472658	1.83	54.97	0.003	1.29	1.94	1.68	2.73	0.31	0.002	0.000
7183	0.87	473306	1.99	50.31	0.004	0.94	1.56	1.47	2.43	0.28	0.001	0.000
4711	0.88	476290	2.16	37.69	0.001	0.33	0.67	0.72	3.76	0.56	0.003	0.000
3993	0.90	477160	1.15	35.07	<0.000	0.16	0.40	0.53	4.35	0.66	0.003	0.000
3817	0.96	477373	0.68	34.83	0.003	0.11	0.35	0.50	4.47	0.68	0.004	0.001
3490	1.00	477772	0.86	30.05	0.006	0.12	0.29	0.40	4.22	0.65	0.003	0.000
5465	1.00	475373	1.75	47.15	0.004	0.58	1.06	1.07	2.86	0.35	0.002	0.000
7453	1.07	472972	1.84	54.85	0.018	0.62	1.07	1.21	3.82	0.54	0.002	0.000
4052	0.97	477095	1.45	36.74	0.006	0.57	0.93	0.88	2.07	0.26	0.002	0.000
4386	0.90	476688	1.13	33.28	0.068	0.26	0.49	0.56	3.87	0.59	0.004	0.001
2776	2.36	478515	2.84	3.34	6.050	0.79	0.42	0.11	0.94	0.15	0.046	0.044
3856	0.86	477336	2.47	30.91	0.008	0.57	0.89	0.80	2.35	0.29	0.002	0.001
3737	1.00	477477	1.92	30.69	0.004	0.31	0.59	0.65	3.19	0.48	0.002	0.000
3573	0.92	477668	0.70	31.82	0.005	0.18	0.36	0.45	4.47	0.69	0.003	0.001
3445	1.49	477803	1.83	33.42	0.010	0.50	0.77	0.86	3.98	0.58	0.005	0.002
2823	4.47	478583	0.43	22.31	0.006	0.99	1.14	0.84	4.77	0.65	0.003	0.000
3431	0.84	477861	2.95	21.94	0.003	0.67	0.95	0.79	1.63	0.22	0.001	0.001
5880	3.61	474666	4.98	9.25	23.470	1.47	0.90	0.41	1.67	0.28	0.158	0.154
7584	1.47	472792	2.52	68.76	0.078	1.39	2.12	2.08	4.23	0.57	0.004	0.001
4422	1.03	476641	1.42	38.52	0.001	0.29	0.56	0.67	4.85	0.74	0.003	0.000
5633	1.62	475172	0.97	31.06	0.018	0.32	0.57	0.60	2.89	0.45	0.003	0.001
4358	1.56	476713	0.75	29.39	0.003	0.17	0.33	0.42	5.31	0.91	0.004	0.001
6482	1.48	474136	2.28	49.73	0.029	0.69	1.13	1.25	3.85	0.51	0.006	0.003
5318	1.44	475553	1.05	41.77	0.010	0.10	0.27	0.45	6.54	1.01	0.005	0.001
6148	1.64	474445	2.08	45.90	0.006	0.61	1.03	1.25	3.89	0.53	0.003	0.001

Uncorrected Ratios						
176Lu/176Hf corr	**2s**	**177Hf/176Hf**	**2s**	**Rho**	**176Hf/176Lu**	**2s**
82.343	9.852	0.922	0.143	0.003	0.012	0.002
74.266	9.544	0.567	0.116	0.060	0.013	0.003
91.137	8.443	0.429	0.070	0.153	0.011	0.001
69.642	16.607	1.395	0.313	0.224	0.014	0.003
101.878	16.281	0.465	0.127	0.305	0.010	0.002
5.242	0.777	3.205	0.183	0.070	0.192	0.027
82.260	8.559	0.302	0.058	0.237	0.012	0.002
78.048	10.808	0.416	0.092	0.140	0.013	0.002
109.330	15.964	0.232	0.051	0.047	0.009	0.001
6.429	1.060	3.140	0.180	0.005	0.154	0.019
63.221	11.366	0.655	0.145	-0.089	0.016	0.005
97.749	18.315	0.608	0.157	0.181	0.010	0.002
90.361	16.107	0.366	0.092	0.059	0.011	0.002
60.657	10.256	0.434	0.094	0.139	0.017	0.005
52.960	10.763	1.175	0.317	-0.053	0.019	0.004
74.127	12.376	0.862	0.166	0.226	0.014	0.002
110.209	26.024	0.617	0.168	0.203	0.009	0.002
93.073	12.253	0.256	0.063	0.119	0.011	0.001
103.033	13.351	0.273	0.062	0.270	0.010	0.001
86.412	9.478	0.778	0.105	0.234	0.012	0.001
102.827	10.806	0.352	0.070	0.088	0.010	0.001
90.275	32.177	0.409	0.100	0.125	0.011	0.002
101.243	15.118	0.498	0.113	0.417	0.010	0.001
76.254	20.796	0.387	0.118	0.669	0.013	0.002
58.984	7.202	0.874	0.312	0.151	0.017	0.004
1.512	0.093	3.464	0.213	0.319	0.661	0.053
83.389	15.628	1.394	0.279	0.401	0.012	0.002
95.754	15.886	0.337	0.081	0.464	0.010	0.002
93.570	11.234	0.746	0.118	-0.465	0.011	0.002
48.799	7.882	1.132	0.369	0.240	0.021	0.005
97.687	12.517	0.551	0.114	0.660	0.010	0.001
74.040	13.876	1.470	0.336	0.079	0.014	0.002
0.811	0.017	3.477	0.086	0.239	1.233	0.031
61.445	8.959	0.825	0.244	0.463	0.016	0.004
98.126	10.269	0.107	0.035	0.127	0.010	0.001
69.461	11.163	1.412	0.280	-0.040	0.014	0.002
95.458	9.630	0.636	0.096	0.207	0.011	0.002
39.060	8.258	1.998	1.011	0.318	0.025	0.002
94.655	13.242	0.800	0.139	-0.185	0.011	0.002
74.490	10.792	1.229	0.400	0.226	0.013	0.003

Sample ID	Mineral	Analytical ID	Note	Sm (ppm)	Nd (ppm)	147Sm/144Nd	143Nd/144Nd
2022330033	Fluorite	YC1	fluo	5.46	8.55	0.3863	0.512994
2022330033	Fluorite	YC4	fluo + gal	4.17	7.92	0.3184	0.512737
2022330033	Fluorite	YC8	fluo	6.62	10.79	0.3711	0.512941
2022330033	Fluorite	YC9	fluo	6.87	11.57	0.3593	0.512870
2022330033	Fluorite	YC11	fluo+cc	2.67	5.82	0.2778	0.512637
2022330033	Fluorite	YC12	alteration	2.37	9.18	0.1560	0.512231

2se	eNd_{meas}	Rb (ppm)	Sr (ppm)	87Rb/86Sr	87Sr/86Sr	2se
0.000011	7.1	11.90	65.73	0.524	0.717246	0.000013
0.000009	2.1	77.80	63.93	3.531	0.738123	0.000013
0.000006	6.1	2.17	58.02	0.108	0.715156	0.000014
0.000011	4.7	2.11	55.03	0.111	0.715086	0.000015
0.000009	0.1	13.03	56.21	0.671	0.717391	0.000015
0.000010	-7.8	222.3	119.6	5.403	0.751620	0.000017

Interplay between supercontinents and accretionary orogens recorded in 200 million years of metallogeny

Appendix 2B Isochron plots of geochronology of samples from mineral deposits in the Delamerian convergent margin, southeast Australia

Yanbo Cheng[1] *, Phil Gilmore[1, 2], Michael Doublier[1], Karol Czarnota[1], Chris Lewis[1], Holly Taylor[1], Andrew Clark[1], Liam Pitt[1], David Mole[1], Yue Wang[3], Sebastien Meffre[4], Adrienne Brotodewo[5], Ross Cayley[6], Cameron Cairns[6], Antony Burhnam[1, 3], Tom Wise[7], Adrian Fabris[7]

1 Geoscience Australia, Canberra 2609, Australia
2 Geoscience, Exploration and Mineral Systems, Newcastle 2300, Australia
3 Research School of Earth Sciences, The Australian National University, Canberra 2601, Australia 4 Earth Sciences, University of Tasmania, Hobart 7006, Australia
5 MinEx CRC, Future Industries Institute, Adelaide University, Adelaide 5005, Australia
6 The Geological Survey of Victoria, Melbourne 3002, Australia
7 The Geological Survey of South Australia, Adelaide, 5000, Australia

* Correspondence: yanbo.cheng@ga.gov.au

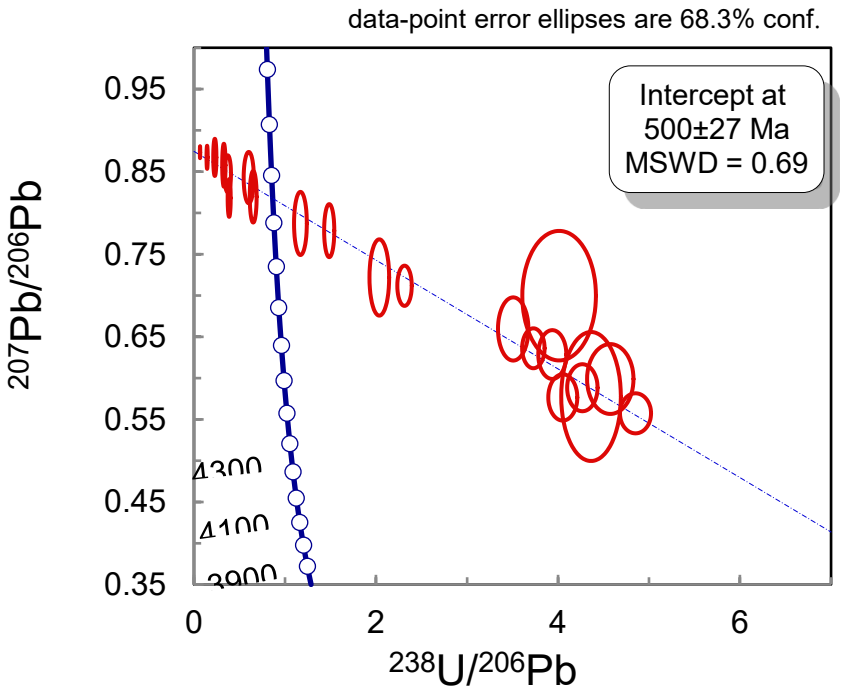

Figure 1 U-Pb Tera-Wasserburg concordia diagram for apatite grains from the mineralised sample 2023440012 of the Glenlye epithermal Au-Ag deposit, Grampian-Stavely Belt, Victoria. Corrected data define a mixing line (isochron) anchored at a common $^{207}Pb/^{206}Pb$ composition of 0.852 ± 0.015. The lower intercept yields a crystallization age of 500 ± 27 Ma (2σ sigma, MSWD = 0.69). Data point error ellipses are 68% confidence level.

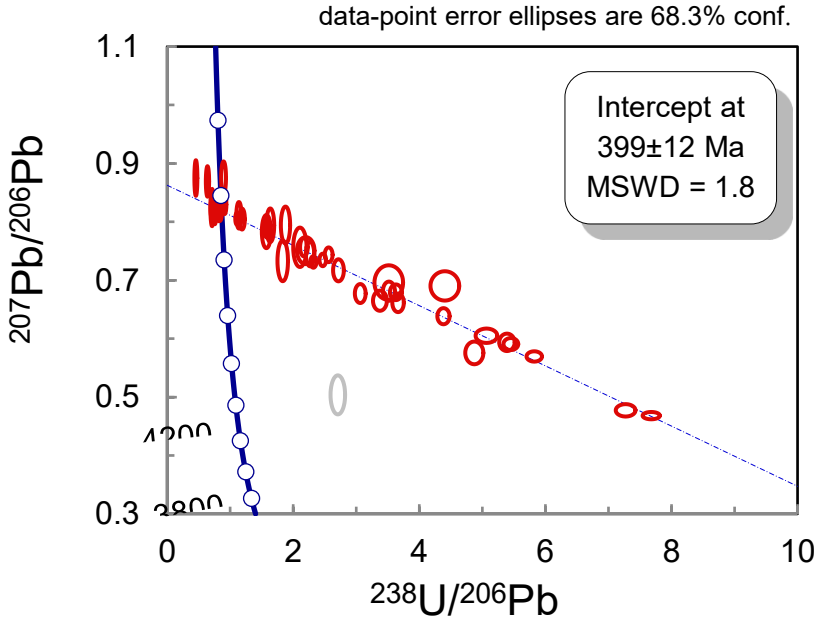

Figure 2 U-Pb Tera-Wasserburg concordia diagram for apatite grains from the mineralised sample 2023440018 of the Stawell intrusion related Au deposit, Grampian-Stavely Belt, Victoria. Corrected data define a mixing line (isochron) anchored at a common $^{207}Pb/^{206}Pb$ composition of 0.852 ± 0.015. The lower intercept yields a crystallization age of 399 ± 12 Ma (2σ sigma, MSWD = 1.8). Data point error ellipses are 68% confidence level.

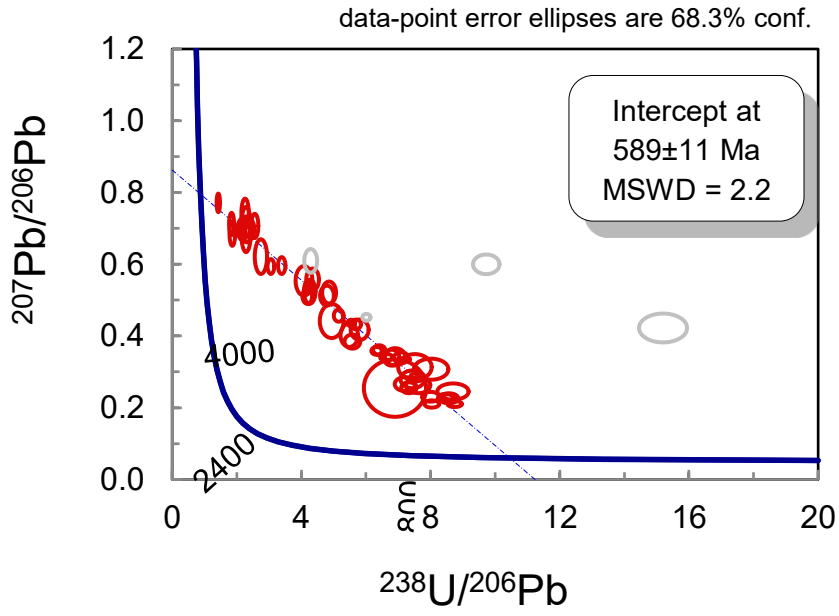

Figure 3 U-Pb Tera-Wasserburg concordia diagram for apatite grains from the mineralised sample 2022440213 of the Mount Arrowsmith orthomagmatic Ni-Cu prospect, Koonenberry Belt, New South Wales. Corrected data define a mixing line (isochron) anchored at a common $^{207}Pb/^{206}Pb$ composition of 0.852 ± 0.015. The lower intercept yields a crystallization age of 589 ± 11 Ma (2σ sigma, MSWD = 2.2). Data point error ellipses are 68% confidence level.

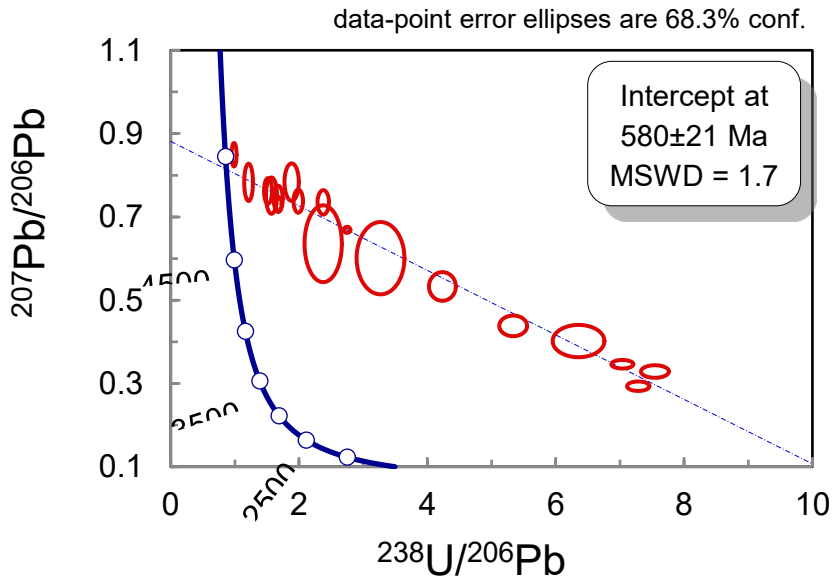

Figure 4 U-Pb Tera-Wasserburg concordia diagram for apatite grains from the mineralised sample 2022440202 of the Mount Arrowsmith orthomagmatic Ni-Cu prospect, Koonenberry Belt, New South Wales. Corrected data define a mixing line (isochron) anchored at a common $^{207}Pb/^{206}Pb$ composition of 0.852 ± 0.015. The lower intercept yields a crystallization age of 580 ± 21 Ma (2σ sigma, MSWD = 1.7). Data point error ellipses are 68% confidence level.

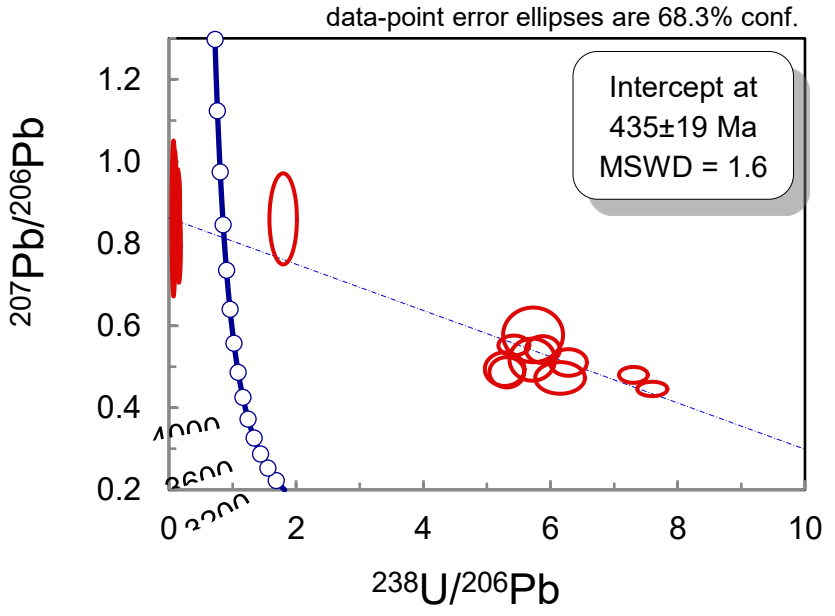

Figure 5 U-Pb Tera-Wasserburg concordia diagram for apatite grains from the mineralised sample 2022440190 of the Eclipse porphyry Cu-Au prospect, Koonenberry Belt, New South Wales. Corrected data define a mixing line (isochron) anchored at a common $^{207}Pb/^{206}Pb$ composition of 0.852 ± 0.015. The lower intercept yields a crystallization age of 435 ± 19 Ma (2σ sigma, MSWD = 1.6). Data point error ellipses are 68% confidence level.

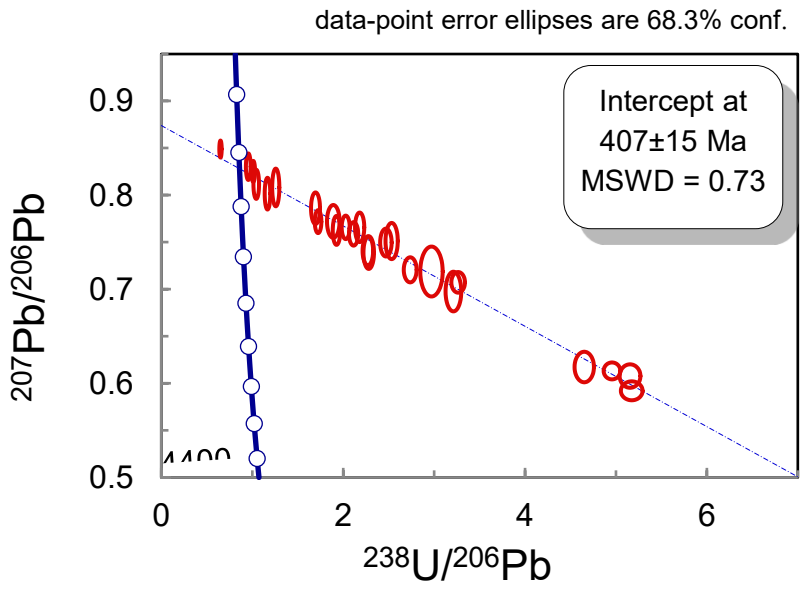

Figure 6 U-Pb Tera-Wasserburg concordia diagram for apatite grains from the mineralised sample 322128 of the Mt Ararat VHMS Cu-Zn prospect, Grampian-Stavely Belt, Victoria. Corrected data define a mixing line (isochron) anchored at a common $^{207}Pb/^{206}Pb$ composition of 0.852 ± 0.015. The lower intercept yields a crystallization age of 407 ± 15 Ma (2σ sigma, MSWD = 0.73). Data point error ellipses are 68% confidence level.

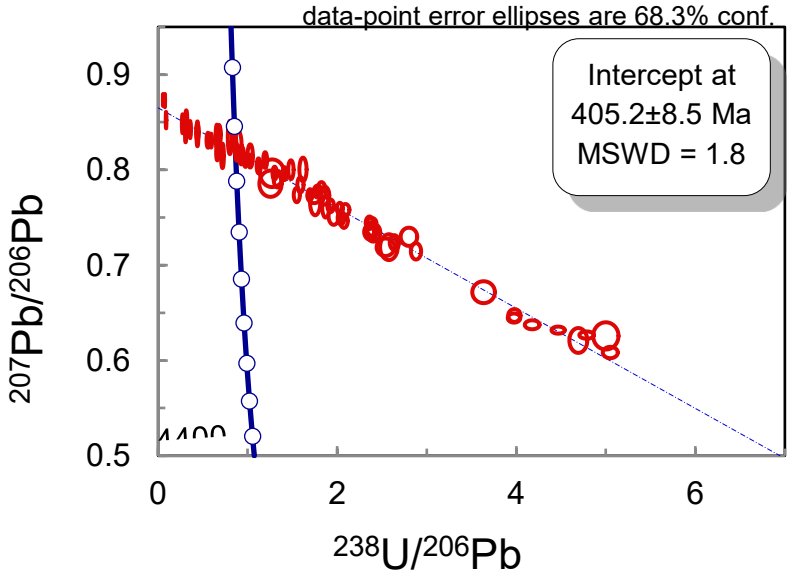

Figure 7 U-Pb Tera-Wasserburg concordia diagram for apatite grains from the mineralised sample 322130 of the Mt Ararat VHMS Cu-Zn prospect, Grampian-Stavely Belt, Victoria. Corrected data define a mixing line (isochron) anchored at a common $^{207}Pb/^{206}Pb$ composition of 0.852 ± 0.015. The lower intercept yields a crystallization age of 405 ± 9 Ma (2σ sigma, MSWD = 1.8). Data point error ellipses are 68% confidence level.

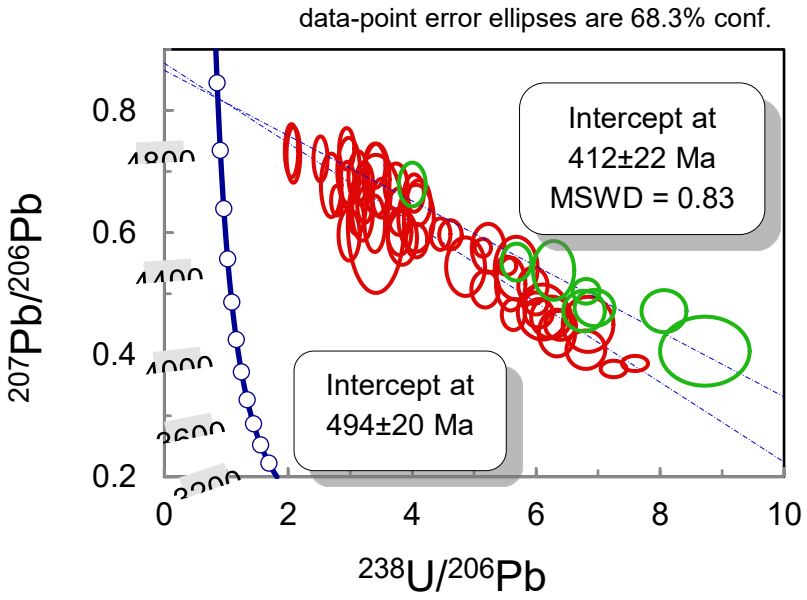

Figure 8 U-Pb Tera-Wasserburg concordia diagram for titanite grains from the mineralised sample 321864 of the Gerang Gerung skarn Zn prospect, Grampian-Stavely Belt, Victoria. Corrected data define a mixing line (isochron) anchored at a common $^{207}Pb/^{206}Pb$ composition of 0.852 ± 0.015. The lower intercept yields two crystallization ages: 412 ± 22 Ma (2σ sigma, MSWD = 0.83), and 494 ± 20 Ma (2σ sigma, MSWD = 1.9). Data point error ellipses are 68% confidence level.

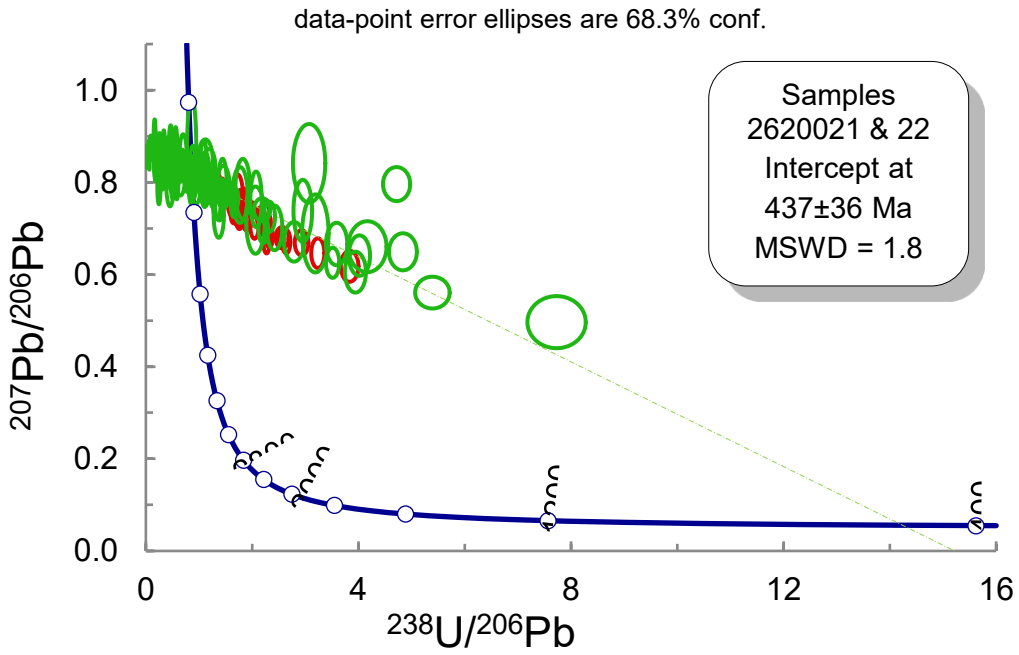

Figure 9 U-Pb Tera-Wasserburg concordia diagram for titanite grains from the mineralised sample 2620021 from the MinEX CRC NDI NDILLK09 drill hole, Loch lilly-Kars Belt, New South Wales. Corrected data define a mixing line (isochron) anchored at a common $^{207}Pb/^{206}Pb$ composition of 0.852 ± 0.015. The lower intercept yields a crystallization age 437 ± 36 Ma (2σ sigma, MSWD = 1.8). Data point error ellipses are 68% confidence level.

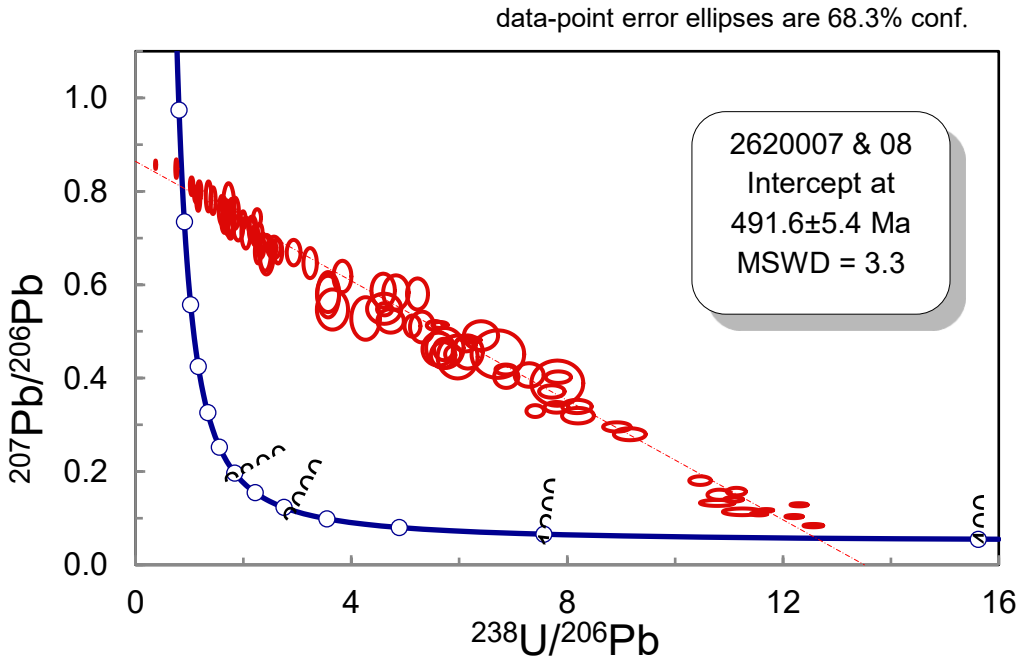

Figure 10 U-Pb Tera-Wasserburg concordia diagram for titanite grains from the mineralised sample 2620007 from the MinEX CRC NDI NDIWMP02 drill hole, Loch lilly-Kars Belt, New South Wales. Corrected data define a mixing line (isochron) anchored at a common $^{207}Pb/^{206}Pb$ composition of 0.852 ± 0.015. The lower intercept yields a crystallization age 492 ± 5 Ma (2σ sigma, MSWD = 3.3). Data point error ellipses are 68% confidence level.

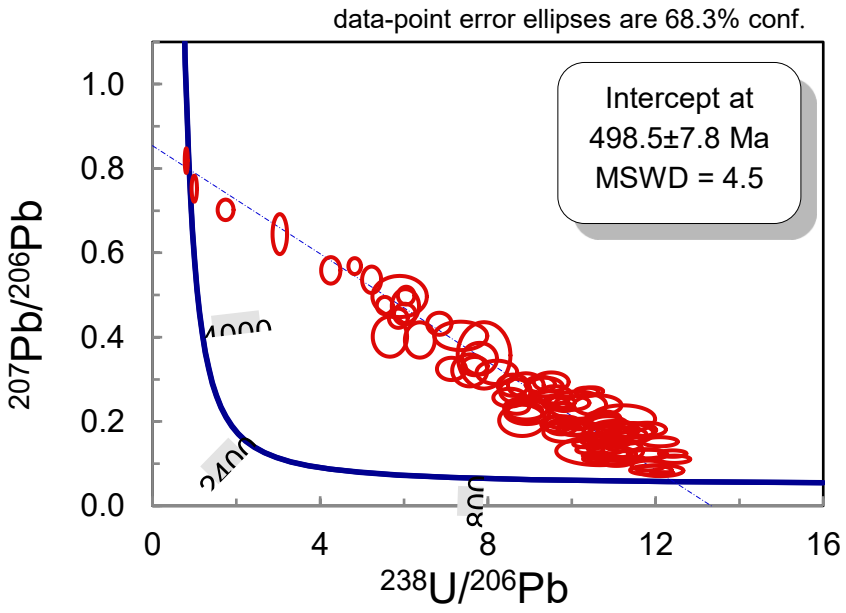

Figure 11 U-Pb Tera-Wasserburg concordia diagram for titanite grains from the mineralised sample 2022330094 from the Quondong porphyry Cu-Au prospect, Loch lilly-Kars Belt, New South Wales. Corrected data define a mixing line (isochron) anchored at a common $^{207}Pb/^{206}Pb$ composition of 0.852 ± 0.015. The lower intercept yields a crystallization age 499 ± 8 Ma (2σ sigma, MSWD = 4.5). Data point error ellipses are 68% confidence level.

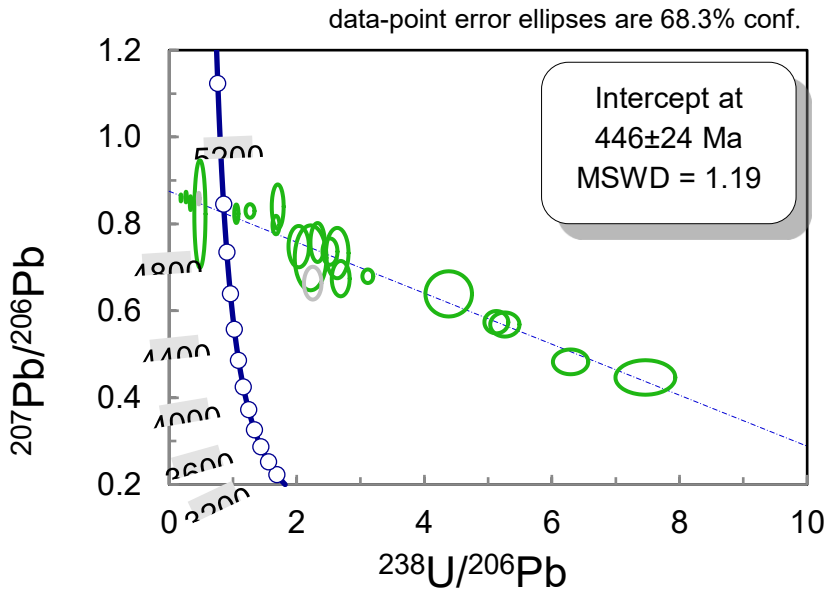

Figure 12 U-Pb Tera-Wasserburg concordia diagram for titanite grains from the mineralised sample 321889 from the Eclipse porphyry Cu-Au prospect, Grampian-Stavely Belt, Victoria. Corrected data define a mixing line (isochron) anchored at a common $^{207}Pb/^{206}Pb$ composition of 0.852 ± 0.015. The lower intercept yields a crystallization age 446 ± 24 Ma (2σ sigma, MSWD = 1.2). Data point error ellipses are 68% confidence level.

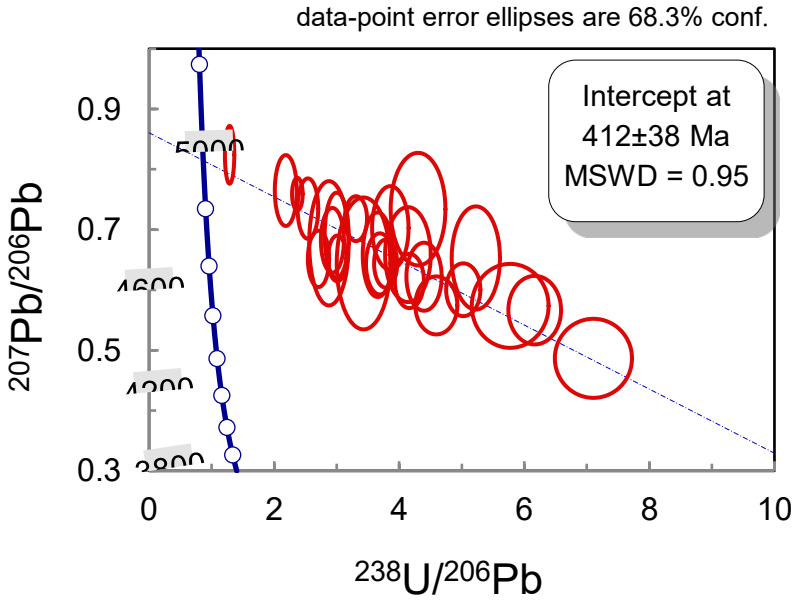

Figure 13 U-Pb Tera-Wasserburg concordia diagram for titanite grains from the mineralised sample 2022440190 from the Eclipse porphyry Cu-Au prospect, Koonenberry Belt, New South Wales. Corrected data define a mixing line (isochron) anchored at a common $^{207}Pb/^{206}Pb$ composition of 0.852 ± 0.015. The lower intercept yields a crystallization age 412 ± 38 Ma (2σ sigma, MSWD = 1.0). Data point error ellipses are 68% confidence level.

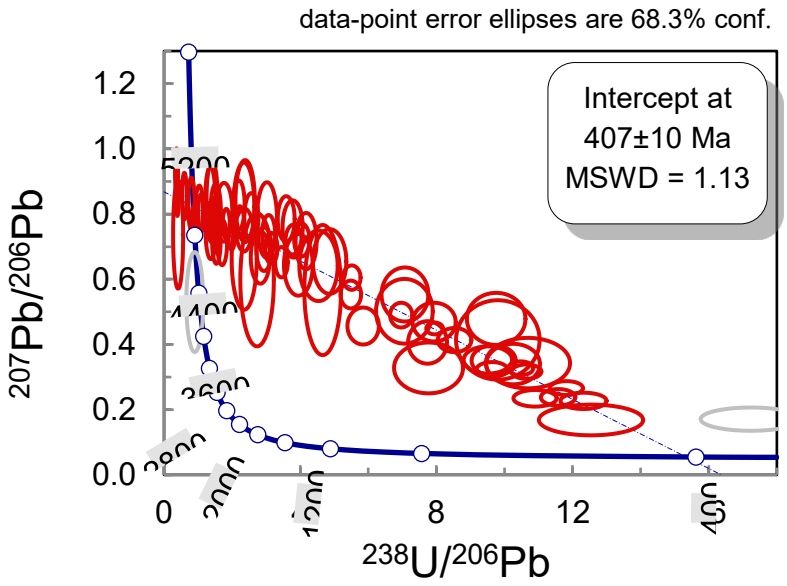

Figure 14 U-Pb Tera-Wasserburg concordia diagram for titanite grains from the mineralised sample 2022440196 from the Bunker Hill porphyry Cu-Au prospect, Koonenberry Belt, New South Wales. Corrected data define a mixing line (isochron) anchored at a common $^{207}Pb/^{206}Pb$ composition of 0.852 ± 0.015. The lower intercept yields a crystallization age 407 ± 10 Ma (2σ sigma, MSWD = 1.1). Data point error ellipses are 68% confidence level.

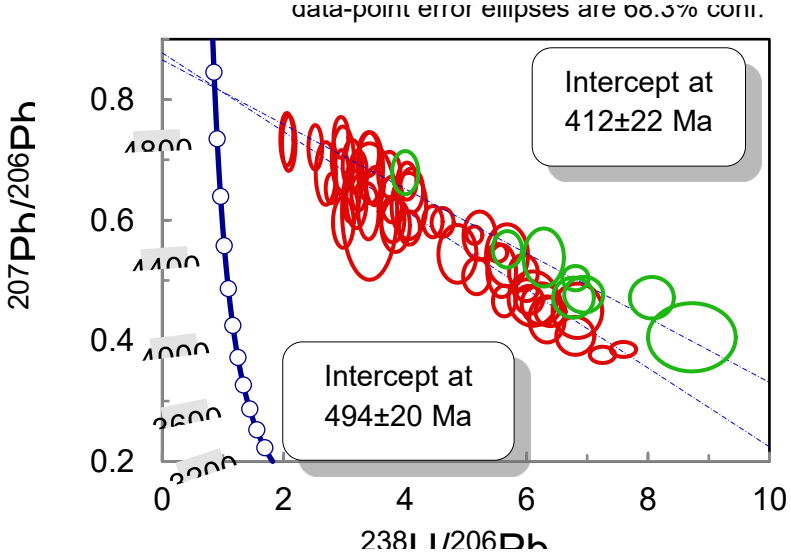

Figure 15 U-Pb Tera-Wasserburg concordia diagram for titanite grains from the mineralised sample 321864 from the Gerang Gerung skarn Zn prospect, Grampian-Stavely Belt, Victoria. Corrected data define a mixing line (isochron) anchored at a common $^{207}Pb/^{206}Pb$ composition of 0.852 ± 0.015. The lower intercept yields two crystallization ages, including 412 ± 22 Ma (2σ sigma, MSWD = 0.8), and 494 ± 20 Ma (2σ sigma, MSWD = 1.9). Data point error ellipses are 68% confidence level.

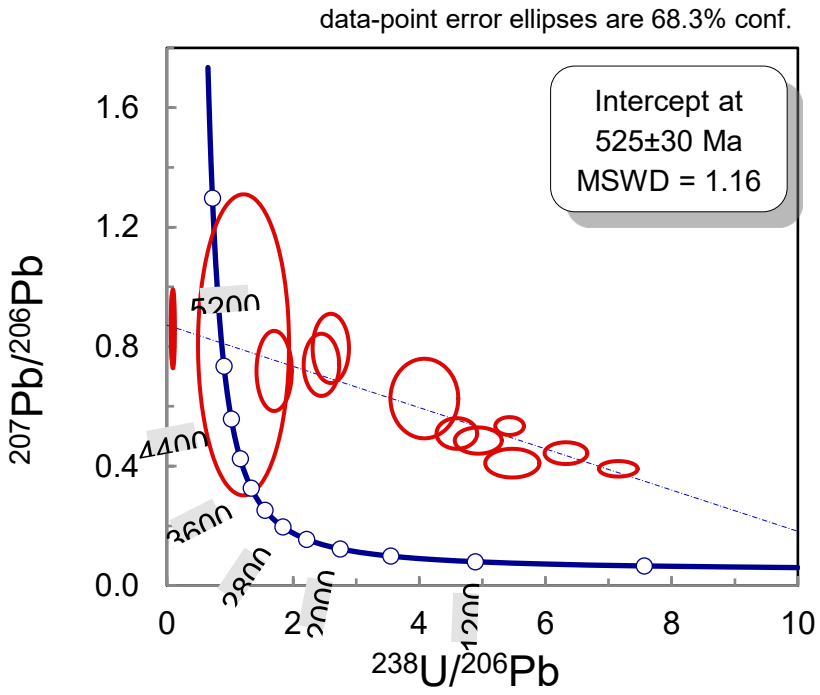

Figure 16 U-Pb Tera-Wasserburg concordia diagram for titanite grains from the mineralised sample 4351206 from the Sherlock VHMS Cu-Zn prospect, Nanyah-Glenelg Belt, South Australia. Corrected data define a mixing line (isochron) anchored at a common $^{207}Pb/^{206}Pb$ composition of 0.852 ± 0.015. The lower intercept yields a crystallization age 525 ± 30 Ma (2σ sigma, MSWD = 1.2). Data point error ellipses are 68% confidence level.

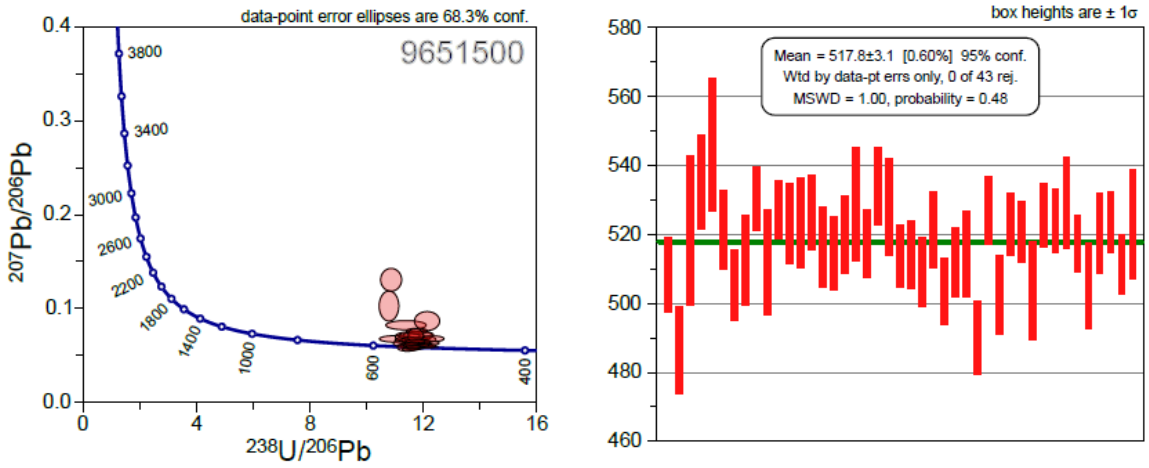

Figure 17 U-Pb Tera-Wasserburg concordia diagram for titanite grains from the mineralised sample 2022330070 from the Wahratta porphyry Cu-Au prospect, Loch Lilly-Kars Belt, New South Wales. Corrected data define a mixing line (isochron) anchored at a common $^{207}Pb/^{206}Pb$ composition of 0.852 ± 0.015. The lower intercept yields a crystallization age 518 ± 3 Ma (2σ sigma, MSWD = 1.0). Data point error ellipses are 68% confidence level.

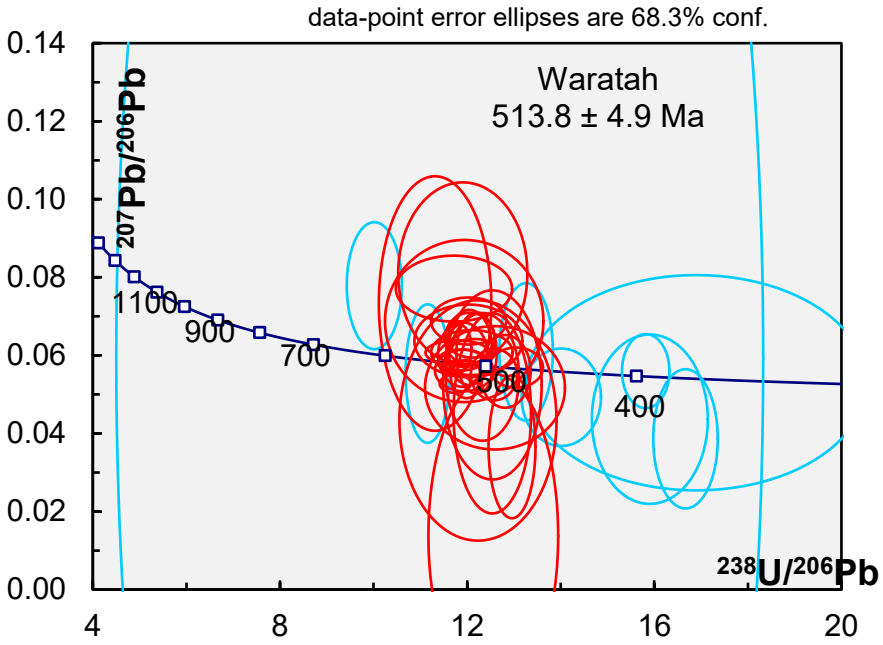

Figure 18 U-Pb Tera-Wasserburg concordia diagram for titanite grains from the mineralised sample 2022330070 from the Wahratta porphyry Cu-Au prospect, Loch Lilly-Kars Belt, New South Wales. Corrected data define a mixing line (isochron) anchored at a common $^{207}Pb/^{206}Pb$ composition of 0.852 ± 0.015. The lower intercept yields a crystallization age 514 ± 5 Ma (2σ sigma, MSWD = 1.0). Data point error ellipses are 68% confidence level.

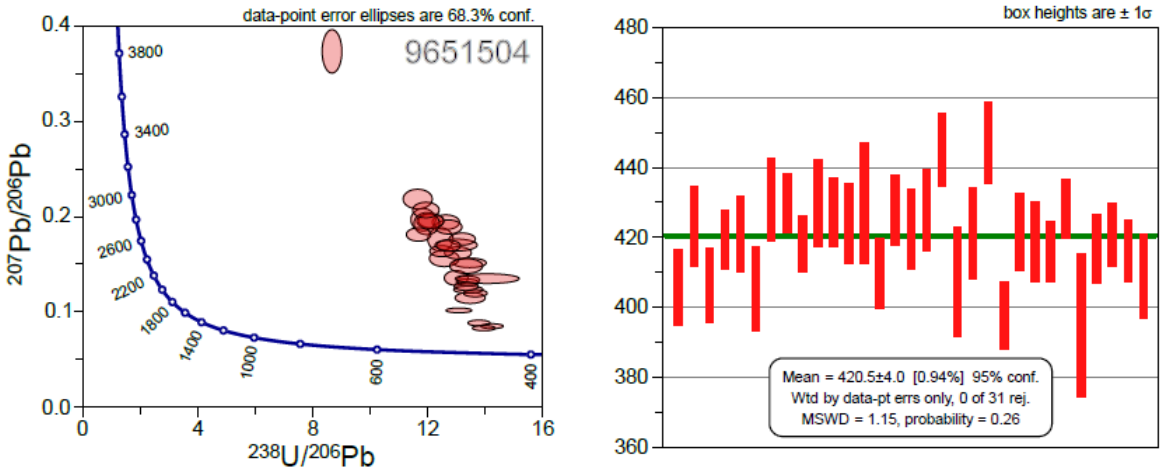

Figure 19 U-Pb Tera-Wasserburg concordia diagram for titanite grains from the mineralised sample 2022330048 from the Eaglehawk skarn Cu-Au prospect, Loch Lilly-Kars Belt, New South Wales. Corrected data define a mixing line (isochron) anchored at a common $^{207}Pb/^{206}Pb$ composition of 0.852 ± 0.015. The lower intercept yields a crystallization age 421 ± 4 Ma (2σ sigma, MSWD = 1.2). Data point error ellipses are 68% confidence level.

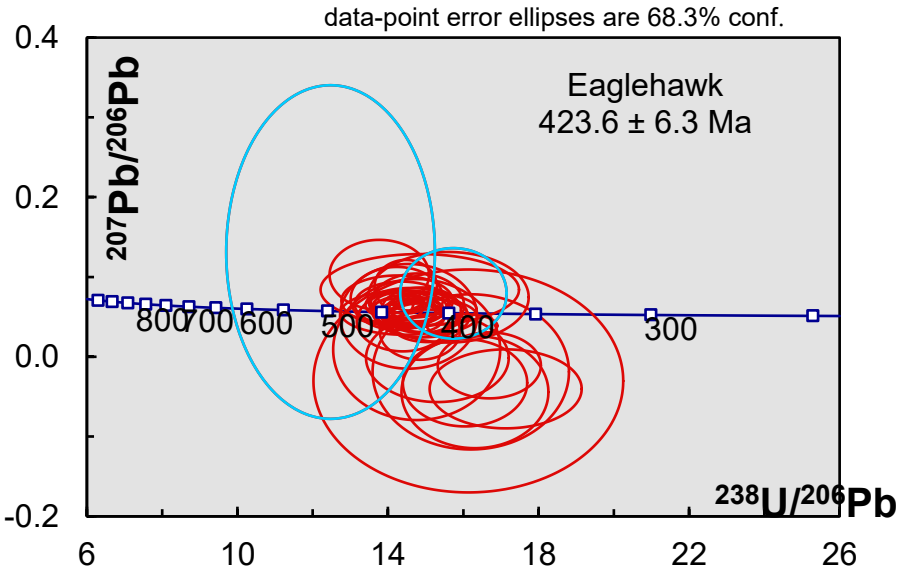

Figure 20 U-Pb Tera-Wasserburg concordia diagram for titanite grains from the mineralised sample 2022330048 from the Eaglehawk skarn Cu-Au prospect, Loch Lilly-Kars Belt, New South Wales. Corrected data define a mixing line (isochron) anchored at a common $^{207}Pb/^{206}Pb$ composition of 0.852 ± 0.015. The lower intercept yields a crystallization age 424 ± 6 Ma (2σ sigma, MSWD = 1.2). Data point error ellipses are 68% confidence level.

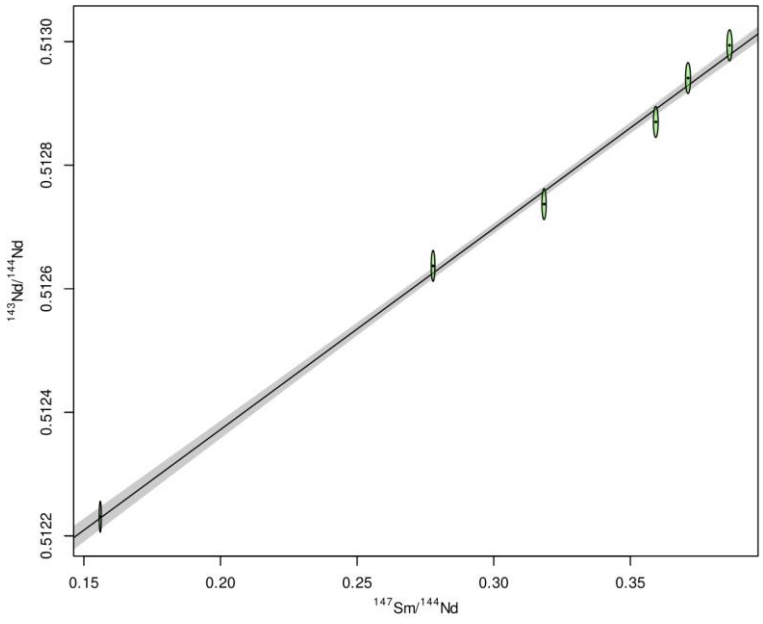

Figure 21 Sm-Nd whole-rock isochron diagram for the fluorite of the Scropes Range skarn Zn-Pb prospect, Loch Lilly-Kars Belt, New South Wales. The calculated age is 498 ± 16 Ma (2σ sigma, MSWD = 3.2) with an initial $^{143}Nd/^{144}Nd$ ratio of 0.51042 ± 0.00005 (εNd = +3.4) and an MSWD of 1.2. Ellipses denote 2σ analytical uncertainties. Where error ellipses are not visible, the uncertainty is smaller than the symbol size. The ^{147}Sm decay constant used is 6.54 × 10^{-12} yr^{-1}.

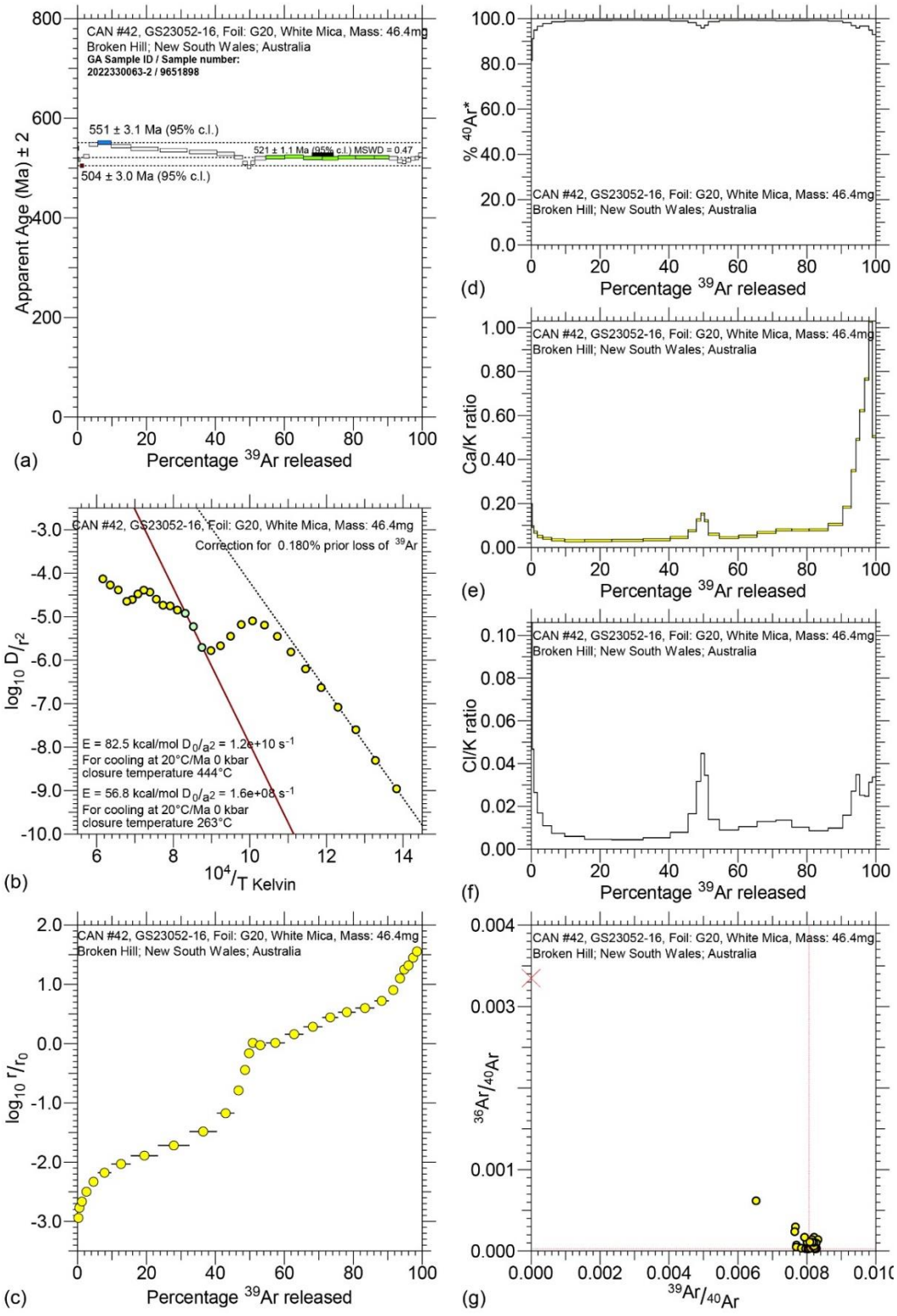

Figure 22 Ar-Ar age of the mica sample 2022330063 from Wahratta porphyry Cu-Au prospect of the Loch Lilly-Kars Belt, New South Wales. The calculated age is 521 ± 1.1 Ma (2σ sigma, MSWD = 2.2)

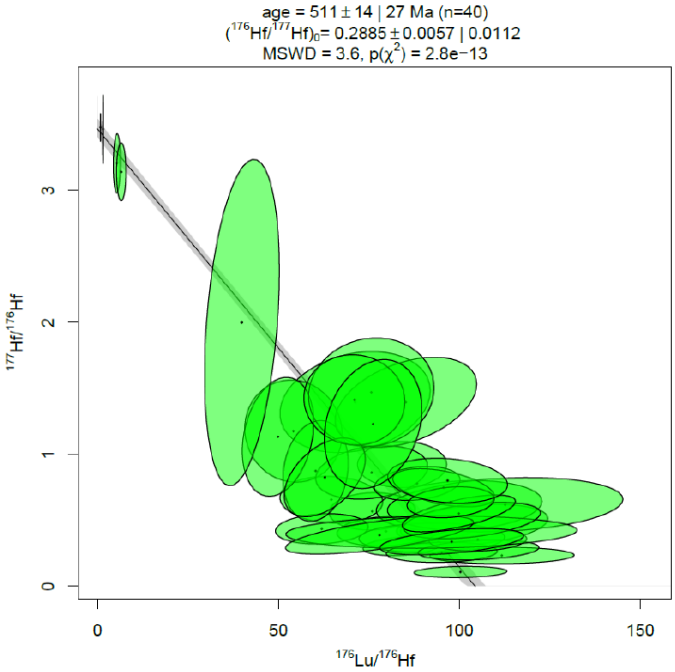

Figure 23 LA-ICP-MS Rb-Sr age of the siderite sample 2023440366 from Thackaringa Ag-Pb-Zn prospect of the Loch Lilly-Kars Belt, New South Wales. The calculated age is 511 ± 14 Ma (2σ sigma, MSWD = 3.6)

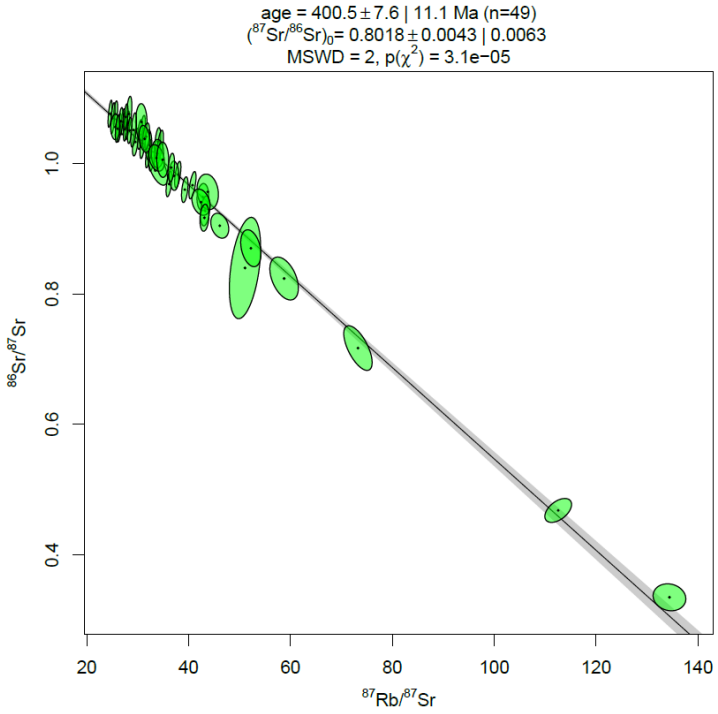

Figure 24 LA-ICP-MS Rb-Sr age of the siderite sample 2023440367 from Thackaringa Ag-Pb-Zn prospect of the Loch Lilly-Kars Belt, New South Wales. The calculated age is 401 ± 8 Ma (2σ sigma, MSWD = 2.0)

Four discr

Scope
Data quality flags
Key thresholds

Appendix 3 — Geochemical fertility data compilation

Delamerian convergent margin vs. global tectono-metallogenic analogues

rimination diagrams: Sr/Y vs La/Yb, V/Sc vs SiO_2 , ΔFMQ vs Sr/Y, (Eu/Eu*)/Yb vs (Ce/Nd)/Y

Individual data points (whole-rock or mean zircon analyses) for all suites plotted in the four geochemical fertility discrimination diagrams. Global analogues: Andean porphyry Cu giants, Oyu Tolgoi (CAOB), Erdenet (CAOB), Kuroko/Green Tuff Belt (Japan). Delamerian Orogen: Zones 1-4 (Koonenberry, Loch Lilly-Kars, Anabama-Glenelg, Stavely).
Literature-confirmed: value explicitly reported or calculated from reported from isotopic systematics or analogue deposits.
Cu-fertile: Sr/Y >35 (Loucks 2014); V/Sc >32.5−0.385×SiO_2 (Loucks 2014); ΔFMQ >+1 (Richards 2015); (Eu/Eu*)/Yb >0.7 AND (Ce/Nd)/Y >0.09 (Lu et al. 2016; Loucks et al. 2024). ND = not determined. All Sr/Y, La/Yb, V/Sc ratios are dimensionless.

Sample ID	System	Belt / Deposit	Suite / Phase	Age (Ma)	SiO_2 (wt%)
GS-01	Delamerian	Stavely (Zone 4)	GS late porphyry (Victor QMD)	503.8	62.0
GS-02	Delamerian	Stavely (Zone 4)	GS late porphyry (Victor QMD)	503.8	64.0
GS-03	Delamerian	Stavely (Zone 4)	GS late porphyry (Victor QMD)	503.8	61.0
GS-04	Delamerian	Stavely (Zone 4)	GS arc MSVC (pre-porphyry)	507.3	63.0
LK-01	Delamerian	Loch Lilly–Kars (Zone 2)	LK Devonian monzodiorite (fertile)	424.0	60.0
LK-02	Delamerian	Loch Lilly–Kars (Zone 2)	LK Devonian monzodiorite (fertile)	421.0	58.0
LK-03	Delamerian	Loch Lilly–Kars (Zone 2)	LK Cambrian arc (non-fertile)	496.0	57.0
NG-01	Delamerian	Anabama–Glenelg (Zone 3)	NG S-type (Port Elliot Granite)	508.0	72.0
NG-02	Delamerian	Anabama–Glenelg (Zone 3)	NG I-type (Tanunda Creek/Palmer)	510.0	67.0
KB-01	Delamerian	Koonenberry (Zone 1)	KB Mt Wright Arc (calc-alkaline)	510.0	63.0
KB-02	Delamerian	Koonenberry (Zone 1)	KB Tibooburra A-type rhyolite	424.0	75.0
AND-01	Andes	El Teniente, Chile	El Teniente intrusive complex	6.0	64.0
AND-02	Andes	El Teniente, Chile	El Teniente ore-stage porphyry	5.5	62.0
AND-03	Andes	Los Pelambres, Chile	Los Pelambres porphyry	9.0	64.0
AND-04	Andes	Los Pelambres, Chile	Los Pelambres late porphyry	8.0	65.0
AND-05	Andes	Don Javier / Toquepala arc, Peru	Don Javier dacite porphyry (~60 Ma)	60.0	65.0
AND-06	Andes	Don Javier / Toquepala arc, Peru	Toquepala pre-mineral arc magmas	65.0	63.0
AND-07	Andes	Quellaveco, Peru	Quellaveco syn-mineral porphyry	56.0	64.0
OT-01	CAOB	Oyu Tolgoi, Mongolia	Hugo North QMD porphyry	372.0	62.0
OT-02	CAOB	Oyu Tolgoi, Mongolia	Hugo North QMD (mean)	372.0	63.0

ERD-01	CAOB	Erdenet, Mongolia	Erdenet granodiorite Gr-2	240.0	62.0
ERD-02	CAOB	Erdenet, Mongolia	Erdenet granodiorite Gr-11	240.0	64.0
KUR-01	Japan	Kuroko / Green Tuff Belt, Japan	Kuroko felsic host rhyolite	15.0	76.0
KUR-02	Japan	Kuroko / Green Tuff Belt, Japan	Kuroko felsic volcanics (bimodal)	14.0	78.0
DEL-01	Delamerian	Anabama Hill, South Australia	Anabama Hill granodiorite	509.0	65.0
DEL-02	Delamerian	Anabama Hill, South Australia	Anabama Hill porphyritic diorite	509.0	63.0
DEL-03	Delamerian	Netley Hill, South Australia	Netley Hill granodiorite	507.0	64.0
DEL-04	Delamerian	Bendigo, South Australia	Bendigo granodiorite	505.0	66.0
DEL-05	Delamerian	Colebatch, South Australia	Colebatch A-type granite	490.0	74.0

Sr (ppm)	Y (ppm)	Sr/Y	La (ppm)	Yb (ppm)	La/Yb	V (ppm)	Sc (ppm)	V/Sc	ΔFMQ	(Eu/Eu*)/Yb (zircon)	(Ce/Nd)/Y (zircon)
490	10.0	49.0	35.0	0.70	50.0	180	13.0	13.8	2.0	1.20	0.130
520	9.0	57.8	40.0	0.75	53.3	195	12.0	16.3	2.5	1.35	0.140
440	14.0	31.4	30.0	0.68	44.1	160	11.0	14.5	1.5	1.10	0.118
320	16.0	20.0	22.0	0.90	24.4	120	16.0	7.5	1.2	0.85	0.090
520	11.0	47.3	34.0	0.82	41.5	230	18.0	12.8	2.0		
580	12.0	48.3	36.0	0.79	45.6	255	20.0	12.8	1.8		
260	18.0	14.4	16.0	1.10	14.5	95	22.0	4.3	0.5		
95	14.0	6.8	25.0	2.20	11.4	30	8.0	3.8	-0.7	0.42	0.068
310	12.0	25.8	28.0	1.20	23.3	85	14.0	6.1	1.0	0.78	0.095
215	20.0	10.8	14.0	1.40	10.0	60	18.0	3.3	0.4		
80	22.0	3.6	8.0	1.90	4.2	15	6.0	2.5	-0.2		
1100	7.0	157.1	38.0	0.90	42.2	140	10.0	14.0	2.2	1.40	0.145
980	9.0	108.9	33.0	0.80	41.3	130	10.0	13.0	2.0	1.30	0.142
760	8.0	95.0	34.0	0.70	48.6	120	11.0	10.9	2.1	1.25	0.138
850	7.0	121.4	40.0	0.65	61.5	125	12.0	10.4	2.3	1.20	0.140
720	7.0	102.9	30.0	0.85	35.3	135	13.0	10.4	1.1	1.05	0.120
210	18.0	11.7	16.0	1.30	12.3	70	15.0	4.7	-0.5	0.40	0.070
680	9.0	75.6	29.0	0.72	40.3	115	12.0	9.6	2.0	1.15	0.125
620	10.0	62.0	28.0	0.65	43.1	165	13.0	12.7	2.0	1.15	0.128
580	9.0	64.4	26.0	0.62	41.9	155	12.0	12.9	2.2	1.20	0.130

460	8.0	57.5				175	14.0	12.5	5.2	0.62	0.105
490	7.0	70.0				180	15.0	12.0	5.8	0.68	0.112
55	35.0	1.6	12.0	2.80	4.3	18	12.0	1.5	0.5	0.30	0.055
40	42.0	1.0	10.0	3.20	3.1	12	10.0	1.2	0.8	0.25	0.048
									2.1	0.72	0.118
									1.9	0.58	0.108
									1.4	0.45	0.092
									1.3	0.40	0.088
									0.4	0.22	0.065

εHf(t)	$\delta^{18}O$ zrc (‰)	Cu-Fertility	Reference
11.0	6.5	YES	Schofield et al. (2018)
12.5	6.8	YES	Schofield et al. (2018)
8.5	6.2	YES	Schofield et al. (2018)
5.0	6.0	PARTIAL	Schofield et al. (2018)
2.5	6.8	YES	Baatar et al. (2020)
1.5	7.0	YES	Baatar et al. (2020)
1.5	6.5	NO	Baatar et al. (2020)
-8.0	7.8	Sn-W	Turner et al. (2022)
-2.0	7.0	PARTIAL	Turner et al. (2022)
5.0	5.8	NO	Gilmore et al. (2025)
		NO	Gilmore et al. (2025)
		YES	Rabbia et al. (2000)
		YES	Rabbia et al. (2000)
		YES	Reich et al. (2003)
		YES	Reich et al. (2003)
		YES	Chen et al. (2022)
		NO	Chen et al. (2023)
		YES	Nathwani et al. (2021)
13.0	6.5	YES	Wainwright et al. (2011)
12.5	6.3	YES	Dolgopolova et al. (2013)

		YES	Shen et al. (2015)
		YES	Shen et al. (2015)
		NO	Agangi et al. (2022)
		NO	Agangi et al. (2022)
		YES	Hong et al. (2024)
		YES	Hong et al. (2024)
		YES	Hong et al. (2024)
		YES	Hong et al. (2024)
		NO	Hong et al. (2024)

Full Reference	DOI
Schofield A et al. (2018) Regional geology and mineral systems of the Stavely Arc, western Victoria. Geoscience Australia Record 2018/02, GeoCat 115622	10.11636/Record.2018.002
Schofield A et al. (2018) Regional geology and mineral systems of the Stavely Arc, western Victoria. Geoscience Australia Record 2018/02, GeoCat 115622	10.11636/Record.2018.002
Schofield A et al. (2018) Regional geology and mineral systems of the Stavely Arc, western Victoria. Geoscience Australia Record 2018/02, GeoCat 115622	10.11636/Record.2018.002
Schofield A et al. (2018) Regional geology and mineral systems of the Stavely Arc, western Victoria. Geoscience Australia Record 2018/02, GeoCat 115622	10.11636/Record.2018.002
Baatar B, Parra-Avila LA, Fiorentini ML, Polito P, Crawford AJ (2020) Porphyry Cu fertility of the Loch Lilly-Kars Belt, western NSW, Australia. Aust J Earth Sci 67(1):75-87	10.1080/08120099.2019.1637937
Baatar B, Parra-Avila LA, Fiorentini ML, Polito P, Crawford AJ (2020) Porphyry Cu fertility of the Loch Lilly-Kars Belt, western NSW, Australia. Aust J Earth Sci 67(1):75-87	10.1080/08120099.2019.1637937
Baatar B, Parra-Avila LA, Fiorentini ML, Polito P, Crawford AJ (2020) Porphyry Cu fertility of the Loch Lilly-Kars Belt, western NSW, Australia. Aust J Earth Sci 67(1):75-87	10.1080/08120099.2019.1637937
Turner S et al. (2022) A comparison of granite genesis in the Adelaide Fold Belt and Glenelg River Complex using U-Pb, Hf and O isotopes in zircon. J Petrology 63(11):egac102	10.1093/petrology/egac102
Turner S et al. (2022) A comparison of granite genesis in the Adelaide Fold Belt and Glenelg River Complex using U-Pb, Hf and O isotopes in zircon. J Petrology 63(11):egac102	10.1093/petrology/egac102
Gilmore PJ et al. (2025) The Delamerian Orogen on mainland Australia plotted in time and space. Geoscience Australia Record 2025/03	10.26186/149699
Gilmore PJ et al. (2025) The Delamerian Orogen on mainland Australia plotted in time and space. Geoscience Australia Record 2025/03	10.26186/149699
Rabbia OM et al. (2000) High-Al TTG-like suite at the El Teniente porphyry copper deposit, Chile. Proc IX Congreso Geológico Chileno 2:740-744	N/A
Rabbia OM et al. (2000) High-Al TTG-like suite at the El Teniente porphyry copper deposit, Chile. Proc IX Congreso Geológico Chileno 2:740-744	N/A
Reich M, Parada MA et al. (2003) Adakite-like signature of Late Miocene intrusions at the Los Pelambres giant porphyry Cu deposit, Andes of central Chile. Mineral Deposita 38(7):876-885	10.1007/s00126-003-0369-9
Reich M, Parada MA et al. (2003) Adakite-like signature of Late Miocene intrusions at the Los Pelambres giant porphyry Cu deposit, Andes of central Chile. Mineral Deposita 38(7):876-885	10.1007/s00126-003-0369-9
Chen J et al. (2022) Rapid transition to fertile magma and promotion of porphyry mineralization: A case study from the Don Javier deposit. Ore Geol Rev 143:104777	10.1016/j.oregeorev.2022.104777
Chen J et al. (2023) Arc magmatic evolution and porphyry copper deposit formation under compressional regime: Toquepala arc, Southern Peru. Earth-Science Reviews 240:104378	10.1016/j.earscirev.2023.104378
Nathwani CL et al. (2021) From long-lived batholith construction to giant porphyry copper deposit formation: petrological and zircon chemical evolution of the Quellaveco District, Southern Peru. Contrib Mineral Petrol 176(1):12	10.1007/s00410-020-01766-1
Wainwright AJ et al. (2011) Devonian and Carboniferous arcs of the Oyu Tolgoi porphyry Cu-Au district, South Gobi region, Mongolia. Gondwana Res 19(3):764-787	10.1016/j.gr.2010.08.003
Dolgopolova A et al. (2013) Sr-Nd-Pb-Hf isotope systematics of the Hugo Dummett Cu-Au porphyry deposit (Oyu Tolgoi, Mongolia). Lithos 164-167:47-64	10.1016/j.lithos.2012.11.017

Shen P et al. (2015) Oxidation condition and metal fertility of granitic magmas: Zircon trace-element data from porphyry Cu deposits in the Central Asian Orogenic Belt. Econ Geol 110(7):1861-1878	10.2113/econgeo.110.7.1861
Shen P et al. (2015) Oxidation condition and metal fertility of granitic magmas: Zircon trace-element data from porphyry Cu deposits in the Central Asian Orogenic Belt. Econ Geol 110(7):1861-1878	10.2113/econgeo.110.7.1861
Agangi A et al. (2022) Magmatic evolution and metal systematics of back-arc volcanic rocks of NE Japan and implications for deposition of massive sulphide Kuroko ores. Contrib Mineral Petrol 177:115	10.1007/s00410-022-01980-z
Agangi A et al. (2022) Magmatic evolution and metal systematics of back-arc volcanic rocks of NE Japan and implications for deposition of massive sulphide Kuroko ores. Contrib Mineral Petrol 177:115	10.1007/s00410-022-01980-z
Hong W et al. (2024) Using zircon and apatite chemistry to fingerprint porphyry Cu-Mo±Au mineralization in the Delamerian Orogen, South Australia. Mineral Deposita 59(7):1619-1640	10.1007/s00126-024-01287-y
Hong W et al. (2024) Using zircon and apatite chemistry to fingerprint porphyry Cu-Mo±Au mineralization in the Delamerian Orogen, South Australia. Mineral Deposita 59(7):1619-1640	10.1007/s00126-024-01287-y
Hong W et al. (2024) Using zircon and apatite chemistry to fingerprint porphyry Cu-Mo±Au mineralization in the Delamerian Orogen, South Australia. Mineral Deposita 59(7):1619-1640	10.1007/s00126-024-01287-y
Hong W et al. (2024) Using zircon and apatite chemistry to fingerprint porphyry Cu-Mo±Au mineralization in the Delamerian Orogen, South Australia. Mineral Deposita 59(7):1619-1640	10.1007/s00126-024-01287-y
Hong W et al. (2024) Using zircon and apatite chemistry to fingerprint porphyry Cu-Mo±Au mineralization in the Delamerian Orogen, South Australia. Mineral Deposita 59(7):1619-1640	10.1007/s00126-024-01287-y

Notes
Late porphyry phase, mean of available analyses; V/Sc above Loucks threshold. ΔFMQ estimated from mineral assemblage (Schofield 2018; Baatar 2020). Sr/Y representative mid-range value (25-60 reported).
Higher Sr/Y end of porphyry range; εHf upper end (+14 max).
Lower end of GS porphyry range; still above Sr/Y=35 threshold for most analyses.
Pre-porphyry calc-alkaline arc sequence; moderate ΔFMQ but Sr/Y below threshold.
Devonian fertile suite; 165 WR + 428 zircon analyses underpinning these estimates. Sr/Y 38-55 range; representative mid-point used. ΔFMQ +1.4 to +2.2 (Baatar 2020).
Upper fertile suite; εHf range 0 to +5 (Baatar 2020); δ18O_zrc 6.0-7.5‰.
Cambrian monzonitic suite; below Sr/Y threshold; post-orogenic context.
S-type peraluminous granite; εHf -6 to -10, δ18O 7.5-8.1‰ (Turner 2022; Foden 2020). A/CNK 1.1-1.3; ΔFMQ -0.9 to -0.5; Cu-barren, Sn-W fertile.
I-type tonalite; transitional magmatic character. εHf +2 to -6 (Turner 2022).
Mt Wright Arc medium-K calc-alkaline; Sr/Y 10-25, V/Sc <10, ΔFMQ <+1 (ilmenite-series). VHMS target only.
Post-kinematic A-type rhyolite; Rb/Sr >2, Zr >200 ppm. Fully barren for Cu-Au.
High-Al TTG-like suite; Sr/Y 82-185, representative mean ~130. La/Yb 27-44 reported (Rabbia 2000; Stern et al. 2011).
Syn-mineralisation porphyry; high Sr/Y reflecting crustal thickness ~50-60 km in Andean setting.
Adakite-like signature; Sr 638-869 ppm, Y 6-10 ppm (Reich 2003). Sr/Y 72-126, La/Yb_N 25-60 reported.
Higher-grade late porphyry facies; representative of highest Sr/Y end of suite.
Syn-mineralisation porphyry; ΔFMQ +1.1 (Chen 2022). Toquepala syn-orogenic avg Sr/Y 104.4, La/Yb 29.6 (Chen 2023).
Pre-mineralisation arc; ΔFMQ -0.5 (Chen 2022); Sr/Y 18.6, La/Yb 11.5 (Chen 2023).
Zircon Eu/Eu* >0.3-0.4; Hf 9,000-11,000 ppm; Sr/Y >40 (Nathwani 2021).
Syn-mineral QMD porphyry; εHf +11.6 to +14.5 (Dolgopolova 2013). Sr/Y 'high adakitic' confirmed; representative estimate used (Wainwright 2011). εNd(t) +3.4 to +7.4; 87Sr/86Sr 0.7037-0.7045.
Second representative analysis; εHf toward higher end (+14.5 max).

Zircon: Eu/Eu* 0.54-0.70 (mean ~0.62); Ce4+/Ce3+ 167-492 (mean ~330). ΔFMQ = ΔNNO -0.67 → Shen 2015 reports ΔNNO +3.7 to +7.4; ΔFMQ = ΔNNO - 0.67 → ΔFMQ +3.0 to +6.7; representative mean +4.5 used. 87Sr/86Sr 0.7037-0.7039; adakite-like high Sr/Y (Kavalieris 2017).
Higher end of Erdenet zircon suite; Ce4+/Ce3+ 492 (maximum); Ti-in-zircon T = 684-728°C range (Shen 2015).
Back-arc rhyolite host: SiO2 >75 wt%, La/Yb_N 1-11 (Agangi 2022). Low Sr/Y due to high Y from HFSE-rich back-arc melts. ΔFMQ +1.5 estimated from Agangi 2022; V/Sc well below Loucks threshold.
Higher-SiO2 end of bimodal rhyolite suite; negative Sr anomaly confirmed (plagioclase fractionation dominant). Ishihara (1977) ilmenite-series character.
Zircon ΔFMQ +2.1±0.4; >90% zircons in fertile field for (Eu/Eu*)/Yb and (Ce/Nd)/Y criteria (Hong 2024). Zircon Eu/Eu* 0.2-0.78 range; representative high-end individual shown here.
Porphyritic diorite phase; ΔFMQ +1.9±0.5 (Hong 2024). Lower (Eu/Eu*)/Yb than granodiorite but still in fertile field.
ΔFMQ +1.3 to +1.5 ±0.6 (Hong 2024). Just at fertile boundary.
ΔFMQ +1.3±0.4 (Hong 2024); marginally fertile.
Post-tectonic A-type; ΔFMQ +0.4±1.1; below fertile threshold (Hong 2024). Zircon fertility criteria not satisfied.

Plot 1 — Sr/Y vs. La/Y

Sample ID	System	Belt / Deposit	Suite / Phase	Age (Ma)
GS-01	Delamerian	Grampians–Stavely (Zone 4)	GS late porphyry (Victor QMD)	503.84
GS-02	Delamerian	Grampians–Stavely (Zone 4)	GS late porphyry (Victor QMD)	503.84
GS-03	Delamerian	Grampians–Stavely (Zone 4)	GS late porphyry (Victor QMD)	503.84
GS-04	Delamerian	Grampians–Stavely (Zone 4)	GS arc MSVC (pre-porphyry)	507.34
LK-01	Delamerian	Loch Lilly–Kars (Zone 2)	LK Devonian monzodiorite (fertile)	424
LK-02	Delamerian	Loch Lilly–Kars (Zone 2)	LK Devonian monzodiorite (fertile)	421
LK-03	Delamerian	Loch Lilly–Kars (Zone 2)	LK Cambrian arc (non-fertile)	496
NG-01	Delamerian	Nanyah–Glenelg (Zone 3)	NG S-type (Port Elliot Granite)	508
NG-02	Delamerian	Nanyah–Glenelg (Zone 3)	NG I-type (Tanunda Creek/Palmer)	510
KB-01	Delamerian	Koonenberry (Zone 1)	KB Mt Wright Arc (calc-alkaline)	510
KB-02	Delamerian	Koonenberry (Zone 1)	KB Tibooburra A-type rhyolite	424
AND-01	Andes	El Teniente, Chile	El Teniente intrusive complex	6
AND-02	Andes	El Teniente, Chile	El Teniente ore-stage porphyry	5.5
AND-03	Andes	Los Pelambres, Chile	Los Pelambres porphyry	9
AND-04	Andes	Los Pelambres, Chile	Los Pelambres late porphyry	8
AND-05	Andes	Don Javier / Toquepala arc, Peru	Don Javier dacite porphyry (~60 Ma)	60
AND-06	Andes	Don Javier / Toquepala arc, Peru	Toquepala pre-mineral arc magmas	65
AND-07	Andes	Quellaveco, Peru	Quellaveco syn-mineral porphyry	56
OT-01	CAOB	Oyu Tolgoi, Mongolia	Hugo North QMD porphyry	372
OT-02	CAOB	Oyu Tolgoi, Mongolia	Hugo North QMD (mean)	372
ERD-01	CAOB	Erdenet, Mongolia	Erdenet granodiorite Gr-2	240
ERD-02	CAOB	Erdenet, Mongolia	Erdenet granodiorite Gr-11	240
KUR-01	Japan	Kuroko / Green Tuff Belt, Japan	Kuroko felsic host rhyolite	15
KUR-02	Japan	Kuroko / Green Tuff Belt, Japan	Kuroko felsic volcanics (bimodal)	14
DEL-01	Delamerian	Anabama Hill, South Australia	Anabama Hill granodiorite	509
DEL-02	Delamerian	Anabama Hill, South Australia	Anabama Hill porphyritic diorite	509
DEL-03	Delamerian	Netley Hill, South Australia	Netley Hill granodiorite	507
DEL-04	Delamerian	Bendigo, South Australia	Bendigo granodiorite	505
DEL-05	Delamerian	Colebatch, South Australia	Colebatch A-type granite	490

Threshold: Sr/Y >35 indicates deep garnet-stable fractionation; La/Yb >15 indicates thick crust (>35 km). Reference: Chiarad

/b (crustal thickness proxy; Chiaradia, 2015)

La/Yb (x-axis)	Sr/Y (y-axis)	Cu-Fertile?	Data Quality	Source (short)
50	49	YES	Literature-confirmed	Schofield et al. (2018)
53.3	57.8	YES	Literature-confirmed	Schofield et al. (2018)
44.1	31.4	YES	Literature-confirmed	Schofield et al. (2018)
24.4	20	PARTIAL	Literature-confirmed	Schofield et al. (2018)
41.5	47.3	YES	Literature-confirmed	Baatar et al. (2020)
45.6	48.3	YES	Literature-confirmed	Baatar et al. (2020)
14.5	14.4	NO	Literature-confirmed	Baatar et al. (2020)
11.4	6.8	Sn-W	Literature-confirmed	Turner et al. (2022)
23.3	25.8	PARTIAL	Literature-confirmed	Turner et al. (2022)
10	10.8	NO	Literature-confirmed	Gilmore et al. (2025)
4.2	3.6	NO	Literature-confirmed	Gilmore et al. (2025)
42.2	157.1	YES	Literature-confirmed	Rabbia et al. (2000)
41.3	108.9	YES	Literature-confirmed	Rabbia et al. (2000)
48.6	95	YES	Literature-confirmed	Reich et al. (2003)
61.5	121.4	YES	Literature-confirmed	Reich et al. (2003)
35.3	102.9	YES	Literature-confirmed	Chen et al. (2022)
12.3	11.7	NO	Literature-confirmed	Chen et al. (2023)
40.3	75.6	YES	Literature-confirmed	Nathwani et al. (2021)
43.1	62	YES	Literature-confirmed	Wainwright et al. (2011)
41.9	64.4	YES	Literature-confirmed	Dolgopolova et al. (2013)
	57.5	YES	Literature-confirmed	Shen et al. (2015)
	70	YES	Literature-confirmed	Shen et al. (2015)
4.3	1.6	NO	Literature-confirmed	Agangi et al. (2022)
3.1	1	NO	Literature-confirmed	Agangi et al. (2022)
		YES	Literature-confirmed	Hong et al. (2024)
		YES	Literature-confirmed	Hong et al. (2024)
		YES	Literature-confirmed	Hong et al. (2024)
		YES	Literature-confirmed	Hong et al. (2024)
		NO	Literature-confirmed	Hong et al. (2024)

ia M (2015) Sci Rep 5:8115; Profeta et al. (2015) Sci Rep 5:17786.

Notes
Late porphyry phase, mean of available analyses; V/Sc above Loucks threshold. ΔFMQ estimated from mineral assemblage.
Higher Sr/Y end of porphyry range; εHf upper end (+14 max).
Lower end of GS porphyry range; still above Sr/Y=35 threshold for most analyses.
Pre-porphyry calc-alkaline arc sequence; moderate ΔFMQ but Sr/Y below threshold.
Devonian fertile suite; 165 WR + 428 zircon analyses underpinning these estimates. Sr/Y 38-55 range.
Upper fertile suite; εHf range 0 to +5 (Baatar 2020); δ18O_zrc 6.0-7.5‰.
Cambrian monzonitic suite; below Sr/Y threshold; post-orogenic context.
S-type peraluminous granite; εHf -6 to -10, δ18O 7.5-8.1‰ (Turner 2022; Foden 2020). A/CNK 1.1-1.3; ΔFMQ -0.9 to -0.5.
I-type tonalite; transitional magmatic character. εHf +2 to -6 (Turner 2022).
Mt Wright Arc medium-K calc-alkaline; Sr/Y 10-25, V/Sc <10, ΔFMQ <+1 (ilmenite-series). VHMS target only.
Post-kinematic A-type rhyolite; Rb/Sr >2, Zr >200 ppm. Fully barren for Cu-Au.
High-Al TTG-like suite; Sr/Y 82-185, representative mean ~130. La/Yb 27-44 reported (Rabbia 2000; Stern et al. 2011).
Syn-mineralisation porphyry; high Sr/Y reflecting crustal thickness ~50-60 km in Andean setting.
Adakite-like signature; Sr 638-869 ppm, Y 6-10 ppm (Reich 2003). Sr/Y 72-126, La/Yb_N 25-60 reported.
Higher-grade late porphyry facies; representative of highest Sr/Y end of suite.
Syn-mineralisation porphyry; ΔFMQ +1.1 (Chen 2022). Toquepala syn-orogenic avg Sr/Y 104.4, La/Yb 29.6 (Chen 2023).
Pre-mineralisation arc; ΔFMQ -0.5 (Chen 2022); Sr/Y 18.6, La/Yb 11.5 (Chen 2023).
Zircon Eu/Eu* >0.3-0.4; Hf 9,000-11,000 ppm; Sr/Y >40 (Nathwani 2021).
Syn-mineral QMD porphyry; εHf +11.6 to +14.5 (Dolgopolova 2013).
Second representative analysis; εHf toward higher end (+14.5 max).
Zircon: Eu/Eu* 0.54-0.70 (mean ~0.62); Ce4+/Ce3+ 167-492 (mean ~330). ΔFMQ = ΔNNO -0.67.
Higher end of Erdenet zircon suite; Ce4+/Ce3+ 492 (maximum); Ti-in-zircon T = 684-728°C range (Shen 2015).
Back-arc rhyolite host: SiO2 >75 wt%, La/Yb_N 1-11 (Agangi 2022). Low Sr/Y due to high Y from HFSE-rich back-arc melts.
Higher-SiO2 end of bimodal rhyolite suite; negative Sr anomaly confirmed (plagioclase fractionation dominant).
Zircon ΔFMQ +2.1±0.4; >90% zircons in fertile field for (Eu/Eu*)/Yb and (Ce/Nd)/Y criteria (Hong 2024).
Porphyritic diorite phase; ΔFMQ +1.9±0.5 (Hong 2024). Lower (Eu/Eu*)/Yb than granodiorite but still in fertile field.
ΔFMQ +1.3 to +1.5 ±0.6 (Hong 2024). Just at fertile boundary.
ΔFMQ +1.3±0.4 (Hong 2024); marginally fertile.
Post-tectonic A-type; ΔFMQ +0.4±1.1; below fertile threshold (Hong 2024). Zircon fertility criteria not satisfied.

Plot 2 — V/S

Sample ID	System	Belt / Deposit	Suite / Phase	Age (Ma)
GS-01	Delamerian	Grampians–Stavely (Zone 4)	GS late porphyry (Victor QMD)	503.84
GS-02	Delamerian	Grampians–Stavely (Zone 4)	GS late porphyry (Victor QMD)	503.84
GS-03	Delamerian	Grampians–Stavely (Zone 4)	GS late porphyry (Victor QMD)	503.84
GS-04	Delamerian	Grampians–Stavely (Zone 4)	GS arc MSVC (pre-porphyry)	507.34
LK-01	Delamerian	Loch Lilly–Kars (Zone 2)	LK Devonian monzodiorite (fertile)	424
LK-02	Delamerian	Loch Lilly–Kars (Zone 2)	LK Devonian monzodiorite (fertile)	421
LK-03	Delamerian	Loch Lilly–Kars (Zone 2)	LK Cambrian arc (non-fertile)	496
NG-01	Delamerian	Nanyah–Glenelg (Zone 3)	NG S-type (Port Elliot Granite)	508
NG-02	Delamerian	Nanyah–Glenelg (Zone 3)	NG I-type (Tanunda Creek/Palmer)	510
KB-01	Delamerian	Koonenberry (Zone 1)	KB Mt Wright Arc (calc-alkaline)	510
KB-02	Delamerian	Koonenberry (Zone 1)	KB Tibooburra A-type rhyolite	424
AND-01	Andes	El Teniente, Chile	El Teniente intrusive complex	6
AND-02	Andes	El Teniente, Chile	El Teniente ore-stage porphyry	5.5
AND-03	Andes	Los Pelambres, Chile	Los Pelambres porphyry	9
AND-04	Andes	Los Pelambres, Chile	Los Pelambres late porphyry	8
AND-05	Andes	Don Javier / Toquepala arc, Peru	Don Javier dacite porphyry (~60 Ma)	60
AND-06	Andes	Don Javier / Toquepala arc, Peru	Toquepala pre-mineral arc magmas	65
AND-07	Andes	Quellaveco, Peru	Quellaveco syn-mineral porphyry	56
OT-01	CAOB	Oyu Tolgoi, Mongolia	Hugo North QMD porphyry	372
OT-02	CAOB	Oyu Tolgoi, Mongolia	Hugo North QMD (mean)	372
ERD-01	CAOB	Erdenet, Mongolia	Erdenet granodiorite Gr-2	240
ERD-02	CAOB	Erdenet, Mongolia	Erdenet granodiorite Gr-11	240
KUR-01	Japan	Kuroko / Green Tuff Belt, Japan	Kuroko felsic host rhyolite	15
KUR-02	Japan	Kuroko / Green Tuff Belt, Japan	Kuroko felsic volcanics (bimodal)	14
DEL-01	Delamerian	Anabama Hill, South Australia	Anabama Hill granodiorite	509
DEL-02	Delamerian	Anabama Hill, South Australia	Anabama Hill porphyritic diorite	509
DEL-03	Delamerian	Netley Hill, South Australia	Netley Hill granodiorite	507
DEL-04	Delamerian	Bendigo, South Australia	Bendigo granodiorite	505
DEL-05	Delamerian	Colebatch, South Australia	Colebatch A-type granite	490

Threshold line: V/Sc = 32.5 − 0.385 × SiO_2 (Loucks 2014, AJES 61:5-16). At SiO_2=62%: threshold V/Sc = 8.6; at SiO_2=6

Sc vs. SiO_2 (Cu-fertility threshold; Loucks, 2014)

SiO_2 wt% (x-axis)	V/Sc (y-axis)	Cu-Fertile?	Data Quality	Source (short)
62	13.8	YES	Literature-confirmed	Schofield et al. (2018)
64	16.3	YES	Literature-confirmed	Schofield et al. (2018)
61	14.5	YES	Literature-confirmed	Schofield et al. (2018)
63	7.5	PARTIAL	Literature-confirmed	Schofield et al. (2018)
60	12.8	YES	Literature-confirmed	Baatar et al. (2020)
58	12.8	YES	Literature-confirmed	Baatar et al. (2020)
57	4.3	NO	Literature-confirmed	Baatar et al. (2020)
72	3.8	Sn-W	Literature-confirmed	Turner et al. (2022)
67	6.1	PARTIAL	Literature-confirmed	Turner et al. (2022)
63	3.3	NO	Literature-confirmed	Gilmore et al. (2025)
75	2.5	NO	Literature-confirmed	Gilmore et al. (2025)
64	14	YES	Literature-confirmed	Rabbia et al. (2000)
62	13	YES	Literature-confirmed	Rabbia et al. (2000)
64	10.9	YES	Literature-confirmed	Reich et al. (2003)
65	10.4	YES	Literature-confirmed	Reich et al. (2003)
65	10.4	YES	Literature-confirmed	Chen et al. (2022)
63	4.7	NO	Literature-confirmed	Chen et al. (2023)
64	9.6	YES	Literature-confirmed	Nathwani et al. (2021)
62	12.7	YES	Literature-confirmed	Wainwright et al. (2011)
63	12.9	YES	Literature-confirmed	Dolgopolova et al. (2013)
62	12.5	YES	Literature-confirmed	Shen et al. (2015)
64	12	YES	Literature-confirmed	Shen et al. (2015)
76	1.5	NO	Literature-confirmed	Agangi et al. (2022)
78	1.2	NO	Literature-confirmed	Agangi et al. (2022)
65		YES	Literature-confirmed	Hong et al. (2024)
63		YES	Literature-confirmed	Hong et al. (2024)
64		YES	Literature-confirmed	Hong et al. (2024)
66		YES	Literature-confirmed	Hong et al. (2024)
74		NO	Literature-confirmed	Hong et al. (2024)

55%: threshold = 7.5.

Notes
Late porphyry phase, mean of available analyses; V/Sc above Loucks threshold. ΔFMQ estimated from mineral assemblage.
Higher Sr/Y end of porphyry range; εHf upper end (+14 max).
Lower end of GS porphyry range; still above Sr/Y=35 threshold for most analyses.
Pre-porphyry calc-alkaline arc sequence; moderate ΔFMQ but Sr/Y below threshold.
Devonian fertile suite; 165 WR + 428 zircon analyses underpinning these estimates. Sr/Y 38-55 range.
Upper fertile suite; εHf range 0 to +5 (Baatar 2020); δ18O_zrc 6.0-7.5‰.
Cambrian monzonitic suite; below Sr/Y threshold; post-orogenic context.
S-type peraluminous granite; εHf -6 to -10, δ18O 7.5-8.1‰ (Turner 2022; Foden 2020). A/CNK 1.1-1.3; ΔFMQ -0.9 to -0.5.
I-type tonalite; transitional magmatic character. εHf +2 to -6 (Turner 2022).
Mt Wright Arc medium-K calc-alkaline; Sr/Y 10-25, V/Sc <10, ΔFMQ <+1 (ilmenite-series). VHMS target only.
Post-kinematic A-type rhyolite; Rb/Sr >2, Zr >200 ppm. Fully barren for Cu-Au.
High-Al TTG-like suite; Sr/Y 82-185, representative mean ~130. La/Yb 27-44 reported (Rabbia 2000; Stern et al. 2011).
Syn-mineralisation porphyry; high Sr/Y reflecting crustal thickness ~50-60 km in Andean setting.
Adakite-like signature; Sr 638-869 ppm, Y 6-10 ppm (Reich 2003). Sr/Y 72-126, La/Yb_N 25-60 reported.
Higher-grade late porphyry facies; representative of highest Sr/Y end of suite.
Syn-mineralisation porphyry; ΔFMQ +1.1 (Chen 2022). Toquepala syn-orogenic avg Sr/Y 104.4, La/Yb 29.6 (Chen 2023).
Pre-mineralisation arc; ΔFMQ -0.5 (Chen 2022); Sr/Y 18.6, La/Yb 11.5 (Chen 2023).
Zircon Eu/Eu* >0.3-0.4; Hf 9,000-11,000 ppm; Sr/Y >40 (Nathwani 2021).
Syn-mineral QMD porphyry; εHf +11.6 to +14.5 (Dolgopolova 2013).
Second representative analysis; εHf toward higher end (+14.5 max).
Zircon: Eu/Eu* 0.54-0.70 (mean ~0.62); Ce4+/Ce3+ 167-492 (mean ~330). ΔFMQ = ΔNNO -0.67.
Higher end of Erdenet zircon suite; Ce4+/Ce3+ 492 (maximum); Ti-in-zircon T = 684-728°C range (Shen 2015).
Back-arc rhyolite host: SiO2 >75 wt%, La/Yb_N 1-11 (Agangi 2022). Low Sr/Y due to high Y from HFSE-rich back-arc melts.
Higher-SiO2 end of bimodal rhyolite suite; negative Sr anomaly confirmed (plagioclase fractionation dominant).
Zircon ΔFMQ +2.1±0.4; >90% zircons in fertile field for (Eu/Eu*)/Yb and (Ce/Nd)/Y criteria (Hong 2024).
Porphyritic diorite phase; ΔFMQ +1.9±0.5 (Hong 2024). Lower (Eu/Eu*)/Yb than granodiorite but still in fertile field.
ΔFMQ +1.3 to +1.5 ±0.6 (Hong 2024). Just at fertile boundary.
ΔFMQ +1.3±0.4 (Hong 2024); marginally fertile.
Post-tectonic A-type; ΔFMQ +0.4±1.1; below fertile threshold (Hong 2024). Zircon fertility criteria not satisfied.

Plot 3 — ΔFMQ vs. Sr/Y (magmatic re

Sample ID	System	Belt / Deposit	Suite / Phase	Age (Ma)
GS-01	Delamerian	Grampians–Stavely (Zone 4)	GS late porphyry (Victor QMD)	503.84
GS-02	Delamerian	Grampians–Stavely (Zone 4)	GS late porphyry (Victor QMD)	503.84
GS-03	Delamerian	Grampians–Stavely (Zone 4)	GS late porphyry (Victor QMD)	503.84
GS-04	Delamerian	Grampians–Stavely (Zone 4)	GS arc MSVC (pre-porphyry)	507.34
LK-01	Delamerian	Loch Lilly–Kars (Zone 2)	LK Devonian monzodiorite (fertile)	424
LK-02	Delamerian	Loch Lilly–Kars (Zone 2)	LK Devonian monzodiorite (fertile)	421
LK-03	Delamerian	Loch Lilly–Kars (Zone 2)	LK Cambrian arc (non-fertile)	496
NG-01	Delamerian	Nanyah–Glenelg (Zone 3)	NG S-type (Port Elliot Granite)	508
NG-02	Delamerian	Nanyah–Glenelg (Zone 3)	NG I-type (Tanunda Creek/Palmer)	510
KB-01	Delamerian	Koonenberry (Zone 1)	KB Mt Wright Arc (calc-alkaline)	510
KB-02	Delamerian	Koonenberry (Zone 1)	KB Tibooburra A-type rhyolite	424
AND-01	Andes	El Teniente, Chile	El Teniente intrusive complex	6
AND-02	Andes	El Teniente, Chile	El Teniente ore-stage porphyry	5.5
AND-03	Andes	Los Pelambres, Chile	Los Pelambres porphyry	9
AND-04	Andes	Los Pelambres, Chile	Los Pelambres late porphyry	8
AND-05	Andes	Don Javier / Toquepala arc, Peru	Don Javier dacite porphyry (~60 Ma)	60
AND-06	Andes	Don Javier / Toquepala arc, Peru	Toquepala pre-mineral arc magmas	65
AND-07	Andes	Quellaveco, Peru	Quellaveco syn-mineral porphyry	56
OT-01	CAOB	Oyu Tolgoi, Mongolia	Hugo North QMD porphyry	372
OT-02	CAOB	Oyu Tolgoi, Mongolia	Hugo North QMD (mean)	372
ERD-01	CAOB	Erdenet, Mongolia	Erdenet granodiorite Gr-2	240
ERD-02	CAOB	Erdenet, Mongolia	Erdenet granodiorite Gr-11	240
KUR-01	Japan	Kuroko / Green Tuff Belt, Japan	Kuroko felsic host rhyolite	15
KUR-02	Japan	Kuroko / Green Tuff Belt, Japan	Kuroko felsic volcanics (bimodal)	14
DEL-01	Delamerian	Anabama Hill, South Australia	Anabama Hill granodiorite	509
DEL-02	Delamerian	Anabama Hill, South Australia	Anabama Hill porphyritic diorite	509
DEL-03	Delamerian	Netley Hill, South Australia	Netley Hill granodiorite	507
DEL-04	Delamerian	Bendigo, South Australia	Bendigo granodiorite	505
DEL-05	Delamerian	Colebatch, South Australia	Colebatch A-type granite	490

Cu-fertile window: BOTH Sr/Y >35 AND ΔFMQ >+1 (green zone in figure). Reference: Richards JP (2015) Lithos 233:27-45

edox and water content; Loucks 2014;

Sr/Y (x-axis)	ΔFMQ (y-axis)	Cu-Fertile?	Source (short)
49	2	YES	Schofield et al. (2018)
57.8	2.5	YES	Schofield et al. (2018)
31.4	1.5	YES	Schofield et al. (2018)
20	1.2	PARTIAL	Schofield et al. (2018)
47.3	2	YES	Baatar et al. (2020)
48.3	1.8	YES	Baatar et al. (2020)
14.4	0.5	NO	Baatar et al. (2020)
6.8	-0.7	Sn-W	Turner et al. (2022)
25.8	1	PARTIAL	Turner et al. (2022)
10.8	0.4	NO	Gilmore et al. (2025)
3.6	-0.2	NO	Gilmore et al. (2025)
157.1	2.2	YES	Rabbia et al. (2000)
108.9	2	YES	Rabbia et al. (2000)
95	2.1	YES	Reich et al. (2003)
121.4	2.3	YES	Reich et al. (2003)
102.9	1.1	YES	Chen et al. (2022)
11.7	-0.5	NO	Chen et al. (2023)
75.6	2	YES	Nathwani et al. (2021)
62	2	YES	Wainwright et al. (2011)
64.4	2.2	YES	Dolgopolova et al. (2013)
57.5	5.2	YES	Shen et al. (2015)
70	5.8	YES	Shen et al. (2015)
1.6	0.5	NO	Agangi et al. (2022)
1	0.8	NO	Agangi et al. (2022)
	2.1	YES	Hong et al. (2024)
	1.9	YES	Hong et al. (2024)
	1.4	YES	Hong et al. (2024)
	1.3	YES	Hong et al. (2024)
	0.4	NO	Hong et al. (2024)

; Loucks RR (2014) AJES 61:5-16.

Richards 2015)

Notes (excerpt)
Late porphyry phase, mean of available analyses; V/Sc above Loucks threshold. ΔFMQ estimated from mineral assemblage.
Higher Sr/Y end of porphyry range; εHf upper end (+14 max).
Lower end of GS porphyry range; still above Sr/Y=35 threshold for most analyses.
Pre-porphyry calc-alkaline arc sequence; moderate ΔFMQ but Sr/Y below threshold.
Devonian fertile suite; 165 WR + 428 zircon analyses underpinning these estimates. Sr/Y 38-55 range.
Upper fertile suite; εHf range 0 to +5 (Baatar 2020); δ18O_zrc 6.0-7.5‰.
Cambrian monzonitic suite; below Sr/Y threshold; post-orogenic context.
S-type peraluminous granite; εHf -6 to -10, δ18O 7.5-8.1‰ (Turner 2022; Foden 2020). A/CNK 1.1-1.3; ΔFMQ -0.9 to -0.5.
I-type tonalite; transitional magmatic character. εHf +2 to -6 (Turner 2022).
Mt Wright Arc medium-K calc-alkaline; Sr/Y 10-25, V/Sc <10, ΔFMQ <+1 (ilmenite-series). VHMS target only.
Post-kinematic A-type rhyolite; Rb/Sr >2, Zr >200 ppm. Fully barren for Cu-Au.
High-Al TTG-like suite; Sr/Y 82-185, representative mean ~130. La/Yb 27-44 reported (Rabbia 2000; Stern et al. 2011).
Syn-mineralisation porphyry; high Sr/Y reflecting crustal thickness ~50-60 km in Andean setting.
Adakite-like signature; Sr 638-869 ppm, Y 6-10 ppm (Reich 2003). Sr/Y 72-126, La/Yb_N 25-60 reported.
Higher-grade late porphyry facies; representative of highest Sr/Y end of suite.
Syn-mineralisation porphyry; ΔFMQ +1.1 (Chen 2022). Toquepala syn-orogenic avg Sr/Y 104.4, La/Yb 29.6 (Chen 2023).
Pre-mineralisation arc; ΔFMQ -0.5 (Chen 2022); Sr/Y 18.6, La/Yb 11.5 (Chen 2023).
Zircon Eu/Eu* >0.3-0.4; Hf 9,000-11,000 ppm; Sr/Y >40 (Nathwani 2021).
Syn-mineral QMD porphyry; εHf +11.6 to +14.5 (Dolgopolova 2013). Sr/Y 'high adakitic' confirmed; representative estimate...
Second representative analysis; εHf toward higher end (+14.5 max).
Zircon: Eu/Eu* 0.54-0.70 (mean ~0.62); Ce4+/Ce3+ 167-492 (mean ~330). ΔFMQ = ΔNNO -0.67
Higher end of Erdenet zircon suite; Ce4+/Ce3+ 492 (maximum); Ti-in-zircon T = 684-728°C range (Shen 2015).
Back-arc rhyolite host: SiO2 >75 wt%, La/Yb_N 1-11 (Agangi 2022). Low Sr/Y due to high Y from HFSE-rich back-arc melts.
Higher-SiO2 end of bimodal rhyolite suite; negative Sr anomaly confirmed (plagioclase fractionation dominant).
Zircon ΔFMQ +2.1±0.4; >90% zircons in fertile field for (Eu/Eu*)/Yb and (Ce/Nd)/Y criteria (Hong 2024).
Porphyritic diorite phase; ΔFMQ +1.9±0.5 (Hong 2024). Lower (Eu/Eu*)/Yb than granodiorite but still in fertile field.
ΔFMQ +1.3 to +1.5 ±0.6 (Hong 2024). Just at fertile boundary.
ΔFMQ +1.3±0.4 (Hong 2024); marginally fertile.
Post-tectonic A-type; ΔFMQ +0.4±1.1; below fertile threshold (Hong 2024). Zircon fertility criteria not satisfied.

Plot 4 — Zircon (Eu/Eu*)/Yb vs. (Ce/Nd

Sample ID	System	Belt / Deposit	Suite / Phase	Age (Ma)
GS-01	Delamerian	Grampians–Stavely (Zone 4)	GS late porphyry (Victor QMD)	503.84
GS-02	Delamerian	Grampians–Stavely (Zone 4)	GS late porphyry (Victor QMD)	503.84
GS-03	Delamerian	Grampians–Stavely (Zone 4)	GS late porphyry (Victor QMD)	503.84
GS-04	Delamerian	Grampians–Stavely (Zone 4)	GS arc MSVC (pre-porphyry)	507.34
LK-01	Delamerian	Loch Lilly–Kars (Zone 2)	LK Devonian monzodiorite (fertile)	424
LK-02	Delamerian	Loch Lilly–Kars (Zone 2)	LK Devonian monzodiorite (fertile)	421
LK-03	Delamerian	Loch Lilly–Kars (Zone 2)	LK Cambrian arc (non-fertile)	496
NG-01	Delamerian	Nanyah–Glenelg (Zone 3)	NG S-type (Port Elliot Granite)	508
NG-02	Delamerian	Nanyah–Glenelg (Zone 3)	NG I-type (Tanunda Creek/Palmer)	510
KB-01	Delamerian	Koonenberry (Zone 1)	KB Mt Wright Arc (calc-alkaline)	510
KB-02	Delamerian	Koonenberry (Zone 1)	KB Tibooburra A-type rhyolite	424
AND-01	Andes	El Teniente, Chile	El Teniente intrusive complex	6
AND-02	Andes	El Teniente, Chile	El Teniente ore-stage porphyry	5.5
AND-03	Andes	Los Pelambres, Chile	Los Pelambres porphyry	9
AND-04	Andes	Los Pelambres, Chile	Los Pelambres late porphyry	8
AND-05	Andes	Don Javier / Toquepala arc, Peru	Don Javier dacite porphyry (~60 Ma)	60
AND-06	Andes	Don Javier / Toquepala arc, Peru	Toquepala pre-mineral arc magmas	65
AND-07	Andes	Quellaveco, Peru	Quellaveco syn-mineral porphyry	56
OT-01	CAOB	Oyu Tolgoi, Mongolia	Hugo North QMD porphyry	372
OT-02	CAOB	Oyu Tolgoi, Mongolia	Hugo North QMD (mean)	372
ERD-01	CAOB	Erdenet, Mongolia	Erdenet granodiorite Gr-2	240
ERD-02	CAOB	Erdenet, Mongolia	Erdenet granodiorite Gr-11	240
KUR-01	Japan	Kuroko / Green Tuff Belt, Japan	Kuroko felsic host rhyolite	15
KUR-02	Japan	Kuroko / Green Tuff Belt, Japan	Kuroko felsic volcanics (bimodal)	14
DEL-01	Delamerian	Anabama Hill, South Australia	Anabama Hill granodiorite	509
DEL-02	Delamerian	Anabama Hill, South Australia	Anabama Hill porphyritic diorite	509

DEL-03	Delamerian	Netley Hill, South Australia	Netley Hill granodiorite	507
DEL-04	Delamerian	Bendigo, South Australia	Bendigo granodiorite	505
DEL-05	Delamerian	Colebatch, South Australia	Colebatch A-type granite	490

Fertile field: (Eu/Eu)/Yb >0.7 AND (Ce/Nd)/Y >0.09. Reference: Lu Y-J et al. (2016) SEG Spec Publ 19:329-347; Louck*

d)/Y (zircon fertility; Lu et al. 2016; Loucks

(Ce/Nd)/Y zircon (x-axis)	(Eu/Eu*)/Yb zircon (y-axis)	Cu-Fertile?	Source (short)
0.13	1.2	YES	Schofield et al. (2018)
0.14	1.35	YES	Schofield et al. (2018)
0.118	1.1	YES	Schofield et al. (2018)
0.09	0.85	PARTIAL	Schofield et al. (2018)
		YES	Baatar et al. (2020)
		YES	Baatar et al. (2020)
		NO	Baatar et al. (2020)
0.068	0.42	Sn-W	Turner et al. (2022)
0.095	0.78	PARTIAL	Turner et al. (2022)
		NO	Gilmore et al. (2025)
		NO	Gilmore et al. (2025)
0.145	1.4	YES	Rabbia et al. (2000)
0.142	1.3	YES	Rabbia et al. (2000)
0.138	1.25	YES	Reich et al. (2003)
0.14	1.2	YES	Reich et al. (2003)
0.12	1.05	YES	Chen et al. (2022)
0.07	0.4	NO	Chen et al. (2023)
0.125	1.15	YES	Nathwani et al. (2021)
0.128	1.15	YES	Wainwright et al. (2011)
0.13	1.2	YES	Dolgopolova et al. (2013)
0.105	0.62	YES	Shen et al. (2015)
0.112	0.68	YES	Shen et al. (2015)
0.055	0.3	NO	Agangi et al. (2022)
0.048	0.25	NO	Agangi et al. (2022)
0.118	0.72	YES	Hong et al. (2024)
0.108	0.58	YES	Hong et al. (2024)

0.092	0.45	YES	Hong et al. (2024)
0.088	0.4	YES	Hong et al. (2024)
0.065	0.22	NO	Hong et al. (2024)

s RR et al. (2024) Econ Geol 119(3):511-523.

s et al. 2024)

Notes (excerpt)
Late porphyry phase, mean of available analyses; V/Sc above Loucks threshold. ΔFMQ estimated from mineral assemblage (Sc...
Higher Sr/Y end of porphyry range; εHf upper end (+14 max).
Lower end of GS porphyry range; still above Sr/Y=35 threshold for most analyses.
Pre-porphyry calc-alkaline arc sequence; moderate ΔFMQ but Sr/Y below threshold.
Devonian fertile suite; 165 WR + 428 zircon analyses underpinning these estimates. Sr/Y 38-55 range; representative mid-...
Upper fertile suite; εHf range 0 to +5 (Baatar 2020); δ18O_zrc 6.0-7.5‰.
Cambrian monzonitic suite; below Sr/Y threshold; post-orogenic context.
S-type peraluminous granite; εHf -6 to -10, δ18O 7.5-8.1‰ (Turner 2022; Foden 2020). A/CNK 1.1-1.3; ΔFMQ -0.9 to -0.5; C...
I-type tonalite; transitional magmatic character. εHf +2 to -6 (Turner 2022).
Mt Wright Arc medium-K calc-alkaline; Sr/Y 10-25, V/Sc <10, ΔFMQ <+1 (ilmenite-series). VHMS target only.
Post-kinematic A-type rhyolite; Rb/Sr >2, Zr >200 ppm. Fully barren for Cu-Au.
High-Al TTG-like suite; Sr/Y 82-185, representative mean ~130. La/Yb 27-44 reported (Rabbia 2000; Stern et al. 2011).
Syn-mineralisation porphyry; high Sr/Y reflecting crustal thickness ~50-60 km in Andean setting.
Adakite-like signature; Sr 638-869 ppm, Y 6-10 ppm (Reich 2003). Sr/Y 72-126, La/Yb_N 25-60 reported.
Higher-grade late porphyry facies; representative of highest Sr/Y end of suite.
Syn-mineralisation porphyry; ΔFMQ +1.1 (Chen 2022). Toquepala syn-orogenic avg Sr/Y 104.4, La/Yb 29.6 (Chen 2023).
Pre-mineralisation arc; ΔFMQ -0.5 (Chen 2022); Sr/Y 18.6, La/Yb 11.5 (Chen 2023).
Zircon Eu/Eu* >0.3-0.4; Hf 9,000-11,000 ppm; Sr/Y >40 (Nathwani 2021).
Syn-mineral QMD porphyry; εHf +11.6 to +14.5 (Dolgopolova 2013). Sr/Y 'high adakitic' confirmed; representative estimate...
Second representative analysis; εHf toward higher end (+14.5 max).
Zircon: Eu/Eu* 0.54-0.70 (mean ~0.62); Ce4+/Ce3+ 167-492 (mean ~330). ΔFMQ = ΔNNO -0.67 → Shen 2015 reports ΔNNO +3.7 to...
Higher end of Erdenet zircon suite; Ce4+/Ce3+ 492 (maximum); Ti-in-zircon T = 684-728°C range (Shen 2015).
Back-arc rhyolite host: SiO2 >75 wt%, La/Yb_N 1-11 (Agangi 2022). Low Sr/Y due to high Y from HFSE-rich back-arc melts. ...
Higher-SiO2 end of bimodal rhyolite suite; negative Sr anomaly confirmed (plagioclase fractionation dominant). Ishihara ...
Zircon ΔFMQ +2.1±0.4; >90% zircons in fertile field for (Eu/Eu*)/Yb and (Ce/Nd)/Y criteria (Hong 2024). Zircon Eu/Eu* 0....
Porphyritic diorite phase; ΔFMQ +1.9±0.5 (Hong 2024). Lower (Eu/Eu*)/Yb than granodiorite but still in fertile field.

ΔFMQ +1.3 to +1.5 ±0.6 (Hong 2024). Just at fertile boundary.
ΔFMQ +1.3±0.4 (Hong 2024); marginally fertile.
Post-tectonic A-type; ΔFMQ +0.4±1.1; below fertile threshold (Hong 2024). Zircon fertility criteria not satisfied.

Porphyry Cu–Au fertility t		
Parameter	**Threshold / fertile field**	**Physical basis**
Sr/Y (whole-rock)	Sr/Y >35 at SiO_2 >57 wt%	Garnet ± amphibole stable in residue; plagioclase suppressed at depth → Y depleted but Sr retained → high Sr/Y signals deep (>40 km) magma processing
La/Yb (whole-rock)	La/Yb >15 (proxy for crust >35 km)	La enriched by slab-fluid metasomatism; Yb depleted by residual garnet at high P → La/Yb encodes crustal thickness
V/Sc (whole-rock)	V/Sc > 32.5 − 0.385 × SiO_2	V partitions as V^{3+} (compatible) under reducing conditions; V^{5+} (incompatible) under oxidised conditions. Sc is fO_2-insensitive. High V/Sc → oxidised, magnetite-series
ΔFMQ (whole-rock/zircon)	ΔFMQ >+1	Above FMQ+1 buffer, S speciation shifts to SO_4^{2-} dominant → Cu retained in melt as Cu^+ complex until hydrothermal exsolution; below FMQ+1, S^{2-} dominant → early Cu sulphide saturation strips Cu
Zircon Eu/Eu*	Eu/Eu* >0.3–0.4 (individual grains)	Eu^{2+} substitutes for Ca^{2+} in plagioclase; high Eu/Eu* in zircon indicates plagioclase NOT stable during crystallisation → deep (>40 km) hydrous conditions
Zircon Ce^{4+}/Ce^{3+}	Ce^{4+}/Ce^{3+} >120 (ore-forming systems)	Ce^{4+} substitutes for Zr^{4+} in zircon under oxidising conditions; Ce^{3+} dominates under reducing conditions. High Ce^{4+}/Ce^{3+} directly encodes magmatic fO_2
(Eu/Eu*)/Yb (zircon)	(Eu/Eu*)/Yb >0.7	Yb normalisation removes dilution effects of HREE partitioning; (Eu/Eu*)/Yb >0.7 indicates combined deep crystallisation AND oxidised conditions
(Ce/Nd)/Y (zircon)	(Ce/Nd)/Y >0.09	Ce anomaly in zircon (Ce^{4+} enrichment) normalised by adjacent REE and Y; decouples oxidation state from degree of fractionation
εHf(t) (zircon)	εHf(t) >+5 (juvenile arc signature)	Positive εHf indicates depleted mantle-derived source (no ancient crustal recycling); juvenile arc setting maximises Cu endowment potential
$\delta^{18}O$ zircon	$\delta^{18}O$_zrc 5.2–7.0‰ (juvenile arc Cu-Au field)	$\delta^{18}O$ tracks crustal assimilation of sedimentary material; <5.2‰ = mantle peridotite; 5.2–7‰ = juvenile arc; >7.5‰ = sedimentary input → Sn-W fertile

hresholds

Key reference	Formula / note
Loucks (2014), AJES 61:5-16	Threshold = 35; supergiant class typically >80 (requires crust >50 km)
Chiaradia (2015), Sci Rep 5:8115	Empirical relationship: thickness (km) = 20.17 × ln(La/Yb_N) + 10.42
Loucks (2014), AJES 61:5-16	At SiO_2=63%: threshold V/Sc = 8.2; at SiO_2=65%: threshold = 7.5
Richards (2015), Lithos 233:27-45	ΔFMQ = $\log_{10}(fO_2) - \log_{10}(fO_2_FMQ)$; porphyry-fertile range +1 to +3
Ballard et al. (2002), CMP 144:347-364	Whole-rock Eu/Eu* and zircon Eu/Eu* positively correlated; fertile suites >0.4 in zircon
Ballard et al. (2002), CMP 144:347-364	Large systems (>10 Mt Cu) typically Ce^{4+}/Ce^{3+} >300 (Shen 2015)
Lu et al. (2016), SEG Spec Publ 19:329-347; Loucks et al. (2024), Econ Geol 119:511-523	Y-axis of Plot 4; combined hydration+oxidation proxy
Lu et al. (2016), SEG Spec Publ 19:329-347	X-axis of Plot 4; pure oxidation proxy
Gardiner et al. (2017), Sci Rep 7:46250	Oyu Tolgoi: +11.6 to +14.5; GS Zone 4: +8 to +14 (near-identical)
Gardiner et al. (2017), Sci Rep 7:46250	GS Zone 4: 6.0–7.0‰ (Cu-Au field); NG S-type: 7.5–8.1‰ (Sn-W field)

Sample ID	Analysis ID	Mineral	Deposit	$^{34}S/^{32}S$_measured
321921	321921_1	Pyrite	Balbeggie, VIC	0.044938641
321921	321921_2	Pyrite	Balbeggie, VIC	0.045071591
321921	321921_3	Pyrite	Balbeggie, VIC	0.04504556
321921	321921_4	Pyrite	Balbeggie, VIC	0.044944043
321921	321921_5	Pyrite	Balbeggie, VIC	0.044964621
321921	321921_6	Pyrite	Balbeggie, VIC	0.045029067
321921	321921_7	Pyrite	Balbeggie, VIC	0.044953156
321921	321921_8	Pyrite	Balbeggie, VIC	0.044997572
321921	321921_9	Pyrite	Balbeggie, VIC	0.045077572
321921	321921_10	Pyrite	Balbeggie, VIC	0.045083364
321921	321921_11	Pyrite	Balbeggie, VIC	0.04508231
321921	321921_12	Pyrite	Balbeggie, VIC	0.045027841
321921	321921_13	Pyrite	Balbeggie, VIC	0.045114711
321921	321921_14	Pyrite	Balbeggie, VIC	0.045052467
2022440196	2022440196.1	Pyrite	Bunker Hill, Wertago, NSW	0.045044292
2022440196	2022440196.2	Pyrite	Bunker Hill, Wertago, NSW	0.045121742
2022440196	2022440196.3	Pyrite	Bunker Hill, Wertago, NSW	0.04509805
2022440196	2022440196.4	Pyrite	Bunker Hill, Wertago, NSW	0.045104241
2022440196	2022440196.5	Pyrite	Bunker Hill, Wertago, NSW	0.04514227
2022440196	2022440196.6	Pyrite	Bunker Hill, Wertago, NSW	0.045276225
2022440196	2022440196.7	Pyrite	Bunker Hill, Wertago, NSW	0.045130682
2022440196	2022440196.8	Pyrite	Bunker Hill, Wertago, NSW	0.045133253
2022440196	2022440196.9	Pyrite	Bunker Hill, Wertago, NSW	0.045085691
2022440196	2022440196.10	Pyrite	Bunker Hill, Wertago, NSW	0.045041222
2022440196	2022440196.11	Pyrite	Bunker Hill, Wertago, NSW	0.045064687
2022440196	2022440196.12	Pyrite	Bunker Hill, Wertago, NSW	0.045045256
2022440196	2022440196.13	Pyrite	Bunker Hill, Wertago, NSW	0.045051673
2022440196	2022440196.14	Pyrite	Bunker Hill, Wertago, NSW	0.045065144
2022440196	2022440196.15	Pyrite	Bunker Hill, Wertago, NSW	0.045062182
2022440196	2022440196.16	Pyrite	Bunker Hill, Wertago, NSW	0.045068005
2022440196	2022440196.17	Pyrite	Bunker Hill, Wertago, NSW	0.045082433
2022440196	2022440196.18	Pyrite	Bunker Hill, Wertago, NSW	0.045078293
2022440196	2022440196.19	Pyrite	Bunker Hill, Wertago, NSW	0.04508383
2022440196	2022440196.20	Pyrite	Bunker Hill, Wertago, NSW	0.045068413
2022440196	2022440196.21	Pyrite	Bunker Hill, Wertago, NSW	0.045118929
2022440196	2022440196.22	Pyrite	Bunker Hill, Wertago, NSW	0.045077665
2022440196	2022440196.23	Pyrite	Bunker Hill, Wertago, NSW	0.045080734
2022440196	2022440196.24	Pyrite	Bunker Hill, Wertago, NSW	0.045083088
2022440196	2022440196.25	Pyrite	Bunker Hill, Wertago, NSW	0.045109937
2022440196	2022440196.26	Pyrite	Bunker Hill, Wertago, NSW	0.045078216
2022440196	2022440196.27	Pyrite	Bunker Hill, Wertago, NSW	0.045170136
2022440196	2022440196.28	Pyrite	Bunker Hill, Wertago, NSW	0.045123546
2022440196	2022440196.29	Pyrite	Bunker Hill, Wertago, NSW	0.045102204
2022440196	2022440196.30	Pyrite	Bunker Hill, Wertago, NSW	0.045096734
2022330048	048-1.1	Pyrite	Eaglehawk, NSW	0.045064093
2022330048	048-1.2	Pyrite	Eaglehawk, NSW	0.045016475
2022330048	048-1.3	Pyrite	Eaglehawk, NSW	0.045068813
2022330048	048-1.4	Pyrite	Eaglehawk, NSW	0.045051584
2022330048	048-1.5	Pyrite	Eaglehawk, NSW	0.045010421

2022330048	048-1.6	Pyrite	Eaglehawk, NSW	0.04502831
2022330048	048-1.7	Pyrite	Eaglehawk, NSW	0.045039319
2022330048	048-1.8	Pyrite	Eaglehawk, NSW	0.045018683
2022330048	048-1.9	Pyrite	Eaglehawk, NSW	0.04505495
2022330048	048-1.10	Pyrite	Eaglehawk, NSW	0.045051376
2022330048	048-1.11	Pyrite	Eaglehawk, NSW	0.045054048
2022330048	048-1.12	Pyrite	Eaglehawk, NSW	0.045017827
2022330048	048-1.13	Pyrite	Eaglehawk, NSW	0.044999867
2022330048	048-1.14	Pyrite	Eaglehawk, NSW	0.045005219
2022330048	048-1.15	Pyrite	Eaglehawk, NSW	0.045024868
2022330048	048-1.1	Chalcopyrite	Eaglehawk, NSW	0.045038975
2022330048	048-1.2	Chalcopyrite	Eaglehawk, NSW	0.044991267
2022330048	048-1.3	Chalcopyrite	Eaglehawk, NSW	0.045043644
2022330048	048-1.4	Chalcopyrite	Eaglehawk, NSW	0.045026429
2022330048	048-1.5	Chalcopyrite	Eaglehawk, NSW	0.044985252
2022330048	048-1.6	Chalcopyrite	Eaglehawk, NSW	0.04500314
2022330048	048-1.7	Chalcopyrite	Eaglehawk, NSW	0.045014197
2022330048	048-1.8	Chalcopyrite	Eaglehawk, NSW	0.044993577
2022330048	048-1.9	Chalcopyrite	Eaglehawk, NSW	0.045029779
2022330048	048-1.10	Chalcopyrite	Eaglehawk, NSW	0.045026211
2022330048	048-1.11	Chalcopyrite	Eaglehawk, NSW	0.045028917
2022330048	048-1.12	Chalcopyrite	Eaglehawk, NSW	0.044992746
2022330048	048-1.13	Chalcopyrite	Eaglehawk, NSW	0.044974744
2022330048	048-1.14	Chalcopyrite	Eaglehawk, NSW	0.044980041
2022330048	048-1.15	Chalcopyrite	Eaglehawk, NSW	0.044999752
2022330043	43-5c.1	Pyrite	Eaglehawk, NSW	0.045014606
2022330043	43-5c.2	Pyrite	Eaglehawk, NSW	0.045049495
2022330043	43-5r.1	Pyrite	Eaglehawk, NSW	0.045137896
2022330043	43-5r.2	Pyrite	Eaglehawk, NSW	0.045042353
2022330043	43-5r.3	Pyrite	Eaglehawk, NSW	0.045077899
2022330043	43-5c.3	Pyrite	Eaglehawk, NSW	0.045008809
2022330043	43-5c.4	Pyrite	Eaglehawk, NSW	0.045016929
2022330043	43-5c.5	Pyrite	Eaglehawk, NSW	0.045037324
2022330043	43-5c.6	Pyrite	Eaglehawk, NSW	0.045027221
2022330043	43-5r.4	Pyrite	Eaglehawk, NSW	0.045206198
2022330043	43-5r.5	Pyrite	Eaglehawk, NSW	0.045027453
2022330043	43-5r.6	Pyrite	Eaglehawk, NSW	0.045135996
2022330043	43-5r.7	Pyrite	Eaglehawk, NSW	0.045053592
2022330043	43-5c.7	Pyrite	Eaglehawk, NSW	0.045003402
2022330043	43-5c.8	Pyrite	Eaglehawk, NSW	0.04503148
2022330043	43-5c.9	Pyrite	Eaglehawk, NSW	0.04502114
2022330043	43-5c.10	Pyrite	Eaglehawk, NSW	0.045009982
2022330043	43-5c.11	Pyrite	Eaglehawk, NSW	0.045037467
2022330043	43-5v.1	Pyrite	Eaglehawk, NSW	0.045038697
2022330043	43-5cpy.1	Chalcopyrite	Eaglehawk, NSW	0.045019999
2022330043	43-5c.1	Chalcopyrite	Eaglehawk, NSW	0.044989486
2022330043	43-5c.2	Chalcopyrite	Eaglehawk, NSW	0.045024351
2022330043	43-5r.1	Chalcopyrite	Eaglehawk, NSW	0.045112716
2022330043	43-5r.2	Chalcopyrite	Eaglehawk, NSW	0.045017207
2022330043	43-5r.3	Chalcopyrite	Eaglehawk, NSW	0.045052782

2022330043	43-5c.3	Chalcopyrite	Eaglehawk, NSW	0.044983723
2022330043	43-5c.4	Chalcopyrite	Eaglehawk, NSW	0.044991774
2022330043	43-5c.5	Chalcopyrite	Eaglehawk, NSW	0.045012116
2022330043	43-5c.6	Chalcopyrite	Eaglehawk, NSW	0.045002076
2022330043	43-5r.4	Chalcopyrite	Eaglehawk, NSW	0.045181009
2022330043	43-5r.5	Chalcopyrite	Eaglehawk, NSW	0.045002268
2022330043	43-5r.6	Chalcopyrite	Eaglehawk, NSW	0.045110757
2022330043	43-5r.7	Chalcopyrite	Eaglehawk, NSW	0.045028443
2022330043	43-5c.7	Chalcopyrite	Eaglehawk, NSW	0.044978282
2022330043	43-5c.8	Chalcopyrite	Eaglehawk, NSW	0.045006338
2022330043	43-5c.9	Chalcopyrite	Eaglehawk, NSW	0.044996052
2022330043	43-5c.10	Chalcopyrite	Eaglehawk, NSW	0.044984879
2022330043	43-5c.11	Chalcopyrite	Eaglehawk, NSW	0.045012345
2022330043	43-5v.1	Chalcopyrite	Eaglehawk, NSW	0.045013616
321889	321889.cpy.1	Chalcopyrite	Eclipse, VIC	0.04476701
321889	321889.cpy.2	Chalcopyrite	Eclipse, VIC	0.044724164
321889	321889.cpy.3	Chalcopyrite	Eclipse, VIC	0.044668967
321889	321889.cpy.4	Chalcopyrite	Eclipse, VIC	0.044747938
321889	321889.cpy.5	Chalcopyrite	Eclipse, VIC	0.044703623
321889	321889.cpy.6	Chalcopyrite	Eclipse, VIC	0.044669036
321893	321893.1	Pyrite	Eclipse, VIC	0.043086491
321893	321893.2	Pyrite	Eclipse, VIC	0.043125521
321893	321893.3	Pyrite	Eclipse, VIC	0.043007094
321893	321893.4	Pyrite	Eclipse, VIC	0.043047934
321893	321893.5	Pyrite	Eclipse, VIC	0.043024097
321893	321893.6	Pyrite	Eclipse, VIC	0.043048727
321893	321893.7	Pyrite	Eclipse, VIC	0.043076701
321893	321893.8	Pyrite	Eclipse, VIC	0.043058299
321893	321893.9	Pyrite	Eclipse, VIC	0.043059558
321893	321893.10	Pyrite	Eclipse, VIC	0.04303843
321893	321893.11	Pyrite	Eclipse, VIC	0.043071408
321893	321893.12	Pyrite	Eclipse, VIC	0.043042099
321893	321893.13	Pyrite	Eclipse, VIC	0.043060834
321893	321893.14	Pyrite	Eclipse, VIC	0.043006261
321893	321893.15	Pyrite	Eclipse, VIC	0.043014356
321893	321893.16	Pyrite	Eclipse, VIC	0.043057639
321893	321893.17	Pyrite	Eclipse, VIC	0.043007142
321889	321889.1	Pyrite	Eclipse, VIC	0.044699068
321889	321889.2	Pyrite	Eclipse, VIC	0.044754676
321889	321889.3	Pyrite	Eclipse, VIC	0.04488821
321889	321889.4	Pyrite	Eclipse, VIC	0.044756579
321889	321889.5	Pyrite	Eclipse, VIC	0.044721848
321889	321889.6	Pyrite	Eclipse, VIC	0.044764528
321889	321889.7	Pyrite	Eclipse, VIC	0.044714508
2022440191	2022440191.1	Pyrite	Eclipse, Wertago, NSW	0.043418999
2022440191	2022440191.2	Pyrite	Eclipse, Wertago, NSW	0.043419275
2022440191	2022440191.3	Pyrite	Eclipse, Wertago, NSW	0.043434819
2022440191	2022440191.4	Pyrite	Eclipse, Wertago, NSW	0.043444976
2022440191	2022440191.5	Pyrite	Eclipse, Wertago, NSW	0.043434048
2022440191	2022440191.6	Pyrite	Eclipse, Wertago, NSW	0.043452165

2022440191	2022440191.7	Pyrite	Eclipse, Wertago, NSW	0.04344005
2022440191	2022440191.8	Pyrite	Eclipse, Wertago, NSW	0.043454633
2022440191	2022440191.9	Pyrite	Eclipse, Wertago, NSW	0.043461143
2022440191	2022440191.10	Pyrite	Eclipse, Wertago, NSW	0.043470137
2022440191	2022440191.11	Pyrite	Eclipse, Wertago, NSW	0.043436818
2022440191	2022440191.12	Pyrite	Eclipse, Wertago, NSW	0.043429772
2022440191	2022440191.13	Pyrite	Eclipse, Wertago, NSW	0.043437673
2022440191	2022440191.14	Pyrite	Eclipse, Wertago, NSW	0.043455588
2022440191	2022440191.15	Pyrite	Eclipse, Wertago, NSW	0.043448399
2202440189B	2202440189B.1	Pyrite	Eclipse, Wertago, NSW	0.043541354
2202440189B	2202440189B.2	Pyrite	Eclipse, Wertago, NSW	0.043470236
2202440189B	2202440189B.3	Pyrite	Eclipse, Wertago, NSW	0.043432903
2202440189B	2202440189B.4	Pyrite	Eclipse, Wertago, NSW	0.043403289
2202440189B	2202440189B.5	Pyrite	Eclipse, Wertago, NSW	0.043401069
2202440189B	2202440189B.6	Pyrite	Eclipse, Wertago, NSW	0.043421703
2202440189B	2202440189B.7	Pyrite	Eclipse, Wertago, NSW	0.043439309
2022440189	2022440189A.1	Pyrite	Eclipse, Wertago, NSW	0.043504327
2022440189	2022440189A.2	Pyrite	Eclipse, Wertago, NSW	0.0435376
2022440189	2022440189A.3	Pyrite	Eclipse, Wertago, NSW	0.043521341
2022440189	2022440189A.4	Pyrite	Eclipse, Wertago, NSW	0.043541629
2022440189	2022440189A.5	Pyrite	Eclipse, Wertago, NSW	0.043502489
2022440189	2022440189A.6	Pyrite	Eclipse, Wertago, NSW	0.04353518
2022440189	2022440189A.7	Pyrite	Eclipse, Wertago, NSW	0.043506829
2022440189	2022440189A.8	Pyrite	Eclipse, Wertago, NSW	0.04354641
2022440189	2022440189A.9	Pyrite	Eclipse, Wertago, NSW	0.043445654
2022440189	2022440189A.10	Pyrite	Eclipse, Wertago, NSW	0.043478581
2022440189	2022440189A.11	Pyrite	Eclipse, Wertago, NSW	0.043491462
2022440189	2022440189A.12	Pyrite	Eclipse, Wertago, NSW	0.04341096
2022440189	2022440189A.13	Pyrite	Eclipse, Wertago, NSW	0.043386403
2022440189	2022440189A.14	Pyrite	Eclipse, Wertago, NSW	0.043452738
2022440189	2022440189A.15	Pyrite	Eclipse, Wertago, NSW	0.043514201
2022440189	2022440189A.16	Pyrite	Eclipse, Wertago, NSW	0.043485357
2022440189	2022440189A.17	Pyrite	Eclipse, Wertago, NSW	0.043503802
2022440189	2022440189A.18	Pyrite	Eclipse, Wertago, NSW	0.043513431
321905	321905.1	Pyrite	Fiddlers Reef, VIC	0.04616657
321905	321905.2	Pyrite	Fiddlers Reef, VIC	0.046203113
321905	321905.3	Pyrite	Fiddlers Reef, VIC	0.046163614
321905	321905.4	Pyrite	Fiddlers Reef, VIC	0.04622793
321905	321905.5	Pyrite	Fiddlers Reef, VIC	0.045875875
321905	321905.6	Pyrite	Fiddlers Reef, VIC	0.045902676
321905	321905.7	Pyrite	Fiddlers Reef, VIC	0.046184648
321905	321905.8	Pyrite	Fiddlers Reef, VIC	0.04624997
321905	321905.9	Pyrite	Fiddlers Reef, VIC	0.046227661
321905	321905.1	Pyrite	Fiddlers Reef, VIC	0.0462277
321905	321905.11	Pyrite	Fiddlers Reef, VIC	0.04620667
321905	321905.12	Pyrite	Fiddlers Reef, VIC	0.046231041
321905	321905.13	Pyrite	Fiddlers Reef, VIC	0.046233903
321905	321905.14	Pyrite	Fiddlers Reef, VIC	0.046223894
321905	321905.15	Pyrite	Fiddlers Reef, VIC	0.046271769
321905	321905.16	Pyrite	Fiddlers Reef, VIC	0.046266205

321905	321905.4B	Pyrite	Fiddlers Reef, VIC	0.045934919
321905	321905.17	Pyrite	Fiddlers Reef, VIC	0.045922427
321905	321905.18	Pyrite	Fiddlers Reef, VIC	0.045862564
321905	321905.19	Pyrite	Fiddlers Reef, VIC	0.045875273
321905	321905.20	Pyrite	Fiddlers Reef, VIC	0.045958105
321905	321905.21	Pyrite	Fiddlers Reef, VIC	0.045911306
321905	321905.22	Pyrite	Fiddlers Reef, VIC	0.045897309
321905	321905.23	Pyrite	Fiddlers Reef, VIC	0.045940957
321905	321905.24	Pyrite	Fiddlers Reef, VIC	0.045894473
321903	321903_1	Pyrite	Fiddlers Reef, VIC	0.046155725
321903	321903_2	Pyrite	Fiddlers Reef, VIC	0.046115907
321903	321903_3	Pyrite	Fiddlers Reef, VIC	0.046117714
321903	321903_4	Pyrite	Fiddlers Reef, VIC	0.04611567
321903	321903_5	Pyrite	Fiddlers Reef, VIC	0.046097894
321903	321903_6	Pyrite	Fiddlers Reef, VIC	0.046095576
321903	321903_7	Pyrite	Fiddlers Reef, VIC	0.046118608
321903	321903_8	Pyrite	Fiddlers Reef, VIC	0.046103703
321903	321903_9	Pyrite	Fiddlers Reef, VIC	0.046090393
321903	321903_10	Pyrite	Fiddlers Reef, VIC	0.046069687
321903	321903_11	Pyrite	Fiddlers Reef, VIC	0.046090153
321903	321903_12	Pyrite	Fiddlers Reef, VIC	0.04611289
321903	321903_13	Pyrite	Fiddlers Reef, VIC	0.04613747
321903	321903_14	Pyrite	Fiddlers Reef, VIC	0.045776169
321903	321903_15	Pyrite	Fiddlers Reef, VIC	0.046220982
321903	321903_16	Pyrite	Fiddlers Reef, VIC	0.046242067
321903	321903_17	Pyrite	Fiddlers Reef, VIC	0.046182597
321903	321903_18	Pyrite	Fiddlers Reef, VIC	0.046160996
321903	321903_19	Pyrite	Fiddlers Reef, VIC	0.046219614
321903	321903_20	Pyrite	Fiddlers Reef, VIC	0.046186888
321903	321903_21	Pyrite	Fiddlers Reef, VIC	0.046113444
321903	321903_22	Pyrite	Fiddlers Reef, VIC	0.046128743
321903	321903_23	Pyrite	Fiddlers Reef, VIC	0.046138528
321903	321903_24	Pyrite	Fiddlers Reef, VIC	0.046159063
321903	321903_25	Pyrite	Fiddlers Reef, VIC	0.046210012
321864	321864.sph.1	Sphalerite	Gerang Gerung, VIC	0.04558892
321864	321864.sph.2	Sphalerite	Gerang Gerung, VIC	0.045559677
321864	321864.sph.3	Sphalerite	Gerang Gerung, VIC	0.045633061
321864	321864.sph.4	Sphalerite	Gerang Gerung, VIC	0.045661104
321864	321864.sph.5	Sphalerite	Gerang Gerung, VIC	0.045540701
321864	321864.sph.6	Sphalerite	Gerang Gerung, VIC	0.045656323
321864	321864A.Sph.1	Sphalerite	Gerang Gerung, VIC	0.045599079
321864	321864A.Sph.2	Sphalerite	Gerang Gerung, VIC	0.045531646
321864	321864A.Sph.3	Sphalerite	Gerang Gerung, VIC	0.045627157
321864	321864A.Sph.4	Sphalerite	Gerang Gerung, VIC	0.045555973
321864	321864A.Sph.5	Sphalerite	Gerang Gerung, VIC	0.045652447
321864	321864A.Sph.6	Sphalerite	Gerang Gerung, VIC	0.045615934
321864	321864A.Sph.7	Sphalerite	Gerang Gerung, VIC	0.045540956
321864	321864A.Sph.8	Sphalerite	Gerang Gerung, VIC	0.045678905
321864	321864.1	Pyrite	Gerang Gerung, Vic	0.043915957
321864	321864.2	Pyrite	Gerang Gerung, Vic	0.043978488

321864	321864.3	Pyrite	Gerang Gerung, Vic	0.043933735
321864	321864.4	Pyrite	Gerang Gerung, Vic	0.043826236
321864	321864.5	Pyrite	Gerang Gerung, Vic	0.04382157
321864	321864.1	Pyrite	Gerang Gerung, Vic	0.043913843
321864	321864.2	Pyrite	Gerang Gerung, Vic	0.043879609
321864	321864.3	Pyrite	Gerang Gerung, Vic	0.043863216
321864	321864.4	Pyrite	Gerang Gerung, Vic	0.043858066
321864	321864.5	Pyrite	Gerang Gerung, Vic	0.04387425
321864	321864.6	Pyrite	Gerang Gerung, Vic	0.043893165
2023440012	2023440012.Sph.1	Sphalerite	Glenlyle, VIC	0.04516959
2023440012	2023440012.Sph.2	Sphalerite	Glenlyle, VIC	0.04516275
2023440012	2023440012.Sph.3	Sphalerite	Glenlyle, VIC	0.045199155
2023440012	2023440012.Sph.4	Sphalerite	Glenlyle, VIC	0.045116363
2023440012	2023440012.Sph.5	Sphalerite	Glenlyle, VIC	0.045243867
2023440012	2023440012.Sph.6	Sphalerite	Glenlyle, VIC	0.045101205
2023440012	2023440012.Sph.7	Sphalerite	Glenlyle, VIC	0.045348787
2022440012	2022440012.1	Pyrite	Glenlyle, VIC	0.045242232
2022440012	2022440012.2	Pyrite	Glenlyle, VIC	0.045202394
2022440012	2022440012.3	Pyrite	Glenlyle, VIC	0.045213022
2022440012	2022440012.4	Pyrite	Glenlyle, VIC	0.045228574
2022440012	2022440012.5	Pyrite	Glenlyle, VIC	0.045230759
2022440012	2022440012.6	Pyrite	Glenlyle, VIC	0.045235823
2022440012	2022440012.7	Pyrite	Glenlyle, VIC	0.045307915
2022440012	2022440012.8	Pyrite	Glenlyle, VIC	0.045264855
2022440012	2022440012.9	Pyrite	Glenlyle, VIC	0.04520864
2022440012	2022440012.10	Pyrite	Glenlyle, VIC	0.045093858
2022440012	2022440012.11	Pyrite	Glenlyle, VIC	0.045046781
2022440012	2022440012.12	Pyrite	Glenlyle, VIC	0.045173797
2022440012	2022440012.13	Pyrite	Glenlyle, VIC	0.045205051
2022440012	2022440012.14	Pyrite	Glenlyle, VIC	0.045196325
2022440012	2022440012.15	Pyrite	Glenlyle, VIC	0.045101731
2022440012	2022440012.16	Pyrite	Glenlyle, VIC	0.045148509
2022440012	2022440012.17	Pyrite	Glenlyle, VIC	0.045030362
2022440119	2022440119C.cpy.1	Chalcopyrite	Grasmere, NSW	0.045214641
2022440119	2022440119C.cpy.2	Chalcopyrite	Grasmere, NSW	0.045218289
2022440119	2022440119C.cpy.3	Chalcopyrite	Grasmere, NSW	0.045223737
2022440119	2022440119C.cpy.4	Chalcopyrite	Grasmere, NSW	0.045213767
2022440119	2022440119C.cpy.5	Chalcopyrite	Grasmere, NSW	0.04521236
2022440119	2022440119C.cpy.6	Chalcopyrite	Grasmere, NSW	0.045216787
2022440119	2022440119A.cpy.1	Chalcopyrite	Grasmere, NSW	0.045243096
2022440119	2022440119A.cpy.2	Chalcopyrite	Grasmere, NSW	0.045179732
2022440119	2022440119A.cpy.3	Chalcopyrite	Grasmere, NSW	0.045305581
2022440119	2022440119A.cpy.4	Chalcopyrite	Grasmere, NSW	0.045200128
2022440119	2022440119A.cpy.6	Chalcopyrite	Grasmere, NSW	0.045262946
2022440119	2022440119A.cpy.7	Chalcopyrite	Grasmere, NSW	0.045222861
2022440119	2022440119A.cpy.8	Chalcopyrite	Grasmere, NSW	0.045189459
2022440119	2022440119A.cpy.9	Chalcopyrite	Grasmere, NSW	0.045214595
2022440117	2022440117A.cpy.1	Chalcopyrite	Grasmere, NSW	0.045293457
2022440117	2022440117A.cpy.2	Chalcopyrite	Grasmere, NSW	0.045252308
2022440117	2022440117A.cpy.3	Chalcopyrite	Grasmere, NSW	0.045304918

2022440117	2022440117A.cpy.4	Chalcopyrite	Grasmere, NSW	0.045278482
2022440117	2022440117A.cpy.5	Chalcopyrite	Grasmere, NSW	0.045305042
2022440117	2022440117A.cpy.6	Chalcopyrite	Grasmere, NSW	0.045324495
2022440117	2022440117A.cpy.7	Chalcopyrite	Grasmere, NSW	0.045302848
2022440117	2022440117A.cpy.8	Chalcopyrite	Grasmere, NSW	0.045315037
2022440117	2022440117A.cpy.10	Chalcopyrite	Grasmere, NSW	0.045299784
2022440115	2022440115.1	Pyrite	Grasmere, NSW	0.043783057
2022440115	2022440115.2	Pyrite	Grasmere, NSW	0.043803949
2022440115	2022440115.3	Pyrite	Grasmere, NSW	0.043803526
2022440115	2022440115.4	Pyrite	Grasmere, NSW	0.043792034
2022440115	2022440115.5	Pyrite	Grasmere, NSW	0.043808684
2022440115	2022440115.6	Pyrite	Grasmere, NSW	0.043803995
2022440115	2022440115.7	Pyrite	Grasmere, NSW	0.04383008
2022440115	2022440115.8	Pyrite	Grasmere, NSW	0.043762586
2022440115	2022440115.9	Pyrite	Grasmere, NSW	0.043828616
2022440075	2022440075.1	Pyrite	Grasmere, NSW	0.043649562
2022440075	2022440075.2	Pyrite	Grasmere, NSW	0.043660795
2022440075	2022440075.3	Pyrite	Grasmere, NSW	0.0436754
2022440075	2022440075.4	Pyrite	Grasmere, NSW	0.043736396
2022440075	2022440075.5	Pyrite	Grasmere, NSW	0.04373616
2022440075	2022440075.6	Pyrite	Grasmere, NSW	0.043639939
2022440075	2022440075.7	Pyrite	Grasmere, NSW	0.043626789
2022440075	2022440075.8	Pyrite	Grasmere, NSW	0.043752414
2022440075	2022440075.9	Pyrite	Grasmere, NSW	0.043624433
2022440075	2022440075.10	Pyrite	Grasmere, NSW	0.04365142
2022440117	2022440117B.1	Pyrite	Grasmere, NSW	0.045355104
2022440117	2022440117B.2	Pyrite	Grasmere, NSW	0.045366847
2022440117	2022440117B.3	Pyrite	Grasmere, NSW	0.045388666
2022440117	2022440117B.4	Pyrite	Grasmere, NSW	0.045371076
2022440117	2022440117B.5	Pyrite	Grasmere, NSW	0.045229311
2022440117	2022440117B.6	Pyrite	Grasmere, NSW	0.045397908
2022440117	2022440117B.7	Pyrite	Grasmere, NSW	0.04535876
2022440117	2022440117B.8	Pyrite	Grasmere, NSW	0.045392833
2022440117	2022440117B.9	Pyrite	Grasmere, NSW	0.045358533
2022440119	2022440119A.1	Pyrite	Grasmere, NSW	0.045219911
2022440119	2022440119A.2	Pyrite	Grasmere, NSW	0.045171873
2022440119	2022440119A.3	Pyrite	Grasmere, NSW	0.04520046
2022440119	2022440119A.4	Pyrite	Grasmere, NSW	0.045244671
2022440119	2022440119A.5	Pyrite	Grasmere, NSW	0.045248274
2022440119	2022440119A.6	Pyrite	Grasmere, NSW	0.045257272
2022440119	2022440119A.7	Pyrite	Grasmere, NSW	0.04526051
2022440119	2022440119A.8	Pyrite	Grasmere, NSW	0.045238762
2022440119	2022440119A.9	Pyrite	Grasmere, NSW	0.045204664
2022440119	2022440119A.10	Pyrite	Grasmere, NSW	0.045211221
2022440119	2022440119A.11	Pyrite	Grasmere, NSW	0.045210987
2022440119	2022440119A.12	Pyrite	Grasmere, NSW	0.045225506
2022440119	2022440119A.13	Pyrite	Grasmere, NSW	0.045257678
2022440119	2022440119A.14	Pyrite	Grasmere, NSW	0.045239985
2022440119	2022440119B.1	Pyrite	Grasmere, NSW	0.045264973
2022440119	2022440119B.2	Pyrite	Grasmere, NSW	0.045261051

2022440119	2022440119B.3	Pyrite	Grasmere, NSW	0.045268974
2022440119	2022440119B.4	Pyrite	Grasmere, NSW	0.045281517
2022440119	2022440119B.5	Pyrite	Grasmere, NSW	0.045254819
2022440119	2022440119B.6	Pyrite	Grasmere, NSW	0.045271783
2022440119	2022440119B.7	Pyrite	Grasmere, NSW	0.045254814
2022440119	2022440119B.8	Pyrite	Grasmere, NSW	0.045237484
2022440119	2022440119B.9	Pyrite	Grasmere, NSW	0.045253326
2022440119	2022440119B.10	Pyrite	Grasmere, NSW	0.045235217
2022440119	2022440119B.11	Pyrite	Grasmere, NSW	0.045302479
2022440119	2022440119B.12	Pyrite	Grasmere, NSW	0.045291555
2022440119	2022440119B.13	Pyrite	Grasmere, NSW	0.045325256
2022440119	2022440119C.1	Pyrite	Grasmere, NSW	0.045326549
2022440119	2022440119C.2	Pyrite	Grasmere, NSW	0.045264284
2022440119	2022440119C.3	Pyrite	Grasmere, NSW	0.04526127
2022440119	2022440119C.4	Pyrite	Grasmere, NSW	0.04524712
2022440119	2022440119C.5	Pyrite	Grasmere, NSW	0.045241776
2022440119	2022440119C.6	Pyrite	Grasmere, NSW	0.045310586
4351174	4351174A.cpy.1	Chalcopyrite	Haylands, SA	0.045757706
4351174	4351174A.cpy.2	Chalcopyrite	Haylands, SA	0.045665113
4351174	4351174A.cpy.3	Chalcopyrite	Haylands, SA	0.045515441
4351174	4351174A.cpy.4	Chalcopyrite	Haylands, SA	0.045440827
4351174	4351174A.cpy.5	Chalcopyrite	Haylands, SA	0.04572728
4351174	4351174A.cpy.6	Chalcopyrite	Haylands, SA	0.045693153
4351174	4351174A.cpy.7	Chalcopyrite	Haylands, SA	0.045772571
4351177	4351177.1	Pyrite	Haylands, SA	0.043885098
4351177	4351177.2	Pyrite	Haylands, SA	0.043915016
4351177	4351177.3	Pyrite	Haylands, SA	0.043889731
4351177	4351177.4	Pyrite	Haylands, SA	0.043927323
4351177	4351177.5	Pyrite	Haylands, SA	0.043894671
4351177	4351177.6	Pyrite	Haylands, SA	0.043893417
4351177	4351177.7	Pyrite	Haylands, SA	0.04390637
4351177	4351177.8	Pyrite	Haylands, SA	0.043872378
4351177	4351177.9	Pyrite	Haylands, SA	0.043889584
4351177	4351177.1	Pyrite	Haylands, SA	0.043906256
4351177	4351177.11	Pyrite	Haylands, SA	0.043876543
4351177	4351177.12	Pyrite	Haylands, SA	0.043881261
4351177	4351177.13	Pyrite	Haylands, SA	0.043900535
4351177	4351177.14	Pyrite	Haylands, SA	0.043895742
4351177	4351177.15	Pyrite	Haylands, SA	0.043883765
4351177	4351177.16	Pyrite	Haylands, SA	0.043873746
4351177	4351177.17	Pyrite	Haylands, SA	0.043863446
4351177	4351177.18	Pyrite	Haylands, SA	0.043880111
4351177	4351177.19	Pyrite	Haylands, SA	0.043930815
4351177	4351177.2	Pyrite	Haylands, SA	0.043897584
4351177	4351177.21	Pyrite	Haylands, SA	0.043907306
4351177	4351177.22	Pyrite	Haylands, SA	0.043894592
4351177	4351177.23	Pyrite	Haylands, SA	0.043886857
4351177	4351177.24	Pyrite	Haylands, SA	0.04387192
4351177	4351177.25	Pyrite	Haylands, SA	0.043885083
4351177	4351177.26	Pyrite	Haylands, SA	0.043893519

4351177	4351177.27	Pyrite	Haylands, SA	0.043863937
4351177	4351177.28	Pyrite	Haylands, SA	0.043870334
4351177	4351177.29	Pyrite	Haylands, SA	0.04389434
4351177	4351177.3	Pyrite	Haylands, SA	0.043898478
4351177	4351177.31	Pyrite	Haylands, SA	0.043904498
4351177	4351177.32	Pyrite	Haylands, SA	0.043894117
4351177	4351177.33	Pyrite	Haylands, SA	0.043886775
4351177	4351177.34	Pyrite	Haylands, SA	0.043928575
4351177	4351177.35	Pyrite	Haylands, SA	0.043911574
4351177	4351177.36	Pyrite	Haylands, SA	0.043934833
4351177	4351177.37	Pyrite	Haylands, SA	0.043907835
4351177	4351177.38	Pyrite	Haylands, SA	0.043941023
4351177	4351177.39	Pyrite	Haylands, SA	0.043916186
4351177	4351177.4	Pyrite	Haylands, SA	0.043936014
4351177	4351177.41	Pyrite	Haylands, SA	0.043937323
4351177	4351177.42	Pyrite	Haylands, SA	0.043905534
4351177	4351177.43	Pyrite	Haylands, SA	0.043913888
4351177	4351177.44	Pyrite	Haylands, SA	0.043934812
4351177	4351177.45	Pyrite	Haylands, SA	0.043930008
4351177	4351177.46	Pyrite	Haylands, SA	0.043945846
4351177	4351177.47	Pyrite	Haylands, SA	0.043923219
4351177	4351177.48	Pyrite	Haylands, SA	0.043930209
4351177	4351177.49	Pyrite	Haylands, SA	0.043925468
4351174	4351174A.1	Pyrite	Haylands, SA	0.045703021
4351174	4351174A.2	Pyrite	Haylands, SA	0.045784523
4351174	4351174A.3	Pyrite	Haylands, SA	0.04574958
4351174	4351174A.4	Pyrite	Haylands, SA	0.045859225
4351174	4351174A.5	Pyrite	Haylands, SA	0.045904592
4351174	4351174A.6	Pyrite	Haylands, SA	0.045826908
4351174	4351174A.7	Pyrite	Haylands, SA	0.045913797
4351174	4351174A.8	Pyrite	Haylands, SA	0.045946209
4351174	4351174A.9	Pyrite	Haylands, SA	0.045941666
4351174	4351174A.10	Pyrite	Haylands, SA	0.04595033
4351174	4351174A.11	Pyrite	Haylands, SA	0.045696162
4351174	4351174A.12	Pyrite	Haylands, SA	0.045696241
4351174	4351174A.13	Pyrite	Haylands, SA	0.045701791
4351174	4351174A.14	Pyrite	Haylands, SA	0.045752245
4351174	4351174A.15	Pyrite	Haylands, SA	0.045780042
4351174	4351174A.16	Pyrite	Haylands, SA	0.045780284
322128	322128.1	Pyrite	Mt Ararat, VIC	0.045633316
322128	322128.2	Pyrite	Mt Ararat, VIC	0.045538197
322128	322128.3	Pyrite	Mt Ararat, VIC	0.045535213
322128	322128.4	Pyrite	Mt Ararat, VIC	0.045555834
322128	322128.5	Pyrite	Mt Ararat, VIC	0.045542963
322128	322128.6	Pyrite	Mt Ararat, VIC	0.045579434
322128	322128.7	Pyrite	Mt Ararat, VIC	0.045566455
322128	322128.sph.1	Sphalerite	Mt Ararat, VIC	0.04565984
322128	322128.sph.2	Sphalerite	Mt Ararat, VIC	0.045672315
322128	322128.sph.3	Sphalerite	Mt Ararat, VIC	0.045663943
322128	322128.sph.4	Sphalerite	Mt Ararat, VIC	0.045691016

322128	322128.sph.5	Sphalerite	Mt Ararat, VIC	0.045694292
322128	322128.sph.6	Sphalerite	Mt Ararat, VIC	0.045566502
322132	322132A.cpy.1	Chalcopyrite	Mt Ararat, VIC	0.045448544
322132	322132A.cpy.2	Chalcopyrite	Mt Ararat, VIC	0.045387876
322132	322132A.cpy.3	Chalcopyrite	Mt Ararat, VIC	0.045408455
322132	322132C.cpy.1	Chalcopyrite	Mt Ararat, VIC	0.045366583
322132	322132C.cpy.2	Chalcopyrite	Mt Ararat, VIC	0.045486651
322132	322132C.cpy.3	Chalcopyrite	Mt Ararat, VIC	0.045409093
322132	322132C.cpy.4	Chalcopyrite	Mt Ararat, VIC	0.045408499
322132	322132C.cpy.5	Chalcopyrite	Mt Ararat, VIC	0.045379814
322132	322132C.cpy.6	Chalcopyrite	Mt Ararat, VIC	0.045382564
322132	322132C.cpy.7	Chalcopyrite	Mt Ararat, VIC	0.045406441
322132	322132C.cpy8	Chalcopyrite	Mt Ararat, VIC	0.045400254
322132	322132C.cpy9	Chalcopyrite	Mt Ararat, VIC	0.045426293
322132	322132B.cpy.1	Chalcopyrite	Mt Ararat, VIC	0.045388061
322132	322132B.cpy.2	Chalcopyrite	Mt Ararat, VIC	0.045385458
322132	322132B.cpy.3	Chalcopyrite	Mt Ararat, VIC	0.045403203
322132	322132B.cpy.4	Chalcopyrite	Mt Ararat, VIC	0.045396069
322129	322129A.cpy.1	Chalcopyrite	Mt Ararat, VIC	0.04547661
322129	322129A.cpy.2	Chalcopyrite	Mt Ararat, VIC	0.045491577
322129	322129B.cpy.1	Chalcopyrite	Mt Ararat, VIC	0.045471655
322129	322129B.cpy.2	Chalcopyrite	Mt Ararat, VIC	0.045458874
322129	322129B.cpy.3	Chalcopyrite	Mt Ararat, VIC	0.045436375
322128	322128.cpy.1	Chalcopyrite	Mt Ararat, VIC	0.045586937
322128	322128.cpy.2	Chalcopyrite	Mt Ararat, VIC	0.045539234
322128	322128.cpy.3	Chalcopyrite	Mt Ararat, VIC	0.045480517
322128	322128.cpy.4	Chalcopyrite	Mt Ararat, VIC	0.045482293
322128	322128.cpy.5	Chalcopyrite	Mt Ararat, VIC	0.045458405
322128	322128.cpy.6	Chalcopyrite	Mt Ararat, VIC	0.045444148
322129	322129A.1	Pyrite	Mt Ararat, VIC	0.045533232
322129	322129A.2	Pyrite	Mt Ararat, VIC	0.045486511
322129	322129A.3	Pyrite	Mt Ararat, VIC	0.045520703
322129	322129A.4	Pyrite	Mt Ararat, VIC	0.045512092
322129	322129A.5	Pyrite	Mt Ararat, VIC	0.045498278
322129	322129A.6	Pyrite	Mt Ararat, VIC	0.04551629
322129	322129A.7	Pyrite	Mt Ararat, VIC	0.045547652
322129	322129A.8	Pyrite	Mt Ararat, VIC	0.045555249
322129	322129A.9	Pyrite	Mt Ararat, VIC	0.045547821
322129	322129B.1	Pyrite	Mt Ararat, VIC	0.04553796
322129	322129B.2	Pyrite	Mt Ararat, VIC	0.045736657
322129	322129B.3	Pyrite	Mt Ararat, VIC	0.045679286
322129	322129B.4	Pyrite	Mt Ararat, VIC	0.04568215
322129	322129B.5	Pyrite	Mt Ararat, VIC	0.045708593
322129	322129C.1	Pyrite	Mt Ararat, VIC	0.045403784
322129	322129C.2	Pyrite	Mt Ararat, VIC	0.045263135
322129	322129C.3	Pyrite	Mt Ararat, VIC	0.045241393
322129	322129C.4	Pyrite	Mt Ararat, VIC	0.04537179
322129	322129C.5	Pyrite	Mt Ararat, VIC	0.045513489
322129	322129C.6	Pyrite	Mt Ararat, VIC	0.045353473
322129	322129C.7	Pyrite	Mt Ararat, VIC	0.045410932

322129	322129C.8	Pyrite	Mt Ararat, VIC	0.045357357
322129	322129C.9	Pyrite	Mt Ararat, VIC	0.045510904
322129	322129C.10	Pyrite	Mt Ararat, VIC	0.045354428
322132	322132A.1	Pyrite	Mt Ararat, VIC	0.04545735
322132	322132A.2	Pyrite	Mt Ararat, VIC	0.0454406
322132	322132A.3	Pyrite	Mt Ararat, VIC	0.045472425
322132	322132A.4	Pyrite	Mt Ararat, VIC	0.045453054
322132	322132A.5	Pyrite	Mt Ararat, VIC	0.045485268
322132	322132B.1	Pyrite	Mt Ararat, VIC	0.045517907
322132	322132B.2	Pyrite	Mt Ararat, VIC	0.045358161
322132	322132B.3	Pyrite	Mt Ararat, VIC	0.045369813
322132	322132B.4	Pyrite	Mt Ararat, VIC	0.045373274
322132	322132B.5	Pyrite	Mt Ararat, VIC	0.045359371
322132	322132B.6	Pyrite	Mt Ararat, VIC	0.045372976
322132	322132B.7	Pyrite	Mt Ararat, VIC	0.045405993
322132	322132B.8	Pyrite	Mt Ararat, VIC	0.045390156
322132	322132B.9	Pyrite	Mt Ararat, VIC	0.045383875
322132	322132B.10	Pyrite	Mt Ararat, VIC	0.0453788
322132	322132B.11	Pyrite	Mt Ararat, VIC	0.045366155
322132	322132B.12	Pyrite	Mt Ararat, VIC	0.04538173
322132	322132B.13	Pyrite	Mt Ararat, VIC	0.045403572
322132	322132B.14	Pyrite	Mt Ararat, VIC	0.045420268
322132	322132B.15	Pyrite	Mt Ararat, VIC	0.045393781
322132	322132B.16	Pyrite	Mt Ararat, VIC	0.045423825
322132	322132C.1	Pyrite	Mt Ararat, VIC	0.045420173
322132	322132C.2	Pyrite	Mt Ararat, VIC	0.046388146
322132	322132C.3	Pyrite	Mt Ararat, VIC	0.045589063
322132	322132C.4	Pyrite	Mt Ararat, VIC	0.045867504
322132	322132C.5	Pyrite	Mt Ararat, VIC	0.046996637
322132	322132C.6	Pyrite	Mt Ararat, VIC	0.04579264
322132	322132C.7	Pyrite	Mt Ararat, VIC	0.045435538
322132	322132C.8	Pyrite	Mt Ararat, VIC	0.045462796
322132	322132C.9	Pyrite	Mt Ararat, VIC	0.045508448
322132	322132C.10	Pyrite	Mt Ararat, VIC	0.045505357
322132	322132C.11	Pyrite	Mt Ararat, VIC	0.045035119
2022440201	2022440201.cpy.1	Chalcopyrite	Mt Arrowsmith, NSW	0.045044754
2022440201	2022440201.cpy.2	Chalcopyrite	Mt Arrowsmith, NSW	0.044996968
2022440201	2022440211.cpy.1	Chalcopyrite	Mt Arrowsmith, NSW	0.044974537
2022440201	2022440211.cpy.2	Chalcopyrite	Mt Arrowsmith, NSW	0.044968389
2022440201	2022440211.cpy.3	Chalcopyrite	Mt Arrowsmith, NSW	0.044982903
2022440201	2022440211.cpy.4	Chalcopyrite	Mt Arrowsmith, NSW	0.044978011
2022440201	2022440211.cpy.5	Chalcopyrite	Mt Arrowsmith, NSW	0.044979483
2022440213	2022440213.cpy.1	Chalcopyrite	Mt Arrowsmith, NSW	0.044977855
2022440213	2022440213.cpy.2	Chalcopyrite	Mt Arrowsmith, NSW	0.04502115
2022440213	2022440213.cpy.3	Chalcopyrite	Mt Arrowsmith, NSW	0.044937656
2022440213	2022440213.cpy.4	Chalcopyrite	Mt Arrowsmith, NSW	0.044939355
2022440213	2022440213.cpy.5	Chalcopyrite	Mt Arrowsmith, NSW	0.045029532
2022440213	2022440213.cpy.6	Chalcopyrite	Mt Arrowsmith, NSW	0.044997138
2022440213	2022440213.cpy.7	Chalcopyrite	Mt Arrowsmith, NSW	0.044988228
2022440213	2022440213.cpy.8	Chalcopyrite	Mt Arrowsmith, NSW	0.044965834

2022440201	2022440201.1	Pyrite	Mt Arrowsmith, NSW	0.045025128
2022440201	2022440201.2	Pyrite	Mt Arrowsmith, NSW	0.044974684
2022440201	2022440201.3	Pyrite	Mt Arrowsmith, NSW	0.044969581
2022440201	2022440201.4	Pyrite	Mt Arrowsmith, NSW	0.044986613
2022440201	2022440201.5	Pyrite	Mt Arrowsmith, NSW	0.044999762
2022440201	2022440201.6	Pyrite	Mt Arrowsmith, NSW	0.04501561
2022440201	2022440201.7	Pyrite	Mt Arrowsmith, NSW	0.045006194
2022440201	2022440201.8	Pyrite	Mt Arrowsmith, NSW	0.044989748
2022440211	2022440211.1	Pyrite	Mt Arrowsmith, NSW	0.045016351
2022440211	2022440211.2	Pyrite	Mt Arrowsmith, NSW	0.045014974
2022440211	2022440211.3	Pyrite	Mt Arrowsmith, NSW	0.045006149
2022440211	2022440211.4	Pyrite	Mt Arrowsmith, NSW	0.04501156
2022440211	2022440211.5	Pyrite	Mt Arrowsmith, NSW	0.044976125
2022440211	2022440211.6	Pyrite	Mt Arrowsmith, NSW	0.045008596
2022440213	2022440213.1	Pyrite	Mt Arrowsmith, NSW	0.044998877
2022440213	2022440213.2	Pyrite	Mt Arrowsmith, NSW	0.044967427
2022440213	2022440213.3	Pyrite	Mt Arrowsmith, NSW	0.044988791
2022440213	2022440213.4	Pyrite	Mt Arrowsmith, NSW	0.044969927
2022440213	2022440213.5	Pyrite	Mt Arrowsmith, NSW	0.044987367
2022440213	2022440213.6	Pyrite	Mt Arrowsmith, NSW	0.045021217
2022440213	2022440213.7	Pyrite	Mt Arrowsmith, NSW	0.045002233
2022440213	2022440213.8	Pyrite	Mt Arrowsmith, NSW	0.045014059
2022440151	2022440151B.1	Pyrite	New Bendigo, NSW	0.045449114
2022440151	2022440151B.2	Pyrite	New Bendigo, NSW	0.04542695
2022440151	2022440151B.3	Pyrite	New Bendigo, NSW	0.045633605
2022440151	2022440151B.4	Pyrite	New Bendigo, NSW	0.04547487
2022440151	2022440151B.5	Pyrite	New Bendigo, NSW	0.045489892
2022440151	2022440151B.6	Pyrite	New Bendigo, NSW	0.045465928
2022440151	2022440151B.7	Pyrite	New Bendigo, NSW	0.045475403
2022440151	2022440151B.8	Pyrite	New Bendigo, NSW	0.04555043
2022440151	2022440151B.9	Pyrite	New Bendigo, NSW	0.045465564
2022440151	2022440151B.10	Pyrite	New Bendigo, NSW	0.045447091
2022440151	2022440151B.11	Pyrite	New Bendigo, NSW	0.045485935
2022440151	2022440151B.12	Pyrite	New Bendigo, NSW	0.045338222
2022440151	2022440151B.13	Pyrite	New Bendigo, NSW	0.045412608
2022440151	2022440151B.14	Pyrite	New Bendigo, NSW	0.04540443
2022440151	2022440151B.15	Pyrite	New Bendigo, NSW	0.045380116
2022440151	2022440151B.16	Pyrite	New Bendigo, NSW	0.045369599
2022440151	2022440151B.17	Pyrite	New Bendigo, NSW	0.045377608
2022440151	2022440151B.18	Pyrite	New Bendigo, NSW	0.04536139
2022440151	2022440151B.19	Pyrite	New Bendigo, NSW	0.045359125
2022440151	2022440151B.20	Pyrite	New Bendigo, NSW	0.045360424
2022440151	2022440151A.1	Pyrite	New Bendigo, NSW	0.043828963
2022440151	2022440151A.2	Pyrite	New Bendigo, NSW	0.043856739
2022440151	2022440151A.3	Pyrite	New Bendigo, NSW	0.043846116
2022440151	2022440151A.4	Pyrite	New Bendigo, NSW	0.043782942
2022440151	2022440151A.5	Pyrite	New Bendigo, NSW	0.043783608
2022440151	2022440151A.6	Pyrite	New Bendigo, NSW	0.043746442
2022440151	2022440151A.7	Pyrite	New Bendigo, NSW	0.043761066
2022440151	2022440151A.8	Pyrite	New Bendigo, NSW	0.043757393

2022440151	2022440151A.9	Pyrite	New Bendigo, NSW	0.043749343
2022440151	2022440151A.10	Pyrite	New Bendigo, NSW	0.04373743
2022440151	2022440151A.11	Pyrite	New Bendigo, NSW	0.043709416
2022440151	2022440151A.12	Pyrite	New Bendigo, NSW	0.043777468
2022440151	2022440151A.13	Pyrite	New Bendigo, NSW	0.043694619
2022440151	2022440151A.14	Pyrite	New Bendigo, NSW	0.043764855
2022440151	2022440151A.15	Pyrite	New Bendigo, NSW	0.043739186
2022440151	2022440151A.16	Pyrite	New Bendigo, NSW	0.043790039
2022440151	2022440151A.17	Pyrite	New Bendigo, NSW	0.043791968
2022440151	2022440151A.18	Pyrite	New Bendigo, NSW	0.043753815
2022440151	2022440151A.19	Pyrite	New Bendigo, NSW	0.043802083
2022440151	2022440151A.20	Pyrite	New Bendigo, NSW	0.043784538
2022440144	2022440144.1	Pyrite	Pioneer, NSW	0.045059311
2022440144	2022440144.2	Pyrite	Pioneer, NSW	0.045077065
2022440144	2022440144.3	Pyrite	Pioneer, NSW	0.045045787
2022440144	2022440144.4	Pyrite	Pioneer, NSW	0.045043544
2022440144	2022440144.5	Pyrite	Pioneer, NSW	0.045053638
2022440144	2022440144.6	Pyrite	Pioneer, NSW	0.045027757
2022440144	2022440144.7	Pyrite	Pioneer, NSW	0.045034514
2022440144	2022440144.8	Pyrite	Pioneer, NSW	0.045029749
2022440144	2022440144.9	Pyrite	Pioneer, NSW	0.045043731
2022440144	2022440144.10	Pyrite	Pioneer, NSW	0.045060359
2022440144	2022440144.11	Pyrite	Pioneer, NSW	0.045079899
2022440144	2022440144.12	Pyrite	Pioneer, NSW	0.045045469
2022440144	2022440144.13	Pyrite	Pioneer, NSW	0.045114626
2022440144	2022440144.14	Pyrite	Pioneer, NSW	0.04506323
2022440144	2022440144.15	Pyrite	Pioneer, NSW	0.045032584
2022440144	2022440144.16	Pyrite	Pioneer, NSW	0.045065724
2022440144	2022440144.17	Pyrite	Pioneer, NSW	0.045048989
2022440144	2022440144.18	Pyrite	Pioneer, NSW	0.045017458
2022440144	2022440144.19	Pyrite	Pioneer, NSW	0.045072597
2022440144	2022440144.20	Pyrite	Pioneer, NSW	0.045043442
2022440144	2022440144.21	Pyrite	Pioneer, NSW	0.045059641
2022440144	2022440144.22	Pyrite	Pioneer, NSW	0.044985064
2022440144	2022440144.23	Pyrite	Pioneer, NSW	0.044967125
2022440144	2022440144.24	Pyrite	Pioneer, NSW	0.044986662
2022440144	2022440144.25	Pyrite	Pioneer, NSW	0.045067007
2022440144	2022440144.26	Pyrite	Pioneer, NSW	0.045019977
2022440144	2022440144.27	Pyrite	Pioneer, NSW	0.045031161
2022440144	2022440144.28	Pyrite	Pioneer, NSW	0.044996916
2022440144	2022440144.29	Pyrite	Pioneer, NSW	0.044984037
2022440144	2022440144.30	Pyrite	Pioneer, NSW	0.044984863
2022440144	2022440144.31	Pyrite	Pioneer, NSW	0.044986403
2022440144	2022440144.32	Pyrite	Pioneer, NSW	0.044975984
2022440144	2022440144.33	Pyrite	Pioneer, NSW	0.045029036
2022440144	2022440144.34	Pyrite	Pioneer, NSW	0.045017652
2022440144	2022440144.35	Pyrite	Pioneer, NSW	0.044982777
2022440144	2022440144.36	Pyrite	Pioneer, NSW	0.044961017
2022440144	2022440144.37	Pyrite	Pioneer, NSW	0.04502859
2022440144	2022440144.38	Pyrite	Pioneer, NSW	0.045055813

2022440144	2022440144.39	Pyrite	Pioneer, NSW	0.045040059
2022440144	2022440144.40	Pyrite	Pioneer, NSW	0.045042985
2022440144	2022440144.41	Pyrite	Pioneer, NSW	0.045086721
2022330094	2022330094A.1	Pyrite	Quondong, NSW	0.04369126
2022330094	2022330094A.2	Pyrite	Quondong, NSW	0.043683992
2022330094	2022330094A.3	Pyrite	Quondong, NSW	0.043676186
2022330094	2022330094A.4	Pyrite	Quondong, NSW	0.043686556
2022330094	2022330094A.5	Pyrite	Quondong, NSW	0.043710828
2022330094	2022330094A.6	Pyrite	Quondong, NSW	0.043661962
2022330094	2022330094A.7	Pyrite	Quondong, NSW	0.043792211
2022330094	2022330094A.8	Pyrite	Quondong, NSW	0.043796402
2022330094	2022330094A.9	Pyrite	Quondong, NSW	0.043793341
2022330094	2022330094A.10	Pyrite	Quondong, NSW	0.043800086
2022330094	2022330094A.11	Pyrite	Quondong, NSW	0.043813145
2022330094	2022330094A.12	Pyrite	Quondong, NSW	0.043779621
2022330094	2022330094B.1	Pyrite	Quondong, NSW	0.043767283
2022330094	2022330094B.2	Pyrite	Quondong, NSW	0.043817731
2022330094	2022330094B.3	Pyrite	Quondong, NSW	0.043769772
2022330094	2022330094B.4	Pyrite	Quondong, NSW	0.043759082
2022330094	2022330094B.5	Pyrite	Quondong, NSW	0.043810764
2022330094	2022330094B.6	Pyrite	Quondong, NSW	0.043739666
2022330094	2022330094B.7	Pyrite	Quondong, NSW	0.043702313
2022330094	2022330094B.8	Pyrite	Quondong, NSW	0.043742297
2022330094	2022330094B.9	Pyrite	Quondong, NSW	0.043767952
2022330094	2022330094B.10	Pyrite	Quondong, NSW	0.043730518
2022330094	2022330094B.11	Pyrite	Quondong, NSW	0.043769411
2022330094	2022330094B.12	Pyrite	Quondong, NSW	0.043726454
4351225	4351225.Sph.1	Sphalerite	Sherlock, SA	0.045384
4351225	4351225.Sph.2	Sphalerite	Sherlock, SA	0.045385423
4351225	4351225.Sph.3	Sphalerite	Sherlock, SA	0.045347982
4351225	4351225.Sph.4	Sphalerite	Sherlock, SA	0.045295501
4351225	4351225.Sph.5	Sphalerite	Sherlock, SA	0.045385402
4351225	4351225.Sph.6	Sphalerite	Sherlock, SA	0.045404962
4351225	4351225.Sph.7	Sphalerite	Sherlock, SA	0.045479595
4351225	4351225.1	Pyrite	Sherlock, SA	0.043690818
4351225	4351225.2	Pyrite	Sherlock, SA	0.043696953
4351225	4351225.3	Pyrite	Sherlock, SA	0.04371836
4351225	4351225.4	Pyrite	Sherlock, SA	0.043731672
4351225	4351225.5	Pyrite	Sherlock, SA	0.043711436
4351225	4351225.6	Pyrite	Sherlock, SA	0.04372612
4351225	4351225.7	Pyrite	Sherlock, SA	0.043690209
4351203	4351203.1	Pyrite	Sherlock, SA	0.043648892
4351203	4351203.2	Pyrite	Sherlock, SA	0.043711106
4351203	4351203.3	Pyrite	Sherlock, SA	0.043672137
4351203	4351203.4	Pyrite	Sherlock, SA	0.043664777
4351203	4351203.5	Pyrite	Sherlock, SA	0.04367843
4351203	4351203.6	Pyrite	Sherlock, SA	0.043608192
4351202	4351202_1	Pyrite	Sherlock, SA	0.045295939
4351202	4351202_2	Pyrite	Sherlock, SA	0.045248275
4351202	4351202_3	Pyrite	Sherlock, SA	0.045248987

4351202	4351202_4	Pyrite	Sherlock, SA	0.045267328
4351202	4351202_5	Pyrite	Sherlock, SA	0.045262322
4351202	4351202_6	Pyrite	Sherlock, SA	0.045267037
4351202	4351202_7	Pyrite	Sherlock, SA	0.045268606
4351202	4351202_8	Pyrite	Sherlock, SA	0.045278602
4351202	4351202_9	Pyrite	Sherlock, SA	0.045261447
4351202	4351202_10	Pyrite	Sherlock, SA	0.04528458
4351202	4351202_11	Pyrite	Sherlock, SA	0.04526436
4351202	4351202_12	Pyrite	Sherlock, SA	0.045277318
4351202	4351202_13	Pyrite	Sherlock, SA	0.04528432
4351202	4351202_14	Pyrite	Sherlock, SA	0.045234047
4351202	4351202_15	Pyrite	Sherlock, SA	0.045220608
4351202	4351202_16	Pyrite	Sherlock, SA	0.045240334
4351202	4351202_17	Pyrite	Sherlock, SA	0.04521071
4351202	4351202_18	Pyrite	Sherlock, SA	0.045268058
4351202	4351202_19	Pyrite	Sherlock, SA	0.045296955
4351202	4351202_20	Pyrite	Sherlock, SA	0.045226691
4351202	4351202_21	Pyrite	Sherlock, SA	0.045281995
4351202	4351202_22	Pyrite	Sherlock, SA	0.045226219
4351202	4351202_23	Pyrite	Sherlock, SA	0.04524621
4351202	4351202_24	Pyrite	Sherlock, SA	0.045288164
4351202	4351202_25	Pyrite	Sherlock, SA	0.045242693
2023440018	2023440018.1	Pyrite	Stawell, VIC	0.043381265
2023440018	2023440018.2	Pyrite	Stawell, VIC	0.043384721
2023440018	2023440018.3	Pyrite	Stawell, VIC	0.043400464
2023440018	2023440018.4	Pyrite	Stawell, VIC	0.04339625
2023440018	2023440018.5	Pyrite	Stawell, VIC	0.043388834
2023440018	2023440018.6	Pyrite	Stawell, VIC	0.043392376
2023440018	2023440018.7	Pyrite	Stawell, VIC	0.043341705
2023440018	2023440018.8	Pyrite	Stawell, VIC	0.043365282
2023440018	2023440018.9	Pyrite	Stawell, VIC	0.043361376
2023440018	2023440018.10	Pyrite	Stawell, VIC	0.043367787
2023440018	2023440018.11	Pyrite	Stawell, VIC	0.04337933
2023440018	2023440018.12	Pyrite	Stawell, VIC	0.043351351
2022330048	048-1.1	Pyrite	Mt Arrowsmith, NSW	0.045064093
2022330048	048-1.2	Pyrite	Mt Arrowsmith, NSW	0.045016475
2022330048	048-1.3	Pyrite	Mt Arrowsmith, NSW	0.045068813
2022330048	048-1.4	Pyrite	Mt Arrowsmith, NSW	0.045051584
2022330048	048-1.5	Pyrite	Mt Arrowsmith, NSW	0.045010421
2022330048	048-1.6	Pyrite	Mt Arrowsmith, NSW	0.04502831
2022330048	048-1.7	Pyrite	Mt Arrowsmith, NSW	0.045039319
2022330048	048-1.8	Pyrite	Mt Arrowsmith, NSW	0.045018683
2022330048	048-1.9	Pyrite	Mt Arrowsmith, NSW	0.04505495
2022330048	048-1.10	Pyrite	Mt Arrowsmith, NSW	0.045051376
2022330048	048-1.11	Pyrite	Mt Arrowsmith, NSW	0.045054048
2022330048	048-1.12	Pyrite	Mt Arrowsmith, NSW	0.045017827
2022330048	048-1.13	Pyrite	Mt Arrowsmith, NSW	0.044999867
2022330048	048-1.14	Pyrite	Mt Arrowsmith, NSW	0.045005219
2022330048	048-1.15	Pyrite	Mt Arrowsmith, NSW	0.045024868
2022330043	43-5c.1	Pyrite	Mt Arrowsmith, NSW	0.045014606

2022330043	43-5c.2	Pyrite	Mt Arrowsmith, NSW	0.045049495
2022330043	43-5r.1	Pyrite	Mt Arrowsmith, NSW	0.045137896
2022330043	43-5r.2	Pyrite	Mt Arrowsmith, NSW	0.045042353
2022330043	43-5r.3	Pyrite	Mt Arrowsmith, NSW	0.045077899
2022330043	43-5c.3	Pyrite	Mt Arrowsmith, NSW	0.045008809
2022330043	43-5c.4	Pyrite	Mt Arrowsmith, NSW	0.045016929
2022330043	43-5c.5	Pyrite	Mt Arrowsmith, NSW	0.045037324
2022330043	43-5c.6	Pyrite	Mt Arrowsmith, NSW	0.045027221
2022330043	43-5r.4	Pyrite	Mt Arrowsmith, NSW	0.045206198
2022330043	43-5r.5	Pyrite	Mt Arrowsmith, NSW	0.045027453
2022330043	43-5r.6	Pyrite	Mt Arrowsmith, NSW	0.045135996
2022330043	43-5r.7	Pyrite	Mt Arrowsmith, NSW	0.045053592
2022330043	43-5c.7	Pyrite	Mt Arrowsmith, NSW	0.045003402
2022330043	43-5c.8	Pyrite	Mt Arrowsmith, NSW	0.04503148
2022330043	43-5c.9	Pyrite	Mt Arrowsmith, NSW	0.04502114
2022330043	43-5c.10	Pyrite	Mt Arrowsmith, NSW	0.045009982
2022330043	43-5c.11	Pyrite	Mt Arrowsmith, NSW	0.045037467
2022330043	43-5v.1	Pyrite	Mt Arrowsmith, NSW	0.045038697
2022330043	43-5cpy.1	Chalcopyrite	Mt Arrowsmith, NSW	0.045019999

Sample ID	**Analysis ID**	**Mineral**	**Deposit**	**$\delta^{33}S_{CDT}$(‰)**
GNTP_023	GNTP_023-1	Pyrite	Kamantoo, SA	5.48
GNTP_023	GNTP_023-2	Pyrite	Kamantoo, SA	5.36
GNTP_023	GNTP_023-3	Pyrite	Kamantoo, SA	5.39
GNTP_023	GNTP_023-4	Pyrite	Kamantoo, SA	5.44
GNTP_023	GNTP_023-5	Pyrite	Kamantoo, SA	5.34
GNTP_023	GNTP_023-6	Pyrite	Kamantoo, SA	5.41
GNTP_023	GNTP_023-7	Pyrite	Kamantoo, SA	5.53
GNTP_023	GNTP_023-8	Pyrite	Kamantoo, SA	5.40
GNTP_023	GNTP_023-9	Pyrite	Kamantoo, SA	5.22
GNTP_023	GNTP_023-10	Pyrite	Kamantoo, SA	5.41
GNTP_023	GNTP_023-11	Pyrite	Kamantoo, SA	5.54
GNTP_023	GNTP_023-12	Pyrite	Kamantoo, SA	5.64
GNTP_023	GNTP_023-13	Pyrite	Kamantoo, SA	5.33
GNTP_023	GNTP_023-14	Pyrite	Kamantoo, SA	5.50
GNTP_023	GNTP_023-15	Pyrite	Kamantoo, SA	5.57
GNTP_023	GNTP_023-16	Pyrite	Kamantoo, SA	5.83
GNTP_023	GNTP_023-17	Pyrite	Kamantoo, SA	5.66
GNTP_023	GNTP_023-18	Pyrite	Kamantoo, SA	5.75
GNTP_023	GNTP_023-19	Pyrite	Kamantoo, SA	5.83
GNTP_023	GNTP_023-20	Pyrite	Kamantoo, SA	5.67
GNTP_023	GNTP_023-21	Pyrite	Kamantoo, SA	5.94
GNTP_023	GNTP_023-22	Pyrite	Kamantoo, SA	6.11
GNTP_023	GNTP_023-23	Pyrite	Kamantoo, SA	6.19
GNTP_023	GNTP_023-24	Pyrite	Kamantoo, SA	6.26
GNTP_023	GNTP_023-25	Pyrite	Kamantoo, SA	5.63

GNTP_023	GNTP_023-26	Pyrite	Kamantoo, SA	5.44
GNTP_023	GNTP_023-27	Pyrite	Kamantoo, SA	5.49
GNTP_023	GNTP_023-28	Pyrite	Kamantoo, SA	5.41
GNTP_023	GNTP_023-29	Pyrite	Kamantoo, SA	5.62
GNTP_023	GNTP_023-30	Pyrite	Kamantoo, SA	5.55
GNTP_023	GNTP_023-31	Pyrite	Kamantoo, SA	5.87
GNTP_023	GNTP_023-32	Pyrite	Kamantoo, SA	6.08
GNTP_023	GNTP-023-32a	Pyrite	Kamantoo, SA	6.01
GNTP_023	GNTP_023-33	Pyrite	Kamantoo, SA	5.88
GNTP_023	GNTP_023-34	Pyrite	Kamantoo, SA	5.96
GNTP_023	GNTP_023-35	Pyrite	Kamantoo, SA	5.73
GNTP_023	GNTP_023-36	Pyrite	Kamantoo, SA	6.18
GNTP_023	GNTP-023-36a	Pyrite	Kamantoo, SA	6.30
GNTP_023	GNTP_023-37	Pyrite	Kamantoo, SA	5.85
GNTP_023	GNTP_023-38	Pyrite	Kamantoo, SA	6.27
GNTP_023	GNTP_023-39	Pyrite	Kamantoo, SA	6.04
GNTP_023	GNTP_023-40	Pyrite	Kamantoo, SA	5.29
GNTP_023	GNTP_023-41	Pyrite	Kamantoo, SA	5.24
GNTP_023	GNTP_023-42	Pyrite	Kamantoo, SA	5.54
GNTP_023	GNTP_023-71	Pyrite	Kamantoo, SA	6.99
GNTP_023	GNTP_023-72	Pyrite	Kamantoo, SA	6.09
GNTP_023	GNTP_023-73	Pyrite	Kamantoo, SA	7.08
GNTP_023	GNTP_023-74	Pyrite	Kamantoo, SA	5.64
GNTP_023	GNTP_023-75	Pyrite	Kamantoo, SA	5.14
GNTP_023	GNTP_023-76	Pyrite	Kamantoo, SA	5.77
GNTP_023	GNTP_023-77	Pyrite	Kamantoo, SA	5.75
GNTP_023	GNTP_023-78	Pyrite	Kamantoo, SA	5.96
GNTP_023	GNTP_023-79	Pyrite	Kamantoo, SA	5.50
GNTP_023	GNTP_023-80	Pyrite	Kamantoo, SA	5.90
GNTP_023	GNTP_023-81	Pyrite	Kamantoo, SA	5.68
GNTP_023	GNTP_023-82	Pyrite	Kamantoo, SA	6.49
GNTP_023	GNTP_023-83	Pyrite	Kamantoo, SA	6.07
GNTP_023	GNTP_023-84	Pyrite	Kamantoo, SA	6.02
GNTP_023	GNTP_023-85	Pyrite	Kamantoo, SA	5.82
GNTP_023	GNTP_023-43	Pyrite	Kamantoo, SA	5.67
GNTP_023	GNTP_023-44	Pyrite	Kamantoo, SA	5.91
GNTP_023	GNTP_023-45	Pyrite	Kamantoo, SA	6.09
GNTP_023	GNTP_023-46	Pyrite	Kamantoo, SA	5.59
GNTP_023	GNTP_023-47	Pyrite	Kamantoo, SA	5.35
GNTP_023	GNTP_023-48	Pyrite	Kamantoo, SA	5.71
GNTP_023	GNTP_023-49	Pyrite	Kamantoo, SA	5.69
GNTP_023	GNTP_023-50	Pyrite	Kamantoo, SA	5.59
GNTP_023	GNTP_023-51	Pyrite	Kamantoo, SA	5.38
GNTP_023	GNTP_023-52	Pyrite	Kamantoo, SA	5.34
GNTP_023	GNTP_023-53	Pyrite	Kamantoo, SA	5.49
GNTP_023	GNTP_023-54	Pyrite	Kamantoo, SA	5.61
GNTP_023	GNTP_023-55	Pyrite	Kamantoo, SA	5.78
GNTP_023	GNTP_023-56	Pyrite	Kamantoo, SA	6.19
GNTP_023	GNTP_023-57	Pyrite	Kamantoo, SA	5.78
GNTP_023	GNTP_023-58	Pyrite	Kamantoo, SA	5.77

GNTP_023	GNTP_023-59	Pyrite	Kamantoo, SA	5.82
GNTP_023	GNTP_023-60	Pyrite	Kamantoo, SA	5.79
GNTP_023	GNTP_023-61	Pyrite	Kamantoo, SA	6.13
GNTP_023	GNTP_023-62	Pyrite	Kamantoo, SA	6.05
GNTP_023	GNTP_023-63	Pyrite	Kamantoo, SA	5.93
GNTP_023	GNTP_023-64	Pyrite	Kamantoo, SA	6.00
GNTP_023	GNTP_023-65	Pyrite	Kamantoo, SA	5.89
GNTP_023	GNTP_023-66	Pyrite	Kamantoo, SA	5.78
GNTP_023	GNTP_023-67	Pyrite	Kamantoo, SA	5.79
GNTP_023	GNTP_023-68	Pyrite	Kamantoo, SA	5.99
GNTP_023	GNTP_023-69	Pyrite	Kamantoo, SA	5.76
GNTP_023	GNTP_023-70	Pyrite	Kamantoo, SA	6.02

Sample ID	**Analysis ID**	**Mineral**	**RT (Sec)**	**Height (nA)**
2022330033	39505	Galena	81.0	5.43
2022330048	39506	Pyrite	82.4	3.55
2022330047	39507	Pyrrhotite	84.0	3.82
2022330030-1	39508	Galena	80.0	4.70
2022330030-2a	39509	Pyrite	82.2	2.90
2022330030-2b	39510	Pyrite	82.5	3.18
2022330030-2c	39511	Pyrite	83.8	1.04
2022330043-1	39513	Pyrite	81.1	2.51
2022330043-2	39514	Chalcopyrite	82.4	5.71
2022330037	39515	Pyrite	81.4	5.68
2022330070	39516	Pyrite	81.0	3.78

$^{34}S/^{32}S$_true	$\delta^{34}S_{CDT}$(‰)	± internal precision(95% conf.)
0.043234866	**-1.4**	0.07
0.043362775	**1.6**	0.09
0.043337731	**1.0**	0.15
0.043240063	**-1.2**	0.13
0.04325986	**-0.8**	0.10
0.043321863	**0.6**	0.10
0.043248831	**-1.0**	0.09
0.043291563	**-0.1**	0.11
0.043368529	**1.7**	0.11
0.043374102	**1.9**	0.09
0.043373088	**1.8**	0.09
0.043320684	**0.6**	0.14
0.043404261	**2.5**	0.10
0.043344376	**1.2**	0.12
0.043491894	**1.0**	0.12
0.043566674	**2.7**	0.09
0.043543798	**2.2**	0.05
0.043549776	**2.3**	0.08
0.043586495	**3.2**	0.13
0.043715833	**6.1**	0.13
0.043575306	**2.9**	0.07
0.043577788	**3.0**	0.13
0.043531865	**1.9**	0.07
0.043488929	**0.9**	0.14
0.043511586	**1.4**	0.06
0.043492824	**1.0**	0.11
0.043499019	**1.1**	0.07
0.043512027	**1.4**	0.05
0.043509167	**1.4**	0.09
0.043514789	**1.5**	0.11
0.04352872	**1.8**	0.09
0.043524723	**1.7**	0.11
0.043530068	**1.9**	0.13
0.043515183	**1.5**	0.02
0.043563958	**2.6**	0.12
0.043524115	**1.7**	0.07
0.043527079	**1.8**	0.06
0.043529352	**1.8**	0.10
0.043555275	**2.4**	0.06
0.043524648	**1.7**	0.08
0.0436134	**3.8**	0.07
0.043568416	**2.7**	0.04
0.043547809	**2.3**	0.12
0.043542528	**2.1**	0.13
0.044226612	**1.4**	0.27
0.044179879	**0.4**	0.21
0.044231244	**1.5**	0.16
0.044214335	**1.1**	0.15
0.044173938	**0.2**	0.23

0.044191494	**0.6**	0.17
0.044202298	**0.9**	0.16
0.044182046	**0.4**	0.22
0.044217639	**1.2**	0.25
0.044214131	**1.1**	0.18
0.044216754	**1.2**	0.14
0.044181206	**0.4**	0.13
0.044163579	**0.0**	0.18
0.044168832	**0.1**	0.20
0.044188116	**0.6**	0.20
0.04422664	**0.9**	0.70
0.044179793	**-0.2**	0.55
0.044231226	**1.0**	0.41
0.04421432	**0.6**	0.40
0.044173887	**-0.3**	0.60
0.044191452	**0.1**	0.43
0.044202309	**0.3**	0.42
0.044182061	**-0.1**	0.56
0.04421761	**0.7**	0.63
0.044214107	**0.6**	0.47
0.044216763	**0.6**	0.36
0.044181245	**-0.2**	0.33
0.044163568	**-0.6**	0.47
0.044168769	**-0.4**	0.51
0.044188125	**0.0**	0.51
0.044178044	**0.3**	0.15
0.044212285	**1.1**	0.15
0.044299043	**3.1**	0.19
0.044205277	**0.9**	0.20
0.044240162	**1.7**	0.17
0.044172356	**0.2**	0.12
0.044180324	**0.4**	0.18
0.044200341	**0.8**	0.21
0.044190425	**0.6**	0.18
0.044366076	**4.6**	0.27
0.044190653	**0.6**	0.17
0.044297179	**3.0**	0.14
0.044216306	**1.2**	0.19
0.044167049	**0.1**	0.18
0.044194605	**0.7**	0.09
0.044184457	**0.5**	0.18
0.044173507	**0.2**	0.15
0.044200481	**0.8**	0.15
0.044201688	**0.9**	0.13
0.044207985	**0.4**	0.16
0.044178044	**-0.2**	0.38
0.04421228	**0.5**	0.38
0.044299052	**2.5**	0.50
0.044205265	**0.4**	0.53
0.044240198	**1.2**	0.44

0.044172385	**-0.4**	0.32
0.04418029	**-0.2**	0.46
0.044200265	**0.3**	0.54
0.044190406	**0.0**	0.45
0.044366113	**4.0**	0.70
0.044190595	**0.1**	0.45
0.044297128	**2.5**	0.35
0.044216298	**0.6**	0.50
0.044167043	**-0.5**	0.47
0.044194592	**0.1**	0.24
0.044184491	**-0.1**	0.45
0.04417352	**-0.3**	0.40
0.04420049	**0.3**	0.38
0.044201738	**0.3**	0.32
0.043153689	**-5.2**	0.09
0.043112387	**-6.1**	0.10
0.043059179	**-7.4**	0.05
0.043135304	**-5.6**	0.12
0.043092587	**-6.6**	0.07
0.043059246	**-7.4**	0.07
0.044671702	**-7.3**	0.09
0.044712168	**-6.4**	0.06
0.044589384	**-9.1**	0.07
0.044631727	**-8.2**	0.07
0.044607013	**-8.7**	0.04
0.044632549	**-8.2**	0.05
0.044661552	**-7.5**	0.09
0.044642473	**-7.9**	0.09
0.044643779	**-7.9**	0.09
0.044621873	**-8.4**	0.03
0.044656065	**-7.6**	0.10
0.044625676	**-8.3**	0.04
0.044645102	**-7.9**	0.11
0.04458852	**-9.1**	0.05
0.044596914	**-9.0**	0.12
0.044641789	**-8.0**	0.08
0.044589434	**-9.1**	0.10
0.043031981	**-6.7**	0.09
0.043085515	**-5.5**	0.11
0.043214069	**-2.5**	0.08
0.043087347	**-5.4**	0.10
0.043053912	**-6.2**	0.14
0.043095	**-5.2**	0.09
0.043046846	**-6.3**	0.12
0.045016443	**0.4**	0.10
0.04501673	**0.4**	0.11
0.045032846	**0.7**	0.08
0.045043376	**1.0**	0.11
0.045032047	**0.7**	0.12
0.04505083	**1.1**	0.11

0.045038269	**0.9**	0.09
0.045053389	**1.2**	0.09
0.045060138	**1.3**	0.08
0.045069463	**1.5**	0.08
0.045034919	**0.8**	0.09
0.045027613	**0.6**	0.14
0.045035805	**0.8**	0.08
0.045054379	**1.2**	0.10
0.045046925	**1.0**	0.07
0.0451433	**3.2**	0.10
0.045069566	**1.5**	0.05
0.045030859	**0.7**	0.08
0.045000156	**0.0**	0.03
0.044997854	**0.0**	0.06
0.045019247	**0.4**	0.11
0.045037501	**0.8**	0.10
0.045104911	**2.3**	0.10
0.045139408	**3.1**	0.05
0.04512255	**2.7**	0.12
0.045143586	**3.2**	0.07
0.045103005	**2.3**	0.08
0.045136899	**3.0**	0.09
0.045107505	**2.4**	0.06
0.045148542	**3.3**	0.12
0.04504408	**1.0**	0.07
0.045078218	**1.7**	0.07
0.045091573	**2.0**	0.09
0.045008109	**0.2**	0.11
0.044982648	**-0.4**	0.06
0.045051424	**1.1**	0.09
0.045115148	**2.6**	0.09
0.045085243	**1.9**	0.06
0.045104366	**2.3**	0.07
0.04511435	**2.5**	0.05
0.044617789	**25.9**	0.10
0.044653107	**26.7**	0.10
0.044614932	**25.9**	0.16
0.044677091	**27.3**	0.12
0.044336847	**19.5**	0.15
0.044362748	**20.1**	0.10
0.044635261	**26.3**	0.14
0.044698392	**27.8**	0.15
0.044676831	**27.3**	0.08
0.044676869	**27.3**	0.11
0.044656544	**26.8**	0.07
0.044680098	**27.4**	0.05
0.044682864	**27.4**	0.07
0.04467319	**27.2**	0.04
0.044719459	**28.3**	0.10
0.044714082	**28.1**	0.13

0.04439391	**20.8**	0.09
0.044381837	**20.5**	0.08
0.044323983	**19.2**	0.07
0.044336265	**19.5**	0.11
0.044416318	**21.3**	0.08
0.044371089	**20.3**	0.11
0.044357561	**19.9**	0.06
0.044399746	**20.9**	0.11
0.044354821	**19.9**	0.02
0.044405806	**25.7**	0.08
0.044367498	**24.8**	0.08
0.044369236	**24.8**	0.12
0.04436727	**24.8**	0.10
0.044350168	**24.4**	0.10
0.044347937	**24.3**	0.14
0.044370097	**24.9**	0.07
0.044355756	**24.5**	0.16
0.044342951	**24.2**	0.11
0.04432303	**23.8**	0.11
0.04434272	**24.2**	0.09
0.044364595	**24.7**	0.09
0.044388243	**25.3**	0.05
0.04404064	**17.2**	3.27
0.044468589	**27.1**	0.09
0.044488875	**27.6**	0.05
0.044431659	**26.3**	0.14
0.044410878	**25.8**	0.07
0.044467273	**27.1**	0.13
0.044435787	**26.4**	0.13
0.044365128	**24.7**	0.13
0.044379847	**25.1**	0.11
0.044389261	**25.3**	0.10
0.044409018	**25.8**	0.11
0.044458035	**26.9**	0.07
0.044034561	**13.1**	0.01
0.044006315	**12.4**	0.06
0.044077198	**14.1**	0.04
0.044104284	**14.7**	0.02
0.043987987	**12.0**	0.01
0.044099666	**14.6**	0.05
0.044044374	**13.3**	0.02
0.04397924	**11.8**	0.03
0.044071495	**13.9**	0.03
0.044002738	**12.4**	0.04
0.044095923	**14.5**	0.02
0.044060655	**13.7**	0.01
0.043988233	**12.0**	0.03
0.044121478	**15.1**	0.02
0.045531685	**11.8**	0.07
0.045596517	**13.3**	0.07

0.045550118	**12.2**	0.08
0.045438663	**9.7**	0.03
0.045433826	**9.6**	0.10
0.045529494	**11.8**	0.06
0.045494	**11.0**	0.09
0.045477004	**10.6**	0.05
0.045471664	**10.5**	0.08
0.045488444	**10.9**	0.07
0.045508055	**11.3**	0.03
0.043629529	**3.8**	0.46
0.043622922	**3.6**	0.15
0.043658086	**4.4**	0.20
0.043578116	**2.6**	0.11
0.043701273	**5.4**	0.19
0.043563475	**2.2**	0.31
0.043802616	**7.8**	0.10
0.043683011	**5.4**	0.09
0.043644547	**4.5**	0.04
0.043654808	**4.7**	0.04
0.043669824	**5.1**	0.11
0.043671934	**5.1**	0.04
0.043676823	**5.2**	0.14
0.04374643	**6.8**	0.05
0.043704855	**5.9**	0.05
0.043650577	**4.6**	0.05
0.043539751	**2.1**	0.09
0.043494297	**1.0**	0.05
0.043616934	**3.9**	0.11
0.043647111	**4.6**	0.08
0.043638686	**4.4**	0.09
0.043547353	**2.3**	0.03
0.043592518	**3.3**	0.17
0.043478443	**0.7**	0.07
0.043585188	**4.8**	0.11
0.043588705	**4.9**	0.07
0.043593957	**5.0**	0.04
0.043584346	**4.8**	0.06
0.043582989	**4.7**	0.08
0.043587257	**4.8**	0.04
0.043612618	**5.4**	0.09
0.043551538	**4.0**	0.07
0.043672852	**6.8**	0.10
0.043571198	**4.4**	0.09
0.043631753	**5.8**	0.08
0.043593112	**5.0**	0.08
0.043560914	**4.2**	0.08
0.043585144	**4.8**	0.09
0.043661164	**6.5**	0.11
0.043621498	**5.6**	0.07
0.043672212	**6.8**	0.10

0.043646729	**6.2**	0.07
0.043672332	**6.8**	0.10
0.043691083	**7.2**	0.08
0.043670217	**6.7**	0.12
0.043681967	**7.0**	0.07
0.043667263	**6.7**	0.10
0.045393895	**8.8**	0.05
0.045415557	**9.2**	0.11
0.045415118	**9.2**	0.13
0.045403203	**9.0**	0.06
0.045420466	**9.3**	0.06
0.045415604	**9.2**	0.09
0.045442648	**9.8**	0.09
0.045372672	**8.3**	0.09
0.045441132	**9.8**	0.04
0.045255489	**5.7**	0.09
0.045267135	**5.9**	0.11
0.045282278	**6.3**	0.10
0.045345518	**7.7**	0.06
0.045345273	**7.7**	0.04
0.045245512	**5.5**	0.07
0.045231879	**5.2**	0.11
0.045362125	**8.0**	0.08
0.045229436	**5.1**	0.10
0.045257416	**5.7**	0.07
0.04366355	**7.9**	0.10
0.043674855	**8.2**	0.14
0.04369586	**8.6**	0.12
0.043678926	**8.2**	0.07
0.043542449	**5.1**	0.09
0.043704757	**8.8**	0.10
0.043667069	**8.0**	0.10
0.043699872	**8.7**	0.10
0.043666851	**8.0**	0.07
0.043533399	**4.9**	0.10
0.043487153	**3.8**	0.12
0.043514673	**4.5**	0.08
0.043557235	**5.4**	0.13
0.043560704	**5.5**	0.09
0.043569366	**5.7**	0.09
0.043572484	**5.8**	0.11
0.043551547	**5.3**	0.10
0.043518721	**4.5**	0.07
0.043525033	**4.7**	0.13
0.043524808	**4.7**	0.19
0.043538785	**5.0**	0.19
0.043569757	**5.7**	0.14
0.043552725	**5.3**	0.12
0.043554377	**5.9**	0.12
0.043550603	**5.8**	0.11

0.043558226	**6.0**	0.06
0.043570296	**6.3**	0.08
0.043544607	**5.7**	0.11
0.043560929	**6.0**	0.12
0.043544602	**5.7**	0.09
0.043527926	**5.3**	0.15
0.04354317	**5.6**	0.07
0.043525745	**5.2**	0.10
0.043590466	**6.7**	0.10
0.043579954	**6.5**	0.11
0.043612382	**7.2**	0.15
0.043613626	**7.3**	0.13
0.043553714	**5.9**	0.10
0.043550814	**5.8**	0.10
0.043537198	**5.5**	0.07
0.043532056	**5.4**	0.14
0.043598266	**6.9**	0.11
0.044108682	**16.8**	0.14
0.044019427	**14.8**	0.12
0.043875148	**11.5**	0.06
0.043803223	**9.8**	0.14
0.044079353	**16.2**	0.09
0.044046456	**15.4**	0.10
0.044123012	**17.2**	0.15
0.045499691	**11.1**	0.07
0.04553071	**11.8**	0.08
0.045504494	**11.2**	0.07
0.045543469	**12.1**	0.06
0.045509617	**11.3**	0.03
0.045508317	**11.3**	0.09
0.045521746	**11.6**	0.09
0.045486504	**10.8**	0.09
0.045504342	**11.2**	0.09
0.045521627	**11.6**	0.05
0.045490821	**10.9**	0.03
0.045495713	**11.0**	0.07
0.045515696	**11.5**	0.10
0.045510727	**11.3**	0.04
0.045498309	**11.1**	0.08
0.045487921	**10.8**	0.10
0.045477242	**10.6**	0.20
0.045494521	**11.0**	0.11
0.04554709	**12.2**	0.06
0.045512637	**11.4**	0.07
0.045522717	**11.6**	0.05
0.045509535	**11.3**	0.05
0.045501515	**11.1**	0.04
0.045486028	**10.8**	0.05
0.045499675	**11.1**	0.06
0.045508422	**11.3**	0.12

0.045477752	**10.6**	0.06
0.045484384	**10.8**	0.06
0.045509273	**11.3**	0.09
0.045513564	**11.4**	0.13
0.045519805	**11.6**	0.08
0.045509042	**11.3**	0.13
0.045501429	**11.1**	0.04
0.045544768	**12.1**	0.10
0.045527142	**11.7**	0.11
0.045551256	**12.3**	0.07
0.045523264	**11.6**	0.05
0.045557674	**12.4**	0.09
0.045531922	**11.8**	0.03
0.045552481	**12.3**	0.05
0.045553838	**12.3**	0.08
0.045520879	**11.6**	0.04
0.045529541	**11.8**	0.11
0.045551234	**12.2**	0.12
0.045546254	**12.1**	0.05
0.045562674	**12.5**	0.07
0.045539215	**12.0**	0.04
0.045546462	**12.1**	0.06
0.045541546	**12.0**	0.07
0.043998491	**15.6**	0.07
0.044076953	**17.4**	0.10
0.044043313	**16.7**	0.08
0.044148869	**19.1**	0.09
0.044192545	**20.1**	0.09
0.044117758	**18.4**	0.12
0.044201406	**20.3**	0.06
0.04423261	**21.0**	0.10
0.044228236	**20.9**	0.09
0.044236576	**21.1**	0.08
0.043991888	**15.5**	0.05
0.043991964	**15.5**	0.04
0.043997307	**15.6**	0.08
0.04404588	**16.7**	0.12
0.044072639	**17.3**	0.04
0.044072873	**17.3**	0.08
0.043931385	**14.1**	0.04
0.043839815	**12.0**	0.05
0.043836941	**11.9**	0.05
0.043856793	**12.4**	0.04
0.043844403	**12.1**	0.07
0.043879513	**12.9**	0.05
0.043867018	**12.6**	0.03
0.044103063	**14.7**	0.04
0.044115113	**14.9**	0.06
0.044107027	**14.8**	0.03
0.044133177	**15.4**	0.01

0.044136341	**15.4**	0.04
0.044012908	**12.6**	0.06
0.043810662	**10.0**	0.11
0.04375218	**8.6**	0.11
0.043772018	**9.1**	0.06
0.043731655	**8.1**	0.12
0.043847396	**10.8**	0.07
0.043772633	**9.1**	0.08
0.04377206	**9.1**	0.10
0.043744408	**8.4**	0.05
0.04374706	**8.5**	0.10
0.043770077	**9.0**	0.11
0.043764113	**8.9**	0.09
0.043789212	**9.5**	0.08
0.043752359	**8.6**	0.07
0.043749849	**8.6**	0.05
0.043766955	**9.0**	0.13
0.043760078	**8.8**	0.07
0.043837717	**10.6**	0.05
0.043852144	**10.9**	0.09
0.04383294	**10.5**	0.15
0.04382062	**10.2**	0.11
0.043798932	**9.7**	0.08
0.043944067	**13.0**	0.07
0.043898084	**12.0**	0.13
0.043841482	**10.7**	0.08
0.043843195	**10.7**	0.13
0.043820168	**10.2**	0.12
0.043806424	**9.9**	0.06
0.043835034	**11.8**	0.20
0.043790056	**10.8**	0.08
0.043822973	**11.6**	0.09
0.043814683	**11.4**	0.12
0.043801384	**11.1**	0.10
0.043818724	**11.5**	0.10
0.043848917	**12.2**	0.08
0.04385623	**12.3**	0.11
0.043849079	**12.2**	0.07
0.043839587	**12.0**	0.08
0.044030872	**16.4**	0.12
0.043975641	**15.1**	0.18
0.043978399	**15.2**	0.11
0.044003855	**15.7**	0.12
0.043710415	**9.0**	0.09
0.043575011	**5.8**	0.08
0.04355408	**5.4**	0.08
0.043679614	**8.3**	0.21
0.043816028	**11.4**	0.12
0.04366198	**7.9**	0.10
0.043717295	**9.1**	0.13

0.043665719	**7.9**	0.14
0.043813539	**11.4**	0.10
0.0436629	**7.9**	0.16
0.043761983	**10.2**	0.10
0.043745857	**9.8**	0.11
0.043776495	**10.5**	0.15
0.043757847	**10.1**	0.07
0.043788859	**10.8**	0.07
0.043820281	**11.5**	0.06
0.043666493	**8.0**	0.12
0.04367771	**8.2**	0.10
0.043681042	**8.3**	0.08
0.043667658	**8.0**	0.08
0.043680755	**8.3**	0.10
0.043712541	**9.0**	0.06
0.043697295	**8.7**	0.09
0.043691248	**8.5**	0.12
0.043686362	**8.4**	0.07
0.043674189	**8.1**	0.07
0.043689183	**8.5**	0.11
0.04371021	**9.0**	0.08
0.043726284	**9.3**	0.11
0.043700784	**8.8**	0.09
0.043729708	**9.4**	0.09
0.043726192	**9.3**	0.11
0.044658063	**30.8**	0.12
0.043888783	**13.1**	0.07
0.04415684	**19.3**	0.09
0.04524386	**44.4**	0.04
0.044084768	**17.6**	0.12
0.043740984	**9.7**	0.08
0.043767225	**10.3**	0.10
0.043811175	**11.3**	0.10
0.043808199	**11.2**	0.06
0.043355499	**0.8**	0.11
0.043421424	**1.0**	0.12
0.04337536	**-0.1**	0.07
0.043353737	**-0.6**	0.07
0.04334781	**-0.7**	0.05
0.043361802	**-0.4**	0.07
0.043357086	**-0.5**	0.07
0.043358505	**-0.5**	0.09
0.043356936	**-0.5**	0.07
0.04339867	**0.5**	0.19
0.043318185	**-1.4**	0.05
0.043319823	**-1.3**	0.08
0.04340675	**0.7**	0.08
0.043375524	**-0.1**	0.15
0.043366935	**-0.3**	0.11
0.043345347	**-0.8**	0.08

0.04334588	**0.6**	0.06
0.043297318	**-0.6**	0.10
0.043292406	**-0.7**	0.06
0.043308802	**-0.3**	0.10
0.04332146	**0.0**	0.09
0.043336718	**0.3**	0.09
0.043327653	**0.1**	0.06
0.043311821	**-0.2**	0.07
0.043337431	**0.4**	0.03
0.043336105	**0.3**	0.05
0.043327609	**0.1**	0.07
0.043332819	**0.3**	0.07
0.043298706	**-0.5**	0.07
0.043329965	**0.2**	0.07
0.043320609	**0.0**	0.06
0.043290331	**-0.7**	0.04
0.043310898	**-0.2**	0.12
0.043292738	**-0.7**	0.08
0.043309528	**-0.3**	0.10
0.043342115	**0.5**	0.08
0.04332384	**0.0**	0.04
0.043335225	**0.3**	0.05
0.043882764	**10.0**	0.09
0.043861363	**9.5**	0.13
0.044060896	**14.1**	0.11
0.043907632	**10.6**	0.06
0.043922136	**10.9**	0.09
0.043898998	**10.4**	0.06
0.043908146	**10.6**	0.05
0.043980587	**12.2**	0.13
0.043898647	**10.3**	0.05
0.04388081	**9.9**	0.09
0.043918316	**10.8**	0.06
0.043775693	**7.5**	0.06
0.043847516	**9.2**	0.13
0.043839619	**9.0**	0.06
0.043816144	**8.4**	0.10
0.043805988	**8.2**	0.10
0.043813722	**8.4**	0.14
0.043798063	**8.0**	0.03
0.043795876	**8.0**	0.05
0.04379713	**8.0**	0.06
0.045441491	**9.8**	0.12
0.045470289	**10.5**	0.06
0.045459275	**10.2**	0.08
0.045393776	**8.8**	0.10
0.045394468	**8.8**	0.08
0.045355934	**7.9**	0.08
0.045371096	**8.2**	0.08
0.045367288	**8.2**	0.05

0.045358942	**8.0**	0.10
0.04534659	**7.7**	0.02
0.045317545	**7.1**	0.12
0.045388101	**8.6**	0.07
0.045302205	**6.7**	0.05
0.045375024	**8.3**	0.08
0.045348411	**7.7**	0.07
0.045401135	**8.9**	0.06
0.045403135	**9.0**	0.02
0.045363578	**8.1**	0.06
0.045413622	**9.2**	0.06
0.045395431	**8.8**	0.07
0.043547677	**1.3**	0.07
0.043564835	**1.7**	0.07
0.043534606	**1.0**	0.05
0.043532438	**1.0**	0.12
0.043542194	**1.2**	0.06
0.043517181	**0.6**	0.10
0.043523711	**0.8**	0.08
0.043519106	**0.7**	0.11
0.043532619	**1.0**	0.07
0.043548689	**1.3**	0.08
0.043567574	**1.8**	0.08
0.043534299	**1.0**	0.07
0.043601135	**2.5**	0.07
0.043551465	**1.4**	0.10
0.043521846	**0.7**	0.06
0.043553874	**1.5**	0.11
0.043537701	**1.1**	0.09
0.043507228	**0.4**	0.10
0.043560517	**1.6**	0.10
0.043532339	**1.0**	0.05
0.043547995	**1.3**	0.09
0.04347592	**-0.3**	0.06
0.043458583	**-0.7**	0.14
0.043477464	**-0.3**	0.12
0.043555114	**1.5**	0.12
0.043509662	**0.4**	0.12
0.043520471	**0.7**	0.09
0.043487375	**-0.1**	0.07
0.043474928	**-0.4**	0.08
0.043475726	**-0.3**	0.09
0.043477214	**-0.3**	0.08
0.043467145	**-0.5**	0.11
0.043518417	**0.6**	0.08
0.043507416	**0.4**	0.11
0.04347371	**-0.4**	0.11
0.04345268	**-0.9**	0.07
0.043517986	**0.6**	0.06
0.043544296	**1.2**	0.11

0.04352907	**0.9**	0.09
0.043531898	**1.0**	0.11
0.043574167	**1.9**	0.07
0.045298721	**6.6**	0.08
0.045291186	**6.5**	0.07
0.045283093	**6.3**	0.06
0.045293845	**6.5**	0.07
0.045319009	**7.1**	0.10
0.045268345	**6.0**	0.04
0.045403387	**9.0**	0.06
0.045407732	**9.1**	0.05
0.045404559	**9.0**	0.10
0.045411551	**9.1**	0.14
0.04542509	**9.4**	0.09
0.045390333	**8.7**	0.06
0.045377542	**8.4**	0.08
0.045429845	**9.6**	0.10
0.045380122	**8.4**	0.17
0.045369038	**8.2**	0.09
0.045422623	**9.4**	0.06
0.045348908	**7.8**	0.07
0.045310181	**6.9**	0.05
0.045351637	**7.8**	0.07
0.045378235	**8.4**	0.09
0.045339424	**7.5**	0.07
0.045379748	**8.4**	0.07
0.045335211	**7.4**	0.09
0.043836629	**8.5**	0.09
0.043838003	**8.6**	0.09
0.043801839	**7.7**	0.10
0.043751147	**6.6**	0.02
0.043837983	**8.6**	0.06
0.043856876	**9.0**	0.03
0.043928964	**10.7**	0.02
0.045298263	**6.6**	0.11
0.045304624	**6.8**	0.09
0.045326818	**7.3**	0.10
0.04534062	**7.6**	0.08
0.04531964	**7.1**	0.07
0.045334864	**7.4**	0.06
0.045297632	**6.6**	0.08
0.045254795	**5.7**	0.11
0.045319298	**7.1**	0.06
0.045278895	**6.2**	0.09
0.045271264	**6.0**	0.06
0.045285419	**6.3**	0.06
0.045212597	**4.7**	0.11
0.043578617	**6.6**	0.07
0.04353276	**5.5**	0.09
0.043533445	**5.5**	0.06

0.043551092	**5.9**	0.10
0.043546275	**5.8**	0.12
0.043550811	**5.9**	0.20
0.04355232	**6.0**	0.12
0.043561938	**6.2**	0.10
0.043545433	**5.8**	0.08
0.043567689	**6.3**	0.13
0.043548235	**5.9**	0.14
0.043560702	**6.2**	0.13
0.043567439	**6.3**	0.17
0.043519072	**5.2**	0.18
0.043506142	**4.9**	0.04
0.043525121	**5.3**	0.12
0.04349662	**4.7**	0.05
0.043551794	**6.0**	0.06
0.043579595	**6.6**	0.15
0.043511994	**5.0**	0.12
0.043565202	**6.3**	0.10
0.043511541	**5.0**	0.06
0.043530774	**5.5**	0.12
0.043571137	**6.4**	0.13
0.04352739	**5.4**	0.08
0.044977322	**-0.5**	0.05
0.044980905	**-0.4**	0.02
0.044997227	**-0.1**	0.06
0.044992858	**-0.2**	0.04
0.044985169	**-0.3**	0.04
0.044988841	**-0.2**	0.04
0.044936306	**-1.4**	0.02
0.04496075	**-0.9**	0.07
0.0449567	**-1.0**	0.01
0.044963347	**-0.8**	0.03
0.044975315	**-0.5**	0.04
0.044946307	**-1.2**	0.04
0.044226612	**1.4**	0.27
0.044179879	**0.4**	0.21
0.044231244	**1.5**	0.16
0.044214335	**1.1**	0.15
0.044173938	**0.2**	0.23
0.044191494	**0.6**	0.17
0.044202298	**0.9**	0.16
0.044182046	**0.4**	0.22
0.044217639	**1.2**	0.25
0.044214131	**1.1**	0.18
0.044216754	**1.2**	0.14
0.044181206	**0.4**	0.13
0.044163579	**0.0**	0.18
0.044168832	**0.1**	0.20
0.044188116	**0.6**	0.20
0.044178044	**0.3**	0.15

0.044212285	**1.1**	0.15
0.044299043	**3.1**	0.19
0.044205277	**0.9**	0.20
0.044240162	**1.7**	0.17
0.044172356	**0.2**	0.12
0.044180324	**0.4**	0.18
0.044200341	**0.8**	0.21
0.044190425	**0.6**	0.18
0.044366076	**4.6**	0.27
0.044190653	**0.6**	0.17
0.044297179	**3.0**	0.14
0.044216306	**1.2**	0.19
0.044167049	**0.1**	0.18
0.044194605	**0.7**	0.09
0.044184457	**0.5**	0.18
0.044173507	**0.2**	0.15
0.044200481	**0.8**	0.15
0.044201688	**0.9**	0.13
0.044207985	**0.4**	0.16

± internal precision(95% conf.)	**$\delta^{34}S_{CDT}$(‰)**	**± internal precision(95% conf.)**
0.03	**10.6**	0.09
0.03	**10.5**	0.07
0.03	**10.5**	0.04
0.03	**10.4**	0.05
0.04	**10.2**	0.04
0.02	**10.5**	0.05
0.03	**10.7**	0.11
0.02	**10.3**	0.06
0.03	**10.2**	0.06
0.02	**10.5**	0.10
0.03	**10.6**	0.06
0.02	**10.8**	0.04
0.03	**10.4**	0.08
0.02	**10.6**	0.08
0.02	**10.7**	0.11
0.03	**11.2**	0.18
0.04	**11.1**	0.09
0.03	**11.1**	0.16
0.02	**11.4**	0.11
0.03	**11.3**	0.13
0.02	**11.4**	0.08
0.04	**11.7**	0.13
0.02	**11.9**	0.06
0.04	**12.0**	0.10
0.04	**11.1**	0.14

0.03	**10.6**	0.16
0.05	**10.8**	0.22
0.02	**10.4**	0.16
0.03	**10.9**	0.19
0.05	**10.8**	0.13
0.03	**11.4**	0.12
0.02	**11.6**	0.15
0.04	**11.7**	0.13
0.03	**11.4**	0.18
0.03	**11.5**	0.12
0.03	**10.9**	0.15
0.02	**11.8**	0.17
0.03	**12.1**	0.13
0.04	**11.3**	0.11
0.01	**12.1**	0.08
0.03	**11.6**	0.18
0.03	**10.3**	0.12
0.03	**10.2**	0.13
0.02	**10.7**	0.18
0.03	**13.4**	0.16
0.02	**11.5**	0.08
0.03	**13.8**	0.17
0.03	**11.2**	0.18
0.04	**10.0**	0.21
0.03	**11.1**	0.13
0.04	**11.1**	0.11
0.04	**11.5**	0.17
0.03	**10.8**	0.15
0.03	**11.5**	0.11
0.03	**10.9**	0.16
0.02	**12.5**	0.07
0.03	**11.6**	0.16
0.02	**11.5**	0.13
0.04	**11.4**	0.10
0.04	**10.9**	0.20
0.03	**11.2**	0.17
0.04	**11.3**	0.12
0.03	**10.7**	0.12
0.04	**10.2**	0.20
0.03	**10.9**	0.16
0.04	**10.8**	0.19
0.04	**10.6**	0.16
0.03	**10.4**	0.05
0.03	**10.0**	0.08
0.03	**10.6**	0.08
0.03	**10.8**	0.13
0.03	**11.1**	0.12
0.02	**11.8**	0.11
0.02	**11.1**	0.19
0.02	**11.1**	0.12

0.03	**11.1**	0.16
0.04	**11.1**	0.07
0.03	**11.9**	0.13
0.03	**11.7**	0.13
0.02	**11.4**	0.11
0.03	**11.6**	0.14
0.03	**11.2**	0.18
0.04	**11.3**	0.20
0.03	**11.3**	0.17
0.03	**11.5**	0.08
0.03	**11.1**	0.11
0.03	**11.4**	0.15

Weight (mg)	**Raw ^{34}S**	**Corrected $\delta^{34}S_{CDT}$**
1.2700	-1.93	**-3.6**
0.3100	2.89	**1.3**
0.4000	2.09	**0.5**
1.2400	-1.60	**-3.3**
0.3000	2.71	**1.1**
0.3200	1.12	**-0.5**
0.2700	0.83	**-0.8**
0.3400	-11.11	**-12.9**
0.3600	3.37	**1.8**
0.3400	38.86	**37.9**
4.4200	8.58	**8.0**

^{32}S (cps)
3.44E+08
3.53E+08
3.52E+08
3.54E+08
3.56E+08
3.49E+08
3.50E+08
3.53E+08
3.36E+08
3.19E+08
3.38E+08
3.15E+08
3.43E+08
3.55E+08
6.95E+08
7.23E+08
6.97E+08
7.18E+08
7.55E+08
2.94E+08
7.19E+08
6.87E+08
6.53E+08
7.01E+08
7.27E+08
6.95E+08
6.82E+08
7.02E+08
7.25E+08
7.18E+08
7.15E+08
7.26E+08
7.22E+08
7.19E+08
7.13E+08
7.07E+08
7.06E+08
6.91E+08
7.28E+08
6.97E+08
6.77E+08
7.02E+08
6.73E+08
6.98E+08
4.07E+08
3.86E+08
3.99E+08
3.80E+08
3.95E+08

4.10E+08
4.00E+08
3.88E+08
3.90E+08
3.92E+08
3.86E+08
3.61E+08
3.50E+08
3.56E+08
3.66E+08
4.07E+08
3.86E+08
3.99E+08
3.80E+08
3.95E+08
4.10E+08
4.00E+08
3.88E+08
3.90E+08
3.92E+08
3.86E+08
3.61E+08
3.50E+08
3.56E+08
3.66E+08
3.55E+08
3.65E+08
3.97E+08
3.76E+08
3.85E+08
3.68E+08
3.64E+08
3.70E+08
3.70E+08
4.61E+08
3.68E+08
4.27E+08
3.95E+08
3.67E+08
3.68E+08
3.60E+08
3.54E+08
3.71E+08
3.58E+08
5.39E+08
3.55E+08
3.65E+08
3.97E+08
3.76E+08
3.85E+08

3.68E+08
3.64E+08
3.70E+08
3.70E+08
4.61E+08
3.68E+08
4.27E+08
3.95E+08
3.67E+08
3.68E+08
3.60E+08
3.54E+08
3.71E+08
3.58E+08
6.17E+08
6.13E+08
5.75E+08
6.21E+08
5.76E+08
5.44E+08
4.56E+08
4.58E+08
4.55E+08
4.25E+08
4.59E+08
4.42E+08
4.56E+08
4.63E+08
4.62E+08
4.60E+08
4.71E+08
4.60E+08
4.45E+08
4.53E+08
4.57E+08
4.65E+08
4.45E+08
4.30E+08
4.62E+08
3.97E+08
3.93E+08
4.19E+08
3.88E+08
4.06E+08
5.08E+08
4.99E+08
5.08E+08
5.06E+08
5.12E+08
5.27E+08

4.98E+08
5.03E+08
5.17E+08
5.14E+08
5.13E+08
5.00E+08
5.02E+08
5.02E+08
4.83E+08
4.67E+08
4.69E+08
4.70E+08
4.59E+08
4.73E+08
4.82E+08
4.89E+08
4.55E+08
4.59E+08
4.59E+08
4.53E+08
4.65E+08
4.69E+08
4.71E+08
4.64E+08
4.58E+08
4.60E+08
4.64E+08
4.72E+08
4.76E+08
4.66E+08
4.62E+08
4.62E+08
4.59E+08
4.54E+08
7.82E+08
8.03E+08
7.72E+08
7.67E+08
7.76E+08
7.62E+08
7.73E+08
7.77E+08
7.83E+08
7.76E+08
7.56E+08
7.70E+08
7.66E+08
7.45E+08
7.77E+08
7.91E+08

7.51E+08
7.70E+08
7.59E+08
7.30E+08
7.58E+08
7.52E+08
7.54E+08
7.57E+08
7.46E+08
3.57E+08
3.53E+08
3.51E+08
3.52E+08
3.55E+08
3.55E+08
3.53E+08
3.54E+08
3.51E+08
3.51E+08
3.51E+08
3.67E+08
3.52E+08
7.29E+07
3.41E+08
3.49E+08
3.55E+08
3.60E+08
3.52E+08
3.55E+08
3.50E+08
3.42E+08
3.52E+08
3.50E+08
3.50E+08
1.08E+09
1.13E+09
1.15E+09
1.18E+09
9.77E+08
1.11E+09
1.10E+09
1.24E+09
1.26E+09
1.01E+09
1.14E+09
8.46E+08
1.12E+09
1.25E+09
4.78E+08
5.20E+08

5.03E+08
4.65E+08
4.79E+08
5.04E+08
4.74E+08
4.67E+08
4.68E+08
4.62E+08
4.90E+08
2.84E+07
6.83E+07
3.91E+07
8.51E+07
7.98E+07
2.90E+07
1.24E+08
6.82E+08
6.91E+08
6.77E+08
7.05E+08
6.99E+08
7.07E+08
6.97E+08
6.85E+08
6.96E+08
7.14E+08
8.02E+08
8.00E+08
6.65E+08
6.77E+08
7.26E+08
7.36E+08
8.51E+08
5.30E+08
5.60E+08
5.42E+08
5.88E+08
5.61E+08
5.60E+08
5.70E+08
5.51E+08
6.33E+08
5.53E+08
5.33E+08
5.50E+08
5.54E+08
5.49E+08
5.49E+08
5.50E+08
5.76E+08

5.67E+08
5.61E+08
6.03E+08
5.59E+08
5.60E+08
5.51E+08
4.62E+08
4.72E+08
4.64E+08
4.67E+08
4.64E+08
4.68E+08
4.65E+08
4.67E+08
4.68E+08
4.51E+08
4.63E+08
5.05E+08
4.54E+08
4.55E+08
4.58E+08
4.54E+08
4.61E+08
4.55E+08
4.74E+08
3.99E+08
4.04E+08
4.05E+08
4.09E+08
4.06E+08
4.09E+08
4.06E+08
4.08E+08
4.07E+08
3.92E+08
3.87E+08
3.88E+08
3.90E+08
3.90E+08
3.92E+08
3.92E+08
3.90E+08
3.87E+08
3.89E+08
3.83E+08
3.91E+08
4.44E+08
3.88E+08
3.67E+08
3.64E+08

3.67E+08
3.62E+08
3.54E+08
3.60E+08
3.58E+08
3.66E+08
3.67E+08
3.62E+08
3.65E+08
3.63E+08
3.64E+08
3.63E+08
3.69E+08
3.65E+08
3.66E+08
3.59E+08
3.67E+08
5.93E+08
5.88E+08
5.87E+08
5.80E+08
5.54E+08
5.60E+08
5.58E+08
4.79E+08
4.85E+08
4.85E+08
4.82E+08
4.83E+08
4.89E+08
4.83E+08
4.88E+08
4.82E+08
4.82E+08
4.79E+08
4.79E+08
4.78E+08
4.78E+08
4.71E+08
4.76E+08
4.74E+08
4.71E+08
4.70E+08
4.75E+08
4.67E+08
4.64E+08
4.68E+08
4.67E+08
4.63E+08
4.70E+08

4.64E+08
4.68E+08
4.65E+08
4.73E+08
4.76E+08
4.75E+08
4.67E+08
4.71E+08
4.70E+08
4.71E+08
4.65E+08
4.69E+08
4.69E+08
4.74E+08
4.79E+08
4.72E+08
4.74E+08
4.80E+08
4.77E+08
4.62E+08
4.71E+08
4.70E+08
4.71E+08
3.81E+08
3.85E+08
3.79E+08
3.85E+08
3.88E+08
3.79E+08
3.87E+08
3.91E+08
3.93E+08
3.93E+08
3.87E+08
3.86E+08
3.86E+08
3.89E+08
3.91E+08
3.91E+08
5.40E+08
5.59E+08
5.59E+08
5.55E+08
5.59E+08
5.65E+08
5.78E+08
1.04E+09
9.87E+08
1.31E+09
1.10E+09

1.05E+09
6.26E+08
5.82E+08
5.89E+08
5.87E+08
5.73E+08
5.79E+08
5.64E+08
5.70E+08
5.64E+08
5.67E+08
5.93E+08
5.75E+08
5.61E+08
5.64E+08
5.63E+08
5.64E+08
5.64E+08
5.64E+08
5.61E+08
5.52E+08
5.63E+08
5.62E+08
5.83E+08
5.77E+08
5.73E+08
5.63E+08
5.58E+08
5.44E+08
4.01E+08
3.95E+08
4.03E+08
4.03E+08
4.06E+08
4.09E+08
4.14E+08
4.09E+08
3.95E+08
4.06E+08
4.14E+08
4.09E+08
4.49E+08
4.21E+08
3.82E+08
3.95E+08
3.92E+08
3.94E+08
4.18E+08
3.89E+08
3.91E+08

3.85E+08
3.75E+08
3.96E+08
3.92E+08
3.92E+08
3.99E+08
4.05E+08
4.05E+08
4.03E+08
4.07E+08
4.03E+08
4.05E+08
4.07E+08
4.11E+08
4.20E+08
4.14E+08
4.19E+08
4.04E+08
4.08E+08
4.05E+08
4.04E+08
4.02E+08
4.13E+08
4.02E+08
3.94E+08
3.99E+08
3.96E+08
3.97E+08
3.96E+08
3.95E+08
3.92E+08
3.95E+08
3.98E+08
4.04E+08
4.00E+08
6.23E+08
5.65E+08
5.62E+08
5.55E+08
5.60E+08
5.62E+08
5.65E+08
5.55E+08
5.97E+08
5.44E+08
5.49E+08
5.88E+08
5.75E+08
5.35E+08
5.47E+08

4.29E+08
4.08E+08
4.17E+08
4.27E+08
4.07E+08
4.22E+08
4.25E+08
4.16E+08
4.39E+08
4.20E+08
4.27E+08
4.33E+08
4.36E+08
4.31E+08
4.25E+08
3.96E+08
4.03E+08
4.07E+08
4.18E+08
4.16E+08
4.20E+08
4.26E+08
6.71E+08
6.64E+08
6.92E+08
7.03E+08
7.34E+08
7.16E+08
7.10E+08
6.73E+08
6.88E+08
7.00E+08
6.96E+08
6.82E+08
7.30E+08
6.50E+08
6.80E+08
6.83E+08
6.81E+08
6.89E+08
6.77E+08
6.93E+08
5.10E+08
5.17E+08
5.06E+08
5.07E+08
4.23E+08
5.07E+08
4.96E+08
5.07E+08

5.02E+08
5.01E+08
4.89E+08
4.92E+08
4.71E+08
5.30E+08
4.87E+08
4.87E+08
4.88E+08
4.96E+08
4.96E+08
4.88E+08
7.31E+08
7.66E+08
7.47E+08
7.46E+08
7.42E+08
7.49E+08
7.30E+08
7.18E+08
7.29E+08
7.30E+08
7.69E+08
7.50E+08
7.39E+08
7.48E+08
7.15E+08
7.32E+08
7.27E+08
7.24E+08
7.27E+08
7.08E+08
7.10E+08
7.12E+08
7.01E+08
7.02E+08
7.02E+08
7.04E+08
7.02E+08
7.14E+08
7.01E+08
7.13E+08
7.17E+08
7.08E+08
7.16E+08
7.09E+08
7.02E+08
7.08E+08
7.22E+08
7.30E+08

7.30E+08
7.34E+08
7.60E+08
4.57E+08
4.54E+08
4.60E+08
4.58E+08
4.63E+08
4.63E+08
4.61E+08
4.64E+08
4.59E+08
4.84E+08
4.50E+08
4.57E+08
4.61E+08
4.61E+08
4.70E+08
4.54E+08
4.67E+08
4.63E+08
4.58E+08
4.62E+08
4.67E+08
4.58E+08
4.63E+08
4.67E+08
7.67E+08
7.64E+08
7.42E+08
3.49E+08
8.00E+08
6.96E+08
9.95E+08
4.88E+08
4.91E+08
4.92E+08
4.89E+08
4.97E+08
4.89E+08
4.86E+08
4.81E+08
4.73E+08
4.81E+08
4.90E+08
4.71E+08
4.71E+08
3.52E+08
3.60E+08
3.56E+08

3.54E+08
3.60E+08
3.57E+08
3.45E+08
3.51E+08
3.50E+08
3.53E+08
3.52E+08
3.56E+08
3.50E+08
3.52E+08
3.45E+08
3.56E+08
3.47E+08
3.60E+08
3.53E+08
3.56E+08
3.55E+08
3.56E+08
3.52E+08
3.35E+08
3.48E+08
6.52E+08
6.54E+08
6.59E+08
6.59E+08
6.33E+08
6.23E+08
6.20E+08
6.50E+08
6.49E+08
6.65E+08
6.67E+08
6.18E+08
4.07E+08
3.86E+08
3.99E+08
3.80E+08
3.95E+08
4.10E+08
4.00E+08
3.88E+08
3.90E+08
3.92E+08
3.86E+08
3.61E+08
3.50E+08
3.56E+08
3.66E+08
3.55E+08

3.65E+08
3.97E+08
3.76E+08
3.85E+08
3.68E+08
3.64E+08
3.70E+08
3.70E+08
4.61E+08
3.68E+08
4.27E+08
3.95E+08
3.67E+08
3.68E+08
3.60E+08
3.54E+08
3.71E+08
3.58E+08
5.39E+08

$\delta^{36}S_{CDT}$(‰)	± internal precision(95% conf.)	$\Delta^{33}S_{CDT}$(‰)
19.68	0.38	0.04
19.44	0.18	-0.02
19.73	0.26	-0.01
19.30	0.16	0.08
19.16	0.16	0.10
20.20	0.28	0.00
20.33	0.35	0.03
19.50	0.24	0.12
19.23	0.27	-0.02
19.83	0.19	0.01
20.32	0.21	0.12
20.36	0.29	0.07
19.03	0.21	-0.02
19.88	0.18	0.06
20.15	0.22	0.05
21.11	0.23	0.05
20.63	0.28	-0.03
21.07	0.21	0.07
21.34	0.29	-0.02
20.55	0.30	-0.12
21.28	0.25	0.08
22.09	0.29	0.11
22.48	0.23	0.06
23.04	0.33	0.12
20.91	0.21	-0.07

20.16	0.38	-0.01
20.25	0.33	-0.03
19.54	0.25	0.05
20.02	0.28	0.02
20.10	0.20	-0.01
21.09	0.18	0.03
22.15	0.22	0.15
22.06	0.26	-0.01
21.84	0.20	0.02
22.60	0.31	0.04
21.44	0.24	0.11
22.58	0.21	0.11
23.26	0.19	0.07
21.32	0.22	0.07
22.81	0.13	0.07
22.07	0.19	0.09
19.18	0.23	0.00
18.86	0.27	0.00
20.05	0.18	0.06
25.46	0.21	0.13
21.64	0.29	0.20
26.34	0.30	0.00
21.12	0.25	-0.11
18.63	0.26	-0.01
21.71	0.26	0.05
19.58	0.35	0.04
21.58	0.25	0.03
20.42	0.25	-0.04
22.27	0.26	0.00
20.62	0.35	0.10
23.87	0.31	0.08
21.76	0.28	0.13
21.18	0.32	0.13
20.97	0.35	-0.01
21.37	0.25	0.04
21.53	0.22	0.16
21.56	0.18	0.31
20.20	0.27	0.07
19.11	0.15	0.12
20.20	0.26	0.12
20.55	0.26	0.14
19.88	0.21	0.14
18.73	0.30	0.03
18.36	0.25	0.20
19.74	0.22	0.05
20.29	0.19	0.08
20.78	0.21	0.07
22.46	0.22	0.12
20.69	0.25	0.08
21.45	0.27	0.05

20.15	0.36	0.13
20.15	0.22	0.11
22.40	0.25	0.03
22.22	0.30	0.04
21.29	0.21	0.06
21.44	0.29	0.07
21.13	0.26	0.15
21.16	0.21	0.00
21.65	0.24	0.00
21.83	0.24	0.10
20.60	0.30	0.04
21.63	0.27	0.15

Elemental content sulphur
12.03
30.41
21.35
10.18
24.16
25.14
2.87
20.13
46.49
47.38
1.08

± internal precision(95% conf.)	$\Delta^{36}S_{CDT}$(‰)	± internal precision(95% conf.)
0.03	-0.54	0.34
0.03	-0.56	0.18
0.03	-0.32	0.24
0.03	-0.61	0.18
0.03	-0.32	0.17
0.02	0.09	0.25
0.03	-0.14	0.33
0.03	-0.12	0.25
0.03	-0.25	0.27
0.03	-0.20	0.19
0.03	0.17	0.23
0.03	-0.33	0.21
0.03	-0.86	0.21
0.02	-0.32	0.20
0.02	-0.37	0.24
0.04	-0.37	0.25
0.03	-0.52	0.27
0.04	-0.06	0.21
0.02	-0.42	0.28
0.03	-0.97	0.34
0.03	-0.49	0.25
0.04	-0.24	0.23
0.02	-0.32	0.22
0.04	0.17	0.28
0.03	-0.27	0.20

0.03	-0.10	0.37
0.04	-0.30	0.36
0.03	-0.40	0.26
0.03	-0.77	0.30
0.05	-0.60	0.21
0.03	-0.63	0.20
0.03	0.09	0.24
0.04	-0.32	0.28
0.03	0.04	0.21
0.03	0.59	0.26
0.03	0.54	0.23
0.02	0.01	0.21
0.03	0.08	0.21
0.03	-0.17	0.20
0.01	-0.26	0.13
0.03	-0.04	0.20
0.03	-0.45	0.27
0.04	-0.60	0.27
0.02	-0.31	0.19
0.03	-0.10	0.22
0.03	-0.23	0.25
0.03	-0.01	0.32
0.03	-0.25	0.24
0.04	-0.51	0.28
0.03	0.46	0.22
0.04	-1.65	0.37
0.04	-0.48	0.29
0.03	-0.18	0.27
0.03	0.32	0.25
0.03	-0.11	0.32
0.03	0.04	0.30
0.04	-0.33	0.27
0.02	-0.72	0.30
0.04	-0.71	0.32
0.04	0.47	0.23
0.03	0.13	0.23
0.03	0.04	0.20
0.03	-0.30	0.25
0.03	-0.32	0.17
0.03	-0.58	0.27
0.03	-0.07	0.25
0.04	-0.37	0.21
0.03	-1.15	0.27
0.03	-0.73	0.26
0.03	-0.48	0.23
0.03	-0.29	0.20
0.03	-0.45	0.24
0.02	-0.11	0.25
0.02	-0.52	0.26
0.02	0.19	0.24

0.03	-0.98	0.28
0.04	-0.95	0.24
0.03	-0.29	0.28
0.04	-0.15	0.31
0.02	-0.53	0.21
0.03	-0.63	0.23
0.03	-0.19	0.25
0.04	-0.33	0.22
0.03	0.13	0.23
0.03	-0.06	0.23
0.03	-0.66	0.26
0.03	-0.21	0.27

Interplay between supercontinents and accretionary orogens recorded in 200 million years of metallogeny

Appendix 6 Analytical Methods

Yanbo Cheng[1] *, Phil Gilmore[1, 2], Michael Doublier[1], Karol Czarnota[1], Chris Lewis[1], Holly Taylor[1], Andrew Clark[1], Liam Pitt[1], David Mole[1], Yue Wang[3], Sebastien Meffre[4], Adrienne Brotodewo[5], Ross Cayley[6], Cameron Cairns[6], Antony Burhnam[1, 3], Tom Wise[7], Adrian Fabris[7]

1 Geoscience Australia, Canberra 2609, Australia

2 Geoscience, Exploration and Mineral Systems, Newcastle 2300, Australia

3 Research School of Earth Sciences, The Australian National University, Canberra 2601, Australia

4 Earth Sciences, University of Tasmania, Hobart 7006, Australia

5 MinEx CRC, Future Industries Institute, Adelaide University, Adelaide 5005, Australia

6 The Geological Survey of Victoria, Melbourne 3002, Australia

7 The Geological Survey of South Australia, Adelaide, 5000, Australia

* Correspondence: yanbo.cheng@ga.gov.au

Part 1 Geochronology

1. SHRIMP U-Pb measurement on titanite at the SHRIMP laboratory, Research School of Earth Sciences, the Australian National University (ANU)

1) Matrix correction

Ling et al. (2022) reported significant matrix effects in the U-Pb dating of titanite using the Cameca 1280 SIMS at CAS, Beijing. The calibrated ratio $^{206}Pb/^{238}U$ measured by SIMS was shown to differ by as much as ±15% from that measured by TIMS, depending upon the difference in Fe content between the reference and sample titanite respectively. Using five titanites of known age, Ling et al. defined a reference curve showing a well-defined curvilinear relationship between Pb/U_{TIMS} / Pb/U_{SIMS} and FeO_{sa}/FeO_{std}.

Before we attempted to date the Waratah and Eaglehawk titanites at RSES, therefore, a day was spent analysing titanite samples of known age, with a range of Fe contents, to see whether the RSES SHRIMP 2 showed a matrix effect, and if it did, whether the effect was similar to that reported for the 1280. The samples tested were recognised standards BLR-1 (1047 Ma), Khan (516 Ma) and MKED1 (1517 Ma). Titanite from two additional samples, both with zircon ages of 395 Ma, was also included: Moruya tonalite (06-057) and Bingie Bingie gabbroic diorite (98-106).

The analyses were done without energy filtering, at a mass resolution of about 5000, with a negative O_2 primary ion beam and a normal zircon U-Th-Pb run table, with Zr_2O replaced by $^{56}Fe^{16}O$ and $^{40}Ca^{48}Ti_2{}^{16}O_4$, respectively, the former providing an empirical estimate of relative Fe content, and the latter a reference mass for the jump to ^{204}Pb. Because time was short, the analyses were done using only 4 scans, and counting times were short, no more than 5 seconds on any isotope. The data were processed using POXI.

The analyses of BLR-1, used as the primary reference standard, were particularly coherent, and gave a clear indication that the slope of the lnPb/U – lnUO/U calibration line was 1.4, not 2.0 as found for zircon. The calibrated measurements of Khan Pb/U, with its relatively high Fe content, were on average about 3.5% higher than expected, and those of MKED1, with its relatively low Fe, about 5% lower than expected, although with quite a bit of scatter. This pattern was broadly consistent with matrix effect reported by Ling et al. The analyses of 06-057 were also scattered, but those of 98-106 were not too bad, considering the low Pb contents. To calculate the correction equation for SHRIMP 2, the FeO count rate for each spot was normalised to a constant primary beam strength (6 nA), the FeO count rate for BLR1 averaged, then FeO_{sa}/FeO_{std} calculated for each spot. The results, when plotted against Pb/U_{exp} / Pb/U_{meas} were more consistent with a straight-line relationship than the curve reported for the 1280. This is a very preliminary interpretation, but for the purpose of correcting the Waratah and Eaglehawk data, a straight-line relationship between the FeO ratio and matrix correction factor [Factor = $1.0952 – 0.0979*(FeO_{sa}/FeO_{std})$] was assumed.

2) Sample analyses

The Waratah and Eaglehawk titanites were run over the following two days, with 5 scans per spot and increased counting times on the Pb isotopes. Each day the FeO count rates were normalised to a constant PBM, and the FeO_{sa}/FeO_{std} ratios for each spot calculated relative to the mean FeO count rate for BLR1, the primary standard contained in the same epoxy mount as the samples. Khan and 98-106 in an adjacent mount were analysed a few times as secondary standards. PRAWN was used in preference to POXI to determine the isotope ratios and their uncertainties, primarily as a way of assessing the chemical and isotopic uniformity (or otherwise) of the analysed spots.

Two analyses of Waratah titanite and three analyses of Eaglehawk titanite were discarded because of unacceptably high intraspot heterogeneity. The corrections applied to the measured Pb/U ranged from 0.75 to 1.06 for Waratah titanites and 0.96 to 1.06 for Eaglehawk titanites, consistent with the more uniform Fe content in the latter. All spots selected for analysis were tested for FeO content prior to analysis, resulting in a small number of titanite grains in the Waratah sample not being analysed because their very high FeO was well beyond the range over which the matrix correction equation had been defined. Validation of the corrections applied to the other analyses was provided by the lack of correlation between FeO_{sa}/FeO_{std} and corrected Pb/U in the titanites from either sample.

The U content of each analysed spot was estimated from the UO count rate from the spot relative to that from BLR1, normalised to a constant PBM and assuming 260 ppm U in BLR1. No Th content for BLR1 was available, so Th ppm and Th/U for each spot was estimated assuming that ThO/UO = Th/U. In the absence of a validated Pb/Th calibration, Pb-Th dates could not be calculated.

a) ***Waratah altered monzonite***: Four rock blocks were included on the Waratah mount. Between 6 and 14 titanite grains from each block were analysed, 39 grains in all. Analyses from all blocks were combined in the final assessment.

Prior to correction for common Pb, the analyses were broadly distributed along a mixing line between radiogenic and common Pb compositions. Three analyses deviated from the array, indicative of either a younger component or radiogenic Pb loss. Corrected for 515 Ma common Pb using ^{204}Pb the analyses clustered on or close to concordia, with the three deviants distinctly offset from the main group. The radiogenic $^{206}Pb/^{238}U$ values for the main group calculated by correcting for common Pb using ^{207}Pb scattered more than expected from the analytical uncertainties (MSWD = 2.2). The scatter could be eliminated by omitting the two lowest and two highest analyses in the group, giving a weighted mean age of 513.8 ± 4.5 Ma (n = 30, MSWD = 1.2). Adding in the 0.19% uncertainty in the measured mean composition of BLR1 increased the 95% confidence limits to ± 4.9 Ma. The weighted mean radiogenic $^{206}Pb/^{238}U$ age of the three younger grains was 394 ± 37 Ma (MSWD = 0.2), the large uncertainty resulting mostly from the large t multiplier (4.3) required to calculate 95% confidence limits for a mean based on only three estimates.

b) ***Eaglehawk altered granodiorite***: Two rock blocks were included on the Eaglehawk mount. Most of the analyses (30) were done on titanite crystals in one block. Eight crystals were analysed in the second block. Dates from both blocks were combined in the final assessment.

Prior to correction for common Pb, the analyses were distributed, within analytical uncertainty, along a mixing line between radiogenic and common Pb compositions. Regression of the data (Isoplot) yielded a lower intercept equivalent to a mean radiogenic $^{206}Pb/^{238}U$ age of 425 ± 11 Ma. Corrected for 425 Ma common Pb using ^{204}Pb, most of the analyses plotted within uncertainty of concordia, a small number requiring the largest corrections plotting below, consistent with slight overcorrection. Corrected for common Pb using ^{207}Pb, all the analyses (n

= 35) yielded the same radiogenic $^{206}Pb/^{238}U$ within uncertainty (MSWD = 0.57), equivalent to a weighted mean age of 422.1 ± 5.4 Ma. Including the uncertainty in the measurement of the mean composition of BLR1 (0.38%) increased the 95% confidence limits to ± 6.2 Ma.

2. SHRIMP U-Pb measurement on titanite at the SHRIMP laboratory, Geoscience Australia

1) Methods

Two samples (9651900, from Wahratta, and 9651904, from Eaglehawk) were prepared as polished thin sections. Titanite crystals were identified by standard optical petrographic techniques (Sorby, 1851). The areas of interest in each thin section were subsequently extracted using an ultrasonic drill bit and mounted alongside a pre-polished puck of titanite U-Pb reference materials in a 1" epoxy mount (one sample per mount). The samples were carbon coated for examination using a Hitachi SU7000 scanning electron microscope. Qualitative mineral compositions were obtained by energy dispersive spectroscopy and images were obtained using backscattered electrons (BSE) to observe textural variations, compositional zoning and cracks and inclusions in the titanite crystals. The modal mineralogy was assessed using the AMICS software package.

Following the completion of SEM imaging, the carbon coat was removed and replaced with a 35 nm Au coat for analysis using the SHRIMP IIe at Geoscience Australia. A total of 44 analyses were conducted on titanite grains in sample 9651900 and 33 analyses were conducted on sample 9651904. The masses analysed were: 72 ($^{56}Fe^{16}O^+$, 1 s), 141 (Pr^+, 1 s), 200 ($CaTi_2O_4^+$, 5 s), 204 (Pb^+, 20 s), 204.05 (background, 20 s), 206 (Pb^+, 15 s), 207 (Pb^+, 40 s), 208 (Pb^+, 5 s), 238 (U^+, 5 s), 248 (ThO^+, 2 s), 251 ($ThF^+ + {}^{235}U^{16}O$, 5 s), 254 ($^{238}U^{16}O^+$, 2 s), 270 (UO_2^+, 2 s). Each analysis comprised six scans of the mass range, with autocentring on the first scan for all masses except 204, 204.05, 207, 208 and 251. Ling et al. (2022) identified a matrix effect in SIMS analysis of titanite, whereby U-Pb ages measured relative to a reference material may be offset to younger or older ages that those obtained by TIMS. This offset correlated best with the Fe content of the titanite. The present study used MKED1 (Spandler et al., 2016) as the primary reference material, and the secondary reference materials were BLR-1 (Aleinikoff et al., 2007), OLT1 (Kennedy et al., 2010), Khan River and Bear Lake (Mazoz et al., 2022) and Separation Point (Harrison and McDougall, 1980), and glasses TNT150 and TNT1500 from Klemme et al. (2008) for trace element concentrations.

Data were reduced using SQUID 2.50.11.02.03, using ^{207}Pb as the reference isotope for Stacey-Kramers common Pb correction. The Pr concentration was approximated assuming a linear relationship between Pr concentration and the $Pr/CaTi_2O_4$ peak using TNT1500 (Klemme et al.,2008) as the primary reference material, with no attempt to correct for deviations from ideal $CaTiSiO_5$ stoichiometry, which was beyond the scope of this work. The Fe_2O_3 concentration was estimated from FeO cps using the average published compositions of Bear Lake, BLR1, Khan River and MKED1: this and the estimated Pr concentration are probably only accurate to within 10 %. $^{206}Pb/^{238}U$ was calculated on the basis of $\ln(^{206}Pb^*/^{238}U)$ versus UO_2/UO with a fixed slope of 0.9 (Kinny, 1997), the U concentration was estimated using the equivalent power-law relationship established for zircon (Claoue-Long et al., 1995) and the Th/U ratio was estimated using the equivalent zircon expression from Williams et al. (1996). The average U-Pb ages for all analyses on the secondary reference materials were compared to their expected (ID-TIMS) ages and regressed against their average FeO^+ count rates (counts per second, cps).

The resulting expression was applied to the unknowns on a spot-by-spot basis to minimise the influence of matrix effects on the measured result.

2) Results

The titanite crystals analysed in 9651900 ranged from ~50 to ~500 µm in length. They were variable in their morphology. Some crystals had domains with abundant cavities, possibly representing exposed fluid inclusions, and some crystals had abundant inclusions of other minerals; some crystals had internal domains of apparently skeletal growth with chlorite; some crystals had ragged irregular margins; some crystals lacked inclusions and had euhedral habits. Internal zonation features, as observed in the backscattered electron images, were also variable, with textures varying from irregular or convolute zoning to euhedral oscillatory and sector zoning. Some titanite occurred as rims on or veins crosscutting ilmenite and other phases in the Fe-Ti-O system.

The titanite crystals analysed in 9651904 ranged from ~50 to ~500 µm in length and varied from anhedral to euhedral. Titanite was commonly associated with irregularly-zoned diopside. Internal zoning was typically more subtle than in 9651900 and, where detectable, was irregular or convolute. In several cases titanite occurred as aggregates of euhedral crystals.

In calculating the uncertainty on the weighted average, the component of uncertainty arising from the regression of U-Pb age against FeO cps must be included. As the physical basis of this effect is not well established, and BLR-1 is reported to be heterogeneous on a crystal-to-crystal basis, the uncertainty on the correction factor is likely to comprise a mixture of systematic and random effects. The standard deviation of the residual deviation of the reference material ages from their ID-TIMS ages, after correcting for the FeO effect, was 1.0 %. This error was added in quadrature to the uncertainty from counting statistics on each spot, and after calculating a weighted mean the uncertainty on the Pb/U calibration constant from the primary standard was further added in quadrature. As the change in ages from the raw values to the corrected values is small, with an average absolute change of 4.5 Ma for 9651900 and 2.5 Ma for 9651904. Further work is required to understand the FeO effect better and assess whether it is more appropriate to add it on to the weighted mean age rather than at an individual spot level. One analysis (9651900-2.4) was rejected because the peak autocentring at nominal mass 200 had selected the $CeSiO_2^+$ peak, 24 mDa heavier than the intended $CaTi_2O_4^+$ peak, and thus the data for ^{204}Pb and background were measured at incorrect masses. All other analyses of 9651900 formed a statistically acceptable group and no analyses were excluded. For 9651904, two analyses were excluded for scattering to young and old ages (9651904-1.5 and 9651904-1.9, respectively).

On the basis of the above calculations and exclusions, the weighted mean ^{207}Pb-corrected $^{206}Pb/^{238}U$ age for 9651900 (Wahratta) is 517.8 ± 3.7 Ma (2-sigma error of the mean; n = 43; MSWD = 1.00; probability of fit = 0.48) and the weighted mean ^{207}Pb-corrected $^{206}Pb/^{238}U$ age for 9651904 is 420.5 ± 4.0 Ma (2-sigma error of the mean; n = 31; MSWD = 1.15; probability = 0.26). The two samples show striking differences in their composition. Sample 9651900 has some crystal cores with Fe_2O_3 > 2.0 %, and these have 1398 ± 664 ppm Pr (1s) and 542 ± 404 ppm U (1s), but the majority of analyses have 1.0 – 1.5 % Fe_2O_3, 946 ± 295 ppm Pr and 63 ± 62 ppm U. Th is highly variable, ranging from 30 – 1920 ppm. The fraction of common Pb (calculated from ^{207}Pb) averages 1.1 % and was elevated in regions with a higher density of fluid inclusions. Sample 9651904 (Eaglehawk) has a maximum Fe_2O_3 of 1.9% and lacks a correlation between Fe_2O_3 and Pr, U or Th. Pr is significantly lower than in 9651900, at 100 ±

12 ppm; U and Th are somewhat lower and more uniform at 34 ± 19 ppm and 47 ± 13 ppm, respectively. Common Pb is significantly higher than in 9651900, at 13 ± 7 % (1s). These differences are likely due to the contrasting host rocks, as titanite from felsic igneous rocks typically has higher concentrations of REE such as Pr than titanite from mafic rocks (Scibiorski and Cawood, 2022).

3. U-Pb laser ablation inductively coupled plasma mass spectrometry (LA-ICP-MS) dating of titanite and apatite at the Adelaide Microscopy, University of Adelaide

Sample 2023440366 from Thackaringa Pb-Zn-Ag deposit was submitted to Adelaide Microscopy Rb-Sr dating of muscovite and Lu-Hf dating of siderite by LA-ICP-MS/MS. The hand specimen was cut and prepared into a 1-inch round polished epoxy block – two pieces were mounted one perpendicular to the marginal muscovite vein and the other parallel (e.g., exposing the planar surface of the vein).

Laser ablation inductively coupled plasma mass spectrometry (LA-ICP-MS) analyses were done using a RESOlution-SE 193 nm ArF excimer laser ablation system with a S155 large format sample chamber, coupled to an Agilent 8900 ICP-MS/MS. He and Ar were used as the ablation and carrier gasses respectively, and 4 ml/min N_2 was added to the carrier gas to enhance sensitivity for isotope analyses.

For Lu-Hf analysis, NH_3 was used as the reaction gas to chemically separate the isobaric overlap between ^{176}Lu and ^{176}Hf (Simpson et al. 2022). For Rb-Sr analysis, N_2O was used as the reaction gas to chemically separate the isobaric overlap between ^{87}Rb and ^{87}Sr (Redaa et al., 2021). Muscovite was analysed for Rb-Sr with a spot size of 67 μm, a fluence of ~3.5 J/cm^2 and a repetition rate of 5 Hz. Siderite was analysed for Lu-Hf with a spot size of 257 μm, a fluence of ~10 J/cm^2 and a repetition rate of 10 Hz. NIST610 was used as the primary reference material for Rb-Sr and Lu-Hf dating, with matrix correction against secondary standards of known age: Entire Creek biotite (312 Ma), and Mt Elliott calcite (1531 Ma). All data was processed using LADR software and isochrons plotted using isoplotR.

4 U-Pb laser ablation inductively coupled plasma mass spectrometry (LA-ICP-MS) dating of titanite and apatite at the Centre for Ore Deposits and Earth Sciences (CODES) Analytical Laboratories, University of Tasmania

Selected areas on each 25 mm diameter polished mounts containing apatite or titanite were analysed using an Agilent 7700 quadrupole ICPMS with a 193 nm Coherent Ar-F gas laser and the RESOlution S155 ablation cell at the University of Tasmania in Hobart. The laser was operated using a 29 μm spot size, pulsing at 5 Hz with a fluence of 2 Jcm^{-2}. Each analysis on the minerals began with a 30 s blank gas measurement followed by a further 30 s of analysis time when the laser was switched on.

When analysing apatite, the following elements and isotopes were analysed: ^{23}Na, ^{31}P, ^{43}Ca, ^{51}V, ^{56}Fe, ^{88}Sr, ^{89}Y, ^{139}La, ^{140}Ce, ^{141}Pr, ^{146}Nd, ^{147}Sm, ^{150}Nd ,^{153}Eu,^{157}Gd, ^{159}Tb, ^{163}Dy, ^{165}Ho, ^{166}Er, ^{169}Tm, ^{172}Yb, ^{175}Lu, ^{204}Pb, ^{206}Pb, ^{207}Pb, ^{208}Pb, ^{232}Th, ^{235}U and ^{238}U. These were chosen to optimise the geochronological and geochemical information collected and enable determination of the trace element content of apatite and the recognition mineral inclusions that could interfere with the geochronology.

The downhole fractionation, instrument drift and mass bias correction factors for Pb/U ratios on apatite were calculated using the OD306 apatite as the primary reference material for calibration of the Pb/U ratios, downhole fractionation and to correct instrumental drift (Huang et al., 2015; Thompson et al., 2016). The correction factor for the $^{207}Pb/^{206}Pb$ ratio was calculated using large spot of NIST610 analysed throughout the day and corrected using the values recommended by Baker et al. (2004). The Durango (McDowell et al., 2005), McClure Mountain (Schoene & Bowring, 2007), and 401 apatite (Thompson et al., 2016) apatite were used as secondary geochronological reference materials to check the calibrations. The data was processed using the LADR software (Norris and Danyushevsky 2018) using standard quantification protocols.

Trace element concentrations were calculated using Ca as the internal standard element assuming stoichiometric proportions in apatite. GSD-1g and BCR-2G reference glasses were also used as secondary standards for the trace element calculations (Jochum et al., 2011; Rocholl, 1998).

Titanite analyses were performed using the same equipment, analytical conditions, and similar techniques. The primary standards used for calibration of the U/Pb ratios was the 19686 titanite (Thompson et al., 2016). Secondary standards, including AUR100606 (Best 2012), Fish Canyon 3 (Daze et al. 2003) and Mt Dromedary (Kohn et a 1990) were used to check the calibrations.

The elements analysed also differed from that used for apatite. These included ^{27}Al, ^{29}Si, ^{43}Ca, ^{49}Ti, ^{55}Mn, ^{56}Fe, ^{89}Y, ^{90}Zr, ^{93}Nb,^{139}La, ^{140}Ce, ^{141}Pr, ^{146}Nd, ^{147}Sm, ^{150}Nd ,^{153}Eu,^{157}Gd, ^{159}Tb, ^{163}Dy, ^{165}Ho, ^{166}Er, ^{169}Tm, ^{172}Yb, ^{175}Lu, ^{178}Hf, ^{181}Ta, ^{204}Pb, ^{206}Pb, ^{207}Pb, ^{208}Pb, ^{232}Th, ^{235}U and ^{238}U.

The isoplot software (Ludwig et al 1994) was used to calculate weighted averages and plot Concordia diagrams.

5 Sm-Nd and Rb-Sr isotope analysis of fluorite at the University of Melbourne

Five samples of fluorite (0.5-1.5 mm fragments, 18-171 mg) and one sample of fluorite-poor vein/alteration material (quartz, chlorite, calcite) handpicked from coarsely crushed vein material were briefly cleaned with dilute nitric acid (<0.1M HNO_3) and then dissolved in concentrated distilled HCl at high pressure (170°C, 48 hrs). Fluorite dissolved well in the HCl; where impurities of other minerals were present (notably in the fragments of mixed vein/alteration material), the samples were further reacted with hydrofluoric and nitric acid. Based on preliminary trace element data, the 6 solutions were mixed with ^{149}Sm-^{150}Nd and ^{85}Rb-^{84}Sr spikes and dried down. The elements of interest were extracted using Eichrom TRU- and LN-resin (Sm, Nd) and Eichrom Sr-resin and BioRad AG50-X8 (200-400) cation resin (Sr, Rb, e.g., Maas et al., 2022). Procedural blanks (<0.1 ng) were negligible in all cases.

Isotopic data were acquired on a Nu Instruments Sapphire multi-collector ICP-MS with sample uptake via a Glass Expansion PFA nebuliser and a CETAC Aridus desolvating system (e.g., Sudholz et al., 2023). Instrumental mass bias for spiked Sr and Nd fractions was corrected by normalizing to $^{88}Sr/^{86}Sr = 8.37521$ and $^{146}Nd/^{145}Nd = 2.0719425$ (equivalent to the more familiar $^{146}Nd/^{144}Nd = 0.7219$, Vance and Thirlwall, 2002), using the exponential law as part of an on-line iterative spike-stripping/internal normalization procedure. Data are reported relative to SRM987 Sr = 0.710230 and La Jolla Nd = 0.511860, respectively. External precision (reproducibility, 2sd) is ±0.000040 (Sr) and ±0.000020. Isotope dilution analyses of spiked Rb were done using the Zr-doping method of Waight et al. (2002); $^{87}Rb/^{86}Sr$ and $^{147}Sm/^{144}Nd$

measured by isotope dilution have external precisions of ±0.5 and ±0.2% (2sd), respectively. ƐNd values are calculated relative to modern CHUR composition with $^{147}Sm/^{144}Nd = 0.1960$ and $^{143}Nd/^{144}Nd = 0.512630$, (Bouvier et al., 2008). Decay constants are: ^{87}Rb $1.397x10^{-11}$/yr; ^{147}Sm $6.54x10^{-12}$/yr.

Part 2 Sulphur isotopes

1 Sulphur isotopes analysis of pyrite and chalcopyrite at The Central Science Laboratory, University of Tasmania

1) Sample preparation

The samples were delivered into the CSL-IRMS lab as coarsely crushed material (Figure 17), containing previously identified type of sulphide. A small subsample of bits visibly containing sulphide grains was selected, ground up using agate mortar and pestle and used for analysis. Based on the estimated average element content in the samples, between 0.3 and 0.4 mg of finely powdered sample was weighed on an ultra-micro balance (MCA2.7S-2S00-M, Sartorius, DE, readability 0.1 µg) into tin cups (Elemental Microanalysis, UK, 8 x 5 mm).

2) Sulphur isotope analysis

The samples were loaded into the autosampler of an EA-IRMS system (pyroCube - Isoprime 100, Elementar, DE). In the Elemental Analyser the samples are flash combusted at 1120°C in an oxidation column filled with granular tungsten (VI)oxide. Oxidated species are reduced at 850°C to CO_2, N_2 and SO_2 in a copper filled reduction column. In a 99.9995% helium carrier gas flow the produced gaseous species are stripped of water in traps filled with indicator loaded Sicapent® (Merck, DE). The SO_2 component is separated from other combustion products by a purge and trap system, it's release occurs when the desorption column is heated to 220°C. The sample gas then bypasses the CO_2 column (where it could potentially be retained), passes through a second water trap and enters the IRMS. Reference gas pulses of SO_2 (99.9%, 15 psi) were delivered through a dual reference gas injector module (Isoprime, Elementar, DE), with carrier gas helium regulated to 1.5 psi. Instrument Control and data evaluation is carried out using Vario PyroCube v4.0.9 and IonVantage v1.7.3.0 software packages (Elementar, DE). All consumables were obtained from Elemental Microanalysis, UK, all gases by BOC, AU).

3) Traceability

Elemental data is factored using sulfanilamide standards every 6th sample. Blank values obtained for an empty tin cup is subtracted to each peak area. Stable isotope abundances are reported by Skrzypek et al. (2022) in delta (∂) values as the deviations from conventional standards in parts per mil (‰) from the following equation (Coplen, 2011):

$\delta^{34}S$ (‰) = $[(R_{sample}/R_{standard} -1) \times 1000]$
where R = the ratio $^{34}S/^{32}S$

For calibration of sulphur isotopic data, the following Certified Reference Materials and $\delta^{34}S_{CDT}$ values by Meija and Chartrand (2018) were used: IAEA-S1 (-0.3, by definition), IAEA-S2 (22.66 ± 0.13‰), IAEA-S3 (-32.3 ± 0.12‰), IAEA-S4 (16.86 ± 0.03‰), IAEA-SO5 (0.49 ±

0.09‰), IAEA-SO6 (-34.18 ± 0.07‰), NBS-123 (17.44 ± 0.13‰) and NBS-127 (20.32± 0.34‰). At least two CRMs are measured in duplicate at the beginning and the end of each daily group of analyses. Obtained samples data is only considered when within the calibration bracket of the used reference materials.

2 Sulphur isotopes analysis of pyrite and chalcopyrite at The Sensitive High Resolution Ion Microprobe (SHRIMP) Laboratory, Australian National University

1) Sample preparation

The thin section samples are degreased before coating. The samples are washed in ethanol and followed by 30s ultrasound. Then scrub the samples with degreaser solution (mixing warm water with several drops RBS 50 detergent) using kimiwipe, followed by 30s ultrasound. Afterwards, rinse with hot water then distilled water followed by 30s ultrasound. The last step is to dry the samples in 60-degree oven for 30 minutes.

2) Sulphur isotope analysis

Thin sections were then coated with 10 nm thick Al alyer to be analysed in the SHRIMP SI ion microscope at the RSES SHRIMP laboratory of the Australian National University. The primary beam was Cs^+ with a source current around 1.5nA. The primary ion optics was configured with a 200 μm Kohler aperture to produce a ~22 μm diameter spot on the surface of thin section. The primary beam was optimized by adjusting deflection lens of Cs source and Source steering lens of primary column. The secondary beam was maximizing its signal on post-ESA monitor (PESAM), and the source slit was set to 120 μm.

Peak shapes were optimized to their best collector position and focuses, yielding peaks with high resolution and low residual. Two Faraday cups were used to collect each S isotope peak at the same magnetic field after peak alignment. HM Faraday cup was assigned to collect ^{34}S with 10E12Ω resistor while the LM Faraday cup collected ^{32}S with 10E11Ω resistor. 200μm collector slits were applied on each Faraday cup.

For measurement, 1 minute after raster burn time was applied after 20 seconds background measurement, following with 10 seconds peaks auto-centring on each spot. The S isotope ratio was measured in 6 scans of 20 seconds counting time, with a total measuring time of 120 seconds per spot. Ruttan and Balmat pyrite were analysed as primary and secondary standards every 5 spots on samples, and S isotope ratios of samples were then calibrated by the weighted mean value of Ruttan pyrite standard in each session.